Improving the Design of Diarylethene Photoswitches and their Exploitation as Remote-Controlled Building Blocks

DISSERTATION

zur Erlangung des akademischen Grades
doctor rerum naturalium
(Dr. rer. nat.)
im Fach Chemie

eingereicht an der
Mathematisch-Naturwissenschaftlichen Fakultät
der Humboldt-Universität zu Berlin

von
Dipl.-Chem. Martin Herder

Präsident der Humboldt-Universität zu Berlin
Prof. Dr. Jan-Hendrik Olbertz

Dekan der Mathematisch-Naturwissenschaftlichen Fakultät
Prof. Dr. Elmar Kulke

Gutachter: 1. Prof. Stefan Hecht, Ph.D.
2. Prof. Dr. Nikolaus P. Ernsting
3. Prof. Dr. Ben L. Feringa

Tag der mündlichen Prüfung: 20.04.2015

Die vorliegende Arbeit wurde in der Zeit von Oktober 2010 bis Februar 2015 am Institut für Chemie der Humboldt-Universität zu Berlin unter der Anleitung von Prof. Stefan Hecht, Ph.D. angefertigt.

Danksagung

An dieser Stelle möchte ich mich bei allen bedanken, die mich bei der Anfertigung meiner Dissertation tatkräftig unterstützt haben.

Besonderer Dank gilt Prof. Stefan Hecht für das große in mich gesetzte Vertrauen, die zahlreichen Gespräche, in denen ich sehr viel gelernt habe und immer motiviert wurde, die hervorragenden Arbeitsbedingungen und die stete Hilfe bei Problemen jeder Art.

Allen derzeitigen und ehemaligen Mitgliedern der Arbeitsgruppe danke ich für die tolle Arbeitsatmosphäre, die gegenseitige Unterstützung und den freundschaftlichen Umgang im und außerhalb des Labors. Ein großer Dank geht an Micha und Lutz. Danke für die enge Zusammenarbeit, die vielen wissenschaftlichen und nicht-wissenschaftlichen Gespräche, die zahlreichen spektroskopischen und elektrochemischen Messungen, die große Unterstützung für meine Arbeit und dafür, immer ein offenes Ohr zu haben. Meinen Laborkollegen Robert, Sonia, Henry, Anne, Bernd, Fabian und Derk-Jan gilt großer Dank für die tolle Zusammenarbeit, den (meist) exzellenten Musikgeschmack und dafür über lange Tage das Rotlicht ausgehalten zu haben. Philipp danke ich für die Freundschaft und die zahlreichen leidenschaftlichen Gespräche über Chemie und anderes, Björn für die eine oder andere Lektion im Skat und Doppelkopf sowie für die schönen Abende im Garten und Robert für die inspirierende Zusammenarbeit und Unterstützung. Bei Herrn Leistner möchte ich mich für die stete Hilfe bei analytischen Problemen bedanken. Für die synthetische Unterstützung bedanke ich mich bei Jutta, Jana und Henry. Meiner Forschungspraktikantin Anne sowie meinen Bachelorstudenten Fabian und Anna danke ich für das Engagement und die gute Zusammenarbeit. Großer Dank gilt auch allen Mitarbeitern in den analytischen Abteilungen des Instituts für Chemie, deren tägliche Arbeit die Grundlage für meine Dissertation ist. Vielen Dank auch an die Korrekturleser meiner Arbeit Maren, Philipp und Fabian.

I am very grateful to Prof. Paolo Samorì and the people in his group, especially Emanuele, Núria, Mirella, Karl, Sara and Thomas, for the very inspiring and fruitful collaboration. Manuel Utecht danke ich für quantenmechanische Rechnungen sowie Johannes Frisch für die UPS Messungen.

Ein herzlicher Dank gilt meiner Familie, die mir das Studium ermöglicht und mich immer unterstützt hat. Meinen Freunden und Kommilitonen danke ich für die schöne Zeit während meines Studiums und meiner Promotion.

Zu guter Letzt möchte ich einen ganz besonderen Dank an Maren richten. Vielen Dank für deine Liebe, dein Vertrauen und die Kraft, die du mir gibst.

Abstract

Among molecular units that can be reversibly switched between two states by light, diarylethenes have the unique property that the π-electronic structure of their molecular backbone significantly alters during the isomerization process, resulting in a marked shift of HOMO and LUMO levels. The incorporation of diarylethene switches into more complex molecular systems would allow for the reversible light-controlled manipulation of specific functions, such as catalytic activity, association behavior, or charge transport, due to the modulation of inherent electronic properties. However, to fulfill this task the photochromic scaffold has to be improved in terms of its switching efficiency, fatigue resistance, and extent of electronic modulation.

In this work, a series of diarylethenes is synthesized by systematically varying the constituents of the hexatriene core and the terminal substituents. By the in-depth characterization of the photochemical reaction to a by-product, an ubiquitous phenomenon of diarylethene photochromism, fatigue resistant structures are identified that allow for the reliable operation of the photochrome over many switching cycles and at the same time guarantee a high degree of structural and synthetic flexibility. Furthermore, a distinct substitution pattern is found to enable the orthogonal electro- and photochemically mediated isomerization of diarylethenes. By proper modulation of the structure, the fatigue observed during the oxidative cyclization reaction is minimized and insights into the underlying mechanism are gained. The impact of different substitution patterns on the π-electronic structure of the diarylethene core is studied and it is shown that HOMO and LUMO levels can be tuned over a broad energy range.

Finally, the electronically tuned diarylethenes are applied as active building blocks in light-controllable organic thin film transistors, which show a modulation of the output current upon isomerization of the photochrome. In a second approach to exploit the isomerization induced electronic modulations, a potentially catalytically active guanidine unit is coupled to the diarylethene core in order to construct a photoswitchable organocatalyst.

Kurzzusammenfassung

Unter Molekülen, die durch Licht reversibel zwischen zwei Zuständen geschaltet werden können, haben Diarylethene die einzigartige Eigenschaft, dass ihr π-Elektronensystem durch den Isomerisierungsprozess stark verändert wird, was zu einer Verschiebung von HOMO und LUMO Niveaus führt. Die Verwendung von Diarylethenen in komplexeren Systemen würde die Steuerung von bestimmten Funktionen, wie katalytische Aktivität, supramolekulare Assoziation oder Ladungstransport, mit Hilfe von Licht durch die Änderung inhärenter elektronischer Eigenschaften ermöglichen. Allerdings muss die photochrome Baueinheit den spezifischen Anforderungen angepasst und ihre Schalteigenschaften, die Ermüdungsresistenz sowie das Ausmaß der elektronischen Modulation verbessert werden.

In dieser Arbeit wird durch systematische Variation der zentralen Komponenten und der terminalen Substituenten eine Serie von elektronisch modulierten Diarylethenen synthetisiert. Durch umfangreiche Untersuchungen zur photochemischen Bildung eines Nebenprodukts, ein Prozess der bei nahezu allen Diarylethenen auftritt, können Strukturen identifiziert werden, die über eine große Zahl von Schaltzyklen ermüdungsresistent sind und gleichzeitig eine hohe strukturelle und synthetische Flexibilität bieten. Weiterhin erlauben bestimmte Substitutions-muster die orthogonale elektro- und photochemische Steuerung des Isomerisierungsprozesses. Durch geeignete strukturelle Modulation wird die Nebenproduktbildung bei der oxidativen Zyklisierungsreaktion unterdrückt und es kann ein Einblick in den zugrunde liegenden Mechanismus erhalten werden. Der Einfluss verschiedener Substitutionsmuster auf das π-Elektronensystem von Diarylethenen wird untersucht und es wird gezeigt, dass HOMO und LUMO Level über einen großen Energiebereich moduliert werden können.

Schließlich werden die so erhaltenen, elektronisch modulierten Diarylethene als aktive Elemente in Licht gesteuerten organischen Dünnschichttransistoren eingesetzt. Diese zeigen eine Änderung im Strom-Ausgangssignal durch die lichtinduzierte Isomerisierung der photochromen Moleküle. In einem zweiten Ansatz die schaltbaren elektronischen Änderungen in Diarylethenen zu nutzen, wird ein potentiell katalytisch aktives Guanidin mit der photochromen Einheit gekoppelt, mit dem Ziel einen photoschaltbaren Organokatalysator zu konstruieren.

Table of contents

1. Introduction

Since the beginning of modern organic chemistry the major task of a synthetic chemist is designing and making molecules, such as reagents, catalysts, drugs, or dyes, as well as materials, *i.e.* ensembles of molecules such as polymers, crystals, or (metal) organic frameworks, which fulfill specific functions. These functions are often based on macroscopic physical properties, such as morphology, color, or charge transport ability, as well as specific chemical properties, for example a certain reactivity or binding affinity. Nowadays there is an increasing demand for complexity and at the same time specificity of these functions, which cannot be met by ordinary molecules or materials only passively interacting with their surroundings. However, imparting responsiveness to external stimuli to a molecule or material enables them to dynamically adapt their properties upon changing surrounding conditions or to exert their function on-demand and in a highly controlled fashion. Stimuli used to control such "smart" systems may be temperature, pressure, the presence of chemical substances, such as protons or metal ions, or an electrochemical potential. Moreover, light is a highly interesting external stimulus due to a number of advantages: It is non-invasive, can be applied over large distances, can easily be tuned in terms of intensity as well as photon energy, and with modern laser techniques an extraordinarily high time resolution can be achieved.

To create "smart" responsiveness of matter to light a molecular interface is needed that dynamically interacts with the photons giving rise to the desired property change.[1] Conventional chromophores may be considered for this, *i.e.* the alternated properties of their excited states are utilized, for example in photoredox catalysis. However, as excited states generally have short lifetimes, a change of properties in the ground state upon light irradiation is desirable. Prominent examples for this are photoacids and photocleavable protecting groups irreversibly setting free a reactive species upon interaction with a photon. Nevertheless, to fully exploit dynamic light responsiveness for the construction and the control of complex molecular systems, a reversible nature of the interaction of molecules with photons is mandatory. For this purpose photochromic compounds, *i.e.* molecules that can be switched reversibly between two or more states with differing physical and chemical properties,[2] have to be used.

Different classes of photochromic compounds have been developed on the basis of a number of reversible photochemical reactions (Scheme 1).[2] The largest family is based on pericyclic reactions such as 6π-electrocyclizations (*e.g.* diarylethenes, spiropyrans and -oxazines, furyl fulgides and fulgimides) or [4+4] and [4+2] cycloadditions (*e.g.* polycyclic hydrocarbons such as anthracene and helianthrene). Another important family evolves from the *E/Z* isomerization of a double bond in azobenzenes, imines and hydrazones, stilbenes, or naturally occurring retinal. Moreover, a number of other photochemical reactions give rise to

interesting photochromes, for example a hydrogen transfer reaction in anils or a homolytic bond cleavage in triarylimidazole dimers. Upon irradiation all of these molecules significantly change their properties, such as absorbance and emission, molecular shape and flexibility, redox potentials, or dipole moment.

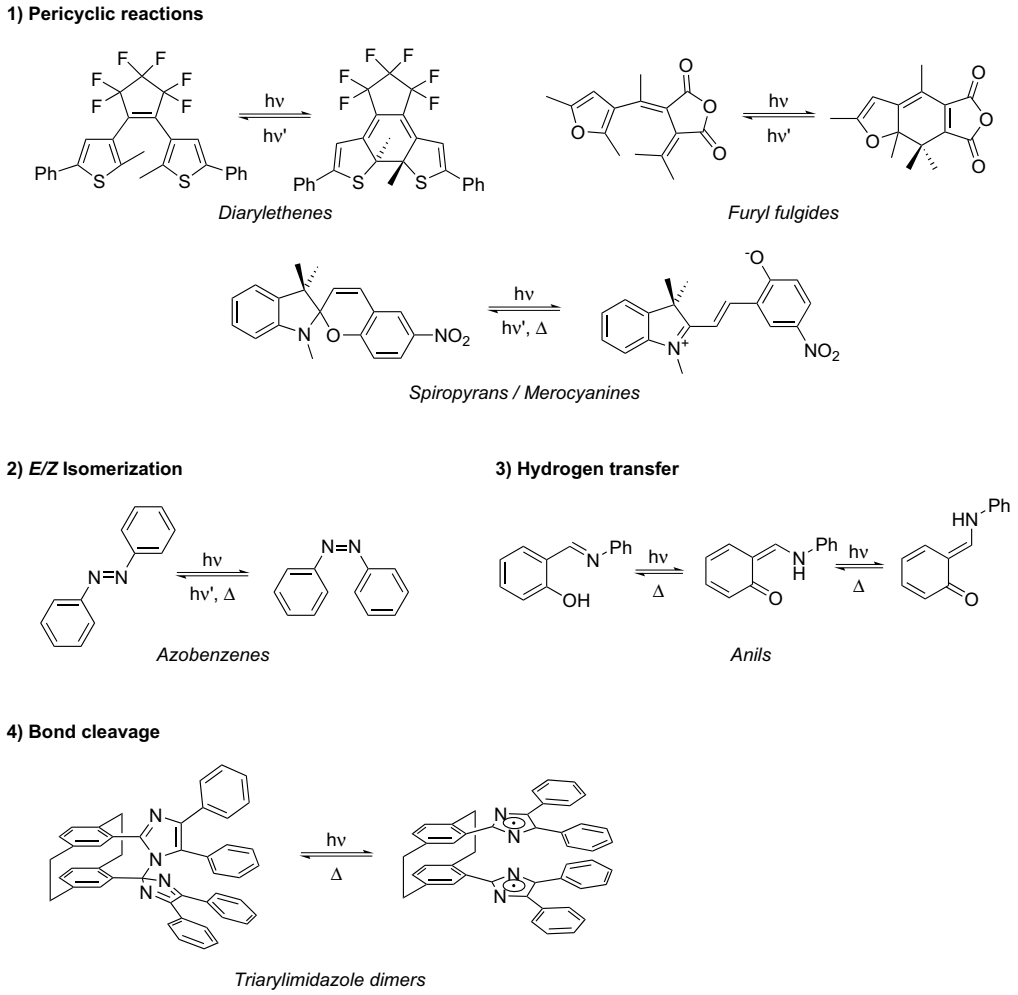

Scheme 1. Important types of photochemical reactions and derived classes of photochromic compounds.

The versatility of photochromic compounds leads to their application in diverse fields of natural sciences. They are used to remote-control functions on the molecular scale, such as reactivity and catalysis allowing for the precise regulation of chemical reactions,[1,3] single molecule fluorescence being utilized in sensing applications and superresolution microscopy,[4] or specific binding interactions for the photocontrol of self-assembled structures and biological systems.[5] Additionally, intriguing light responsive functionalities arising from molecular ensembles containing photochromes can be realized, such as photoactuation and –mechanics,[6] optical memory elements, as well as light-controllable organic electronic devices.[7] However, in order to achieve such functional systems with technological relevance it is mandatory to optimize the utilized photochromic compounds in terms of the desired property change, their switching

efficiency, and, often overlooked, their resistance to fatigue, *i.e.* the decomposition of the photochromic material over a large number of switching cycles.

In this work the class of photochromic diarylethenes (DAEs) is exploited in terms of their applicability as light responsive gates for the construction of remote controllable functional systems and devices. DAEs are one of the most potent families of photochromic compounds with a number of properties that make them superior to others: In general, the photochemical interconversion between the two isomers is highly efficient, both isomers are thermally stable, and they are regarded to be one of the classes of photochromes possessing outstanding fatigue resistance.[8] Additionally, in contrast to azobenzenes, they undergo only a small structural change during their isomerization reaction, which makes them ideally suited for applications in the solid phase.[9] However, the outstanding feature of DAEs is the pronounced change of their π-electronic system during the isomerization reaction accompanied by a significant alternation of electronic levels and thus redox potentials.

In this work the change of electronic properties of DAEs upon isomerization shall be utilized in two ways: On the one hand the different energy level alignment of the two isomers is employed to switch the charge transport of organic semiconducting matrices, thus implementing an additional remote-control for the function of a molecular ensemble (Chapter 4.6). On the other hand the alternation of electron density shall be transduced to a specific site of the photochromic molecule, modulating its chemical reactivity or even catalytic activity (Chapter 4.7). Prior to that, a central part of this work is concerned with the modification and improvement of the design of the parent DAE motif in order to meet criteria identified to be crucial for any application: Although generally regarded as highly fatigue resistant in the literature, it is found during this work that most DAE derivatives undergo a photochemical side reaction, and therefore strategies are developed to minimize the fatigue (Chapter 4.3). Additionally, fine tuning of the electronic changes occurring during the isomerization reaction as well as orthogonal photochemical and electrochemical switching of the DAE motif is realized (Chapters 4.4 and 4.5). In advance to these results some background on the photochemistry of diarylethenes and their utilization in light-responsive functional systems (Chapter 2) and a more detailed introduction into the molecular design (Chapter 3) are given. The syntheses of all diarylethene structures investigated are collected in Chapter 4.1, while Chapter 4.2 describes procedures for the conduction and evaluation of quantitative photochemical measurements that were established during this work.

2. Theoretical background

2.1 Diarylethene photoswitches

2.1.1 General structure-property relationships

The photochromism of diarylethenes is based on the 6π-electrocyclization and –cycloreversion reaction between a 1,3,5-hexatriene and a 1,3-cyclohexadiene core, which proceeds according to the Woodward-Hoffmann rules for the conservation of orbital symmetry[10] in a disrotatory manner when performed thermally and conrotatory after photochemical excitation. As the hexatriene core is incorporated in a tricyclic structure normally containing two (hetero)aromatic moieties, its thermal cyclization to the disrotatory ring-closed isomer has an endergonic character, thus only the photochemical reaction pathway is available (Figure 1a). Assuming a thermal equilibrium between the energetically similar antiparallel and parallel conformer of the ring-open isomer, only 50% of the molecules can undergo the conrotatory reaction after excitation, which results in a theoretical maximum quantum yield of 0.5. In fact, typical quantum yields for ring-closure of DAEs are in the range 0.1 – 0.6.[8a,11] However, the value may be significantly higher if an energetic preference for the antiparallel conformer exists in the ground state.[12] As the activation energy of a conrotatory cyclization/cycloreversion in the ground state is very high, generally both isomers are thermally stable, even at elevated temperatures.[8a]

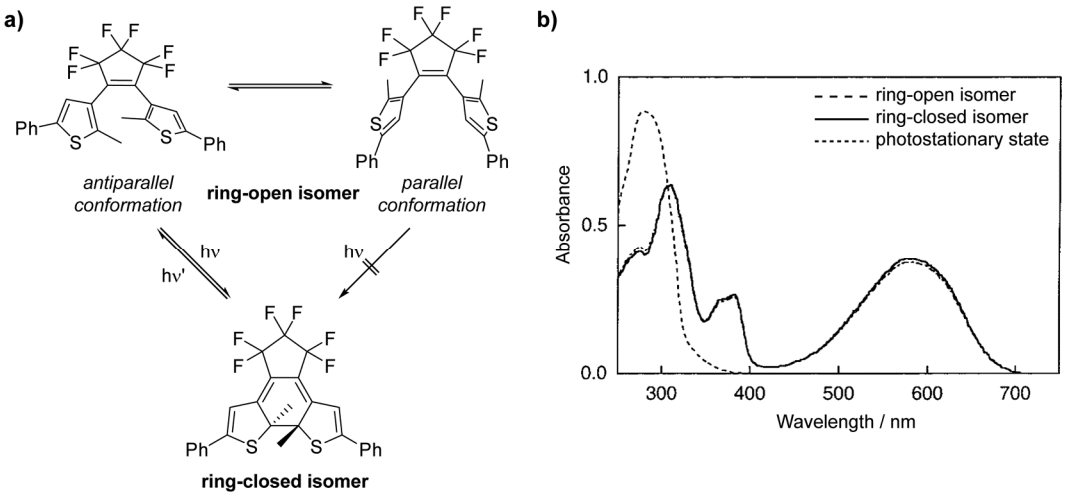

Figure 1. a) Conrotatory cyclization of the antiparallel conformer of a prototype DAE. b) UV/Vis spectra of the ring-open and ring-closed isomer as well as the photostationary state after irradiation with 313 nm light in hexane.[13]

Typically the ring-open isomer of a DAE strongly absorbs in the UV range of the electromagnetic spectrum (Figure 1b), which is characteristic for its electronically decoupled, cross-conjugated (hetero)aryl moieties. Excitation with UV light results in a fast development of a broad absorption band in the visible range, which can be ascribed to the ring-closed isomer with its π-electrons delocalized over the entire molecular backbone. As both isomers generally absorb UV light, a photostationary state (PSS) evolves, with its composition being highly dependent on the quantum yields of the forward and back reaction. Often on the DAE core a substitution pattern is chosen (*vide infra)* that effects a quantum yield for the cycloreversion around one magnitude smaller than that for the cyclization resulting in a conversion of >90% to the ring-closed isomer in the PSS upon UV light irradiation.[11] During the visible light driven back reaction a quantitative conversion is achieved, as only the ring-closed isomer absorbs at the excitation wavelength.

The principle structure of DAEs was already derived in the mid-1960s from detailed investigations of the photochemistry of stilbenes and hetarylstilbenes forming dihydrophenanthrene derivatives upon excitation.[14] In the late 1980s Irie and coworkers recognized the potential of 1,2-dihetarylethenes as thermally stable photochromic switches[15] and systematically developed their basic design principles. Since then, plenty of research has been done revealing fundamental structure-property relationships, which shall be briefly described in the following paragraphs. In Scheme 2 an overview of the structural versatility of DAEs is given, divided into four building blocks out of which the photochromic core has to be assembled, *i.e.* a bridging moiety, two hetaryl rings, substituents R^1 at the ring-closing carbons, and substituents R^2 in the periphery of the DAE.

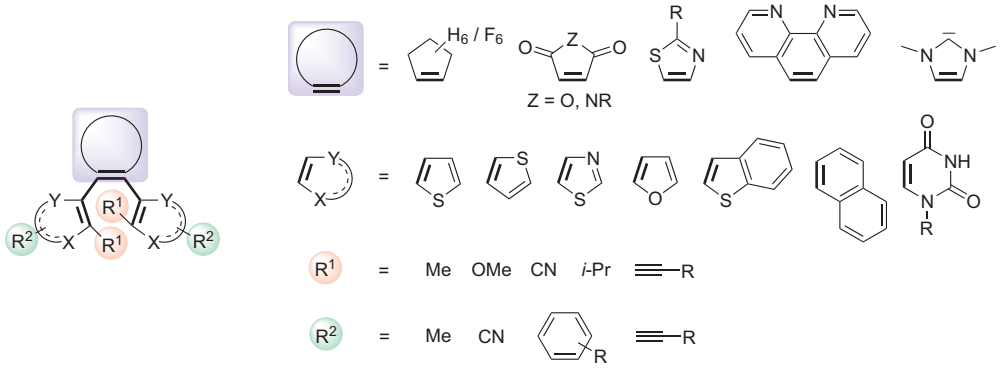

Scheme 2. Structural composition of photochromic DAEs and examples for the nature of the different building blocks.

Role of the bridge

The incorporation of the central double bond of the hexatriene system into a cyclic structure eliminates its photochemical *E/Z* isomerization, which would compete with the desired cyclization reaction. Thus, early DAE derivatives were functionalized with maleic anhydride,[16]

maleimide,[17] and perfluorocyclopentene[18] as bridging moiety. In particular, the perfluorocyclopentene bridge enjoys a huge popularity in the DAE community up to the present day, as it combines good photochemical stability with high switching efficiencies. Feringa and coworkers developed DAEs possessing non-fluorinated cyclopentene as bridging moiety, which broadens the synthetic flexibility and imparts advantageous electrochemical properties to the parent structure (see Section 2.1.4) while showing a comparable photochemistry.[19] Another milestone in the development of modern DAEs was the implementation of a third hetaryl moiety in place of the central double bond resulting in so called "terarylenes".[20] Since the additional group loses its aromaticity during ring-closure, terarylenes were identified to be thermally reversible, while the thermal rate constants can be fine-tuned by varying the nature of the hetaryl rings. Additionally, terarylenes allow for distinct functionalization of the bridging moiety leading to highly interesting structures, *e.g.* possessing extraordinarily large quantum yields for the ring-closure reaction.[21]

In principle, any cyclic structure possessing a localized double bond can be used as bridging moiety, as has been demonstrated by DAEs functionalized with a phenanthroline[22] or an *N*-heterocyclic carbene moiety.[23] These examples point to the potential of bridge modifications for implementing chemical functionalities into DAEs that shall be modulated by the photochromic reaction (see Section 2.2).

Role of the hetaryl rings

Placing two double bonds of the hexatriene system into 5-membered hetaryl rings ensures the endergonic nature of the disrotatory cyclization reaction, while at the same time providing a π-electronic system absorbing UV light at reasonable wavelengths and extinction coefficients. It is mandatory to use heteroaromatics with relatively low aromatic stabilization energy to retain the thermal irreversibility of the photochromic reaction.[15b] Although most DAE compounds found in the literature possess thiophene or benzothiophene rings, a variety of other hetaryl structures such as thiazole, furan, imidazole, or pyrrole as well as their benzannulated analogues can be used. It has been shown that thiazoles, exhibiting less aromatic stabilization energy than thiophene, significantly increase the thermal half-lifes of ring-closed isomers at elevated temperatures.[20a,24] Interesting structural modifications can be made when choosing an unsymmetrical substitution pattern: By placing only one hetaryl ring as one "arm" of the DAE it is possible to use a different double bond containing structure as the other "arm" while retaining the photoswitchability and thermal stability. Thus, unsymmetrical DAEs were realized which possess highly aromatic benzene and naphthalene rings[25] or which are functionalized with nucleosides ready to be incorporated into DNA.[26]

The mode of connection between the hetaryl rings and the bridging moiety has huge impact on the photochemical properties of DAEs. If in case of thiophene the connection is done

via the β-positions of the hetarenes, *i.e.* X = S and Y = CH in Scheme 2, so called "normal type" DAEs are obtained, which this work generally refers to. However, a connection via the α-positions (X = CH and Y = S) yields "inverse type" DAEs with markedly different photochemical properties.[27] Whereas for normal type DAEs there is no direct conjugation path between the two hetaryl moieties in the ring-open isomer due to cross-conjugation with the bridge, in inverse type DAEs the π-electron density is more delocalized resulting in a significant bathochromic shift of the absorbance. However, the absorbance of the ring-closed isomer is shifted hypsochromically compared to normal type DAEs, because after cyclization the conjugation path is interrupted. This also has interesting implications on the observed quantum yields for ring-closure and ring-opening. While for normal type DAEs usually ring-closure is very efficient and ring-opening is significantly slower, the opposite situation holds for inverse type DAEs.[27a,27b] This observation is attributed to changes of activation barriers in the excited state (see Section 2.1.2).

Besides the distinction between normal and inverse type DAEs there are no systematic investigations in the literature on the dependency of quantum yields and other photochemical properties on the nature of the hetaryl moieties.

Role of substituents R^1 at the reactive carbon atoms

Substitution at the reactive carbon atoms is obligatory to avoid oxidation of the ring-closed isomer to phenanthrene analogues.[14b,14c] Thus, in the vast majority of DAEs reported in the literature the protons on the inner α-positions of the hetaryl rings are replaced by methyl groups. Nevertheless, variation of this substituent yields structures with modulated properties: Placing a bulky substituent, for example an isopropyl group, at this position improves the quantum yield for ring-closure due to an increased population of the antiparallel conformer in the ground state.[12b] However, thermal reversibility is induced as well due to weakening of the formed C-C bond by the increased steric strain.[28] Other derivatives demonstrate that substituents exerting a +M effect on the reactive carbon atoms, e.g. methoxy groups[28b,29] or fluorine[30], significantly stabilize the ring-closed isomer resulting in a marked decrease of the quantum yield for ring-opening. On the contrary, attaching electron withdrawing cyano groups has been shown to accelerate the photochemical cycloreversion.[31]

Role of substituents R^2 in the periphery

Substitution in the periphery of DAE structures may significantly influence their photochemical properties and thermal reversibility. In case of normal type DAEs a great variety of substituents has been installed in the α-position of the heterocyclic rings opposite to the reactive carbons, reaching from simple methyl groups over substituted phenyl groups to almost any type of functional group, *e.g.* chlorine, aldehyde, carboxylic acid, dicyanoethylene, or alkyne moieties.

Generally two trends can be observed: First, strong electron accepting moieties in the periphery significantly decrease the thermal stability of the ring-closed isomer as reported for dicyanoethylene, N-methylpyridinium or protonated amine groups.[32] Second, the more the conjugated π-system of the DAE backbone is enlarged by the substituent, the more the absorbance of both the ring-open and ring-closed isomer is shifted to longer wavelengths, eventually allowing for the operation of DAEs solely with visible light.[33] However, with an increasing π-electron delocalization the ring-closed isomer gets stabilized resulting in decreasing quantum yields for cycloreversion up to the situation in which it is essentially zero.[34] As mentioned earlier, decreasing the ring-opening quantum yield to some extent is beneficial if a large conversion to the ring-closed isomer is desired. Thus, in many DAE structures (substituted) phenyl rings are used as substituents R^2 effecting a decrease in the cycloreversion quantum yield of about one order of magnitude.[11b]

Besides the fine tuning of the photochromic properties the peripheral substituents generally serve as an anchoring point for the implementation of diverse chemical functionalities that shall be remote controlled by operation of the switch (see Section 2.2)

2.1.2 Excited state properties

The mechanism of the photochemical isomerization of DAEs has been subject to intensive research in the past two decades. A huge number of experimental investigations give a concise picture of the excited state properties. Transient absorption spectroscopy revealed that generally the ring-closed isomer is formed within a few picoseconds after excitation of the ring-open isomer.[35] Additionally, the temperature independence of both the lifetime of the excited state of the ring-open isomer[36] as well as cyclization quantum yields[27a,36-37] points to an essentially barrierless reaction pathway. Thus, the cyclization efficiency of DAEs is mainly dependent on the ratio of the antiparallel and parallel conformer in the ground state (*vide supra*), as within the short lifetime of the excited state a conformational equilibration is not possible.[35a] Consequently, it has been shown that the cyclization quantum yields were dramatically increased up to values close to unity by thermodynamically stabilizing and thus increasing the population of the antiparallel conformer[21] or by preparative isolation of the antiparallel conformer of a rotationally hindered DAE.[12a] Due to fast deactivation of the excited state via the cyclization reaction fluorescence of the ring-open isomer is generally weak, although there are a number of exceptions.[38] It could be shown for a prototype DAE that weak fluorescence originates from the excited state of the non-reactive parallel conformer.[35a]

For DAE structures possessing a pronounced donor-acceptor character the cyclization reaction may be strongly inhibited, accompanied by an increase of the lifetime of the excited state.[11b,16,39] This behavior was attributed to the charge transfer character of the excitation and

subsequent stabilization of the excited state by rotation of the hetaryl rings orthogonal to the cyclization reaction coordinate to form a *twisted intramolecular charge transfer* (TICT) state.[40]

As mentioned earlier, the photochemical ring-opening of DAEs is generally much less efficient than ring-closure. Ultrafast dynamics of the excited state of the ring-closed isomer show that during its lifetime within the picosecond range more than one deactivation pathway can be followed.[36] On the one hand cycloreversion via the same conical intersection that is populated during ring-closure can happen; on the other hand competitive non-radiative deactivation via a different conical intersection is discussed. Importantly, the lifetime of the excited state as well as quantum yields for ring-opening depend strongly on temperature[11b,27a,34b,36-37,41] and the excitation wavelength.[11a,41b,42] This indicates the presence of an activation barrier on the excited state potential energy surface.

Already in the mid-1990s high level quantum mechanical calculations were performed in order to rationalize the photochemical interconversion between *cis/Z/cis*-1,3,5-hexatriene (HT) and 1,3-cyclohexadiene (CHD).[43] The principal findings are summarized in Figure 2. After excitation of both HT and CHD to the accessible S_2(1B) state, rapid relaxation within the Frank-Condon region to the energetically near S_1(2A) surface takes place. On this surface the minima HT* and CHD* are reached. While the structure of CHD* is very similar to the structure of CHD, in HT* the distance between the ring-closing carbons is significantly shorter than in HT. The CHD* minimum is shallow, as only a very small activation barrier exists along the reaction coordinate (*i.e.* the distance between the ring-closing carbons) that is easily overcome (Figure 2b). This finally results in the population of the same HT* minimum from both sides of the PES. Importantly, from the energy profile along the reaction coordinate it can be deduced that this coordinate is not sufficient for the description of the excited state dynamics, as no minimum pointing to a conical intersection with the S_0(1A) surface exists. Thus, an orthogonal coordinate, *i.e.* the lowest frequency normal mode of HT* describing a bending of the hexatriene core, has to be considered. After redistribution of the vibrational energy in the HT* minimum, movement along the second coordinate takes place and finally a conical intersection (CI_{CHD}) is reached, from where both ground state minima are accessible (Figure 2c). The fact that starting from both sides the reaction proceeds through the same excited state intermediates implies that the sum of the quantum yields for the forward and backward reaction cannot exceed unity and the ratio between both is determined by the branching of the S_0(1A) surface at the conical intersection. A distinct feature of the structure of the hexatriene at the CI is recognized: The C_1, C_5, and C_6 carbons form an isosceles triangle with the distances C_1-C_5 and C_1-C_6 being almost identical. Importantly, theory predicts that bond formation between C_1 and C_5 could also happen from CI_{CHD} leading to the formation of the methylcyclopentene diradical (MCPD) which may react to bicyclohexene (BCH), an intermediate structure discussed for the fatigue reaction of DAEs (see Section 2.1.3).

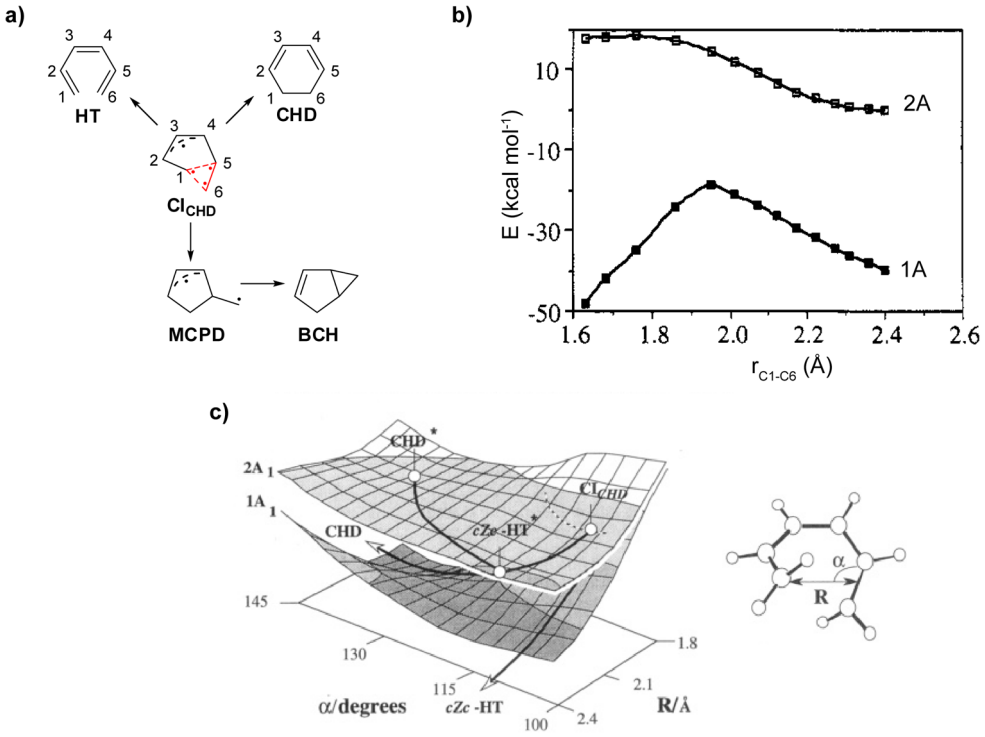

Figure 2. Mechanism of the photochemical **HT-CHD** interconversion. a) Structure of $\mathbf{CI_{CHD}}$ and possible reaction products. b) CASSCF(6,6)/4-31G energy profiles along the **CHD→HT** reaction coordinate in the 1A ground state and 2A excited state. c) Cross section of 2A and 1A potential energy surfaces (CASSCF(6,6)/4-31G) spanned by the geometrical parameters R and α. Solid lines represent reaction paths connecting the different regions of the 2A surface, the dashed line marks the region where the two surfaces are degenerate.[43c]

Theoretical treatment of the excited state of DAEs[44] gives a very similar mechanistic picture, though some decisive differences to the HT-CHD system exist. Calculations on model DAE I (Figure 3a)[44b] show that the isomerization reaction starting from both the ring-open isomer (HT form) and ring-closed isomer (CHD form) proceeds via the same minimum HT* and conical intersection $ConInt_1$ on the $S_1(2A)$ surface (Figure 3b). At the latter point the ground state PES branches between the HT and CHD minima. Again $ConInt_1$ does not lie directly on the reaction coordinate but is accessed by bending of the DAE structure forming an isosceles triangle between C_1, C_5, and C_6 (Figure 3c). Starting from the HT side, the reaction path to $ConInt_1$ is barrierless. Nevertheless, starting from the CHD side, a significant barrier (TS_5 in Figure 3b) between CHD* and HT* has to be overcome, which is in stark contrast to the simple hexatriene-cyclohexadiene system. Besides, additional conical intersections near the CHD* and HT* minima were identified, which lead to deactivation of the excited state without undergoing isomerization. Together these two facts explain the experimentally observed poor quantum yields for ring-opening as well as their temperature and wavelength dependence. The barrier between CHD* and HT* represents a "bottleneck" for ring-opening, which has to be hit by CHD* competing with other possible geometries leading to deactivation.

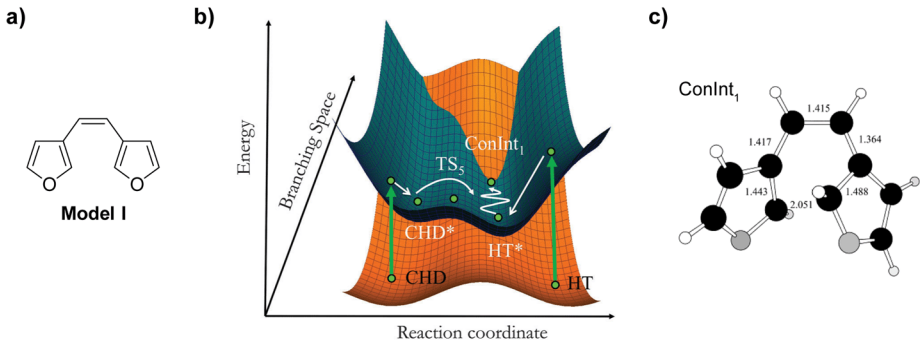

Figure 3. Mechanism for the photochemical isomerization of DAEs. a) Structure of model DAE I. b) CASSCF(10,10)/4-31G potential energy surfaces of the S_0(1A) and S_1(2A) states. The surface is spanned along the reaction coordinate (distance between C_1 and C_6) and the branching space of the conical intersection (*i.e.* the linear combination of the gradient difference vector and derivative coupling vector) corresponding to a bending motion of the DAE. c) Distortion from C_2-symmetry at the conical intersection $ConInt_1$.[44b,45]

To overcome the efficiency limitation for the ring-opening process several strategies are suggested: As mentioned earlier, distinct substitution at the ring-closing carbon atoms may alternate the energy of the ring-closed isomer, influencing the height of the barrier in the excited state.[31b] Other experiments show that significantly increased cycloreversion quantum yields are obtained by a stepwise multiphoton excitation into higher excited states[46] or by plasmonic enhancement near gold or silver nanoparticles.[47] Another strategy utilizing photoredox catalysis to induce ring-opening is described in Section 2.1.4 of this work.

Besides the thoroughly investigated singlet reaction pathway, DAEs were also found to cyclize in the triplet state. A number of studies concerning DAEs bound as ligands to different heavy metal atoms prove that ring-closure proceeds with high quantum yields upon excitation of the MLCT band, subsequent intersystem crossing, and triplet energy transfer to the DAE ligand.[22,48]. Population of the DAE triplet state may also be induced by intersystem crossing of the DAE chromophore itself[48b] or by inter-[49] or intramolecular[50] sensitization with an organic sensitizer. From quantum mechanical modeling of the triplet reaction pathway it can be deduced that a barrier exists between minima corresponding to the ring-open and ring-closed isomers.[48b] However, the barrier is relatively small from the side of the ring-open isomer and can be overcome during the long lifetime (several µs) of the triplet state. Ring-opening is not observed due to the significantly larger stability of the triplet state of the ring-closed isomer. All in all, the cyclization reaction of DAEs in the triplet state represents an attractive alternative to the singlet photochemistry as it can be induced by irradiation with visible light using sensitizers, proceeds with comparably high quantum yields, and gives quantitative conversion to the ring-closed isomer.

2.1.3 Fatigue behavior[1]

For the application of photoswitches to construct functional systems with technological relevance a crucial property is the resistance to fatigue, *i.e.* the stability of the photochrome against bleaching and side reactions over a large number of switching cycles. Even the occurrence of a slow side reaction, which is hardly observed when the isomerization is performed only once, will lead over tens or hundreds of switching cycles to a significant loss of photochromic material. In this respect, DAEs are generally regarded to possess outstanding properties. Some derivatives are reported to withstand more than 10^4 switching cycles without any sign of degradation.[8a] In particular, for the motifs shown in Scheme 3 exhibiting either benzothiophene[18] or β-methyl substituted thiophenes[51] as aryl moieties in conjunction with the hexafluorocyclopentene bridge no by-product formation is observed.

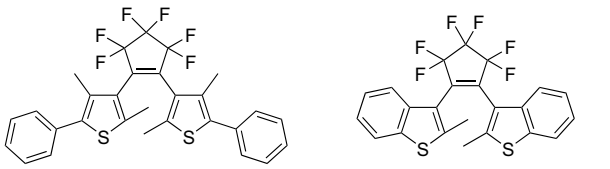

Scheme 3. Fatigue resistant diarylperfluorocyclopentenes.

However, it has been noted by several groups that distinct DAE derivatives show different types of photochemical side reactions, *e.g.* oxidation or elimination reactions of the ring-closed isomer.[52] In particular, the formation of an annulated ring system (Scheme 4) has been reported for perfluorocyclopentene and perhydrocyclopentene derivatives.[51,53] The structure of the by-product has been proven by X-ray crystallography.[51,53g] It is formed upon excitation of the ring-closed isomer with UV light by a formal 1,2-dyotropic rearrangement,[54] *i.e.* two substituents are exchanged along the central C-C single bond. The rearrangement may proceed via radical intermediates formed either after homolytic C-S bond cleavage in one of the thiophene rings or reaction of the cyclohexadiene core to the methylcyclopentene diradical (MCPD) intermediate, as discussed before (Scheme 5 top and middle).[53g] Both reactions would lead to the bicyclohexene intermediate BCH, which eventually forms the annulated by-product. However, a concerted mechanism for the 1,2-dyotropic rearrangement (Scheme 5 bottom)[55] or ionic intermediates are also conceivable.

[1] Parts of this section have been published in M. Herder *et al*,. *J. Am. Chem. Soc.* **2015**, *137*, 2738-2747.

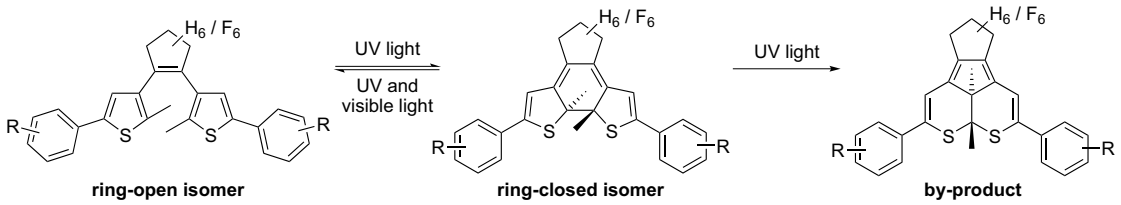

Scheme 4. Formation of an annulated isomer as a by-product of DAE photochromism.

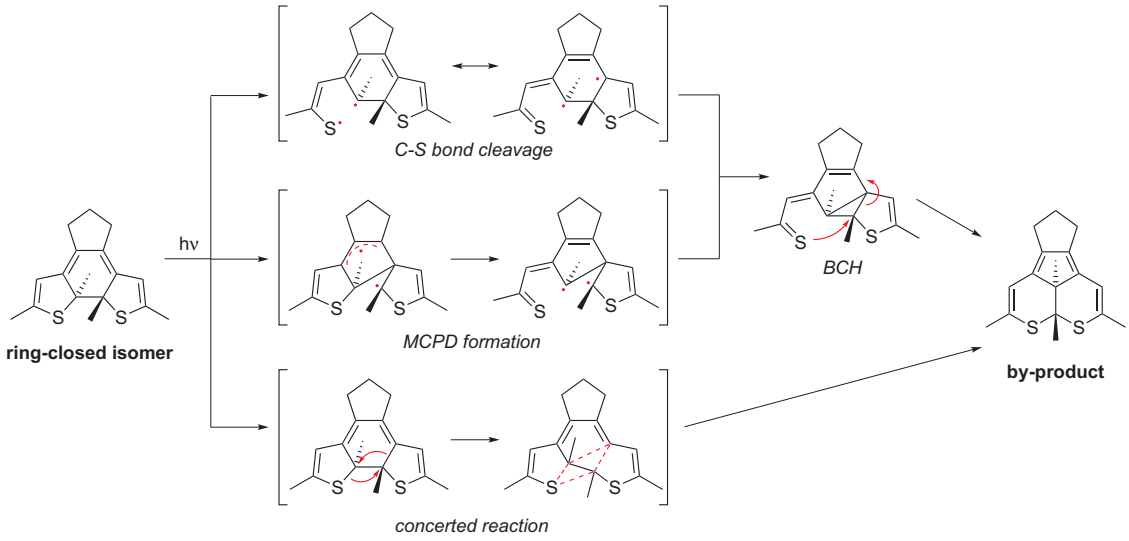

Scheme 5. Possible mechanisms for by-product formation.[53g,55]

A recent theoretical work by Jacquemin and coworkers[45] examines the cleavage of the C-S bond as reaction coordinate in the excited state of the ring-closed isomer (Figure 4). Due to performance restrictions the calculations on the CASSCF(10,10)/6-31G(d) level of theory were based on model DAE II bearing CH_2 groups instead of sulfur atoms after showing that the exchange has only minor effects compared to model DAE III. In analogy to an older work[56] a ground state reaction path between the ring-closed isomer (CHD) and the by-product (BP) via the BCH intermediate has been identified, which is characterized by a huge thermal barrier for the initial bond cleavage (Figure 4b). However, in the $S_1(2A)$ excited state (Figure 4c) the C-CH_2 bond cleavage proceeds via a barrier TS_4 that is only slightly larger than the barrier TS_5 leading to ring-opening. Behind TS_4 a conical intersection leads to the ground state PES at geometries near the planar minimum PM and transition state TS_2, which are shown in Figure 4b. From this region the molecule may react back to the ring-closed isomer or form the by-product. It was suggested that sterical hindrance between the hetaryl ring and the bridge, as it is present in the structures shown in Scheme 3, increases the barrier TS_3 between the BCH intermediate and the by-product, making both structures much more fatigue resistant than other DAEs.[56]

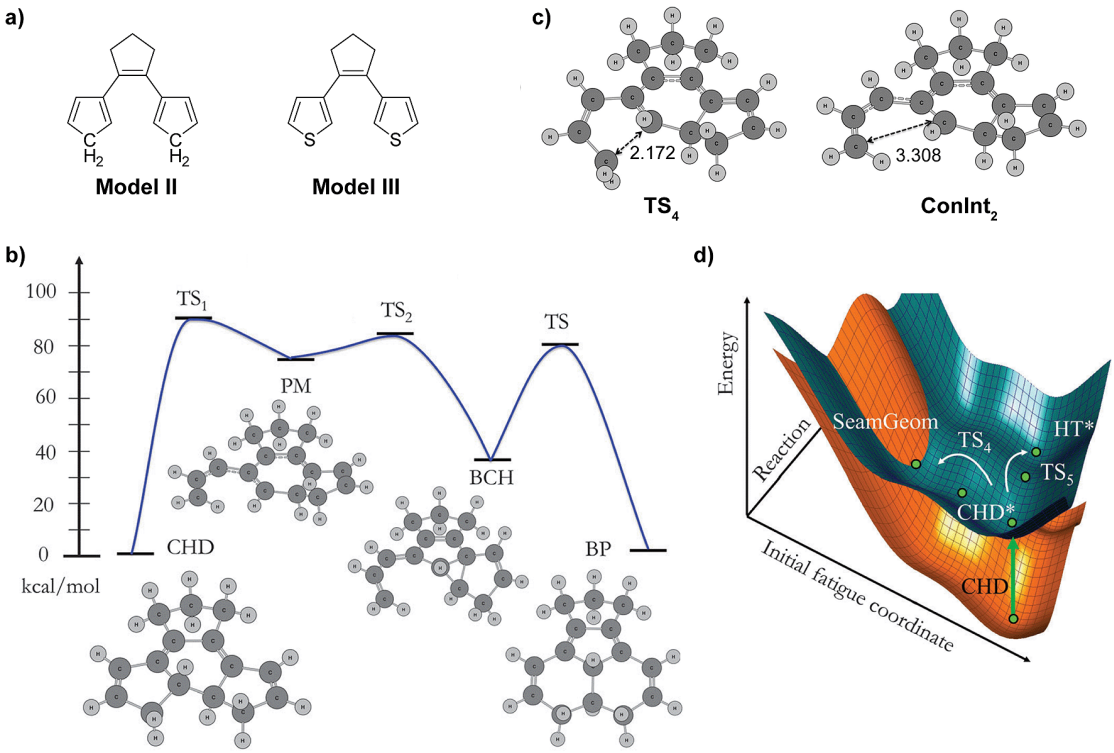

Figure 4. Quantum mechanical modelling of by-product formation. a) Structure of model DAEs investigated. b) Ground state reaction path of model DAE II for the formation of the by-product (BP) from the ring-closed isomer (CHD) via a planar minimum structure (PM) and a bicyclohexene intermediate (BCH). c) CASSCF(10,10)/6-31G(d) potential energy surfaces of the S_0(1A) and S_1(2A) states of model DAE II. The surface is spanned along the reaction coordinate (distance between C_1 and C_6) and the initial fatigue coordinate (distance between C_1 and the CH_2 group). d) Structure of model DAE II at TS_4 and $ConInt_2$ showing the elongation of the C_1-CH_2 distance.[45]

Besides this finding there are hardly any systematic investigations of the dependency of by-product formation on the molecular structure of DAEs. It has been noted earlier that dithienylperhydrocyclopentenes suffer more from fatigue than the respective perfluorocyclopentene derivatives.[19b] Only the combination of β-methyl substituted thiophenes or benzothiophenes with the perfluorocyclopentene bridge completely prevents the formation of the annulated isomer in the structures shown in Scheme 3. Additionally, oxidation of one thiophene or benzothiophene unit to the *S,S*-dioxide may lead to an improved photochemical stability.[57] For the photoconversion of DAEs in the single crystalline state the formation of the annulated by-product has not been observed.[51]

2.1.4 Electrochemical properties[2]

The strong alternation of the π-electronic system of DAEs during their isomerization, changing from isolated aromatic cores in the ring-open isomer to an extended conjugation over the whole molecular backbone in the ring-closed isomer, can easily be observed by electrochemical investigations using cyclic voltammetry. Typically the ring-open isomer is oxidized and reduced

[2] Parts of this section have been published in M. Herder *et al.*, *Chem. Sci.* **2013**, *4*, 1028-1040.

at significantly higher positive or negative potentials, respectively, than the ring-closed isomer, reflecting the reduction of the HOMO-LUMO gap during cyclization.

An interesting feature of many, though not all, DAE structures is the possibility of triggering their isomerization reaction not only by light, but also by electrochemical oxidation or reduction. DAEs bearing thiophenes as hetaryl rings (dithienylethenes, DTEs) often undergo oxidative cyclization, which can be observed in cyclic voltammograms that consist of several consecutive scans (Figure 5a).[58] After a two-electron oxidation of the ring-open isomer has been performed, cathodic waves as well as anodic waves in the second scan cycle corresponding to the ring-closed isomer appear. Depending on the substitution pattern of the DTE oxidative cycloreversion has also been reported.[58c,58g,58h,59] In addition, DTEs substituted with redox active metal centers show a similar behavior.[60] A reductive cyclization reaction was reported for DAEs substituted with cationic N-methylpyridinium units in the periphery of the photochromic core.[61] The combination of the different structural motifs in one molecular scaffold afforded a fully bidirectionally switchable DAE that undergoes isomerization in both directions either by excitation with light or by the electrochemical pathway.[62]

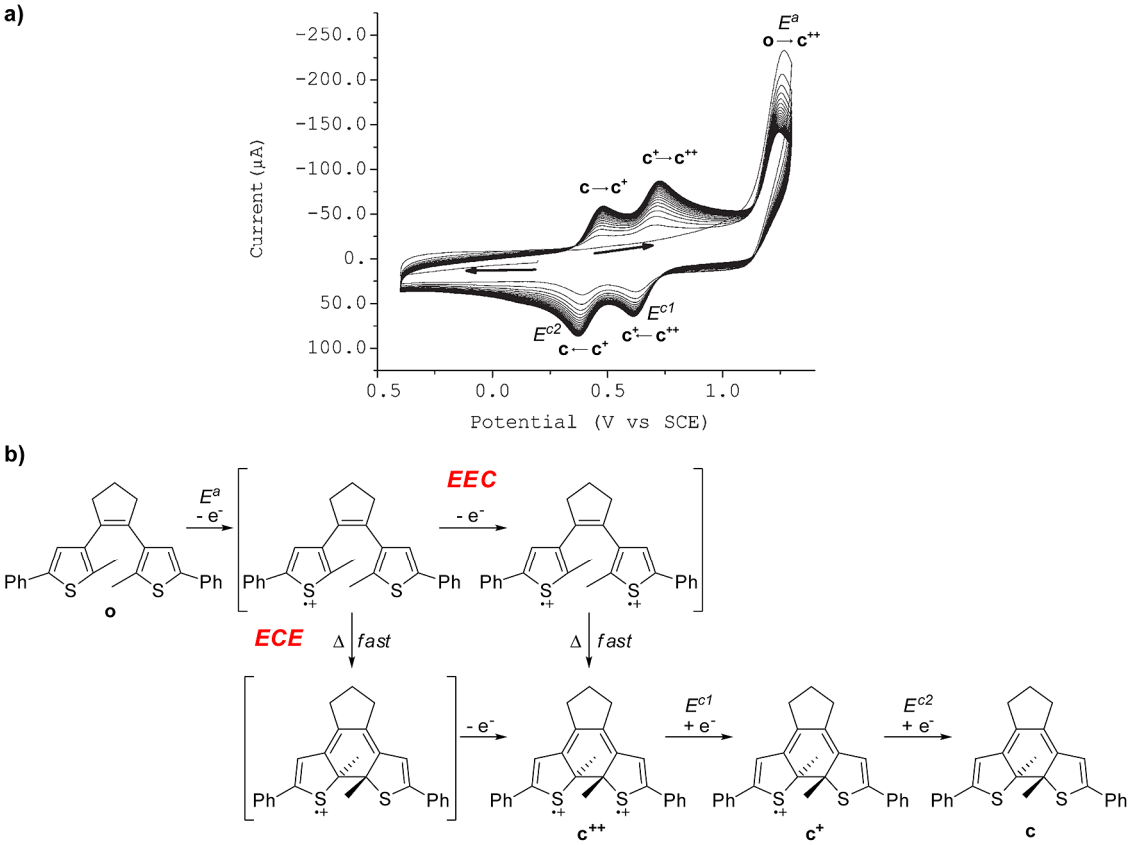

Figure 5. a) Typical cyclic voltammogram of a DAE showing oxidative cyclization during consecutive scan cycles.[58f] b) Possible intermediates of the oxidative cyclization following an *EEC* or an *ECE* mechanism.

The mechanistic pathway for the oxidative ring-closure or ring-opening of DAEs is still under discussion. Both radical cationic intermediates[58e-h,59a,59b] and dicationic intermediates[58a,58b,60a,60e] were postulated to be the species undergoing the thermal isomerization reaction. Thereby, it is assumed that an equilibrium exists between oxidized ring-open and ring-closed isomers which is shifted to either side depending on the substituents. For the oxidative cyclization reaction shown in Figure 5a both radical cationic or dicationic intermediates would experimentally lead to the same observation: For a reaction via a monocationic state one would postulate an *ECE*-mechanism consisting of an initial electron transfer (*E*) from the ring-open isomer giving the radical cation, which subsequently undergoes a fast chemical reaction (*C*), *i.e.* cyclization (Figure 5b). As the resulting ring-closed isomer possesses a lower oxidation potential, a second electron is immediately transferred to the electrode resulting in the ring-closed dicationic species. Nevertheless, an *EEC*-mechanism might also be possible: Supposing both thienyl moieties of the ring-open isomer are electronically decoupled by twisting of the ring-planes and cross-conjugation with the bridge, they can be regarded as independent redox centers that in case of a symmetrical molecule get oxidized simultaneously or at least at very similar potentials.[63] Thus a diradical dication of the open isomer is formed that cyclizes to the dicationic ring-closed isomer. In both cases, cyclic voltammetry shows an irreversible two-electron oxidation of the ring-open isomer.

It was proposed that the oxidative ring-opening of some DAEs, generally assumed to occur in the monoradical cationic state, might be utilized as an alternative to the inefficient photochemical cycloreversion (see Section 2.1.2).[59] In principle, the oxidative isomerization reaction in direction of the ring-open isomer is "catalytic in electrons", *i.e.* only some oxidation events are needed to induce a reaction chain resulting in complete ring-opening (Scheme 6). At a certain potential the radical cation of the ring-closed isomer is formed, which thermally ring-opens resulting in a shift of its oxidation potential to higher values. Thus, it gets reduced by another ring-closed molecule which itself is oxidized to the radical cationic state, proceeding the reaction chain. In recent works by Fukuzumi and Nam[64] this concept was combined with organic and inorganic photoredox catalysts, which upon excitation with visible light induce the primary oxidative event (Scheme 6). Effective quantum yields up to 0.38 have been obtained for this process, depending on the catalyst and concentration. In principle, with this strategy it is possible to overcome the intrinsic limitation of the DAE photochemistry that the sum of quantum yields for the forward and backward reaction cannot exceed unity.

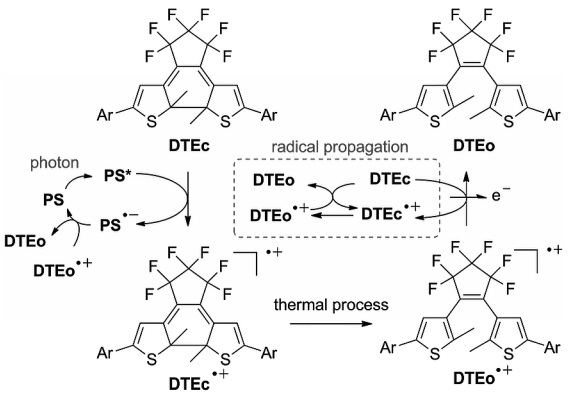

Scheme 6. Photoelectrocatalytic ring-opening of DAEs using a photoredox catalyst (PS).[64a]

The electrochemistry cannot only be used to enhance the efficiency of the isomerization reaction, but also may serve as a stimulus orthogonal to the photochemistry. Thus, by oxidative cyclization of a DAE dimer the singly ring-closed compound was selectively obtained whereas by irradiation only the doubly ring-closed isomer was accessible.[60b] Though these examples demonstrate the huge potential of the electrochemical pathway, there are only few systematic studies concerning its mechanism and efficiency. In particular nothing is known about fatigue during electrochemical operation of DAEs.

2.2 Application of diarylethenes to remote-control functions

2.2.1 General principles

The simplest remote-controllable function of a *photochromic* molecule is the absorption of light of distinct wavelengths and thus the emergence of color. However, as there are more physical and chemical properties that are altered upon the isomerization reaction many other functions exerted either by single photochromic molecules or by molecular ensembles containing the photochrome can be modulated by irradiation with light. The superior photochromic properties of DAEs make them ideal candidates for the construction of such smart functional systems. Indeed, in the last two decades academic interest in their application in all fields of natural sciences has grown enormously. Looking into the literature four principle strategies can be identified how the photochromic reaction of DAEs can be translated into a remote-controllable function (Figure 6). Some examples rely on the geometrical modulation of the DAE core upon isomerization, though it is generally relatively small compared to other photochromic molecules (strategies A and B). The vast majority of applications, however, utilize the marked electronic changes occurring during isomerization (strategies C and D). In the following the different strategies will be briefly discussed.

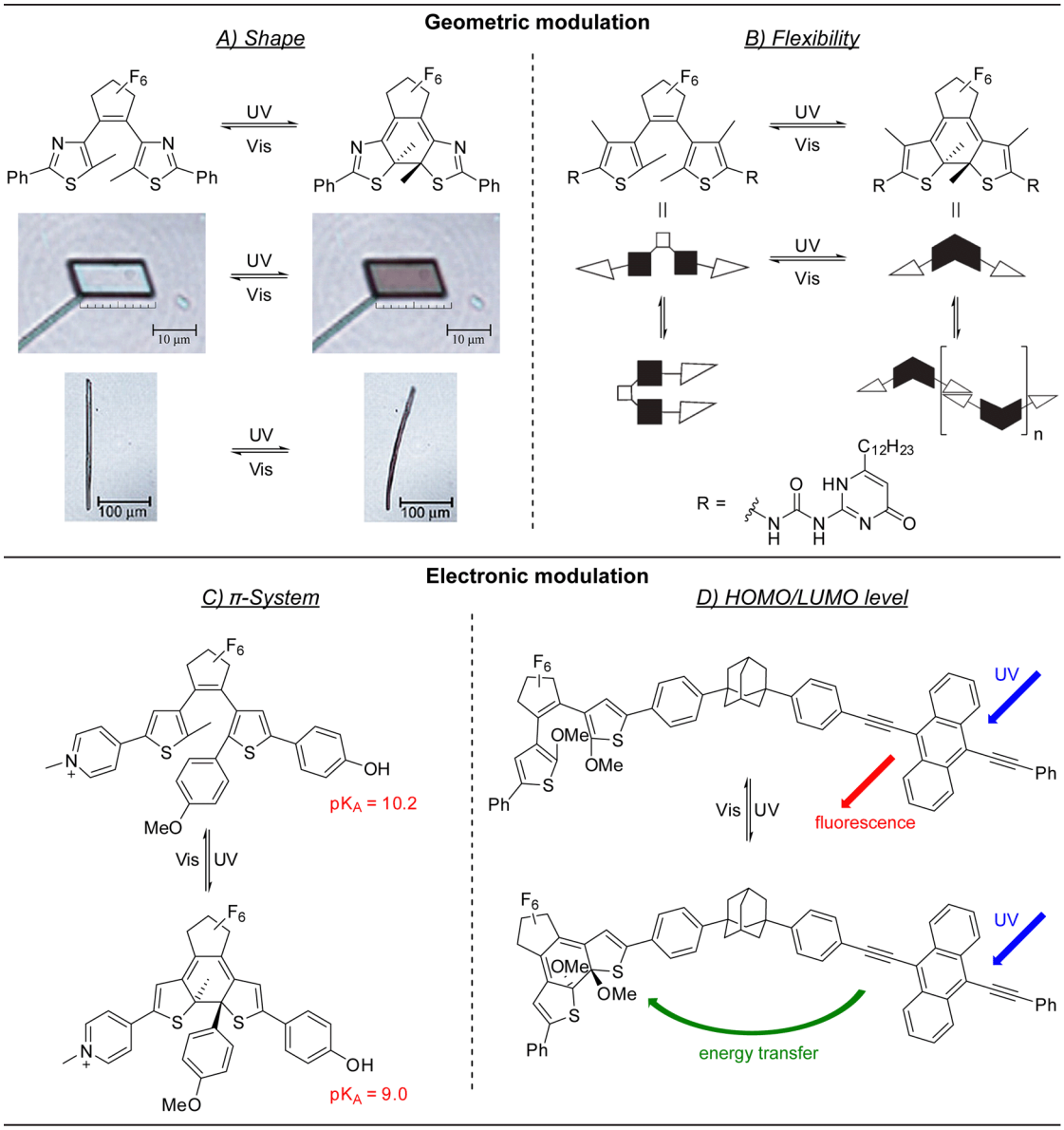

Figure 6. Examples for remote-controlling functions using DAEs based on their geometrical and electronic changes upon isomerization. A) Changing molecular shape leads to shrinking and bending of DAE single crystals observed under a microscope.[65] B) Reduced flexibility of a ring-closed isomer prevents intramolecular hydrogen bonding and thus induces supramolecular polymerization.[66] C) Altered π-conjugation pathways lead to coupling of a phenol to an electron acceptor reducing its pK_A value.[67] D) The reduced energy gap of the ring-closed isomer allows for energy transfer from an excited fluorophor quenching its emission.[68]

A) Change of molecular shape: In fact, the geometrical difference between the ring-open isomer and the ring-closed isomer is only very small, in contrast to many other photochromic compounds such as azobenzenes. This allows for the remarkable feature of some DAE derivatives to isomerize in the single crystalline state.[9] However, the mechanical stress resulting from the subtle change of molecular shape of some DAE molecules undergoing isomerization in the crystal lattice can result in impressive macroscopic morphology changes of the single crystal, such as shrinking, bending, or twisting, making DAE single crystals potential photoactuators converting light into mechanical work.[65,69]

B) Change of molecular flexibility: While in the ring-open isomer rotations around the single bonds are possible leading to an equilibrium between the parallel and antiparallel conformer, the ring-closed isomer is a stiff and flat molecule. This can have dramatic effects on the self-aggregation behavior[70] or on the geometry of specific association motifs.[66,71] As an example, while the ring-open form of a DAE functionalized with ureidopyrimidinone moieties undergoes intramolecular hydrogen-bonding in the parallel conformer, in the ring-closed form only intermolecular association is possible leading to the formation of supramolecular polymers.[66] Changes in molecular flexibility of DAEs were also demonstrated to lead to a differing binding affinity of the DAE isomers to biological receptors[72] or a modulation of the coordination sphere of metals bound to DAE ligands.[73]

C) Change of the π-electronic system: By isomerization of the DAE core the conjugation pathways through the molecular backbone are significantly altered making it possible to reversibly couple and decouple EWGs or EDGs with groups that exert a function. In Figure 6c this principle is shown by means of a phenol moiety whose acidity is increased after coupling with an electron accepting N-methylpyridinium unit in the ring-closed isomer.[67,74] By utilizing this coupling/decoupling principle or the general reshuffling of double bonds during isomerization, it was demonstrated that the reactivity or catalytic activity of certain functional groups can be effectively modulated (see Section 2.2.3). In a diploma thesis preceding this work, it was shown that the strength of supramolecular association via hydrogen bonding may also be modulated using this strategy.[75]

D) Change of energy levels: The different π-electronic structures of the isomers induce a marked alternation of the HOMO and LUMO energy levels. Besides inducing different light absorption of the two isomers, this property can be used in manifold ways. The emission of fluorophores attached to DAEs can be quenched by energy transfer or electron transfer typically to the ring-closed isomer with its reduced energy gap, as shown in Figure 6d.[68,76] This gives rise to a huge number of potential applications in *e.g.* information storage and processing, sensing, or superresolution microscopy.[4,38b] Moreover, the excited states of other functional moieties such as triplet sensitizers can be reversibly quenched using DAEs.[77] Additionally, by alternating HOMO and LUMO levels the mobility of charge carriers in organic electronic devices or the conductance through single molecules can be efficiently affected (see Section 2.2.2).

2.2.2 Diarylethenes in organic electronic devices

Given the strong alternation of the electronic properties of DAEs during their isomerization it is obvious that they may be advantageously used as active building blocks to construct light-controllable electric circuits and devices. This opens up the emerging field of active

optoelectronic materials and devices that promise manifold applications in information processing, memory elements, or sensing technologies.[7,78]

In a number of reports the binary modulation of electrical conductance by light induced isomerization of DAEs was demonstrated at the single molecular level with the help of STM,[79] conducting AFM,[80] and molecular junctions sandwiching single DAE molecules between nanoscale electrodes[81] or nanoparticle networks.[82] Typically, DAE molecules are contacted to gold electrodes or nanoparticles via thiol anchor groups, though covalent functionalization of carbon nanotubes or graphene has also been reported. However, it turned out that it can be difficult to retain full photoswitchability while bringing the DAE in close contact with the electrode due to quenching of the excited state by the metal surface.[81c,83] Additionally, single molecular junctions are difficult to fabricate and are prone to large statistical fluctuations.

It is much easier to measure conductance of bulk DAE materials, such as single crystals, amorphous and polycrystalline films,[84] as well as polymeric materials containing DAEs in their main chain.[85] Indeed, significant changes of the electrical properties of these materials upon light irradiation have been observed. However, their applicability may be limited due to poor intrinsic conductivity[84b] or low conversions to the ring-closed isomer in the solid state.[85a]

For these reasons it is advantageous to combine the photochromic molecule with established organic semiconductors and thus to construct light responsive organic electronic devices, such as two-terminal devices like simple diodes and OLEDs, or three-terminal devices like OFETs. For implementing a photochromic compound into a device different strategies can be found in the literature (Figure 7).[78a] First of all the photochromic molecule may be used itself as an organic semiconductor, optionally in combination with other emissive or hole- and electron-transporting layers. This has been realized using DAEs to construct photo-programmable diodes[86] and OLEDs[87] that can be applied as high density memory elements. The basic principle of operation of these devices is shown in Figure 8a for the example of an OLED that was designed by the group of Meerholz.[87b] A crosslinked DAE layer is fabricated in between the anode and the emissive layer of the device. By photoisomerization of the DAE the valence level of this layer, i.e. the HOMO energy, is shifted, thus allowing for hole injection into the DAE layer in the ring-closed form (ON-state), while it comprises a hole-blocking layer in the ring-open form (OFF-state). Only in the ON-state the holes arrive at the emissive layer where they recombine with electrons to emit photons. In seminal works[86f,87c] Meerholz and coworkers demonstrated the huge potential of photo-programmable diodes and OLEDs to store information, as a multitude of differentiable states could be obtained for one device by controlling the irradiation time. The readout process can be accomplished by simple current detection in case of the diode or optical photography of the OLED emission.

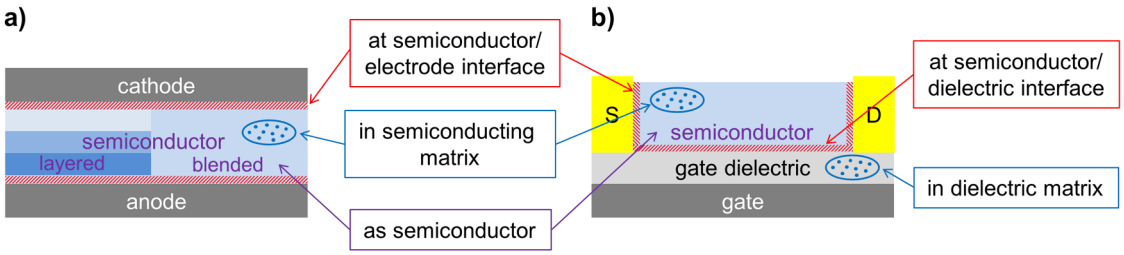

Figure 7. Possibilities to implement photochromic compounds into organic electronic devices. a) Two-terminal device (*e.g.* diode, OLED). b) Three-terminal device (*e.g.* OFET). The figure was taken and modified from Wakayama *et al.*[78a]

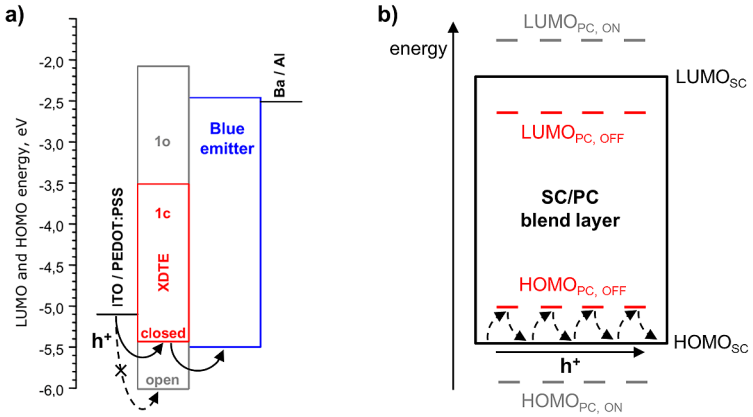

Figure 8. Mechanisms for photocontrol of organic electronic devices. a) Switchable hole-blocking layer consisting of a DAE (XDTE) in its ring-open or ring-closed form in a photo-programmable OLED with a layered architecture.[87b] b) Hole trapping in a blend of an organic semiconductor (SC) and a photochrome (PC) with switchable HOMO levels. Solid arrows show unhindered hole injection and trap-free hole transport (ON-state) while dashed arrows indicate blocking of hole injection and charge trapping (OFF-state) in a) and b) respectively. Figure b) was adapted from Crispin *et al.*[88]

An OFET using a neat DAE layer as semiconductor that comprises a large switching ratio of the drain current of 100 between the photochemical ON and OFF state has recently been realized by the group of Wakayama.[89] However, the hole mobility of the device was very low ($1 \cdot 10^{-5}$ cm² V^{-1} s^{-1}), which shows the poor semiconducting properties of the DAE itself. In 2010 a layered OFET device consisting of a DAE layer between the dielectric and a layer of pentacene as semiconductor was reported, which showed a higher hole mobility but significantly lower ON/OFF ratios.[90] The reduction of drain current in the OFF state was attributed to hole injection into the poorly semiconducting DAE layer occurring after isomerization to the ring-closed isomer.

To improve the interaction of the photochrome with a highly efficient organic semiconductor a second strategy was theoretically proposed[88] consisting of simple blending of both components into one layer. By precise alignment of the energy levels in a way that the HOMO of the photochrome in one isomerization state lies above the HOMO level of the semiconductor its hole mobility should decrease due to charge trapping at the photochrome sites (Figure 8b). By isomerization the HOMO level of the photochrome is lowered and unhindered

hole transport via the valence level of the semiconductor is possible. That this principle might work using DAEs as photochromes can be deduced from experiments on blends with polyoctylthiophene[91] or F8BT[92] as semiconducting matrices showing a variation of photocurrent upon isomerization. Besides, the results presented in this work (section 4.6) are the first example of utilizing the blending approach to implement DAEs in highly efficient photomodulable electronic devices. Blends of other photochromes, in particular of the spiropyran/spirooxazine type, with semiconductors were reported earlier and in parallel to this work, however, they generally exhibit relatively low photochemical ON/OFF ratios in OFET device configurations.[93]

Further possibilities to implement photoresponsivity into devices are the modification of the electrode semiconductor interface or, in case of OFET configurations, the modulation of the gate dielectric by blending or interface engineering. While the former was successfully realized using self-assembled monolayers (SAMs) of DAEs on gold electrodes,[94] the latter was only reported using spiropyran photoswitches.[95]

2.2.3 Diarylethenes for reactivity control and catalysis

The reversible control over chemical reactivity using photochromic compounds demands that the properties of a specific functional group are modulated to a large extent by the photo-isomerization.[1,3] In particular, designing switchable systems that show reasonable reactivity in the ON-state and are completely unreactive in the OFF-state is difficult. However, such systems possess a huge potential to enable chemists to control where and when a specific reaction takes place. In terms of information processing such systems would be the interface to translate an external optical signal to a chemical signal. Especially the situation of a switchable molecule serving as a catalyst for a distinct reaction, with its activity being highly different in the two switching states, is advantageous. An optical signal consisting of few photons would be amplified by orders of magnitude giving a huge chemical response.

In a number of reports it was shown that azobenzenes and other photochromic units can be utilized to modulate catalytic activity based on geometrical changes.[3b] In contrast, there are only some very recent reports on photoswitchable catalysts based on the electronic modulation of the active functional group using DAEs.[23a-d,96] However, it was shown earlier that chemical reactivity of distinct functional groups being part of or attached to the DAE scaffold can be modulated.

One strategy consists of the reversible electronic coupling/decoupling of a donor or acceptor group to the reactive moiety, modulating its nucleo-/electropilicity or its (Lewis) basicity/acidity. Besides the photocontrol over pK_A values of a phenolic group (*i.e.* the photocontrol over acid/base equilibria, see Figure 6c),[67,74] there are reports demonstrating the modulation of the reactivity of an alkyne towards tetracyanoethylene[97] as well as the

nucleophilicity and Lewis basicity of a pyridine moiety[98] by coupling/decoupling with an electron donating *N,N*-dimethylaniline or an electron accepting *N*-methylpyridinium moiety. In terms of photoswitchable catalysis, Branda and coworkers. used the latter structural motif to modulate the racemization of *L*-alanine mediated by a DAE linked aldehyde with an ON/OFF ratio of 10 (Scheme 7a).[96a] However, the authors did not conduct any control experiments to reveal whether it is the reduced electrophilicity of the carbonyl moiety or the reduced acidity of the imine intermediate which leads to the strongly suppressed catalytic activity in the ring-open state of the DAE. Yashima and coworkers ascribed differences in the catalytic acetylation of 2-decanol mediated by *N*-methylimidazole coupled to a DAE core to electronic changes occurring during the isomerization reaction.[96b]

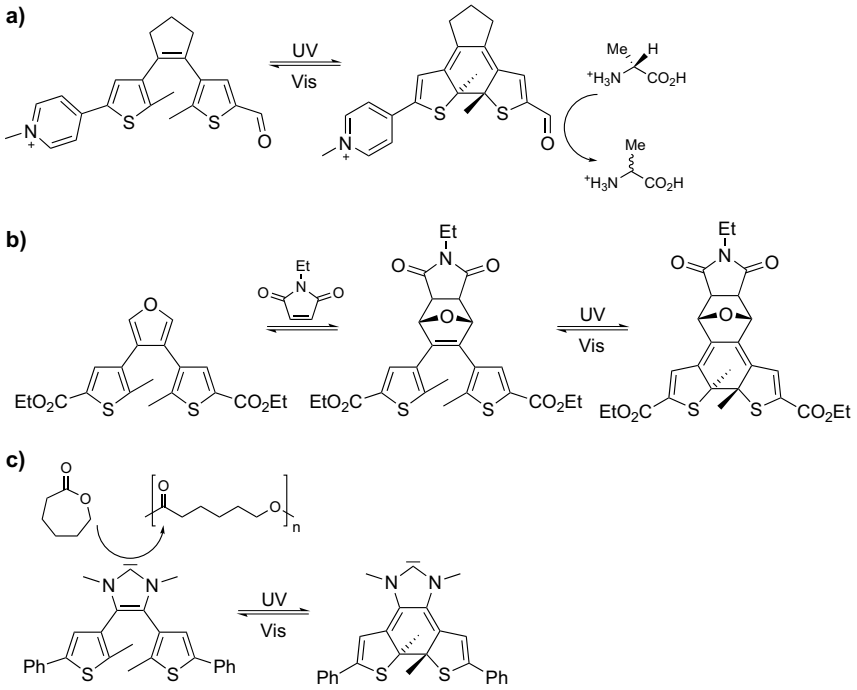

Scheme 7. Reactivity control using DAEs: a) Catalytic racemization of *L*-alanine by the ring-closed isomer.[96a] b) Retro-Diels-Alder reaction that proceeds only after ring-opening.[99] c) ROP of lactones catalyzed by the ring-open isomer of a DAE coupled NHC.[23b]

A second way to accomplish modulated reactivity/catalytic activity using DAEs is to profit from the change between single and double bond character of one of the C-C bonds within the hexatriene/cyclohexadiene core. Thus, in specifically designed systems pericyclic reactions such as the (retro-)Diels-Alder reaction (Scheme 7b)[99-100] or the Bergmann cyclization[101] were demonstrated to proceed only in the DAE state which possesses a double bond in the right position. Furthermore, the reactivity of heterocyclic structures used as bridging moiety of the DAE scaffold can be modulated by changing the central C-C bond from a double bond in the ring-open isomer to a single bond in the ring-closed isomer. Thus, the Lewis acidity of an aromatic 1,3,2-dioxaborole ring is drastically increased by isomerizing it to a

1,3,2-dioxaborolane with exocyclic double bonds.[102] Likewise, the electrophilicity of an 1,3-disubstituted imidazolium salt was demonstrated to increase when being transformed to an imidazolinium moiety after ring-closure.[103] In a series of reports the group of Bielawski recently demonstrated the modulation of reactivity and catalytic activity of a dimethyl substituted N-heterocyclic carbene (NHC) used as bridge of a DAE scaffold (Scheme 7c).[23a-d] Upon changing the backbone from a conjugated to the cross-conjugated structure the nucleophilicity/electron donating capability of the NHC is reduced. This effect was explored by using the photochromic NHC as switchable organocatalyst for transesterification reactions and the ring-opening polymerization (ROP) of lactones, as well as by using it as a ligand in a Rh metal complex allowing the photocontrol over hydroboration reactions.

A very different approach for the photocontrol over chemical reactivity and catalysis consists in using DAEs as photoreversible inhibitors of biological receptors such as enzymes. Thereby, binding to the enzyme and with this the inhibition of its catalytic activity is modulated by changes in the the molecular shape and flexibility of the DAE upon the isomerization.[72]

3. Motivation

In the preceding chapter a picture of the huge versatility of DAEs as photochromic compounds has been drawn. Much is known about how to tune the photochemical properties of DAEs and work has been done on the multifunctional addressing of the isomerization reaction using UV light, triplet sensitizers, or electrochemistry. By utilizing geometric and in particular electronic changes occurring during the isomerization reaction, many potential applications for DAEs in various fields of natural sciences are conceivable. However, there are certain aspects of DAE photochromism that demand further understanding and tuning in order to successfully realize the exploitation of DAEs as remote-controllable building blocks in functional systems (Scheme 8).

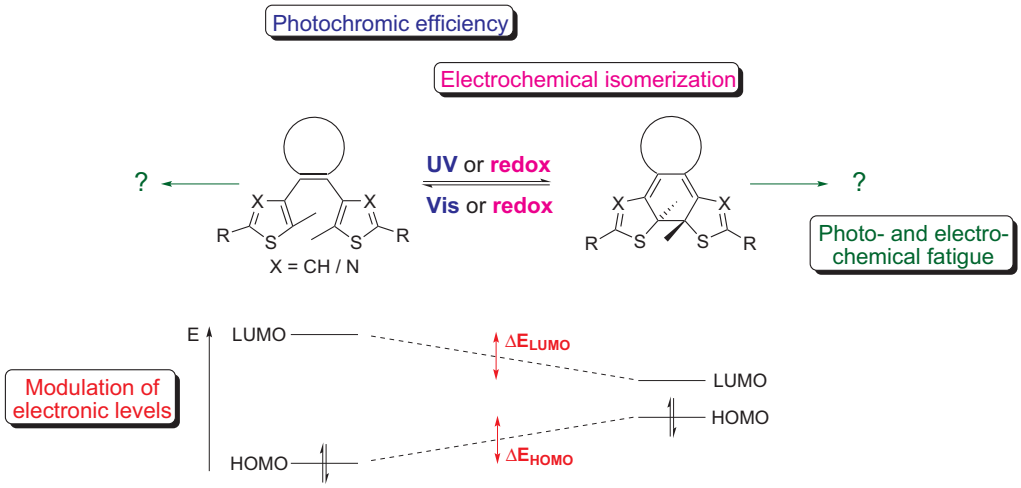

Scheme 8. Aspects of DAE photochromism to be tuned by structural design.

- *Photochromic efficiency.* As described in sections 2.1.1 and 2.1.2, a lot of studies have been performed in order to understand spectral shifts, quantum yields, and the thermal stability of the ring-closed isomer. However, high quantum yields for ring-closure often go in line with inefficient ring-opening and are highly dependent on the solvent. To improve photochromic efficiency general concepts are needed to realize high quantum yields for ring-closure *and* ring-opening that are independent of the surrounding conditions. To retain high conversion to the ring-closed isomer in the PSS the spectral overlap between the isomers in the UV region has to be minimized. These problems are currently being addressed by the research projects of other coworkers in the Hecht group,[104] while always being a side aspect of *this* work.
- *Photochemical fatigue.* The fatigue reaction of DAEs to the annulated isomer is well known (see Section 2.1.3) and comprises a serious handicap for any application of DAEs

in which more than just a few switching cycles are needed. Until the present day no quantification or systematic investigation of its dependency on structural parameters has been performed yet. The goal of this work is to precisely quantify by-product formation of DAEs and to find generally applicable strategies to improve their fatigue resistance, in particular for structures *not* possessing the perfluorocyclopentene bridge.

- *Electrochemical isomerization.* The operation of DAEs by redox chemistry has been reported, but there is some dissent in the literature about the mechanisms (see Section 2.1.4). Furthermore, nothing has been reported on potential fatigue reactions. Thus, during the electrochemical investigation of DAEs synthesized in this work, special attention shall be paid on this topic. By specific design of the DAE scaffold insights into the mechanism shall be gained.
- *Modulation of electronic levels.* The literature shows that the photoinduced modulation of HOMO and LUMO levels is a unique and highly interesting property of DAEs. By structural variation a library of DAE structures shall be obtained, which covers a broad range of level energies, allowing for the precise tuning of electronic interactions with other compounds. Furthermore, structures shall be identified for which the shift in HOMO or LUMO energy during the isomerization reaction is maximal. An estimation on how much the electronic changes in the DAE core can be transduced to adjacent functional groups shall give hints for the optimal geometry and substitution pattern of functionalized DAEs.

In this work structural variation of the DAE scaffold is achieved at four different sites (Scheme 9). As bridging moiety perhydrocyclopentene is chosen, which has the advantage over the perfluorinated analogue that it is an electron neutral substituent, thus not influencing the reactivity of other functional groups, facilitating electronic communication between the two hetaryl rings in the ring-closed isomer, and leading to significantly higher HOMO energies. Comparisons with perfluorocyclopentene and *N*-*tert*-butyl maleimide derivatives are made, the latter bridge motif having been extensively used in a diploma thesis preceeding this work.[75a]

The nature of the hetaryl rings is varied by comparing standard dithienylethene switches with their thiazole analogues. It is known that thiazoles as hetaryl moieties impart higher thermal stability to the ring-closed isomer, however, nothing has been reported on the fatigue behavior or the electrochemical isomerization of dithiazolylethenes. Furthermore, the additional nitrogen in the heterocycle induces subtle changes in the electronic levels.

A significant structural modification is made by replacing the methyl groups on the reactive carbon atoms with CF_3 groups. Though this substitution pattern has been used previously in an inverse type dithiazolylethene,[105] nothing has been reported on its influence on

the photochemical properties, the fatigue resistance, and electrochemistry. A significant alteration of electronic levels is expected.

Last but not least, substituents R^2 are chosen to be substituted phenyl rings. This shall guarantee beneficial photochemical properties (high extinction coefficients, high quantum yield for ring-closure, lower quantum yield for ring-opening to obtain high conversions in the PSS), while modulation of the electronic properties is obtained by donor and acceptor substitution. By using strongly donating morpholino substituents instead of phenyl rings photochemical and electrochemical properties of dithiazolylethenes are dramatically altered.

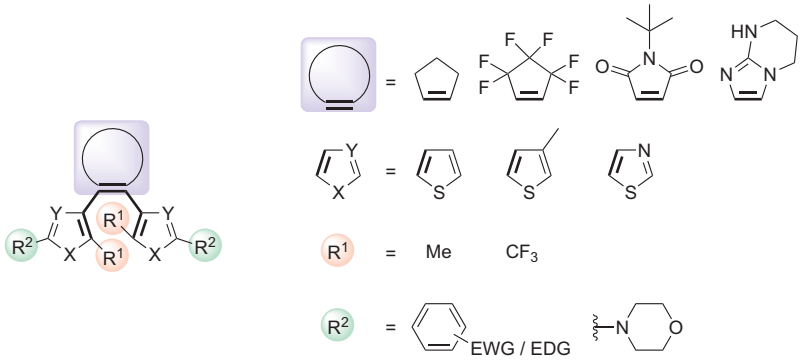

Scheme 9. Structural variation of the DAE scaffold in this work.

Finally, the goal of this work is to exploit the electronic modulation occurring during the isomerization reaction of DAEs to remote-control functional systems, in particular organic electronic devices and an organocatalyst. The first concept, developed and conducted in collaboration with the group of Prof. Paolo Samorì, is based on implementing DAE switches into semiconducting matrices and let them act as photoswitchable trapping centers in transistor device geometries (see Section 2.2.2, Figure 8b). This shall be realized using both p-type and n-type semiconducting matrices and is achieved by fine tuning of the absolute HOMO/LUMO levels of the DAE compounds with respect to the semiconductor. Although theoretically predicted,[88] at the beginning of this work this had not been realized using DAEs as active compounds.

Secondly, based on a structural motif developed in a diploma thesis preceding this work,[75a] the potential catalytic activity of a bicyclic guanidine used as bridging moiety of a DAE shall be modulated by changing the π-electronic system upon isomerization. Though recently photoswitchable catalysis using NHC, carbonyl, and imidazole moieties coupled to DAEs has been reported (see Section 2.2.3), at the beginning of this work there was no example exploiting the electronic modulation of DAEs.

4. Results and Discussion

4.1 Synthesis of all DAE derivatives

4.1.1 General synthetic strategies

The structures of all DAE compounds, which will be discussed in the later sections of this work, are collected in in Scheme 10 – Scheme 12. Their syntheses were accomplished following three common strategies and shall be described here in detail. Thereby the question why a specific substitution pattern has been chosen will be omitted, and the reader is referred to the subsequent sections.

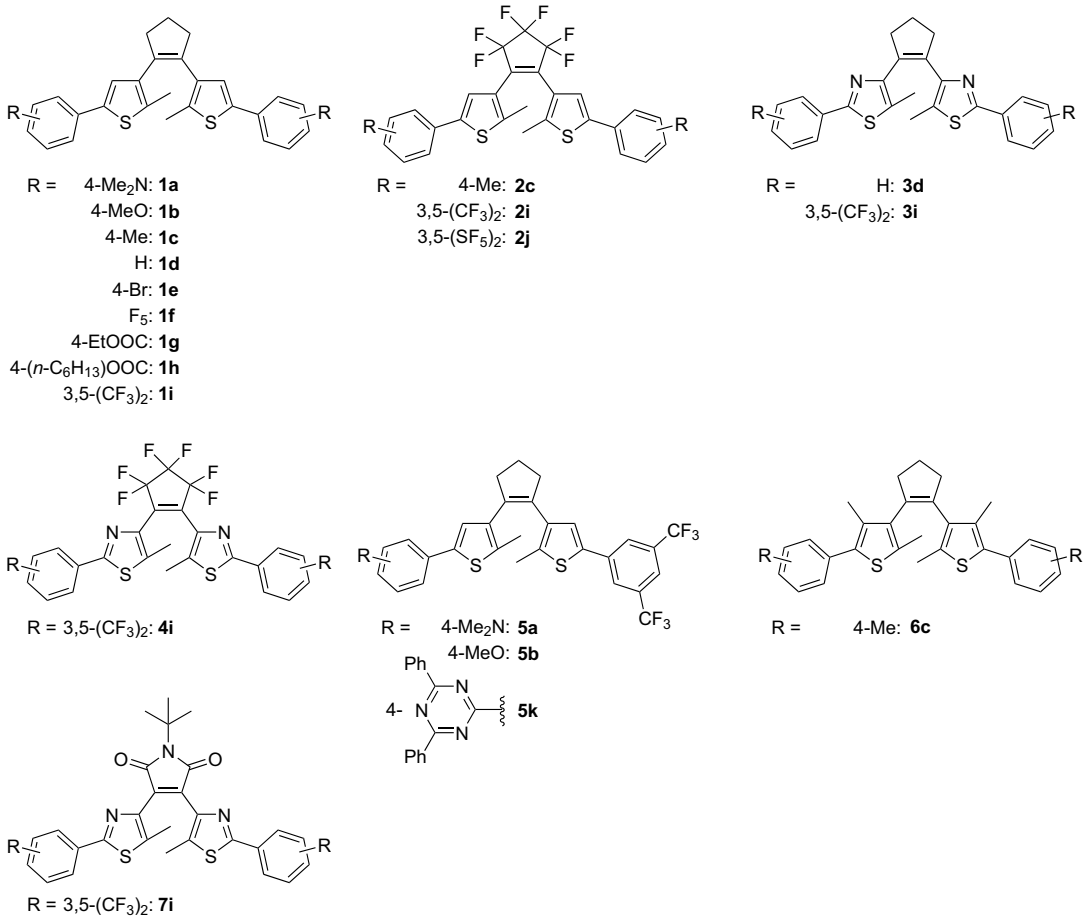

Scheme 10. Electronically modulated DAE structures discussed in this work.

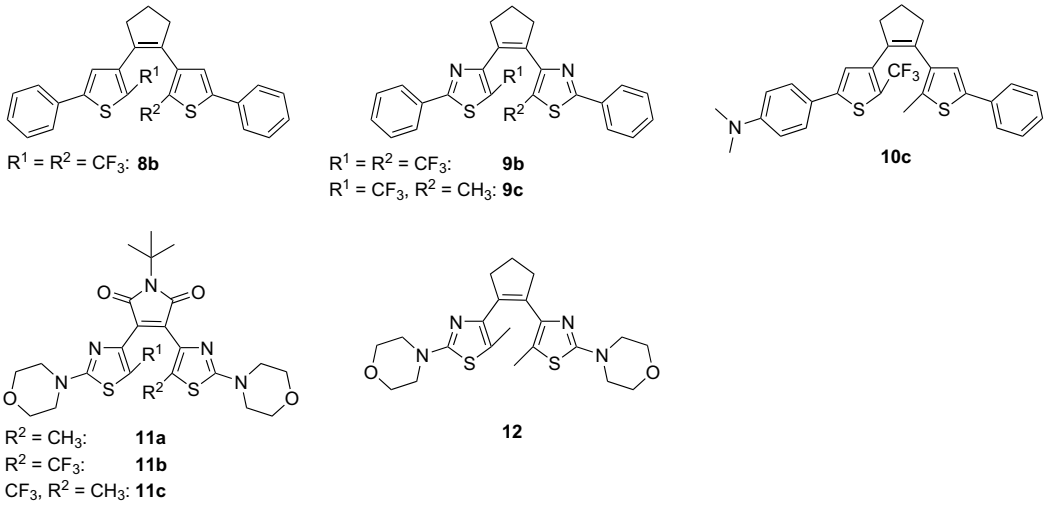

Scheme 11. DAE compounds bearing CF_3 groups at the ring-closing carbons and related reference structures.

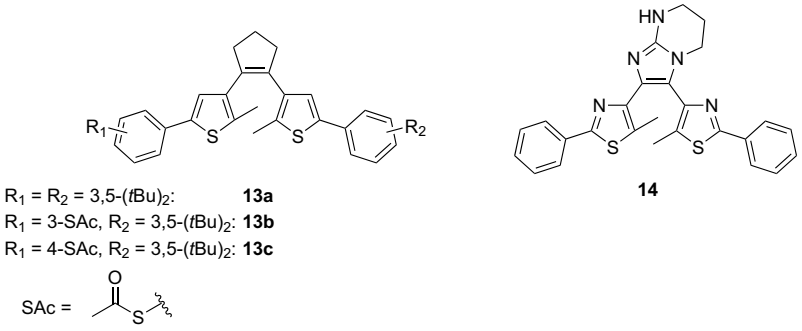

Scheme 12. *tert*-Butyl, thioacetyl, and bicyclic guanidine functionalized DAEs.

In the literature there are four established strategies for the synthesis of DAEs (Scheme 13).[106] The "classic" synthesis of DAEs bearing the perfluorocyclopentene bridge initially reported by Irie and coworkers[11b,18] consists of reacting a lithiated heterocyclic precursor with octafluorocyclopentene **15** in an addition elimination mechanism (strategy A in Scheme 13). Thereby the symmetric photochromic core is assembled in one step or the reaction is conducted stepwise to access unsymmetrically substituted DAEs, *i.e.* possessing different substitution patterns on the left and right "arm". However, often the reaction is accompanied with unsatisfactory yields and it is restricted to substitution patterns insensitive to lithium organyls. Furthermore, the heterocyclic building blocks have to be preassembled, making the synthesis inflexible. Thus, strategy A was not followed in this work.

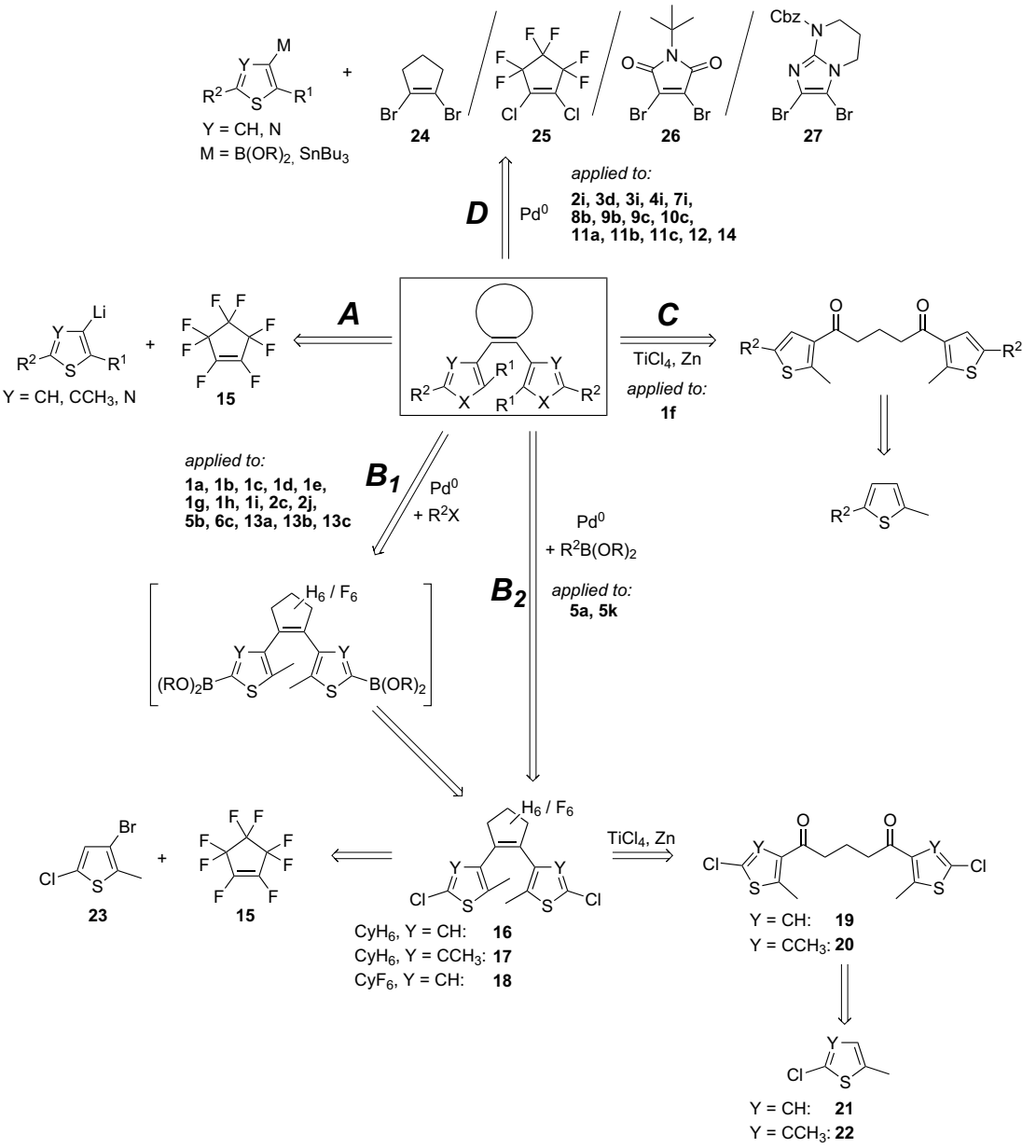

Scheme 13. Retrosynthetic pathways for the assembly of DAEs.

A very versatile synthetic route initially proposed by the group of Feringa[19,107] consists of using 1,2-bisthienylcyclopentene and 1,2-bisthienylperfluorocyclopentene building blocks that bear chlorine groups at the outer α-positions of the thiophene rings, *i.e.* compounds **16**, **17**, and **18**, respectively. These synthetic intermediates can easily be functionalized in the periphery by chlorine-lithium exchange, transformation into the boronic ester, and subsequent cross coupling with aryl halides (strategy B_1 in Scheme 13). Using this flexible route, which also tolerates sensitive functional groups on the aryl halides, a number of differently substituted DAEs were prepared in this work. The synthesis of unsymmetrically substituted DAEs can be accomplished by stepwise lithiation, borylation, and cross coupling of the dichloro-intermediates. However, it was found during this work that a reversal of the polarity in the cross coupling step, *i.e.* using the α-chlorinated thiophene and an aryl boronic acid as coupling

partners, can be advantageous (strategy B_2). The bis-chlorinated perhydrocyclopentene intermediates **16** and **17** are available by Friedel-Crafts acylation of 2-chloro-5-methylthiophenes **21** and **22** and subsequent McMurry coupling of the resulting 1,5-diketones.[19a] The perfluorinated analogue **18** is obtained by lithiation of 3-bromo-5-chloro-2-methylthiophene **23** and reaction with octafluorocyclopentene **15**.[108] One drawback of strategies B_1 and B_2 is that only thiophene-containing DAEs can be prepared. In the case of perhydrocyclopentene derivatives the Friedel-Crafts acylation step does not work with thiazole heterocycles due to the nucleophilic nitrogen atom. Furthermore, a selective lithiation of thiazole in the 4-position and quenching with an electrophile while the 2-position is free or substituted with chlorine may be difficult due to occurring lithium shifts, halogen dance reactions, or nucleophilic attacks in the 2-position of the thiazole.[109] As a second drawback, the introduction of CF_3 groups at the inner α-position of the thiophene rings is not feasible via these routes, because regioselectivity and reactivity in the Friedel-Crafts acylation would be strongly diminished, and the synthesis of halogenated, CF_3 decorated heterocycles with low molecular mass turned out to be difficult due to their high volatility (see section 4.1.4).

As a modification of strategies B_1 and B_2, in one case the Friedel-Crafts acylation and subsequent McMurry coupling have been performed on a preassembled thiophene building block to synthesize DAE structure **1f** (strategy C). While strategy C cannot be followed in general due to poor regioselectivity of the Friedel-Crafts acylation when substituted thiophenes are used, in case of **1f** this has been done to profit from the high yielding oxidative cross coupling between 2-methylthiophene and pentafluorobenzene.[110]

In order to vary the bridging moiety, but also in cases where strategies A – C cannot be employed, *e.g.* in the presence of sensitive functional groups, when using thiazoles as heterocycles, or CF_3 substitution at the ring-closing carbons, the assembly of the DAE structure by cross coupling between a dihalogenated bridging moiety and hetaryl boronic esters or stannanes has to be used (strategy D). In particular, cross couplings on 1,2-dibromo-cyclopentene **24**,[26c] 1,2-dichloroperfluorocyclopentene **25**,[111] 3,4-dibromo-*N*-*tert*-butylmaleimide **26**,[75,112] and Cbz protected 8,9-dibromo-1,5,7-triazabicyclo[4.3.0]-nona-6,8-diene **27**[75a] have been performed in this work. The heteroaromatic organoboron and organotin precursors can be synthesized using lithiation reactions. For obtaining boronic esters the Pd catalyzed Miyaura borylation[113] can also be used in cases where organolithium intermediates are not accessible.

In general, the cross coupling approach is extremely flexible as the photoresponsive hexatriene system is assembled in one step and the hetaryl moieties as well as the bridging unit can easily be exchanged. Furthermore, it is highly tolerant to sensitive functional groups on the building blocks. However, drawbacks of the cross coupling strategy are the need for preassembling the heterocyclic building blocks, which makes it inflexible in terms of

substitution in the periphery of the DAE, and the notorious sensitivity of heterocyclic boronic acids and esters against protodeboronation,[114] significantly lowering the reaction yields and making purification difficult. Though unsymmetrical substitution can be achieved by conducting the two cross coupling reactions stepwise, in case of symmetrical bridges the first step is a statistical reaction associated with lowered yields and purification problems.

In the following sections details on the synthethic procedures following strategies B_1/B_2 and D are given.[3]

4.1.2 Syntheses via post-functionalization (routes B_1 and B_2)

For obtaining dithienylperhydrocyclopentene derivatives the route established by the group of Feringa was followed.[19] The dichloro-substituted intermediate **16** was treated with two equivalents of *n*-BuLi and subsequently quenched with tri-*n*-butylborate to yield the bis(dibutyl borate), which *in situ* was reacted with an excess of the aryl bromide under conventional Suzuki coupling conditions (Scheme 14). In most cases UPLC analysis of the crude reaction mixture revealed good conversion to the desired product. However, often the isolated yields were significantly diminished, as usually several column chromatographic separations from by-products had to be performed. A by-product that was observed in all cases, yet in varying amounts, was the monocoupled species, which was hydrolyzed on the second thiophene ring. As during the halogen-metal exchange dry THF was used as solvent, this hints to protodeboronation reactions of the boronic ester under the aqueous Suzuki conditions.

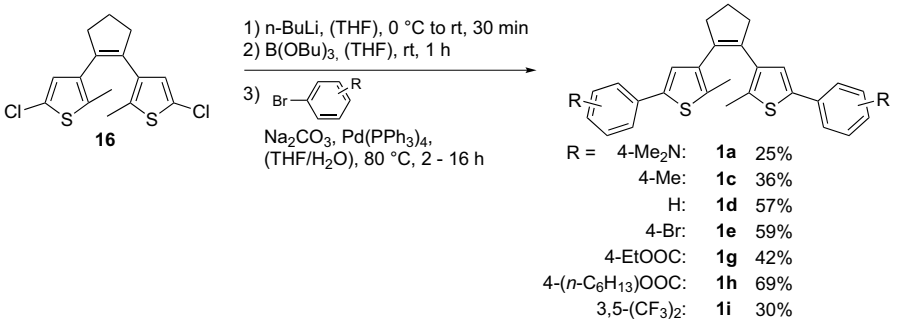

Scheme 14. Synthesis of dithienylperhydrocyclopentenes following the procedure of Feringa *et al.*[19a]

In order to start the Suzuki coupling from a defined species and to use different conditions, eventually preventing protodeboronation reactions, the bis(pinacol boronate) **29** was isolated (Scheme 15). According to conditions reported by Buchwald and coworkers,[115] the Suzuki coupling was performed without the addition of water using $Pd(OAc)_2$ together with the

[3] Details on the synthesis of compounds **1f** and **6c** will not be reported in this work. The synthesis of **1f** via strategy C was conducted by Dr. Bernd Schmidt and can be found in: M. Herder *et al*,. *J. Am. Chem. Soc.* **2015**, *137*, 2738-2747. Synthesis of **6c** via the intermediates **17**, **20**, and **22** was conducted by Jutta Schwarz and has been published.[104a]

SPhos ligand as catalyst, solid K_3PO_4 as base and toluene as solvent. Thereby, the solvent was intentionally used without employing any drying procedures, as it is believed that trace amounts of water are needed to activate boronic esters for cross coupling.[4] However, in case of compound **13a** the yield was again diminished by the chromatographic separation of the highly unpolar compound from unpolar by-products resulting from protodeboronation. In case of compound **1b,** the bis(pinacol boronate) **29** was reacted with only one equivalent of 4-bromoanisole, as initially the monocoupling was intended. However, only the hydrolyzed monocoupled species could be isolated besides 9% of the biscoupled species **1b**.

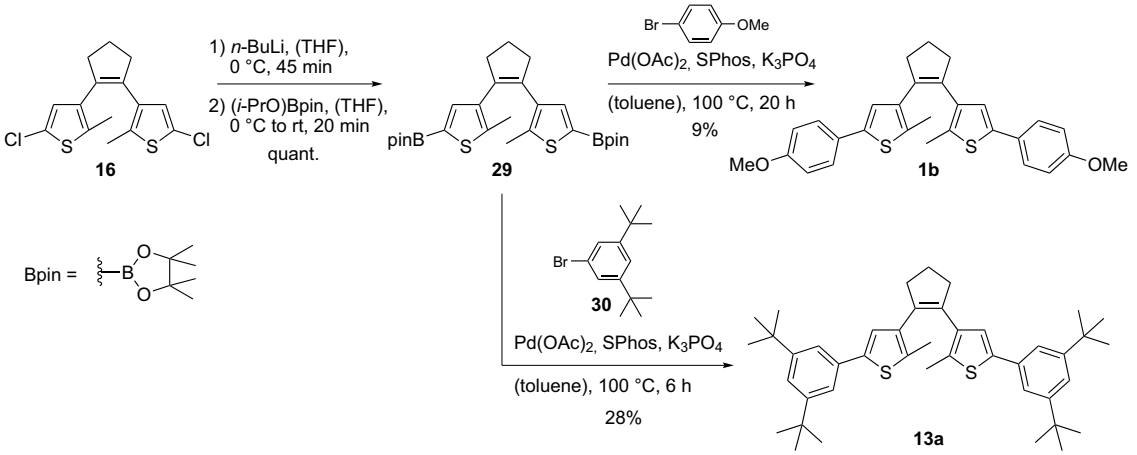

Scheme 15. Synthesis of dithienylperhydrocyclopentenes via the isolated bis(pinacol boronate) **29**.

For synthesizing dithienylperfluorocyclopentenes the dichlorinated intermediate **18** was obtained from the lithiation of 3-bromo-5-chloro-2-methylthiophene **23** via halogen-metal exchange and reaction with octafluorocyclopentene **15**.[108] Subsequent treatment of **18** according to the *in situ* lithiation/borylation/cross coupling protocol applied to the perhydrocyclopentene derivatives was not successful. Thus, the bis(pinacol boronate) **31** was isolated (Scheme 16). Thereby, it proved to be essential to perform the halogen-lithium exchange in diethyl ether instead of THF to avoid decomposition reactions. Furthermore, the bis(pinacol boronate) **31** seemed to be much less stable than the perhydrocyclopentene analogue **29**, as slow decomposition was observed during the workup in the presence of water and during TLC analysis. However, by coupling of compound **31** using the Buchwald

[4] The role of water and the nature of the active species during the Suzuki coupling are under debate.[116] In case of free boronic acids $RB(OH)_2$ a recent study[117] indicates that it is the neutral form, which undergoes transmetalation to an oxo-palladium intermediate $[L_2Pd(Ar)(OH)]$ (L = ligand, Ar = aryl) that is formed after oxidative addition of ArX (X = halogen) and substitution of X^- with OH^-. Transmetalation of the base activated boronate $RB(OH)_3^-$ on $[L_2Pd(Ar)(X)]$ is shown to be much slower. However, in both cases trace amounts of water would be needed to generate the OH^- ion. Note that for free boronic acids also fully anhydrous conditions have been applied.[118]
Importantly, no mechanistic studies have been performed on boronic esters regarding the question if they have to get (partially) hydrolyzed by water or if they can be activated directly in order to undergo transmetalation. In fact, in the literature Suzuki couplings employing boronic esters always are conducted in aqueous solvent mixtures or under conditions not ruling out trace amounts of water.[116,119]

conditions with *p*-tolylbromide and 3,5-bis(pentafluorosulfanyl)bromobenzene, respectively, DAEs **2c** and **2j** could successfully be isolated.

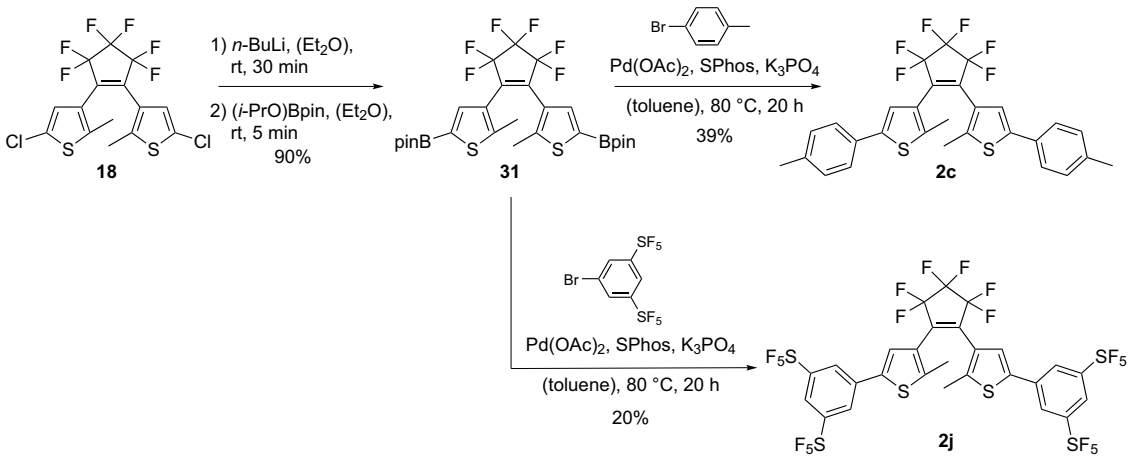

Scheme 16. Synthesis of dithienylperfluorocyclopentenes via the isolated bis(pinacol boronate) **31**.

Synthesis of unsymmetrically substituted DAEs

In principle, unsymmetrically substituted DAEs are easily accessible via the postfunctionalization route, as the dichlorinated intermediate **16** can selectively be mono-lithiated using only one equivalent of *n*-BuLi and the subsequent Suzuki coupling proceeds only on the added aryl bromide. Thus, monocoupled compounds **32** and **33** were obtained in satisfactory yields (Scheme 17). However, in both cases halogen metal exchange on the second thiophene ring was hindered by the presence of the aryl moiety. In case of the *p*-methoxyphenyl substituted DAE **32** it was noted earlier that two equivalents of *n*-BuLi were needed to achieve substitution of the chlorine group. After cross coupling with 3,5-bis(trifluoromethyl)-bromobenzene two products were obtained which showed an UV-induced coloration reaction. As the separation of the two products was not successful using conventional column chromatography due to very similar R_f-values, preparative GPC had to be used. By NMR spectroscopy and UPLC/MS the products were assigned to the desired DAE **5b** and the analogous compound **5x** substituted with an additional 3,5-bis(trifluoromethyl)phenyl group in *ortho* position to the methoxy group. Thus, it is the *ortho* lithiation of compound **32** which hinders efficient access to unsymmetrically substituted DAEs of this type.

Turning around the order of the coupling steps was not possible, as lithiation of compound **33** employing *n*-BuLi or *tert*-BuLi and subsequent quenching with different trialkylborates or the much more reactive tributyltin chloride mainly resulted in decomposition of the starting material. This might be due to nucleophilic attack of the organolithium species on the highly electron poor 3,5-bis(trifluoromethyl)phenylthiophene scaffold, as also observed with analogous thiazole compounds (see section 4.1.3).

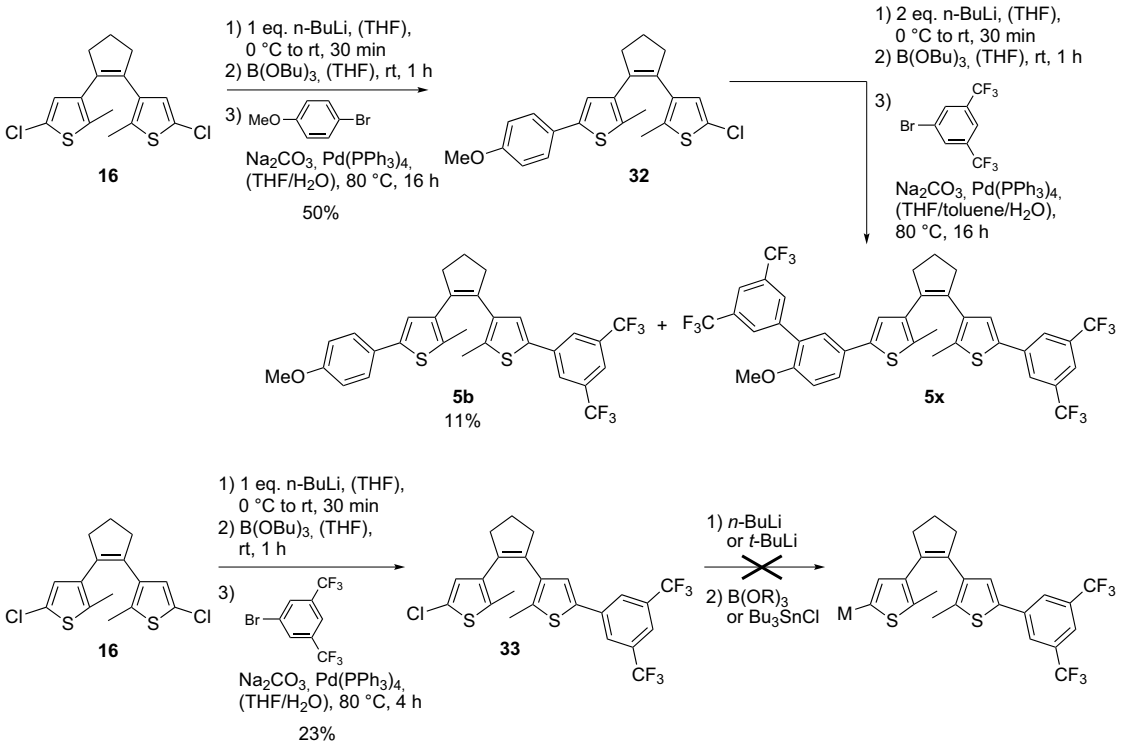

Scheme 17. Synthesis of unsymmetrically substituted DAEs via stepwise lithiation, borylation, and cross coupling.

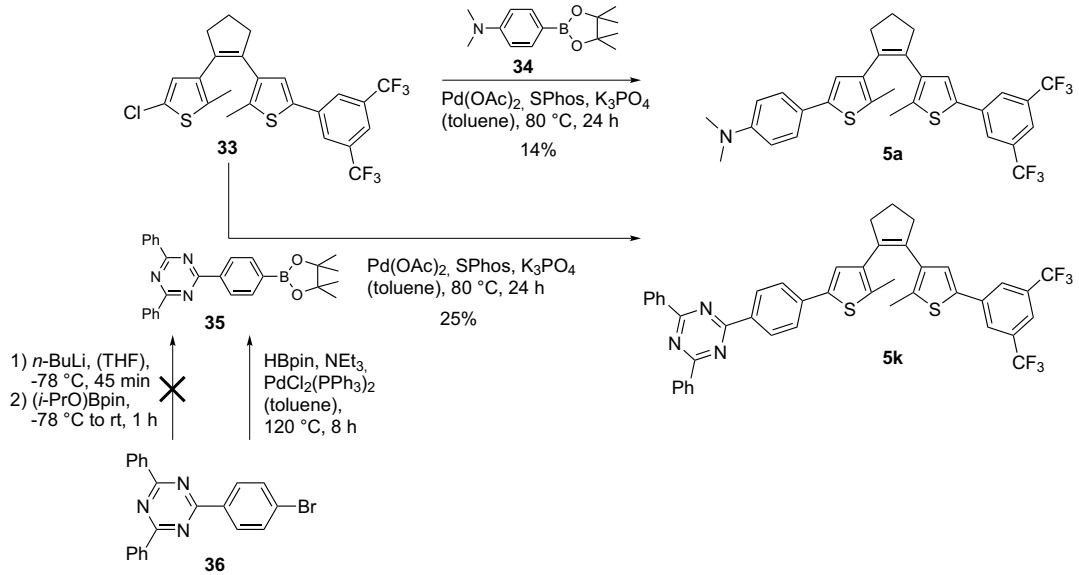

Scheme 18. Synthesis of unsymmetrically substituted DAE via cross coupling with inverse polarity in the second step.

In order to access unsymmetrically substituted DAEs from intermediate **33**, the polarity of the cross coupling reaction was changed (Scheme 18). Using the $Pd(OAc)_2$/SPhos catalyst and K_3PO_4 as base the α-chlorinated thiophene can serve as aryl halide in couplings with arylboronic acids or esters. Thus, DAEs **5a** and **5k**[5] were obtained by reaction with the pinacol

[5] Compound **5k** was synthesized by Anna Grafl in a Bachelor thesis.

boronates **34** and **35** derived from 4-bromo-*N,N*-dimethylaniline and 2-(4-bromophenyl)-4,6-diphenyltriazine **36**, respectively. Due to sensitivity of the triazine ring against nucleophilic attack, pinacol boronate **35** could not be prepared by halogen metal exchange, but a Pd-catalyzed borylation reaction analogous to the Miyaura borylation had to be used. Compound **35** could be isolated only in a mixture with minor amounts of the starting material **36**. However, it was used in excess for the subsequent Suzuki coupling.

In contrast to the above mentioned examples, the stepwise lithiation/cross coupling protocol worked when inert 3,5-bis(*tert*-butyl)bromobenzene was used as coupling partner in the first step, yielding intermediate **37** (Scheme 19). The second lithiation/cross coupling with 3-bromoiodobenzene and 4-bromoiodobenzene afforded the isomeric DAEs **38** and **39**. These were converted to the acetyl protected thiols **13b**[6] and **13c** by two different protocols: In case of *para* substitution of the phenyl ring, halogen metal exchange using *n*-BuLi, quenching with elemental sulfur and *in-situ* protection with acetyl chloride[83] afforded **13c**. For the *meta* substituted derivative **13b** a Pd-catalyzed thioacetylation[120] of the bromophenyl moiety was conducted. In both cases satisfactory conversions to the desired products were obtained. However, purification by column chromatography decreased the yields due to unwanted deprotection and oxidation of the thiol groups.

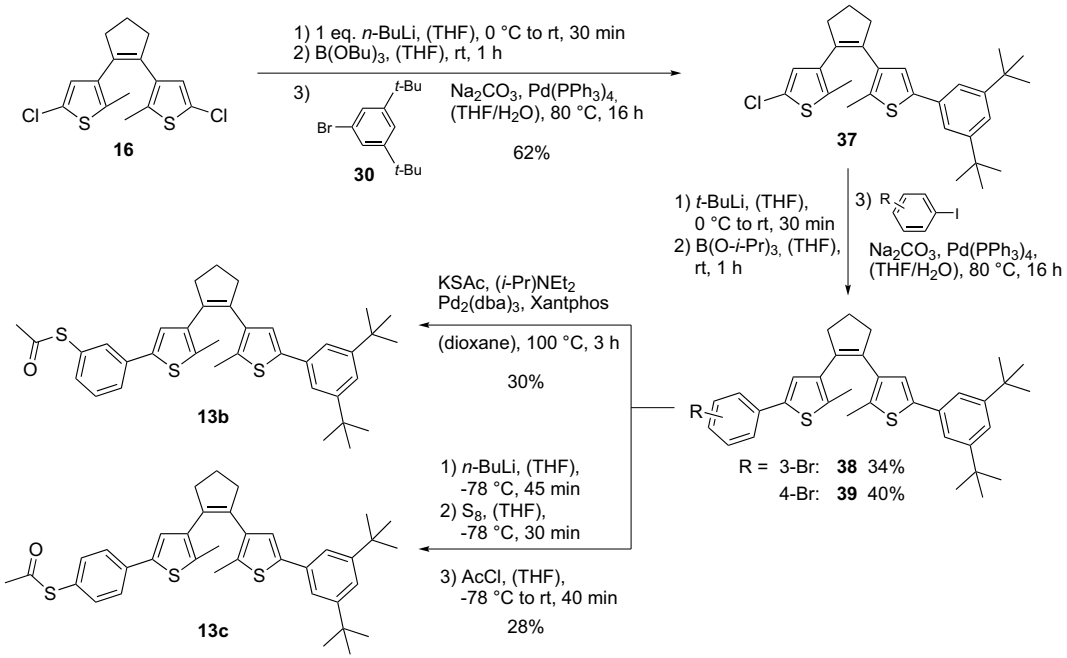

Scheme 19. Synthesis of unsymmetrically thioacetyl substituted DAEs.

[6] Compound **13b** was synthesized by Jana Hildebrandt.

4.1.3 Syntheses via cross coupling with dihalogenated bridges (route D)

Cross couplings with 1,2-dibromocyclopentene

In a diploma thesis preceding this work[75a] compound **3d** was synthesized by preassembly of the thiazole building block **41** via high yielding Hantzsch thiazole synthesis starting from thiobenzamide and 2-bromopropionaldehyde diethyl acetal **40**, direct metallation of **41** in the 4-position of the thiazole using *tert*-BuLi, quantitative conversion to the corresponding pinacol boronic ester **42**, and finally Suzuki cross coupling with 1,2-dibromocyclopentene **24** (Scheme 20, entry 1 of Table 1). For the last step it was noted that the reactivity of 1,2-dibromocyclopentene **24** in cross coupling reactions is poor and that using standard Suzuki coupling conditions, *i.e.* $Pd(PPh_3)_4$ or $PdCl_2(dppf)$ as palladium source and aqueous Na_2CO_3 as base, did not lead to the formation of the desired product. Thus, "anhydrous" conditions were applied using DMF as solvent, $PdCl_2(PPh_3)_2$ as palladium source, and Cs_2CO_3 as base without the addition of water, which allowed for the isolation of **3d** in 55% yield.[75a]

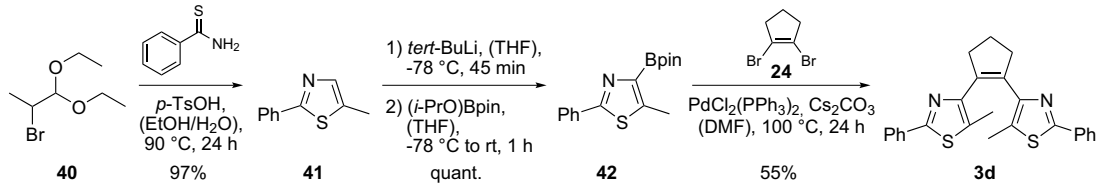

Scheme 20. Hantzsch thiazole synthesis and cross coupling with 1,2-dibromocyclopentene **24** to obtain dithiazolylethene **3d**.[75a]

While trying to synthesize larger quantities of DAE **3d** the cross coupling reaction under these conditions proved to be highly unreliable. In several trials the parent thiazole **41** was the only reaction product that could be detected by TLC or UPLC/MS, indicating quantitative protodeboronation of the pinacol boronate **42** (Table 1, entry 2). Changing the solvent to THF and using solid Na_2CO_3 as base led to the formation of only small amounts of the desired DAE **3d** (7% isolated yield) besides the monocoupled compound **43** (36% isolated yield) and the parent thiazole **41** as major products (entry 3). The monocoupled species **43** was again subjected to the cross coupling using the initial DMF/$PdCl_2(PPh_3)_2$/Cs_2CO_3 reaction conditions (entry 4). This time good conversion to DAE **3d** was observed and it was isolated in 45% yield. However, also the protodeboronation product and homocoupling of the thiazole to compound **44** were observed. Other conditions for the Suzuki reaction were also tested, *i.e.* the $PdCl_2(PPh_3)_2$/Cs_2CO_3 system using microwave irradiation (entry 5) as well as the $Pd(OAc)_2$/SPhos/K_3PO_4 system in an intended monocoupling to **43** (entry 6), which both led to the formation of the desired products. In particular the latter Buchwald conditions promised to be a good alternative as compound **43** could be isolated in 61% yield. However, in a second trial

using these conditions to directly access **3d** in one step again the protodeboronated thiazole **41** was the only reaction product (entry 7).

Table 1. Conditions employed for cross coupling of thiazolyl pinacol boronate **42** with 1,2-dibromocyclopentene **24**.

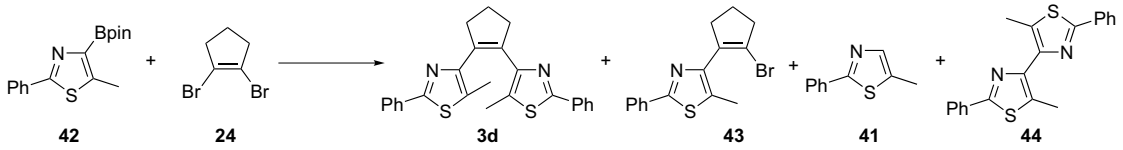

42 **24** **3d** **43** **41** **44**

Entry	Conditions	Main products detected by TLC or UPLC (isolated yields in brackets)
1[75a]	**24** + 3 eq. **42** $PdCl_2(PPh_3)_2$, Cs_2CO_3, (DMF), 100 °C, 24 h	**3d** (55%)
2	**24** + 3 eq. **42** $PdCl_2(PPh_3)_2$, Cs_2CO_3, (DMF), 100 °C, 24 h	only **41**
3	**24** + 3 eq. **42** $PdCl_2(PPh_3)_2$, Na_2CO_3, (THF), 80 °C, 20 h	**3d** (7%), **41**, **43** (36%)
4	**43** + 2 eq. **42** $PdCl_2(PPh_3)_2$, Cs_2CO_3, (DMF), 100 °C, 20 h	**3d** (45%), **41**, **43**, **44**
5	**24** + 3 eq. **42** $PdCl_2(PPh_3)_2$, Cs_2CO_3, (DMF/toluene), 110 °C, 20 min, microwave	**3d** (14%), **41**, **44**
6	3 eq. **24** + **42** $Pd(OAc)_2$, SPhos, K_3PO_4, (toluene), 16 h, 100 °C	**43** (61%), **3d**, **44**
7	**24** + 3 eq. **42** $Pd(OAc)_2$, SPhos, K_3PO_4, (toluene), 24 h, 90 °C	only **41**

All in all, the observed irreproducibility of the cross coupling indicates that there is an aspect of the reaction conditions that was not precisely controlled. As in all cases thiazole **41** was observed as reaction product in varying amounts up to quantitative conversion, it seems that thiazolylboronate **42** is highly sensitive under cross coupling conditions and that the rate of protodeboronation is a crucial factor for the success of the reaction.[7] The rate will strongly depend on the water content in the reaction mixture, which indeed was not precisely controlled in the described examples. Note that though "anhydrous" conditions were employed by avoiding the use of aqueous base, intentionally no excessive drying of the solvents and the carbonate or phosphate salts was conducted, as it is generally believed that trace amounts of water are necessary to activate boronate esters for the Suzuki reaction. In parallel experiments trying to cross couple pinacol boronate **42** with the bicyclic bridge **27** it was found that adding a defined amount of water to the reaction mixture improves conversion to the desired product (*vide infra*).

[7] Though acid catalyzed protodeboronation of free boronic acids is well known[121] and it was noted early that sterically hindered boronic acids protodeboronate under Suzuki coupling conditions,[122] only recently systematic studies on this reaction were undertaken.[123] However, only one study was found on the stability of boronic esters under basic conditions[124] and nothing is known on the interplay between their hydrolysis, transmetalation, and competing protodeboronation in a Suzuki coupling in the presence of water and a palladium catalyst.

As an alternative to the precarious Suzuki cross coupling on 1,2-dibromocyclopentene **24** the Stille reaction starting from stable thiazol-4-yl stannanes has been used previously for the synthesis of DAE **3d** as well as for DAE **12**.[75a] In the latter case morpholinothiazole **46**, obtained via Hantzsch thiazole synthesis, was metallated using *tert*-BuLi and converted to the tributylstannane **47**, which then was coupled to give DAE **12** in 6% isolated yield (Scheme 21). The low yield resulted from side reactions and purification issues typical for Stille cross couplings, as the thiazolylstannane underwent homocoupling and it was difficult to eliminate organotin residues from the final product.

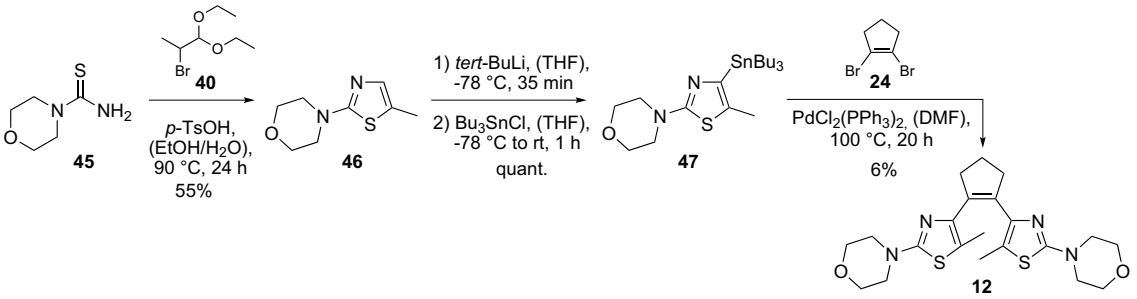

Scheme 21. Synthesis of **12** via Stille cross coupling.[75a]

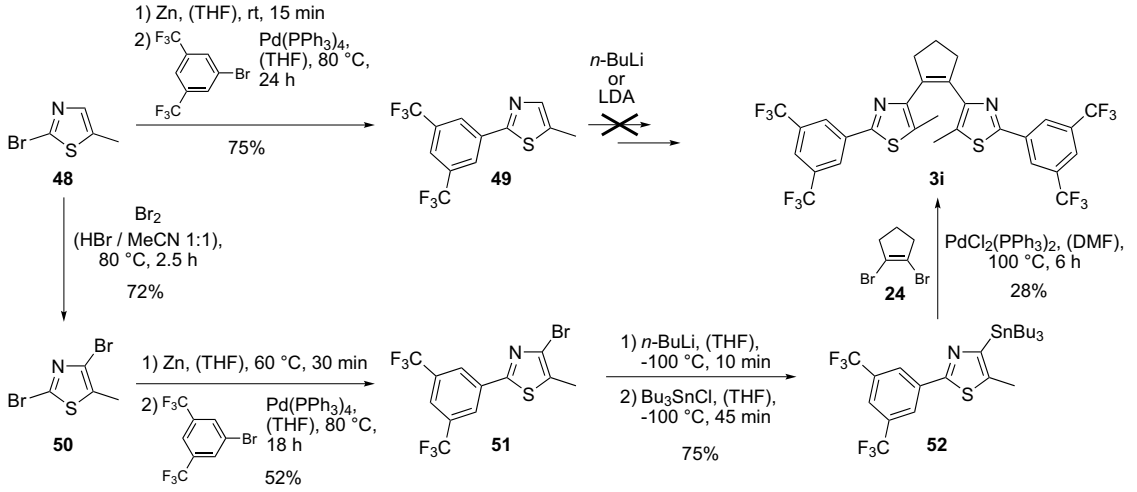

Scheme 22. Unsuccessful direct metalation of thiazole precursor **49** and synthesis of **3i** via halogen metal exchange on **51**, stannylation and Stille cross coupling.

Also for the synthesis of DAE **3i** a final Stille cross coupling on 1,2-dibromocyclopentene **24** was employed (Scheme 22). For the assembly of the thiazole building block, 2-bromo-5-methylthiazole **48**, obtained from commercially available 2-amino-5-methylthiazole by a Sandmeyer reaction, was converted to an organozinc intermediate by insertion of elemental zinc into the 2-position,[125] *in situ* followed by Negishi cross coupling with 3,5-bis(trifluoromethyl)bromobenzene to yield thiazole **49** in good yields. Unfortunately, lithiation of **49** using *n*-BuLi or LDA resulted in decomposition of the starting material, presumably due to nucleophilic attack of intermediate organolithium species at the electron

deficient 2-position of the thiazole ring. Additionally a poor regioselectivity of proton abstraction on **49** would be expected. Thus, the 4-position of the thiazole had to be substituted with bromine in order to conduct a selective halogen metal exchange. This is done by bromination of the precursor **48** to 2,4-dibromo-5-methylthiazole **50** and subsequent regioselective zincation and *in-situ* Negishi cross coupling to yield bromothiazole **51**. Importantly, the halogen metal exchange on **51** using *n*-BuLi could only be accomplished at -100 °C. At slightly higher temperatures, *i.e.* at -80 °C, the lithiated intermediate started to decompose. This is the reason why **51** could only be converted to the organostannane **52** by quenching with tributyltin chloride, which is able to react at these low temperatures in contrast to boronation agents such as isopropoxy pinacol borate. Finally, Stille cross coupling with 1,2-dibromocyclopentene **24** yielded DAE **3i** in 28% yield.

Cross couplings with 1,2-dichlorohexafluorocyclopentene

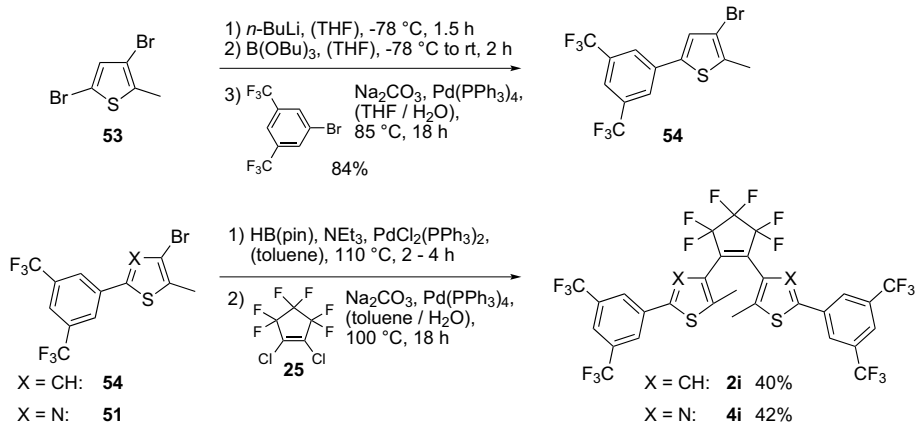

Scheme 23. Functionalization of thiophene and thiazole precursors via *in situ* Miyaura borylation and Suzuki cross coupling.

For the synthesis of the diarylperfluorocyclopentenes **2i** and **4i** the strategy of performing Suzuki cross coupling on 1,2-dichlorohexafluorocyclopentene **25**, recently reported by Shinokubo and coworkers,[111] was employed. It has the advantages that compound **25** is much cheaper and easier to handle than octafluorocyclopentene **15** and that organolithium intermediates may be avoided, which especially proved to be important in the handling of the thiazole building block **51** (*vide supra*). Though Shinokubo and coworkers optimized the reaction starting from pre-synthesized boronic acids and esters by using bulky ligands on the catalyst, such as XPhos and PCy_3, the coupling reaction was attempted using an *in situ* Pd-catalyzed borylation and Suzuki coupling protocol (Scheme 23). Thus, starting from thiophene and thiazole precursors **54** and **51**, respectively, the boronation was conducted using pinacol borane (HBpin), triethylamine and $PdCl_2(PPh_3)_2$ as catalyst.[113b] After confirming the conversion of the starting material by TLC, excess borane was quenched by the addition of

aqueous Na_2CO_3, before 1,2-dichlorohexafluorocyclopentene **25** was added together with $Pd(PPh_3)_4$ to conduct the Suzuki coupling. It seems to be necessary to add fresh Pd-catalyst for the second step, because at the end of the boronation reaction usually a black precipitate forms indicative of decomposition of the catalytically active Pd-complex.[8]

Thiophene precursor **54** was synthesized by selective halogen-metal exchange in the 2-position of 2,4-dibromo-5-methylthiophene **53**, *in situ* boronation, and cross coupling with 3,5-bis(trifluoromethyl)bromobenzene. As expected, the latter is much more reactive in the cross coupling than the thiophene itself at its 4-position.

Cross couplings with 3,4-dibromo-*N*-*tert*-butylmaleimide

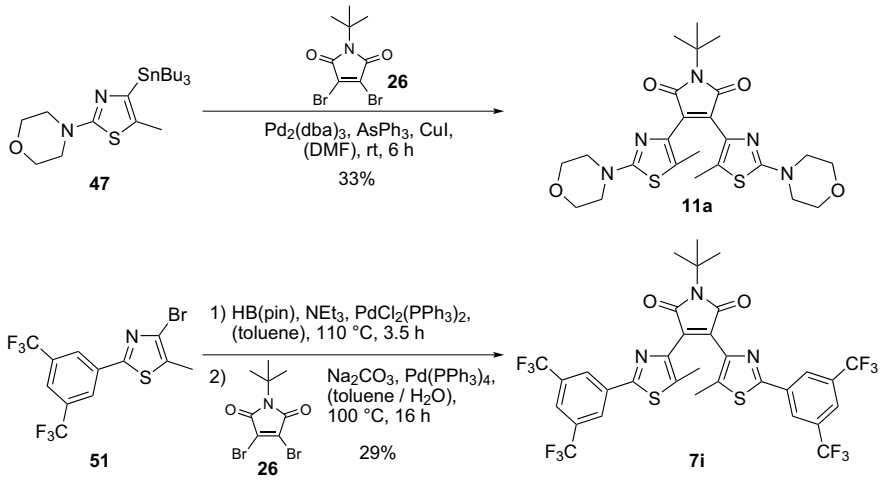

Scheme 24. Synthesis of dithiazolylmaleimides via Stille cross coupling[75a] and *in situ* Miyaura borylation/Suzuki cross coupling.

In a diploma thesis preceding this work[75a] a number of cross couplings on 3,4-dibromo-*N*-*tert*-butylmaleimide **26** were performed using Suzuki as well as Stille protocols, *e.g.* for the synthesis of DAE **11a** from thiazolylstannane **47** (Scheme 24). Using thiazolylstannane **52** also a Stille reaction was performed in order to synthesize DAE **7i**. However, the crude product could not be purified from organotin residues. Thus, for obtaining DAE **7i** from bromothiazole **51** the *in situ* borylation/Suzuki cross coupling protocol described above was applied and **7i** could be isolated in 29% yield (Scheme 24).

[8] In principle, it is possible that formed Pd-nanoparticles actually are the catalytically active species, as well in the second reaction step. However, no systematic investigations about this issue have been made.

Cross couplings with bicyclic bridge 27

The synthesis of the dibrominated bicyclic bridge **27**, consisting of alkylation of tribromoimidazole **55** and a subsequent copper catalyzed intramolecular amidation reaction was described before (Scheme 25).[75a] Thereby, the usage of Cbz as protection group was essential as it ensures reactivity in the intramolecular coupling and the compound analogous to **27** bearing a Boc protection group was difficult to purify. Furthermore, clean acidic deprotection of the final DAE could not be achieved due to side reactions.

In the diploma thesis[75a] Suzuki cross coupling of **27** with pinacol boronate **42** was performed yielding the Cbz protected DAE **61**. However, as already experienced during synthesis of dithiazolylcyclopentene **3d** (*vide supra*), the Suzuki cross coupling using boronate **42** was not reproducible and in a second attempt only 6% of the desired DAE besides 24% of a monocoupled species **62**[9] could be isolated (Table 2, entry 1). By UPLC/MS analysis of the crude reaction mixture mainly protodeboronation of boronate **42** and homocoupling to dithiazole **44** was detected. As the dibrominated bridge **27** was completely consumed it seems that the first coupling step to the monocoupled species **62** proceeds fast while the second coupling is significantly slower, thus competing with the degradation of the boronic ester.

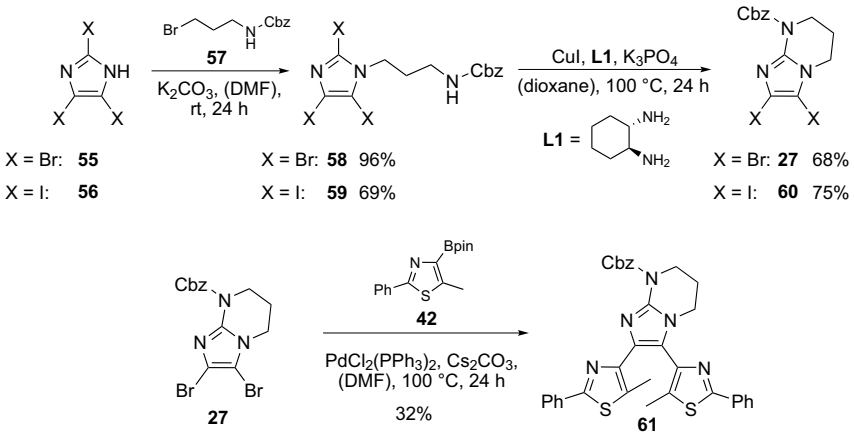

Scheme 25. Synthesis of dibrominated triazabicyclononadiene **27** and its Suzuki cross coupling to **61**[75a] as well as synthesis of diiodinated triazabicyclononadiene **60**.

[9] Due to electronic reasons Suzuki cross coupling on N-substituted 4,5-dihalogenated imidazoles should proceed in the 5-position first, which has also been observed in the literature.[126] It is assumed that monocoupled compound **62** has the according structure. However, no clear structural proof could be obtained by NMR spectroscopy. By UPLC/MS analysis of the crude reaction mixture two isomers with a *m/z* ratio corresponding to **62** were identified, with one of them being present only in trace amounts.

Table 2. Employed conditions for the cross coupling of pinacol boronate **42** and dibrominated bridge **27**.

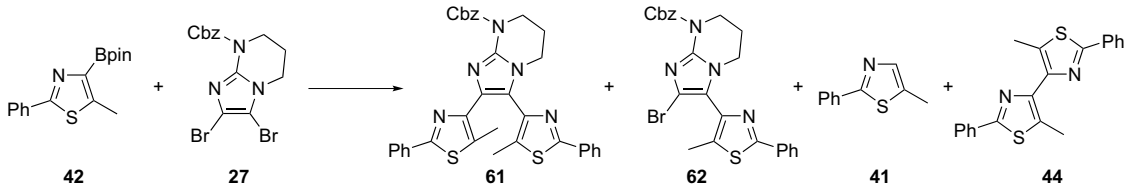

Entry	Conditions	Product distribution[a,b]				
		61	**62**[c]	**41**	**44**	**42**
1	3 eq. **42** + **27** $PdCl_2(PPh_3)_2$, Cs_2CO_3, DMF, 100 °C, 24 h	13% (6%)	23% (24%)	47%	17%	-
2	3 eq. **42** + **27** $Pd(OAc)_2$, SPhos, K_3PO_4, toluene, 90 °C, 16 h	15%	21%	53%	11%	-
3	3 eq. **42** + **27** $Pd(OAc)_2$, SPhos, K_3PO_4, toluene ***(dry)***, 100 °C, 16 h	29%	23%	32%	15%	-
4	3 eq. **42** + **27** $Pd(OAc)_2$, SPhos, K_3PO_4 ***(dry)***, toluene ***(dry)***, 100 °C, 16 h	6%	16%	13%	7%	59%
5	3 eq. **42** + **27** + 3 eq. H_2O $Pd(OAc)_2$, SPhos, K_3PO_4 ***(dry)***, toluene ***(dry)***, 100 °C, 16 h	65% (45%)	-	23%	13%	-
6	3 eq. **42** + **27** $Pd(PPh_3)_4$, K_3PO_4, dioxane, microwave, 30 min, 110 °C	28% (25%)	35%	23%	13%	-
7	3 eq. **42** + **27** $Pd(PPh_3)_4$, K_3PO_4 ***(dry)***, dioxane, microwave, 15 min, 110 °C	55%	13%	20%	13%	-
8	3 eq. **42** + **27** $Pd(PPh_3)_4$, K_3PO_4 ***(dry)***, toluene ***(dry)***, microwave, 15 min, 110 °C	38%	13%	11%	7%	31%

[a] Obtained from UPLC/MS analysis of the crude reaction mixtures. Relative integrals of the major peaks in the diode array detector trace are given.
[b] Values in brackets give isolated yields after work up and purification by column chromatography.
[c] Sum of both regioisomers.

In order to optimize the conditions for a double Suzuki coupling on bridge **27** phenyl boronic acid was used as a test substrate and a number of different reaction conditions varying the catalyst, base, and solvent were screened (Table 3). During most reactions mainly the monocoupled species **65** was formed while only small amounts of the biscoupled compound **64** were present. Importantly, using the $Pd(OAc)_2$/SPhos/K_3PO_4 system in toluene (Table 3, entry 6) or $Pd(PPh_3)_4$/K_3PO_4 in dioxane under microwave irradiation (Table 3, entry 7) gave high conversion to the desired product and only minor amounts of the monocoupled species were detected. Thus, with the former method compound **64** could be isolated in 66% yield.

Table 3. Optimization of conditions for Suzuki cross coupling on dibrominated bridge **27**.

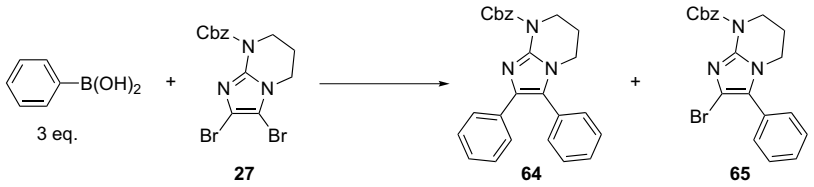

Entry	Conditions	Product distribution[a,b] 64	65	27
1	$PdCl_2(PPh_3)_2$, Cs_2CO_3, (DMF), 100 °C, 3 h	12%	44%	-
2	$PdCl_2(PPh_3)_2$, Cs_2CO_3, (DMF), 100 °C, 20 h	16%	28%	-
3	$Pd(PPh_3)_4$, Na_2CO_3 (DMF/H_2O), 100 °C, 20 h	10%	30%	-
4	$PdCl_2(PPh_3)_2$, CsF, Et_3BnNCl, (toluene/H_2O 1:1), 60 °C, 24 h	17%	34%	-
5	Pd/C, Na_2CO_3 (EtOH/H_2O 1:1), 100 °C, 4 h	6%	21%	43%
6	Pd(OAc), SPhos, K_3PO_4 (toluene), 100 °C, 20 h	84% (66%)	2%	-
7	$Pd(PPh_3)_4$, K_3PO_4, (dioxane), microwave, 110 °C, 30 min	82%	3%	-
8	$PdCl_2(PPh_3)_2$, Cs_2CO_3, (DMF), microwave, 110 °C, 30 min	-[c]	-[c]	-[c]

[a] Obtained from UPLC/MS analysis of the crude reaction mixtures. Relative integrals of peaks in the diode array detector trace are given, normalized to the total integral of all peaks in the chromatogram.
[b] Values in brackets give isolated yields after work up and purification by column chromatography.
[c] Complete decomposition.

Consequently, both reaction protocols that were identified to promote the second coupling step were applied to the reaction of **27** with thiazolyl pinacol boronate **42** (Table 2, entries 1 and 6). In both reactions conversion to the desired DAE **61** was detected, however, still significant amounts of the monocoupled species **62** as well as the protodeboronated thiazole **41** were formed. To investigate the role of trace amounts of water in the reaction mixture, efforts were made to dry the solvent and the solid base.[10] Using the anhydrous solvent while taking K_3PO_4 from the bench the conversion to the desired DAE increased but still large amounts of monocoupled species and deboronated thiazole were formed (entry 3). By using both anhydrous solvent and K_3PO_4 the conversion to the DAE and to the monocoupled species significantly dropped and large amounts of the starting material **42** were detected in the reaction mixture (entry 4). Reactions performed using the microwave based protocol gave a similar trend (entries 6 and 7). This finding indicates that water is needed in the reaction mixture to activate the boronic ester. Remarkably, using anhydrous toluene and K_3PO_4 and then adding to the reaction mixture one equivalent of water per boronic ester gave excellent conversion to the

[10] Pre-dried toluene was stored over activated molecular sieves (4 Å) for three days resulting in a residual water content below 10 ppm, as determined by Karl Fischer titration. K_3PO_4 was kept at 160 °C under high vacuum for three days and then handled under argon atmosphere.

biscoupled DAE while no monocoupled compound and only small amounts of the deboronated thiazole were detected (entry 5). With this method DAE **61** could be isolated in 45% yield.

As a second approach to improve the Suzuki coupling step the diiodinated bridge building block **60** was synthesized starting from triiodoimidazole **56** and following the same strategy that was used for the dibrominated analogue **27** (Scheme 25). However, as the reaction with guanidine **27** could finally be accomplished with satisfying yields by controlling the water content of the reaction mixture, no further investigations into the reactivity of compound **60** were conducted.

The final cleavage of the Cbz group of compound **61** to yield the free bicyclic guanidine substituted DAE **14** was not straight forward. First, hydrogenation in the presence of palladium on charcoal in an autoclave at 20 bar pressure was attempted. While after 24 h ca. 30% of the starting material was converted to DAE **14**, a further increase of the reaction time, the addition of more catalyst, or the use of a different solvent did not lead to completion of the reaction. Secondly, cleavage of the carbamate using trimethylsilyliodide (TMSI)[127] was tested. The starting material was rapidly consumed but a number of by-products were formed along with the desired compound **14**. Eventually, transfer hydrogenation using excess ammonium formate in the presence of 10 mol% Pd/C,[128] either performed in the microwave or in a flask put into a preheated oil bath, led to the selective and almost quantitative cleavage of the Cbz group. After workup and column chromatography DAE **14** was obtained in 77% yield. Note that during the chromatographic purification some material was lost due to adsorption on the silica gel.

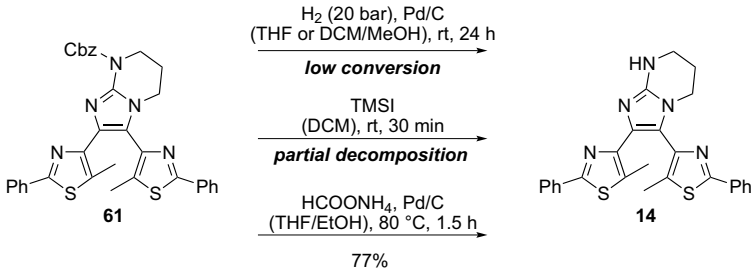

Scheme 26. Cbz deprotection on **61** to yield bicyclic guanidine substituted DAE **14**.

4.1.4 Synthesis of α-trifluoromethylated DAEs

The central step in the synthesis of α-CF_3 substituted DAEs is the conversion of halogenated thiazole or thiophene precursors to the trifluoromethylated analogues. Though since the late 1960s copper mediated trifluoromethylation of iodoarenes has been known,[129] highly effective, functional group tolerant and cheap trifluoromethylation procedures have been developed only very recently.[130] The vast majority of reports are based on the use of Cu(I) to form a "$CuCF_3$" intermediate that is able to transfer the CF_3 group onto the arene. It has been noted that the chemistry of "$CuCF_3$" in solution is very complex, tending to form higher perfluoroalky-copper homologues such as "$CuCF_2CF_3$" and to decompose at higher temperatures.[131] Thus the stabilization of the "$CuCF_3$" species by the solvent or ligands is essential to successfully conduct the desired reaction. CF_3 sources may be cheap trifluoroacetate salts,[132] CF_3I and CF_3Br,[129] or $FSO_2CF_2CO_2Me$,[133] the latter efficiently forming "$CuCF_3$" upon decarboxylation. However, because of harsh conditions needed (CF_3COONa), their difficult handling (CF_3I), or high costs ($FSO_2CF_2CO_2Me$) most modern procedures employ trifluoromethyltrimethylsilane ($TMSCF_3$, "Ruppert's reagent") to transfer the CF_3 group onto the metal complex.[130] In particular, a protocol initially developed by Urata and Fuchikami in 1991[134] using CuI in combination with $TMSCF_3$ and stabilizing the "$CuCF_3$" species by using excess KF and a 1:1 mixture of DMF/NMP as solvent proved to be highly efficient for trifluoromethylation of activated iodoarenes. A recent milestone in trifluoromethylation chemistry was laid in 2011 by Hartwig and coworkers[135] in synthesizing a [(phen)$CuCF_3$] (phen = 1,10-phenanthroline) complex, one of the few structurally well-defined "$CuCF_3$" complexes. It is capable of trifluoromethylating also unactivated iodoarenes and activated bromoarenes in almost quantitative yields while tolerating a very broad range of functional groups. Drawbacks of these and many other trifluoromethylation protocols are the need for iodo substituents on the arene and the use of stoichiometric amounts of copper. However, procedures catalytic in Cu or Pd as well as starting from arylboronic esters have been described recently.[136] Note that most trifluoromethylation reactions found in the literature were performed on benzene derivatives while only few examples on heteroaromatic compounds such as thiophene have been reported.[130]

In order to synthesize the desired α-halogenated hetaryl precursor a Hantzsch thiazole synthesis was conducted using morpholinothioamide **45** and 2-bromoacetaldehyd diethylacetal to yield the unsubstituted 2-morpholinothiazole **66** (Scheme 27a). Subsequent bromination gave bromothiazole **67**, which was used in first trials to introduce the CF_3 group. After reactions using CF_3COONa[132] and $FSO_2CF_2CO_2Me$[133] as CF_3 sources failed, trifluoromethylation was accomplished using the protocol by Urata and Fuchikami.[134] However, trifluoromethylated thiazole **69** could not be obtained pure, as higher perfluoroalkyl homologues, mainly the C_2F_5 substituted compound, were formed as inseparable by-products. Probably by-product formation was due to the long reaction times and slightly elevated temperatures needed for the reaction to

proceed on electron-rich bromothiazole **67**. Consequently, iodothiazole **68** was prepared and its trifluoromethylation was accomplished without forming higher perfluoroalkyl by-products. However, the yield of **69** was only 36%, as a significant portion of the starting material reacted in an Ullmann coupling to the 5,5'-dithiazole or was deiodinated. Trifluoromethylated thiazole **69** could be lithiated in the 4-position using *tert*-BuLi and converted to the tributylstannane **70**.

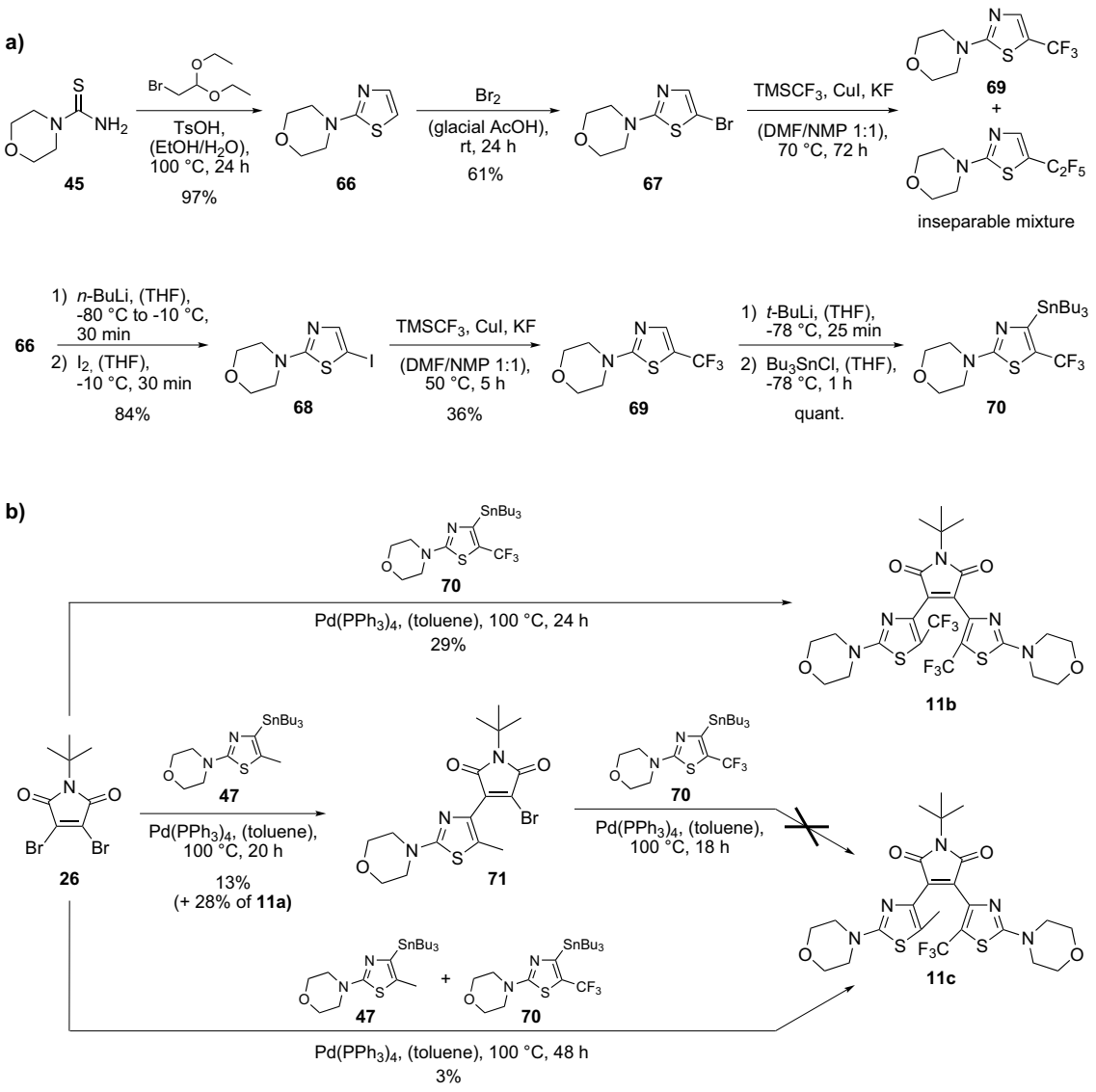

Scheme 27. a) Synthesis of α-trifluoromethylated morpholinothiazole **68** and corresponding stannane **70**. b) Cross coupling to symmetrical substituted DAE **11b** as well as unsymmetrical substituted DAE **11c**.

The Stille cross coupling between dibromomaleimide **26** and stannane **70** was performed using standard conditions yielding the symmetrically α-trifluoromethylated DAE **11b** in 29% yield (Scheme 27b). Formation of the homocoupled dithiazole and purification problems regarding organotin residues diminished the yield of the reaction. In order to synthesize DAE **11c**, which is unsymmetrically substituted with a CH_3 group on one morpholinothiazole and a CF_3 group on the other, a stepwise cross coupling was conducted. First, dibromomaleimide **26**

and CH_3-thiazolylstanne **47** were reacted to yield the monocoupled DAE **71**. However, though dibromomaleimide **26** was used in excess, the main product of this cross coupling was the symmetrical DAE **11a**, indicating that the second coupling step is significantly faster than the first. Unfortunately, by isolating **71** and performing the second coupling with CF_3-thiazolylstannane **70** the desired DAE **11c** could not be isolated. UPLC/MS analysis of the reaction mixture showed that monocoupled DAE **71** was quantitatively debrominated during the reaction. In a second attempt to synthesize DAE **11c** the two stannanes **47** and **70** were mixed in a 1:1 ratio and reacted in a statistical reaction with 0.8 equivalents of dibromomaleimide **26**. Unsurprisingly, UPLC/MS analysis of the reaction mixture revealed that the main product was the symmetrically CH_3-substituted DAE **11a** besides smaller amounts of the monocoupled DAE **71**. However, while no traces of the symmetrical CF_3 substituted DAE **11b** were formed, a small amount of unsymmetrical DAE **11c** was detected. Eventually, DAE **11c** could be isolated from the reaction mixture in 3% yield. The outcome of this reaction demonstrates the strong influence of the CF_3 group on the nucleophilicity and thereby the reactivity of the thiazolylstannanes.

The synthesis of α-trifluoromethylated DAEs was also attempted in the 2-phenylthiazole series. For this purpose Hantzsch thiazole synthesis was conducted to form 2-phenylthiazole **72**. Iodination in the 5-position was easily accomplished using *n*-BuLi and iodine giving iodothiazole **73** in good yield. As the trifluoromethylation procedure by Urata and Fuchikami gave only modest yields in case of the morpholinothiazole series, the protocol by Hartwig and coworkers,[135] published at the same time when these experiments were conducted, was applied. Thus, generating the reactive [(phen)$CuCF_3$] complex *in situ*, iodothiazole **73** was converted in 77% yield to the trifluoromethylated analogue **74**, which proved the applicability of the [(phen)$CuCF_3$] "trifluoromethylator" to 5-membered heteroaromatic compounds. However, attempts to scale up the reaction from the 0.5 mmol scale, as reported in the study by Hartwig and coworkers, failed. Performing the reaction on a 1 mmol scale drastically reduced the yield to ca. 30%, while reactions on an even larger scale failed completely, which reveals a sincere limitation of this procedure. Interestingly, CF_3-thiazole **74** could not be lithiated by proton abstraction using *tert*-BuLi like the 2-morpholino analogue **69** and the non-trifluoromethylated 5-methyl-2-phenylthiazole **42** (*vide supra*). The starting material decomposed during the reaction. This hints to a nucleophilic attack of *tert*-BuLi at the electron deficient 2-position of the thiazole ring, activated by the CF_3 group. On the other hand, the CF_3 group facilitates proton abstraction using LDA as base and subsequent transformation to the tributylstannane **78** could be achieved. Nevertheless, during the reaction still some decomposition of the starting material was detected, making a column chromatographic purification mandatory and resulting in the only moderate yield of 68%.

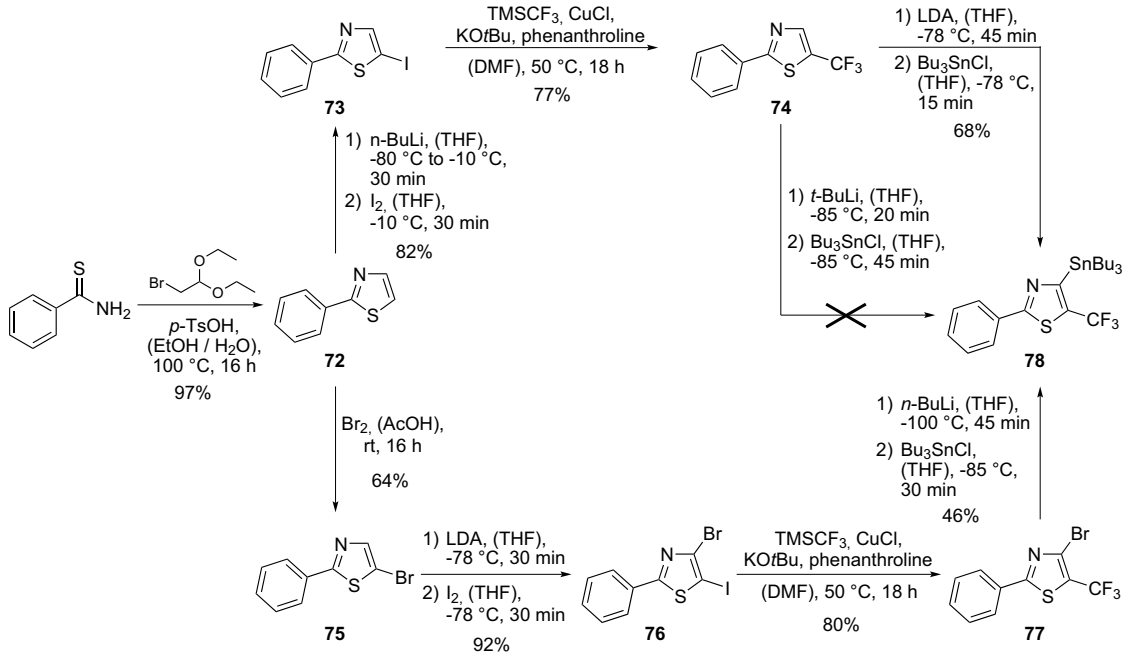

Scheme 28. Synthesis of α-trifluoromethylated thiazoles **74** and **77** and conversion to corresponding stannane **78**.

To improve the stannylation step it was envisioned to implement a bromo substituent in the 4-position of the thiazole to allow for lithiation via halogen-metal exchange which can be conducted at significantly lower temperatures than the proton abstraction with LDA. Furthermore, bromo substitution allows for conducting the final cross coupling with the bridging moiety with inversed polarity, *i.e.* using the trifluoromethylated thiazole as arylhalide instead of metalorganic compound and thus increasing its reactivity (*vide infra*). Introduction of the bromine is advantageously done in the beginning of the synthesis by bromination of 2-phenylthiazole **72** in the 5-position (Scheme 28, bottom). Then, by lithiating the 4-position using LDA a "halogen-dance-reaction"[109] is induced, *i.e.* lithium and bromine exchange positions. By quenching the intermediate with iodine 5-iodo-4-bromothiazole **76** was obtained in excellent yield. Remarkably, using Hartwig's trifluoromethylation the CF_3 group was selectively introduced in the 5-position to yield brominated CF_3-thiazole **77** in high yield. By performing the halogen-metal exchange with *n*-BuLi at -100 °C and subsequent quenching with Bu_3SnCl stannane **78** was obtained. However, also this reaction gave no clean conversion to the stannane resulting in a modest yield of 46%.

Stille cross coupling of excess stannane **78** with 1,2-dibromocyclopentene **24** yielded the symmetrically substituted α-trifluoromethylated DAE **9b** in 18% yield (Scheme 29). The unsymmetrically substituted DAE **9c** was accessed via stepwise cross coupling.[11] First 1,2-dibromocyclopentene was functionalized with the corresponding CH_3-thiazole by reacting it with boronate **42** to afford monocoupled DAE **43** (*vide supra*). This was transformed to the

[11] DAE **9c** and precursors **43**, **79**, and **80** were synthesized by Fabian Eisenreich in a Bachelor thesis. Experimental details can be found there.[137]

pinacol boronate **79** allowing for the Suzuki coupling with 4-bromo-2-phenyl-5-trifluoromethylthiazole **77** with inversed polarity relative to the first coupling step. The reaction yielded DAE **9c** in 10% yield. In order to avoid a statistical reaction during synthesizing unsymmetrically substituted DAEs a protocol recently proposed by the group of Knochel[138] for the selective transformation of 1,2-dibromocyclopentene **24** to the boronic ester **80** via halogen-metal exchange mediated by the "Turbo-Grignard" reagent *i*-PrMgCl·LiCl was tested. Indeed, boronic ester **80** was obtained in 87% yield. However, performing the Suzuki coupling of the boronic ester **80** and bromothiazole **77** gave only trace amounts of the desired monocoupled compound. Instead, a second equivalent of boronic ester **80** reacted with the monocoupled DAE, showing that the second cyclopentene-bromine bond is activated once the electron withdrawing CF_3-thiazole is attached.

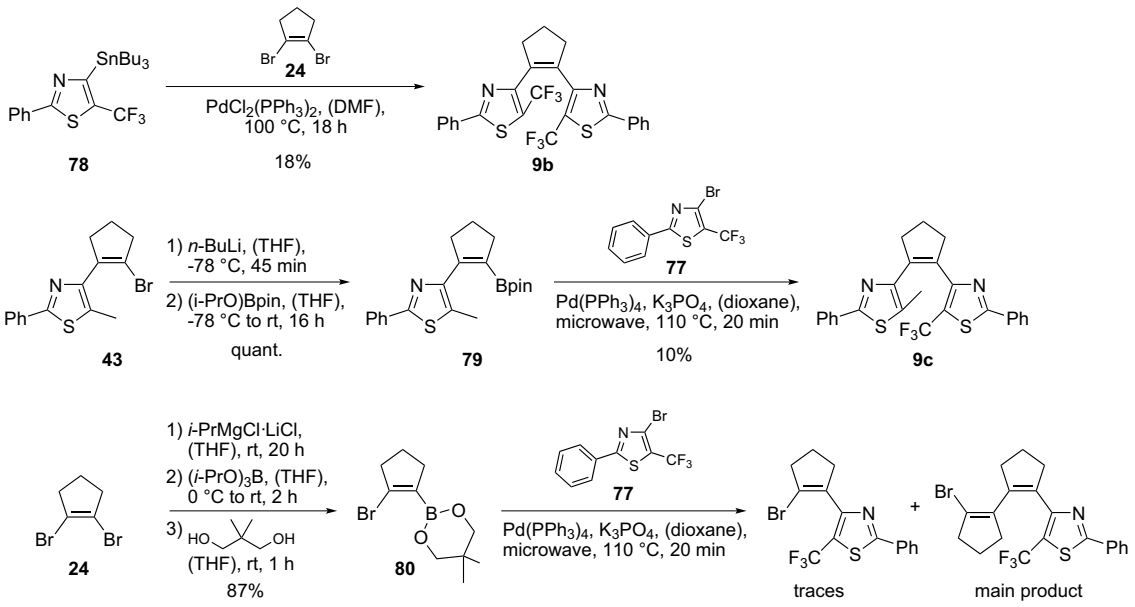

Scheme 29. Synthesis of α-trifluoromethylated dithiazolylcyclopentenes **9b** and **9c**.

In order to obtain α-trifluoromethylated DAEs in the thiophene series it was envisioned that an early introduction of the CF_3 group and construction of the 2,2'-trifluoromethylated and 5,5'-dichlorinated DAE intermediate, analogous to CH_3-bearing compound **16**, would be advantageous, as the peripheral substituents could be altered very easily (Scheme 30a). For this purpose 2-chloro-5-iodothiophene **81** was synthesized by iodination using I_2 and HIO_3.[139] This compound was subjected to Hartwig's trifluoromethylation, which gave clean conversion to a new compound, which was detected in the crude reaction mixture by UPLC. The R_f value of this compound was different to that of the starting material **81** and that of 2-chlorothiophene, thus it was concluded that the trifluoromethylated thiophene **82** may have been formed. However, upon workup of this reaction involving evaporation of the solvent no traces of either a thiophene or of a fluorine containing molecule were found by NMR spectroscopy and the peak

in the UPLC was not detected any more. Presumably, compound **82** is highly volatile making it difficult to isolate. Thus, a later introduction of the CF_3 group in preassembled thiophene building blocks had to be utilized.

Thus, 2-bromothiophene **83** was converted in a Suzuki coupling to 2-phenylthiophene **84**, which then was iodinated in the 5-position using NCS and NaI (Scheme 30b).[140] Iodothiophene **85** was trifluoromethylated using Hartwig's protocol to give CF_3 substituted thiophene **86**. As expected, deprotonation using LDA proceeded regioselectively in α-position to the CF_3 group, which allowed for the synthesis of pinacol boronate **87**, which then was cross coupled with 1,2-dibromocyclopentene **24** to give the symmetrical α-trifluoromethylated dithienylethene **8b**. Unfortunately, DAE **8b** could not be obtained pure, as after several column chromatographic separations still small impurities were detected by NMR spectroscopy and recrystallization was unsuccessful. Nevertheless, DAE **8b** was studied spectroscopically and it was assumed that the impurities do not affect the principal findings.[12]

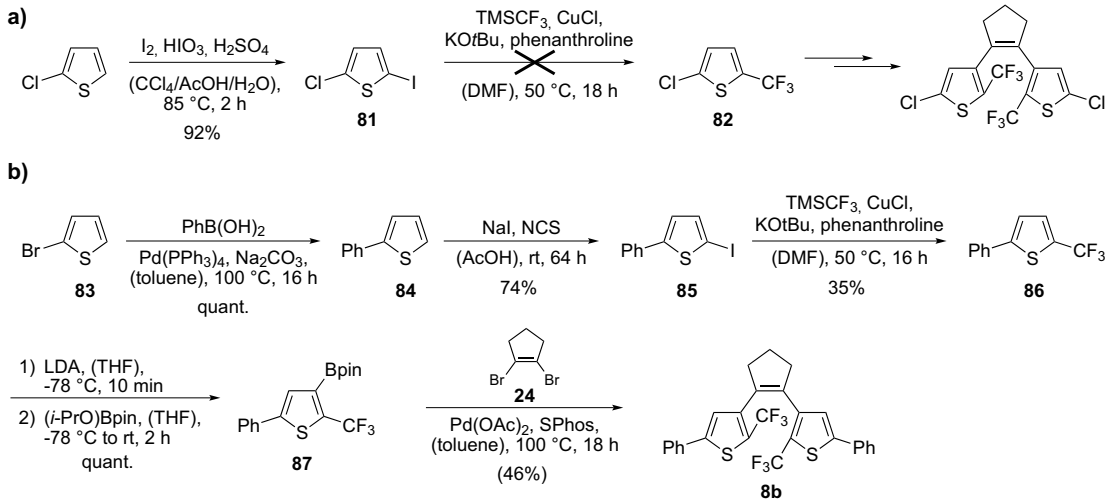

Scheme 30. a) Attempted early trifluoromethylation for the synthesis of α-trifluoromethylated dithienylcyclopentenes. b) Synthesis of DAE **8b**.

Unsymmetrically substituted dithienylethene **10c**, bearing a donor-acceptor substitution pattern composed of a *N,N*-dimethylaniline and a CF_3 group on one of the thiophene moieties, was obtained using a similar strategy (Scheme 31). Thiophene was lithiated in the α-position, converted to the boronic acid, and cross coupled with 4-bromo-N,N-dimethylaniline. The resulting thiophene **88** was iodinated using *n*-BuLi and iodine and then trifluoromethylated using the protocol by Urata and Fuchikami. Despite the substitution with a strong donor group thiophene **90** could be isolated in satisfactory 69% yield. By regioselective lithiation using LDA pinacol boronate **91** was accessed. Eventually, cross coupling of **91** with the monocoupled DAE

[12] DAE **8b** and precursors **83**-**87** were synthesized by Fabian Eisenreich in a Bachelor thesis. Experimental details can be found there.[137]

94, obtained from a low yielding statistical reaction on 1,2-dibromocyclopentene, allowed for the isolation of DAE **10c** in 28% yield starting from thiophene **90**.

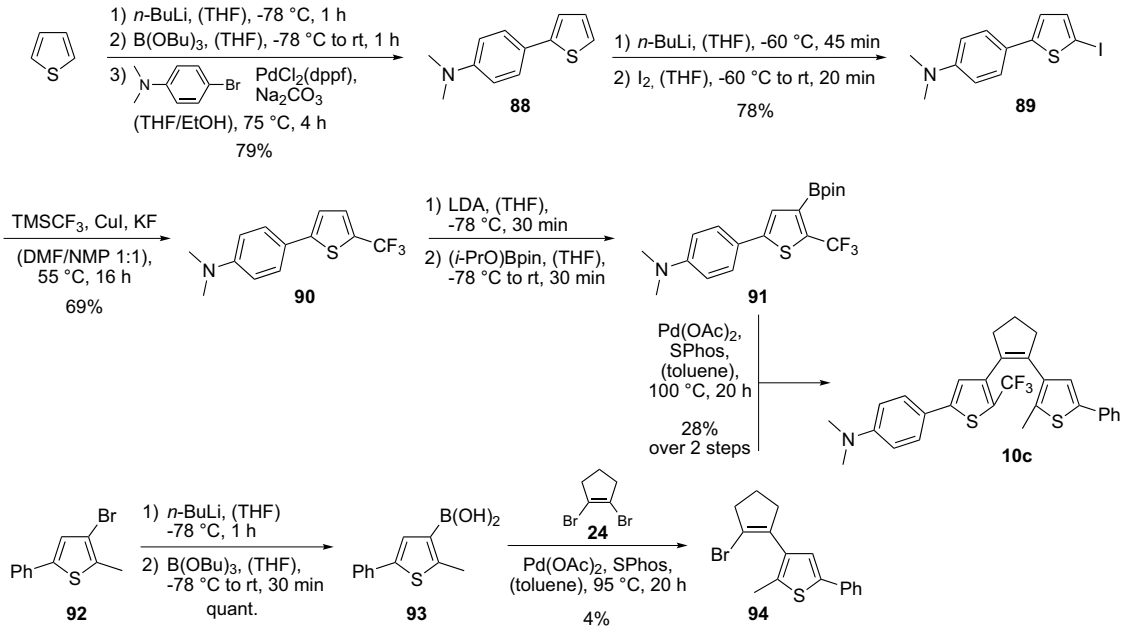

Scheme 31. Synthesis of donor substituted, α-trifluoromethylated dithienylcyclopentene **10c**.

4.1.5 Isolation of ring-closed isomers and by-products

Ring-closed isomers and by-products of three diarylcyclopentenes were isolated by irradiation in a preparative scale (Scheme 32). For this purpose ca. $1 - 2 \cdot 10^{-3}$ M solutions of the corresponding ring-open isomers in acetonitrile were placed in quartz tubes and irradiated in a photochemical reactor with 300 nm light. Thereby working under an argon atmosphere and with degassed solvents was essential, in particular for electron rich DAE **1c**. In order to isolate the ring-closed isomer in case of **1c** also the irradiation time had to be kept short to a maximum conversion of ca. 50%, as at longer irradiation times significant amounts of the by-product **1c(bp)** were formed, which were difficult to separate. For this reason and due to partly decomposition of **1c(c)** during column chromatographic purification a yield of only 33% was obtained. Notably, strict oxygen free conditions had to be applied during the column chromatographic purification of **1c(c)**, as in the presence of oxygen the compound immediately decomposed on the silica gel. Compounds **1h(c)** and **3d(c)** as well as the by-products **1c(bp)** and **3d(bp)** were much less sensitive. Detailed analytical characterization of isomers of **1c** and **3d** will be discussed in section 4.3.

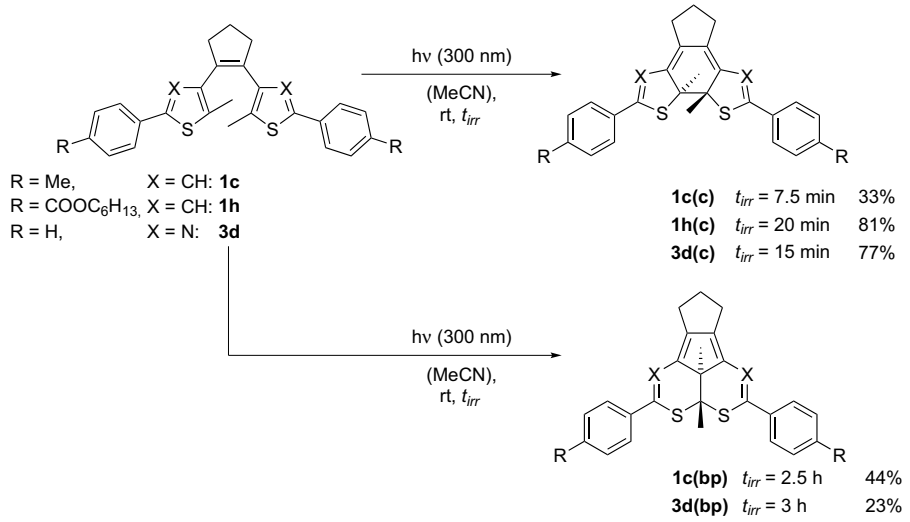

Scheme 32. Isolation of ring-closed isomers and by-products by irradiation in a preparative scale.

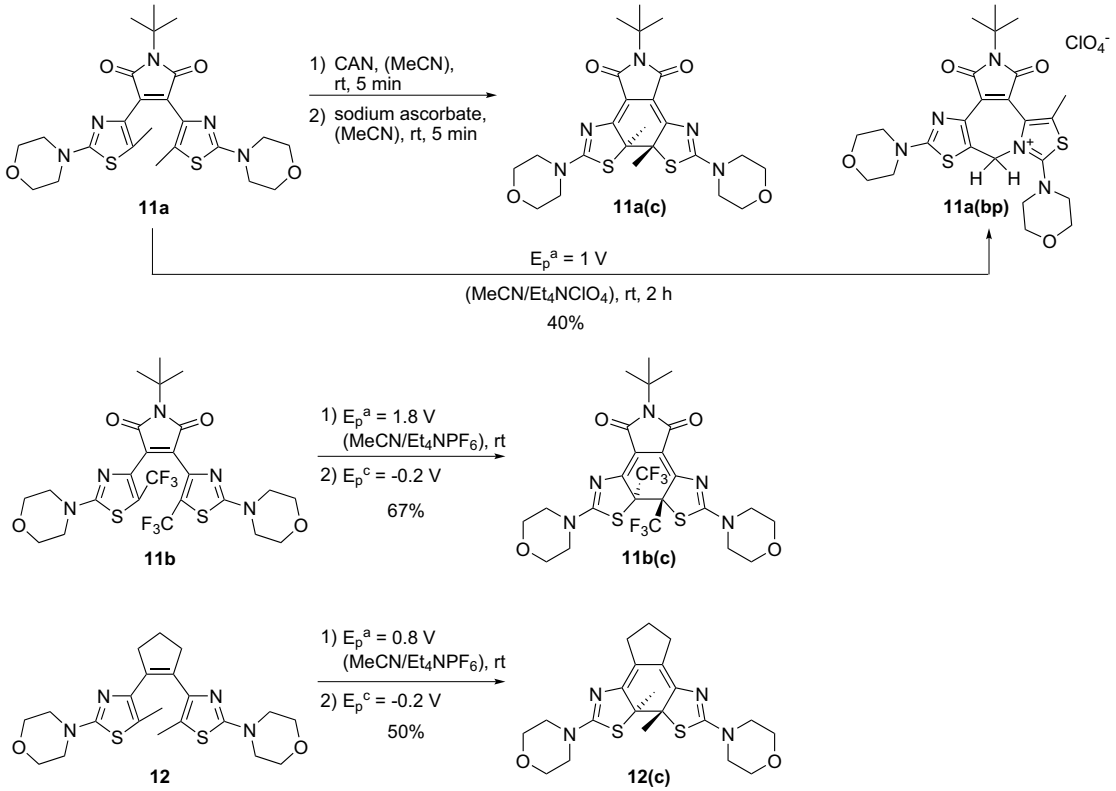

Scheme 33. Synthesis of ring-closed dimorpholinothiazolylethenes by oxidation and re-reduction.

As morpholinothiazole substituted DAEs cannot be cyclized photochemically (see section 4.4), chemical and electrochemical oxidation was used (Scheme 33). Compound **11a** was oxidized using ceric(IV) ammonium nitrate (CAN) and re-reduced with sodium ascorbate to yield a mixture of the ring-open and ring-closed isomers and a by-product **11a(bp)**. From this mixture an analytical sample of **11a(c)** was isolated using preparative HPLC. The by-product **11a(bp)** was obtained in 40% yield by electrochemical oxidation of the ring-open isomer and stirring in the dicationic state for 2 h without the re-reduction step. Compounds **11b(c)** and

12(c) were isolated after electrochemical oxidation to the dicationic state and subsequent re-reduction in 67% and 50% yield, respectively. For a detailed discussion on the observed by-product formation and its analytical characterization see section 4.4.

4.1.6 Summary and Outlook

By using post-functionalization in the periphery of the dithienyl(perfluoro)cyclopentene cores **16** and **18**, according to the route proposed by Feringa and coworkers, a series of DAEs was successfully synthesized bearing a broad range of donor and acceptor groups on the phenyl rings. In general, the reactions worked in satisfactory yields, however, in some cases purification problems arose due to formation of monocoupled by-products with very similar polarity. Unsymmetrical substitution of the DAE core could be achieved by stepwise reactions, but it was observed that the second halogen-metal exchange/cross coupling step may be hindered or prevented depending on the nature of the first phenyl substituent. To circumvent this problem, cross couplings with inverted polarity, using the 2-chlorothiophene moiety as aryl halide, were explored, which represent an attractive alternative for the post-functionalization of DAEs.

The second strategy to assemble the DAE scaffold consisted in cross couplings between pre-assembled heterocyclic boronic esters or stannanes and dihalogenated bridging moieties. While this strategy is very flexible in terms of alternating the bridge and is particularly interesting for the synthesis of perfluorocyclopentene bridged DAEs, for some bridging motifs the reaction conditions had to be precisely optimized. In particular, for cross couplings on the less reactive 1,2-dibromocyclopentene **24** and 8,9-dibromo-1,5,7-triazabicyclo[4.3.0]-nona-6,8-diene **27** bridges the notorious sensitivity of thiazolylboronic esters towards protodeboronation massively diminishes the yields. In the latter case precise control of the water content in the reaction mixture led to a significant improvement of the outcome of the reaction. Alternatively, in cases for which the boronic esters were difficult to obtain, Stille cross couplings using stable organostannanes were applied. These, however, often lead to problems during purification of the desired compounds due to formation of homocoupled by-products and organotin residues.

To improve the cross coupling a systematic screening of reaction conditions concerning solvent, catalyst, ligands, and the base has to be performed. In addition, inverting the polarity by using the bridging moiety as organoboronic ester or stannane, if synthetically accessible, may lead to higher yields. To face the problem of protodeboronation the controlled slow addition of the heterocyclic boronic ester to the reaction mixture or the use of more stable organotrifluoroborates (R-BF_3K) and MIDA boronates (R-B[$CH_3N(CH_2COO)_2$]), the latter slowly releasing the free boronic acid during the reaction, is promising.

The introduction of CF_3 substituents in the α-position of the thiophene and thiazole heterocycles was accomplished utilizing protocols by Urata and Fuchikami as well as Hartwig

and coworkers. Although the former was not always high yielding, it could be applied on large scales. With the latter high yields could be achieved, but reactions were successful only on very small scales. This problem may be avoided by not generating the [(phen)$CuCF_3$] complex *in situ* but isolating it in advance to the reaction using glovebox techniques. Already during the synthesis the remarkable modulation of electronic properties by the CF_3 group was observed: The CF_3 containing stannanes were highly deactivated in Stille cross coupling compared to the methyl substituted analogues. On the other hand, CF_3-thiazole derivatives were activated against nucleophilic attack and deprotonation of the 4-position using LDA.

4.2 Quantitative photochemical measurements[13]

4.2.1 Introduction

Often the performance of photochromic compounds is characterized by recording their electronic spectra before and after certain times of irradiation, analyzing the composition of the PSS that is reached, and determining the rate of the thermal back-reaction, if present. However, parameters such as the composition of the PSS and the irradiation time needed to reach it are only qualitative, as they are highly dependent on the experimental conditions such as concentration, molar absorptivities of all isomers, light intensity, and temperature. Therefore, to assess definite structure-property relationships an in-depth quantification of the underlying isomerization reactions, *i.e.* ring-closure, ring-opening, and by-product formation in case of DAEs, by determining their partial reaction quantum yields[141] is essential. While quantum yields for ring-closure and ring-opening of a large number of DAE derivatives are reported in the literature,[8b] a quantification of by-product formation has not been performed before.

The main difficulty in the quantification of DAE photochromism arises from the fact that generally the absorbance bands of the ring-open and ring-closed isomers fully overlap in the UV-range of the electromagnetic spectrum, *i.e.* there is no wavelength found where only the ring-open isomer absorbs. This prevents the quantification from pure spectrophotometric data as the molar absorptivity of the ring-closed isomer cannot be determined. To assess the needed extinction coefficients the preparative isolation of the ring-closed isomer (as well as the by-product) is necessary. However, this is laborious and in some cases very difficult due to their highly similar structure and susceptibility to oxidation. Alternatively, careful determination of the composition of samples taken during different stages of the isomerization reaction using a secondary method, *e.g.* UPLC or NMR, allows for the calculation of the molar absorptivities. Also approximations, in particular using "Fischer's method",[142] can be used for their estimation. Note that though theoretically the pure spectrum of the irreversibly formed by-product could be determined by simply irradiating the sample until everything has been converted, this is not practicable due to the long irradiation times needed and unspecific photobleaching.

As part of *this* work procedures for the quantitative characterization of DAEs and other photochromes have been established in the Hecht research group. This was done by assembling a spectroscopic setup allowing for the simultaneous irradiation of a sample and measurement of its absorbance spectra, establishing literature known actinometric procedures, and evaluating different procedures for the determination of molar absorptivities of the unknown isomers and quantum yields for the single isomerization reactions of DAEs. Thereby a special focus was laid

[13] Parts of this section have been published in M. Herder *et al*,. *J. Am. Chem. Soc.* **2015**, *137*, 2738-2747.

on the quantification of the by-product formation. Also the applicability of Singular Value Decomposition (SVD) for the evaluation of photokinetic data of DAEs was tested and a procedure was identified that gives the spectra of the unknown isomers as well as quantum yields without the need of secondary methods.

In the following DAE **3d** shall serve as model compound for the demonstration of the different evaluation procedures and the application of SVD to DAE photochromism. A discussion of the experimental uncertainties is included for procedures relating to the quantification of by-product formation.

4.2.2 Spectroscopy setup

Stepwise irradiation and measurement of electronic spectra was routinely performed using a 1000 W high pressure Xe arc lamp equipped with collimating lenses to ensure a parallel orientation of the emitted light. A timed electronic shutter allowed for the precise control of irradiation times. For wavelength selection combinations of different interference, bandpass, and cutoff filters were used. The complete front area of 3 mL quartz cuvettes (10x10 mm) containing the sample solution was illuminated. UV/Vis spectra were recorded on a Cary50 spectrophotometer equipped with a Peltier thermostated cell holder at 25 °C.

For quantitative photokinetic measurements using simultaneous irradiation and recording of UV/Vis spectra a setup was assembled consisting of a 500 W high pressure Hg(Xe) lamp (LOT Oriel) coupled to a monochromator (LOT Oriel MSH-300), which was equipped with an electronic shutter. The light output of the monochromator was transferred to the cell compartment of a Cary60 spectrophotometer using an optical fiber. The irradiation beam was assembled orthogonal to the measurement beam of the spectrophotometer illuminating ca. 1 cm² of the front area of a 3 mL quartz cuvette (10x10 mm), which was thermostated at 25 °C. During photokinetic measurements effective stirring of the sample was ensured. The minimal time resolution of the Cary60 spectrophotometer while scanning a wavelength range of 300 nm is 3 s. The intensity of the irradiation beam was kept low enough that no inhomogeneities due to illumination of only a part of the cuvette front area were detected and the spectral changes within the time resolution of the spectrometer could be neglected.

4.2.3 Photokinetic rate laws

In Table 4 physical quantities that are used for the following discussion are collected.

Table 4. Nomenclature of physical quantities used in this chapter.

quantity	unit	
$a(t), b(t), c(t)$	mol L^{-1}	concentrations of species A, B, and C
a_0	mol L^{-1}	overall concentration
$\Phi_{AB}, \Phi_{BA}, \Phi_{BC}$		quantum yields of ring-closure, ring-opening, and by-product formation
$\varepsilon'_A, \varepsilon'_B, \varepsilon'_C$	L mol^{-1} cm^{-1}	decadic extinction coefficents of A, B, and C at the irradiation wavelength
$\varepsilon_A^{obs}, \varepsilon_B^{obs}, \varepsilon_C^{obs}$	L mol^{-1} cm^{-1}	decadic extinction coefficents of A, B, and C at the observation wavelength
l', l^{obs}	cm	path lengths of the irradiation and observation beams
A', A^{obs}		overall absorbance at the irradiation and observation wavelengths
$F(t) = \frac{\left(1-10^{-A'(t)}\right)}{A'(t)}$		photokinetic factor
I_0	E s^{-1} cm^{-3}	light intensity[a]
$I_{abs,X}$	E s^{-1} cm^{-3}	light intensity absorbed by species X[a]

[a] here the unit Einstein (E) denotes "mole of photons".

The quantum yield of a photochemical reaction is defined as the ratio of the number of molecules of a species A undergoing the reaction and the number of photons absorbed by the sample:

$$\Phi = \frac{\#\ molecules\ reacted}{\#\ photons\ absorbed} = \frac{\Delta n_A}{n_P} \qquad (1)$$

To obtain values independent from the irradiation conditions every linear independent step *k* of the photoreaction has to be considered.[141] Furthermore, the change in the number of molecules can be referred to the volume of the sample, *i.e.* the change of concentration, and to an infinitesimally small time *dt* giving

$$\Phi_k = \frac{-da(t)/dt}{1000\ I_{abs,A}} \qquad (2)$$

with $I_{abs,A}$ being the light intensity absorbed by species A. A factor of 1000 cm^3 dm^{-3} was introduced to match the units typically used for concentration (mol dm^{-3}) and light intensity (E s^{-1} cm^{-3}). According to Lambert-Beer's law the amount of absorbed light by a sample of the path length l' is:

$$I_{abs} = I_0 - I_{l'} = I_0(1 - 10^{-A'}) \qquad (3)$$

If more than one species in the sample absorbs at the irradiation wavelength the contribution of species A to the total extinction has to be considered to determine the light intensity absorbed by A:

$$I_{abs,A} = I_0\left(1 - 10^{-A'}\right)\frac{A'_A}{A'} = I_0\left(1 - 10^{-A'}\right)\frac{\varepsilon'_A\, a\, l'}{A'} \qquad (4)$$

Combining equations *(2)* and *(4)* and using the photokinetic factor *F(t)*, which is time-dependent due to the changing extinction at the irradiation wavelength in case of non-isosbestic irradiation, gives the kinetic rate law for the photochemical reaction step *k* starting from species A:

$$\frac{da(t)}{dt} = -1000\, I_0\, F(t)\, \varepsilon'_A\, \Phi_k\, a(t)\, l' \qquad (5)$$

The photochromism of DAEs is described by an AB(2*Φ*) isomerization scheme consisting of two independent photochemical reaction steps between species A (ring-open isomer) and B (ring-closed isomer) while neglecting a possible thermal back-reaction (Scheme 34a). If the by-product formation is to be considered, the scheme is extended to an ABC(3*Φ*) system with an additional irreversible photochemical step from B to the by-product C (Scheme 34b).

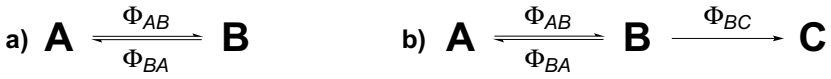

Scheme 34. General isomerization schemes for photochromic systems of the a) AB(2*Φ*) and b) ABC(3*Φ*) type.

According to these reaction schemes the following sets of rate equations are derived from equation *(5)*:

For AB(2Φ):

$$\frac{da(t)}{dt} = 1000\, I_0\, F(t)\, l' \left(-\varepsilon'_A\, \Phi_{AB}\, a(t) + \varepsilon'_B\, \Phi_{BA}\, b(t)\right) \qquad (6a)$$

$$\frac{db(t)}{dt} = 1000\, I_0\, F(t)\, l' \left(\varepsilon'_A\, \Phi_{AB}\, a(t) - \varepsilon'_B\, \Phi_{BA}\, b(t)\right) \qquad (6b)$$

For ABC(3Φ):

$$\frac{da(t)}{dt} = 1000\, I_0\, F(t)\, l' \left(-\varepsilon'_A\, \Phi_{AB}\, a(t) + \varepsilon'_B\, \Phi_{BA}\, b(t)\right) \qquad (7a)$$

$$\frac{db(t)}{dt} = 1000\, I_0\, F(t)\, l' \left(\varepsilon'_A\, \Phi_{AB}\, a(t) - \varepsilon'_B\, \Phi_{BA}\, b(t) - \varepsilon'_B\, \Phi_{BC}\, b(t)\right) \qquad (7b)$$

$$\frac{dc(t)}{dt} = 1000\, I_0\, F(t)\, l' \left(\varepsilon'_B\, \Phi_{BC}\, b(t)\right) \qquad (7c)$$

In general these rate equations cannot be integrated in a closed form due to the time-dependence of the photokinetic factor.[141,143] However, a solution for the AB(2Φ) system can be found if simplifying assumptions are made in terms of the "initial slope method". An exact solution for both systems can be calculated using numerical procedures (see section 4.2.6).

4.2.4 Actinometry

To determine the intensity of the irradiation beam I_0 three different chemical actinometers[144] were used that cover wavelengths between 254 nm and 600 nm (Figure 9). In the UV range initially azobenzene was chosen as easy-to-handle actinometer[144-145] covering the mercury lines 280 nm, 313 nm, and 334 nm. However, as azobenzene actinometry comes along with certain disadvantages,[14] later during this work the widely-used potassium ferrioxalate actinometry[146] was employed covering a broad wavelength range in the UV region. In the visible range of the spectrum the commercial furyl fulgide Aberchrome 670 (*(E)*-3-(adamantan-2-ylidene)-4-[1-(2,5-dimethyl-3-furyl)ethylidene]dihydro-2,5-furandione)[147] was used as a reference. It was chosen as it covers similar wavelengths as the ring-closed isomers of DAEs and it is much easier to handle than many other actinometers for the visible range.[144a] However, there are only few detailed reports on its photochemical properties.[147-148]

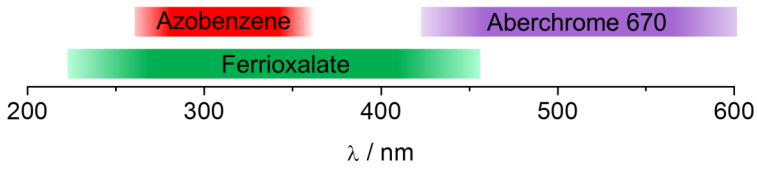

Figure 9. Wavelength ranges for utilized chemical actinometers.

Note that a comparison of I_0-values obtained with azobenzene and ferrioxalate at irradiation wavelengths of 313 nm and 334 nm revealed a maximum discrepancy of 5% showing that values obtained with both methods are fairly comparable. On the other hand, the I_0-value at λ_{irr} = 436 nm obtained using Aberchrome 670 was 16% lower than the value obtained using ferrioxalate under identical irradiation conditions. This demonstrates the uncertainty when comparing quantitative photochemical measurements using different actinometers. Though Aberchrome 670 seems rather unreliable in terms of absolute values due to the lack of literature data, the actinometric procedure was not changed to ensure comparability of ring-opening quantum yields within *this* work. Note that very recently the group of Irie reported detailed

[14] Using azobenzene in total absorbance[144a,145a] turned out to be unreliable due to the necessity of recording very small absorbance changes in the steep low-energy onset of the π-π*-band. In diluted solutions only wavelengths near the maximum of the π-π*-band may be used, in particular actinometry at 365 nm is not practicable.

quantitative photochemical data on the ring-opening of two commercial DAE derivatives, which may be advantageously used for future actinometric measurements.[11a]

Azobenzene actinometry[144-145]

Light intensities at 280 nm, 313 nm, and 334 nm were determined using a $4 \cdot 10^{-5}$ M solution of azobenzene in methanol. Therefore the solution was irradiated in at least 6 steps until the absorbance at 313 nm $A^{313\,nm}$ depleted by 10%. From the recorded values $A^{313\,nm}$ the concentration of the *trans*-Isomer *a* was obtained by:

$$a = \frac{A^{313\,nm} - \varepsilon_{cis}^{313\,nm}\, a_0\, l'}{\varepsilon_{trans}^{313\,nm} - \varepsilon_{cis}^{313\,nm}} \qquad (8)$$

with l' = 1 cm, $\varepsilon_{trans}^{313\,nm}$ = 22020 M^{-1} cm^{-1} and $\varepsilon_{cis}^{313\,nm}$ = 2715 M^{-1} cm^{-1}. The obtained concentration was plotted against the time and linear regression was performed to determine the slope *da/dt*. According to the "initial slope method" the light intensity I_0 was calculated by:

$$I_0 = -\frac{da}{dt} \cdot \frac{1}{1000\, \phi^{\lambda}\, (1 - 10^{-A'})} \qquad (9)$$

Thereby quantum yields ϕ^{λ} = 0.12 (280 nm), 0.13 (313 nm), and 0.15 (334 nm) were used.

Ferrioxalate actinometry

The "micro-version"[144b] of potassium ferrioxalate actinometry[146] was used under conditions of total absorbance. It consists of irradiation of 3 mL of a fresh potassium ferrioxalate solution (0.006 M in 0.05 M H_2SO_4) in a cuvette for 2 - 4 min, subsequent addition of 0.5 mL of 1,10-phenanthroline buffer (0.1 wt% in 0.5 M H_2SO_4/1.6 M NaOAc), and absorbance readout at 510 nm. I_0 is obtained from:

$$I_0 = \frac{\Delta A^{510\,nm}}{\Delta t\; 1000\, \phi^{\lambda}\, \varepsilon^{510\,nm}} \cdot \frac{3.5\,mL}{3\,mL} \qquad (10)$$

with $\Delta A^{510\,nm}$ being the difference in absorbance between the sample and a non-irradiated reference, $\varepsilon^{510\,nm}$ = 11100 M^{-1} cm^{-1}, and ϕ^{λ} = 1.24 (280 – 313 nm), 1.23 (334 nm), 1.21 (365 nm), or 1.11 (436 nm). In case λ_{irr} = 436 nm an additional factor $1/(1-10^{-A'})$ was introduced into eq. (10) due to the lack of total absorbance.

For the described Hg(Xe) lamp setup light intensities of $I_0 = 4.0 \cdot 10^{-10}$ – $1.1 \cdot 10^{-9}$ E s^{-1} cm^{-3} have been obtained. The maximum relative error of the actinometry is 2% assuming uncertainties of 0.3% for $\Delta A^{510\,nm}$ (ΔA = 0.8 – 1.0, $\Delta\Delta A$ = 0.002), 1% for Δt

(Δt = 120 – 240 s, $\Delta\Delta t$ = 1 s), and 0.3% for the sample volume (V = 3.5 mL, ΔV = 0.0060 mL / V = 3.0 mL, ΔV = 0.0045 mL). The actual error may be lower as in a series of eight independent actinometric measurements at λ_{irr} = 313 nm under identical irradiation conditions I_0 was obtained with a standard deviation of 0.8%.

Aberchrome 670 actinometry

Light intensities at 436 nm and 546 nm were determined using the commercial furyl fulgide Aberchrome 670[147] as reference. Therefore 3 mL of a toluene solution of Aberchrome 670 ($1.0 \cdot 10^{-4}$ M) were irradiated for 4 min at 365 nm (1000 W Xe, interference filter) before irradiation with visible light was performed in 6 steps each consisting of 5% conversion (15 s irradiation time). I_0 is obtained from the depletion of absorbance at 519 nm:

$$I_0 = -\frac{\Delta A^{519\,nm}}{\Delta t} \cdot \frac{1}{1000\,\phi^{\lambda}\,\varepsilon^{519\,nm}\,(1-10^{-A'})} \qquad (11)$$

with A' the initial absorbance at the irradiation wavelength, ϕ^{λ} = 0.32 (436 nm) or 0.29 (546 nm), and $\varepsilon^{519\,nm}$ = 7760 M^{-1} cm^{-1}. The typical standard deviation of the six measurements is 2%.

4.2.5 Determination of molar absorptivities using UPLC

The molar absorptivity of the ring-open isomer ε_A^{λ} is obtained by careful preparation of a standard solution and calculation according to equations *(12)* and *(13)*.

$$a_0 = \frac{m}{M\,V} \qquad (12) \qquad\qquad \varepsilon_A^{\lambda} = \frac{A^{\lambda}}{a_0\,l'} \qquad (13)$$

The concentration of the spectroscopic solution a_0 can be determined with a relative error of 2% assuming uncertainties for the sample weight of 1% ($m \approx$ 1-2 mg, Δm = 0.01 mg) and the solvent volume of 1%, (V = 100 mL, ΔV = 1 mL). Thus the error of the molar absorptivity of the ring-open isomer ε_A^{λ} does not exceed 3% assuming a maximum uncertainty of the absorbance measurement of 1% ($A \approx$ 0.1-1.0, ΔA = 0.001).

Extinction coefficients of the unknown isomers were calculated by determining conversions of the ring-open isomer to ring-closed isomer and by-product after varying times of UV-irradiation by means of ultra-high performance liquid chromatography (UPLC). For this purpose at least 4 samples were taken from an irradiated quartz cuvette during the conversion to the (pseudo-)PSS between the ring-open and ring-closed isomer. Another 4 samples were taken

during the successive conversion to the by-product upon prolonged UV-irradiation.[15] The solutions in spectroscopic concentrations (typically $3 \cdot 10^{-5}$ M) were directly injected into the UPLC and separated on reversed phase columns (Acquity UPLC BEH C18/ BEH Phenyl) using solvent gradients of 20 – 5% 0.1 M NH_4HCO_3 (pH = 9) / 80 – 95% acetonitrile. It was ensured that under these conditions absorbance of the involved species recorded by the diode array detector in the water/acetonitrile gradient is identical compared to spectra obtained from UV/Vis spectroscopy in pure acetonitrile. Integration of the obtained diode array signal was performed using isosbestic wavelengths observed during conversion from ring-open isomer to the PSS and from the PSS to the by-product, respectively (see Figure 10a-b and Figure 11a-b for exemplary spectra and chromatograms of DAE **3d**).

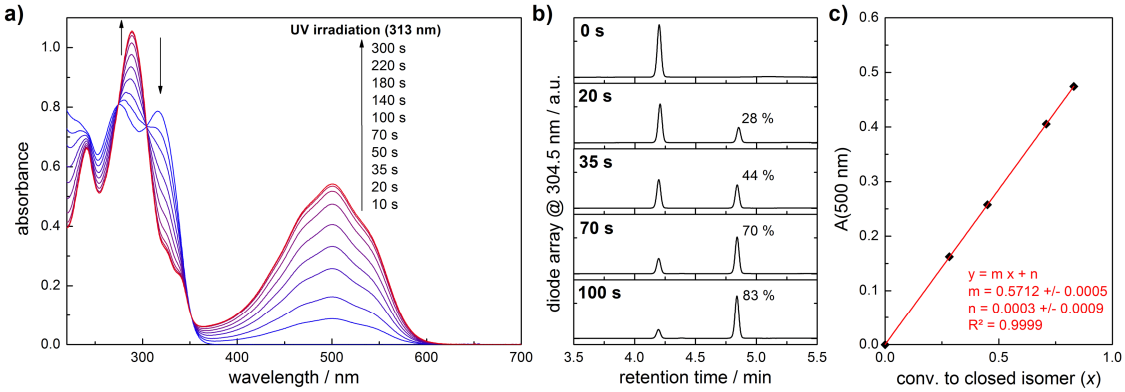

Figure 10. a) UV/Vis spectra of **3d** (acetonitrile, $3.70 \cdot 10^{-5}$ M) during irradiation with 313 nm light (1000 W Xe) *until reaching the PSS*. b) UPLC traces of samples taken after different irradiation times. c) Determination of the absorbance of the pure ring-closed isomer by liner regression according to eq. *(14)*.

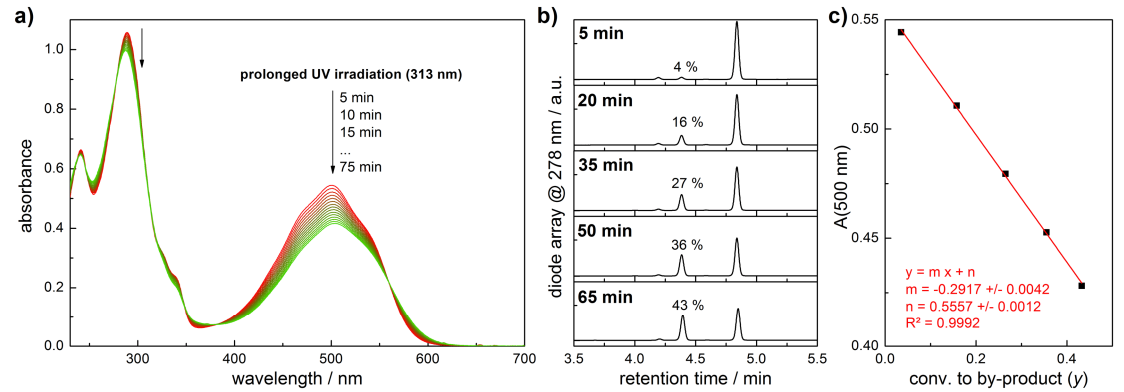

Figure 11. a) UV/Vis spectra of **3d** (acetonitrile, $3.70 \cdot 10^{-5}$ M) during prolonged irradiation with 313 nm light (1000 W Xe) *after reaching the PSS*. b) UPLC traces of samples taken after different irradiation times. c) Determination of the absorbance of the pure by-product by linear regression according to eq. *(15)*.

[15] For a detailed discussion of the spectroscopic behavior of DAEs under prolonged UV-irradiation see section 4.3.

Note that although three isomers with differing UV/Vis spectra are present in the reaction mixture the occurrence of isosbestic points during the progressive formation of the by-product follows from the fact that once the photostationary equilibrium between the ring-open and ring-closed isomers is reached, the concentration ratio of these two isomers remains constant. Thus, during prolonged UV irradiation the absorbance spectrum of the mixture uniformly changes from the spectrum of the "pure" PSS to that of the by-product.

For any wavelength λ_{obs} the total absorbance A^{obs} during conversion from the pure ring-open isomer to the PSS is given by:

$$A^{obs} = x \cdot A_B^{obs} + (1 - x) \cdot A_A^{obs} = \left(A_B^{obs} - A_A^{obs}\right) \cdot x + A_A^{obs} \qquad (14)$$

with A_A^{obs} and A_B^{obs} as the absorbance of the pure ring-open and ring-closed isomer, respectively, and x the mole fraction of the closed isomer. Analogous for prolonged UV-irradiation after reaching the PSS A^{obs} is given by:

$$A^{obs} = y \cdot A_C^{obs} + (1 - y) \cdot A_{PSS}^{obs} = \left(A_C^{obs} - A_{PSS}^{obs}\right) \cdot y + A_{PSS}^{obs} \qquad (15)$$

with A_{PSS}^{obs} as the absorbance of the pure photostationary mixture of the ring-open and ring-closed isomer, A_C^{obs} as the absorbance of the pure by-product, and y as the mole fraction of the by-product. By plotting A^{obs} against x and y, which were obtained from UPLC at different stages of the irradiation, the spectra of the individual components can be obtained from the intercept and slope according to eq. *(14)* and *(15)* (see Figure 10c and Figure 11c for the exemplary procedure on DAE **3d**).

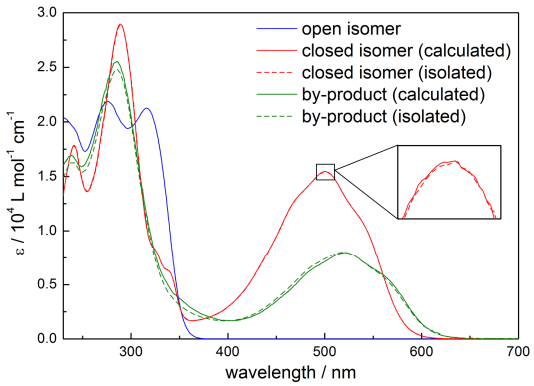

Figure 12. Comparison of UV/Vis spectra of all three isomers of **3d** in acetonitrile obtained by calculation from UPLC data (solid lines) and by isolation of the ring-closed isomer and by-product (dashed lines).

Note that eq. *(15)* holds as long as the amount of by-product formed during the initial period of UV irradiation before reaching the PSS can be neglected. For all DAEs reported in this work y was < 1% during this period. The comparison of theoretical spectra of the pure isomers with spectra obtained from the respective isolated isomers of compound **3d** shows excellent agreement (Figure 12).

The standard deviations of intercept and slope originating from linear regression of the experimental data using eq. *(14)* and *(15)* are relatively small so that the errors of the values for A_B^{obs} and A_C^{obs} do not exceed 3% (see Table 5 for an exemplary calculation on DAE **3d**). With this, molar absorptivities of the ring-closed isomer and by-product can be calculated with a maximum relative error of 5%. Note that for simplicity an error of 5% for ε_B^{obs} and ε_C^{obs} was assumed for all compounds discussed in section 4.3 although in some cases the actual error was smaller.

It has to be noted that though the outlined procedure is able to determine the molar absorptivities of the unknown isomers very accurately for most DAEs, it has to be applied with care. In particular, it has to be ensured that the compounds do not exhibit solvatochromism, which would make the integration of the diode array detector trace highly unreliable. Furthermore, the thermal stability of the isomers of the photochromic compound has to be sufficiently high and no isomerization reaction should be induced during UPLC analysis by any part of the solvent or the stationary phase.[16]

Table 5. Exemplary determination of $\boldsymbol{\varepsilon_B^{obs}}$ and $\boldsymbol{\varepsilon_C^{obs}}$ via linear regression (y = mx + n) according to eq. *(14)* and *(15)* for compound **3d**.

ring-closed isomer				by-product			
$\mathbf{m^{500\ nm}}$	$\mathbf{n^{500\ nm}}$	$\boldsymbol{A_B^{500\ nm}}$ [a]	$\boldsymbol{\varepsilon_B^{500\ nm}}$ [$\mathbf{M^{-1}\ cm^{-1}}$][b]	$\mathbf{m^{500\ nm}}$	$\mathbf{n^{500\ nm}}$	$\boldsymbol{A_C^{500\ nm}}$ [a]	$\boldsymbol{\varepsilon_C^{500\ nm}}$ [$\mathbf{M^{-1}\ cm^{-1}}$][b]
0.5712 ±0.0005	0.0003 ±0.0009	0.572 ±0.001	15500 ±800	-0.2917 ±0.0042	0.5557 ±0.0012	0.265 ±0.005	7200 ± 400

[a] $A^{500\ nm} = m^{500\ nm} + n^{500\ nm}$

[b] with $a_0 = 3.70 \cdot 10^{-5}$ M, assumed maximum error of 5%

[16] Problems due to solvatochromism were encountered when analyzing azobenzene with the outlined procedure. Analysis of a terarylene-type DAE structure, which is not reported in this work, revealed considerable thermal instability of the ring-closed isomer in the presence of the stationary phase.

4.2.6 Determination of quantum yields

Initial slope method

Quantum yields for ring-closure under UV irradiation as well as ring-opening under visible light irradiation were determined using the "initial slope method". Thereby only the first 10% of the conversion are considered allowing for two simplifying assumptions:[17] 1) The overall absorbance at the irradiation wavelength is considered to be constant ($A'(t) \approx A'(0)$) and 2) the UV-light induced back reaction can be neglected as only a very small amount of isomer B is formed during this period ($\varepsilon'_{\mathrm{B}}\ \Phi_{\mathrm{BA}}\ \mathrm{b(t)} \approx 0$). With these assumptions and under the premise that in the beginning only species A is present ($A'(0) = \varepsilon'_{\mathrm{A}}\ a(t)\ l'$), eq. *(6a)* can be converted into a linear expression:

$$\frac{da(t)}{dt} = -1000\ I_0\left(1 - 10^{-A'(0)}\right)\Phi_{AB} \qquad (16)$$

Substitution of $a(t)$ by the absorbance recorded in the visible range, where only the ring-closed isomer absorbs, gives:

$$\frac{dA^{obs}(t)}{dt} = 1000\ I_0\left(1 - 10^{-A'(0)}\right)\varepsilon_B^{obs}\ \Phi_{AB} \qquad (17)$$

Plotting $A^{obs}(\mathrm{t})$ against the time and determining the slope $dA^{obs}(\mathrm{t})/dt$ for the first 10% of conversion by linear regression easily allows for the calculation of Φ_{AB} using eq. *(17)*.

By testing the outlined procedure against simulated photokinetic data, which represent a typical DAE, the validity of the intial slope method is shown (Figure 13). However, a small systematic error is introduced by the linearization in the 10% region resulting in the calculated value (0.48) being somewhat smaller than the "true" quantum yield used for the simulation (0.50). Accounting for this systematic error and the experimental uncertainties in determining I_0 and $\varepsilon_{\mathrm{B}}^{\mathrm{obs}}$ quantum yields determined by the initial slope method are estimated to possess an uncertainty of 10%.

Numerical integration of rate equations and non-linear regression

Using the photochemical rate constants $k_1 = \varepsilon'_A\ \phi_{AB}\ l'$, $k_2 = \varepsilon'_B\ \phi_{BA}\ l'$, and $k_3 = \varepsilon'_B\ \phi_{BC}\ l'$ rate equations *(6a-b)* and *(7a-c)* can be expressed as:

[17] The approximation holds as long as the absorbance of the photoproduct B at the irradiation wavelength is not much larger than that of A and the quantum yield of the back-reaction is not much larger than that of the forward reaction. Both is fulfilled for typical DAEs.

$$\frac{da(t)}{dt} = 1000\, I_0\, F(t)\left(-k_1\, a(t) + k_2\, b(t)\right) \qquad (18a)$$

$$\frac{db(t)}{dt} = 1000\, I_0\, F(t)\left(k_1\, a(t) - k_2\, b(t)\right) \qquad (18b)$$

$$\frac{da(t)}{dt} = 1000\, I_0\, F(t)\left(-k_1\, a(t) + k_2\, b(t)\right) \qquad (19a)$$

$$\frac{db(t)}{dt} = 1000\, I_0\, F(t)\left(k_1\, a(t) - k_2\, b(t) - k_3\, b(t)\right) \qquad (19b)$$

$$\frac{dc(t)}{dt} = 1000\, I_0\, F(t)\left(k_3\, b(t)\right) \qquad (19c)$$

To numerically integrate these rate equations first the photokinetic factor $F(t)$ is calculated at each point of the measurement from the recorded absorbance at the irradiation wavelength A'.[18] Values in between the data points are obtained by linear interpolation of A'. Then, reasonable values for $k_1 - k_3$ are guessed and for given initial values for the concentration of the species[19] the differential rate equations are solved iteratively using the Runge-Kutta algorithm. With the thus obtained concentration-time profiles $a(t) - c(t)$ the absorbance at the observation wavelength (typically in the visible range where only the ring-closed isomer and by-product absorb) is calculated using Lambert-Beer's law:

$$A^{obs}(t) = \varepsilon_A^{obs}\, a(t)\, l^{obs} + \varepsilon_B^{obs}\, b(t)\, l^{obs} + \varepsilon_C^{obs}\, c(t)\, l^{obs} \qquad (20)$$

Finally the parameters k_1 - k_3 are optimized with a least squares method to fit the calculated $A^{obs}(t)$ with the experimental data. By dividing k_1, k_2, and k_3 with the molar absorptivity at the irradiation wavelength of the ring-open and ring-closed isomers, respectively, quantum yields are obtained. The numerical integration and regression procedure was conducted using the software package Mathematica 8.0 (Wolfram Research Inc.).

The obtained fit is very robust, *i.e.* only one global minimum is found independent of the guessed starting values for $k_1 - k_3$. The test against simulated data shows exact matching of the calculated quantum yields with the "true" values (Figure 13). Also it is shown that a simulated absorbance-time profile with Φ_{AB} deviating by only 3% can already be differentiated by the naked eye.

Application of the procedure on experimental data of DAE **3d**, including by-product formation, is shown in Figure 14. Also one global minimum is found, the experimental data and the fitted function do not show any systematic deviation over time, and standard errors for the obtained parameters k_1 - k_3 are below 0.5% (Table 6).

[18] If the path length of the recording beam and the irradiation beam are different, this has to be corrected here. In the utilized spectroscopic setup both l' and l^{obs} are 1 cm.

[19] Typically $a(0) = a_0$ and $b(0) = c(0) = 0$.

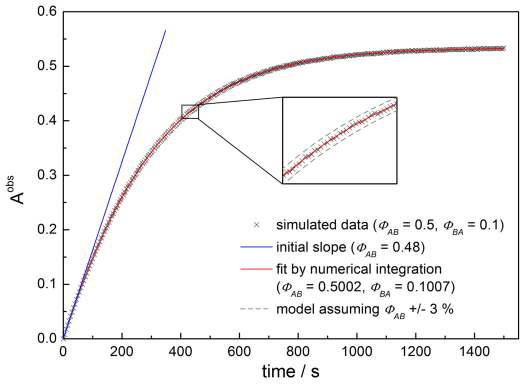

Figure 13. Testing of the initial slope method and non-linear regression by numerical integration of the exact rate equations against simulated photokinetic data. Simulation was performed using equations *(18a-b)* and *(20)* with $a_0 = 3 \cdot 10^{-5}$ M, $\varepsilon'_A = 26300$ M^{-1} cm^{-1}, $\varepsilon'_B = 16100$ M^{-1} cm^{-1}, $\varepsilon_B^{obs} = 20000$ M^{-1} cm^{-1}, $I_0 = 2 \cdot 10^{-10}$ E cm^{-3} s^{-1}, $\Phi_{AB} = 0.5$, and $\Phi_{BA} = 0.1$. Random noise ($\Delta A^{obs} = 0.001$) was added to the obtained photokinetic trace.

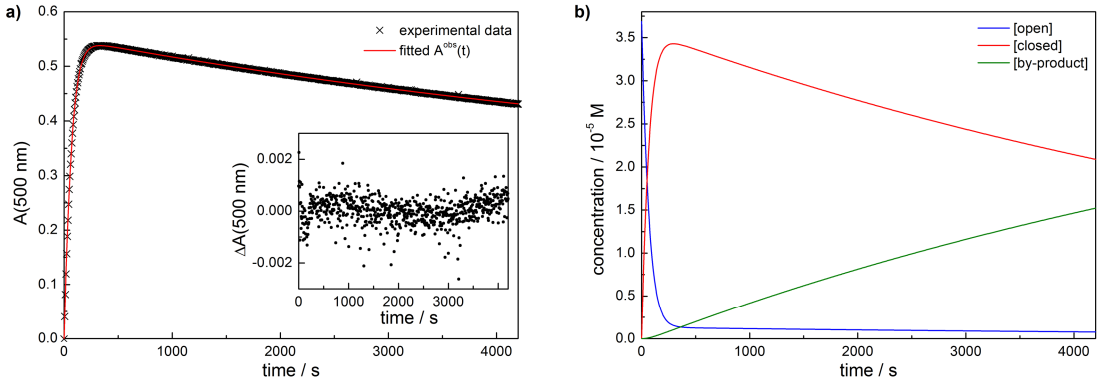

Figure 14. a) Absorbance-time profile during irradiation of **3d** (acetonitrile, $3.70 \cdot 10^{-5}$ M) with 313 nm light ($I_0 = 1.08 \cdot 10^{-9}$ E s^{-1} cm^{-2}, ferrioxalate actinometry) and fitted kinetics according to eq. *(19a-c)*. Inset: Residuals of the fit. b) Calculated concentration profiles *a(t)*, *b(t)*, and *c(t)* corresponding to the fitted kinetics.

Table 6. Error of fitted parameters and derived quantum yields of compound **3d**.

	value[a]	$\left\|\frac{\partial k}{\partial \varepsilon_B^{obs}}\right\| \cdot \Delta\varepsilon_B^{obs}$	$\left\|\frac{\partial k}{\partial \varepsilon_C^{obs}}\right\| \cdot \Delta\varepsilon_C^{obs}$	$\frac{\Delta k}{k}$	$\frac{\Delta \phi}{\phi}$	ϕ
k_1	11125 ± 6	572	30.2	5%	10%	$\phi_{AB} = 0.53 \pm 0.05$
k_2	408 ± 1	551	5.1	136%	143%	$\phi_{BA} = 0.03 \pm 0.05$
k_3	87.9 ± 0.1	4.6	5.0	11%	18%	$\phi_{BC} = 0.007 \pm 0.001$

[a] with standard deviation obtained from non-linear regression analysis

The major source of error in the determination of $k_1 - k_3$ is their dependency on the molar absorptivities ε_B^{obs} and ε_C^{obs} that is not reflected by the negligible standard deviation obtained from the fitting procedure. To estimate this dependency the regression was repeated assuming extreme values for ε_B^{obs} and ε_C^{obs} within their error margins. Thus the errors of the parameters $k_1 - k_3$ were calculated according to:

$$\Delta k = \left|\frac{\partial k}{\partial \varepsilon_B^{obs}}\right| \cdot \Delta\varepsilon_B^{obs} + \left|\frac{\partial k}{\partial \varepsilon_C^{obs}}\right| \cdot \Delta\varepsilon_C^{obs} \quad (21)$$

$$\frac{\partial k}{\partial \varepsilon_X^{obs}} = \frac{k\left(\varepsilon_X^{obs}+\Delta\varepsilon_X^{obs}\right) - k\left(\varepsilon_X^{obs}-\Delta\varepsilon_X^{obs}\right)}{2\,\Delta\varepsilon_X^{obs}} \quad (22)$$

using $\Delta\varepsilon_X^{obs}$ = 5% as the maximum relative error of the calculated molar absorptivities (*vide supra*). In Table 6 an exemplary calculation for compound **3d** is given. As one can expect the accuracy of ε_B^{obs} has a much larger influence on k_1 and k_2 (ring-closure and ring-opening process) compared to the accuracy of ε_C^{obs} whereas the value of k_3 depends on the accuracy of both extinction coefficients. Obviously the chosen method is not able to yield a highly reliable rate for the ring-opening process as the error of k_2 is very large. This can be rationalized by the fact that in contrast to k_1, which is highly descriptive for the initial slope of the absorbance-time profile, k_2 is determined by the plateau that is reached in the (pseudo)PSS. As the (pseudo)PSS contains a very high amount of ring-closed isomer the difference between this plateau and the absorbance of the pure ring-closed isomer is small, thus an error in determining the absorbance of the pure ring-closed isomer has a large effect.

Final quantum yields, which are derived from $k_1 - k_2$, are additionally influenced by errors of the molar absorptivities at the irradiation wavelength (3% for ε'_A, 5% for ε'_B) and by the error in determining I_0 (2%). This is accounted for by adding the relative uncertainties (Table 6).

4.2.7 Application of Singular Value Decomposition to photokinetic data of the AB(2Φ) type

Basic principle[20]

A series of photokinetic spectra can be written as a matrix **M** with the wavelength and the time as the two dimensions. The matrix **M** can be represented by a product of matrices $\mathbf{U}_{full}$ and $\mathbf{V}^{T}_{full}$, possessing orthonormal columns and rows, respectively, and a rectangular diagonal matrix $\mathbf{S}_{full}$ by means of Singular Value Decomposition (SVD) (eq. *(23),* Figure 15).[149] Thereby, columns in $\mathbf{U}_{full}$ can be regarded as "basic spectra" that are linearly combined using time-dependent factors in $\mathbf{V}^{T}_{full}$, *i.e.* the "basic kinetics", to yield the series of spectra **M**. The singular values in $\mathbf{S}_{full}$ give the "weights" by which the components of $\mathbf{U}_{full}$ and $\mathbf{V}^{T}_{full}$ are considered. Application of SVD to photokinetic spectra of the AB(2*Φ*)-type gives only two large singular values, due to the fact that only two independent components are needed to fully

[20] The basic idea and style of representation are adapted from a tutorial by Prof. N. P. Ernsting: *Decomposition of spectra of a thermodynamic equilibrium system*, Humboldt-Universität zu Berlin, 2009-03-25.

represent the data. The other singular values are significantly smaller, representing random noise of the measurement, and can be dropped. Thus, truncated matrices **U** and $\mathbf{V}^T$ are obtained each possessing two columns/rows containing two basic spectra and corresponding basic kinetics, respectively (eq. *(24)*). Note that at this point **U** and $\mathbf{V}^T$ have no physical meaning.

$$\boldsymbol{M} = \boldsymbol{U_{full}} \cdot \boldsymbol{S_{full}} \cdot \boldsymbol{V_{full}^T} \qquad (23)$$

$$\approx \boldsymbol{U} \cdot \boldsymbol{S} \cdot \boldsymbol{V^T} = \boldsymbol{U} \cdot \boldsymbol{S} \cdot \boldsymbol{F} \cdot \boldsymbol{K^T} = \boldsymbol{SAS} \cdot \boldsymbol{K^T} \qquad (24)$$

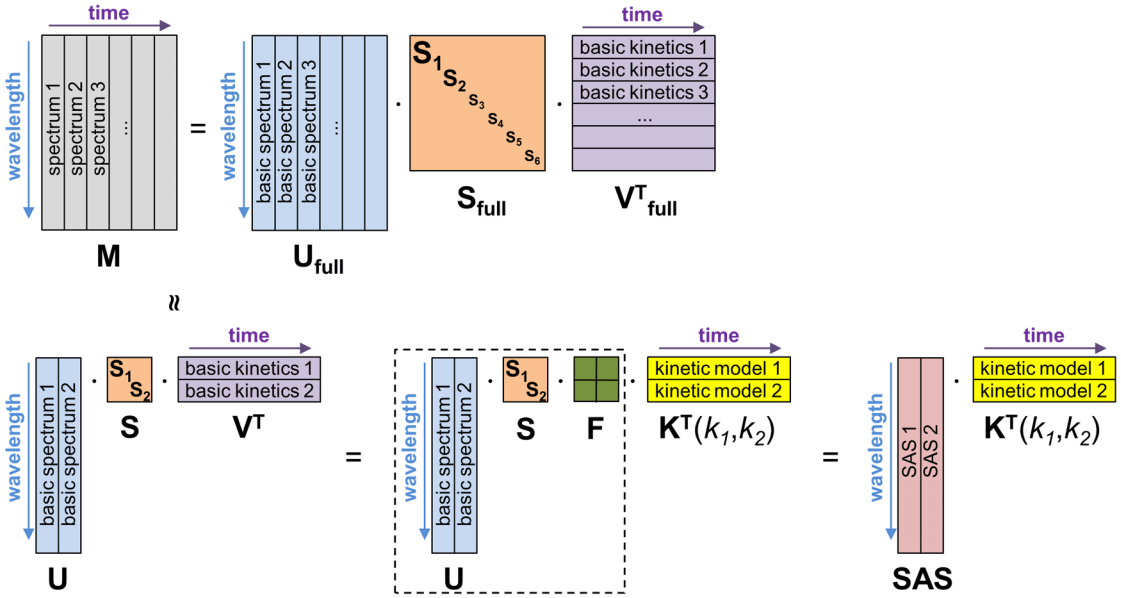

Figure 15. Principle of Singular Value Decomposition of photokinetic spectra and transformation to a product of species associated spectra (**SAS**) and time-dependent concentration profiles $\mathbf{K}^T$.

The photophysical kinetics of the AB(2*Φ*) system can be calculated by numerical integation of equations *(18a-b)*, as described in the preceding section, assuming some reasonable values for the rate constants k_1 and k_2. This kinetic model, represented in a matrix $\mathbf{K}^T$, can be transformed by a factor matrix **F** to the basic kinetics $\mathbf{V}^T$ obtained from the SVD procedure (eq. *(25)*). **F** is calculated via the pseudoinverse $(\mathbf{K}^T)^+$ (eq. *(26)*), *i.e.* the obtained matrix $\mathbf{F}_{opt}$ contains the parameters that give the "best" projection of $\mathbf{K}^T$ on $\mathbf{V}^T$ by means of a least squares procedure. Note thar for arbitrary values of k_1 and k_2 the product $\mathbf{F}_{opt} \cdot \mathbf{K}^T$ is not identical with $\mathbf{V}^T$. Thus, by varying the values for k_1 and k_2, calculation of $\mathbf{K}^T$, $\mathbf{F}_{opt}$, and $\mathbf{V}^T_{opt}$ and finally minimizing the sum of the quadratic errors $E = (\mathbf{V}^T_{opt}-\mathbf{V}^T)^2$ of each element of the matrices (eq. *(28)*) values for k_1 and k_2 are found that fit the kinetics $\mathbf{V}^T$ obtained from SVD and thus describe the full photokinetic data in **M**. If the found kinetics $\mathbf{K}^T(k_1, k_2)$ with optimized values for k_1 and k_2 represent the "true" photokinetics of the system, then the "true" spectra of both species ("species associated spectra", **SAS**) are represented by the product of **U**, **S**, and $\mathbf{F}_{opt}$ (right side of eq. *(24)*, Figure 15).

$$\boldsymbol{V^T = F \cdot K^T} \qquad (25)$$

$$\boldsymbol{F_{opt} = V^T \cdot \left(K^T\right)^+ = V^T \cdot K \cdot \left(K^T \cdot K\right)^{-1}} \qquad (26)$$

$$\boldsymbol{V^T_{opt}}(k_1, k_2) = \boldsymbol{F_{opt} \cdot K^T}(k_1, k_2) \qquad (27)$$

$$E_{total}(k_1, k_2) = \sum_{i,j}\left[\left(\boldsymbol{V^T_{opt}}(k_1, k_2) - \boldsymbol{V^T}\right)^2_{i,j}\right] \qquad (28)$$

It is important to note here that in principle this SVD based and other related procedures are able to decompose a series of spectra recorded during a physicochemical process into the (unknown) pure spectra of the species involved by fitting with a physical model. For example it is successfully applied for complicated protolytic equilibria or analysis of time-resolved absorption spectra.[149-150] However, in case of an reversible photoreaction of the AB(2Φ)-type the pure photokinetic data do not contain enough information to fully determine parameters k_1 and k_2 and thus to obtain the unknown spectrum of the isomer B.[143a] Instead, only the "pseudo rate" $R = k_1 + k_2$ is characteristic for a given series of photokinetic spectra.[141]

Consequently, application of the outlined procedure to a series of spectra of DAE **3d** recorded upon irradiation with 313 nm light (Figure 16a) gives no defined minimum for parameters k_1 and k_2 during the optimization step. A global analysis by systematic variation of the parameters reveals that all pairs of k_1/k_2 fulfilling the relation $k_1 = R - k_2$ fit the experimental data (Figure 16b). Using these pairs of k_1/k_2 the corresponding species associated spectra **SAS** can be calculated. Thus, under the premise that none of the parameters can be negative and the obtained spectra have to be positive or equal zero at any wavelength, for the unknown isomer B only a range of spectra can be defined which contains the true one (Figure 16c).

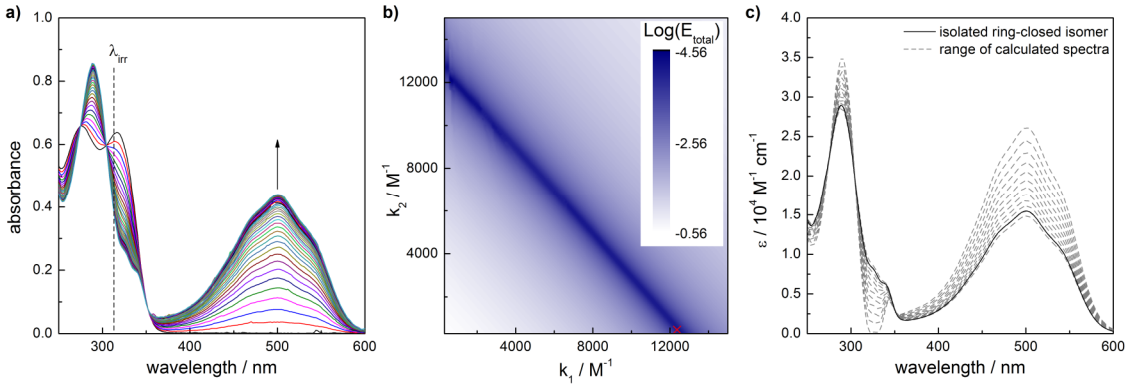

Figure 16. SVD based evaluation of *one set* of photokinetic data of **3d** (λ_{irr} = 313 nm). a) UV/Vis absorbance spectra of a solution of **3d** in acetonitrile ($c = 3.0 \cdot 10^{-5}$ M) recorded under irradiation with 313 nm light ($I_0 = 5.2 \cdot 10\text{-}^{10}$ E s^{-1} cm^{-3}, ferrioxalate actinometry) at 25 °C. Spectra were recorded every 12 s. b) Global analysis of the total quadratic error Log(E_{total}) according to equation *(28)* by systematic variation of k_1 and k_2 in steps of 100 M^{-1}. The red cross marks the "true" values for k_1/k_2 as obtained from fitting with two photokinetic datasets (*vide infra*). c) Range of plausible spectra for the ring-closed isomer as calculated from the **SAS** matrix.

SVD based analysis of photokinetic data recorded with two different irradiation wavelengths

To determine the spectra of the unknown isomers and the quantum yields from pure photokinetic data irradiation with a second wavelength is needed.[143a] Thereby, the assumption is made that quantum yields are wavelength independent.

This assumption is originally used in "Fischer's method" that calculates the spectrum of the unknown isomer from the difference of absorbance in the PSSs that are reached under irradiation with two different wavelengths.[142] Thereby, the ratio of the molar absorptivities of the two isomers has to be different at the two irradiation wavelengths. However, relying solely on the absorbance in the PSS can be erroneous, in particular when the observed difference in absorbance is small or no stable PSS is reached due to by-product formation. Both is typically the case for DAEs. Furthermore, if a thermal back reaction has to be considered Fisher's method can only be applied using high light intensities or low temperatures.[151]

Micheau and coworkers have shown that full evaluation of photochromic equilibria can be performed by simultaneous multi-variable curve fitting of several absorbance-time profiles recorded using two or more irradiation wavelength.[143b,152] For an AB(2Φ) system under irradiation with two different wavelengths λ_1 and λ_2, five variables $(\varepsilon_B^{\lambda 1}, \varepsilon_B^{\lambda 2}, \varepsilon_B^{obs}, \Phi_{AB}, \Phi_{BA})$ are unknown. They can be determined by simultaneously fitting at least 4 different absorbance-time profiles (with the irradiation/observation wavelengths: λ_1/λ_1, λ_1/λ_{obs}, λ_2/λ_2 and λ_2/λ_{obs}). However, following this approach on experimental data of DAE **3d** it was found that although one set of parameters could be identified to give the best fit, multiple local minima were found depending on the initial guess, which makes the fitting procedure unreliable. This is an intrinsic problem of multi-variable curve fitting with five free variables.

Here it is shown that the application of SVD on photokinetic data recorded with two different irradiation wavelengths leads to the situation that only two unknowns (k_1 and k_2) have to be fitted simultaneously while the information on the molar absorptivities of the species is automatically obtained from the species associated spectra **SAS**. This greatly improves the reliability of the fitting procedure as only one global minimum is found, independent of the initial guess. Note that, in analogy to Fischer's method, wavelength independence of the quantum yields is assumed and the ratio of the molar absorptivities of the two isomers has to be different at the two irradiation wavelengths.

From measurements using two different irradiation wavelengths λ_1 and λ_2 two series of photokinetic data $\mathbf{M_{\lambda 1}}$ and $\mathbf{M_{\lambda 2}}$ are obtained. Both are subjected to SVD, as described above, to yield truncated matrices **U**, **S** and $\mathbf{V^T}$ for each set of data (equations *(29)* and *(30)*). At this point matrices **U** and **S** are combined to **US**. As both sets of photokinetic data originate from the same molecular species, the basic spectra collected in the matrices $\mathbf{US_{\lambda 1}}$ and $\mathbf{US_{\lambda 2}}$ have to be identical. Thus $\mathbf{US_{\lambda 2}}$ is replaced by the product of $\mathbf{US_{\lambda 1}}$ and a transformation matrix **X**. Combining **X** and $\mathbf{V_{\lambda 2}^T}$ to a new matrix $\mathbf{V_{\lambda 2,corr}^T}$ allows for the representation of both sets of photokinetic data $\mathbf{M_{\lambda 1}}$

and $\mathbf{M}_{\lambda 2}$ by a matrix product of identical basic spectra $\mathbf{US}_{\boldsymbol{\lambda 1}}$ and two different basic kinetics $\mathbf{V}_{\boldsymbol{\lambda 1}}^{\mathbf{T}}$ and $\mathbf{V}_{\boldsymbol{\lambda 2,corr}}^{\mathbf{T}}$ (right side of eq. *(30)*). The transformation matrix **X** is calculated using the pseudoinverse $(\mathbf{US}_{\boldsymbol{\lambda 1}})^{+}$ (eq. *(31)*).

$$\boldsymbol{M_{\lambda 1}} \approx \boldsymbol{US_{\lambda 1}} \cdot \boldsymbol{V_{\lambda 1}^{T}} \tag{29}$$

$$\boldsymbol{M_{\lambda 2}} \approx \boldsymbol{US_{\lambda 2}} \cdot \boldsymbol{V_{\lambda 2}^{T}} = \boldsymbol{US_{\lambda 1}} \cdot \boldsymbol{X} \cdot \boldsymbol{V_{\lambda 2}^{T}} = \boldsymbol{US_{\lambda 1}} \cdot \boldsymbol{V_{\lambda 2,corr}^{T}} \tag{30}$$

$$\boldsymbol{X} = (\boldsymbol{US_{\lambda 1}})^{+} \cdot \boldsymbol{US_{\lambda 2}} = \left(\boldsymbol{US_{\lambda 1}^{T}} \cdot \boldsymbol{US_{\lambda 1}}\right)^{-1} \cdot \boldsymbol{US_{\lambda 1}^{T}} \cdot \boldsymbol{US_{\lambda 2}} \tag{31}$$

As described above, the basic kinetics $\mathbf{V}_{\boldsymbol{\lambda 1}}^{\mathbf{T}}$ and $\mathbf{V}_{\boldsymbol{\lambda 2,corr}}^{\mathbf{T}}$ can be transformed to a product $\mathbf{F} \cdot \mathbf{K}^{\mathbf{T}}$ with $\mathbf{K}^{\mathbf{T}}$ containing the concentration-time profiles obtained by numerical integration of rate equations and guessing starting values for the rate constants (equations *(32)* and *(33)*). This is done for the first set of photokinetic data assuming some values for k_1 and k_2, $\mathbf{F}_{\mathbf{opt}}$ is determined according to eq. *(26)*, and the matrix **SAS** is calculated. Note that for the second set of photokinetic data $\mathbf{F}_{\mathbf{opt}}$ has to be identical, as in the end the same species associated spectra **SAS** shall be obtained. However, the kinetic model for the second dataset $\mathbf{K}_{\boldsymbol{\lambda 2}}^{\mathbf{T}}$ contains rate constants k_3 and k_4 which are different to k_1 and k_2 due to different absorbance of the species at the irradiation wavelength. Nevertheless, k_3 and k_4 are related to k_1 and k_2, respectively, by their molar absorptivities at λ_1 and λ_2 (equations *(33)* and *(34)*). Importantly, the information on molar absorptivites can be found in the species associated spectra **SAS**, already calculated from $\mathbf{US}_{\boldsymbol{\lambda 1}}$ and $\mathbf{F}_{\mathbf{opt}}$.

$$\boldsymbol{M_{\lambda 1}} \approx \boldsymbol{US_{\lambda 1}} \cdot \boldsymbol{F_{opt}} \cdot \boldsymbol{K_{\lambda 1}^{T}}(k_1, k_2) = \boldsymbol{SAS} \cdot \boldsymbol{K_{\lambda 1}^{T}}(k_1, k_2) \tag{32}$$

$$\boldsymbol{M_{\lambda 2}} \approx \boldsymbol{US_{\lambda 1}} \cdot \boldsymbol{F_{opt}} \cdot \boldsymbol{K_{\lambda 2}^{T}}(k_3, k_4) = \boldsymbol{SAS} \cdot \boldsymbol{K_{\lambda 2}^{T}}(k_3, k_4) \tag{33}$$

$$k_3 = \left[\frac{\varepsilon_A^{\lambda 2}}{\varepsilon_A^{\lambda 1}}\right]_{\boldsymbol{SAS}} \cdot k_1 \tag{34}$$

$$k_4 = \left[\frac{\varepsilon_B^{\lambda 2}}{\varepsilon_B^{\lambda 1}}\right]_{\boldsymbol{SAS}} \cdot k_2 \tag{35}$$

Thus, the overall optimization procedure is the following:

1) Starting values for k_1 and k_2 are guessed and $\mathbf{K}_{\boldsymbol{\lambda 1}}^{\mathbf{T}}$ is determined by numerical integration of rate equations *(18a-b)*.
2) $\mathbf{F}_{\mathbf{opt}}$ is calculated according to eq. *(26)* using $\mathbf{V}_{\boldsymbol{\lambda 1}}^{\mathbf{T}}$.
3) $\mathbf{US}_{\boldsymbol{\lambda 1}}$ and $\mathbf{F}_{\mathbf{opt}}$ are combined to yield species associated spectra **SAS**.

4) From the **SAS** matrix information on the molar absorptivities of the two species at the two irradiation wavelengths is taken to calculate k_3 and k_4 (eq. *(34)* and *(35)*), and hence to determine $\mathbf{K}^{\mathbf{T}}_{\boldsymbol{\lambda 2}}$ by numerical integration of rate equations *(18a-b)*.
5) The matrices $\mathbf{V}^{\mathbf{T}}_{\mathbf{opt},\boldsymbol{\lambda 1}}$ and $\mathbf{V}^{\mathbf{T}}_{\mathbf{opt},\boldsymbol{\lambda 2}}$ are calculated (eq. *(36)* and *(37)*) and the overall sum of quadratic errors E_{total} is determined according to eq. *(38)*.
6) E_{total} is minimized by variation of k_1 and k_2 and repetition of steps 1) - 5).

$$\boldsymbol{V}^{\boldsymbol{T}}_{\boldsymbol{opt},\boldsymbol{\lambda 1}}(k_1,k_2) = \boldsymbol{F}_{\boldsymbol{opt}} \cdot \boldsymbol{K}^{\boldsymbol{T}}_{\boldsymbol{\lambda 1}}(k_1,k_2) \qquad (36)$$

$$\boldsymbol{V}^{\boldsymbol{T}}_{\boldsymbol{opt},\boldsymbol{\lambda 2}}(k_1,k_2) = \boldsymbol{F}_{\boldsymbol{opt}} \cdot \boldsymbol{K}^{\boldsymbol{T}}_{\boldsymbol{\lambda 2}}(k_3,k_4) \qquad (37)$$

$$E_{total}(k_1,k_2) = \sum_{i,j}\left[\left(\boldsymbol{V}^{\boldsymbol{T}}_{\boldsymbol{opt},\boldsymbol{\lambda 1}}(k_1,k_2) - \boldsymbol{V}^{\boldsymbol{T}}_{\boldsymbol{\lambda 1}}\right)^2_{i,j}\right] + \sum_{i,j}\left[\left(\boldsymbol{V}^{\boldsymbol{T}}_{\boldsymbol{opt},\boldsymbol{\lambda 2}}(k_3,k_4) - \boldsymbol{V}^{\boldsymbol{T}}_{\boldsymbol{\lambda 2,corr}}\right)^2_{i,j}\right] \qquad (38)$$

The procedure was applied to two series of photokinetic data, the first under 313 nm (Figure 16a) and the second under 297 nm irradiation (Figure 17a). As can be seen from the irradiation spectra, molar absorptivities of the two isomers are fairly different at these two wavelengths. Importantly, SVD of both datasets and subsequent fitting of the kinetics provides a single global minimum for the parameters k_1 and k_2 (Figure 16b). The spectra of both isomers are obtained from the **SAS** matrix after the parameter optimization. Comparison of the calculated spectra with the spectra of the isolated isomers of **3d** shows excellent agreement (Figure 16c). Finally the quantum yields are easily obtained by dividing k_1 and k_2 with molar absorptivities of the isomers at the irradiation wavelength, as given in the **SAS** matrix.

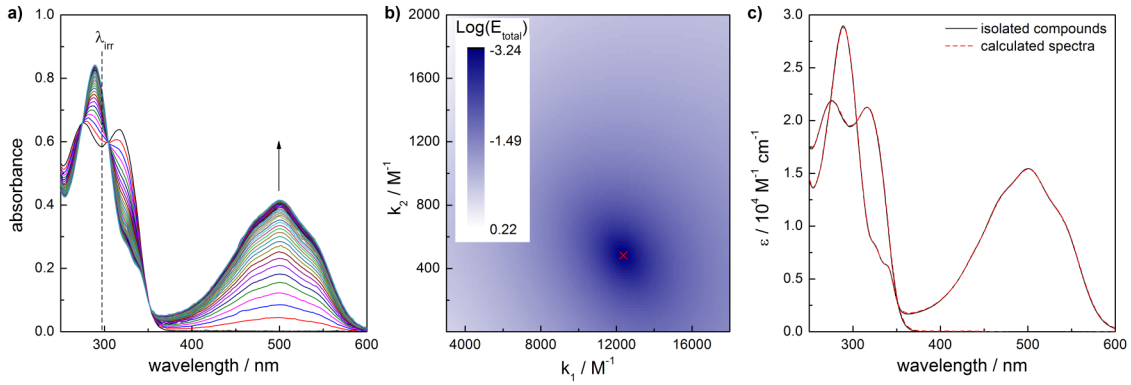

Figure 17. SVD based evaluation of *two sets* of photokinetic data of **3d** (λ_1 = 313 nm, λ_2 = 297 nm). a) UV/Vis absorbance spectra of a solution of **3d** in acetonitrile ($c = 3.0 \cdot 10^{-5}$ M) recorded under irradiation with 297 nm light ($I_0 = 6.6 \cdot 10\text{-}^{10}$ E s^{-1} cm^{-3}, ferrioxalate actinometry) at 25 °C. Spectra were recorded every 12 s. b) Global analysis of the total quadratic error Log(E_{total}) according to equation *(38)* by systematic variation of k_1 and k_2 in steps of 100 M^{-1} (k_1) and 20 M^{-1} (k_2). The red cross marks the minimum found during the optimization procedure. c) Comparison of spectra obtained from the **SAS** matrix after optimization and spectra of the isolated isomers of **3d**.

4.2.8 Summary

In order to quantify the photochromic isomerization reactions of DAEs, in particular the by-product formation, a spectroscopic setup was assembled allowing for the precise recording of photokinetic data under simultaneous irradiation. For measuring the light intensity literature known chemical actinometry procedures were followed. A method was developed to determine the unknown spectra of the ring-closed and by-product isomers by separation of samples taken during the irradiation process using UPLC. The recorded diode array traces were carefully integrated and the thus calculated spectra were shown to excellently agree with the spectra of the isolated isomers in case of compound **3d**.

Quantum yields under UV irradiation for the single isomerization steps were assessed by evaluation of full absorbance-time profiles using numerical integration of the exact rate equations describing the photochromic system. Importantly, this procedure enables the precise determination of the quantum yield of by-product formation. An estimation of the experimental errors shows that the quantum yields for ring-closure and by-product formation possess relative uncertainties of ca. 10% and 20%, respectively, while the uncertainty of the quantum yield for ring-opening is significantly larger for a typical DAE.

In order to find a general way for the quantification of photochromic compounds which possess a fast thermal back reaction or cannot be analyzed by UPLC, an SVD based analysis of pure photokinetic data was developed. While the information contained in one set of photokinetic data is not sufficient, the implementation of "Fischer's method", *i.e.* the utilization of two irradiation wavelengths under the assumption of wavelength independence of the quantum yields, allowed for the precise determination of the spectra of the unknown isomers of DAE **3d**. Thereby, the SVD based analysis of the data significantly reduces the number of free variables compared to earlier reported methods based on multi-variable curve fitting. This makes the non-linear regression analysis much more robust and a unique best-fit is obtained. Currently the SVD based method is applied in the Hecht group to quantify the photochromic reactions of thermally reversible DAEs and spiropyrans.

4.3 Improving the fatigue resistance of diarylethenes[21]

4.3.1 Introduction

The fatigue of DAEs due to the formation of the annulated isomer, as described in section 2.1.3 of this work, is an often disregarded feature of their photochromic behavior. In contrast, DAEs are generally described as highly fatigue resistant. However, during earlier studies on DAEs in the Hecht group, it was noted that the formation of the annulated isomer is a ubiquitous phenomenon for a large variety of DAE structures. Only if β-methyl substituted thiophenes or benzothiophenes are utilized as hetaryl moieties in combination with the perfluorocyclopentene bridge, highly fatigue resistant DAEs can be constructed.[18,51]

As literature shows (see section 2.2), many interesting properties or functions can be implemented to DAEs by structural variation of the photochromic core itself, *e.g.* the incorporation of the bridging double bond into a reactive or catalytically active moiety, the use of a heteroaromatic ring as bridging moiety, or the use of any double bond containing structure instead of the parent thiophene or benzothiophene motif. Thus, it is of high importance to find a general strategy to impart fatigue resistance to DAE photochromes while maintaining a maximum degree of structural and synthetic flexibility. As a first step, the construction of fatigue resistant perhydrocyclopentene bridged DAEs is desirable due to their advantageous electronic properties and synthetic accessibility.

To accomplish this goal, a precise quantitative analysis of the fatigue reaction is mandatory in order to establish distinct structure-property relationships. Therefore, the spectroscopic procedures outlined in the preceding section 4.2 were developed and applied on a series of DAEs obtained by systematic structural variation (Scheme 35). Starting with the parent dithienylperhydrocyclopentene structure **1** substituents on the phenyl rings were varied from strongly donating (4-Me_2N, **1a**) to strongly accepting (3,5-$(CF_3)_2$, **1i**) moieties. To study the effect of the perfluorocyclopentene bridge, derivatives **2c**, **2i**, and **2j** were prepared. In addition, thiazole analogues **3d, 3i** and **4i** as well as two non-symmetrically substituted dithienylcyclopentenes **5a** and **5b** were investigated. Last but not least, dithienylcyclopentene **6c** was studied to determine the effect of the additional β-methyl group in the case the perhydrocyclopentene bridge is used.

[21] Large parts of this section have been published: M. Herder *et al,. J. Am. Chem. Soc.* **2015**, *137*, 2738-2747.

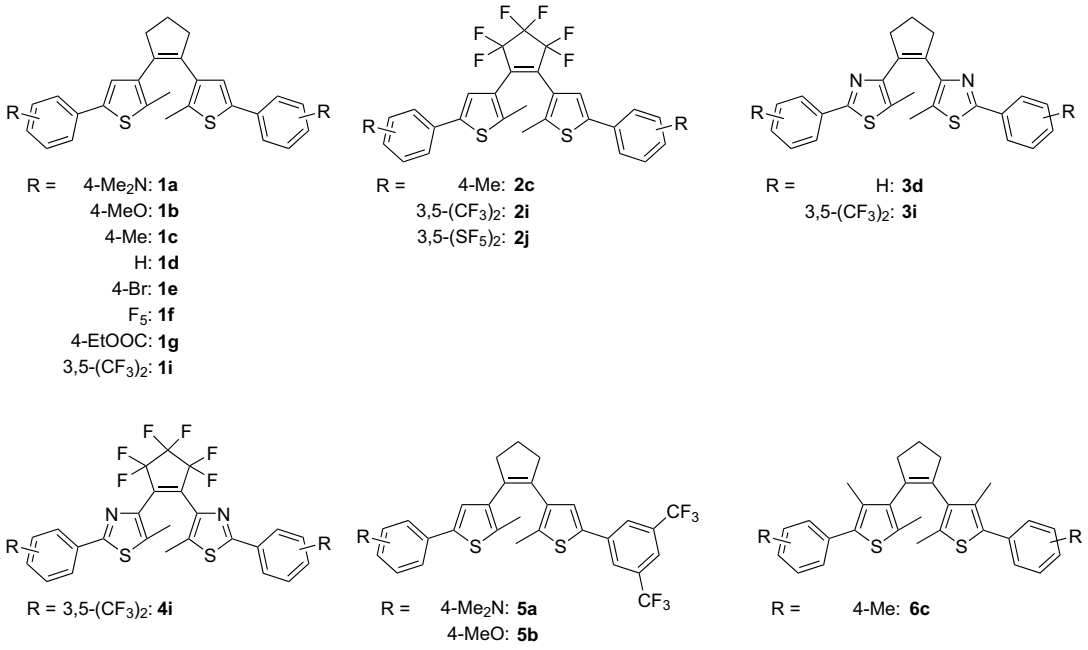

Scheme 35. DAE structures discussed in terms of their fatigue behavior.

4.3.2 General fatigue behavior

The typical spectral response of DAE switches upon irradiation with UV light is exemplarily shown in Figure 18 for the methyl substituted compound **1c**. While the ring-open isomer possesses a strong absorbance in the UV range, upon irradiation with 313 nm light a new broad band centered at 522 nm builds up that is characteristic for the ring-closed isomer with its extended π-conjugation (Figure 18a). The fast growth of the visible band is completed after 60 s when a plateau is reached, *i.e.* the absorbance does not increase upon further UV illumination. This is the expected behavior for a photochemical equilibrium between the ring-open and ring-closed isomer leading to a photostationary state (PSS). Importantly, when the sample after reaching the PSS is further subjected to UV illumination a slow decrease of the visible absorbance can be observed accompanied by a small hypsochromic shift of the band maximum (Figure 18b). Analysis of the irradiated solution by ultra-performance liquid chromatography (UPLC) reveals the emergence of a second photoproduct upon longer irradiation times (Figure 18d). In contrast to the formation of the ring-closed isomer this process is not reversible, *i.e.* upon visible light irradiation to induce the ring-opening reaction a weak absorbance in the visible range is retained and corresponds to the formed by-product. Although the observed by-product formation seems to be very slow it leads to a significant loss of photochromic material already after few switching cycles, which consist of short UV-irradiation until reaching the (pseudo)PSS and subsequent visible light irradiation until no further spectral change can be observed (Figure 18c).

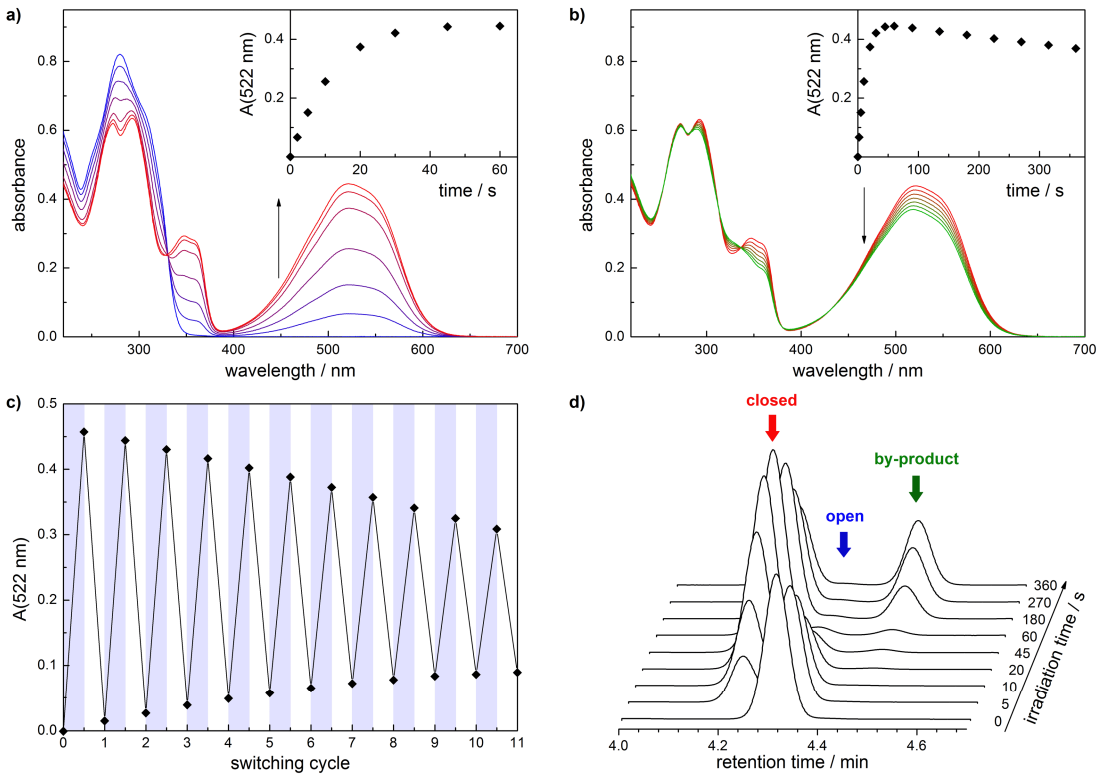

Figure 18. UV/Vis spectroscopy of an acetonitrile solution of **1c** ($2.38 \cdot 10^{-5}$ M, 25 °C): a) Irradiation with UV-light (310 nm, 1000 W Xe) until reaching maximum absorbance in the visible range. b) Prolonged UV-irradiation (310 nm, 1000 W Xe) after reaching maximum absorbance. c) Evolution of absorbance in the visible range during repetitive switching cycles consisting of alternating UV- (310 nm, 90 s, 1000 W Xe) and Vis- irradiation(> 500 nm, 600 s, 1000 W Xe). d) Evolution of UPLC-traces (absorbance monitoring by diode array detector integrated between 250 – 800 nm) upon continuous UV-irradiation (310 nm, 1000 W Xe).

The identity of the formed by-product with the condensed ring system which was reported earlier by the group of Irie[51] (see section 2.1.3), was proven by its preparative isolation and subsequent NMR spectroscopic examination. While ^{1}H NMR spectra of the ring-open and ring-closed isomers of **1c** show only one signal for the methyl groups attached to the reactive carbons, two separated singlets each integrating for 3 protons appear in the spectrum of the isolated by-product (Figure 19). Also in ^{13}C NMR spectra two quaternary carbon signals are detected for **1c(bp)** in contrast to **1c(c)**. Furthermore the cyclopentene protons give a complicated signal pattern, probably due to the highly strained structure of **1c(bp)**. 2D NMR spectroscopy proves the structure by unambiguous assignment of the observed signals and analysis of the coupling paths between the methyl groups, adjacent quaternary carbon atoms, and thiophene protons (see Figure A1-1 and Figure A1-2 in Appendix 1). Notably, the downfield shifted part of the ^{1}H NMR spectrum of the by-product is nearly identical to that of the ring-closed isomer, which is an indication for their similar π-electronic structure.

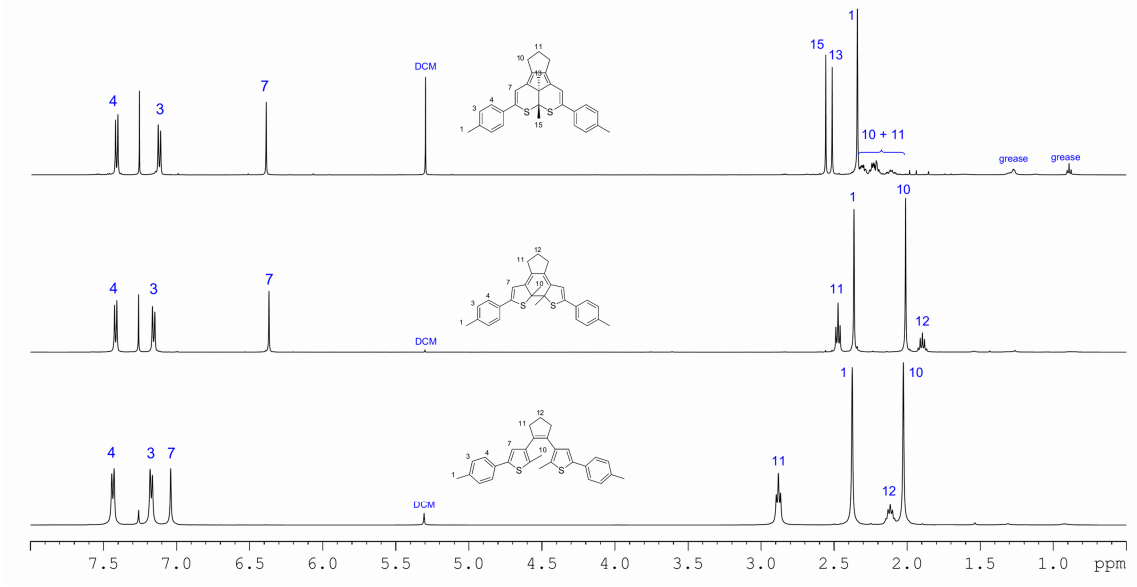

Figure 19. Comparison of ^{1}H NMR spectra ($CDCl_3$, 500 MHz) of all isomers of **1c**.

From inspection of the irradiation spectra of *all* other DAE derivatives discussed here (collected in Appendix 2), it can be deduced that the fatigue exemplified in Figure 18 for compound **1c** is a general feature of DAEs, independent of the nature of their aryl moieties or of their bridging unit.[22] While, as discussed in section 2.1.3, the formation of the annulated ring-system has been noted earlier for some dithienylethene derivatives, for DAEs bearing thiazoles as aryl moieties the formation of a by-product has not been reported yet. In contrast, they were originally characterized as highly fatigue resistant.[153]

To prove that the photochemical by-product formed from dithiazolylethene **3d** is structurally analogous to the thiophene counterpart, it has been isolated by irradiation and subsequent chromatography on a preparative scale. Again, ^{1}H NMR spectroscopy shows signals for two magnetically inequivalent methyl groups (Figure 20) while ^{13}C NMR shows two signals for quaternary carbon atoms at high field. Long range couplings observed in 2D NMR spectra are similar to those observed for the by-product of **1c** (Figure A1-3 and Figure A1-4 in Appendix 1). Note that for *all* compounds reported in this study UPLC/MS analysis of irradiated samples verifies that the emerging by-product is an additional isomer of the parent structure possessing a *m/z* ratio identical to that of the respective ring-open and ring-closed forms. Given the close similarities between all compounds in the observed UV/Vis spectra and corresponding UPLC/MS traces it is assumed that in any case the fatigue of the photochrome is based on the formation of the same condensed ring-system as a by-product. Only in case of electron-rich dithienylcyclopentenes (**1a-f** and **5a-b**) some additional unspecific by-product formation in the form of oxidation reactions can be detected by UPLC/MS (peaks corresponding

[22] Note that besides cyclopentene and perfluorocyclopentene bridged DAEs discussed in this section also for DAE **7i**, possessing an *N*-*tert*-butylmaleimide bridge, and DAEs **14** and **61**, possessing an aromatic imidazole bridge, by-product formation upon UV irradiation was detected. See sections 4.5 and 4.7.

to $[M+16]^+$ and $[M+32]^+$). However, in argon saturated solutions the emergence of the rearranged isomer is much faster than photooxidation.

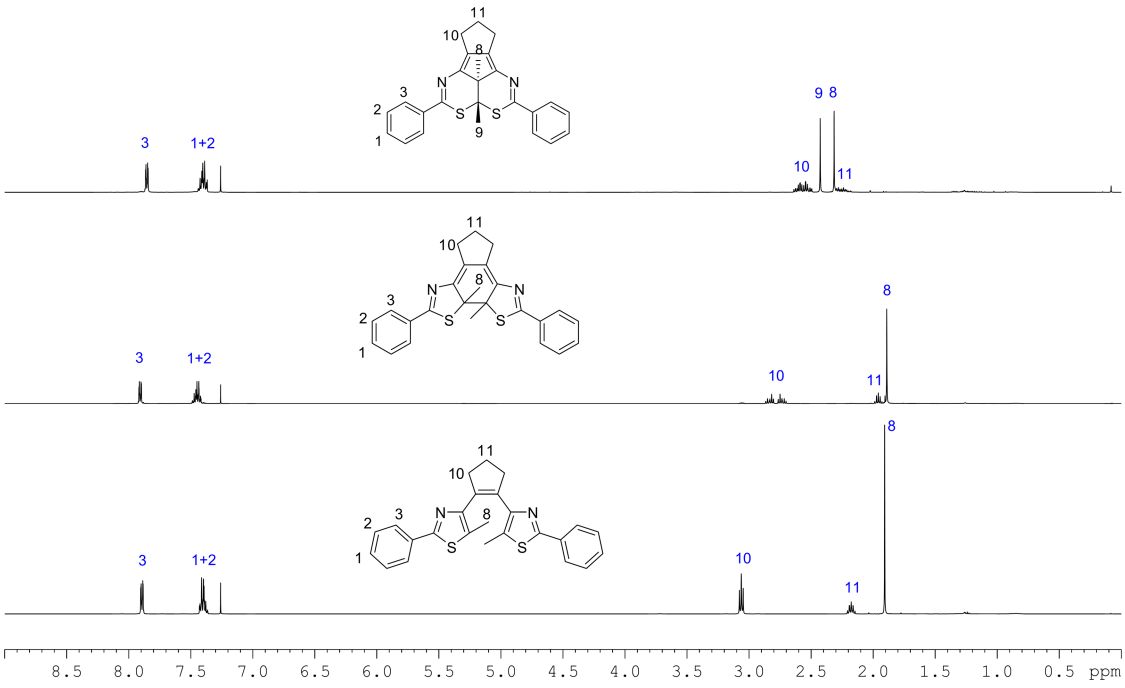

Figure 20. Comparison of ^{1}H NMR spectra ($CDCl_3$, 500 MHz) of all isomers of **3d**

Interestingly, close inspection of UV/Vis spectra (Appendix 2) reveals subtle differences in the spectroscopic characteristics of the by-product when comparing dithienylethenes **1c**, **1i**, and **2i** with their thiazole analogues **3d**, **3i**, and **4i**. For all compounds both the ring-closed isomer and the by-product possess a very similar absorbance in the visible region due to analogous π-conjugation pathways throughout their molecular backbone. Nevertheless, the molar absorptivity of the by-product is significantly lower leading to the typical decrease of the absorption band upon prolonged UV irradiation. For thiophene derivatives the decrease is accompanied by a hypsochromic shift, which is more pronounced for electron deficient derivatives ($\Delta\lambda_{max}$ = 14 nm for **1d**, $\Delta\lambda_{max}$ = 41 nm for **2i**). However, thiazole derivatives show a bathochromic shift of 21 nm and 18 nm for **3d** and **3i**, respectively, or in the case of **4i** λ_{max} of the ring-closed form and the by-product are identical.

To gain further insight into the spectroscopic characteristics calculations were performed on the prototype thiophene and thiazole containing structures **1c** and **3d**. Thereby a three step procedure previously used by Jacquemin and coworkers[154] for the modelling of electronic spectra of DAEs was followed:

1 Full optimization of ground state energies on the B3LYP/6-311G(d,p) level of theory. The effect of acetonitrile as solvent was included using the polarizable continuum model (PCM).

2 Calculation of vibrational frequencies to prove that the optimized structure corresponds to a true minimum on the potential energy surface

3 Computation of the first 20 singlet excited states using the vertical TD-DFT approach on the CAM-B3LYP/PCM(acetonitrile)/6-311+G(2d,p) and PBE0/PCM(acetonitrile)/6-311+G(2d,p) levels of theory.

It has been shown that CAM-B3LYP and PBE0 functionals give a good agreement between experimental spectra and calculated vertical transition energies of DAEs.[155] In the case of **1c** and **3d** CAM-B3LYP reproduced the experimentally observed λ_{max} for all three isomers very accurately (Figure 21 and Figure 22) while the PBE0 functional significantly underestimates the transition energies (Figure A3-3, Figure A3-4, and Table A3-1 in Appendix 3). Nevertheless, both methods confirm a hypsochromic shift of λ_{max} for **1c** (11 nm with CAM-B3LYP / 15 nm with PBE0) and a bathochromic shift of λ_{max} for **3d** (24 nm with CAM-B3LYP / 21 nm with PBE0) when going from the ring-closed isomer to the by-product. The reduced oscillator strength of the lowest energy transition of the by-products is demonstrated as well.

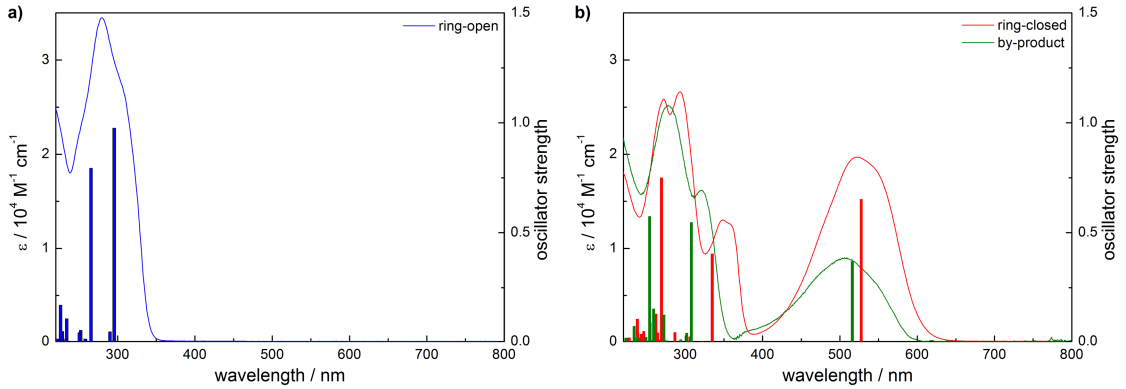

Figure 21. Experimental UV/Vis spectra of **1c** (acetonitrile, 25 °C) and vertical transitions computed on the CAM-B3LYP/PCM(acetonitrile)/6-311+G(2d,p) level of theory: a) ring-open isomer, b) ring-closed isomer and by-product.

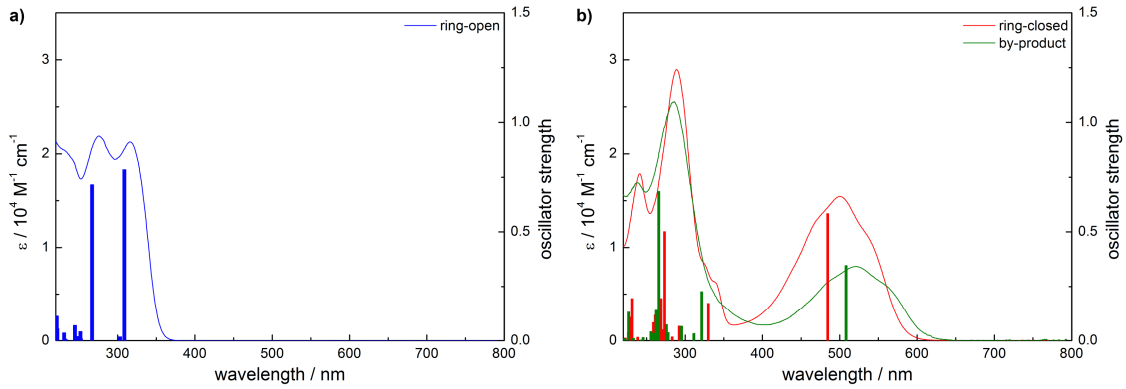

Figure 22. Experimental UV/Vis spectra of **3d** (acetonitrile, 25 °C) and vertical transitions computed on the CAM-B3LYP/PCM(acetonitrile)/6-311+G(2d,p) level of theory: a) ring-open isomer, b) ring-closed isomer and by-product.

Inspecting the optimized geometries one finds that the major difference between isomers of **1c** and **3d** lies in the twisting of the adjacent phenyl groups while deviations in the central hexatriene/cyclohexadiene core are small (strucutral parameters are collected in Table 7, see also Figure A3-1 and Figure A3-2 in Appendix 3). In general, the dihedral angle θ between thiophenes and phenyl rings in **1c** is larger for all isomers than that between thiazoles and phenyl rings in **3d**. Importantly, θ increases on going from the ring-closed isomer to the by-product due to increased steric repulsion by expanding the former thiophene/thiazole 5-membered to a 6-membered ring. While for **3d** the increase is moderate (θ = 4° for the ring-closed isomer / θ = 20° for the by-product) it is larger for **1c** (θ = 13° for the ring-closed isomer / θ = 40° for the by-product). Thus, a smaller increase of the dihedral angle of **3d** due to less steric repulsion by the nitrogen atom may lead to a better delocalization of π-electron density resulting in the experimentally observed bathochromic shift while a stronger twisting of the phenyl group shifts the absorbance maximum of the by-product of **1c** to shorter wavelengths. This can easily be visualized by re-optimization of the structure of **3d(bp)** using frozen dihedral angles θ and subsequent calculation of the vertical transitions. Upon increasing the dihedral angle beyond the value of the minimum structure, the lowest energy vertical transition is significantly shifted to higher wavelengths (Figure 23).

Table 7. Geometric parameters of optimized structures of **1c** and **3d** on the B3LYP/PCM(acetonitrile)/ 6-311G(d,p) level of theory.

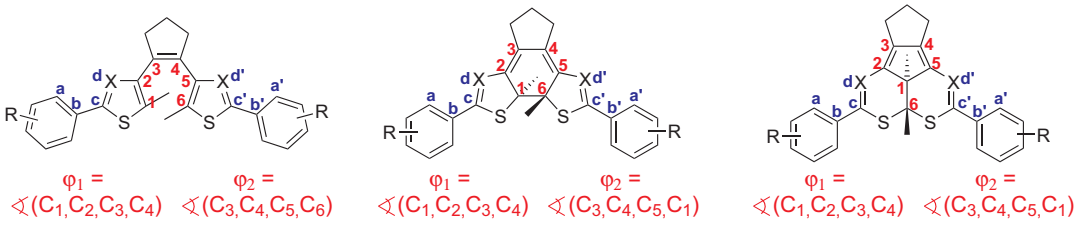

	1c(o)	1c(c)	1c(bp)	3d(o)	3d(c)	3d(bp)
E^a / kJ mol^{-1}	0	48.92	92.03	0	45.61	123.56
$r_{C1\text{-}C6}$ / Å	3.64	1.54	1.53	3.63	1.54	1.53
φ_1 / φ_2	50.2° / 49.2°	7.6° / 7.4°	-5.9° / 5.9°	49.0° / 48.3°	7.2° / 6.8°	-5.2° / 5.2°
θ_1 / θ_2	-25.6° / -25.4°	13.6° / 12.2°	36.9° / -36.9°	-4.4° / -5.5°	3.4° / 3.5°	19.9° / -19.9°

a) Energy relative to ring-open isomer including zero-point correction.

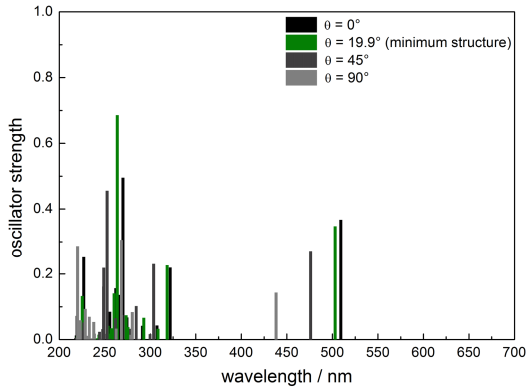

Figure 23. Vertical transitions (CAM-B3LYP/PCM(acetonitrile)/6-311+G(2d,p)) of **3d(bp)** computed from structures optimized at the B3LYP/PCM(acetonitrile)/6-311G(d,p) level of theory with frozen dihedral angles θ_1/ θ_2.

4.3.3 Quantification of by-product formation

Along the whole series of DAE derivatives possessing electronically different substitution patterns significant differences in the rate of by-product formation have been observed. At first glance a good indication for the performance of a switch is the amount of by-product formed after a certain time of UV irradiation under comparable conditions, which can readily be determined by UPLC. Although this can only serve as a crude estimate since the exact amount of by-product depends on the sample concentration, molar absorptivities at the irradiation wavelength, and quantum yields for all photochemical reactions, the obtained conversions clearly show a strong correlation of the fatigue behavior on the substitution pattern (Figure 24, Table 8). After 30 min of high intensity UV irradiation using a 1000 W Xe arc lamp together with a 310 nm interference filter the most electron rich dithienylethenes **1a-1d** bearing perhydrocyclopentene bridges and electron donating or electron neutral substituents on the adjacent phenyl rings are almost quantitatively converted to the by-product. For analogous compounds possessing substituents with increasing acceptor strength, e.g. bromine (**1e**), fluorine (**1f**), ester (**1g**), or trifluoromethyl (**1i**) groups, the yield of by-product is more and more suppressed down to a minimum amount of ca. 6% for compound **1i**. Notably, structurally analogous DAEs of the thiophene and thiazole series possess a comparable fatigue resistance. Introduction of the perfluorocyclopentene bridge strongly reduces by-product formation for donor or electron neutral substituted compounds while no further suppression is observed for trifluoromethyl substituted compound **2i** when compared to the respective perhydrocyclopentene **1i**.

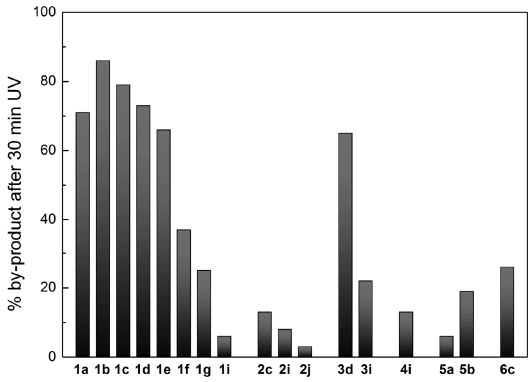

Figure 24. Amount of by-product built upon 30 min of UV irradiation (310 nm, 1000 W Xe, $I_0 = 5.67 \cdot 10^{-9}$ E s^{-1} cm^{-3} determined by ferrioxalate actinometry) of acetonitrile solutions ($c = 2.5 \cdot 10^{-5}$ M) of diarylethenes **1a**-**6c**.

In order to obtain more precise information on the dependency of fatigue behavior on the substitution pattern a precise quantification of the rate of by-product formation is needed. Therefore, molar absorptivities of all isomers were determined using a combination of UV/Vis spectroscopy and UPLC, as described in detail in section 4.2.5 of this work. Quantum yields for all photochemical steps involved in the isomerization and fatigue reaction have been determined by means of measurement of absorbance time profiles under continuous UV irradiation and their evaluation by numerical nonlinear regression, as discussed in detail in section 0. As a kinetic model for the nonlinear regression a photochromic ABC(3Φ) system was assumed, consisting of a photochemical equilibrium between species A and B and a subsequent irreversible photochemical reaction from species B to C. By fitting the theoretical model to the experimental data quantum yields Φ_{AB} for ring-closure, Φ_{BA} for ring-opening, and Φ_{BC} for by-product formation were obtained (Table 8). Note that assuming a different model with the by-product being formed parallel to the ring-closed isomer by excitation of the ring-open isomer does not lead to a satisfying fit of the experimental data in accordance to previous findings.[53g]

Quantum yields for ring-opening and ring-closure

The data in Table 8 show that the majority of the investigated compounds possess the expected photochemical behavior of DAEs substituted with methyl groups and phenyl rings at the inner and outer α-positions of the hetaryl groups, respectively.[11b,19b] Quantum yields for ring-closure are in the range of $0.4 - 0.6$ reflecting the thermal equilibrium between the parallel and antiparallel conformer of the ring-open isomer, with only the latter being photoactive.[8a] Quantum yields for ring-opening are more than one magnitude smaller and strongly wavelength-dependent, *i.e.* the ring-opening reaction performed upon irradiation with visible light proceeds much more slowly than the reaction with UV light.[11a,42] Due to the ratio of $\Phi_{AB} : \Phi_{BA}$ the amount of ring-closed isomer in the PSS generally exceeds 90%, although both isomers absorb UV light.

Table 8. Photochemical properties of investigated diarylethenes in acetonitrile.

comp.	λ_{max} / nm (ε / 10^4 M^{-1} cm^{-1})			PSS (310 nm)[a]	by-product (310 nm)[b]	Φ_{AB} (313 nm)[c]	Φ_{BA} (313 nm)[c]	Φ_{BC} (313 nm)[c]	Φ_{BA} (546 nm)[d]
	ring-open isomer	ring-closed isomer	by-product						
1a	331 (4.33)	537 (2.66)	530 (1.44)	99%	71%	0.74 ± 0.09	0.03 ± 0.06	0.008 ± 0.003	0.0029 ± 0.0002
1b	283 (3.19)	520 (1.90)	509 (0.84)	89%	86%	0.47 ± 0.05	0.03 ± 0.03	0.007 ± 0.002	0.0072 ± 0.0006
1c	279 (3.45)	522 (1.97)	508 (1.13)	94%	79%	0.43 ± 0.05	0.01 ± 0.03	0.009 ± 0.003	0.008 ± 0.0006
1d	278 (3.25)	520 (1.78)	510 (0.94)	98%	73%	0.47 ± 0.05	0.02 ± 0.05	0.013 ± 0.003	0.0093 ± 0.0007
1e	284 (3.71)	532 (2.16)	514 (1.17)	96%	66%	0.42 ± 0.05	0.02 ± 0.03	0.006 ± 0.002	0.0055 ± 0.0004
1f	273 (2.83)	512 (1.18)	476 (0.51)	96%	37%	0.41 ± 0.04	0.01 ± 0.05	0.006 ± 0.001	0.020 ± 0.002
1g	334 (3.58)	556 (2.32)	532 (1.18)	98%	25%	0.65 ± 0.07	0.06 ± 0.05	0.0013 ± 0.0003	0.0021 ± 0.0002
1i	284 (3.16)	548 (1.96)	524 (0.95)	97%	6%	0.44 ± 0.04	0.02 ± 0.06	0.0004 ± 0.0001	0.0046 ± 0.0004
2c	289 (3.87)	588 (1.79)	550 (0.85)	94%	13%	0.62 ± 0.08	0.03 ± 0.03	0.0006 ± 0.0002	0.015 ± 0.001
2i	300 (3.45)	590 (1.54)	549 (0.72)	96%	8%	0.58 ± 0.06	0.05 ± 0.05	0.0004 ± 0.0001	0.017 ± 0.001
2j	302 (3.43)	590 (1.58)	545 (0.76)	96%	3%	0.50 ± 0.05	0.04 ± 0.05	0.00019 ± 0.00004	0.018 ± 0.001
3d	316 (2.13)	500 (1.55)	521 (0.80)	94%	65%	0.53 ± 0.05	0.03 ± 0.05	0.007 ± 0.001	0.021 ± 0.002
3i	332 (1.80)	522 (1.34)	540 (0.77)	95%	22%	0.56 ± 0.06	0.03 ± 0.05	0.002 ± 0.0005	0.015 ± 0.001
4i	307 (3.11)	538 (1.13)	538 (0.64)	89%	13%	0.45 ± 0.05	0.06 ± 0.04	0.0008 ± 0.0002	0.039 ± 0.003
5a	326 (3.37)	570 (2.54)	539 (1.22)	97%	6%	0.051 ± 0.005	0.005 ± 0.008	0.0009 ± 0.0002	0.0022 ± 0.0002
5b	282 (3.04)	546 (1.82)	515 (0.82)	99%	19%	0.56 ± 0.06	0.02 ± 0.04	0.0013 ± 0.0002	0.0058 ± 0.0005
6c	271 (2.75)	483 (1.29)	459 (0.35)	91%	26%	0.47 ± 0.05	0.04 ± 0.03	0.004 ± 0.001	0.043 ± 0.003

a) Amount of ring-closed isomer in the (pseudo)PSS reached after UV-irradiation (310 nm, 1000 W Xe), obtained by UPLC.
b) Amount of by-product after 30 min of UV-irradiation (310 nm, 1000 W Xe), obtained by UPLC.
c) Quantum yields obtained by nonlinear regression of photokinetic data under UV-irradiation (313 nm, 500 W Xe(Hg), ferrioxalate actinometry).
d) Ring-opening quantum yields under visible light irradiation (546 nm, 500 W Xe(Hg), Aberchrome 670 actinometry) obtained from the initial slope of photoconversion.

Only compounds **1a** and **5a** deviate from the described behavior, with the former possessing a slightly larger quantum yield for ring-closure of 0.74 and the latter showing a significantly reduced photoreactivity with Φ_{AB} being only 0.05. Whereas a differing population of the antiparallel and parallel conformers in the electronic ground state may serve as explanation for these deviations, for compound **5a** an electronic reason due to the pronounced donor-acceptor character of the π-electronic system seems plausible as well. This is manifested in the fact that quantum yields for *both* ring-closure and ring-opening are reduced by approximately one order of magnitude. In addition, compound **5a** shows a strong bathochromic

shift of the absorption bands of all three isomers pointing to a charge transfer character of the excitation.

Quantum yields for by-product formation

The measured quantum yields for by-product formation (Table 8) confirm the qualitatively observed trends. The largest values for Φ_{BC} are found for donor substituted and unsubstituted dithienylethenes possessing the perhydrocyclopentene bridge (**1a-1d**) with values between 0.007 – 0.013. Thus, for these structures the rate of by-product formation is in the same order of magnitude as the rate of the ring-opening reaction leading to the observed fast depletion of the photochromic material under continuous UV irradiation and high irreversibility during full switching cycles (Figure 18c, Figure 25). A comparison between structures **1d** and **3d** shows that employing less electron-rich thiazoles instead of thiophenes increases the fatigue resistance only marginally. In contrast, the perfluorination of the cyclopentene bridge has a much larger effect. Compared to perhydrocyclopentene **1c** Φ_{BC} is reduced by a factor of 15 to a value of 0.0006 for perfluorocyclopentene **2c**.

Importantly, in the perhydrocyclopentene series by-product formation is suppressed to the same degree by introduction of acceptor groups on the adjacent phenyl rings. While a small effect is observed for substitution with *p*-bromophenyl groups (**1e**) and pentafluorophenyl groups (**1f**), substitution with an ester group in *para* position of the phenyl ring (**1g**), exerting a –M effect, reduces Φ_{BC} to a value of 0.001. An exceptional improvement of the fatigue behavior is found when chemically inert trifluoromethyl groups, exerting a strong –I effect, are attached at the *meta* positions of the phenyl rings. With $\Phi_{BC} = 0.0004$ for compound **1i** by-product formation is suppressed by a factor of 20-30 when compared to the unsubstituted or donor substituted analogues **1a-1d**. Importantly, the CF_3 substitution does not alter the rates of the desired photochemical isomerization reactions between the ring-open and ring-closed isomer and has only minor influence on the electronic spectra (see Appendix 2). The positive effect of the 3,5-bis(trifluoromethyl)phenyl groups can be observed in the dithiazolylethene series as well. However, compared to the parent structure **3d** the quantum yield of by-product formation of compound **3i** is reduced by only a factor of 3. The combination of the 3,5-bis(trifluoromethyl)phenyl substituents with the perfluorocyclopentene bridge in DAE structures **2i** and **4i** gives a further reduction of Φ_{BC} only in case of the thiazole containing compound. In the thiophene series the performances of the perhydro- and perfluorocyclopentene switches **1i** and **2i** are very similar. The large improvement of fatigue resistance for structures **1i**, **2i**, **3i**, and **4i** is manifested as well in the excellent reversibility during full switching cycles (Figure 25).

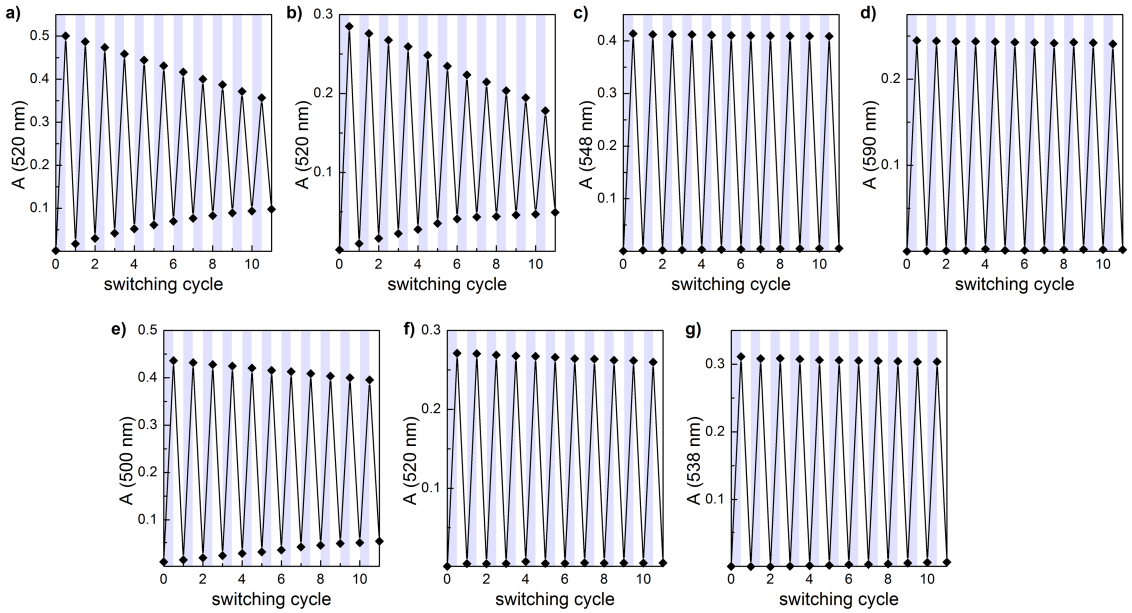

Figure 25. Evolution of absorbance in the visible range upon alternating UV- (310 nm, 90 s, 1000 W Xe) and Vis- (> 500 nm, 600 s, 1000 W Xe) irradiation of acetonitrile solutions of compounds a) **1b**, b) **1d**, c) **1i**, d) **2i**, e) **3d**, f) **3i**, and g) **4i**.

In an attempt to further suppress by-product formation by substitution with strong acceptor groups compound **2j** was synthesized, possessing pentafluorosulfanyl groups. Compared to CF_3 the SF_5 group is an even stronger electron acceptor while being structurally related and chemically inert.[156] In fact, comparing structures **2i** and **2j** by introduction of SF_5 groups Φ_{BC} is further reduced by a factor of 2. Thus far, compound **2j** shows the highest fatigue resistance of all DAE structures investigated during this work. Note that similar to CF_3 groups SF_5 substitution only marginally alters the photochromic properties of the parent unsubstituted compound.

Given the outstanding performance of CF_3 and SF_5 substituted DAEs in terms of fatigue resistance it was speculated that it could be sufficient to functionalize only one hetaryl terminus of the structure with this motif while still suppressing by-product formation. This would enable a flexible choice of the structure of the second terminus, thus allowing for implementing any desired chemical functionality to be modulated by the photochromic reaction. To answer this question unsymmetrically substituted dithienylethenes **5a** and **5b** were synthesized possessing the 3,5-bis(trifluoromethyl)phenyl group on one thiophene ring and a 4-*N,N*-dimethylamino or 4-methoxy substituted phenyl group on the other. In terms of fatigue this substitution pattern combines one of the best-performing acceptor with poor-performing donor substituents. Besides the modulation of the rates of ring-closure and ring-opening in case of compound **5a** (*vide supra*) it was found that for both structures by-product formation is strongly suppressed compared to the symmetrically donor substituted compounds. This strategy of using a nonsymmetrical substitution pattern to implement fatigue resistance via the 3,5-bis(trifluoromethyl)phenyl group on one side and a functional moiety on the other side of

the DAE was recently applied in the Hecht group to remote-control of the reactivity of a furan in a Diels-Alder reaction.[100c,157] Importantly, in this particular case a perfluorinated bridge could not be used to provide improved fatigue resistance for electronic reasons as it would significantly reduce the Diels-Alder reactivity of the attached furan. This nicely demonstrates the power of imparting fatigue resistance via the DAE termini and not the bridge.

The second previously known strategy to impart fatigue resistance to DAEs making use of β-methyl substituted thiophenes was reported only for compounds possessing the perfluorocyclopentene bridge.[51] To test if the β-methyl substituent has an effect on the fatigue behavior when other bridges are used, the photochemistry of compound **6c**, possessing β-methyl substituted thiophenes and the perhydrocyclopentene bridge, was investigated. In fact, **6c** shows significant by-product formation with a quantum yield only slightly lower than that of compound **1c** without β-methyl substituents. This finding supports theoretical investigations,[56] which attribute the lack of fatigue of β-methyl substituted dithienylperfluorocyclopentenes to steric hindrance between the β-methyl group and the fluorine atoms, which are not present in compound **6c**.

Solvent and wavelength dependence of Φ_{BC}

The photochemistry of dithiazolylethene **3d** was investigated in different solvents and under different irradiation conditions (Table 9). Using solvents with lower polarity than acetonitrile causes a small increase of the quantum yield for ring-closure, while quantum yields for ring-opening as well as by-product formation are not altered. Interestingly, quantum yields for all three isomerization reactions are not affected within the error of measurement by the choice of the irradiation wavelength in the UV range. For photochemical ring-closure of DAEs the insensitivity to the irradiation wavelength was expected.[42] The previously observed wavelength dependence of the quantum yield for the ring-opening process[11a,42] is manifested in the much lower values for excitation with visible light (Table 8), yet probably could not be resolved in the experiments within the UV range due to the high statistical error of this parameter.

In accordance to previous reports[51,53g] it is found that by-product formation is not induced by irradiation of the ring-closed isomer using visible light. This can be shown by using a purified photostationary mixture of **3d**, which was obtained by preparative irradiation of **3d(o)** with UV light and subsequent column chromatographic separation of the by-product. The purified photostationary mixture was subjected to visible light irradiation at 546 nm (Figure 26). Assuming the same ratio Φ_{BC}/Φ_{BA}, which is observed under UV irradiation, for the visible light irradiation experiment, one would expect that ca. 10-20% of the material converts to the by-product upon photolysis of the ring-closed isomer at 546 nm. However, UPLC traces recorded before and after the experiment show that no by-product is formed. Furthermore, UV/Vis

spectra show the complete depletion of the absorbance in the visible range, indicative for quantitative ring-opening.

The lack of by-product formation upon visible light irradiation may be ascribed to a thermal barrier in the S_1 excited state making excitation to a higher excited state by UV light necessary to deliver sufficient kinetic energy upon internal conversion to the S_1 state to overcome the barrier (see section 2.1.3).[45] Thus, one would also expect a dependence of the quantum yield for by-product formation on the wavelength within the UV range. However, it is found that Φ_{BC} is essentially wavelength independent between 297 and 334 nm (Table 9).

Table 9. Solvent and wavelength dependence of quantum yields of compound **3d**.

solvent	λ_{irr}	PSS[a]	Φ_{AB}[b]	Φ_{BA}[b]	Φ_{BC}[b]
MeCN	313 nm	94%	0.53 ± 0.05	0.03 ± 0.05	0.007 ± 0.001
CH_2Cl_2	313 nm	94%	0.59 ± 0.06	0.03 ± 0.04	0.007 ± 0.001
C_6H_{12}	313 nm	96%	0.73 ± 0.07	0.02 ± 0.06	0.008 ± 0.002
MeCN	297 nm	88%	0.51 ± 0.05	0.04 ± 0.03	0.007 ± 0.001
MeCN	334 nm	96%	0.60 ± 0.06	0.04 ± 0.08	0.008 ± 0.001

a) Amount of ring-closed isomer in the (pseudo)PSS reached after UV irradiation (310 nm, 1000 W Xe), obtained by UPLC.
b) Quantum yields obtained by nonlinear regression of photokinetic data under UV-irradiation (313 nm, 500 W Xe(Hg), ferrioxalate actinometry).

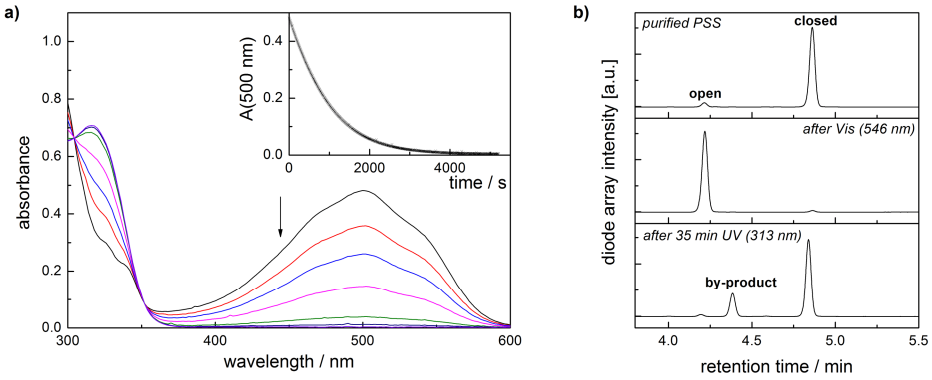

Figure 26. a) UV/Vis spectra of a purified photostationary mixture of **3d(o)** and **3d(c)** in acetonitrile during irradiation with 546 nm light (500 W Xe(Hg)). Inset: Corresponding absorbance-time profile. b) UPLC traces (diode-array detector integrated between 250-800 nm) of the photostationary mixture before irradiation (top), after irradiation with 546 nm light (middle), and after subsequent irradiation with 313 nm light (1000 W Xe).

4.3.4 By-product formation in the triplet excited state?

From the theoretical standpoint[45] it seems possible, that by-product formation is induced by intersystem crossing of the excited state, facilitated by the presence of sulfur atoms, and subsequent relaxation of the triplet species to a different conical intersection than that leading to ring-opening. To address this question the fatigue behavior of compound **1c** in the presence of triplet sensitizers was investigated. Note that the triplet sensitized cyclization reaction of DAEs is well known in the literature (see section 2.1.2).

Butane-2,3-dione (biacetyl, **BA**) was chosen as an intermolecular sensitizer undergoing quantitative intersystem crossing ($\Phi_{ISC} = 1$[158]). It can be selectively excited at 405 nm in the presence of the ring-open or ring-closed isomers of **1c**. Although its absorption is red shifted to that of the ring-open isomer of **1c** the triplet energy of **BA** is within the range of the triplet energy of **1c(o)** which was estimated by TD-DFT calculation (Table 10). Thus, effective triplet energy transfer from **BA** to the ring-open isomer of **1c** can be expected.

In fact, irradiation of a thoroughly degassed mixture of **1c** and excess **BA** in acetonitrile with 405 nm light results in efficient formation of the ring-closed isomer (Figure 27a). Importantly, when irradiating **1c** alone or the mixture of **1c** and **BA** in the presence of oxygen no changes in the absorption spectra can be observed. A significant difference in the rate of conversion can be observed comparing a sample that was thoroughly degassed by freeze-pump-thaw cycles and one that was only treated with a stream of argon for 10 min (Figure 28a). The observed impact of traces of oxygen and the fact that in presence of the ring-open isomer of **1c** the phosphorescence of **BA** is quenched (Figure 27b) proves the involvement of triplet species and the efficient energy transfer from the **BA** moiety to the DAE.

Table 10. Experimental and calculated singlet and triplet energies of **1c**, **BA**, and **MB**.

comp.	E_S *(exp.)*	E_S *(calc.)*[a]	E_T *(exp.)*	E_T *(calc.)*[a]
1c(o)[b]	4.05 eV (306 nm)	4.21 eV (294 nm)		2.52 eV (492 nm)
1c(c)[b]	2.37 eV (523 nm)	2.36 eV (526 nm)		0.71 eV (1736 nm)
1c(bp)[b]	2.44 eV (508 nm)	2.42 eV (513 nm)		0.88 eV (1411 nm)
BA	2.83 eV (438 nm)[b] 2.77 eV (448 nm)[d]		2.55 eV (486 nm)[c] 2.45 eV (507 nm)[d]	
MB	1.89 eV (656 nm)[b] 1.87 eV (665 nm)[d]		1.43 eV (867 nm)[d]	

a) TD-DFT/PCM(acetonitrile)/CAM-B3LYP/6-311+G(2d,p).
b) from absorbance spectrum in acetonitrile.
c) high energy onset of phosphorescence spectrum in acetonitrile.
d) "in polar solvent", taken from reference [158].

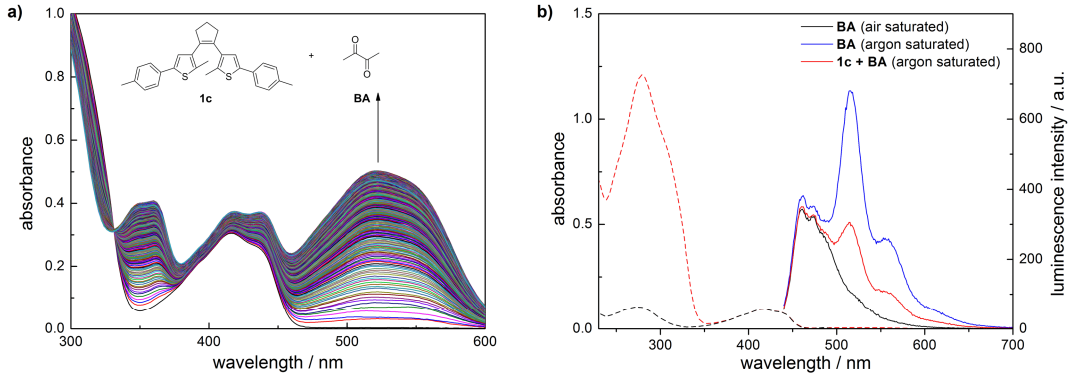

Figure 27. a) UV/Vis spectra recorded during irradiation with 405 nm light (500 W Xe(Hg), $I_0 = 7.29 \cdot 10^{-10}$ E s^{-1} cm^{-2}) of a solution of **1c** ($c = 3.1 \cdot 10^{-5}$ M) and biacetyl **BA** ($c = 1.0 \cdot 10^{-2}$ M) in acetonitrile, degassed by three freeze-pump-thaw cycles. b) Absorbance and emission ($\lambda_{exc} = 416$ nm) spectra of biacetyl **BA** ($c = 5.7 \cdot 10^{-3}$ M) and a mixture of **1c** ($c = 3.1 \cdot 10^{-5}$ M) and **BA** ($c = 5.7 \cdot 10^{-3}$ M) in acetonitrile.

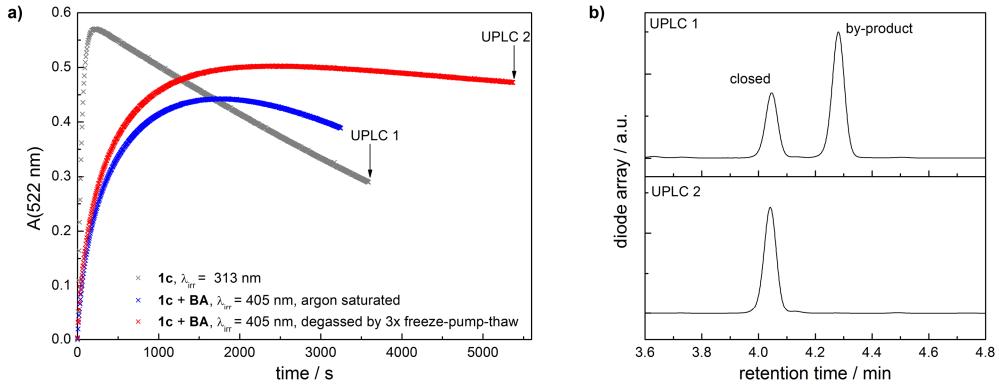

Figure 28. a) Evolution of visible absorbance of a mixture of **1c** ($c = 3.1 \cdot 10^{-5}$ M) and biacetyl B**A** ($c = 1.0 \cdot 10^{-2}$ M) in acetonitrile, degassed by three freeze-pump-thaw cycles or by passing a slow stream of argon through the solution for 10 min, respectively, during irradiation with 405 nm light (500 W Xe(Hg), $I_0 = 7.29 \cdot 10^{-10}$ E s^{-1} cm^{-2}) as well as of a solution of **1c** ($c = 3.1 \cdot 10^{-5}$ M) in acetonitrile during irradiation with 313 nm light (500 W Xe(Hg), $I_0 = 1.25 \cdot 10^{-9}$ E s^{-1} cm^{-2}). b) UPLC traces (diode array detector integrated between 250 nm – 800 nm) of samples of **1c/BA** and **1c** taken at the end of the irradiation with 405 nm and 313 nm light, respectively.

Due to the low absorbance of **BA** the absolute rate of conversion to the ring-closed isomer via the triplet pathway is relatively low compared to the isomerization of **1c** alone with 313 nm light (Figure 28a). However, determination of an effective quantum yield for the cyclization at 405 nm with the initial slope method gave a surprisingly high value of $\Phi_{AB,eff} = 0.40$. Of course this value is highly dependent on concentrations, light intensity, and triplet lifetimes due to the bimolecular triplet energy transfer process. Nevertheless, the fact that the effective quantum yield of the sensitized ring-closure in this experiment is as high as the quantum yield for ring closure by direct excitation with 313 nm light ($\Phi_{AB} = 0.43$, see Table 8) shows that the cyclization reaction of **1c** within the triplet state is highly efficient. Kinetic traces recorded during irradiation of **1c** alone with 313 nm light or the mixture of **1c** and **BA** with 405 nm light both show the emergence of a (pseudo)PSS with a subsequent decrease of the

absorbance in the visible range. However, UPLC analysis of the irradiated samples reveals that the by-product is exclusively formed upon excitation with 313 nm light (Figure 28b). Note that the decrease in absorbance during the sensitized cyclization can be attributed to residual traces of oxygen in the degassed solution, being transformed into singlet oxygen by the sensitizer and thus unspecifically degrading the DAE.

In a second experiment methylene blue (**MB**, $\Phi_{ISC} = 0.52$[158]) was used to sensitize the formation of the triplet selectively for the ring-closed isomer of **1c**, whose triplet energy was calculated to lie way below that of **MB** (Table 10). Importantly, **MB** can be selectively excited at longer wavelengths than **1c(c)**, thus preventing (singlet) resonance energy transfer. As expected, during irradiation of a mixture of **1c(o)** and **MB** or a mixture of **1c(c)** and **MB** with 654 nm light no changes in the absorbance spectra could be observed (Figure 29). While triplet energy transfer from **MB** to **1c(o)** is not possible and thus no reaction can take place, the latter result points to the inability of the triplet excited state of the ring-closed isomer either to undergo ring-opening or to form the by-product. For the ring-opening reaction this has been attributed earlier to the presence of a barrier on the triplet reaction pathway.[48b] From the photochemistry of the singlet excited state of the ring-closed isomer can be deduced that the barrier for by-product formation is even higher than the barrier for ring-opening[45] as excess energy in terms of excitation with UV light is needed. In analogy to ring-opening, by-product formation in the triplet excited state following the same pathway would not be expected.

The singlet and triplet pathways for the isomerization and by-product formation of DAEs are summarized in Scheme 36. It shows that the sensitized cyclization of a DAE via its triplet state in combination with low energy excitation of the ring-closed isomer for the reverse ring-opening reaction may represent an alternative way to guarantee high fatigue resistance while efficiently operating the switch, given strict oxygen-free conditions are applied.

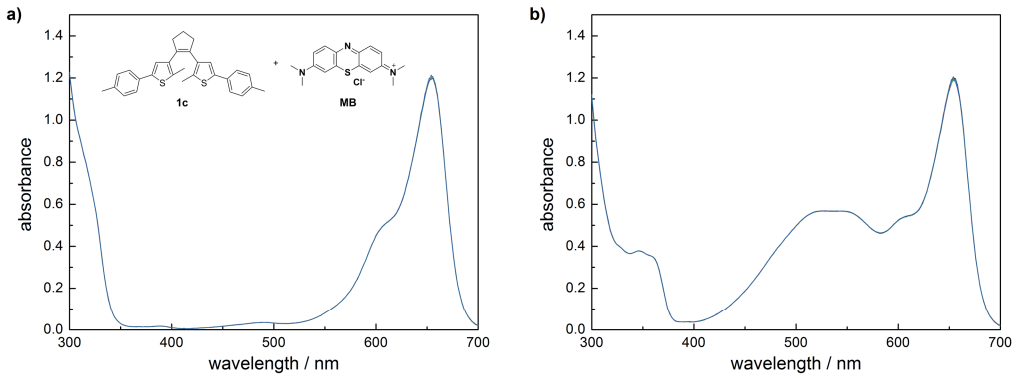

Figure 29. UV/Vis spectra recorded during irradiation with 654 nm light (500 W Xe(Hg)) of a solution of **1c** ($c = 3.1 \cdot 10^{-5}$ M) and methylene blue **MB** ($1.5 \cdot 10^{-5}$ M) in acetonitrile, degassed by passing a slow stream of argon through the solution for 10 min, a) before and b) after irradiation with 313 nm light to induce ring-closure.

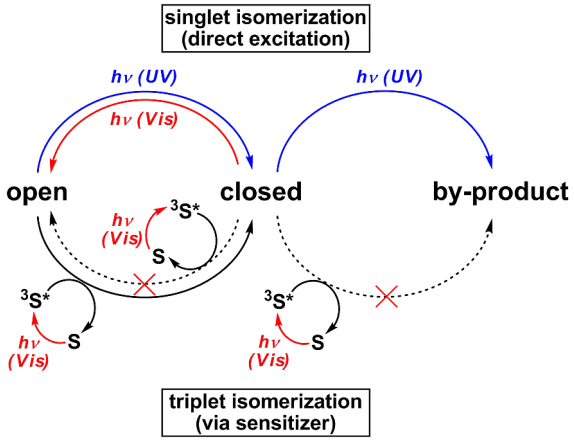

Scheme 36. Singlet and triplet pathways for the isomerization and by-product formation of diarylethenes (S = triplet sensitizer).

4.3.5 Electronic effects of the substituents

To estimate the effects of the substituents on the DAEs' electronic structure cyclic voltammetry was performed. Cyclic voltammograms of all compounds are collected in Appendix 4. Perhydrocyclopentene substituted dithienylethenes **1a-1e**, **5a**, **5b**, and **6c** show the expected electrochemical behavior consisting of an irreversible oxidation of the ring-open isomer followed by the appearance of cathodic waves at similar potentials as the two reversible oxidations of the respective ring-closed isomers, which indicates a thermal cyclization reaction (see section 2.1.4).[23] For the acceptor substituted analogues **1f**, **1g**, and **1i** the oxidative cyclization cannot be observed. The same holds for thiazole substituted compounds **3d** and **3i**. For the perfluorocyclopentene derivatives an oxidative cyclization takes place only for the most electron-rich derivative **2c**. Reductions, which are generally observed within the accessible potential range for all ring-closed isomers and only for acceptor substituted ring-open isomers, do not induce isomerization reactions.

Peak potentials (against Fc/Fc^{+}) reported in Table 11 show that by changing the substitution pattern the electron density within the π-electronic system is varied over a broad range. Thus, ring-open isomers become oxidized between 0.13 V in case of strong donor substitution (**1a**) and around 2.00 V in case when the perfluorocyclopentene bridge is used (**2i**, **2j**, **4i**). The same trend is observed for ring-closed isomers with their first oxidation potential E_p^{a1} between -0.37 V (**1a**) and 1.35 V (**4i**). In particular, oxidation potentials of ring-closed isomers may relate with the observed trends in the fatigue behavior of the photochromes. In fact, starting from the parent dithienylcylopentene **1c**, the largest effect on oxidation potentials

[23] For all compounds oxidative cyclization was further proven by performing two consecutive cyclic voltammetric scans on the ring-open isomer. Upon the second scan anodic waves corresponding to the ring-closed isomer are observed.

has the perfluorination of the cyclopentene bridge shifting E_p^{a1} of the ring-closed isomer by 520 mV (**1c** vs. **2c**) to more positive values, accompanied by the massive improvement of fatigue resistance. Introduction of CF_3 groups in **1i**, exerting the same effect on the fatigue, gives a potential shift of 260 mV. Comparing **1i** and **2i** one finds again a shift of 520 mV arising from the perfluorination of the bridge, nevertheless there is no difference in the rate of by-product formation between these two structures. The replacement of CF_3 with SF_5 groups, giving rise to the structure with the lowest rate of by-product formation, is accompanied by a further increase of the oxidation potential by 110 mV.

In contrast to this general trend, the thiazole containing structure **3d** becomes oxidized at slightly higher potentials than **1i**, although showing a much higher rate of by-product formation. Again, introduction of CF_3 groups in **3i** shifts the potential by 210 mV.

Table 11. Anodic and cathodic peak potentials determined by cyclic voltammetry in acetonitrile. All values are reported against the ferrocene/ferrocenium redox couple as external standard.

comp.	open isomer		closed isomer		
	E_p^{a1} / V	E_p^{c1} / V	E_p^{a1} / V	E_p^{a2} / V	E_p^{c1} / V
1a	0.13	< -2.80	-0.37	-	-2.40
1b	0.62	< -2.80	-0.07	0.06	-2.30
1c	0.79	< -2.80	-0.02	0.20	-2.25
1d	0.79	< -2.80	0.03	0.27	-2.17
1e	0.81	-2.86	0.07	0.31	-2.18
1f	1.08	-2.79	0.29	0.55	-1.90
1g	0.87	-2.48	0.13	0.39	-1.87
1i	1.08	< -2.80	0.24	0.53	-1.84
2c	1.08	-2.53	0.50	-	-1.56
2i	1.79	-2.40	0.76	-	-1.27
2j	> 2.00	-2.63	0.87	1.02	-1.20
3d	0.84	-2.85	0.40	0.61	-1.99
3i	1.06	-2.38	0.61	0.88	-1.61
4i	> 2.00	-2.11	1.35	-	-1.08
5a	0.22[a]	-2.71	-0.13	0.09	-2.02
5b	0.74	< -2.80	0.05	0.28	-2.02
6c	0.77	< -2.80	-0.02	0.22	-2.45

[a] E_p^{a2} = 0.64 V

Another example showing that there is no straightforward correlation between electrochemical oxidation potentials and photochemical fatigue is the pentafluorophenyl substituted compound **1f**. It was synthesized with the expectation that the pentafluorophenyl group would have a similar effect as the 3,5-bis(trifluoromethyl)phenyl group in **1i**. Indeed, both structures are oxidized at very similar potentials in the ring-open and ring-closed state. However, for **1f** the quantum yield for by-product formation is larger by more than one order of magnitude.

DFT calculations on the B3LYP/6-31G(d) level of theory were performed to estimate the influence of the substituents on the geometry and relative ground state stability of the three isomers. Therefore, the hypothetical derivatives **1j** (R = 3,5-$(SF_5)_2$), **2d** (R = H), and **3c** (R = Me) were also included. Remarkably, in all cases except for DAE **1f**[24] the geometry optimization led to very similar structures of the DAE cores independent of the substituents on the phenyl rings, with only small, non-systematic variations in geometric parameters such as dihedral angles, the distance between the ring-closing carbons, or the lengths of the C-S bonds (Table 12). Computed NICS values[159] of the thiophene or thiazole rings in the ring-open isomers, indicative for their aromatic stabilization energy, also show only minimal variation upon exchange of substituents (Table 12). However, ground state energies of the ring-closed isomers and by-products, relative to the respective ring-open isomers, slightly rise within a series of similar structures by going from donor to acceptor substitution (Figure 30, Table 12). While the by-products are generally much less stable than the ring-closed isomers, their further destabilization by acceptor substitution may lead to an increased fatigue resistance. Nevertheless, comparing the different series (cyclopentene vs perfluorocyclopentene and thiophene vs. thiazole switches) it is obvious that for compounds experimentally possessing similar fatigue behavior (*e.g.* **1i** and **2i**) the stabilities of the by-products are very different. Thus, more advanced quantum mechanical calculations concerning stabilities in the excited state and reaction barriers will be needed to rationalize the experimental trends.

[24] For the pentafluorophenyl substituted DAE **1f** ground state geometries of the ring-closed isomer and by-product significantly deviate in the dihedral angle θ between the thiophene and phenyl ring. With values of 28° and 61° for **1f(c)** and **1f(bp)**, respectively, θ is significantly increased compared to other dithienylethenes showing values between 12-21° and 35-38°, respectively. This is also reflected in increased relative ground state energies for the ring-closed isomer and by-product. Strong twisting of the pentafluorophenyl group may also explain the hypsochromically shifted UV/Vis spectra experimentally observed for all isomers of **1f**.

Table 12. Energies, geometrical parameters, and NICS values of DFT-optimized structures on the B3LYP/6-31G(d) level of theory.

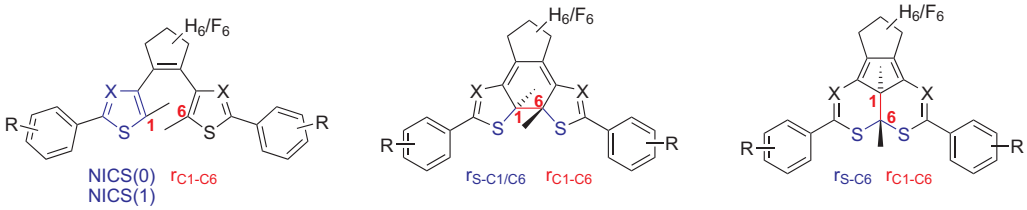

comp.	ring-open isomer			ring-closed isomer			by-product		
	r_{C1-C6} / Å	NICS(0)	NICS(1)	E^a / kJ mol^{-1}	r_{C1-C6} / Å	$r_{S-C1/C6}$ / Å	E^a / kJ mol^{-1}	r_{C1-C6} / Å	r_{S-C6} / Å
1a	3.651	-9.75	-7.66	43.23	1.546	1.874	88.03	1.537	1.872
1b	3.658	-9.83	-7.77	47.44	1.545	1.874	89.66	1.537	1.872
1c	3.664	-9.79	-7.80	49.07	1.546	1.875	91.53	1.537	1.872
1d	3.666	-9.79	-7.81	50.62	1.545	1.875	92.30	1.537	1.872
1e	3.657	-9.84	-7.87	50.32	1.545	1.875	91.62	1.537	1.872
1f	3.664	n.d.	n.d.	66.72	1.545	1.873	108.90	1.538	1.874
1g	3.661	-9.64	-7.79	51.65	1.546	1.874	93.75	1.536	1.872
1i	3.669	-9.75	-7.85	53.00	1.545	1.876	92.87	1.538	1.873
1j	3.672	-9.74	-7.87	54.34	1.545	1.876	93.65	1.538	1.874
2c	3.674	-9.90	-7.86	54.35	1.548	1.870	110.40	1.533	1.872
2d	3.676	-9.90	-7.87	56.90	1.548	1.871	112.32	1.533	1.872
2i	3.687	-9.89	-7.94	63.43	1.548	1.872	117.83	1.534	1.873
2j	3.693	-9.90	-7.97	67.05	1.548	1.873	120.40	1.535	1.874
3c	3.642	-8.44	-7.96	40.76	1.546	1.864	121.03	1.530	1.868
3d	3.647	-8.44	-7.99	42.15	1.546	1.865	121.77	1.530	1.868
3i	3.644	-8.55	-8.15	46.12	1.545	1.866	121.85	1.530	1.870

a) Energy relative to ring-open isomer including zero-point correction.

Figure 30. Energies (including zero-point corrections) of ring-closed isomers and by-products, relative to the corresponding ring-open isomers, as obtained from DFT calculations on the B3LYP/6-31G(d) level of theory. Calculations were also performed on the hypothetical derivatives **1j**, **2d**, and **3c**. Compound **1f** was omitted due to deviations in its ground state geometry.

4.3.6 Summary

A detailed investigation of the photochemistry of a series of DAEs, systematically varying the nature of the hetaryl moieties, the substituents on the adjacent phenyl rings, and the bridging moiety, allowed for the identification of the previously known annulated by-product as the major source of fatigue appearing ubiquitously over the broad range of structures. Photokinetic measurements and evaluation of quantum yields for the elementary photochemical processes revealed a strong dependency of the rate of by-product formation on the electronic properties of the substituents. It appears that the more and the stronger electron-accepting units are introduced to the parent structure the less fatigue due to formation of the annulated isomer is observed. While the stabilizing effect of the perfluorocyclopentene compared to perhydrocyclopentene bridge was recognized earlier, it is found that in the latter structures an equally high fatigue resistance can be imparted by substitution with 3,5-bis(trifluoromethyl)phenyl groups. By exchanging CF_3 with SF_5 groups a further improvement can be observed, making compound **2j** the DAE structure with the highest fatigue resistance studied in this work. Importantly, CF_3 or SF_5 groups are chemically inert and their introduction into DAEs does not alter their efficient isomerization between the ring-open and ring-closed isomers.

While the results show a clear correlation between the electronic nature of the substituents and the fatigue behavior of DAE photochromes, they are only phenomenological at the current point. Correlations with ground state properties such as electrochemical redox potentials or computed geometric parameters and relative stabilities are not straight forward. From a mechanistic standpoint substitution of the DAE core with donor or acceptor groups may alternate the relative stability of intermediates or transition state structures on pathways leading to either ring-opening or by-product formation after excitation of the ring-closed isomer.[45] However, for obtaining a deeper understanding the observation of by-product formation using time-resolved spectroscopic techniques together with a theoretical rationalization supported by high level quantum mechanical calculations of the excited state potential energy surface will be needed.

Based on the experimental results a strategy is proposed for imparting excellent fatigue resistance to DAEs while allowing a high flexibility in the choice of the components out of which the photochromic system may be assembled. Unsymmetrically substituted derivatives **5a** and **5b** show that it is sufficient to substitute one hetaryl ring with a 3,5-bis(trifluoromethyl)phenyl group, leaving the other aryl ring and the bridging moiety of the DAE structure open to modifications. Notably, the reported compounds demonstrate that the performance of dithienylperhydrocyclopentenes, which typically show a low reversibility in their switching behavior, can be massively improved. Experiments using an organic sensitizer to induce the cyclization reaction of the ring-open isomer via its triplet state revealed that the by-

product is not formed at all under these conditions, rendering triplet sensitized isomerization an attractive alternative for the operation of DAEs.

4.4 Orthogonally switchable DAEs and electrochemical fatigue[25]

4.4.1 Introduction

As shown in section 2.1.4 of this work, many dithienylethenes offer the possibility to induce their isomerization reaction not only by light but also by oxidation or reduction of the molecule. In principle the combination of different stimuli for the operation of switchable molecules is highly promising in terms of information storage and signal processing.[160] Furthermore, it may allow for a high selectivity in addressing ensembles of different switches, which is difficult to achieve when using purely photochromic compounds relying on their full spectral separation.[161] Especially in this context, the *orthogonal* implementation of photochemical and electrochemical responsiveness to a single molecule or a molecular ensemble, *i.e.* the two stimuli lead to a different reaction outcome, is highly interesting, as it would allow for the selective addressing of a multitude of different states.[60b] Note that for simple dithienylethenes reported in the literature the redox induced isomerization is a process *parallel* to the light induced reactions, *i.e.* both yield the same isomerization product.

In a diploma thesis preceding this work[75a] DAE motif **11a** (Scheme 37), possessing electron rich morpholino substituted thiazole heterocycles and an electron deficient *N-tert*-butylmaleimide bridge, was synthesized during studies concerned with the effect of different bridging moieties and donor or acceptor substituents on dithiazolylethenes. Thereby, DAE **11a** was identified to be non-photochromic in acetonitrile solvent, *i.e.* no isomerization reaction takes place upon UV-irradiation. However, by cyclic voltammetry oxidative ring closure was observed, which is very untypical for DAEs bearing thiazole heterocycles.[26]

Here the potential of DAE motif **11a** as a molecular switch orthogonally operated by electrochemical (for ring-closure) and photochemical (for ring-opening) stimuli is investigated in detail. By introduction of trifluoromethyl groups on the ring-closing carbons, leading to compound **11b**, the fatigue resistance of the switching process is significantly enhanced. Investigation of an unsymmetrically substituted analogue **11c** gives insights into the mechanism of the oxidative ring-closure. The perhydrocyclopentene bridged derivative **12**[75a] serves as a reference compound showing both photochemical and electrochemical ring-closure.

[25] Large parts of this section have been published: M. Herder *et al.*, *Chem. Sci.* **2013**, *4*, 1028-1040.

[26] All other dithiazolylethene motifs investigated in this work and before give irreversible oxidations in their ring-open and ring-closed forms with no sign of an isomerization reaction. See CV data of compounds **3d**, **3i**, and **4i** in Appendix 4 as well as CV data of other dithiazolylmaleimides in reference [75a].

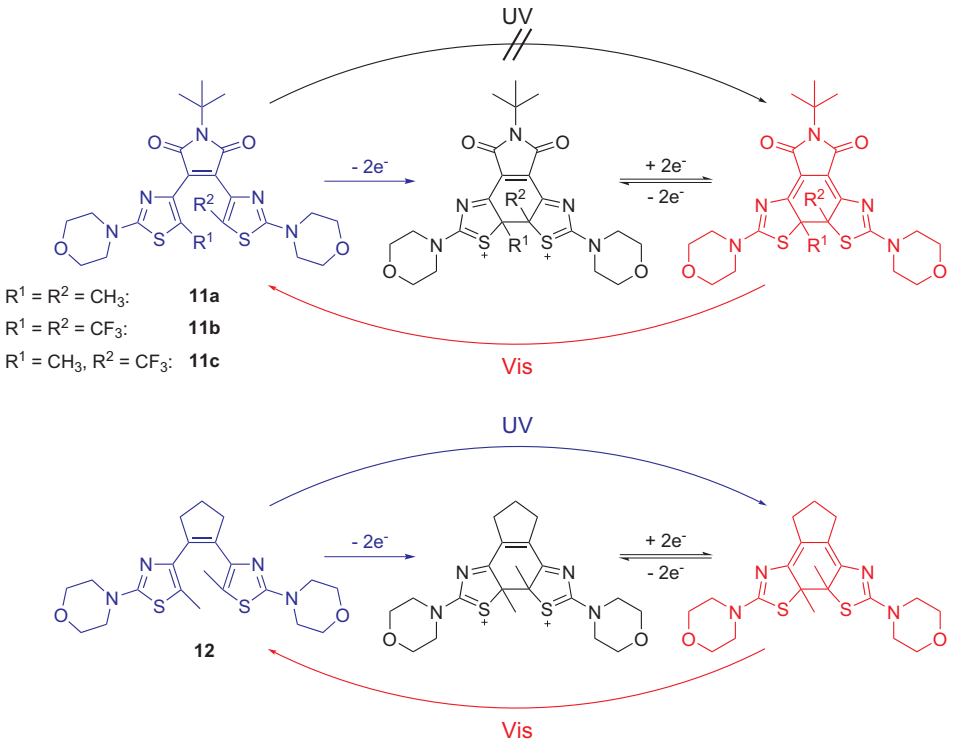

Scheme 37. Isomerization behavior of morpholino substituted dithiazolylethenes.

4.4.2 Photochemical behavior

UV/Vis-spectra of ring-open isomers of **11a**, **11b**, **11c**, and **12** were recorded in acetonitrile (Figure 31, Table 13). Besides an intense absorption in the UV originating from the aromatic thiazole moieties the structurally related compounds **11a**, **11b**, and **11c** show a broad absorption band in the visible range between 350 – 500 nm. This band can be attributed to the charge-transfer from the electron-rich morpholinothiazoles to the strongly electron-deficient *tert*-butylmaleimide bridge (*vide infra*). Compared to the parent structure **11a**, for compounds **11b** and **11c** the intensity of the CT-band is significantly lower and its position is shifted hypsochromically by 40 nm and 10 nm, respectively, reflecting the reduced electron-density of the CF_3 substituted morpholinothiazole cores.

As proposed in the literature for analogous dithienylmaleimides,[39a] such a pronounced CT-behavior between the aryl moieties and the bridge moiety of DAEs can lead to a diminished photochemical cyclization efficiency due to the formation of a TICT (Twisted Intramolecular Charge Transfer) excited state, which is characterized by a pronounced twisting of the single bond between the electron donating and the electron accepting parts of the molecule.[40] In fact, during irradiation of a yellow solution of **11a** in acetonitrile with UV light (λ_{irr} = 280 nm) or with visible light (λ_{irr}= 436 nm) no changes in the UV/Vis spectrum could be observed (Figure 31a). Furthermore, analysis of the reaction mixture by UPLC did not show any new photoproduct. Only when exposed to UV irradiation over an extended time period using a 1000 W Xe arc lamp with a broad UV bandpass filter some unspecific degradation (bleaching)

took place. According to the TICT-model, the usage of cyclohexane as a non-polar solvent allowed for the photochemical cyclization reaction to take place to some extent (Figure 32, Table 14). Nevertheless, its efficiency was extremely low with a quantum yield of 0.05 for the ring-closure of **11a** and a conversion of only 16% in the PSS. A similar lack of photochemical reactivity for the ring-open isomers was also observed for the CF_3 substituted derivatives **11b** and **11c**.

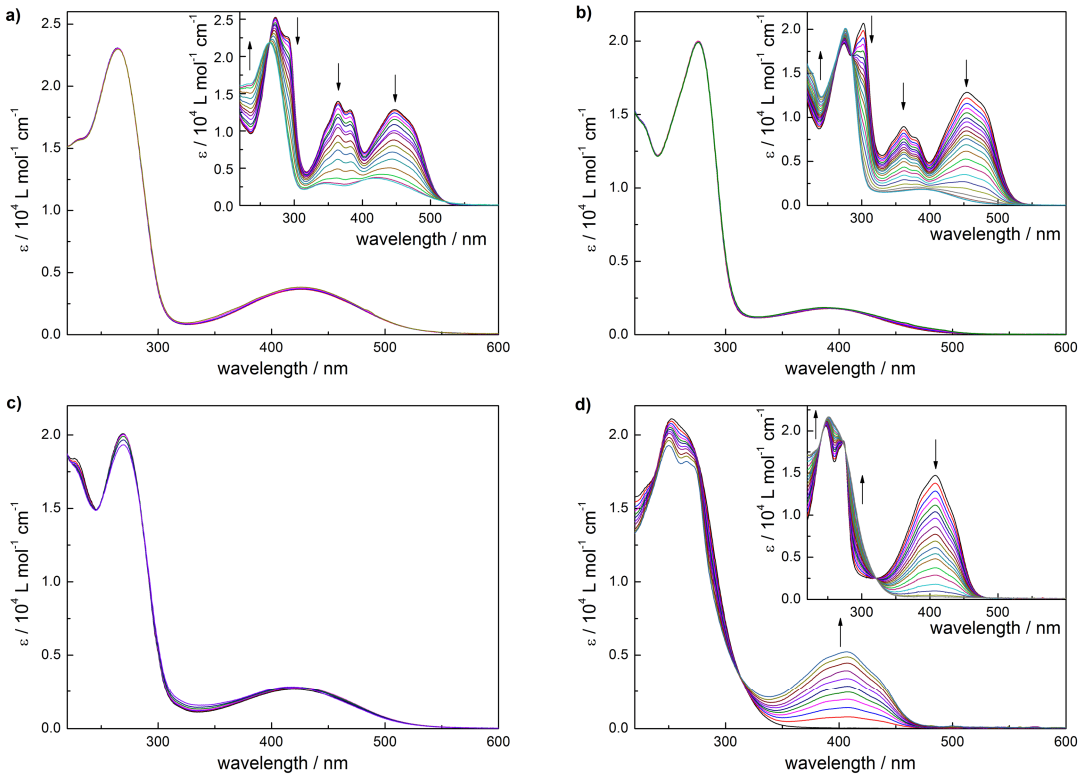

Figure 31. UV/Vis-spectra during the course of irradiation of acetonitrile solutions of a) **11a**, b) **11b**, c) **11c**, and d) **12** with UV light (280 nm, 1000 W Xe, interference filter). Insets show UV/Vis spectra in acetonitrile during the irradiation with visible light (436 nm, 1000 W Xe, interference filter) of the respective isolated ring-closed isomers **11a(c)**, **11b(c)**, and **12(c)**, which were prepared separately via oxidation of the ring-open compounds. All concentrations $5.0 \cdot 10^{-5}$ M.

Table 13. Photophysical properties of DAEs **11a**, **11b**, **11c**, and **12** in acetonitrile.

comp.	λ_{max} / nm (ε / 10^4 M^{-1} cm^{-1})		Φ_{AB} (280 nm)[a]	Φ_{BA} (436 nm)[a]	PSS (280 nm)[b]
	ring-open isomer	ring-closed isomer			
11a	265 (2.31), 430 (0.39)	364 (1.40), 447 (1.29)	< 0.001	0.13	< 1%
11b	276 (2.01); 390 (0.18)	361 (0.89); 454 (1.29)	< 0.001	0.37	< 1%
11c	269 (1.89), 420 (0.25)	n.d.[c]	< 0.001	n.d.[c]	< 1%
12	252 (2.11), 268 (shoulder)	408 (1.47)	0.13	0.26	36%

a) Quantum yields obtained from the initial slope of photoconversion (500 W Xe(Hg), azobenzene and Aberchrome 670 actinometry).
b) Conversion to the ring-closed isomer in the PSS reached after UV irradiation (280 nm, 1000 W Xe).
c) Compound **11c(c)** was not isolated.

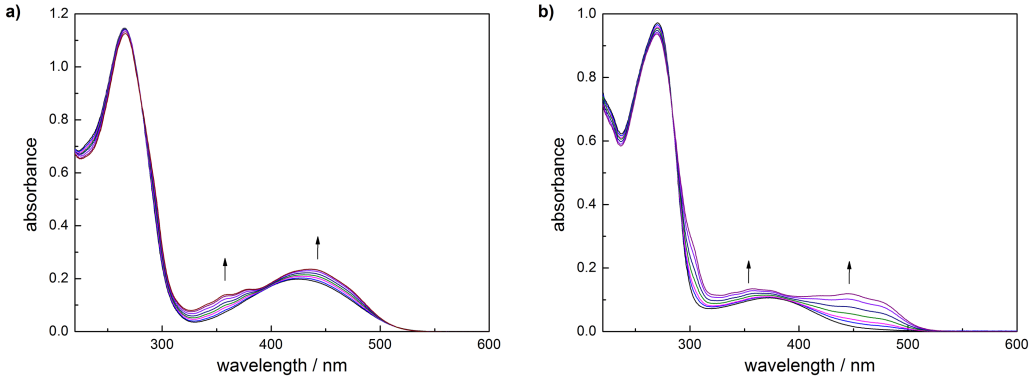

Figure 32. UV/Vis spectra during the course of irradiation of solutions of a) **11a** and b) **11b** in cyclohexane (c = $5 \cdot 10^{-5}$ M) with UV-light (λ_{irr} = 280 nm, 1000 W Xe) until reaching the PSS.

Table 14. Photophysical properties of DAEs **11a** and **11b** in cyclohexane.

comp.	λ_{max} / nm (ε / 10^4 M^{-1} cm^{-1})		Φ_{AB} (280 nm)[a]	PSS (280 nm)[b]
	ring-open isomer	ring-closed isomer		
11a	266 (2.44), 425 (0.42)	356 (1.04), 443 (1.02)	0.05	16%
11b	270 (2.07), 373 (0.23)	449 (1.16)	0.05	16%

a) Quantum yields obtained from the initial slope of photoconversion (500 W Xe(Hg), azobenzene).
b) Conversion to the ring-closed isomer in the PSS reached after UV irradiation (280 nm, 1000 W Xe).

Nevertheless, the ring-closed isomers **11a(c)** and **11b(c)** could be isolated via oxidation of the respective ring-open isomers (see section 4.1.5). They show an intense absorption in the visible region split into two bands (insets of Figure 31a-b). Upon illumination of acetonitrile solutions of **11a(c)** and **11b(c)** with visible light (λ_{irr}= 436 nm) both bands diminish rapidly and the spectra of the respective ring-open compounds are obtained. Although the spectra of the ring-closed and the ring-open isomers overlap significantly at the irradiation wavelength complete conversion to the ring-open isomers is achieved, as the latter are photochemically inactive. The quantum yields for the ring-opening of **11a(c)** and **11b(c)** with 436 nm light were determined to be relatively high with values of 0.13 and 0.37, respectively. Notably, the ring-opening process is significantly enhanced for compound **11b(c)**, which may be attributed to the strong electron-withdrawing character of the CF_3 groups attached on the reactive carbon atoms.[31b], [27]

Contrasting this unidirectional photochemical switching behavior of DAEs **11a**, **11b**, and **11c,** bearing a maleimide bridge, compound **12**, possessing a cyclopentene as bridging unit, shows photochemical bidirectionality to some extent (Figure 31d). UV/Vis spectra as well as UPLC-traces recorded during irradiation of a colorless solution of **12(o)** in acetonitrile with UV

[27] See also section 4.5.3 for photochemical properties of α-CF_3 substituted DAEs.

light (λ_{irr}= 280 nm) indicate the formation of the ring-closed isomer **12(c)**. However, only 36% of **12(c)** are formed in the PSS due to a high ring-opening quantum yield of 0.26 while the ring-closing quantum yield was determined to be 0.13. Obviously, the lack of a charge transfer between the thiazole moieties and the cyclopentene bridge, indicated by the absence of a visible absorption in the case of the ring-open isomer, restores the reversibility of the photochemical reaction typical for DAEs. An intramolecular charge transfer interaction is clearly essential to install unidirectional photochemical behavior.

To get further insight into the photochemical processes that lead to the observed lack of cyclization efficiency theoretical investigations were performed.[28] Ground state structures were optimized, vertical excitation energies were calculated, and structures in the first excited state were optimized using (TD-)DFT on the CAM-B3LYP/PCM(acetonitrile)/6-31G(d) level of theory. The weak, broad band in the visible range for ring-open isomers of **11a**, **11b**, and **11c** is reproduced by vertical excitation energies and can be attributed to a HOMO→LUMO transition. Isocontour plots of the frontier molecular orbitals (exemplarily shown for **11a** in Figure 33, left) show that the HOMO and LUMO are localized on the morpholinothiazoles and the maleimide bridge, respectively. Note also that for the LUMO, which dominates the photochemical pericyclic reaction according to the Woodward-Hoffman rules, only small coefficients are found on the ring-closing carbon atoms. For compounds **11b** and **11c** the HOMO energies are lowered due to the electron accepting CF_3 groups, reproducing the experimentally observed blue shift of the CT band. For compound **12** no such CT transition is found and the HOMO and the LUMO are delocalized over the whole hexatriene backbone (Figure 33, right). Notably, for compounds **11a** and **11c** geometry optimization in the first excited state lead to stable minimum structures showing a certain twist between the thiazole rings and the maleimide bridge, while for **12** no stable minimum could be found. Instead the calculations converged towards a conical intersection with a decreased distance between the ring-closing carbons. However, in gasphase calculations the same behavior was observed for **11a**, making a clear assignment of TICT states by theory difficult.

[28] All quantum mechanical calculations discussed in this section were performed by Manuel Utecht in the group of Prof. Peter Saalfrank, Department of Chemistry, Universität Potsdam. They shall be briefly discussed here, for details the reader is referenced to: M. Herder *et al.*, *Chem. Sci.* **2013**, *4*, 1028-1040.

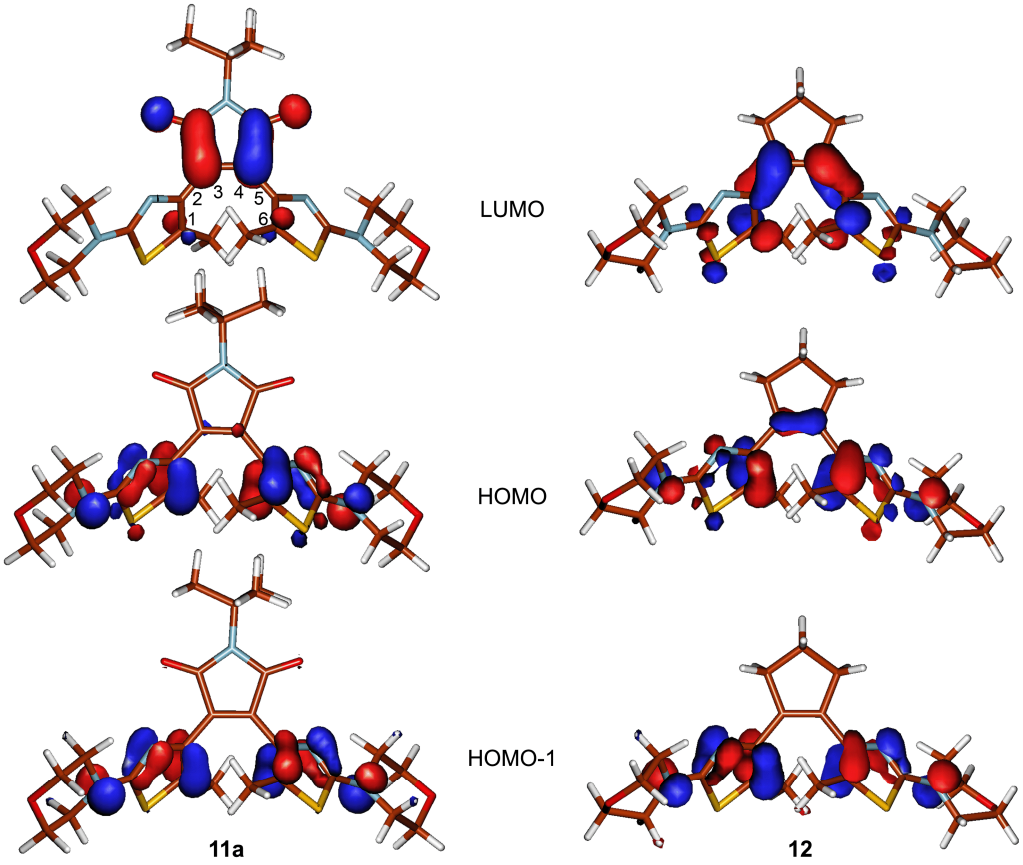

Figure 33. Isocontour plots of frontier molecular orbitals for compounds **11a** (left) and **12** (right) obtained on the CAM-B3LYP/PCM(acetonitrile)/6-31G(d) level of theory.

4.4.3 Electrochemical behavior

Upon oxidation of **11a** a single irreversible oxidation wave at a potential of 0.57 V is observed (Figure 34a, Table 15), which is associated with a charge transfer of two electrons per molecule, as determined by controlled potential coulometry. The parent 5-methyl-2-morpholinothiazole **46** is oxidized at a very similar potential of 0.52 V, thus it can be assumed that the maleimide bridge has only minor influence on the oxidation potential of **11a** and that the electron transfer originates from both electron-rich morpholinothiazole moieties. During the return scan the stepwise reduction of a new species can be observed at potentials of 0.26 V and 0.09 V corresponding to two one-electron processes. When a second scan-cycle is performed reversible oxidation waves arise at 0.15 V and 0.32 V (Figure 34a, inset). In analogy to the known behaviour of dithienylethenes this observation can be explained by a fast thermal reaction of oxidized **11a(o)** to its ring-closed analogue that is subsequently reduced in two steps to **11a(c)**, which possesses significantly lower oxidation potentials due to its conjugated structure. A charge of 2 C mol^{-1} is required during oxidation to fully convert the ring-open isomer to its ring-closed analogue. In fact, **11a(c)** could be isolated by oxidation of the ring-open isomer on a preparative scale using two equivalents of ceric ammonium nitrate as oxidant and subsequent reduction with ascorbic acid (see section 4.1.5). The structure was confirmed via NMR-

spectroscopy and HRMS and its isomerization to the ring-open isomer is observed upon irradiation with 436 nm light (*vide supra*).

The oxidative ring-closure of **11a** was also followed using spectroelectrochemistry (Figure 35). While increasing the potential up to the return point, the formation of an absorption band centered at 360 nm, which is characteristic for the dicationic ring-closed isomer **11a(c)**$^{++}$, can be observed. During the following reduction a bathochromically shifted absorption band around 550 – 750 nm evolves, indicating the presence of the monoradical cation **11a(c)**$^{\bullet+}$. Upon further reduction of the potential this band diminishes again and the characteristic absorption spectrum of **12a(c)** can be observed.

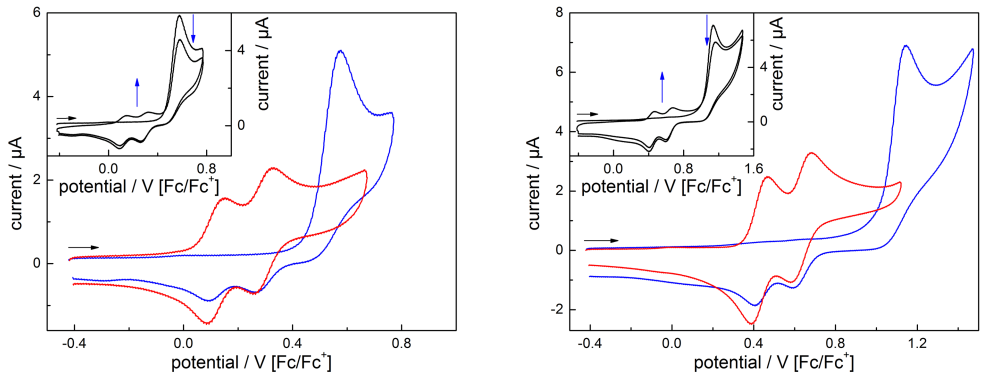

Figure 34. Cyclic voltammograms of the isolated ring-open isomer (blue) and ring-closed isomer (red) of a) **11a** and b) **11b** in acetonitrile/0.1 M Bu_4NPF_6 (c = $1 \cdot 10^{-3}$ M, dE/dt = 1V s^{-1}). Insets show two oxidative cycles consecutively performed on the respective ring-open isomer.

Table 15. Anodic peak potentials of **11a**, **11b**, **11c**, and **12** determined by cyclic voltammetry in acetonitrile. All values are reported against the ferrocene/ferrocenium redox couple as external standard (rev = reversible, qr = quasireversible, irr = irreversible).

comp.	E_p^a / V	
	ring-open isomer	ring-closed isomer
11a	0.57 (irr)	0.15 (rev), 0.32 (rev)
11b	1.14 (irr)	0.47 (rev), 0.69 (rev)
11c	0.70 (qr), 1.23(irr)	0.30 (rev), 0.52(rev)
12	0.27 (irr)	-0.29 (rev), -0.19 (rev)

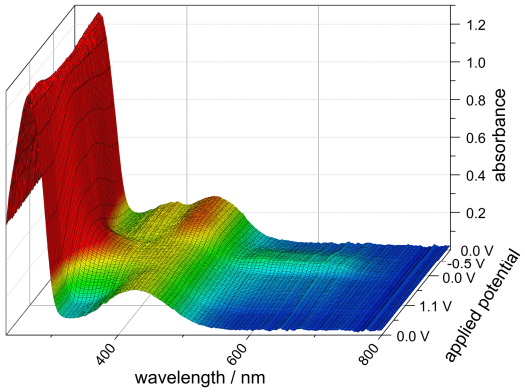

Figure 35. UV/Vis spectral changes during cyclic voltammetry of compound **11a** in acetonitrile/0.1 M Bu_4NPF_6 ($c = 5 \cdot 10^{-4}$ M, $dE/dt = 10$ mV s^{-1}). The potential scan was performed starting from 0 V with return points at 1.1 V and -0.5 V. Potentials are given against the $Ag/AgNO_3$ reference electrode.

To test the potential of **11a** as a switch with orthogonal stimuli it was subjected to several switching cycles consisting of electrochemical oxidation and re-reduction of an acetonitrile solution of **11a(o)** in a divided H-cell and subsequent irradiation of the cell with visible light in front of an 1000 W Xe arc lamp equipped with a longpass filter ($\lambda_{irr} > 430$ nm). During this process UPLC traces as well as UV/Vis spectra of small samples of the reaction mixture were recorded (Figure 36). After the initial oxidation/re-reduction step an absorption band in the visible region corresponding to the ring-closed isomer appeared. UPLC of the reaction mixture indicated a conversion of 51% to the ring-closed isomer **11a(c)**, but showed as well the presence of 32% of a second product **11a(bp)** (Figure 36a). Upon irradiation with visible light ring-opening of **11a(c)** was induced, but the initial UV-spectrum of **11a(o)** could not be restored completely due to the photoinactivity of **11a(bp)**. Upon two more switching cycles the compound was almost completely converted to the by-product, indicated by the loss of absorbance in the visible region and by UPLC.

To isolate the by-product an acetonitrile solution of **11a(o)** was subjected to electrochemical oxidation and was subsequently stirred for 2 h at room temperature. During this time the oxidized species almost quantitatively converted to **11a(bp)**, which was then precipitated in water. Analysis of a low quality x-ray crystal structure of this material recrystallized from chloroform suggests an ionic nature of **11a(bp)** (Figure 36c and Appendix 6). A possible mechanism for its formation is depicted in Scheme 38: In the ring-closed dicationic state **11a(c)**$^{++}$, which is immediately formed upon oxidation of **11a(o)**, one of the thiazole methyl groups loses one proton and a subsequent nucleophilic attack of the neighboring thiazole nitrogen leads to the formation of a 7-membered ring. This assignment is supported by high resolution mass spectrometry proving the loss of one proton. Additionally, NMR spectroscopy of the rearranged product clearly indicates the presence of two different morpholinothiazole moieties and shows a new CH_2 group as a broad signal at room-

temperature. At lower temperatures this signal splits into two doublets showing the restricted conformational flexibility of the 7-membered ring (see Appendix 5)

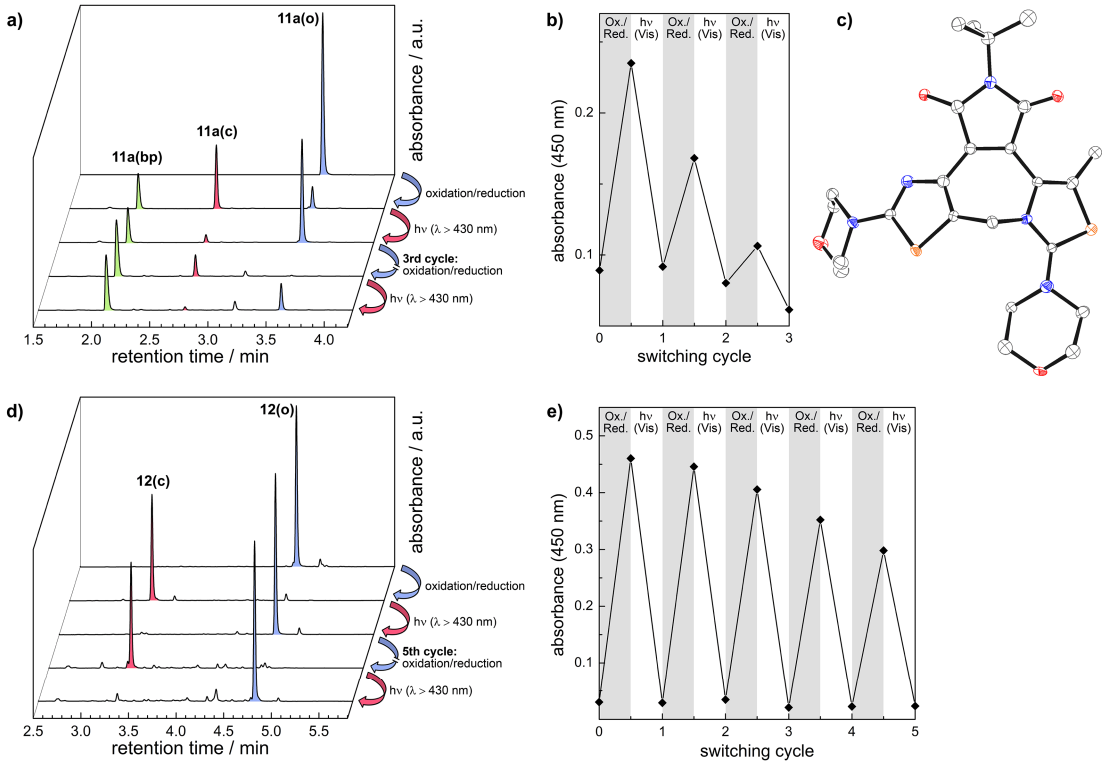

Figure 36. a) UPLC-traces (diode array detector between 250-800 nm) and b) absorbance in the visible region of the reaction mixture recorded during three cycles of electrochemical ring-closure and subsequent photochemical ring-opening of **11a** in acetonitrile/0.1 M Bu_4NPF_6. c) Single-crystal X-ray structure of low quality crystals of by-product **11a(bp)** (ORTEP-drawing, 50% probability thermal ellipsoids, hydrogen atoms and the ClO_4^- anion were omitted for clarity, CCDC 904568). d) UPLC-traces (diode array detector between 250-800 nm) and e) absorbance in the visible region of the reaction mixture recorded during five cycles of electrochemical ring-closure and subsequent photochemical ring-opening of **11b** in acetonitrile/0.1 M Bu_4NPF_6.

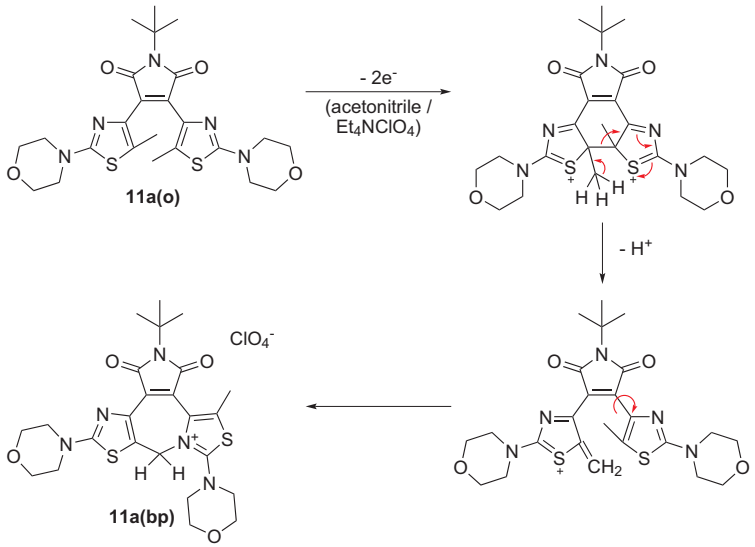

Scheme 38. Proposed mechanism for by-product formation during oxidative ring-closure of **11a(o)**.

In order to increase the fatigue resistance of the overall switching cycle it was investigated if a substitution of the methyl groups in **11a** by trifluoromethyl groups would stabilize the dicationic species by preventing its deprotonation. In fact, the ring-open isomer **11b(o)**, possessing trifluoromethyl groups on both thiazole rings, shows an oxidation wave centered at a peak potential of 1.14 V (Figure 34b). Compared to **11a(o)** this is a relatively large shift by 570 mV to higher potentials proving the strongly electron-withdrawing nature of the CF_3 groups. Nevertheless, the two-electron oxidation of **11b(o)** results as well in ring closing to **11b(c)** as can be seen from the presence of two new reversible oxidation waves in a second scan cycle. These oxidation waves show a significantly smaller shift to higher potentials of 320 mV when compared to **11a(c)**. This is due to the formation of a quaternary carbon at the 5- and 5'-position of the thiazole moieties during the cyclization separating the CF_3 groups from the π-system.

When **11b** is subjected to repeated electrochemical ring-closure and photochemical ring-opening a clearly enhanced performance of the reported system can be observed. UV/Vis-spectra measured from small samples of the reaction mixture show the reversible formation of the absorption bands in the visible range, which correspond to the ring-closed isomer (Figure 36e). UPLC traces obtained during this experiment show almost quantitative conversion to **11b(c)** after each oxidation/re-reduction step (Figure 36d). Subsequent irradiation with visible light leads to complete cycloreversion to **11b(o)**. There is no indication for the formation of a by-product. Nevertheless, due to diffusion of the compound into the cathode compartment of the divided electrochemical cell and due to unspecific degradation processes of the intermediate radical cationic species a continuous loss in the visible absorbance is observed during five switching cycles. This points to a general drawback of the electrochemical setup that has to be addressed in any future application; however, it does not constitute an intrinsic limitation of the molecular system.

While for the symmetrically substituted compounds **11a** and **11b** an irreversible two-electron oxidation that leads to thermal ring closure is observed in CV, the behavior of the unsymmetrically substituted derivative **11c** is slightly different. Here, the cyclic voltammogram (Figure 37a) shows two well separated one-electron oxidation waves. Based on the observed oxidation potentials for compounds **11a** and **11b** the wave at 0.70 V can be assigned to the oxidation of the morpholinothiazole moiety bearing the CH_3-group while the wave at 1.23 V corresponds to the morpholinothiazole bearing the CF_3 group. The origin of the small shoulder at a potential of 1.05 V is currently unknown. Again, the total oxidative process is irreversible yielding the ring-closed species, indicated by two new oxidative waves arising at 0.42 V and 0.24 V in the second scan cycle. Most importantly, if only the morpholinothiazole bearing a CH_3-group is oxidized and the return point of the potential scan is set before the second oxidation takes place, the observed anodic wave has a quasireversible character. At a scan rate of 1 V s^{-1} the first oxidation step is reversible indicated by a corresponding cathodic wave on the

return scan, while at lower scan rates the formed radical cation undergoes a consecutive reaction (Figure 37b). The linear dependence of the peak current with the square root of the scan rate shows that the one-electronic nature of the oxidation is not altered. The product of the slow irreversible reaction cannot be identified and is *not* identical with the ring-closed isomer, which only forms after extraction of the second electron from the ring-open species.

Note that the introduction of only one CF_3 group into the morpholinothiazole-maleimide architecture does not improve the fatigue resistance of the electrochemical switching process. During the oxidative cyclization of **11c** a by-product similar to that described earlier for **11a** could be observed in UPLC/MS-measurements.

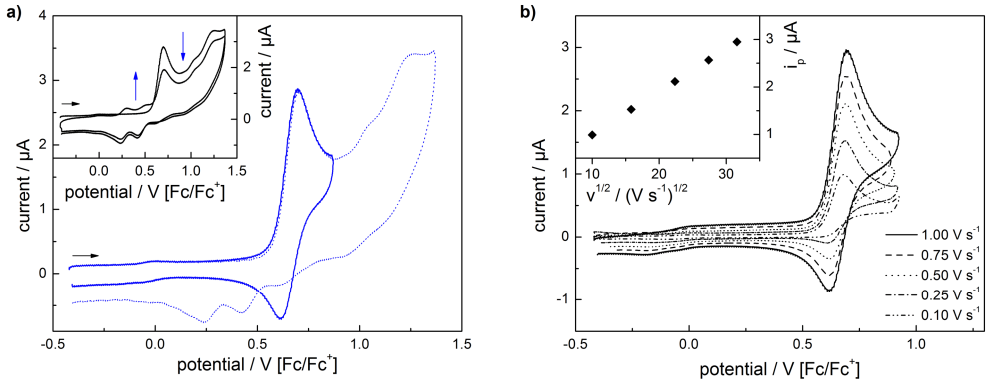

Figure 37. a) Cyclic voltammetry of **11c** in acetonitrile/0.1 M Bu_4NPF_6 ($c = 1 \cdot 10^{-3}$ M, dE/dt = 1 V/s) using a return potential at 0.87 V (solid line) and at 1.37 V (dotted line), respectively. The inset shows two full oxidative cycles consecutively performed on the ring-open isomer. b) Cyclic voltammetry of **11a** in acetonitrile/0.1 M Bu_4NPF_6 ($c = 1 \cdot 10^{-3}$ M) at varying scan rates.

4.4.4 Mechanistic considerations

As discussed in section 2.1.4 of this work, the mechanism of redox induced ring-closure/ring-opening of DAEs is under debate. Both diradical dicationic and monoradical cationic intermediates are postulated to undergo the thermal isomerization reaction. In case of oxidative ring-closure both possibilities, following either an *EEC* or an *ECE* mechanism (see Figure 5, section 2.1.4), give identical cyclic voltammograms consisting of an irreversible two electron oxidation wave in case of symmetrically substituted derivatives.

A first hint that directs towards the latter *EEC*-mechanism working in case of morpholinothiazole switches **11a-c** is the lack of any bathochromic absorbance during the spectroelectrochemical investigation of the oxidation of **11a** (Figure 35), which would be characteristic for an intermediate monoradical cationic species either in the ring-open or in the ring-closed form. A similar observation has recently been made for a related dithienylethene possessing amine redox centers attached directly to the thiophene rings.[58b]

To further prove the assumption of an operating *EEC* mechanism an unsymmetrically substituted derivative is necessary in order to achieve a maximum difference in the oxidation potentials of both aryl units. The reported derivative **11c** was synthesized specifically for this task. The introduction of the CF_3 unit did not alter the properties of the morpholinothiazole as a redox center apart from a significant shift of its oxidation potential by 570 mV. In fact, from cyclic voltammetry of **11c** as described above (Figure 37) it is clear that the first electron transfer from the molecule has a quasireversible nature and does not lead to a chemical reaction at high scan rates. Therefore, a stepwise double ionization to a dicationic species has to take place in order to induce the ring-closure. Thus it is concluded that the oxidative cyclization of **11c** follows an *EEC* mechanism (Scheme 39).[29]

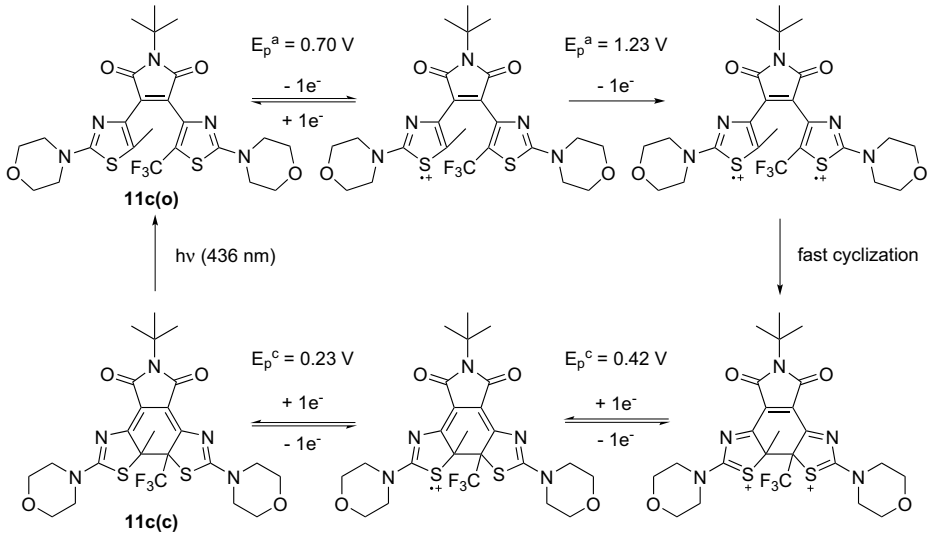

Scheme 39. *EEC* mechanism for the oxidative ring-closure of **11c**.

The preference of the thermal cyclization in the dicationic state of the ring-open isomer was also demonstrated by theory. Energies of the neutral isomers of **11a**, **11b**, **11c**, and **12** as well as closed shell singlet dicationic species ($^{S}X^{2+}$) were calculated on the B3LYP/PCM(acetonitrile)/6-31G(d) level of theory.[30] Doublet monoradical cationic ($^{D}X^{+}$) as well as singlet ($^{SU}X^{2+}$), and triplet ($^{T}X^{2+}$) diradical dicationic species were treated using the unrestricted B3LYP (UB3LYP) method. Besides geometry optimized ionic ring-open and ring-

[29] Note that also unsymmetrically substituted dithienylethene **5a** shows two separated oxidation waves with the first being reversible and the second being irreversible (see Figure A4-15 in Appendix 4). Only after the second oxidation step the ring-closed isomer is formed. In contrast, for compound **5b** only one oxidation wave is observed, *i.e.* the potential splitting between the two oxidation steps is too small to be resolved or allows for a disproportionation reaction in the monoradical cationic state thermodynamically driven by the formation of the ring-closed isomer. However, from both compounds no clear mechanistic information can be gained as due to the presence of an "electroactive" *N,N*-dimehtylaminophenyl or methoxyphenyl group the location of the primary electron transfer may not be within the hexatriene core. For a similar observation see also reference [58e].

[30] Quantum mechnanical calculations were performed by Manuel Utecht in the group of Prof. Peter Saalfrank, Department of Chemistry, Universität Potsdam.

closed isomers, vertical ionization energies were determined without re-optimization of the ions (*e.g.* ($^{SU}X^{2+}$)^{v}). Furthermore, transition state structures (TS) for the conrotatory thermal cyclization reaction were determined using the QST3 method. For compound **11c** also the disrotatory cyclization reaction was considered. Figure 38 exemplarily shows the obtained energy profiles for compound **11c**.[31]

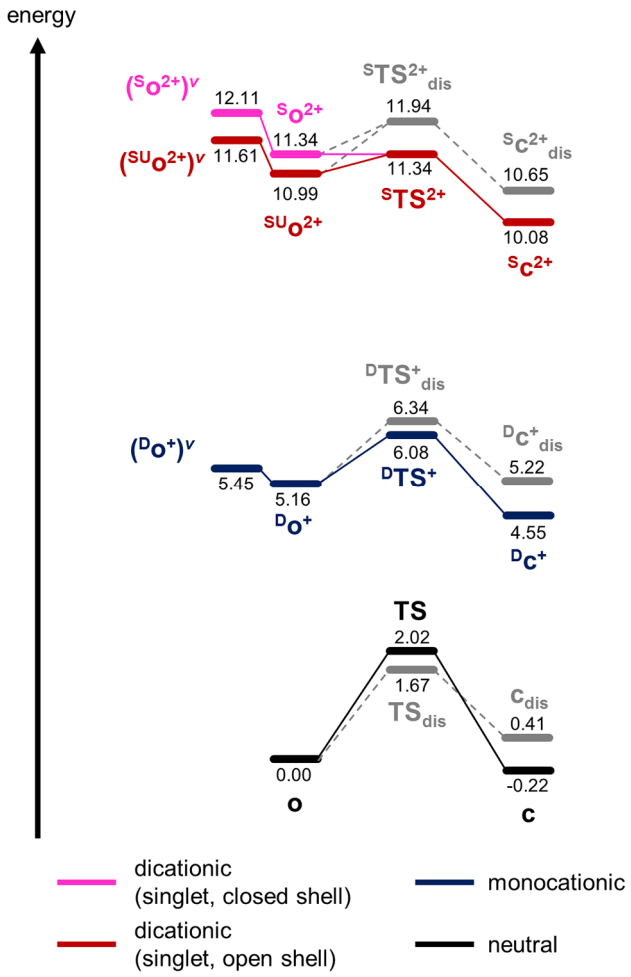

Figure 38. Energy profile for the thermal conrotatory and disrotatory (X_{dis}) cyclization reaction of **11c** in its neutral, monocationic ($^{D}X^{+}$), dicationic singlet closed shell ($^{S}X^{2+}$), and dicationic singlet open shell ($^{SU}X^{2+}$) forms as obtained from calculations on the (U)B3LYP/PCM(acetonitrile)/6-31G(d) level of theory. Vertical (^{v}) and adiabatic ionization potentials of ring-open (o) and ring-closed (c) isomer are shown together with transition states (TS) for the cyclization reaction, which were obtained by the QST3 method. Energies are given relative to the neutral ring-open form in eV.

For all compounds theoretical ionization potentials IP(X→$^{D}X^{+}$) = E(X) – E($^{D}X^{+}$) nicely followed the experimentally observed trends for the first oxidation potentials of the ring-open as well as ring-closed isomers. For ring-open dicationic species it was found that the singlet diradicals ($^{SU}X^{2+}$) were always slightly more stable or as stable as the triplet diradicals ($^{T}X^{2+}$)

[31] Details on calculated energies for all other compounds can be found in: M. Herder *et al.*, *Chem. Sci.* **2013**, *4*, 1028-1040.

and always more stable than the closed shell singlets ($^{S}X^{2+}$). For ring-closed singlet dications UB3LYP and B3LYP gave the same result with only paired electrons, *i.e.* no singlet diradical species exit. Ring-closed triplet diradical dications were always much higher in energy.

The thermal cyclization reaction from ring-open to ring-closed isomers was calculated to be exergonic in the neutral and all ionized states, except for the triplet diradical dications. However, large variations in the activation energies, *i.e.* in the relative energies of the transition states (TS), were obtained. For neutral compounds the activation energies lie in the range of 2 eV, reflecting the fact that a conrotatory cyclization is thermally forbidden by the Woodward-Hoffman rules. In the monocationic state ($^{D}X^{+}$) activation energies lie between 0.77 – 0.92 eV. However, the energy gain by structural reorganization after vertical ionization is significantly smaller, making it improbable that the monocations can overcome this barrier. In contrast, for the closed shell singlet dications ($^{S}X^{2+}$) there is essentially no activation barrier for the cyclization reaction. This can also be rationalized inspecting the HOMO-1 molecular orbital of the neutral compound (Figure 33), which is expected to play a prominent role in the pericyclic reaction of the diacationic species. It has large coefficients with opposite signs on the ring-closing carbon atoms allowing for an easy cyclization reaction. In the singlet diradical dicationic state the small barriers for the conrotatory cyclization between 0.05 – 0.52 eV can easily be overcome due to the considerably larger reorganization energies after vertical ionization of the ring-open compounds. Thus it can be concluded that the conrotatory cyclization only takes place in the singlet dicationic state, whereby due to its lower total energy the singlet diradical dication is the reactive species.

Furthermore, the calculations show that disrotatory cyclization products are not expected due to their endergonic nature. However, as predicted by the Woodward-Hoffman rules, the disrotatory activation barrier for the neutral compounds is smaller than that for the conrotatory pathway, while for the ionic species it is considerably higher.

4.4.5 Summary

A series of dithiazolylethenes was investigated, which show oxidative ring-closure, a property that is exceptional for DAEs possessing thiazole heterocycles. As a common structural motif strongly electron donating morpholino substituents were placed on the thiazole rings, which in combination with an electron withdrawing *N-tert*-butylmaleimide bridge efficiently prohibit a photochemically induced ring-closure reaction due to the charge transfer character of the first excited state. However, photochemical ring-opening proceeds with high quantum yields, rendering these compounds simple orthogonally switchable DAEs with the electrochemical and photochemical triggers working into different directions.

The performance of the orthogonal switching process could be massively improved by exchanging both methyl substituents on the ring-closing carbon atoms by CF_3 groups, which

prevented the emergence of a by-product resulting from a rearrangement of the ring-closed isomer in its doubly oxidized state. Furthermore, the remarkable shift of the oxidation potential of the DAE by introduction of the CF_3 groups allowed for a conclusive experimental evidence for the mechanism underlying oxidative ring-closure by using an unsymmetrically substituted derivative. Supported by theory, the diradical dication of the ring-open form was identified to undergo the thermal cyclization reaction. The remarkable properties of the α-CF_3 substituted compounds initiated further investigations into the general effect of α-CF_3 groups on the photochemical and electrochemical properties of the DAE scaffold, which are reported in section 4.5 of this work.

Besides potential applications in multi-stimuli responsive devices with logic functions, the (orthogonal) combination of the electrochemical and photochemical triggers of DAE isomerism may lead to switchable systems that overcome the limitations in switching efficiency and selectivity of purely photochemically controlled photochromes. Furthermore, systems are conceivable that are energetically driven by photochemical isomerization into a meta-stable state from which the energy could be harvested via the redox induced back-reaction.

4.5 Tuning of energy levels

4.5.1 Introduction

As shown in section 2.2 of this work most applications of DAE photochromes for the remote-control of specific functions rely on the isomerization-induced modulation of the π-electronic system within the DAE core and the thus induced shifts of the HOMO and LUMO energies. For normal-type DAEs the π-conjugation is more extended in the ring-closed state. Thus, upon cyclization the HOMO and LUMO levels are raised and lowered, respectively (Scheme 40a). As a central part of this work the fundamental electronic properties of a series of DAE structures are investigated using cyclic voltammetry. Thereby, three points shall be addressed:

- *Absolute* HOMO and LUMO energies of the two isomers shall be tuned over a broad range by structural modification of the DAE. Thus, a library of structures is obtained, out of which compounds can be selected that fit to specific energetic requirements of prospective applications.
- Structural motifs shall be identified for which *relative* shifts of the HOMO and LUMO energies upon the isomerization reaction are very large in order to induce a maximum effect by the switching process.
- It shall be determined how much of the isomerization-induced electronic changes within the DAE core can be transduced to an adjacent functional unit depending on the DAE architecture.

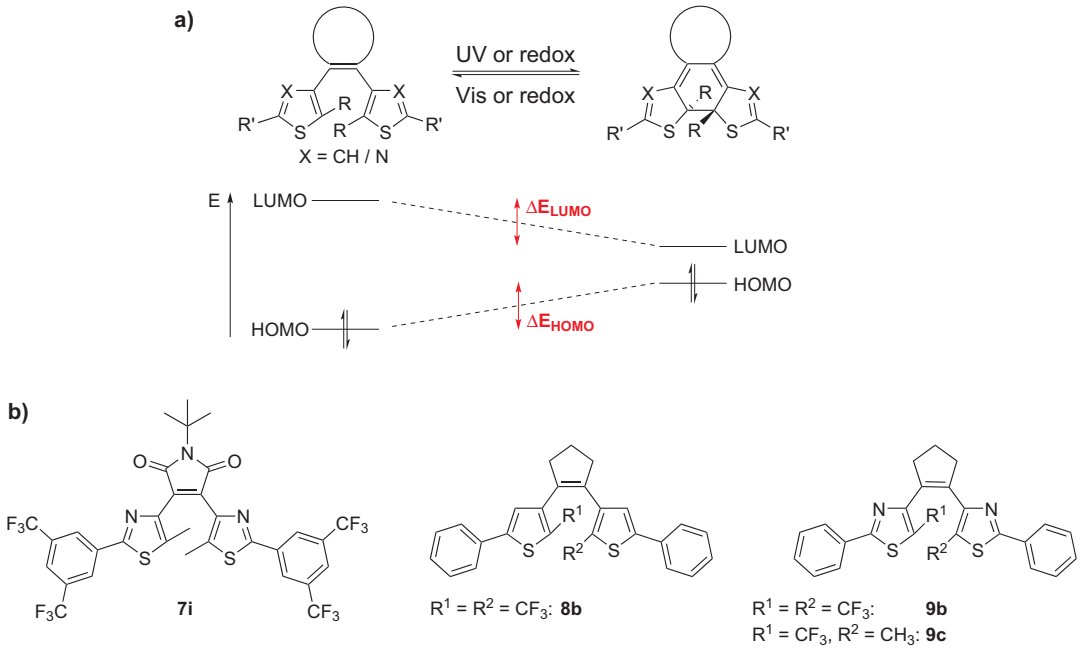

Scheme 40. a) Shift of HOMO and LUMO levels within the DAE core upon isomerization. b) *N*-*tert*-Butylmaleimide bridged and α-CF_3 substituted derivatives for the investigation of the modulation of energy levels.

The series of structurally modified DAE derivatives **1a-i**, **2c-j**, **3d-i**, **4i**, and **5a-b** (see Scheme 35 in section 4.3) has been synthesized not only to study their fatigue behavior, but also to use it as the basis for electrochemical investigations. It is extended by compound **7i** (Scheme 40b), which reveals the electronic effects of the *N*-*tert*-butylmaleimide bridge. Furthermore, inspired by experiences with CF_3 substitution at the ring-closing carbon atoms of morpholino substituted dithiazolylmaleimides (see section 4.4) DAEs **8b**, **9b**, and **9c** have been synthesized and investigated to estimate the effect of α-CF_3 groups on the photochemical and electronic properties of DAEs.

For coupling a functional unit, *e.g.* a binding site or a reactive or catalytically active moiety, with DAE photochromes different architectures are possible (Scheme 41). In many cases (see section 2.2) the functional unit serves as bridge of the DAE scaffold (Scheme 41a). Thereby, the properties of the bridge are modulated upon ring-closure by turning the central double bond into a single bond and by bringing donor or acceptor groups positioned on the hetaryl rings into conjugation.

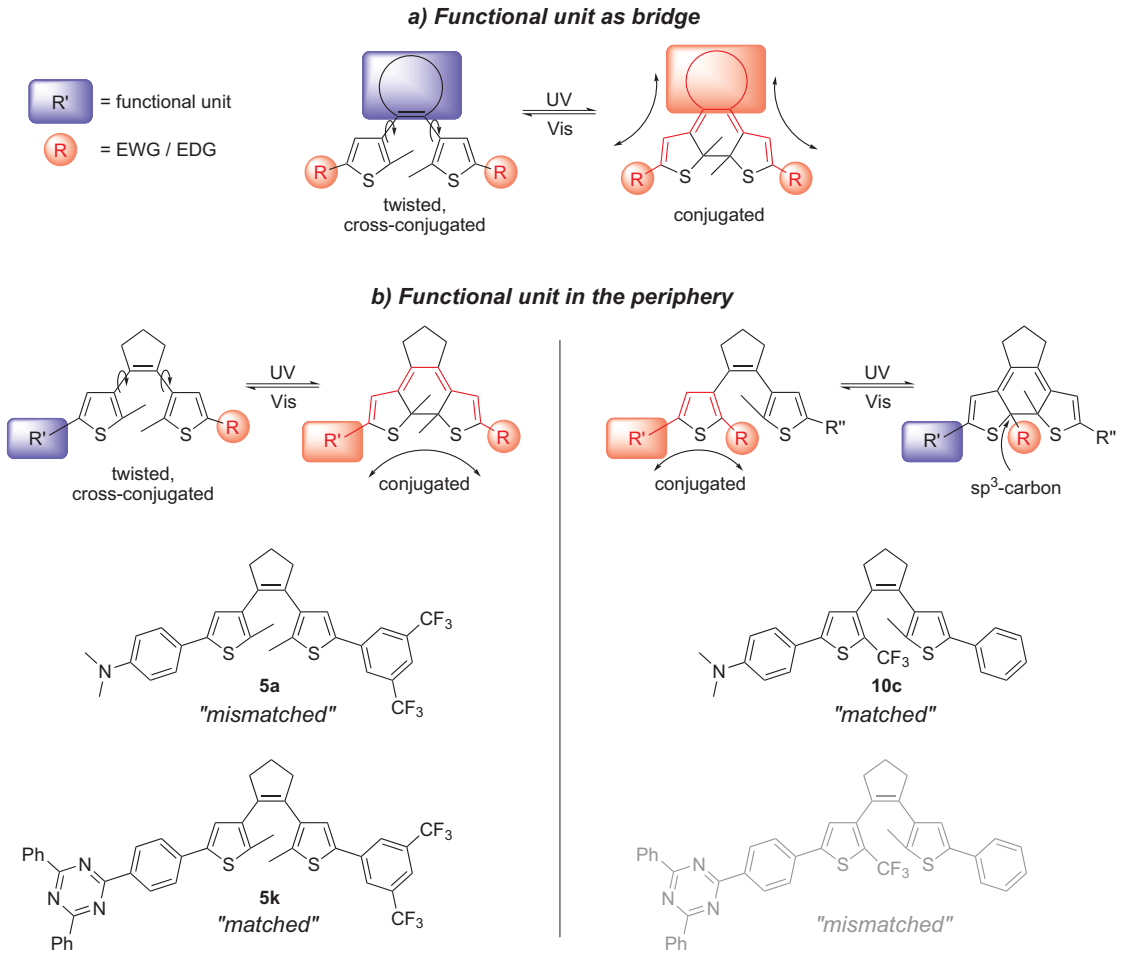

Scheme 41. Structural motifs for the reversible electronic coupling/decoupling of a functional unit with donor/acceptor substituents via the isomerization of DAEs. a) Implementation of the functional unit as bridge. b) Attachment of the functional unit in the periphery using donor/acceptor substituents either on the opposite or on the same thiophene ring. Below structural motifs possessing redox active groups for testing the extent of electronic modulation at the site of the functional unit are shown for each scenario.

The functional unit may also be placed in the periphery of the DAE, *i.e.* as substituent of one hetaryl ring (Scheme 41b). The isomerization reaction effects a coupling/decoupling with donor or acceptor groups, placed either on the opposite hetaryl ring or in the α-position of the same hetaryl ring.

For all three architectures examples can be found in the literature (see section 2.2). However, a direct comparison to evaluate which structure gives the largest transduction of electronic effects to the functional unit resulting from the switching process is difficult. Therefore, model compounds **5a**, **5k**, and **10c** were designed bearing redox active *N,N*-dimethylaminophenyl or triphenyltriazine moieties as "functional units" in the periphery, which report the electronic changes occurring during the isomerization reaction by the change in their oxidation or reduction potential, respectively. CF_3 groups were chosen as acceptor moieties, either in the form of 3,5-bis(trifluoromethyl)phenyl substituents (**5a**, **5k**) or directly attached to the α-position of the thiophene ring (**10c**). Thereby, compound **5a** can be regarded as a "mismatched" case: Generally the π-system of the DAE gets extended by the cyclization reaction leading to a decrease of the oxidation potential of the amine. On the other hand, in the ring-closed state the electronic coupling between the amine and the acceptor group on the second thiophene ring should increase the amine's oxidation potential. In contrast, compounds **10c** and **5k** are "matched" cases, for which the change in conjugation and coupling/decoupling of the acceptor units operate into the same direction, *i.e.* lowering the oxidation or reduction potentials, respectively, upon ring-closure. Thus, for **10c** and **5k** higher potential differences between the isomers are expected.

Note that the bridge-functionalized motif was already investigated during preceding studies.[75] The reduction potential of a bridging maleimide "matched" with acceptor substituents in the periphery was reduced by 240 mV upon ring-closure, while the "mismatched" derivative bearing donor groups showed a change of only 70 mV. This electronic difference was directly related to a difference in the function of the maleimide, *i.e.* the strength of the binding to a receptor via hydrogen bonding interactions.

In the following the photochemistry of compounds **5k** and **7i** is presented and the remarkable impact of α-CF_3 groups on the photochemical properties of DAEs is shown before the electrochemical results are discussed.

4.5.2 Photochemistry of 5k and 7i

As expected from the extended π-system of DAE **5k**, both in the ring-open and ring-closed form its molar absorptivity is much higher than that of the prototype DAE **1d**. In addition, absorption bands of both isomers are bathochromically shifted (Figure 39a, Table 16). Compound **5k** smoothly undergoes cyclization with a quantum yield of 0.59, which is in the expected range of

DAEs. In contrast, the quantum yield for ring-opening is lowered by a factor of 4 compared to **1d**, which is typical for the presence of an extended π-conjugated system.[34]

In analogy to morpholino substituted dithiazolylmaleimides discussed in section 4.4 of this work, the UV/Vis spectrum of the ring-open isomer of **7i** shows a weak, broad charge transfer band besides the π-π*-transition (Figure 39b). However, the CT band is shifted hypsochromically due to the low donor character of the 3,5-bis(trifluoromethyl)phenylthiazole groups. Therefore, in contrast to the morpholino substituted compounds photochemical cyclization is possible with a quantum yield of 0.13, which is in accordance to related structures.[75a]

Remarkably, both **5k** and **7i** show fluorescence in their ring-open states, which is not observed for most other DAE structures studied in this work. Upon prolonged UV irradiation for both derivatives the emergence of an isomeric by-product, presumably the annulated isomer discussed in section 4.3, was observed by UPLC/MS. A precise quantification of by-product formation was not conducted. However, the conversion was estimated to be below 10% after 30 min of UV irradiation (310 nm, 1000 W Xe, interference filter), which renders both acceptor substituted DAEs quite fatigue resistant.

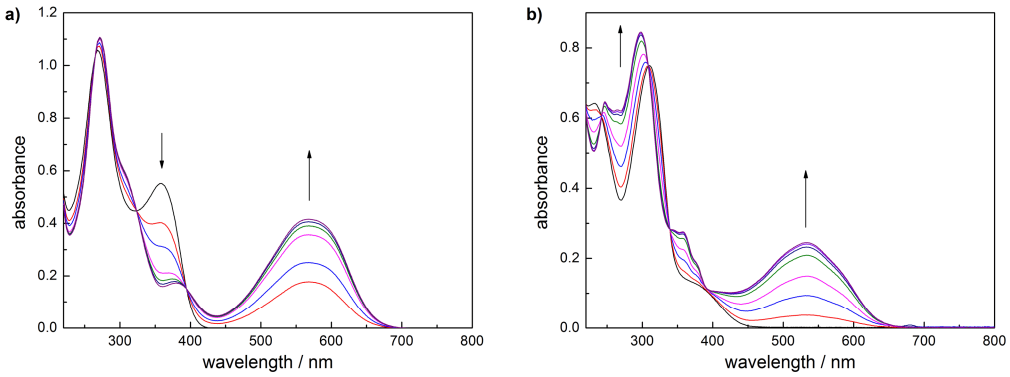

Figure 39. UV/Vis spectra of compounds a) **5k** ($1.69 \cdot 10^{-5}$ M) and b) **7i** ($2.88 \cdot 10^{-5}$ M) in acetonitrile (25 °C) under irradiation with 313 nm light until reaching the PSS.

Table 16. Photophysical properties of DAEs **5k** and **7i** in acetonitrile.

comp.	λ_{max} / nm (ε / 10^4 M^{-1} cm^{-1})		PSS (313 nm)[a]	Φ_{AB} (313 nm)[b]	Φ_{BA} (546 nm)[c]
	ring-open isomer	ring-closed isomer			
5k	269 (6.27), 358 (3.28)	568 (2.63)	97%	0.59	0.0023
7i	310 (2.60), 376 (0.44, shoulder)	532 (1.10)	78%	0.13	n.d.

a) Amount of ring-closed isomer in the PSS reached after UV-irradiation, determined by UPLC.
b) Quantum yields for ring-closure, obtained by the initial slope method using ferrioxalate actinometry.
c) Quantum yields for ring-opening, obtained by the initial slope method using Aberchrome 670 actinometry.

4.5.3 Photochemistry of α-trifluoromethyl substituted DAEs

Compared to the parent dithiazolylcyclopentene **3d**, the doubly CF_3 functionalized compound **9b** shows marked hypsochromic shifts of the lowest energy absorption bands both in the ring-open and ring-closed states (Figure 40a, Table 17). Remarkably, the amount of the ring-closed isomer in the PSS upon UV irradiation is only 31%. This is due to the unfavorable ratio of quantum yields for ring-closure and ring-opening. Compared to **3d**[32] the quantum yield for ring-closure of **9b** under irradiation with 313 nm light is decreased by one order of magnitude. When using 280 nm light, *i.e.* going from the low energy onset near to the maximum of the absorption band, the quantum yield was determined to be only slightly higher. In contrast, the quantum yield for ring-opening of **9b** is almost one order of magnitude higher than that of **3d**, showing the rate increasing effect of the α-CF_3 groups.[33]

Importantly, when only one methyl group of the parent DAE structure is replaced by a CF_3 group, as in compound **9c**, the typical photochemical behavior of DAEs is retained (Figure 40b). Though the quantum yield for ring-closure of **9c** with a value of 0.23 still is somewhat smaller than that of **3d**, it is in a reasonable range. As ring-opening is slow, a PSS of 87% is reached under 313 nm light irradiation. The wavelengths of the maxima of the lowest energy absorption bands lie in-between the values for **3d** and **9b** for both isomers.

Table 17. Photochemical properties of α-CF_3 substituted DAEs and related compounds.

comp.	λ_{max} / nm (ε / 10^4 M^{-1} cm^{-1})		PSS (λ_{irr})[a]	Φ_{AB} (λ_{irr})[b]	Φ_{BA} (λ_{irr})[c]
	ring-open isomer	ring-closed isomer			
1d	278 (3.25)	520 (1.78)	98% (310 nm)	0.50 (313 nm)	0.0093 (546 nm)
3d	316 (2.13)	500 (1.55)	94% (310 nm)	0.57 (313 nm)	0.021 (546 nm)
5a	326 (3.37)	570 (2.54)	97% (310 nm)	0.056 (313 nm)	0.0022 (546 nm)
8b	n.d.	n.d.	61% (300 nm)	n.d.	n.d.
9b	283 (2.42)	469 (1.65)	31% (313 nm)	0.075 (280 nm) 0.060 (313 nm)	0.16 (436 nm)
9c	288 (2.29)	482 (1.29)	87% (313 nm)	0.23 (313 nm)	0.020 (436 nm)
10c	311 (2.39), 346 (2.08)	522 (2.69)	98% (313 nm)	0.70 (313 nm)	0.011.(546 nm)

a) Amount of ring-closed isomer in the PSS reached after UV-irradiation, determined by UPLC.
b) Quantum yields for ring-closure, obtained by the initial slope method using azobenzene actinometry.
c) Quantum yields for ring-opening, obtained by the initial slope method using Aberchrome 670 actinometry.

[32] Note that quantum yields for ring-closure of **1d**, **3d** and **5a** reported in Table 17 slightly differ from the values reported before in section 4.3. To a minor part this is due to application of the initial slope method and to a major part due to the use of azobenzene instead of ferrioxalate as actinometric reference during these independent experiments.

[33] Compare with the increased ring-opening quantum yield of compound **11b** discussed in section 4.4.

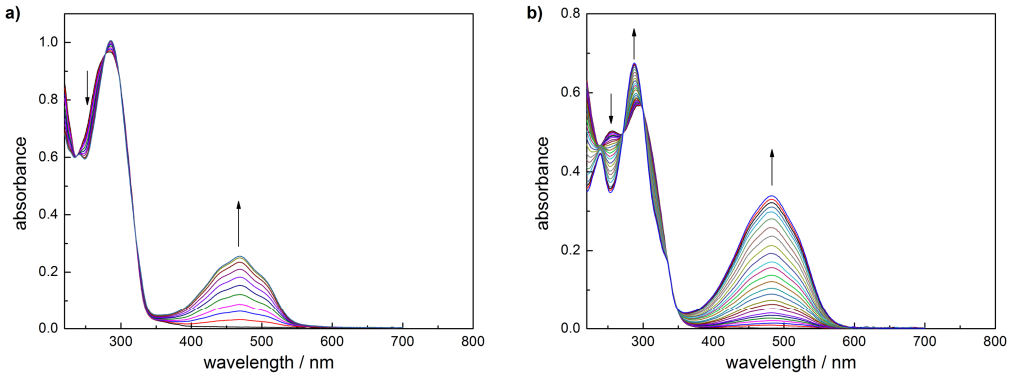

Figure 40. UV/Vis spectra of compounds a) **9b** ($4.00 \cdot 10^{-5}$ M) and b) **9c** ($3.01 \cdot 10^{-5}$ M) in acetonitrile (25 °C) under irradiation with 313 nm light until reaching the PSS.

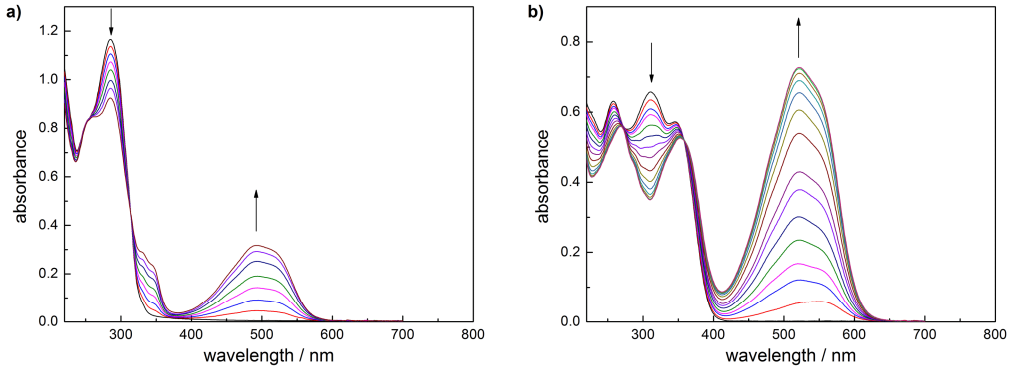

Figure 41. UV/Vis spectra in acetonitrile (25 °C) of compounds a) **8b** (ca. $3.4 \cdot 10^{-5}$ M) under irradiation with 300 nm light and b) **10c** ($2.75 \cdot 10^{-5}$ M) under irradiation with 313 nm light until reaching the PSS.

The doubly CF_3 substituted dithienylethene **8b** shows very similar trends as its thiazole analogue. Compared to the parent dithienylethene **1d** its absorption bands are shifted hypsochromically and the amount of ring-closed isomer in the PSS is significantly reduced (Figure 41a). As compound **8b** was contaminated with a minor impurity, no quantitative measures can be given. However, from photokinetic measurements quantum yields can be estimated to lie in the same order of magnitude as the values for **9b**.

The unsymmetrically substituted DAE **10c** possessing a 4-*N,N*-dimethylaminophenyl and a CF_3 group on the same thiophene ring shows remarkable photochemical properties. Due to the coupling of the donor and acceptor group in the ring-open form, the lowest energy absorbance maximum is shifted by 68 nm to longer wavelengths (Figure 41b) compared to the parent dithienylethene **1d**. Importantly, despite the pronounced donor-acceptor interaction compound **10c** undergoes the photochemical cyclization reaction very efficiently with a quantum yield of 0.70. This is in stark contrast to derivative **5a**, which is substituted with the acceptor group on the opposite thiophene ring. Photochemical ring-opening of **10c** proceeds with a quantum yield of 0.01, a value very similar to DAE **1d**.

Comparison of the UV/Vis spectra of DAEs **1d**, **5a**, and **10c** (Figure 42) reveals the different conjugation paths between the aniline as a "functional unit" and the acceptor moieties, as depicted in Scheme 41b. In the ring-open form compound **10c**, with the donor and the acceptor being electronically coupled, shows the most bathochromically shifted absorbance. However, in the ring-closed form the position of the absorbance band in the visible range is almost identical to that of unsubstituted **1d**. This shows that the CF_3 group is efficiently decoupled from the π-electronic system. In contrast, the absorbance of the ring-closed isomer of **5a** is shifted bathochromically by 50 nm revealing the strong coupling of the donor and the acceptor.

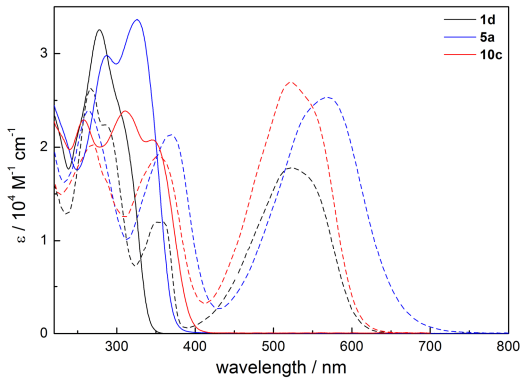

Figure 42. Comparison of UV/Vis spectra in acetonitrile of DAEs **1d**, **5a**, and **10c** in their ring-open (solid lines) and ring-closed (dashed lines) forms.

4.5.4 HOMO and LUMO levels

In this work HOMO and LUMO energy levels of DAE derivatives are calculated from the first oxidation and reduction potentials E_p^{a1} and E_p^{c1}, determined by cyclic voltammetry in acetonitrile, according to the following equation (e = elementary charge):

$$E_{HOMO/LUMO} = -e \cdot E_p^{a1/c1} - 4.8\ eV \qquad (39)$$

The offset of 4.8 eV represents the ionization potential of ferrocene in the vacuum scale as postulated by Pommerehne and coworkers.[162] It is important to note that the utilization of redox potentials as a measure for absolute and relative frontier orbital energies is a rough estimate due to a number of reasons:[163]

1) While HOMO and LUMO energies are scaled in vacuum, redox potentials are generally obtained in solution in the presence of large amounts of an electrolyte. Thus, effects by solvation and interaction with the electrolyte are neglected, which is highly questionable. However, if structurally similar compounds are compared, it can be assumed that solvation and interaction with the electrolyte do not differ too much and that relative energies are quite

accurate within a margin of 0.1 eV.[163] Comparing values obtained in different solvents or between solution and the solid state is more unreliable.

2) Generally, the half-wave potential of a fully reversible peak is taken as a measure for the formal potential of the redox process. However, in case of DAEs also irreversible processes are observed, in particular for oxidations of the ring-open isomers. Therefore, peak potentials are reported for *all* observed redox waves. In case of fully reversible processes the difference between the half-wave potential and the peak potential amounts to 29 mV and can be neglected. For irreversible processes, which are due to a chemical reaction following the electron transfer, *e.g.* ring-closure for many ring-open DAEs, the observed peak potential is shifted to lower values compared to the formal potential of the electron transfer. This shift can amount up to approximately 370 mV for very fast chemical reactions.[164] However, for slower reactions the shift is smaller and in case of quasireversible processes it can be neglected. Thus, HOMO and LUMO levels of ring-open isomers showing fully irreversible redox processes have to be treated with care. In contrast, redox processes of most ring-closed isomers are reversible or quasireversible and can be regarded to be more reliable.

3) The offset of 4.8 eV relating the ferrocene/ferrocenium redox couple to the vacuum scale is under debate and a number of different conversion scales with values between 4.5 - 5.4 eV exist in the literature.[163] Thus, care has to be taken which conversion scale is applied when comparing to literature data.

Though these arguments make the utilization of cyclic voltammetry for the estimation of frontier orbital energies appear very unreliable, the procedure often is successfully applied for the prediction of specific device properties in the field of organic electronics.[165] Additionally, results presented in section 4.6 of this work demonstrate that the method is an easy, cheap, and fast way to select derivatives that fulfill specific energetic requirements out of a library of compounds. Thereby, for the reasons stated above, comparing *relative* energies of structurally similar derivatives is much more precise than their positioning on an *absolute* scale. Note that in the literature[166] correlations between HOMO energies found by cyclic voltammetry with values determined by ultraviolet photoelectron spectroscopy (UPS) generally show a linear dependence even for structurally very different compounds, though the slope may slightly deviate from unity.[34]

Electrochemical data for compounds **1a-i**, **2c-j**, **3d-i**, **4i**, and **5a-b** can be found in Table 11 (section 4.3.5) as well as in the Appendix 4. For compounds **7i** and α-trifluoromethylated DAEs **8b** and **9b-c** the data are collected in Table 18. Derived HOMO and LUMO levels are shown for a representative selection of derivatives of the dithienylethene and dithiazolylethene type in Figure 43.

[34] For compounds **1c** and **1h** HOMO energies obtained from cyclic voltammetry and from UPS show very similar trends when comparing the isomers with each other. Nevertheless, absolute values slightly differ between the two methods, see section 4.6.

Table 18. Anodic and cathodic peak potentials of **7i**, **8b**, and **9b-c**, determined by cyclic voltammetry in acetonitrile. All values are reported against the ferrocene/ferrocenium redox couple as external standard (rev = reversible, qr = quasireversible, irr = irreversible).

comp.	open isomer			closed isomer		
	E_p^{a1} / V	E_p^{a2} / V	E_p^{c1} / V	E_p^{a1} / V	E_p^{a2} / V	E_p^{c1} / V
7i	1.63 (irr)	-	-1.57 (rev)	1.10 (irr)	-	-1.21 (qr)
8b	1.51 (irr)	1.70 (irr)	-2.60 (irr)	0.46 (rev)	0.69 (rev)	-1.87 (irr)
9b	1.64 (irr)	-	-2.35 (irr)	0.60 (irr)	0.90 (irr)	-1.64 (irr)
9c	1.09 (irr)	-	-2.49 (irr)	0.66 (qr)	0.87 (irr)	-1.84 (irr)

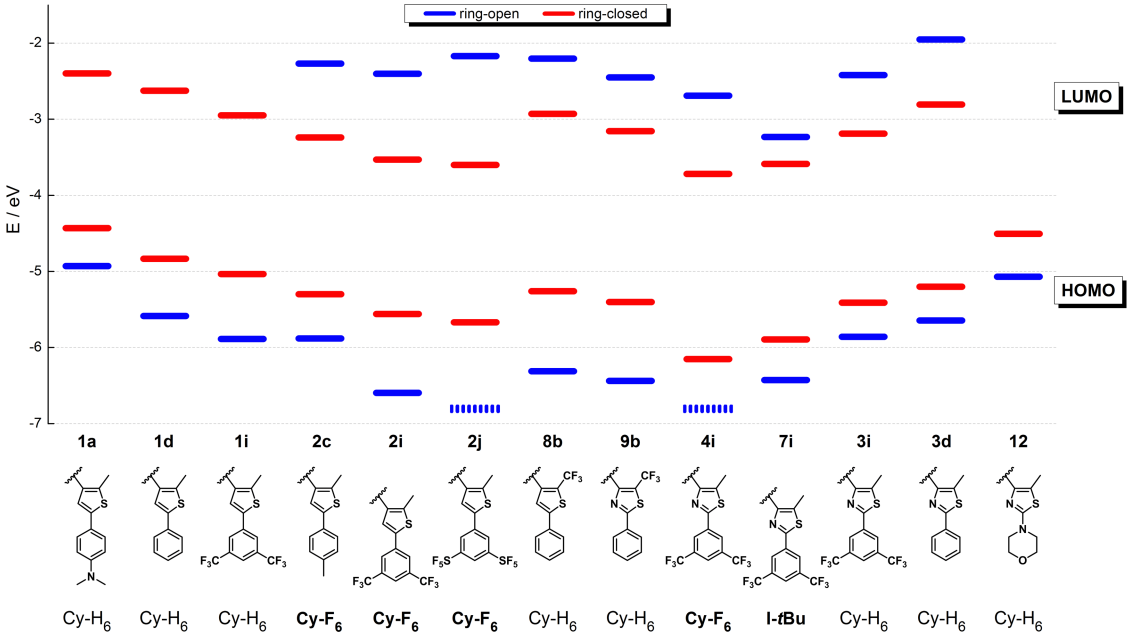

Figure 43. Tuning of HOMO and LUMO levels, as obtained from cyclic voltammetric oxidation and reduction potentials, by donor and acceptor substitution of symmetrical DAEs. For compounds **2j** and **4i** oxidation potentials of the ring-open isomers are in the range of the onset of solvent oxidation, thus only approximate values can be given, indicated by dashed lines. The heterocyclic building blocks as well as the bridging unit of each compound are depicted below. Cy-H_6 = perhydrocyclopentene, Cy-F_6 = perfluorocyclopentene, I-*t*Bu = *N*-*tert*-butylmaleimide.

From Figure 43 the following general trends can be derived:

- The absolute energies of the frontier molecular orbitals can be systematically tuned over a broad range covering more than 2.5 eV for HOMO levels (**1a(c)** vs. **2j(o)**) and at least 1.8 eV for LUMO levels (**4i(c)** vs. **3d(o)**). Note that LUMO levels of ring-open dithienylethenes are expected to lie above -1.9 eV, the limit of accessible potentials in the CV experiment.
- Both the variation between donor and acceptor substituents in the periphery and the nature of the bridging moiety exhibit strong influence on the absolute electronic levels with shifts between 0.5 – 0.9 eV for both ring-open and ring-closed isomers. Comparison of DAEs **1i** and **2c**, both possessing very similar HOMO energies,

shows that the effects exerted by the 3,5-bistrifluoromethyl substitution and the perfluorocyclopentene bridge are of similar magnitudes. Comparison of HOMO levels of compounds **3i**, **4i**, and **7i** shows that the electron-withdrawing capability of the *N-tert*-butylmaleimide bridge is slightly smaller than that of perfluorocyclopentene. However, the electron affinity of the ring-open isomer of **7i** is strongly increased due to the redox active carbonyl groups present in the bridge.

- Substitution with α-CF_3 groups strongly influences HOMO and LUMO levels of ring-open isomers, as can be seen by comparing DAEs **1d** and **8b** as well as **3d** and **9b**, which show shifts between 0.5 – 0.8 eV. In contrast, the effect on ring-closed isomers is significantly smaller with shifts between 0.2 – 0.4 eV. The latter is expected as in the ring-closed state quaternary carbon atoms separate the CF_3 groups from the π-electronic system. Thus, by α-CF_3 substitution the relative shifts of energy levels by the ring-closure reaction are significantly increased.
- Further fine-tuning of absolute energy levels can be achieved by exchanging thiophene with thiazole heterocycles in otherwise identical structures. For analogous substitution patterns HOMO and LUMO levels of thiazole derivatives are between 0.1 – 0.5 eV lower in energy than their thiophene counterparts.
- Large relative shifts in HOMO and LUMO levels comparing ring-open and ring-closed isomers are obtained upon increasing acceptor substitution of the DAE scaffold. Thereby, dithienylethenes generally show a larger isomerization induced variation than their thiazole analogues, if not substituted with α-CF_3 groups. Maximum relative shifts of more than 1 eV are exhibited by the strongly acceptor substituted dithienylethenes **2i** and **2j** as well as α-CF_3 substituted DAEs **8b** and **9b**.

4.5.5 Transduction of electronic changes to redox active groups

The redox behavior of unsymmetrically substituted DAEs **5a**, **10c**, and **5k** was investigated by cyclic voltammetry (Figure 44, Table 19). Compounds **5a** and **10c** represent the "mismatched" and "matched" configuration, respectively, for the transduction of electronic changes appearing within the DAE scaffold to the redox active *N,N*-dimethylaniline group. For both compounds the first oxidation processes are fully reversible in the ring-open and ring-closed forms and can be assumed to be located at the *N,N*-dimethylaniline groups. Note that, similar to symmetrically *N,N*-dimethylaniline substituted compound **1a**, for the ring-closed isomer of **10c** a two-electron oxidation wave is observed. From the difference of the anodic and cathodic peak currents it can be derived that two one-electron oxidation processes with a potential splitting of less than 100 mV are present.

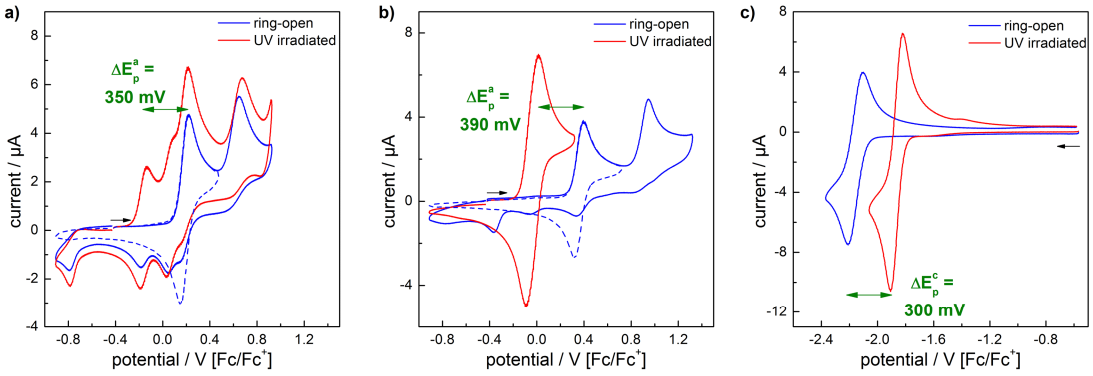

Figure 44. Cyclic voltammograms (dE/dt = 1 V s^{-1}) of DAEs a) **5a** in acetonitrile/0.1M Bu_4NPF_6, b) **10c** in acetonitrile/0.1M Bu_4NPF_6, and c) **5k** in methylene chloride/0.1M Bu_4NPF_6. All concentrations were $1 \cdot 10^{-3}$ M before irradiation. For compound **5a** only low conversion to the ring-closed isomer could be achieved after extended irradiation of the electrochemical cell for 2.5 h. Note that for a) and c) solutions became more concentrated during the irradiation procedure due to long irradiation times needed in case of a) and high volatility of the solvent in case of c).

Table 19. Anodic and cathodic peak potentials of **1a**, **5a**, **5k** and **10c**, determined by cyclic voltammetry in acetonitrile or methylene chloride. All values are reported against the ferrocene/ferrocenium redox couple as external standard (rev = reversible, qr = quasireversible, irr = irreversible).

comp.	open isomer			closed isomer		
	E_p^{a1} / V	E_p^{a2} / V	E_p^{c1} / V	E_p^{a1} / V	E_p^{a2} / V	E_p^{c1} / V
1a[a]	0.13 (irr)	-	< -2.80	-0.37 (rev)	-	-2.40 (irr)
5a[a]	0.22 (rev)	0.64 (irr)	-2.71 (irr)	-0.13 (rev)	0.09 (rev)	-2.02 (rev)
5k[b]	0.93 (irr)	-	-2.21 (rev)	0.11 (rev)	0.46 (rev)	-1.91 (rev)
10c[a]	0.40 (rev)	0.95 (irr)	-	0.01 (rev)	-	-2.23 (irr)

a) in acetonitrile
b) in methylene chloride

The potential of the first oxidation process of the ring-open isomer of **10c** is higher by 180 mV compared to **5a** and by 270 mV compared to **1a**, which is in accordance with the initial expectation (Scheme 41) that the CF_3 group in the α-postion of the thiophene ring would decrease the electron density of the aniline moiety. However, given the much larger electronic effect of α-CF_3 groups on the electron density within the DAE core itself, observed by comparing compounds **1d** and **8b** as well as **3d** and **9b** (*vide supra*), it can already be seen that transduction of the electronic changes to an adjacent functional unit is significantly less pronounced. Note that compared to the ring-open form of **1a** the first oxidation of **5a** is also shifted by 90 mV to higher potentials, although both compounds are expected to possess the same redox behavior in the first step, assuming that in the ring-open form both termini are electronically isolated from each other.

Due to the coupling of the *N,N*-dimethylaniline moiety with the electron-withdrawing 3,5-bis(trifluoromethyl)phenyl group in the ring-closed isomer of **5a**, it was expected that its first oxidation would appear at higher potentials than the first oxidation of the ring-closed isomer of **10c**, for which the aniline is decoupled from the CF_3 group. In contrast, it is

experimentally found that the oxidation of **5a(c)** at E_p^{a1}=-0.13 V occurs at a slightly lower potential than that of **10c(c)** at E_p^{a1} = 0.01 V. As a result, the difference between the two DAE derivatives in the relative potential shift upon ring-closure is relatively small. Though it is larger in the "matched" compound **10c** with a value of 390 mV, the shift of 350 mV for the "mismatched" compound **5a** is only slightly smaller.

A similar potential shift between the ring-open and ring-closed isomer is observed for the reversible reduction of DAE **5k**, which is located at the triphenyltriazine moiety. As this compound already represents the "matched" case, the synthesis of the mismatched analogue (Scheme 41) was not attempted.

4.5.6 Summary

It was demonstrated that the HOMO and LUMO energies of DAE photochromes can be precisely tuned over a broad range by donor/acceptor substitution in the periphery, variation of the bridging moiety, substitution with CF_3 groups in the α-positions of the hetaryl rings, and exchange of thiophene with thiazole heterocycles. Structures were obtained that show remarkable photoisomerization induced shifts of the energies of electronic levels of more than 1 eV. By creating a large collection of electronically modulated DAEs and by estimating the effects of structural modifications it is possible to select specific DAE derivatives or design new structures that fulfill energetic requirements for potential applications, in particular in combination with other optoelectronically active materials to reversibly enable and disable energy transfer or charge transport between the building blocks.

It was shown that transduction of the electronic changes induced within the DAE core upon isomerization to an adjacent, conjugated functional unit is much less pronounced. For model compounds possessing easily oxidizable aniline or reducible triazine moieties potential shifts between 300 – 400 mV were observed upon ring-closure. Thereby, different patterns of substitution with acceptor groups, inducing a "matched" or "mismatched" correlation to the electronic changes within the π-electronic system of the DAE, turned out to have only a small influence. In light of the desired property changes of functional units attached to DAEs, such as binding motifs or catalytically active moieties, a larger modulation of electron density is needed. Therefore, the electronic communication between the functional unit and the DAE core should be increased by restricting dihedral twisting or moving the functional unit closer to the DAE core by omitting the phenyl group or using the functional unit itself instead of one thiophene or thiazole heterocycle. Furthermore, electronic modulation can potentially be increased using -M substituents instead of CF_3 groups or by placing the acceptor group at the free β-position of the thiophene ring. Research into these directions is currently ongoing in the Hecht group.

In addition to the remarkable electronic properties of α-CF_3 substituted DAEs, interesting insights into their photochemistry were obtained. DAEs symmetrically substituted

with α-CF_3 groups on both hetaryl rings showed a strong reduction of the quantum yield for ring-closure, while the quantum yield for ring-opening was significantly increased compared to the methyl substituted derivatives. Importantly, installing only one CF_3 group on one hetaryl ring restores the usual photochemical behavior of DAEs. The combination of a 4-*N,N*-dimethylaniline donor and a CF_3 acceptor placed in the two α-positions of one thiophene ring gave a DAE showing a marked bathochromic shift of the absorbance of the ring-open form and an increased quantum yield for ring-closure. A thorough investigation of the photochemical fatigue behavior of α-CF_3 substituted DAEs has not yet been conducted.

4.6 Realization of photocontrollable OTFTs[35]

4.6.1 Introduction

In collaboration with the group of Paolo Samorì, organic thin film transistors (OTFTs) were designed that incorporate photochromic DAEs in order to reversibly photomodulate the current output of the device. Therefore, established polymeric and small molecule organic semiconductors were simply mixed with appropriate DAE derivatives and the thus obtained blends were used as active layer in the devices. As discussed in section 2.2.2 of this work, the combination of well-known organic semiconducting materials with photochromic molecules is advantageous to the use of pure photochromic compounds as active layer, as devices with a much higher electrical performance, *i.e.* charge carrier mobility, can be constructed. Thereby, the simple blending approach allows for an easy and fast fabrication of the light-responsive OTFTs by a spin-coating procedure. The application of DAE-semiconductor blends for the construction of organic electronic devices is unprecedented in the literature.

In order to photocontrol the charge transport within the device, the energy levels of the organic semiconductor and the DAE have to be precisely aligned (Figure 45). The basis for the energy level alignment was laid by systematically tuning of HOMO and LUMO levels of DAE photochromes by variation of their substitution pattern (see section 4.5). Thus, derivatives could be selected for which the HOMO of the ring-open form is positioned way below the HOMO of the p-type semiconductor to be applied. Importantly, the HOMO of the ring-closed isomer is positioned slightly above that of the semiconductor (Figure 45, left). In this scenario the mobility of charge carriers, *i.e.* holes, introduced into the semiconducting matrix by application of a gate voltage will not be disturbed by the presence of the ring-open isomer and a high drain current will be detected, which resembles the ON state of the transistor. However, the ring-closed isomer of the DAE will serve as a trapping center for the holes, *i.e.* there is a driving force for the transfer of holes to the DAE molecules. As the back-transfer to the semiconductor is energetically unfavorable, the hole mobility is significantly reduced, leading to the OFF state of the transistor.

The same principle can be realized using n-type semiconductors by aligning the LUMO levels of the DAE with the LUMO level of the matrix. In the ring-open state of the DAE electron transport is not influenced as its LUMO is higher in energy than that of the semiconductor. In the ring-closed state trapping centers are introduced by the reduction of the

[35] In this section results are summarized that were obtained in collaboration with the group of Prof. Paolo Samorì at the Institut de Science et d'Ingénerie Supramoléculaire, Université de Strasbourg. Further details can be found in the following publications:
E. Orgiu *et al.*, *Nat. Chem.* **2012**, *4*, 675 – 679.
J. Frisch *et al.*, *Appl. Phys. A* **2013**, *113*, 1-4.
M. El Gemayel *et al.*, *Nat. Commun.* **2015**, 6:6330, DOI: 10.1038/ncomms7330.
K. Börjesson *et al.*, *J. Mater. Chem. C* **2015**, *3*, 4156-4161.

LUMO energy of the DAE and thus charge transport is hindered in the active layer. (Figure 45, right).

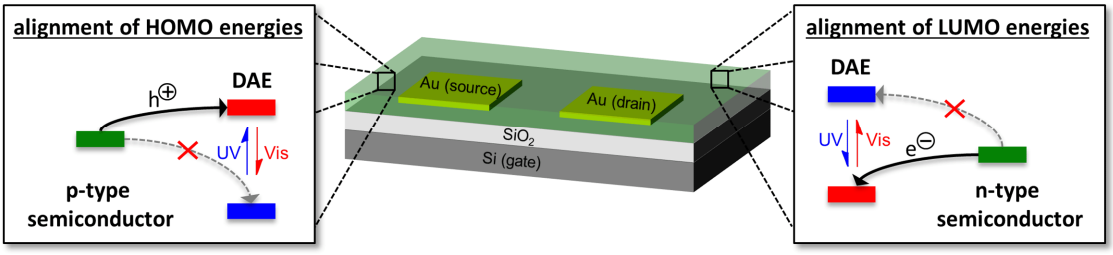

Figure 45. General concept for the photocontrol of charge transport in organic field effect transistors (OTFTs) by isomerization induced trapping of charge carriers within p-type (left) and n-type (right) semiconducting matrices using DAEs.

In the following, results on the realization of the concept using both p-type and n-type semiconducting matrices and carefully selected DAE derivatives possessing high HOMO and low LUMO energies, respectively, are summarized.

4.6.2 Photocontrollable p-type OTFTs

As a starting point, one of the best-performing polymeric semiconductors, regioregular poly(3-hexylthiophene) P3HT[167] (Scheme 42), was chosen as the matrix for the fabrication of photoswitchable p-type OTFTs. From the library of electronically modulated DAEs, compounds **1c** possessing methyl groups and **1h** possessing an *n*-hexyl ester groups in the para-positions of the peripheral phenyl rings were selected. By choosing a non-polar dithienylcyclopentene and by substitution of the ester derivative with long alkyl chains, miscibility with the P3HT matrix should be ensured.

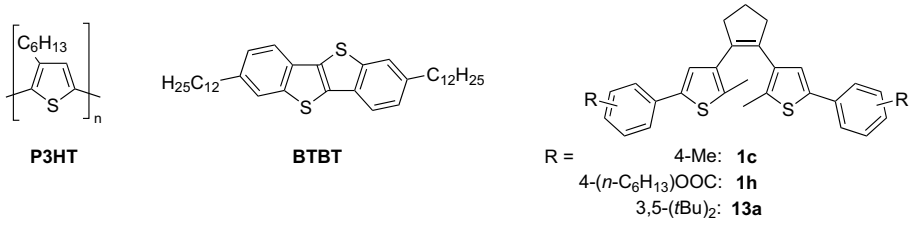

Scheme 42. Semiconducting matrices and DAE derivatives for the construction of photocontrollable p-type OTFTs.

Using cyclic voltammetry the HOMO energy of P3HT was determined to be at -4.8 eV from the onset of the oxidation of a drop-casted film on the electrode (Table 20). In the literature electrochemical HOMO energies between -4.7 and -5.2 eV can be found.[168] The two DAE derivatives were chosen in a way that the HOMO energies of the ring-open forms, obtained from cyclic voltammetry in methylene chloride, are below that of P3HT with values of -5.5 eV for **1c(o)** and -5.7 eV for **1h(o)**. At the same time, the HOMO energy of the ring-closed

isomer **1c(c)** of -4.7 is positioned slightly above that of P3HT while the HOMO of the ring-closed ester derivative **1h(c)** is shifted by 180 meV to lower energies (Table 20, Figure 47a). Note that due to reasons discussed in section 4.5.4 the exact relative and absolute positioning of the HOMO levels of the DAEs and P3HT is somewhat insecure. However, it is expected that the ring-closed isomer of **1c** shows a higher hole trapping efficiency when operating the device than the ring-closed isomer of **1h**.

Ultraviolet photoelectron spectroscopy (UPS) was performed on thin films of isolated ring-open and ring-closed isomers of **1c** and **1h** to compare with the electrochemically obtained energy level alignment (Table 20).[36] The ionization energy (IE) of both DAEs is lowered by 0.8 eV upon ring-closure, in perfect agreement with the electrochemically obtained HOMO energies. Furthermore, IEs of both isomers of **1h** are higher by 0.1 eV than that of DAE **1c**, confirming the relative difference between the two derivatives. On an absolute scale, IEs determined by UPS and HOMO energies determined by cyclic voltammetry differ due to the reasons discussed in section 4.5.4. Moreover, UPS fails to place the IE of P3HT in-between that of the ring-open and ring-closed isomers of the DAEs. Note that the IEs of films of P3HT were found to vary depending on the surface orientation of the molecules.[169]

Table 20. Oxidation potentials and derived HOMO energies of semiconducting matrices and DAE derivatives obtained from cyclic voltammetry as well as ionization energies determined by UPS. Potentials are given in reference to the ferrocene/ferrocenium redox couple (rev = reversible, qr = quasireversible, irr = irreversible).

comp.	acetonitrile		methylene chloride		IE / eV[a]
	E_p^{a1} / V	E_{HOMO} / eV	E_p^{a1} / V	E_{HOMO} / eV	
1c(o)	0.79 (irr)	-5.59	0.69 (irr)	-5.49	-5.9
1c(c)	-0.02 (rev)	-4.78	-0.12 (rev)	-4.68	-5.1
1h(o)	-	-	0.85 (irr)	-5.65	-6.0
1h(c)	-	-	0.06 (rev)	-4.86	-5.2
13a(o)	0.79 (irr)	-5.59	-	-	-
13a(c)	0.02 (rev)	-4.82	-	-	-
P3HT[b]	0.02	-4.82	-	-	-4.4 – -4.9[169-170]
BTBT	-	-	0.87 (rev)	-5.67	-

a) Ionization energies from UPS of thin films of the isolated ring-open and ring-closed isomers.
b) Onset potential of a film on the electrode drop-casted from a $CHCl_3$-solution.

To see to what extent photoisomerization of DAEs in a P3HT matrix is possible, irradiation experiments were carried out using thin films prepared by drop-casting on a quartz substrate and spectral changes were monitored using UV/Vis spectroscopy. First, a film of pure DAE **1c(o)** was prepared by drop casting from a $CHCl_3$-solution (0.3 mg/mL) and irradiated

[36] UPS measurements were performed by Johannes Frisch in the group of Prof. Norbert Koch, Department of Physics, Humboldt-Universität zu Berlin.

with UV light using a 365 nm standard laboratory UV lamp. It showed smooth conversion to the ring-closed isomer, which could be ring-opened again by white light irradiation (> 400 nm, 1000 W Xe arc lamp, longpass filter). Absorption bands for the ring-open and ring-closed isomers were bathochromically shifted by ca. 10 nm. Importantly, irradiation of a bare P3HT film drop-casted from a $CHCl_3$-solution (0.3 mg/mL) showed no spectral changes upon irradiation with UV or white light under the same conditions. In the UV/Vis spectrum of a film obtained from a mixture of P3HT and 40 wt% of DAE **1c(o)** the absorption band of the ring-open isomer of the DAE in the UV range can clearly be differentiated from the P3HT background (Figure 46a). Upon UV irradiation (365 nm) it decreases while a new band evolves at 370 nm and the absorbance between 400 – 600 nm rises, indicating the efficient formation of the ring-closed isomer. The process is almost fully reversible upon subsequent white light irradiation of the film (Figure 46b). To estimate the conversion to the ring-closed isomer upon UV irradiation a film of 40 wt% of the isolated ring-closed isomer **1c(c)** in the P3HT matrix was prepared. After complete ring-opening using white light (Figure 46c) and subsequent ring-closure using UV light (Figure 46d), the initial absorbance in the visible region is not fully reached, indicating that ca. 65% of the ring-open isomer undergo ring-closure in the film.

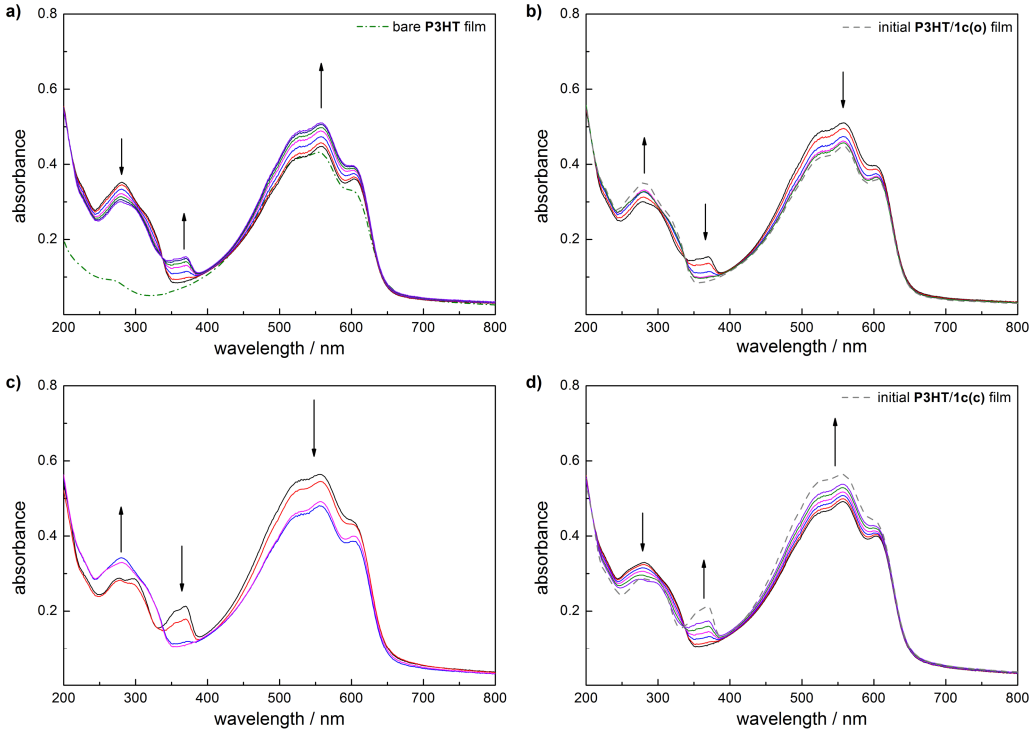

Figure 46. a) UV/Vis spectra of a film of 40 wt% **1c(o)** in P3HT, drop-casted from a $CHCl_3$-solution (0.3 mg/mL) on a quartz substrate, during irradiation with UV-light (365 nm, standard laboratory UV lamp) and b) during subsequent irradiation with white light (> 400 nm, 1000 W Xe, longpass filter). c) UV/Vis spectra of a film of 40 wt% **1c(c)** in P3HT, drop-casted from a $CHCl_3$-solution (0.3 mg/mL) on a quartz substrate, during irradiation with white light and b) during subsequent irradiation with UV light under the same conditions.

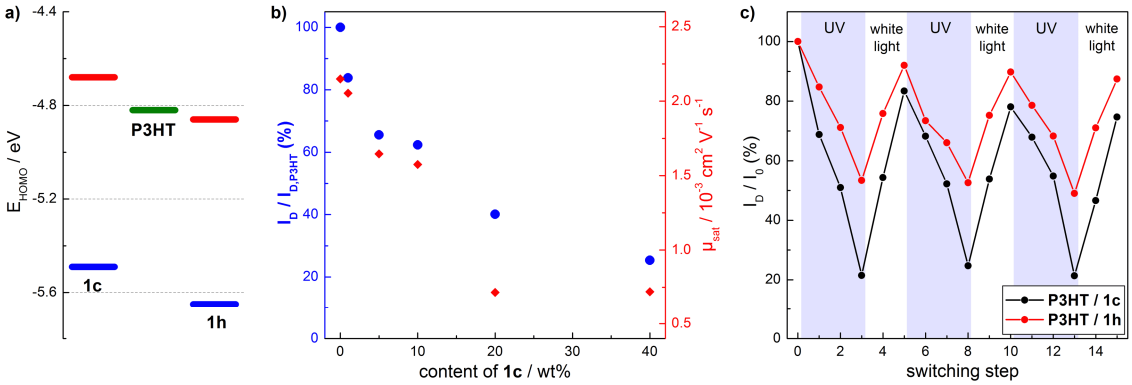

Figure 47. a) HOMO energy alignment between P3HT and ring-open (blue) and ring-closed (red) isomers of DAEs **1c** and **1h**, as obtained from cyclic voltammetry in methylene chloride. b) Drain current (normalized to drain current of bare P3HT, V_D = -60 V, V_G = -80 V) and corresponding field effect mobilities of BG-BC transistors using blends composed of P3HT and varying amounts of DAE **1c**. c) Normalized drain current (V_D = -10 V, V_G = -80 V) during photoswitching of BG-BC OTFT devices containing DAE **1c** (20 wt% in P3HT) or DAE **1h** (20 wt% in P3HT) using UV light (365 nm) and white light (>400 nm). Each switching cycle consisted of 3 steps of UV irradiation (30 s, 2 min, 10 min) and 2 steps of white light irradiation (2 min, 10 min). After each step a transfer curve was measured in the dark.

Transistor devices were fabricated in the bottom gate - bottom contact (BG-BC) geometry by spin coating $CHCl_3$-solutions of P3HT containing varying amounts of DAE **1c(o)** or DAE **1h(o)** on a Si/SiO_2 substrate to form a thin film between pre-patterned gold source and drain electrodes. Compared to the drain current I_D observed for a bare P3HT device, the blended films showed a decrease of I_D at fixed gate (V_G) and drain voltages (V_D) upon increasing the amount of DAE **1c(o)** up to 40 wt%. Corresponding hole mobilities measured in the saturation regime decrease up to a factor of 3 for the 40 wt% blend (Figure 47b). This relatively low decrease of hole mobility is remarkable in view of the high percentage of DAE molecules in the film and shows that the blending does not disrupt significantly the molecular packing of crystalline domains in the P3HT matrix. This was further confirmed by Grazing Incidence X-ray Diffraction (GIXD) measurements which showed similar diffraction patterns for the blended films and bare P3HT. In addition to GIXD, AFM measurements also showed the absence of phase segregation; thus, it is concluded that the DAE molecules are located within the amorphous domains of the P3HT polymer.

Upon UV illumination of the P3HT/**1c(o)** (20 wt%) transistor using 365 nm light the observed drain current is reduced by a maximum of 80% (Figure 47c). It can be restored almost completely by subsequent white light irradiation (> 400 nm) and further switching cycles can be performed. Using alternating short UV and white light irradiation pulses of 5 s each, the I_D output of the transistor was reversibly modulated by more than 10% for 5 switching cycles without any loss of performance. Importantly, the maximum photoresponse of I_D of a bare P3HT transistor was found to be less than 10% and for *both* UV and white light illumination I_D increased with time. Thus, the observed current modulation in the P3HT/**1c(o)** transistor can be attributed to the isomerization of the DAE between the ring-open and the ring-closed isomer

and the reversible formation of charge traps. Notably, the photoinduced current modulation of the P3HT/**1h(o)** device is significantly smaller than that of the P3HT/**1c(o)** transistor (Figure 47c), indicating less efficient hole transfer from the P3HT to the HOMO of **1h(c)**.

The initial experiments on photocontrollable P3HT/DAE OTFTs raised the question if also small molecule organic semiconductors, which typically perform better due to their enhanced crystallinity, can be applied and how the morphology of the resulting blend and potentially increased phase segregation influence the transistor performance. Therefore, 2,7-dodecylbenzothieno(3,2-b)benzothiophene BTBT (Scheme 42) was chosen as small molecule semiconductor, which has been shown in the literature to possess a charge carrier mobility between 0.1 – 16.4 $cm^2\ V^{-1}\ s^{-1}$ depending on the processing conditions.[171] Its performance upon blending with DAEs is compared to the already studied P3HT based transistors. As photoactive compound again DAE **1(c)** was chosen. From HOMO energy levels reported in Table 20 and in Figure 48 can be seen that in contrast to P3HT devices the HOMO of the ring-open form of **1c** is accessible for holes in the BTBT matrix, as their HOMO energies are very similar. Thus, a decrease of hole mobility is expected upon blending BTBT with DEA 1c(o). To study the influence of the blend morphology the 3,5-bis(*tert*-butyl)phenyl substituted DAE **13a** (Scheme 42) was synthesized and investigated. While comprising HOMO energies almost identical to **1c** in the ring-open and the ring-closed form, it is expected that **13a** undergoes less pronounced intermolecular interactions with the BTBT matrix due to the bulkiness of the *tert*-butyl groups.

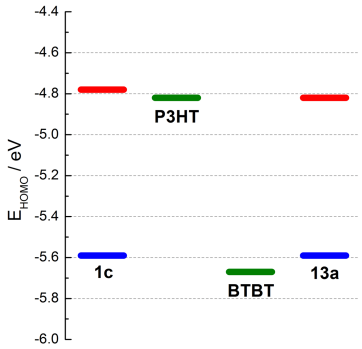

Figure 48. HOMO energy alignment between P3HT, BTBT, as well as DAEs **1c** and **13a** in their ring-open (blue) and ring-closed (red) forms, as determined by cyclic voltammetry.

Transistors using P3HT and BTBT as matrices were fabricated in the bottom-gate top-contact (BG-TC) geometry[37] and included 20 wt% of the respective DAEs in all cases. Compared to the bare semiconductor, blending of P3HT with both DAEs in their ring-open forms did not reduce the hole mobility with values around $1 \cdot 10^{-3}\ cm^2\ V^{-1}\ s^{-1}$, showing that the DAEs are located in the amorphous regions of the polymer and the HOMO levels are not

[37] Note that the experiments reported before ware made on P3HT devices in the BG-BG geometry. However, BG-BG devices using BTBT were found to be non-functioning.

accessible for holes. Blending BTBT with DAE **13a(o)** resulted in a moderate decrease of the hole mobility by a factor of 3 compared to the value of 0.64 $cm^2 V^{-1} s^{-1}$ of the bare semiconductor. In contrast, the hole mobility of the BTBT/**1c(o)** blend was reduced by more than two orders of magnitude. As both ring-open isomers **1c(o)** and **13a(o)** have the same driving force for charge trapping the huge difference in the dark-performance of the BTBT transistors has to originate from differences of the morphology of the blends. Presumably, due to stronger interactions between **1a(o)** and BTBT the crystallinity of the semiconducting matrix is significantly reduced resulting in a charge carrier mobility. Further evidence for this assumption was found by GIXD, AFM, confocal fluorescence microscopy, and measurement of the photokinetics for ring-closure of the DAEs within the BTBT matrix.

Photoswitching of the P3HT/**1c(o)** based devices (Figure 49a) proceeds in a very similar manner to the experiments using BG-BC transistors (*vide supra*). The drain current decreases by 68% upon UV irradiation and it is restored upon visible light irradiation. Notably, the P3HT/**13(a)** blend shows a smaller current variation of only 22% under the same irradiation conditions. Again, this may be attributed to a different interaction between P3HT and DAE **13a**. For BTBT devices the differences between the two DAE derivatives in the isomerization induced current modulation are much more pronounced. While DAE **13a** shows a moderate modulation of I_D of 40%, in case of the BTBT/**1c(o)** blend it is reduced by almost 100% upon UV irradiation (Figure 49b). Thus, for both DAEs the decrease of the drain current is larger for the BTBT devices than for P3HT, indicating that the traps formed by ring-closure are deeper in energy in the BTBT blends, which has been predicted the HOMO energy alignment (Figure 48). Surprisingly, upon irradiation with visible light the drain current did not recover at all for the BTBT/**1c(o)** blend and the switching process showed significant fatigue for the BTBT/**13c(o)** blend. However, by optical spectroscopy on blended films it could be proven that photochemical ring-opening of **1c** and **13a** does take place in the BTBT matrix.

To further understand the observed phenomenon, the time for UV irradiation of the transistors was restricted to a total of 30 s for one switching cycle. Thereby, in the P3HT based transistors only a small current modulation could be observed (Figure 49c). In contrast, for the BTBT/**1c(o)** blend still a maximum decrease of I_D by 90% was detected while the BTBT/**13a(o)** blend showed a current modulation of only 20% (Figure 49d). This is again indicative for a much stronger interaction of DAE **1c** with BTBT resulting in higher charge carrier trapping efficiency. Importantly, when using short UV irradiation times the observed current modulation is fully reversible for both BTBT devices.

In view of these results, the irreversible decrease of I_D in the BTBT/**1c(o)** device upon longer UV irradiation times may be explained by the irreversible formation of small amounts of the photochemical by-product of the DAE (see section 4.3). The annulated isomer has a very similar π-electronic structure as the ring-closed isomer and should therefore act as a charge trap

as well. Obviously, due to the strong interaction between BTBT and DAE **1c** the isomerization of only a small fraction of molecules to the ring-closed isomer is sufficient to induce a strong reduction of the drain current. Thus, upon longer UV irradiation the formation of a small amount of by-product is sufficient to irreversibly induce charge trapping and degrade the photoresponse of the transistor. For the BTBT/**13a** the observed fatigue may be explained analogously. However, in this case the trapping efficiencies of the ring-closed isomer and the by-product are less pronounced, so it takes more switching cycles to irreversibly decrease I_D.

It can be concluded that in order to construct transistors with small molecule semiconductors showing high intrinsic charge carrier mobility, blends of BTBT with weakly interacting DAE **13a** have to be employed at the cost of efficiency for the photomodulation of the output current. If photomodulation of I_D has priority, DAE **1c** interacting more strongly with the matrix is superior. However, due to the strong interaction the dark-performance of the transistor is significantly reduced and sensitivity towards photodegradation of the DAE is increased.

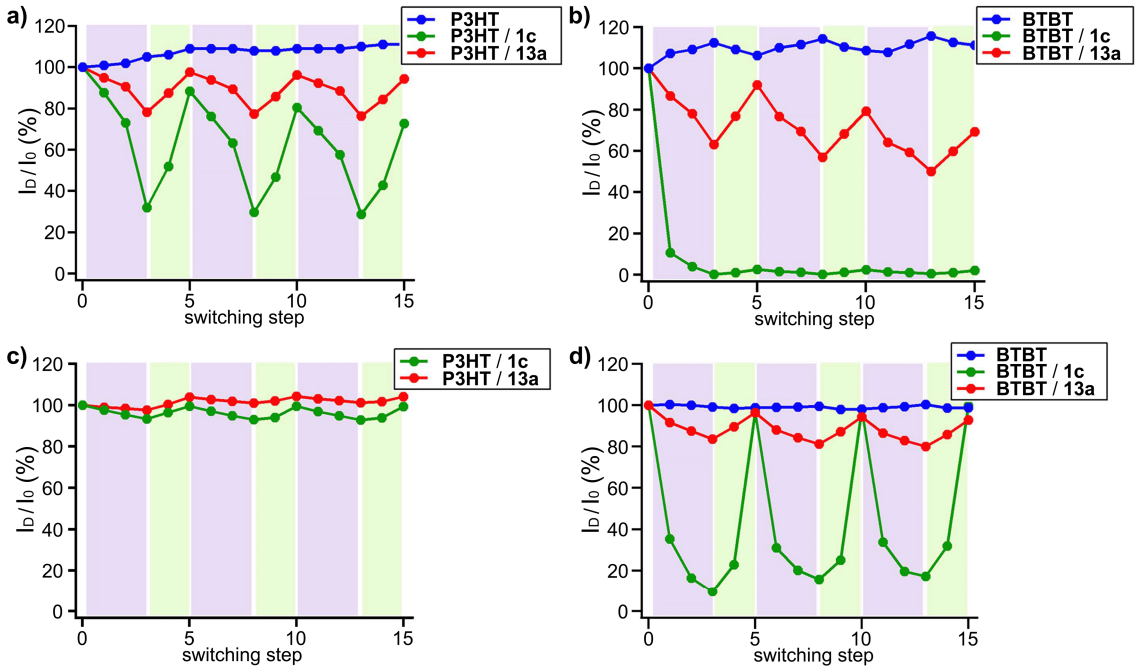

Figure 49. Comparison of the photoswitching of a) P3HT and b) BTBT based TFTs for *long* UV irradiation times and of c) P3HT and d) BTBT based TFTs for *short* UV irradiation times. All devices were in the BG-TC geometry and active layers contained 20 wt% of the respective DAE derivatives. Normalized maximum drain currents were extracted from transfer curves recorded in the dark at fixed gate (V_G = -80 V) and drain (V_D = -10 V) voltages. *Long* UV irradiation cycles consisted of 3 steps of UV irradiation (365 nm, 90 s, 120 s, 600 s) and 2 steps of irradiation with visible light (546 nm, 120 s, 600 s). For *short* UV irradiation cycles the UV irradiation was restricted to 3 steps of each 10 s.

4.6.3 Photocontrollable n-type OTFTs

The concept of introducing photocontrollable trapping states into a semiconducting matrix using DAEs was extended to n-type semiconductors. Therefore, DAEs possessing a strong modulation of their LUMO energies between the ring-open and ring-closed form are needed. Importantly, the absolute LUMO energies have to be very low in order to be compatible with common organic n-type semiconductors. Thus, structurally similar DAEs **2i** and **4i** were chosen, both possessing strongly electron accepting perfluorocyclopentene as bridging moiety and 3,5-bis(trifluoromethyl)phenyl substituents in the periphery (Scheme 43). From the results presented in section 4.5 can be deduced that these DAEs are amongst the structures possessing lowest LUMO energies of all compounds investigated in this work. While DAE **2i** in its ring-closed form possesses a LUMO energy of -3.5 eV, the additional nitrogen of the thiazole rings of DAE **4i** slightly shifts its LUMO energy further down to -3.7 eV (Table 21, Figure 50a). LUMO levels of both ring-open isomers are more than 1 eV higher in energy.

Two fullerene based semiconductors, PCBM and ICBA (Scheme 43), were chosen as matrices for the construction of the OTFTs. Their LUMO energies perfectly align with that of the DAEs in order to fulfill the energetic requirements. Thereby, the LUMO of ICBA is positioned at slightly higher energies than both of the ring-closed DAEs while the LUMO of PCBM is positioned in-between the two ring-closed isomers (Table 21, Figure 50a). This results in the situation that the LUMO energy difference $\Delta E_1 = 290$ meV between ICBA and DAE **4i(c)** represents the largest driving force for electron trapping amongst the four possible fullerene/DAE blends. For the combinations of ICBA and **2i(c)** as well as PCBM and **4i(c)** a smaller driving force with $\Delta E_2 = \Delta E_3 = 100$ meV is predicted. Finally, for the combination of PCBM with **2i(c)** no driving force for electron trapping should exist.

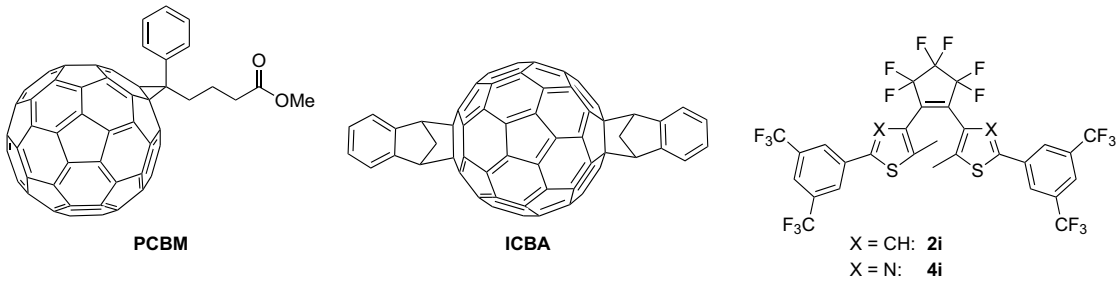

Scheme 43. Semiconducting matrices and DAE derivatives for the construction of photocontrollable n-type OTFTs.

Table 21. Reduction potentials and derived LUMO energies of semiconducting matrices and DAE derivatives, obtained from cyclic voltammetry. Potentials are given in reference to the ferrocene/ferrocenium redox couple (rev = reversible, qr = quasireversible, irr = irreversible).

comp.	E_p^{c1} / V	E_{LUMO} / eV
2i(o)[a]	-2.56 (irr)	-2.24
2i(c)[a]	-1.27 (qr)	-3.53
4i(o)[a]	-2.11 (irr)	-2.69
4i(c)[a]	-1.08 (qr)	-3.72
PCBM[b]	-1.18 (rev)	-3.62
ICBA[b]	-1.37 (rev)	-3.43

a) acetonitrile/0.1 M Bu_4NPF_6.
b) toluene/acetonitrile 3:1/0.1 M Bu_4NPF_6.

OTFTs with active layers composed of blends of the four possible combinations between the two semiconductors and the ring-open DAE isomers were fabricated in the BG-BC geometry by spin-coating from chlorobenzene solutions. Thereby, all blends contained 20 wt% of the respective DAE derivatives. For PCBM based devices electron mobilities were essentially unaffected by the presence of the DAEs and amounted to 0.04 $cm^2 V^{-1} s^{-1}$. In contrast, electron mobilities of the two blended ICBA devices were reduced by a factor of 6 compared to the pristine semiconductor, which possessed a mobility of $8 \cdot 10^{-3}$ $cm^2 V^{-1} s^{-1}$. GIXD measurements showed that all investigated films were completely amorphous. AFM measurements and Scanning Auger Microscopy indicated a higher degree of phase segregation for the PCBM blends, explaining that the presence of the DAEs did not reduce their electron mobility.

By irradiation of the transistors with UV (320nm) and visible (540 nm) light the expected photoresponse is observed. The pristine semiconductors show only negligible variation of the drain current upon irradiation. The same is observed for the PCBM/**2i** blend, which represents the energetically unfavorable combination for electron trapping in the ring-closed state of the DAE. Blends of PCBM with **4i** as well as ICBA with **2i** show a light induced current modulation of 14% and 11%, respectively. Notably, the ICBA/**4i** blend, possessing the largest driving force for electron trapping, shows the by far highest current modulation of 55%. Thus, the four fullerene/DAE combinations demonstrate that the photochemical current switching efficiency critically depends on the energy difference between the LUMO levels of the phohotchromic molecule and the semiconductor.

Both PCBM and ICBA transistors show a slow decrease of the absolute drain current measured over several switching cycles. This fatigue, which is more pronounced in the ICBA case, is attributed to degradation of the semiconductors and not to the degradation or by-product formation of the DAE molecules. Note that DAEs **2i** and **4i** have been characterized as highly fatigue resistant in section 4.3 of this work.

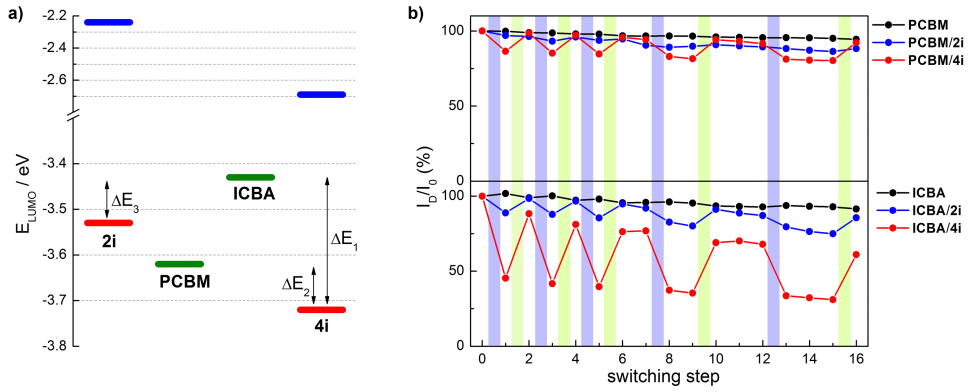

Figure 50. a) LUMO energy alignment between PCBM and ICBA as well as open (blue) and closed (red) isomers of DAEs **2i** and **4i**, as obtained from cyclic voltammetry. b) Normalized drain current ($V_D = 40$ V, $V_G = 80$ V for ICBA, $V_G = 120$ V for PCBM) during photoswitching of OTFT devices containing blends of PCBM (top) and ICBA (bottom) with 20 wt% of DAEs **2i** and **4i**, respectively. Each switching cycle consisted of 30 s of UV irradiation (320 nm) and 10 min of visible light irradiation (540 nm). After each irradiation step the transistor was relaxed for 30 s in the dark before a transfer curve was recorded.

4.6.4 Summary

For the first time photocontrollable OTFTs were constructed by the light-induced reversible energy level modulation of DAEs blended with p-type and n-type semiconductors. The blending approach offers the advantage that each component can be chosen to fulfill specific optoelectronic functions. While the utilization of well-known polymer and small molecule semiconductors enables the electrical operation of the transistor devices with a high efficiency, the DAE component of the blend can be tuned by structural modifications in order to precisely align HOMO and LUMO energy levels with that of the semiconductor. Thereby, the energy difference between the semiconductor and charge carrier traps induced by the DAE directly correlates to the extent of photomodulation of the output current. Furthermore, the delicate interplay between phase segregation within the blended films and strong intermolecular interactions between the DAE and the semiconductor has been demonstrated. Strong phase segregation gives transistors with high charge carrier mobilities but photomodulation of the output current may be diminished. On the other hand, strong intermolecular interactions give large photomodulation but reduce the crystallinity of the semiconductor and thus alternate its electric properties. By proper substitution of the DAE components the morphology of the blended films can be tuned in order to meet the demands on the device. In addition to the compositional flexibility, the blending approach ensures easy and cheap fabrication processes as well as the applicability for large-area electronics.

For p-type transistors photomodulation of the drain current up to 90% using the small molecule BTBT and up to 80% using polymeric P3HT was achieved. In case of n-type transistors photomodulation efficiencies were significantly smaller and degradation of the fullerene matrices was observed.

To increase the transistor performance, DAE derivatives possessing LUMO levels lower in energy than -4.0 eV are of high interest for combining them with high-performing and air-stable n-type semiconductors such as PDIF-CN2[172] or P(NDI2OD-T2).[173] For the construction of photocontrollable p-type OTFTs a broad library of DAE compounds can be accessed. However, it has to be noted that such electron-rich DAEs generally suffer from increased fatigue due to formation of the photochemical by-product (see section 4.3). It remains a challenge to design highly fatigue resistant DAEs possessing HOMO levels suited for charge trapping in p-type semiconducting matrices.

Further, currently ongoing studies are concerned with the immobilization of thiol functionalized DAEs **13b** and **13c** on gold electrodes comprising the source and drain within the transistor geometry. Thus, DAEs within a self-assembled monolayer comprise an interface between the electrode and the semiconductor. By photoinduced changes of energy levels the barriers for charge injection and thus the drain current shall be modulated.

4.7 Towards photoswitchable catalysis

4.7.1 Introduction

The application of photochromic molecules for the photocontrol over chemical reactivity and catalysis increasingly gains attention (see section 2.2.3). Reversibly controlling the outcome of reactions between small molecules with light is interesting for the procession and amplification of optical signals within chemical systems[1] or in the emerging field of photopharmacology.[174] Moreover, photoswitchable catalysts have huge potential when applied to polymerization reactions. In principle, they would constitute a new way to precisely control the microscopic structure of the growing polymer, *i.e.* its molecular weight and distribution, the sequence of monomers, or its tacticity, and consequently would enable the synthesis of new polymeric materials with unique macroscopic properties. Therefore, in the long run, photoswitchable catalysts that not only switch between active and non-active states but also are able to control the chemo- and stereoselectivity of a polymerization reaction are of high interest.

As a first step, activity control over an organic polymerization catalyst shall be realized by utilizing the electronic differences between the ring-open and ring-closed isomers of DAEs.[38] The ring-opening polymerization (ROP) of *L*-lactide to form polylactide (Scheme 44a) is an attractive target, as it is efficiently mediated by a number of organocatalysts, *e.g.* DMAP, NHCs, bifunctional thioureas, amidines, or guanidines, and thereby shows the properties of a living polymerization.[175] In particular, the bicyclic guanidine 1,5,7-triazabicyclo[4.4.0]dec-5-ene (TBD, Scheme 44b) has been shown by the group of Hedrick to be an outstandingly efficient organocatalyst for this reaction.[176] It polymerizes 100 monomer units of *L*-lactide within 20 s reaction time using a catalyst loading of only 0.1 mol%. The resulting polymer shows a narrow polydispersity with a PDI of 1.19. The extraordinary high activity of TBD has been attributed to its bifunctional nature and its bicyclic structure.[177] While the NH-group activates the carbonyl function of the monomer, the basic nitrogen atom undergoes nucleophilic attack and ring-opens the lactide forming an N-acyl intermediate, which subsequently reacts with the alcohol function of the initiator or chain end. Alternatively, a purely hydrogen-bonding mediated mechanism is discussed for which the basic nitrogen atom activates the alcohol that then directly reacts with the activated monomer unit.[176c] The bicyclic structure of TBD provides the advantageous parallel orientation of the acidic NH-group and basic nitrogen lone-pair.[177] In addition to the ROP of lactide and lactones, TBD proved to be an efficient

[38] At the time the project was started no reversible photocontrol over catalysis of a polymerization reaction using a photochromic compound has been reported. In the meantime the group of Bielawski reported the photocontrol over ROP of lactide using an NHC functionalized DAE (see also section 2.2.3).[23b] However, the catalyst showed poor reversibility of the switching process due to degradation.

organocatalyst for many other small molecule reactions, such as aldol, Henry, Michael, and Knoevenagel reactions[177] as well as transesterifications.[178]

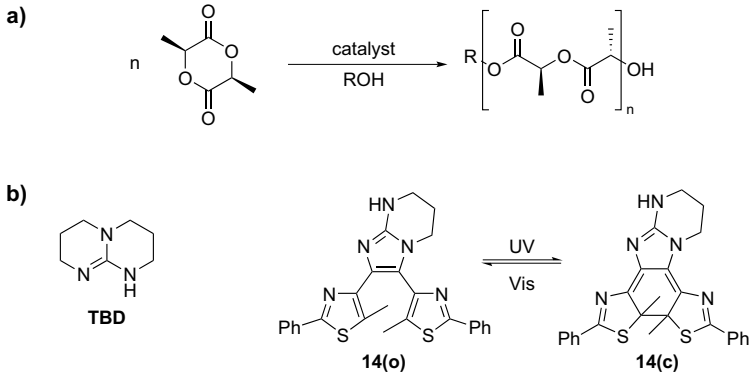

Scheme 44. a) Ring-opening polymerization of *L*-lactide. b) Bicyclic structure of TBD, a highly active organocatalyst for the ROP of lactide and lactones, and a derived structural motif for a photoswitchable bicyclic guanidine.

Inspired by the remarkable properties of TBD the DAE motif **14** (Scheme 44b) has been designed possessing a bicyclic guanidine functionality as bridging moiety. Thereby, the parent structure of TBD has been modified to a bicyclic structure consisting of a 6-membered and a 5-membered ring and an additional double bond has been incorporated into the latter. It is supposed that the decrease of the size of *one* ring only has little influence on the basicity of the bicyclic guanidine, as can be seen from pK_A-values measured in water[179] and nucleophilicity parameters collected by the group of Mayr.[180] The effect of incorporating an additional double bond and thus forming an aromatic imidazole ring presumably reduces the nucleophilicity by one order of magnitude, as can be estimated by comparing the nucleophilicity parameter of 2-methylimidazole[181] and 2-methylimidazoline.[182] However, by ring-closure of compound **14** the 2-aminoimidazole moiety is converted into an "2-aminoimidazoline" possessing two exocyclic double bonds and thus being in conjugation with the extended π-system of the DAE. It is difficult to predict the effect of ring-closure on the basicity, nucleophilicity and hence catalytic activity of the guanidine motif at this point. Note that structurally related 2-aminooxazolines and 2-aminothiazolines showed catalytic activity in the ROP of lactide.[183] To ensure sufficient thermal stability of the ring-closed isomer thiazole heterocycles have been employed for the construction of the DAE **14**.

The synthesis of compound **14** was already developed during a diploma thesis preceding this work.[75a] Further optimization of the synthesis is reported in section 4.1. In the following the photochemical properties of DAE **14** will be presented before studies on the catalytic activity and basicity of the guanidine motif will be discussed.

4.7.2 General properties of DAE 14

After Cbz-deprotection of intermediate **61** to give the free guanidine **14** the compound becomes sensitive towards air. It has to be stored under an argon atmosphere; otherwise some decomposition products can be detected by TLC and UPLC within several days. Notably, after evaporation of the solvent under reduced pressure, the solid material obtained cannot be re-dissolved in any neutral solvent, including CH_2Cl_2, MeOH, DMF, or DMSO, unless relatively large amounts (approximately 100 mL per mg) are used. Once dissolved, the solution can be concentrated by evaporation of the solvent under reduced pressure to a significantly smaller volume before precipitation starts. The solubility of the isolated compound can be increased by adding excess benzene to concentrated solutions and subsequent lyophilization under high vacuum. However, the solubility of the thus obtained solid material is still relatively low and upon storage over few days it further decreases markedly. Best results are obtained using solvent mixtures consisting of CH_2Cl_2 or THF and MeOH, which enable the preparation of solutions with concentrations not higher than 0.01 M.

Note that upon addition of a small amount of acid to the solvent the solubility of compound **14** is massively increased.

4.7.3 Photochemical studies

UV/Vis spectra recorded of DAE **14** and the Cbz-protected analogue **61** in acetonitrile (Figure 51a-b, Table 22) show the typical characteristics of a terarylene,[20a] *i.e.* a DAE with an aromatic heterocycle in the bridge. While the absorbance of the ring-open isomers is not shifted compared to normal DAEs such as dithiazolylcyclopentene **3d**, the low-energy absorption band of the ring-closed isomers is shifted by more than 100 nm to longer wavelengths. The shift is due to an increased conjugated length of the π-system in the ring-closed state including the additional double bond of the bridging heterocycle. The ring-closed isomers of compounds **14** and **61** did not show any thermal cycloreversion at 25 °C.

Quantum yields for ring-closure and ring-opening upon UV irradiation were determined by analysis of the full kinetic traces revealing that the cyclization reaction of Cbz-protected DAE **61** proceeds slightly faster than that of DAE **14** (Table 22). However, for both compounds a PSS consisting of 92% of the ring-closed isomer is reached. Notably, upon prolonged UV irradiation for both DAEs **14** and **61** UPLC/MS showed the fast emergence of an isomeric by-product, presumably the annulated isomer, which is discussed in section 4.3 of this work. Employing the procedures outlined in section 4.2, quantum yields for by-product formation of 0.004 were determined, which demonstrates the relatively low fatigue resistance of DAEs **14** and **61**.

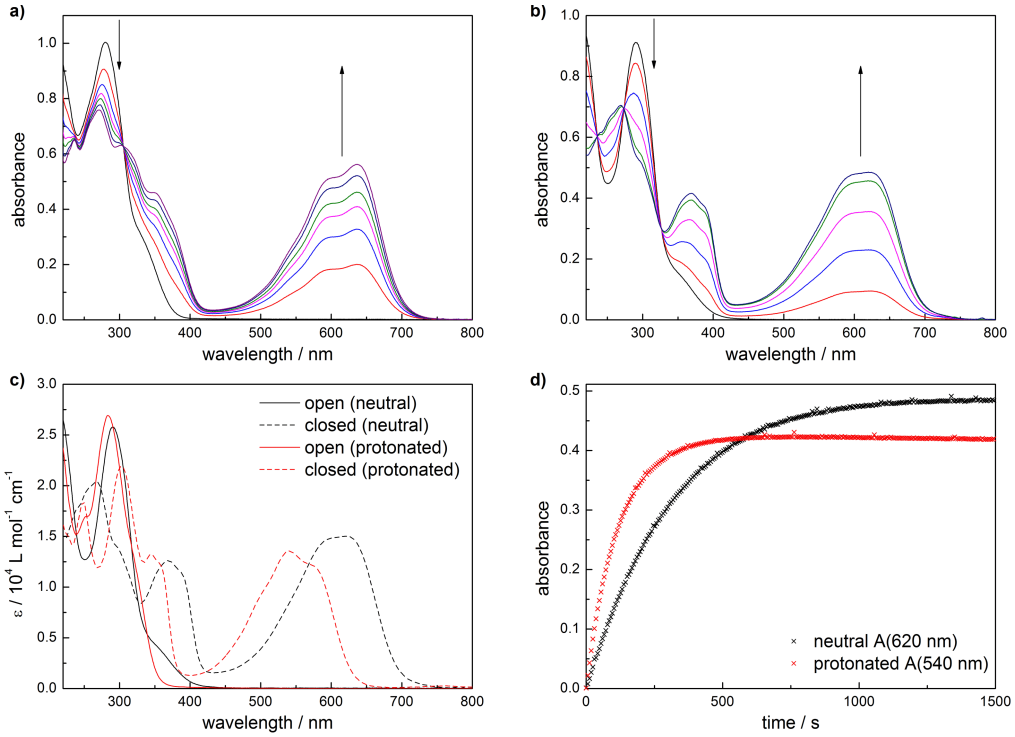

Figure 51. UV/Vis spectra of acetonitrile solutions of a) Cbz-protected DAE **61** ($3.08 \cdot 10^{-5}$ M) and b) DAE **14** ($3.50 \cdot 10^{-5}$ M) during irradiation with 310 nm light (1000 W Xe, interference filter) until reaching the PSS. c) Molar absorptivities of the ring-open and ring-closed isomers of **14** in acetonitrile and in acetonitrile containing $5.5 \cdot 10^{-5}$ M $MeSO_3H$. d) Photokinetic traces of **14** ($3.50 \cdot 10^{-5}$ M) in acetonitrile and in acetonitrile containing $5.5 \cdot 10^{-5}$ M $MeSO_3H$ recorded under irradiation with 313 nm light ($I_0 = 4.20 \cdot 10^{-10}$ E s^{-1} cm^{-3}, ferrioxalate actinometry). All solutions were saturated with argon.

Table 22. Photophysical properties of guanidine substituted DAEs in acetonitrile.

comp.	λ_{max} / nm (ε / 10^4 M^{-1} cm^{-1})		PSS (310 nm)[a]	Φ_{AB} (313 nm)[b]	Φ_{BA} (313 nm)[b]	Φ_{BC} (313 nm)[b]
	ring-open isomer	ring-closed isomer				
61	280 (3.26)	599 (1.80), 637 (1.98)	92%	0.51	0.03	0.004
14	291 (2.57)	620 (1.50)	92%	0.32	0.03	0.004
14[c]	283 (2.69)	540 (1.35)	95%	0.97	0.05	n.d.

a) Conversion to the ring-closed isomer in the PSS reached after UV irradiation (310 nm, 1000 W Xe), determined by UPLC.
b) Quantum yields for ring-closure, ring-opening, and by-product formation obtained by nonlinear regression of photokinetic data under UV-irradiation (313 nm, 500 W Xe(Hg), ferrioxalate actinometry).
c) In acetonitrile/$5.5 \cdot 10^{-5}$ M $MeSO_3H$.

Upon addition of excess methanesulfonic acid to an acetonitrile solution of DAE **14** a marked hypsochromic shift of the absorption bands of the ring-open and ring-closed isomers is observed, indicative for protonation of the guanidine moiety (Figure 51c). In the protonated state the ring-closed isomer thermally reverts to the ring-open form. However, no simple monoexponential kinetics are observed, thus only an approximate half-life of 64 h at 25 °C can be determined. Remarkably, in the protonated state the ring-closure of **14** proceeds with a significantly higher rate than in the neutral form (Figure 51d). A quantum yield of 0.97 was

determined using regression analysis of photokinetic data, indicating that the reaction is nearly photon-quantitative. However, note that the relative error of this parameter usually amounts to 10 – 12%, as discussed in section 4.2. Possibly, after protonation of the guanidine nitrogen a hydrogen-bond to one of the thiazole heterocycles is formed restricting the DAE in its antiparallel conformation, which is in analogy to dithiazolylethenes showing photon-quantitative cyclization reported by the group of Kawai.[21b]

As test experiments on the potential catalytic activity of guanidine **14** in the ROP of lactide shall be performed in methylene chloride solutions, the photochemistry of **14** was also examined in this solvent. In spectroscopic concentrations ($3 \cdot 10^{-5}$ M) irradiation with UV-light lead to the immediate formation of the ring-closed isomer, but with every irradiation step the spectrum of the neutral compound was shifted more and more to the spectrum of the protonated species. Presumably compound **14** is sensitive to acidic trace impurities of the solvent.

For a higher concentration, *i.e.* the concentration that shall be used in test experiments on catalytic activity, the photochemistry of DAE **14** in methylene chloride was probed by NMR spectroscopy (Figure 52). Therefore, a 0.01 M solution of freshly lyophilized DAE **14** was prepared in CD_2Cl_2. The compound initially did not dissolve completely, however upon UV irradiation (300 nm) of the NMR tube in a photochemical reactor the residual solid material disappeared. Before UV irradiation the ^{1}H NMR spectrum showed sharp signals, in particular for the two methyl groups on the thiazole rings at ca. 2.1 ppm. Upon irradiation the sharp signals corresponding to the ring-open isomer gradually disappeared and an overall broadened spectrum evolved in which no distinct features could be identified. After 15 min at a conversion of ca. 73% to the ring-closed isomer no further changes were detected. Importantly, after subsequent visible light irradiation the initial NMR spectrum of the ring-open isomer was almost fully restored with only trace signals for degradation products, showing that the photochemical switching in a concentrated methylene chloride solution is reversible. However, note that after the switching cycle the color of the solution in the NMR tube appeared brownish instead of pale yellow as at the beginning of the experiment.

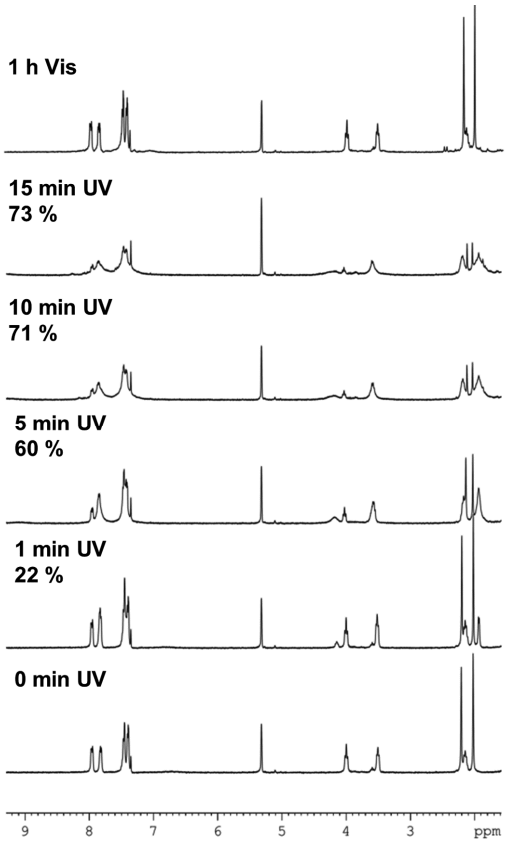

Figure 52. ^{1}H NMR spectra (300 MHz) recorded during irradiation of an NMR tube containing a solution of **14** in CD_2Cl_2 ($c \approx 0.01$ M) using a Rayonet RPR 100 photochemical reactor equipped with 300 nm lamps. Note that optical inspection of the NMR tube showed that a small amount of the material was not dissolved before irradiation. Conversion to the ring-closed isomer is roughly estimated from the relative decrease of the two sharp singlets at ca. 2.1 ppm. After 15 min of UV irradiation the NMR tube was placed in front of a 1000 W Xe arc lamp equipped with a longpass filter (λ>500 nm) for 1 h.

4.7.4 Reactivity studies

ROP of *L*-lactide

To study the ROP of *L*-lactide the procedure reported by Hedrick and coworkers,[176a] which has been established in the Hecht group by Dr. Philipp Viehmann,[184] was followed. For experimental details see section 6.6. 1-Pyrenebutanol was used as the initiator in a ratio of 1:100 to the *L*-lactide monomer. The polymerization conditions were tested by performing the reaction in CD_2Cl_2 using TBD (0.1 mol% relative to *L*-lactide) as the catalyst. After 30 s reaction time the polymerization was quenched by the addition of benzoic acid and a ^{1}H NMR spectrum of the crude reaction mixture was recorded (Figure 53, top). The emergence of a new set of signals for the methyl and methine protons of the lactide backbone, the latter integrating 191:2 to the signal corresponding to the CH_2O group of the initiator, proved the clean formation of the polymer.

In order to test the ability of DAE **14** to catalyze the ROP of *L*-lactide, identical reaction conditions were chosen. Due to the restricted solubility of DAE **14** it could only be used in an

amount of 2 mol% relative to the monomer. After combining the monomer, catalyst and initiator in CD_2Cl_2, the reaction mixture was divided between two NMR tubes and one of the NMR tubes was irradiated with UV light (300 nm) in a photochemical reactor for 15 min. Then, the reaction was followed over a period of 17 h using NMR spectroscopy. Unfortunately, neither the non-irradiated nor the irradiated sample showed any sign of conversion to the polymer (Figure 53, middle and bottom).

Given that the catalytic activity of guanidine **14** is expected to be significantly lower than that of TBD, a catalyst loading of only 2 mol% in the experiment appears to be way too low for an efficient reaction. Thus, due to the restricted solubility of DAE **14** no definite answer on its capability to catalyze the ROP of *L*-lactide can be given.

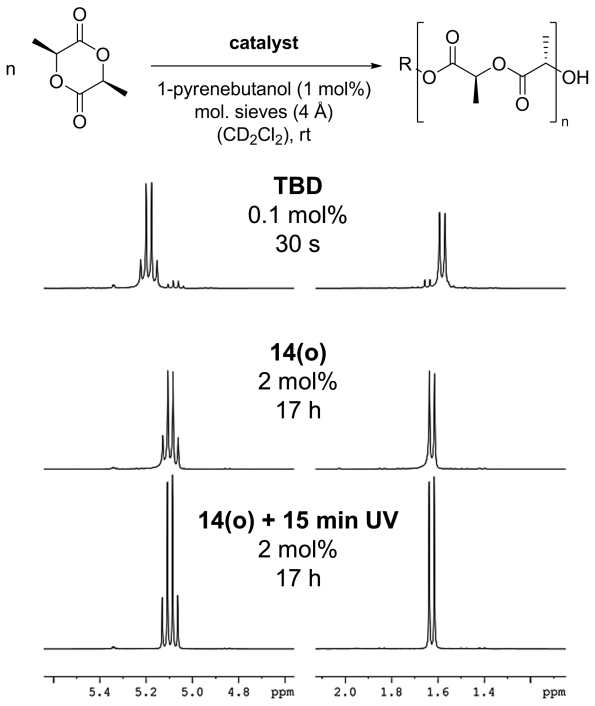

Figure 53. ^{1}H NMR spectra (300 MHz) of the crude reaction mixtures of the attempted ring-opening polymerization of *L*-lactide in CD_2Cl_2. Signals corresponding to the methine protons (left) and methyl protons (right) of the lactide backbone are shown. When using TBD (0.1 mol%) as catalyst clean conversion to the polymer is observed (top). If **14** (2 mol%) is employed as catalyst, no conversion can be observed, neither in the non-irradiated nor in the irradiated NMR tube (middle and bottom).

Determination of pK_a values

In order to compare the properties of DAE **14** with other organic bases and to determine the effect of the isomerization reaction, pK_a values were determined in acetonitrile for both the ring-open and ring-closed isomers. Therefore, the procedure described by Leito and coworkers[185] consisting of titration of the analyte in presence of a reference base with an optically transparent acid and following of the spectral changes using UV/Vis spectroscopy was applied. Thereby, the difference of the pK_a values between the analyte and the reference must not be larger than 2

units. The reference base 2-amino-1-methylbenzimidazole **ABI**, for which a pK_a value of 16.31 in acetonitrile has been reported,[185b] proved to fulfill this condition.

Acetonitrile solutions of **14(o)**, **14(c)**, and **ABI** were titrated with methanesulfonic acid and the spectral changes were recorded by UV/Vis spectroscopy (Figure 54a-c). For experimental simplicity, the titration of the ring-closed isomer **14(c)** was performed using a solution of **14(o)** which was pre-irradiated to the photostationary state. The residual amount of the ring-open isomer was neglected. The absorption spectra of all three titration experiments show smooth conversion to the protonated species with several sharp isosbestic points present.

In a second experiment mixtures of **14(o)** and **ABI** as well as **14(c)** and **ABI** were titrated (Figure 54d-e) and the occurring spectral changes were evaluated at wavelengths at which isosbestic points were observed in the titration spectra of the pure compounds (for details see section 6.1.2). Note that the absolute and relative concentrations of the analyte and the reference are of no importance for the experiment. They were chosen in a way that both species contribute to ca. 50% to the total absorbance. Evaluation of the titration data revealed a ΔpK_a of 0.22±0.15 between **14(o)** and **ABI** and a ΔpK_a of 0.73±0.09 between **ABI** and **14(c)** (Figure 55).

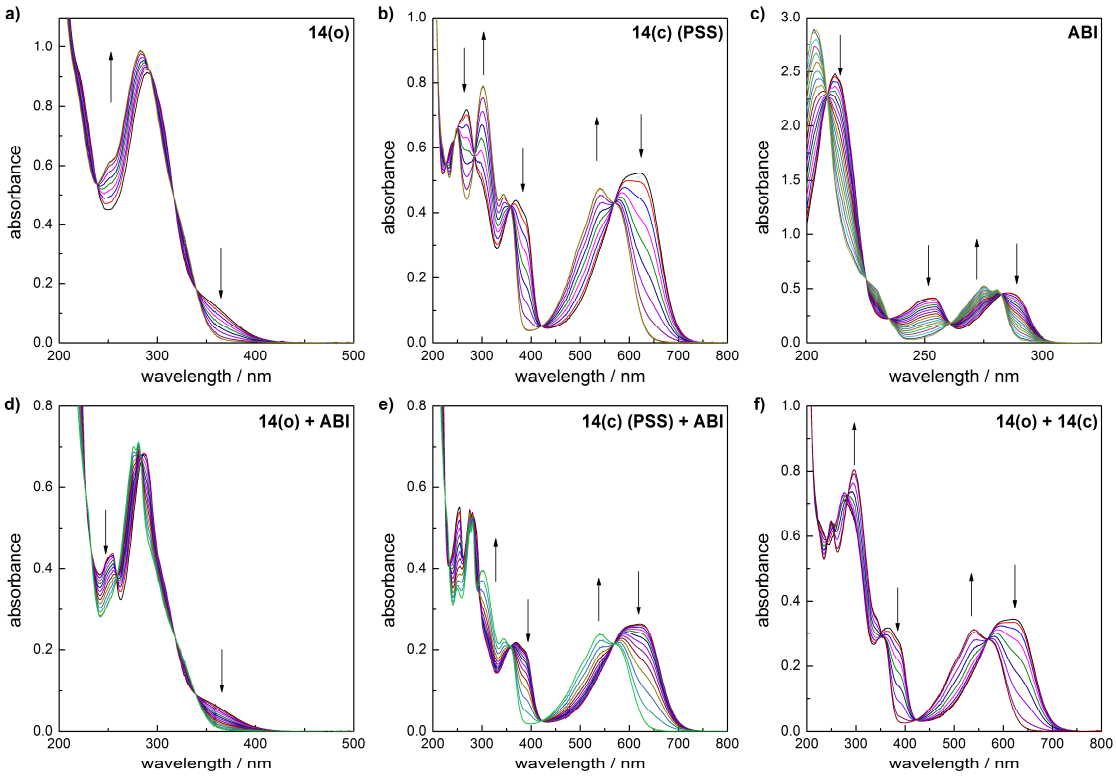

Figure 54. UV/Vis spectra of acetonitrile solutions recorded upon addition of a solution of methanesulfonic acid ($1.08 \cdot 10^{-3}$ M in acetonitrile) in steps of 10 µL: a) Ring-open isomer **14(o)** ($3.50 \cdot 10^{-5}$ M), b) a solution of **14(c)** (ca. $3.5 \cdot 10^{-5}$ M) obtained by pre-irradiation of the ring-open isomer to the PSS, c) 2-amino-1-methylbenzimidazole **ABI** ($6.00 \cdot 10^{-5}$ M), d) a mixture of **14(o)** ($1.75 \cdot 10^{-5}$ M) and **ABI** ($3.00 \cdot 10^{-5}$ M), e) a mixture of **14(c)** ($1.75 \cdot 10^{-5}$ M) and **ABI** ($3.00 \cdot 10^{-5}$ M), f) a mixture of **14(o)** ($1.2 \cdot 10^{-5}$ M) and **14(c)** ($2.3 \cdot 10^{-5}$ M). All spectra have been corrected for dilution by addition of the acid.

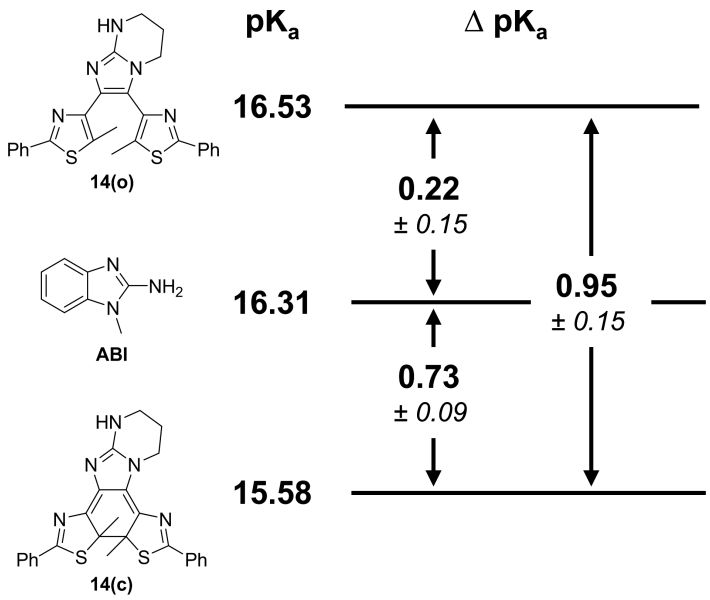

Figure 55. Experimental ΔpK_a and derived absolute pK_a values in reference to 2-amino-1-methylbenzimidazole **ABI**.[185b]

A relative pK_a difference can also be measured directly between the ring-open and ring-closed isomer of DAE **14**. Therefore, a solution of **14(o)** was irradiated using UV light until a conversion of ca. 60% to the ring-closed isomer was reached and the resulting mixture was titrated with methanesulfonic acid (Figure 54f). Thus, a ΔpK_a of 0.95±0.15 was determined, which is in perfect agreement with the values obtained in reference to **ABI** (Figure 55). This also shows that the error by using the photostationary mixture instead of the pure ring-closed isomer of DAE **14** in a titration against the reference base is only marginal and an absolute pK_a value for the ring-closed isomer can be determined.

Remarkably, the results prove that the ring-open and ring-closed isomers of DAE **14** differ in their basicity by almost one order of magnitude, with the ring-closed isomer being the less basic. The observed ΔpK_a is comparable to values reported in the literature for the isomerization induced change of the acidity of phenol[67,74] and carboxylic acid groups[186] coupled to the DAE photochromes. The first photoswitchable bases, which were realized by reversible steric shielding of a piperidine group using an azobenzene tether by the group of Hecht in 2008,[187] showed a comparable pK_a change of 0.7-0.8 in acetonitrile.

On an absolute scale the basicity of the guanidine motif **14** is much smaller than that of the prototype TBD structure (pK_a = 26.03 in acetonitrile[185b]), the latter presumably being very similar to that of the saturated 5-6-bicyclic analogue[179-180] (Scheme 45a). This indicates that the incorporation of an additional double bond into the 5-6-bicyclic structure comprises a major change to the ability of the guanidine motif to stabilize the protonated species. Due to the aromaticity of the 5-membered ring and consequently the delocalization of the nitrogen lone-pairs their capability to stabilize the positive charge on the guanidine carbon atom in the protonated state is significantly reduced (Scheme 45b). Somewhat surprisingly, the basicity of

the ring-closed isomer of DAE **14** is even lower, though the aromaticity of the 5-membered ring is destroyed by the cyclization reaction. However, both nitrogen atoms of the 5-membered ring are now in conjugation with the π-electronic system of the DAE, which obviously reduces their capability to stabilize the charge in the protonated state even more.

Based on the experimental findings and these considerations two improved bicyclic guanidine motifs for the incorporation into the DAE skeleton are proposed. First, the unsaturated bicyclic guanidine could be used as an "arm" of the DAE instead as bridging moiety (Scheme 45c). Therefore, the 5-position of the imidazole ring has to be substituted with a methyl group. While in the ring-open isomer this should not comprise any significant change compared to DAE **14**, in the ring-closed isomer the tertiary nitrogen atom within the 5-membered ring is now electronically isolated from the π-system. Thus, a higher basicity of the ring-closed isomer would be expected.

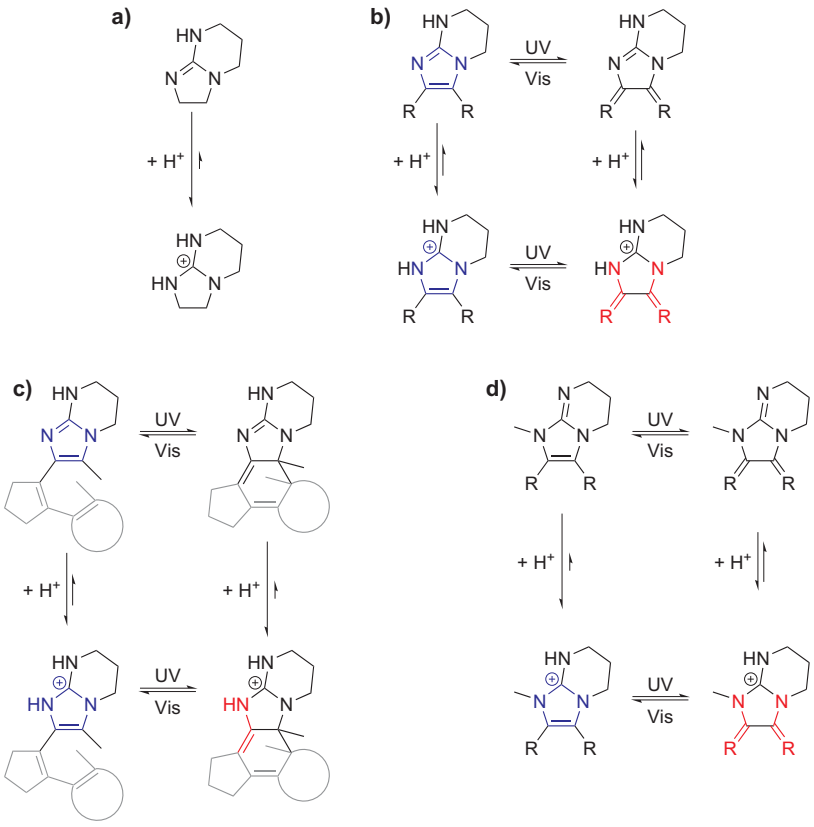

Scheme 45. Protonation equilibria for a) the saturated 5-6-bicyclic guanidine, b) the unsaturated 5-6-bicyclic guanidine used as bridge of a DAE, c) the unsaturated 5-6-bicyclic guanidine used as an "arm" of a DAE, and d) analogous 1,3-dialkylimidazol-2-ylidene amines used as bridge of a DAE. The lengths of the reaction arrows indicate the assumed positions of the equilibria.

Secondly, making a small structural modification, *i.e.* substituting the nitrogen in the 3-position of the imidazole ring with a methyl group, would turn the guanidine bridge of the ring-open isomer into a non-aromatic, cross-conjugated 1,3-dialkylimidazol-2-ylidene amine moiety (Scheme 45d). Upon protonation the 5-membered ring gains aromaticity and

consequently is stabilized. This should result in a significantly higher basicity of the ring-open form. In contrast, in the ring-closed form the lone-pairs of the nitrogen atoms are still in conjugation with the DAE π-system. Thus, a basicity comparable to that of the ring-closed isomer of DAE **14** would be expected. The proposed motif is in analogy to *N*-alkyl-1,3-dialkyl-4,5-dimethylimidazol-2-ylidene amines, which were shown to possess superbasic properties with pK_a constants between 23 – 30 in acetonitrile.[188]

Testing DAE 14 in a Henry reaction

Further reactivity studies using guanidine DAE **14** as a general base catalyst for small molecule reactions were unsuccessful due to the restricted solubility of the compound. In particular, the Henry reaction between 4-nitrobenzaldehyde and nitromethane, a reaction that is catalyzed by a large variety of organic bases[189], was employed. Preliminary tests revealed that TBD (10 mol%) is a highly efficient catalyst for this reaction, triethylamine has moderate activity with full conversion within 24 h, and pyridine shows no activity at all (Table 23). Thus, it was anticipated that the two isomers of DAE **14**, with their pK_a constants being located in-between that of triethylamine and pyridine, would be able to catalyze the Henry reaction with a marked rate difference. Indeed, both isomers showed full conversion within 72 h reaction time, as indicated by TLC. Note that only 5 mol% of catalyst could be used and that a mixture of THF and methanol had to be employed as solvent to ensure solubility of DAE **14**.

Table 23. Preliminary tests for base catalysis of a Henry reaction by TLC.[a]

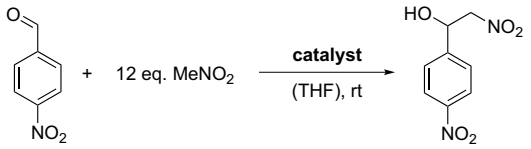

catalyst	pK_a (AN)	time until full conversion (TLC)
TBD (10 mol%)	26.03[185b]	< 2 min
NEt_3 (10 mol%)	18.82[185b]	ca. 24 h
14(o) (5 mol%)[b]	16.53	ca. 72 h
14(c) (5 mol%)[b]	15.58	ca. 72 h
pyridine (10 mol%)	12.53[185b]	no reaction

a) Conditions: 4-Nitrobenzaldehyde (1.0 mmol), nitromethane (0.64 mL, 12.0 mmol) and the catalyst in 2.5 mL of THF at room temperature. TLC eluent: petrol ether/ethyl acetate 3:1.
b) In THF/MeOH 2:1.

Unfortunately, it was not possible to determine the rate difference between the ring-open and ring-closed isomer by following the progress of the reaction in THF-d_8/MeOH using NMR spectroscopy. This was due to equilibration of 4-nitrobenzaldehyde with its dimethyl

acetal in presence of methanol, also taking place under neutral conditions.[190] The equilibration proceeded in parallel to the formation of the nitroaldol product and ^{1}H NMR signals for the dimethyl acetal completely overlapped with that of the starting material and the product. Thus, no quantitative analysis could be conducted.

4.7.5 Summary

After the completion of the synthesis of bicyclic guanidine substituted DAE **14** its properties as a catalyst for the ring-opening polymerization of *L*-lactide were tested. Unfortunately, both the ring-open and ring-closed isomers did not show any catalytic activity in this reaction. However, the low solubility of DAE **14** prevented the utilization of higher catalyst loadings than 2 mol%. In order to quantify the difference between the highly active bicyclic guanidine TBD and DAE **14**, pK_a constants were determined for both isomers in acetonitrile. While the absolute pK_a values were much lower than that of TBD, the difference of the basicity between the ring-open and ring-closed isomer amounted to almost one order of magnitude.

Utilizing DAE **14** as a catalyst in a Henry reaction between 4-nitrobenzaldehyde and nitromethane revealed catalytic activity of both isomers. However, due to the low solubility of DAE **14** the catalyst loading could not be increased and the rate difference between the two isomers could not be determined.

Based on these findings two improved structural designs for photoswitchable bicyclic guanidines are proposed. The motif can either be placed as an "arm" of the DAE or methylation of the imidazole nitrogen converts it into a 1,3-dialkylimidazol-2-ylidene amine. In particular for the latter structure a significant increase of the basicity and thus the potential catalytic activity of the ring-open isomer are predicted. To improve the solubility of the guanidine substituted DAE the utilization of thiophenes as hetaryl rings or the attachment of solubilizing groups should be considered. Furthermore, in a second generation of guanidine substituted DAEs the 3,5-bis(trifluoromethyl)phenyl substituent should be used in the periphery to ensure an increased fatigue resistance.

Another possibility to apply the photoswitchable bicyclic guanidine motif is to exploit its supramolecular association behavior. In the protonated state bicyclic guanidines such as TBD show remarkably high association constants in hydrogen bond mediated complexes with carboxylate and other oxoanions.[177,191] Exploration of the isomerization induced changes of the strengths of hydrogen-bonding interactions of guanidine motif **14** may lead to its application within photoswitchable supramolecular assemblies or polymers.[75b,184]

Research in these directions is currently going on in the Hecht group.

5. Conclusion

With the aim of using DAEs as remote-controllable building blocks in functional systems, basic properties of their photochromic reaction were investigated and tuned in order to design highly efficient switches that fulfill the requirements of potential applications. In particular, the fatigue behavior, the electrochemical isomerization reaction, and the isomerization induced shifts of HOMO and LUMO levels of the DAE core have been studied in this work. Therefore, a large variety of DAEs was synthesized by varying the nature of the bridging unit as well as the heterocycles forming the cyclohexadiene core, by placing different substituents into the DAE's periphery possessing strong electron donating or strong electron-withdrawing character, and by exchanging the methyl substituents at the ring-closing carbons with CF_3 groups. In particular, the synthesis of α-trifluoromethyl substituted DAEs is unprecedented in the literature and they were shown to possess remarkable photochemical properties. α-CF_3 groups were also demonstrated to have strong impact on the DAE's π-electronic system leading to large variations of HOMO and LUMO levels upon ring-closure.

By developing a procedure for the determination of quantum yields for the formation of the known by-product of DAE photochromism, an in-depth characterization of the fatigue properties of the synthesized compounds was conducted. Thereby, the general trend could be revealed that the more and the stronger acceptor substituents are present on the DAE core the lower is the rate of by-product formation. Importantly, structures containing the perhydrocyclopentene bridge were identified which show a similar fatigue resistance as the commonly used perfluorocyclopentene bridged DAEs. This gives high structural and synthetic flexibility for the design of DAEs possessing excellent photochromic properties. The observed experimental trends could not be easily rationalized on the basis of ground state properties, so that further spectroscopic and theoretical investigations have to be performed to reveal the mechanism of by-product formation.

Investigations into the electrochemistry of DAEs lead to the identification of a motif that can be orthogonally switched between the two isomers using redox- and photochemistry. By the incorporation of α-CF_3 substituted heterocyclic building blocks the fatigue of the oxidative ring-closure reaction could be significantly reduced and insights into the underlying mechanism could be gained. Furthermore, screening of the redox properties of the members of the DAE library revealed that HOMO and LUMO levels of the DAE photochromes can be precisely tuned over a broad energy range and that specific structures show an exceptionally high modulation of the electronic levels upon the isomerization reaction.

By precisely aligning HOMO and LUMO energies between specific DAE derivatives and organic semiconductors photocontrollable organic thin film transistors could be realized via

a simple blending approach. Thereby, the trapping of charge carriers within the device was reversibly controlled by the light-induced isomerization of DAE molecules within the semiconducting matrix. The principle was demonstrated to work for both p-type and n-type semiconductors using DAEs possessing high HOMO energies or low LUMO energies, respectively. Moreover, the delicate interplay between strong intermolecular interactions between the DAE and the semiconductor and phase segregation of the blended material was studied. The synthesis of DAEs that possess high HOMO energies for the application in p-type OTFTs and that show a high fatigue resistance at the same time remains a challenge. Furthermore, DAEs showing a modulation of LUMO levels in an energy range below -4.0 eV are of high interest in order to combine them with air-stable, high-performing n-type semiconducting matrices.

In another attempt to exploit the isomerization induced electronic modulations, a bicyclic guanidine bridged DAE was designed as a potentially photoswitchable organocatalyst, in particular for the anionic ring-opening polymerization of lactide and lactones. However, it turned out that the guanidine motif showed no catalytic activity in the polymerization reaction. By determining pK_a constants in acetonitrile it was revealed that the basicity of the guanidine is significantly lower than that of the parent, catalytically active bicyclic guanidine structure due to the electronic coupling with the DAE's π- system. The activity of the guanidine motif may be increased by small structural modifications to limit the electronic coupling with the DAE or to implement superbasic properties. Furthermore, the impact of the photoisomerization on the supramolecular association behavior of the guanidine motif will be topic of future investigations.

6. Experimental Part

6.1 Instrumentation and procedures

6.1.1 UV/Vis spectroscopy

The setup for UV/Vis spectroscopy and irradiation experiments is described in detail in section 4.2.2. Fluorescence spectroscopy was performed using a Cary Eclipse Fluorescence spectrometer. For all experiments spectrophotometric grade solvents were used as received.

6.1.2 Determination of pK_a values

The method described by Leito and coworkers[185] was applied for the determination of pK_a values in acetonitrile. The difference between the pK_a of two acids HB_1^+ and HB_2^+, with their corresponding free bases B_1 and B_2, is given by:

$$\Delta pK_a = pK_a(HB_1^+) - pK_a(HB_2^+) = log\left(\frac{a(HB_2^+)\cdot a(B_1)}{a(B_2)\cdot a(HB_1^+)}\right) = log\left(\frac{[HB_2^+]\cdot[B_1]}{[B_2]\cdot[HB_1^+]}\right) \quad (40)$$

Thereby, it is assumed that the ratio of the activity coefficients *f(HB⁺)/f(B)* is constant for the two bases and molar concentrations can be used instead of molar activities. If both bases change their UV/Vis spectra upon protonation direct measurment of the ratios [HB⁺]/[B] is possible. This is done by recording the UV/Vis spectrum of each base separately and determining the isosbestic points (or wavelengths for which the absorbance does not change) upon protonation with optically transparent methanesulfonic acid. Then, the mixture of the two bases is titrated with the acid and at an isosbestic wavelength λ observed during titration *one* base, the ratio *[HB⁺]/[B]* for the *other* base is calculated by

$$\frac{[HB^+]}{[B]} = \frac{A_n^\lambda - A^\lambda}{A^\lambda - A_i^\lambda} \quad (41)$$

with A_n^λ the absorbance of the neutral mixture, A_i^λ the absorbance of the fully ionized mixture, and A^λ the absorbance of the mixture at a certain point of the titration. Thus, for both bases the ratio *[HB⁺]/[B]* is determined at a certain point of the titration and inserted into equation *(40)* in order to calculate the relative pK_a difference.

For the experiments solutions of DAE **14** ($3.50\cdot10^{-5}$ M), the reference base ($6.00\cdot10^{-5}$ M), and methane sulfonic acid ($1.08\cdot10^{-3}$ M) in spectrophotometry grade acetonitrile were used. The titration consisted of addition of of methanesulfonic acid in steps of 10 µL to

3 mL of the analyte solution. The recorded UV/Vis spectra were corrected for dilution by the addition of the acid. Values determined for $[HB^+]/[B]$ and ΔpK_a at different isosbestic wavelengths and different points of the titration were averaged. The uncertainty of the pK_a constant was estimated by assuming an uncertainty of the absorbance measurement of 0.002.

6.1.3 Cyclic voltammetry

Cyclic voltammetry was performed using a PG310 USB (HEKA Elektronik) potentiostat interfaced to a PC with PotMaster v2x43 (HEKA Elektronik) software for data evaluation. A three-electrode configuration contained in a non-divided cell consisting of a platinum disc (d = 1 mm) as working electrode, a platinum plate as counter-electrode, and a saturated calomel electrode (SCE) with an agar-agar-plug in a Luggin capillary with a diaphragm as reference electrode was used. Measurements were carried out in $1 \cdot 10^{-3}$ M solutions in acetonitrile (HPLC-grade, dried over calcium hydride and distilled) containing 0.1 M Bu_4NPF_6 using a scan rate of $dE/dt = 1\ V\ s^{-1}$. The data is given in reference to the ferrocene redox couple (Fc/Fc^+), which was used as external standard. Cyclic voltammograms of ring-closed isomers of diarylethenes were obtained by irradiation of the electrochemical cell using a standard laboratory UV-lamp equipped with a 313 nm UV-tube (Vilber Lourmat).

6.1.4 Spectroelectrochemistry of 11a

Spectroelectrochemistry was performed using a quarz cuvette with 1 mm pathlength in an Avantes AvaSpec-2048x14 spectrometer combined with an AvaLight-DH-S-BAL light source. The cuvette was equipped with a platinum net as working electrode, a platinum wire as counter electrode, and an $Ag/AgNO_3$ reference electrode connected to an Autolab PGSTAT128N potentiostat from Metrohm GmbH, Germany. An acetonitrile solution of **11a** ($c = 5 \cdot 10^{-4}$ M) containing 0.1 M Bu_4NPF_6 was placed in the cuvette and a potential scan was performed using a scan rate of 10 mV/s while UV/Vis-spectra were recorded every 10 mV. As reference the ferrocene/ferrocenium redox couple was determined to have an oxidation potential of 0.21 V in this configuration.

6.1.5 Repetitive electrochemical and photochemical switching of 11a and 11b

Repetitive switching was performed with an argon saturated solution of the respective ring-open isomer ($c = 5 \cdot 10^{-4}$ M) in acetonitrile containing 0.1 M Bu_4NPF_6, which was placed into a divided H-cell equipped with platinum nets as working and counter electrodes, a standard calomel electrode (SCE) as reference, and a magnetic stir bar. Each switching cycle consisted of an oxidation step by applying a potential of 1.3 V in case of **11a** or a potential of 1.8 V in case of **11b** over a period of 5 min, immediately followed by a reduction at a potential of -0.3 V [SCE]. This procedure led to formation of the ring-closed isomer. Ring-opening was then

accomplished by irradiating the cell with visible light using a 1000 W Xe arc lamp in combination with a longpass-filter ($\lambda > 430$ nm) until no further changes could be observed by UV/Vis spectroscopy. After each reduction step and irradiation step an analytical sample of the mixture was analyzed by UV/Vis spectroscopy and by UPLC.

6.1.6 Computation

All calculations have been performed using the Gaussian09 (Rev. A02 and Rev. C01)[192] software package. For geometry optimizations no symmetry constraints were applied. Optimized structures were proven to correspond to minima on the potential energy surface by frequency calculatios. All energies include zero-point corrections.

6.2 General synthetic methods

Solvents and commercial starting materials were used as received. All reactions requiring inert gas atmosphere were performed under argon atmosphere. Solvents were dried before use, if necessary, employing an Innovative Technologies solvent purification system. THF was further dried by storing over activated molecular sieves (4 Å). Column chromatography was carried out with silica gel (0.035–0.070 mm, 60 Å) using eluents as specified. All experiments involving light-sensitive compounds were carried out in the dark under red light. NMR spectra were recorded on a 500 MHz Bruker AV 500, a 400 MHz Bruker AV 400, or a 300 MHz Bruker DPX 300 spectrometer at 25 °C using residual protonated solvent signals as internal standards for ^{1}H and ^{13}C spectra (^{1}H: $\delta(CHCl_3) = 7.26$ ppm, $\delta(CH_2Cl_2) = 5.32$ ppm and ^{13}C: $\delta(CDCl_3) = 77.16$ ppm, $\delta(CD_2Cl_2) = 53.84$ ppm) or $CFCl_3$ as external standard for ^{19}F spectra ($\delta(CFCl_3) = 0$ ppm). UPLC/MS was performed with a Waters UPLC Acquity equipped with a Waters LCT Premier XE Mass Detector for UPLC-HR-MS, with Waters Alliance systems (consisting of a Waters Separations Module 2695, a Waters Diode Array Detector 996 and a Waters Mass Detector ZQ 2000). Preparative GPC was performed on a LC-9210NEXT preparative recycling GPC (Japan Analytical Industry). Microwave assisted reactions were performed in a CEM Discover 300 W microwave system. Preparative irradiations were performed using 30 mL quartz tubes placed in a Rayonet RPR 100 photochemical reactor equipped with 250 nm, 300 nm, or 350 nm lamps.

The syntheses of compounds **3d**, **11a**, **12**, **27**, **28**, **41**, **42**, **46**, **47**, **48**, **57**, and **58** were described in a diploma thesis preceding this work.[75a] Syntheses of compounds **1f**[193], **6c**[104a], **17**[104a], **20**[104a], and **22**[104a] were reported elsewhere. Compounds **8b**, **9c**, **79**, **80**, and **83** – **87** were reported in a bachelor thesis by Fabian Eisenreich.[137] Compounds **16**[19a], **18**[108], **19**[19a], **21**[19a], **23**[19a], **24**[194], **26**[195], **36**[196], **40**[197], **45**[198], **53**[199], **55**[200], and **92**[13] were prepared as described in the literature.

6.3 Syntheses of DAEs

1,2-Bis(5-(4-*N,N*-dimethylaminophenyl)-2-methylthien-3-yl)cyclopent-1-ene 1a

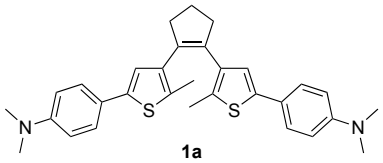

1a

In analogy to a literature procedure,[19a] 1,2-bis(5-chloro-2-methylthiophen-3-yl)cyclopent-1-ene **16** (0.500 g, 1.52 mmol, 1.0 eq.) was dissolved in 15 mL of anhydrous THF and *n*-BuLi (2.2 M in cyclohexane, 2.10 mL, 4.56 mmol, 3 eq.) was added dropwise at room temperature. The dark solution was stirred at room temperature for 30 min. Then, tri(*n*-butyl) borate (1.23 mL, 4.56 mmol, 3 eq.) was added in one portion and the resulting mixture was stirred at room temperature for 1 h. In the meantime, 4-*N,N*-dimethylaminobromobenzene (1.519 g, 7.59 mmol, 5 eq.) was dissolved in 15 mL of toluene, $Pd(PPh_3)_4$ (0.175 g, 0.15 mmol, 0.1 eq.) was added, 5 drops of ethylene glycol were added, and the mixture was stirred at room temperature for 15 min. An aqueous solution of Na_2CO_3 (2 M, 10 mL, 20.0 mmol, 13 eq.) and the previously prepared solution of the borylated bisthienylcyclopentene were added and the mixture was stirred at 80 °C for 16 h. After cooling to room temperature, 100 mL of water were added and the mixture was extracted with 50 mL of ethyl acetate three times. The combined organic phases were washed with brine, dried over $MgSO_4$ and evaporated. Purification by column chromatography (petrol ether/ethyl acetate/triethylamine 100:4:4) afforded compound **1a** (0.189 g, 0.38 mmol, 25%) as a yellow solid.

^{1}H-NMR (500 MHz, $CDCl_3$): δ (ppm) = 7.40 (d, $^3J_{H,H}$ = 9.0 Hz, 4 H, CH_{ar}), 6.90 (s, 2 H, CH_{ar}), 6.71 (d, $^3J_{H,H}$ = 9.0 Hz, 4 H, CH_{ar}), 2.97 (s, 12 H, NCH_3), 2.85 (t, $^3J_{H,H}$ = 7.5 Hz, 4 H, CH_2), 2.07 (p, $^3J_{H,H}$ = 7.5 Hz, 4 H, CH_2), 1.97 (s, 6 H, CH_3).

^{13}C-NMR (126 MHz, $CDCl_3$): δ (ppm) = 149.8, 140.4, 136.6, 134.6, 132.5, 126.4 (CH), 123.5, 121.9 (CH), 112.8 (CH), 40.7 (CH_3), 38.6 (CH_2), 23.2 (CH_2), 14.5 (CH_3).

HRMS (ESI+): *m/z* = 489.213 ($[M]^+$, calcd. 498.216 for $[C_{31}H_{34}N_2S_2]^+$).

1,2-Bis(5-(4-methoxyphenyl)-2-methylthien-3-yl)cyclopent-1-ene 1b[19b]

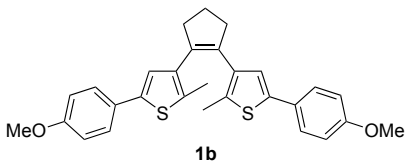

1b

In an intended monocoupling, a mixture of the bis(pinacol boronate) **29** (1.445 g, 2.82 mmol. 1.0 eq.), 4-bromoanisole (0.649 g, 3.47 mmol, 1.2 eq.), $Pd(OAc)_2$ (24 mg, 0.11 mmol, 0.04 eq.), SPhos (89 mg, 0.22 mmol, 0.08 eq.) and K_3PO_4 (ground, 0.921 g, 4.338 mmol, 1.5 eq.) in 8 mL of toluene was degassed by bubbling argon through it for 10 min and then stirred at 100 °C for 20 h. After cooling to room temperature the mixture was filtered through a Celite pad eluting

with ethyl acetate, and the filtrate was evaporated. Purification by column chromatography (petrol ether/ethyl acetate 20:1) afforded compound **1b** (0.124 g, 0.25 mmol, 9%) as a white solid.

^{1}H-NMR (500 MHz, $CDCl_3$): δ (ppm) = 7.43 (d, $^3J_{H,H}$ = 8.8 Hz, 4 H, CH_{ar}), 6.93 (s, 2 H, CH_{ar}), 6.88 (d, $^3J_{H,H}$ = 8.8 Hz, 4 H, CH_{ar}), 3.82 (s, 6 H, CH_3O), 2.85 (t, $^3J_{H,H}$ = 7.4 Hz, 4 H, CH_2), 2.08 (p, $^3J_{H,H}$ = 7.4 Hz, 2 H, CH_2), 2.00 (s, 6 H, CH_3).

^{13}C-NMR (126 MHz, $CDCl_3$): δ (ppm) = 158.9, 139.6, 136.7, 134.7, 133.6, 127.6, 126.7 (*C*H), 123.1 (*C*H), 114.3 (*C*H), 55.5 (*C*H_3), 38.6 (*C*H_2), 23.1 (*C*H_2), 14.5 (*C*H_3).

HRMS (ESI+): m/z = 472.155 ([M]$^+$, calcd. 472.153 for $[C_{29}H_{28}O_2S_2]^+$).

1,2-Bis(2-methyl-5-(4-methylphenyl)thien-3-yl)cyclopent-1-ene 1c

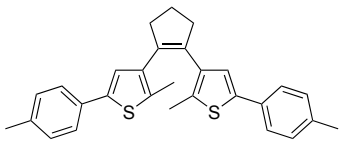

1c

Compound **1c** was synthesized following the procedure described for **1a** using 1,2-bis(5-chloro-2-methylthiophen-3-yl)cyclopent-1-ene **16** (2.806 g, 8.52 mmol, 1.0 eq.) in 40 mL of THF, *n*-BuLi (2.2 M in cyclohexane, 9.68 mL, 21.30 mmol, 2.5 eq.), tri(*n*-butyl) borate (6.90 mL, 25.56 mmol, 3.0 eq.), *p*-tolylbromide (6.995 g, 40.90 mmol, 4.8 eq.) in 20 mL of THF, $Pd(PPh_3)_4$ (0.492 g, 0.42 mmol, 0.05 eq.), and aqueous Na_2CO_3 (2 M, 42.6 mL, 85.2 mmol, 10 eq.). The reaction was performed at 80 °C for 16 h. Column chromatography (petrol ether/methylene chloride 10:1) afforded compound **1c** (1.366 g, 3.10 mmol, 36%) as a white solid.

^{1}H-NMR (500 MHz, $CDCl_3$): δ (ppm) = 7.44 (d, $^3J_{H,H}$ = 7.5 Hz, 4 H, CH_{ar}), 7.17 (d, $^3J_{H,H}$ = 7.5 Hz, 4 H, CH_{ar}), 7.04 (s, 2 H, CH_{ar}), 2.88 (t, $^3J_{H,H}$ = 7.0 Hz, 4 H, CH_2), 2.38 (s, 6 H, CH_3), 2.12 (p, $^3J_{H,H}$ = 7.0 Hz, 2 H, CH_2), 2.03 (s, 6 H, CH_3).

^{13}C-NMR (126 MHz, $CDCl_3$): δ (ppm) = 139.9, 136.9, 136.7, 134.7, 134.0, 131.9, 129.6 (*C*H), 125.4 (*C*H), 123.6 (*C*H), 38.6 (*C*H_2), 23.2 (*C*H_2), 21.2 (*C*H_3), 14.5 (*C*H_3).

HRMS (ESI+): m/z = 440.164 ([M]$^+$, calcd. 440.163 for $[C_{29}H_{28}S_2]^+$).

1,2-Bis(2-methyl-5-phenylthien-3-yl)cyclopent-1-ene 1d[19a]

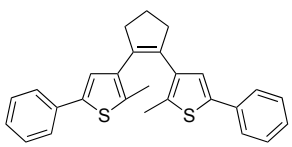

1d

Compound **1d** was synthesized following the procedure described for **1a** using 1,2-bis(5-chloro-2-methylthiophen-3-yl)cyclopent-1-ene **16** (0.770 g, 2.34 mmol, 1.0 eq.) in 20 mL of THF, *n*-BuLi (2.2 M in cyclohexane, 3.20 mL, 7.01 mmol, 3.0 eq.), tri(*n*-butyl) borate (1.89 mL,

7.01 mmol, 3.0 eq.), bromobenzene (1.23 mL, 11.69 mmol, 5.0 eq.) in 10 mL of THF, $Pd(PPh_3)_4$ (0.270 g, 0.23 mmol, 0.1 eq.), and aqueous Na_2CO_3 (2 M, 11.7 mL, 23.4 mmol, 10 eq.). The reaction was performed at 80 °C for 16 h. Column chromatography (petrol ether/methylene chloride 50:1) afforded compound **1d** (0.549 g, 1.33 mmol, 57%) as a white solid.

^{1}H-NMR (500 MHz, $CDCl_3$): δ (ppm) = 7.53 – 7.50 (m, 4 H, CH_{ar}), 7.37 – 7.33 (m, 4 H, CH_{ar}), 7.26 – 7.22 (m, 2 H, CH_{ar}), 7.06 (s, 2 H, CH_{ar}), 2.87 (t, $^3J_{H,H}$ = 7.4 Hz, 4 H, CH_2), 2.10 (p, $^3J_{H,H}$ = 7.4 Hz, 2 H, CH_2), 2.01 (s, 6 H, CH_3).

^{13}C-NMR (126 MHz, $CDCl_3$): δ (ppm) = 139.8, 136.8, 134.8, 134.7, 134.6, 128.9 (*C*H), 127.1 (*C*H), 125.4 (*C*H), 124.1 (*C*H), 38.6 (*C*H_2), 23.2 (*C*H_2), 14.6 (*C*H_3).

HRMS (ESI+): m/z = 412.127 ($[M]^+$, calcd. 412.132 for $[C_{27}H_{24}S_2]^+$).

1,2-Bis(5-(4-bromophenyl)-2-methylthien-3-yl)cyclopent-1-ene 1e[19b]

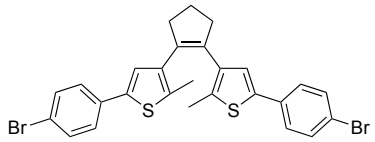

1e

Compound **1e** was synthesized following the procedure described for **1a** using 1,2-bis(5-chloro-2-methylthiophen-3-yl)cyclopent-1-ene **16** (0.728 g, 2.21 mmol, 1.0 eq.) in 12 mL of THF, *n*-BuLi (1.6 M in hexane, 3.70 mL, 5.97 mmol, 2.7 eq.), tri(*n*-butyl) borate (1.61 mL, 5.97 mmol, 2.7 eq.), 1,4-dibromobenzene (2.471 g, 10.48 mmol, 4.74 eq.) in 12 mL of THF, $Pd(PPh_3)_4$ (0.227 g, 0.20 mmol, 0.09 eq.), and aqueous Na_2CO_3 (2 M, 12.3 mL, 24.60 mmol, 11 eq.). The reaction was performed at 80 °C for 2 h. Column chromatography (petrol ether) afforded compound **1e** (0.738 g, 1.29 mmol, 59%) as a white solid.

^{1}H-NMR (500 MHz, $CDCl_3$): δ (ppm) = 7.44 (d, $^3J_{H,H}$ = 8.4 Hz, 4 H, CH_{ar}), 7.34 (d, $^3J_{H,H}$ = 8.4 Hz, 4 H, CH_{ar}), 7.01 (s, 2 H, CH_{ar}), 2.84 (t, $^3J_{H,H}$ = 7.4 Hz, 4 H, CH_2), 2.09 (p, $^3J_{H,H}$ = 7.4 Hz, 2 H, CH_2), 2.00 (s, 6 H, CH_3).

^{13}C-NMR (126 MHz, $CDCl_3$): δ (ppm) = 138.5, 136.9, 135.2, 134.8, 133.6, 132.0 (CH), 126.9 (CH), 124.5 (CH), 120.8, 38.6 (CH_2), 23.2 (CH_2), 14.6 (CH_3).

HRMS (ESI+): m/z = 567.957 ($[M]^+$, calcd. 567.953 for $[C_{27}H_{22}{}^{79}Br_2S_2]^+$), 569.953 ($[M]^+$, calcd. 569.951 for $[C_{27}H_{22}{}^{79}Br^{81}BrS_2]^+$), 571.955 ($[M]^+$, calcd. 571.949 for $[C_{27}H_{22}{}^{81}Br_2S_2]^+$).

1,2-Bis(5-(4-ethyloxycarbonylphenyl)-2-methylthiophen-3-yl)cyclopent-1-ene 1g

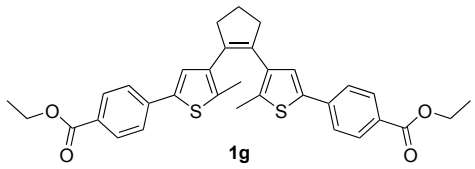

Compound **1g** was synthesized following the procedure described for **1a** using 1,2-bis(5-chloro-2-methylthiophen-3-yl)cyclopent-1-ene **16** (1.000 g, 3.04 mmol, 1.0 eq.) in 30 mL of THF, *n*-BuLi (2.2 M in cyclohexane, 3.73 mL, 8.20 mmol, 2.7 eq.), tri(*n*-butyl) borate (2.46 mL, 9.11 mmol, 3 eq.), ethyl 4-bromobenzoate (2.35 mL, 14.40 mmol, 4.75 eq.) in 10 mL of THF, $Pd(PPh_3)_4$ (0.312 g, 0.27 mmol, 0.09 eq.), and aqueous Na_2CO_3 (2 M, 23.0 mL, 46.00 mmol, 15 eq.). The reaction was performed at 80 °C for 16 h. Column chromatography (petrol ether/ethyl acetate 10:1) afforded compound **1g** (0.716 g, 1.29 mmol, 42%) as a pale yellow solid.

^{1}H-NMR (500 MHz, $CDCl_3$): δ (ppm) = 7.99 (d, $^3J_{H,H}$ = 8.4 Hz, 4 H, CH_{ar}), 7.53 (d, $^3J_{H,H}$ = 8.4 Hz, 4 H, CH_{ar}), 7.12 (s, 2 H, CH_{th}), 4.37 (q, $^3J_{H,H}$ = 7.2 Hz, 4 H, CH_3CH_2O), 2.85 (t, $^3J_{H,H}$ = 7.4 Hz, 4 H, CH_2), 2.10 (p, $^3J_{H,H}$ = 7.4 Hz, 2 H, CH_2), 2.02 (s, 6 H, CH_3), 1.40 (t, $^3J_{H,H}$ = 7.2 Hz, 6 H, CH_3CH_2O).

^{13}C-NMR (126 MHz, $CDCl_3$): δ (ppm) = 166.5, 138.71, 138.69, 137.1, 136.4, 134.9, 130.3 (*C*H), 128.8, 125.6 (*C*H), 124.9 (*C*H), 61.1 (CH_2), 38.6 (CH_2), 23.2 (CH_2), 14.7 (CH_3), 14.5 (CH_3).

HRMS (ESI+): *m/z* = 556.171 ($[M]^+$, calcd. 556.174 for $[C_{33}H_{32}O_4S_2]^+$), 579.160 ($[M+Na]^+$, calcd. 579.164 for $[C_{33}H_{32}NaO_4S_2]^+$).

1,2-Bis(5-(4-hexyloxycarbonylphenyl)-2-methylthiophen-3-yl)cyclopent-1-ene 1h

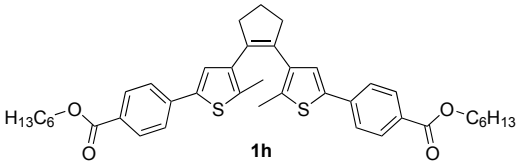

Compound **1h** was synthesized following the procedure described for **1a** using 1,2-bis(5-chloro-2-methylthiophen-3-yl)cyclopent-1-ene **16** (1.000 g, 3.04 mmol, 1.0 eq.) in 40 mL of THF, *n*-BuLi (2.2 M in cyclohexane, 3.73 mL, 8.20 mmol, 2.7 eq.), tri(*n*-butyl) borate (2.21 mL, 8.20 mmol, 2.7 eq.), hexyl 4-bromobenzoate **28** (3.463 g, 12.14 mmol, 4.0 eq.) in 12 mL of THF, $Pd(PPh_3)_4$ (0.312 g, 0.27 mmol, 0.09 eq.), and aqueous Na_2CO_3 (2 M, 17.00 mL, 34.00 mmol, 11 eq.). The reaction was performed at 80 °C for 3 h. Column chromatography (petrol ether/ethyl acetate 30:1) afforded compound **1h** (1.407 g, 2.10 mmol, 69%) as yellow viscous oil.

^{1}H-NMR (300 MHz, $CDCl_3$): δ (ppm) = 8.00 (d, $^3J_{H,H}$ = 8.4 Hz, 4 H, CH_{ar}), 7.54 (d, ^{3}J(H,H) = 8.4 Hz, 4 H, CH_{ar}), 7.14 (s, 2 H, CH_{ar}), 4.31 (t, $^3J_{H,H}$ = 6.6 Hz, 4 H, CH_2), 2.86 (t,

$^{3}J_{H,H}$ = 7.5 Hz, 4 H, CH_2), 2.10 (p, $^{3}J_{H,H}$ = 7.5 Hz, 2 H, CH_2), 2.02 (s, 6 H, CH_3), 1.81 – 1.72 (m, 4 H, CH_2), 1.47 – 1.34 (m, 12 H, CH_2), 0.91 (t, $^{3}J_{H,H}$ = 6.9 Hz, 6 H, CH_3).

^{13}C-NMR (76 MHz, $CDCl_3$): δ (ppm) = 166.5, 138.7, 137.1, 136.3, 134.9, 130.3 (*C*H), 128.8, 125.5 (*C*H), 124.9 (*C*H), 65.2 (*C*H_2), 38.6 (*C*H_2), 31.6 (*C*H_2), 28.8 (*C*H_2), 25.8 (*C*H_2), 23.1 (*C*H_2), 22.7 (*C*H_2), 14.7 (*C*H_3), 14.1 (*C*H_3), the signal of one quaternary carbon was not detected due to signal overlapping.

HRMS (ESI$^+$): *m/z* = 668.299 ([M]$^+$, calcd. 668.299 for $C_{41}H_{48}O_4S_2^+$).

1,2-Bis(5-(3,5-bis(trifluoromethyl)phenyl)-2-methylthien-3-yl)cyclopent-1-ene 1i

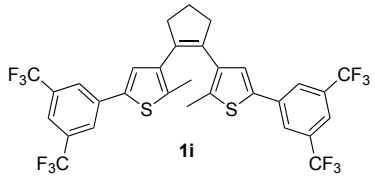

1i

Compound **1i** was synthesized following the procedure described for **1a** using 1,2-bis(5-chloro-2-methylthiophen-3-yl)cyclopent-1-ene **16** (1.000 g, 3.04 mmol, 1.0 eq.) in 20 mL of THF, *n*-BuLi (2.2 M in cyclohexane, 4.14 mL, 9.11 mmol, 3.0 eq.), tri(*n*-butyl) borate (2.46 mL, 9.11 mmol, 3.0 eq.), 3,5-bis(trifluoromethyl)-1-bromobenzene (2.62 mL, 15.18 mmol, 5.0 eq.) in 10 mL of THF, $Pd(PPh_3)_4$ (0.351 g, 0.30 mmol, 0.1 eq.), and aqueous Na_2CO_3 (2 M, 8.00 mL, 16.00 mmol, 5.2 eq.). The reaction was performed at 80 °C for 16 h. Column chromatography (petrol ether) afforded compound **1i** (0.630 g, 0.92 mmol, 30%) as a white solid.

^{1}H-NMR (500 MHz, $CDCl_3$): δ (ppm) = 7.86 (br s, 4 H, CH_{ar}), 7.71 (br s, 2 H, CH_{ar}), 7.15 (s, 2 H, CH_{th}), 2.89 (t, $^{3}J_{H,H}$ = 7.4 Hz, 4 H, *C*H_2), 2.14 (p, $^{3}J_{H,H}$ = 7.4 Hz, 2 H, CH_2), 2.06 (s, 6 H, CH_3).

^{13}C-NMR (126 MHz, $CDCl_3$): δ (ppm) = 137.3, 137.2, 136.6, 136.5, 135.1, 132.4 (q, $^{2}J_{C,F}$ = 34 Hz, *C*CF_3), 126.3 (*C*H), 125.1 (br, *C*H), 123.4 (q, $^{1}J_{C,F}$ = 273 Hz, *C*F_3), 120.4 (br, *C*H), 38.5 (*C*H_2), 23.2 (*C*H_2), 14.7 (*C*H_3).

^{19}F-NMR (470 MHz, $CDCl_3$): δ (ppm) = -63.3 (s, CF_3).

HRMS (ESI+): *m/z* = 684.080 ([M]$^+$, calcd. 684.081 for $[C_{31}H_{20}F_{12}S_2]^+$).

1,2-Bis(2-methyl-5-(4-methylphenyl)thien-3-yl)perfluorocyclopent-1-ene 2c[13]

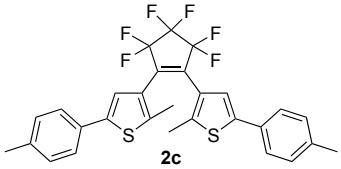

2c

To a Schlenk tube were added the bis(pinacol boronate) **31** (620 mg, 1.00 mmol, 1 eq.), 4-bromotoluene (513 mg, 3.00 mmol, 3 eq.), K_3PO_4 (ground, 637 mg, 3.00 mmol, 3 eq.), $Pd(OAc)_2$ (11 mg, 0.05 mmol, 0.05 eq.), and SPhos (41 mg, 0.10 mmol, 0.1 eq.), and the tube was evacuated and refilled with argon twice. Then, 5 mL of degassed toluene were added and

the mixture was stirred at 80 °C for 20 h. After cooling to room temperature the mixture was diluted with 20 mL of ethyl acetate and filtered through a plug of Celite eluting with ethyl acetate. After evaporation of the solvent the residue was purified by column chromatography (petrol ether/toluene 9:1) affording compound **2c** (213 mg, 0.39 mmol, 39%) as a white solid.

^{1}H-NMR (500 MHz, $CDCl_3$): δ (ppm) = 7.43 (d, $^{3}J_{H,H}$ = 7.9 Hz, 4 H, CH_{ar}), 7.23 (s, 2 H, CH_{ar}), 7.19 (d, $^{3}J_{H,H}$ = 7.9 Hz, 4 H, CH_{ar}), 2.37 (s, 6 H, CH_3), 1.95 (s, 6 H, CH_3).

^{13}C-NMR (126 MHz, $CDCl_3$): δ (ppm) = 142.5, 140.9, 138.0, 130.7, 129.8 (*C*H), 125.9, 125.7 (*C*H), 122.0 (*C*H), 21.3 (CH_3), 14.7 (CH_3), due to C-F couplings not all signals can be detected.

^{19}F-NMR (470 MHz, $CDCl_3$): δ (ppm) = -110.2 (br, 4 F, CF_2), -132.0 (br, 2 F, CF_2).

HRMS (ESI+): *m/z* = 548.100 ([M]$^+$, calcd. 548.107 for $[C_{29}H_{22}F_6S_2]^+$).

1,2-Bis(2-(3,5-bis(trifluoromethyl)phenyl)-5-methylthien-4-yl)hexafluorocyclopent-1-ene 2i[201]

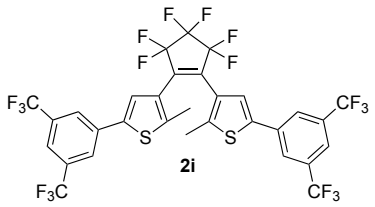

2i

Bromothiophene **54** (1.000 g, 2.57 mmol, 1.0 eq.), triethylamine (2.15 mL, 15.41 mmol, 6.0 eq.) and $Pd(PPh_3)_2Cl_2$ (90 mg, 0.13 mmol, 0.05 eq.) were dissolved in 30 mL of dry toluene and the mixture was degassed by repeated evacuation of the flask and refilling with argon. After the addition of pinacolborane (1.14 mL, 7.71 mmol, 3.0 eq.) the mixture was refluxed for 2 h at 120 °C until TLC indicated consumption of the starting material. After cooling down to 80 °C, an aqueous solution of Na_2CO_3 (2 M, 3.6 mL, 7.2 mmol) was added very slowly due to vigorous gas evolution. Then, 1,2-dichlorohexafluorocylopent-1-ene **25** (208 mg, 0.85 mmol, 0.33 eq.) and $Pd(PPh_3)_4$ (59 mg, 0.05 mmol, 0.02 eq.) were added and the mixture was stirred at 100 °C for 18 h. After cooling to room temperature the mixture was extracted with ethyl acetate and the combined organic layers were washed with brine and dried over $MgSO_4$. Purification by column chromatography (petrol ether) and purification by preparative GPC yielded compound **2i** (270 mg, 0.34 mmol, 40%) as a white solid.

^{1}H-NMR (500 MHz, $CDCl_3$): *δ* (ppm) = 7.91 (br, 4 H, CH_{ar}), 7.80 (br, 2 H, CH_{ar}), 7.39 (s, 2 H, CH_{ar}), 2.05 (s, 6 H, CH_3).

^{13}C-NMR (126 MHz, $CDCl_3$): 143.6, 139.2, 135.3, 132.7 (q, $^{2}J_{C,F}$ = 34 Hz, *C*CF_3), 126.4, 125.6 (*C*H), 124.8 (*C*H), 123.2 (q, $^{1}J_{C,F}$ = 273 Hz, *C*F_3), 121.5 (*C*H), 14.9 (*C*H_3), due to C-F couplings not all signals can be detected.

^{19}F-NMR (471 MHz, $CDCl_3$): *δ* (ppm) = -63.3 (s, 12 F, CF_3), -110.3 (br, 4 F, CF_2), -132.0 (br, 2 F, CF_2).

HRMS (ESI+): *m/z* = 792.019 ([M]$^+$, calcd. 792.025 for $[C_{31}H_{14}F_{18}S_2]^+$).

1,2-Bis(5-(3,5-bis(pentafluorosulfanyl)phenyl)-2-methylthien-3-yl)perfluorocyclopent-1-ene 2j

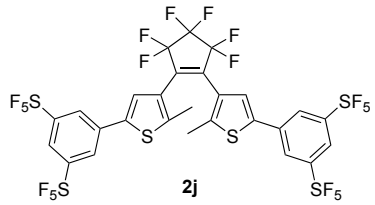

2j

To a Schlenk tube were added the bis(pinacol boronate) **31** (124 mg, 0.20 mmol, 1 eq.), 3,5-bis(pentafluorosulfanyl)-1-bromobenzene (205 mg, 0.50 mmol, 2.5 eq.), K_3PO_4 (ground, 106 mg, 0.50 mmol, 3 eq.), $Pd(OAc)_2$ (3 mg, 0.012 mmol, 0.06 eq.), and SPhos (10 mg, 0.024 mmol, 0.12 eq.), and the tube was evacuated and refilled with argon twice. Then, 1 mL of degassed toluene was added and the mixture was stirred at 80 °C for 20 h. After cooling to room temperature the mixture was diluted with 10 mL of ethyl acetate and filtered through a plug of Celite eluting with ethyl acetate. After evaporation of the solvent the residue was purified by column chromatography (petrol ether/ethyl acetate 100:1) and lyophilized from benzene affording compound **2j** (40 mg, 0.04 mmol, 20%) as a white solid.

^{1}H-NMR (500 MHz, $CDCl_3$): δ (ppm) = 8.04 (m, 2 H, CH_{ar}), 7.97 (m, 4 H, CH_{ar}), 7.34 (s, 2 H, CH_{ar}), 2.09 (s, 6 H, CH_3).

^{13}C-NMR (126 MHz, $CDCl_3$): δ (ppm) = 144.2, 138.4, 135.4, 126.5, 126.0 (br, *C*H), 125.4 (*C*H), 123.1 (br, *C*H), 14.9 (*C*H_3), due to C-F couplings not all signals can be detected.

^{19}F-NMR (470 MHz, $CDCl_3$): δ (ppm) = 81.0 (p, $^2J_{F,F}$ = 151 Hz, 4 F, S*F*$_5$), 62.6 (d, $^2J_{F,F}$ = 151 Hz, 16 F, S*F*$_5$), -110.2 (br, 4 F, C*F*$_2$), -132.0 (br, 2 F, C*F*$_2$).

HRMS (ESI-): *m/z* = 1022.893 ([M-H]$^-$, calcd. 1022.893 for [$C_{27}H_{13}F_{26}S_6$]$^-$).

1,2-Bis(5-methyl-2-phenylthiazol-4-yl)cyclopent-1-ene 3d[75a]

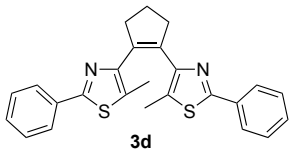

3d

Synthesis using the $PdCl_2(PPh_3)_2/Na_2CO_3$ catalyst system (entry 3 of Table 1):

Pinacol boronate **42** (4.518 g, 15.00 mmol, 3.0 eq.), 1,2-dibromocyclopentene **24** (1.130 g, 5.00 mmol, 1.0 eq.), and $PdCl_2(PPh_3)_2$ (0.175 g, 0.25 mmol, 0.05 eq.) were suspended in 10 mL of THF and degassed by repeated evacuation of the flask and refilling with argon. After the addition of Na_2CO_3 (2.650 g, 25.00 mmol, 5.0 eq.) the mixture was stirred at 80 °C for 20 h. After cooling to room temperature it was filtered through a pad of Celite eluting with ethyl acetate, and the filtrate was evaporated. Purification by column chromatography (petrol ether/ethyl acetate 9:1) afforded compound **3d** (0.152 g, 0.37 mmol, 7%) as a pale yellow solid.

Additionally, by the column chromatographic separation the monocoupled DAE **43** (0.562 g, 1.75 mmol, 36%) was obtained as a pale yellow solid.

*Synthesis starting from monocoupled DAE **43** (entry 4 of Table 1):*

Monocoupled DAE **43** (0.560 g, 1.75 mmol, 1.0 eq), pinacol boronate **42** (1.054 g, 3.50 mmol, 2.0 eq.), and $PdCl_2(PPh_3)_2$ (61 mg, 0.09 mmol, 0.05 eq.) were placed into a Schlenk tube and the tube was evacuated and refilled with argon twice. Then, 6 mL of DMF and Cs_2CO_3 (1.425 g, 4.38 mmol, 2.5 eq.) were added, the mixture was degassed by repeated evacuation and refilling with argon, and it was stirred at 100 °C for 20 h. After cooling to room temperature it was filtered through a pad of Celite eluting with ethyl acetate and the filtrate was evaporated. Purification by column chromatography (petrol ether/ethyl acetate 9:1) and recrystallization from ethanol afforded compound **3d** (0.329 g, 0.79 mmol, 45%) as colorless crystals.

Synthesis using microwave irradiation (entry 5 of Table 1):

Cs_2CO_3 (0.747 g, 2.29 mmol, 4.0 eq.) and $PdCl_2(PPh_3)_2$ (20 mg, 0.03 mmol, 0.05 eq.) were placed into each of 5 microwave tubes. To each tube 3 mL of a solution of pinacol boronate **42** (2.590 g, 8.60 mmol, 3.0 eq.) and 1,2-dibromocyclopentene **24** (0.648 g, 2.87 mmol, 1.0 eq.) in a mixture of 14 mL of DMF and 1 mL of toluene were added. The tubes were degassed by bubbling argon through the mixtures for 5 min before they were heated in a microwave (300 W) to 110 °C for 20 min. The contents of all tubes were combined and filtered through a pad of Celite eluting with ethyl acetate. The filtrate was washed with water and brine. The organic phase was dried over $MgSO_4$ and evaporated. Purification by column chromatography (petrol ether/ethyl acetate 9:1) and recrystallization from ethanol afforded compound **3d** (0.168 g, 0.41 mmol, 14%) as colorless crystals.

^{1}H-NMR (500 MHz, $CDCl_3$): δ (ppm) = 7.91 – 7.87 (m, 4 H, CH_{ar}), 7.43 - 7.36 (m, 6 H, CH_{ar}), 3.06 (t, $^3J_{H,H}$ = 7.5 Hz, 4 H, CH_2), 2.18 (p, $^3J_{H,H}$ = 7.5 Hz, 2 H, CH_2), 1.91 (s, 6 H, CH_3).
^{13}C-NMR (126 MHz, $CDCl_3$): δ (ppm) = 164.0, 150.4, 135.9, 134.1, 129.6 (*C*H), 129.5, 128.9 (*C*H), 126.4 (*C*H), 38.4 (*C*H_2), 22.9 (*C*H_2), 12.2 (CH_3).
HRMS (ESI+): *m/z* = 415.126 ($[M+H]^+$, calcd. 415.130 for $[C_{25}H_{23}N_2S_2]^+$).

1,2-Bis(2-(3,5-bis(trifluoromethyl)phenyl)-5-methylthiazol-4-yl)cyclopent-1-ene 3i

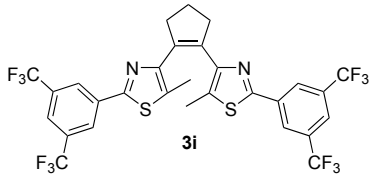

3i

Stannane **52** (270 mg, 0.45 mmol, 3.0 eq.) and 1,2-dibromocyclopentene **24** (34 mg, 0.15 mmol, 1 eq.) were dissolved in 2 mL of DMF and the mixture was degassed by bubbling argon through the solution for 5 min. $PdCl_2(PPh_3)_2$ (15 mg, 0.02 mmol, 0.14 eq.) was added and the mixture

was stirred at 100 °C for 6 h. After cooling to room temperature the mixture was poured into 10 mL of brine and it was extracted 3x with diethyl ether. The combined organic phases were dried over $MgSO_4$ and evaporated. Purification by column chromatography (petrol ether/ethyl acetate 50:1) afforded compound **3i** (29 mg, 0.04 mmol, 28%) as a white solid.

^{1}H-NMR (500 MHz, $CDCl_3$): δ (ppm) = 8.25 (br s, 4 H, CH_{ar}), 7.85 (br s, 2 H, CH_{ar}), 3.07 (t, $^3J_{H,H}$ = 7.5 Hz, 4 H, CH_2), 2.22 (p, $^3J_{H,H}$ = 7.5 Hz, 2 H, CH_2), 2.05 (s, 6 H, CH_3).

^{13}C-NMR (126 MHz, $CDCl_3$): δ (ppm) = 160.2, 151.2, 136.3, 135.8, 132.5 (q, $^2J_{C,F}$ = 34 Hz, CCF_3), 131.4, 126.1 (br, CH), 123.2 (q, $^1J_{C,F}$ = 273 Hz, CF_3), 122.8 (br, CH), 38.1 (CH_2), 23.0 (CH_2), 12.3 (CH_3).

^{19}F-NMR (471 MHz, $CDCl_3$): δ (ppm) = -63.3 (s, CF_3).

HRMS (ESI+): *m/z* = 687.084 ([M+H]$^+$, calcd. 687.080 for $[C_{29}H_{19}F_{12}N_2S_2]^+$).

1,2-Bis(2-(3,5-bis(trifluoromethyl)phenyl)-5-methylthiazol-4-yl)hexafluorocyclopent-1-ene 4i

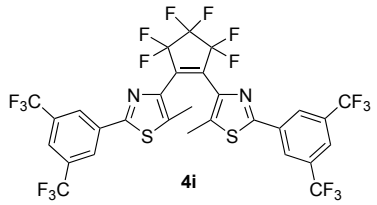

4i

Bromothiazole **48** (0.500 g, 1.28 mmol, 1 eq.), triethylamine (1.10 mL, 7.68 mmol, 6 eq.) and $Pd(PPh_3)_2Cl_2$ (45 mg, 0.06 mmol, 0.05 eq.) were dissolved in 15 mL of dry toluene and the mixture was degassed by repeated evacuation of the flask and refilling with argon. After the addition of pinacolborane (0.57 mL, 3.84 mmol, 3 eq.) the mixture was refluxed for 4 h at 120 °C until TLC indicated consumption of the starting material. After cooling to 80 °C, an aqueous solution of Na_2CO_3 (2 M, 1.8 mL, 3.60 mmol) was added very slowly due to vigorous gas evolution. Then, 1,2-dichlorohexafluorocylopent-1-ene **25** (0.103 g, 0.42 mmol, 0.33 eq.) and $Pd(PPh_3)_4$ (30 mg, 0.03 mmol, 0.02 eq.) were added and the mixture was stirred at 100 °C for 18 h. After cooling down to room temperature the mixture was extracted with ethyl acetate and the combined organic layers were washed with brine and dried over $MgSO_4$. Purification by column chromatography (petrol ether/methylene chloride 7:3) yielded **4i** (140 mg, 0.18 mmol, 42%) as a white solid.

^{1}H-NMR (500 MHz, $CDCl_3$): *δ* (ppm) = 8.20 (br, 4 H, CH_{ar}), 7.90 (br, 2 H, CH_{ar}), 2.32 (s, 6 H, CH_3).

^{13}C-NMR (126 MHz, $CDCl_3$): 162.1, 141.1, 139.0, 134.8, 132.7 (q, $^2J_{C,F}$ = 34 Hz, CCF_3), 126.3 (CH), 123.7 (CH), 123.0 (q, $^1J_{C,F}$ = 273 Hz, CF_3), 12.4 (CH_3), signals for CF_2 groups were not detected due to C-F coupling.

^{19}F-NMR (471 MHz, $CDCl_3$): *δ* (ppm) = -63.4 (s, 12 F, CF_3), -110.3 (br, 4 F, CF_2), -132.2 (br, 2 F, CF_2).

HRMS (ESI+): *m/z* = 795.026 ([M+H]$^+$, calcd. 795.023 for $[C_{29}H_{13}F_{18}N_2S_2]^+$).

1-(5-(3,5-Bis(trifluoromethyl)phenyl)-2-methylthien-3-yl)-2-(5-(4-*N*,*N*-dimethylaminophenyl)-2-methylthien-3-yl)cyclopent-1-ene 5a

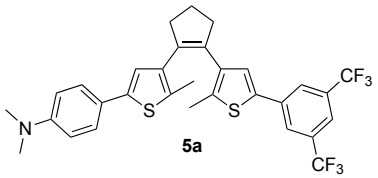

5a

Boronic ester **34** (643 mg, 2.60 mmol, 2.0 eq.), $Pd(OAc)_2$ (15 mg, 0.07 mmol, 0.05 eq.), SPhos (59 mg, 0.14 mmol, 0.10 eq.), and K_3PO_4 (ground, 1.104 g, 5.20 mmol, 4.0 eq.) were added to a Schlenk tube and the tube was evacuated and refilled with argon twice. Then, a solution of mono substituted diarylethene **33** (659 mg, 1.30 mmol, 1.0 eq.) in 8 mL of toluene was added and the mixture was stirred at 80 °C for 24 h. After cooling to room temperature, the mixture was diluted with 20 mL of ethyl acetate, washed with brine, dried over $MgSO_4$, and evaporated. Purification by column chromatography (petrol ether/methylene chloride 50:1 – 4:1) afforded compound **5a** (107 mg, 0.18 mmol, 14%) as a white solid.

^{1}H-NMR (500 MHz, $CDCl_3$): δ (ppm) = 7.88 (br s, 2 H, CH_{ar}), 7.70 (br s, 1 H, CH_{ar}), 7.38 (d, $^3J_{H,H}$ = 8.8 Hz, 2 H, CH_{ar}), 7.18 (s, 1 H, CH_{th}), 6.84 (s, 1 H, CH_{th}), 6.70 (d, $^3J_{H,H}$ = 8.8 Hz, 2 H, CH_{ar}), 2.97 (s, 6 H, NCH_3), 2.86 (ps t, $^3J_{H,H}$ = 7.4 Hz, 4 H, CH_2), 2.10 (ps p, $^3J_{H,H}$ = 7.4 Hz, 2 H, CH_2), 2.03 (s, 3 H, CH_3), 2.00 (s, 3 H, CH_3).

^{13}C-NMR (126 MHz, $CDCl_3$): δ (ppm) = 150.0, 141.0, 137.7, 137.3, 136.8, 136.3, 136.19, 136.17, 133.6, 132.4, 132.3 (q, $^2J_{C,F}$ = 34 Hz, *C*CF_3), 126.5 (2x *C*H), 125.1 (br, *C*H), 123.4 (q, $^1J_{C,F}$ = 273 Hz, *C*F_3), 123.2, 121.8 (*C*H), 120.2 (br, *C*H), 112.8 (*C*H), 40.7 (*C*H_3), 38.63 (*C*H_2), 38.60 (*C*H_2), 23.2 (*C*H_2), 14.7 (*C*H_3), 14.5 (*C*H_3).

^{19}F-NMR (470 MHz, $CDCl_3$): δ (ppm) = -63.2 (s, CF_3).

HRMS (ESI+): *m/z* = 592.154 ([M+H]$^+$, calcd. 592.157 for $[C_{31}H_{28}F_6NS_2]^+$).

1-(5-(3,5-Bis(trifluoromethyl)phenyl)-2-methylthien-3-yl)-2-(5-(4-methoxyphenyl)-2-methylthien-3-yl)-cyclopent-1-ene 5b

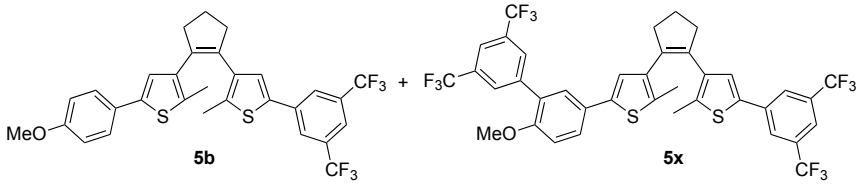

5b **5x**

Compound **5b** was synthesized following the procedure described for **1a** using monosubstituted DAE **32** (230 mg, 0.57 mmol, 1.0 eq.) in 10 mL of THF, *n*-BuLi (2.2 M in cyclohexane, 0.60 mL, 1.26 mmol, 2.2 eq.), tri(*n*-butyl) borate (0.23 mL, 0.86 mmol, 1.5 eq.), 3,5-bis(trifluoromethyl)-1-bromobenzene (0.12 mL, 0.69 mmol, 1.2 eq.) in 5 mL of toluene,

$Pd(PPh_3)_4$ (60 mg, 0.05 mmol, 0.09 eq.), and aqueous Na_2CO_3 (2 M, 5 mL). The reaction was performed at 80 °C for 16 h. Preparative GPC and column chromatography (petrol ether/ethyl acetate 50:1) afforded compound **5b** (34 mg, 0.06 mmol, 11%) as a white solid.

^{1}H-NMR (500 MHz, $CDCl_3$): δ (ppm) = 7.87 (br s, 2 H, CH_{ar}), 7.70 (br s, 1 H, CH_{ar}), 7.44 – 7.40 (m, 2 H, CH_{ar}), 7.17 (s, 1 H, CH_{th}), 6.90 (s, 1 H, CH_{th}), 6.89 – 6.86 (m, 2 H, CH_{ar}), 3.82 (s, 3 H, OCH_3), 2.86 (ps t, $^3J_{H,H}$ = 7.4 Hz, 4 H, CH_2), 2.10 (ps p, $^3J_{H,H}$ = 7.4 Hz, 2 H, CH_2), 2.03 (s, 3 H, CH_3), 2.00 (s, 3 H, CH_3).

^{13}C-NMR (126 MHz, $CDCl_3$): δ (ppm) = 159.1, 140.1, 137.6, 137.2, 136.7, 136.5, 136.2, 135.9, 133.9, 133.5, 132.3 (q, $^2J_{C,F}$ = 34 Hz, *C*CF_3), 127.4, 126.8 (*C*H), 126.4 (*C*H), 125.1 (br, *C*H), 123.4 (q, $^1J_{C,F}$ = 273 Hz, *C*F_3), 122.9 (*C*H), 120.2 (br, *C*H), 114.3 (*C*H), 55.4 (*C*H_3), 38.61 (*C*H_2), 38.57 (*C*H_2), 23.17 (*C*H_2), 14.7 (*C*H_3), 14.5 (*C*H_3).

^{19}F-NMR (471 MHz, $CDCl_3$): δ (ppm) = -63.2 (s, CF_3).

HRMS (ESI+): *m/z* = 578.115 ($[M]^+$, calcd. 578.117 for $[C_{30}H_{24}F_6OS_2]^+$).

During the purification step using preparative GPC a second compound was obtained, which was identified by its NMR signature and its high resolution mass to be the by-product **5x** shown above. However, no efforts were made to obtain it analytically pure.

^{1}H-NMR (500 MHz, $CDCl_3$): 7.97 (br s, 2 H, CH_{ar}-CCF_3), 7.83 (br s, 3 H, 2x CH_{ar}-CCF_3), 7.68 (br s, 1 H, CH_{ar}-CCF_3), 7.51 (dd, $^3J_{H,H}$ = 8.6 Hz, $^4J_{H,H}$ = 2.3 Hz, 1 H, CH_{ar}), 7.41 (d, $^4J_{H,H}$ = 2.3 Hz, 1 H, CH_{ar}), 7.14 (s, 1 H, CH_{th}), 6.99 (d, $^3J_{H,H}$ = 8.6 Hz, 1 H, CH_{ar}-COMe), 6.96 (s, 1 H, CH_{th}), 3.84 (s, 3 H, OCH_3), 2.86 (ps t, $^3J_{H,H}$ = 7.5 Hz, 4 H, CH_2), 2.10 (ps p, $^3J_{H,H}$ = 7.5 Hz, 2 H, CH_2), 2.06 (s, 3 H, CH_3), 2.01 (s, 3 H, CH_3).

HRMS (ESI+): *m/z* = 790.123 ($[M]^+$, calcd. 790.123 for $[C_{38}H_{26}F_{12}OS_2]^+$).

1-(5-(3,5-Bis(trifluoromethyl)phenyl)-2-methylthien-3-yl)-2-(5-(4-(4,6-diphenyltriazin-2-yl)phenyl)-2-methylthien-3-yl)cyclopent-1-ene 5k

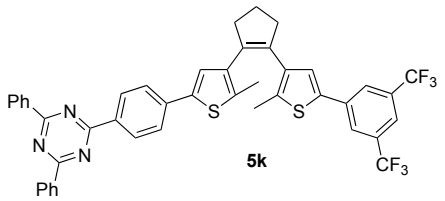

5k

Into a Schlenk tube equipped with a teflon screw cap was put the pinacol boronate **35** (80% of 0.226 g, 0.42 mmol, 1.2 eq.), $Pd(OAc)_2$ (4 mg, 0.02 mmol, 0.05 eq.), SPhos (16 mg, 0.04 mmol, 0.10 eq.), and K_3PO_4 (ground, 0.308 g, 1.45 mmol, 4 eq.) and the tube was evacuated and refilled with argon twice. Then, a solution of the monocoupled DAE **33** (0.184 g, 0.36 mmol, 1.0 eq.) in 10 mL of toluene was added, the screw cap was closed, and the reaction mixture was stirred at 80 °C for 24 h. After cooling to room temperature, water was added and the mixture was extracted with ethyl acetate. The combined organic phases were washed with brine, dried

over $MgSO_4$ and evaporated. Purification by column chromatography in two runs (petrol ether/ethyl acetate 50:1 and hexane/toluene 9:1) afforded compound **5k** (71 mg, 0.09 mmol, 25%) as a white solid.

^{1}H-NMR (500 MHz , CD_2Cl_2): δ (ppm) = 8.79 – 8.75 (m, 4 H, CH_{ar}), 8.73 (d, $^3J_{H,H}$ = 8.4 Hz, 2 H, CH_{ar}), 7.94 (br s, 2 H, CH_{ar}-CCF_3), 7.74 (br s, 1 H, CH_{ar}-CCF_3), 7.69 (d, $^3J_{H,H}$ = 8.4 Hz, 2 H, CH_{ar}), 7.66 – 7.57 (m, 6 H, CH_{ar}), 7.24 (s, 1 H, CH_{th}), 7.23 (s, 1 H, CH_{th}), 2.94 – 2.87 (m, 4 H, CH_2), 2.15 (ps p, $^3J_{H,H}$ = 7.4 Hz, 2 H, CH_2), 2.07 (br s, 6 H, CH_3).

^{13}C-NMR (126 MHz, CD_2Cl_2): δ (ppm) = 171.9, 171.4, 139.3, 138.7, 137.9, 137.6, 137.5, 137.0, 136.64, 136.57, 136.56, 135.8, 135.0, 134.9, 132.9 (*C*H), 132.3 (q, $^2J_{C,F}$ = 34 Hz, *C*CF_3), 129.8 (*C*H), 129.3 (*C*H), 129.0 (*C*H), 126.9 (*C*H), 125.8 (*C*H), 125.5 (*C*H), 125.5 (br *C*H), 123.4 (q, $^1J_{C,F}$ = 273 Hz, *C*F_3), 120.5 (br, *C*H), 38.9 (*C*H_2), 38.8 (*C*H_2), 23.5 (*C*H_2), 14.7 (2x *C*H_3).

^{19}F-NMR (471 MHz, CD_2Cl_2): δ (ppm) = -63.6 (s, CF_3).

HRMS (ESI+): *m/z* = 780.195 ($[M+H]^+$, calcd. 780.194 for $[C_{44}H_{32}F_6N_3S_2]^+$).

3,4-Bis(2-(3,5-bis(trifluoromethyl)phenyl)-5-methylthiazol-4-yl)-1-*tert*-butyl-1*H*-pyrrole-2,5-dione 7i

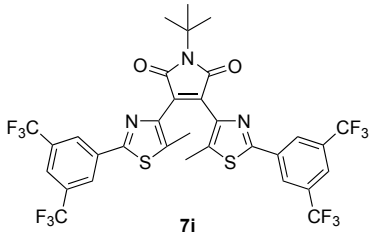

7i

Bromothiazole **48** (0.300 g, 0.77 mmol, 1 eq.), triethylamine (0.64 mL, 4.62 mmol, 6 eq.) and $Pd(PPh_3)_2Cl_2$ (27 mg, 0.04 mmol, 0.05 eq.) were dissolved in 10 mL of dry toluene and the mixture was degassed by repeated evacuation of the flask and refilling with argon. After the addition of pinacolborane (0.34 mL, 2.31 mmol, 3 eq.) the mixture was refluxed for 3.5 h at 120 °C until TLC indicated consumption of the starting material. After cooling down to 80 °C, an aqueous solution of Na_2CO_3 (2 M, 1.16 mL, 2.31 mmol, 3.0 eq.) was added very slowly due to vigorous gas evolution. Then, 3,4-dibromo-1-*tert*-butyl-1*H*-pyrrole-2,5-dione **26** (0.079 g, 0.25 mmol, 0.33 eq.) and $Pd(PPh_3)_4$ (18 mg, 0.02 mmol, 0.02 eq.) were added and the mixture was stirred at 100 °C for 16 h. After cooling down to room temperature the mixture was extracted with ethyl acetate and the combined organic layers were washed with brine and dried over $MgSO_4$. Purification by column chromatography (petrol ether/ethyl acetate 18:1) yielded **7i** (0.057 g, 0.07 mmol, 29%) as a yellow solid.

^{1}H-NMR (500 MHz , $CDCl_3$): δ (ppm) = 8.12 (br s, 4 H, CH_{ar}), 7.83 (br s, 2 H, CH_{ar}), 2.42 (s, 6 H, CH_3), 1.72 (s, 9 H, CH_3).

^{13}C-NMR (126 MHz, $CDCl_3$): δ (ppm) = 170.3, 161.5, 142.4, 138.7, 135.0, 134.9, 132.6 (q, $^2J_{C,F}$ = 34 Hz, *C*CF_3), 126.2 (br, *C*H), 123.3 (br, *C*H), 123.0 (q, $^1J_{C,F}$ = 273 Hz, *C*F_3), 58.5, 29.1 (*C*H_3), 13.0 (*C*H_3).

^{19}F-NMR (471 MHz, $CDCl_3$): δ (ppm) = -63.4 (s, C*F*$_3$).

HRMS (ESI+): *m/z* = 772.097 ([M+H]$^+$, calcd. 772.096 for $[C_{32}H_{22}F_{12}N_3O_2S_2]^+$).

1,2-Bis(2-phenyl-5-trifluoromethylthiazol-4-yl)cyclopent-1-ene 9b

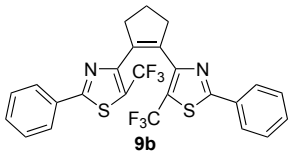

9b

Thiazolylstannane **78** (451 mg, 0.87 mmol, 2.5 eq.) and 1,2-dibromocyclopentene **24** (79 mg, 0.35 mmol, 1.0 eq.) were dissolved in 4 mL of DMF and the mixture was degassed by bubbling argon through it for 10 min. Then, $PdCl_2(PPh_3)_2$ (24 mg, 0.04 mmol, 0.10 eq.) was added and the mixture was stirred at 100 °C for 18 h. After cooling to room temperature, the mixture was poured into 100 mL of water and it was extracted with 4x 30 mL of diethyl ether. The combined organic phases were dried over $MgSO_4$ and the solvent was evaporated. Purification by column chromatography (petrol ether/ethyl acetate 50:1) afforded compound **9b** (32 mg, 0.06 mmol, 18%) as a turbid-white viscous oil.

^{1}H-NMR (500 MHz, $CDCl_3$): δ (ppm) = 7.79 – 7.77 (m, 4 H, C*H*$_{ar}$), 7.42 – 7.39 (m, 2 H, C*H*$_{ar}$), 7.33 – 7.29 (m, 4 H, C*H*$_{ar}$), 3.03 (t, $^3J_{H,H}$ = 7.5 Hz, 4 H, C*H*$_2$), 2.25 (p, $^3J_{H,H}$ = 7.5 Hz, 2 H, C*H*$_2$).

^{13}C-NMR (126 MHz, $CDCl_3$): δ (ppm) = 167.7, 153.7 (q, $^3J_{C,F}$ = 2 Hz, *C*-C-CF_3), 138.4, 132.6, 131.1 (*C*H), 129.0 (*C*H), 126.8 (*C*H), 122.2 (q, $^1J_{C,F}$ = 269 Hz, *C*F_3), 120.6 (q, $^2J_{C,F}$ = 38 Hz, *C*-CF_3), 37.3 (*C*H_2), 23.7 (*C*H_2).

^{19}F-NMR (471 MHz, $CDCl_3$): δ (ppm) = -52.0 (s, C*F*$_3$).

HRMS (ESI+): *m/z* = 523.075 ([M+H]$^+$, calcd. 523.074 for $[C_{25}H_{17}F_6N_2S_2]^+$).

1-(2-(4-*N*,*N*-dimethylaminophenyl)-5-trifluoromethylthiophen-4-yl)-2-(2-methyl-5-phenylthiophen-3-yl)cyclopent-1-ene 10c

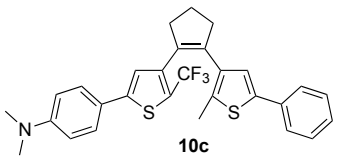

10c

Thienylboronic ester **91** (0.199 g, 0.50 mmol, 1.0 eq.) and monocoupled DAE **94** (0.160 g, 0.50 mmol, 1.0 eq.) were dissolved in 6 mL of toluene. To this solution K_3PO_4 (0.212 g, 1.00 mmol, 2.0 eq.), $Pd(OAc)_2$ (0.011 g, 0.05 mmol, 0.1 eq.), and SPhos (0.041 g, 0.10 mmol, 0.2 eq.) were added. The mixture was degassed by repeated evacuation of the flask and refilling with argon and it was stirred at 100 °C for 20 h. After cooling to room temperature it was diluted with ethyl acetate and filtered through a pad of Celite eluting with ethyl acetate. The

filtrate was evaporated and the residue was purified by column chromatography (petrol ether/methylene chloride 9:1) to afford compound **10c** (0.142 g, 0.28 mmol, 28% over two steps starting from thiophene **90**) as a pale yellow solid.

^{1}H-NMR (500 MHz, $CDCl_3$): δ (ppm) = 7.54 – 7.52 (m, 2 H, CH_{ar}), 7.37 – 7.34 (m, 2 H, CH_{ar}), 7.30 – 7.23 (m, 3 H, CH_{ar}), 7.09 (s, 1 H, CH_{ar}), 6.67 (q, $^{5}J_{H,F}$ = 1.3 Hz, 1 H, CH_{ar}), 6.66 – 6.63 (m, 2 H, CH_{ar}), 2.96 (s, 6 H, CH_3), 2.92 – 2.88 (m, 2 H, CH_2), 2.86 – 2.82 (m, 2 H, CH_2), 2.11 (ps p, $^{3}J_{H,H}$ = 7.3 Hz, 2 H, CH_2), 2.04 (s, 3 H, CH_3).

^{13}C-NMR (126 MHz, $CDCl_3$): δ (ppm) = 150.6, 145.9, 142.1 (br), 139.9, 137.8, 135.8, 135.6, 134.7, 133.7, 128.9 (*C*H), 127.10 (*C*H), 127.07 (*C*H), 125.5 (*C*H), 124.2 (*C*H), 124.1 (*C*H), 123.1 (q, $^{1}J_{C,F}$ = 270 Hz, *C*F_3), 121.4 (q, $^{2}J_{C,F}$ = 36 Hz, *C*CF_3), 121.1, 112.4 (*C*H), 40.4 (*C*H_3), 38.6 (*C*H_2), 38.1 (br, *C*H_2), 23.5 (*C*H_2), 14.3 (*C*H_3).

^{19}F-NMR (471 MHz, $CDCl_3$): δ (ppm) = -52.6 (s, CF_3).

HRMS (ESI+): *m/z* = 510.150 ([M+H]$^+$, calcd. 510.154 for [$C_{29}H_{27}F_3NS_2$]$^+$).

1-*tert*-Butyl-3,4-bis(2-morpholino-5-trifluoromethylthiazol-4-yl)-1*H*-pyrrole-2,5-dione 11b

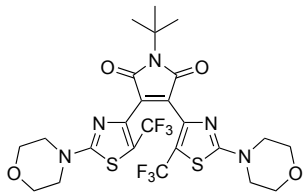

11b

2-Morpholino-4-(tributylstannyl)-5-trifluoromethylthiazole **70** (1.45 g, 2.75 mmol, 2.5 eq.) and 3,4-dibromo-1-*tert*-butyl-1*H*-pyrrole-2,5-dione **26** (0.34 g, 1.10 mmol, 1.0 eq.) were dissolved in 70 mL of toluene and the mixture was degassed by bubbling argon through the solution for 10 min. After the addition of $Pd(PPh_3)_4$ (165 mg, 0.14 mmol, 0.13 eq.) the mixture was stirred at 110 °C for 20 h. After cooling to room temperature, the mixture was diluted with 100 mL of ethyl acetate and washed with 3x 100 mL of water. The organic phase was dried over $MgSO_4$ and evaporated. Purification of the residue by column chromatography (methylene chloride/ethyl acetate 2:1, 1% triethylamine) afforded compound **11b** (203 mg, 0.32 mmol, 29%) as an orange solid.

^{1}H-NMR (500 MHz, $CDCl_3$): δ (ppm) = 3.75 (t, $^{3}J_{H,H}$ = 5.0 Hz, 8 H, CH_2), 3.42 (t, $^{3}J_{H,H}$ = 5.0 Hz, 8 H, CH_2), 1.63 (s, 9 H, CH_3).

^{13}C-NMR (126 MHz, $CDCl_3$): δ (ppm) = 170.6, 169.0, 140.8, 136.2, 121.9 (q, $^{1}J_{C,F}$ = 267 Hz, *C*F_3), 114.1 (q, $^{2}J_{C,F}$ = 37 Hz, *C*CF_3), 66.0 (*C*H_2), 58.5, 48.4 (*C*H_2), 28.9 (*C*H_3).

^{19}F-NMR (471 MHz, $CDCl_3$): δ (ppm) = -52.7 (s, CF_3).

HRMS (ESI+): *m/z* = 626.128 ([M+H]$^+$, calcd. 626.133 for [$C_{24}H_{26}F_6N_5O_4S_2$]$^+$).

1-*tert*-Butyl-3-(5-methyl-2-morpholinothiazol-4-yl)-4-(2-morpholino-5-trifluoromethyl-thiazol-4-yl)-1*H*-pyrrole-2,5-dione 11c

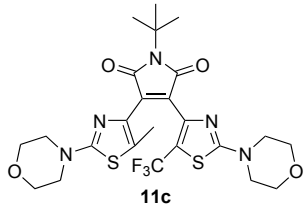

11c

5-Methyl-2-morpholino-4-(tributylstannyl)thiazole **47** (295 mg, 0.62 mmol, 1.2 eq.), 2-morpholino-4-(tributylstannyl)-5-trifluoromethylthiazole **70** (329 mg, 0.62 mmol, 1.2 eq.), and 3,4-dibromo-1-*tert*-butyl-1*H*-pyrrole-2,5-dione **26** (162 mg, 0.52 mmol, 1.0 eq.) were dissolved in 15 mL of dry toluene and degassed by bubbling argon through the solution for 5 min. Then, $Pd(PPh_3)_4$ (36 mg, 0.03 mmol, 0.06 eq.) was added and the mixture was stirred at 100 °C for 48 h. After cooling to room temperature the mixture was filtered through a pad of Celite eluting with ethyl acetate. The filtrate was washed with brine and dried over $MgSO_4$. After evaporation of the solvents the crude mixture was separated by column chromatography (petrol ether/ethyl acetate gradient from 10:1 to 1:1) affording compound **11c** (8 mg, 0.01 mmol, 3%) as a yellow solid.

^{1}H-NMR (300 MHz, $CDCl_3$): δ (ppm) = 3.77 (t, $^3J_{H,H}$ = 5.1 Hz, 4 H, CH_2), 3.72 (t, $^3J_{H,H}$ = 4.8 Hz, 4 H, CH_2), 3.44 (t, $^3J_{H,H}$ = 5.1 Hz, 4 H, CH_2), 3.26 (t, $^3J_{H,H}$ = 4.8 Hz, 4 H, CH_2), 2.29 (s, 3 H, CH_3), 1.63 (s, 9 H, CH_3).

^{13}C-NMR (76 MHz, $CDCl_3$): δ (ppm) = 66.2 (*C*H_2), 66.0 (*C*H_2), 48.5 (*C*H_2), 48.4 (*C*H_2), 29.0 (*C*H_3), 13.3 (*C*H_3), quaternary carbons were not detected due to low concentration.

^{19}F-NMR (282 MHz, $CDCl_3$): δ (ppm) = -52.2 (s, CF_3).

HRMS (ESI+): *m/z* = 572.170 ($[M+H]^+$, calcd. 572.161 for $[C_{24}H_{29}F_3N_5O_4S_2]^+$).

1,2-Bis(5-(3,5-di-*tert*-butylphenyl)-2-methylthiophen-3-yl)cyclopent-1-ene 13a

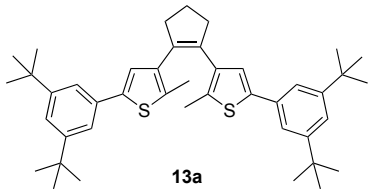

13a

The bis(pinacol boronate) **29** (425 mg, 0.83 mmol, 1.0 eq.), 1-bromo-3,5-di-*tert*-butylbenzene (670 mg, 2.49 mmol, 3 eq.), $Pd(OAc)_2$ (9 mg, 0.04 mmol, 0.05 eq.), SPhos (34 mg, 0.08 mmol, 0.1 eq.), and K_3PO_4 (ground, 705 mg, 3.32 mmol, 4 eq.) were put into a Schlenk tube equipped with a teflon screw cap. The tube was evacuated and refilled with argon twice. Then, 3 mL of degassed toluene were added, the screw cap was closed, and the mixture was stirred at 100 °C for 6 h. After cooling to room temperature the mixture was diluted with ethyl acetate and

filtered through a pad of Celite eluting with ethyl acetate. The filtrate was evaporated and purified by column chromatography (petrol ether) affording **13a** (148 mg, 0.23 mmol, 28%) as a white solid.

^{1}H-NMR (500 MHz , $CDCl_3$): δ (ppm) = 7.33 – 7.31 (m, 6 H, CH_{ar}), 7.02 (s, 2 H, CH_{ar}), 2.89 (t, $^3J_{H,H}$ = 7.5 Hz, 4 H, CH_2), 2.11 (p, $^3J_{H,H}$ = 7.5 Hz, 2 H, CH_2), 2.06 (s, 6 H, CH_3), 1.33 (s, 36 H, CH_3).

^{13}C-NMR (126 MHz, $CDCl_3$): δ (ppm) = 151.3, 140.9, 136.7, 134.9, 134.1, 133.9, 124.0 (CH), 121.5 (CH), 120.1 (CH), 38.5 (CH_2), 35.0, 31.6 (CH_3), 23.2 (CH_2), 14.6 (CH_3).

HRMS (ESI$^+$): m/z = 636.378 ($[M]^+$, calcd. 636.382 for $[C_{43}H_{56}S_2]^+$).

1-(5-(3-(acetylthio)phenyl)-2-methylthien-3-yl)-2-(5-(3,5-di-*tert*-butylphenyl)-2-methyl-thien-3-yl)cyclopent-1-ene 13b

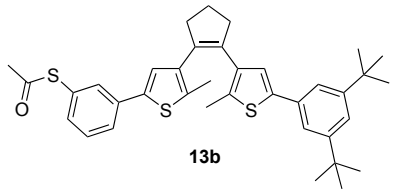

13b

In analogy to a literature procedure,[120] compound **38** (0.850 g, 1.41 mmol, 1.0 eq.), potassium thioacetate (0.241 g, 2.11 mmol, 1.5 eq.), $Pd_2(dba)_3$ (32 mg, 0.035 mmol, 0.025 eq.), and Xantphos (41 mg, 0.07 mmol, 0.05 eq.) were put into a Schlenk flask and the flask was evacuated and refilled with argon twice. A solution of diisopropylethylamine (0.49 mL, 2.82 mmol, 2.0 eq.) in 5 mL of 1,4-dioxane was added and the mixture was stirred at 100 °C for 3 h. After cooling to room temperature ethyl acetate and water were added, the organic phase was separated, and the aqueous phase was extracted with ethyl acetate. The combined organic phases were dried over $MgSO_4$ and evaporated. Purification by column chromatography (cyclohexane/ethyl acetate 20:1) afforded compound **13b** (0.250 g, 0.42 mmol, 30%) as a pale yellow solid.

^{1}H-NMR (500 MHz , $CDCl_3$): δ (ppm) = 7.55 (t, $^4J_{H,H}$ = 1.7 Hz, 1 H, CH_{ar}), 7.53 – 7.51 (m, 1 H, CH_{ar}), 7.37 (ps t, $^3J_{H,H}$ = 7.8 Hz, 1 H, CH_{ar}), 7.32 – 7.30 (m, 3 H, CH_{ar}), 7.28 – 7.25 (m, 1 H, CH_{ar}), 7.08 (s, 1 H, CH_{th}), 6.97 (s, 1 H, CH_{th}), 2.90 – 2.81 (m, 4 H, CH_2), 2.42 (s, 3 H, CH_3), 2.09 (ps p, $^3J_{H,H}$ = 7.4 Hz, 2 H, CH_2), 2.02 (s, 3 H, CH_3), 1.98 (s, 3 H, CH_3), 1.32 (s, 18 H, CH_3).

^{13}C-NMR (126 MHz, $CDCl_3$): δ (ppm) = 194.0, 151.3, 140.9, 138.5, 137.1, 136.5, 135.8, 135.4, 135.2, 134.4, 134.1, 133.8, 132.9, 131.2, 129.7, 128.6, 126.5, 124.8, 123.9, 121.5, 120.1, 38.6, 38.5, 35.0, 31.5, 30.4, 23.2, 14.64, 14.58.

HRMS (ESI$^+$): m/z = 598.243 ($[M]^+$, calcd. 598.240 for $C_{37}H_{42}OS_3^+$), 599.248 ($[M+H]^+$, calcd. 599.248 for $[C_{37}H_{43}OS_3]^+$)

1-(5-(4-(acetylthio)phenyl)-2-methylthien-3-yl)-2-(5-(3,5-di-*tert*-butylphenyl)-2-methyl-thien-3-yl)cyclopent-1-ene 13c

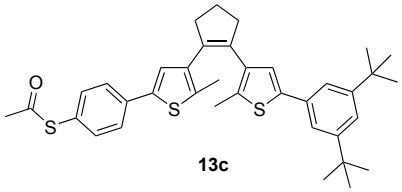

13c

Following a literature procedure,[83] compound **39** (1.026 g, 1.70 mmol, 1.0 eq.) was dissolved in 20 mL of anhydrous THF and cooled to -78 °C. *n*-BuLi (2.2 M in cyclohexane, 1.01 mL, 2.21 mmol, 1.3 eq.) was added dropwise and the mixture was stirred at -78 °C for 45 min. Then, sulfur (0.065 g, 2.04 mmol, 1.2 eq.) was added as a solid and the mixture was stirred at -78 °C for 30 min. Acteyl chloride (0.15 mL, 2.04 mmol, 1.2 eq.) was added, the mixture was stirred for 10 min at -78 °C and then warmed to room temperature over 30 min. It was diluted by addition of diethyl ether and was washed with water and brine. The organic phase was dried over $MgSO_4$ and evaporated. Purification by column chromatography (petrol ether/methylene chloride 9:1) afforded compound **13c** (0.280 g, 0.47 mmol, 28%) as a pale yellow solid.

^{1}H-NMR (500 MHz , $CDCl_3$): δ (ppm) = 7.55 (d, $^3J_{H,H}$ = 8.4 Hz, 2 H, CH_{ar}), 7.38 (d, $^3J_{H,H}$ = 8.4 Hz, 2 H, CH_{ar}), 7.35 – 7.33 (m, 3 H, CH_{ar}), 7.12 (s, 1 H, CH_{th}), 7.01 (s, 1 H, CH_{th}), 2.92 – 2.83 (m, 4 H, CH_2), 2.44 (s, 3 H, CH_3), 2.11 (ps p, $^3J_{H,H}$ = 7.3 Hz, 2 H, CH_2), 2.05 – 2.03 (m, 6 H, 2x CH_3), 1.35 (s, 18 H, CH_3).

^{13}C-NMR (126 MHz, $CDCl_3$): δ (ppm) = 194.3, 151.3, 140.9, 138.6, 137.2, 136.4, 135.8, 135.7, 135.3, 134.9 (*C*H), 134.4, 134.1, 133.8, 126.1, 126.0 (*C*H), 125.0 (*C*H), 123.9 (*C*H), 121.5 (*C*H), 120.0 (*C*H), 38.52 (*C*H_2), 38.50 (*C*H_2), 35.0, 31.5 (*C*H_3), 30.3 (*C*H_3), 23.2 (*C*H_2), 14.62 (*C*H_3), 14.58 (*C*H_3).

HRMS (ESI^+): m/z = 598.241 ($[M]^+$, calcd. 598.240 for $[C_{37}H_{42}OS_3]^+$).

8,9-Bis(5-methyl-2-phenylthiazol-4-yl)-1,5,7-triazabicyclo[4.3.0]-nona-6,8-diene 14

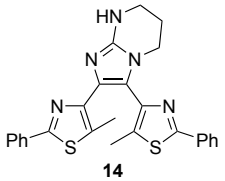

14

Cbz-protected DAE **61** (0.254 g, 0.42 mmol, 1.0 eq.) was dissolved in 15 mL of a 1:1 mixture of THF and ethanol. Ammonium formate (1.059 g, 16.80 mmol, 40 eq.) and palladium (10% on charcoal, 50 mg, 0.04 mmol, 0.1 eq.) were added and the flask was put into a pre-heated oil bath at 90 °C. The mixture was refluxed for 1.5 h until TLC indicated consumption of the starting material. After cooling to room temperature the mixture was filtered through a pad of Celite eluting with methylene chloride/methanol 9:1. The filtrate was evaporated and the residue was

purified by column chromatography (methylene chloride/methanol 9:1). The obtained material was lyophilized twice from benzene to afford compound **14** (0.152 g, 0.32 mmol, 77%) as a yellow solid.

^{1}H-NMR (300 MHz , $CDCl_3$): δ (ppm) = 7.98 – 7.91 (m, 2 H, C*H*$_{ar}$), 7.91 – 7.84 (m, 2 H, C*H*$_{ar}$), 7.51 – 7.42 (m, 3 H, C*H*$_{ar}$), 7.42 – 7.33 (m, 3 H, C*H*$_{ar}$), 4.04 (t, $^{3}J_{H,H}$ = 6.0 Hz, 2 H, C*H*$_2$), 3.51 (t, $^{3}J_{H,H}$ = 5.5 Hz, 2 H, C*H*$_2$), 2.21 – 2.12 (m, 2 H, C*H*$_2$), 2.14 (s, 3 H, C*H*$_3$), 2.01 (s, 3 H, C*H*$_3$).

^{13}C-DEPT-NMR (300 MHz, $CDCl_3$/CF_3COOH): δ (ppm) = 133.7 (*C*H), 132.3 (*C*H), 130.0 (*C*H), 129.7 (*C*H), 127.5 (*C*H), 127.0 (*C*H), 42.5 (*C*H$_2$), 38.6 (*C*H$_2$), 19.8 (*C*H$_2$), 12.2 (*C*H$_3$), 12.1 (*C*H$_3$).

HRMS (ESI^+): m/z = 470.136 ($[M+H]^+$, calcd. 470.147 for $[C_{26}H_{24}N_5S_2]^+$).

6.4 Isolation of ring-closed isomers and by-products

Isolation of 1c(c)

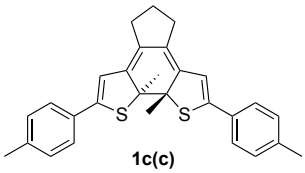

1c(c)

A solution of **1c** (145 mg, 0.33 mmol) in 250 mL of acetonitrile was degassed by evacuating the air in the flask and refilling with argon for several times. The solution was placed in 6 quartz tubes, which were purged with argon prior to use, and irradiated using a Rayonet RPR 100 photochemical reactor equipped with 300 nm lamps over a period of 7.5 min. Prolonged irradiation times led to an increased formation of the by-product **1c(bp)**. After evaporating the solvent the mixture consisting of ca. 50% of the ring-closed isomer was separated by column chromatography (hexane/ethyl acetate/triethylamine 100:1:2). Due to fast oxidation of the material in the presence of silica gel column chromatography was performed with an argon flushed column and thoroughly argon saturated solvents. Compound **1c(c)** (50 mg, 0.11 mmol, 33%) was obtained as a purple solid.

^{1}H-NMR (500 MHz, $CDCl_3$): δ (ppm) = 7.42 (d, $^{3}J_{H,H}$ = 8.0 Hz, 4 H, CH_{ar}), 7.16 (d, $^{3}J_{H,H}$ = 8.0 Hz, 4 H, CH_{ar}), 6.37 (s, 2 H, CH_{ar}), 2.47 (t, $^{3}J_{H,H}$ = 7.0 Hz, 4 H, CH_2), 2.36 (s, 6 H, CH_3), 2.01 (s, 6 H, CH_3), 1.90 (p, $^{3}J_{H,H}$ = 7.0 Hz, 2 H, CH_2).

^{13}C-NMR (126 MHz, $CDCl_3$): δ (ppm) = 146.2, 141.5, 138.6, 133.6, 132.0, 129.3 (*C*H), 126.1 (*C*H), 115.1 (*C*H), 66.1, 29.9 (*C*H_2), 27.3 (*C*H_3), 25.5 (*C*H_2), 21.5 (*C*H_3).

HRMS (ESI+): *m/z* = 440.149 ($[M]^+$, calcd. 440.163 for $C_{29}H_{28}S_2^+$).

Isolation of 1c(bp)

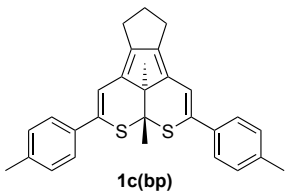

1c(bp)

A solution of **1c** (150 mg, 0.34 mmol) in 200 mL of acetonitrile was degassed by evacuating the air in the flask and refilling with argon for several times. The solution was placed in quartz tubes, which were purged with argon prior to use, and irradiated using a Rayonet RPR 100 photochemical reactor equipped with 300 nm lamps over a period of 2.5 h. After evaporating the solvent the mixture of the ring-closed isomer and by-product was separated by column chromatography (hexane/ethyl acetate/triethylamine 100:1:2). Due to fast oxidation of the material in the presence of silica gel column chromatography was performed with an argon flushed column and thoroughly argon saturated solvents. Compound **1c(bp)** (66 mg, 0.15 mmol, 44%) was obtained as a purple solid.

^{1}H-NMR (500 MHz, $CDCl_3$): δ (ppm) = 7.42 (d, $^{3}J_{H,H}$ = 8.0 Hz, 4 H, CH_{ar}), 7.12 (d, $^{3}J_{H,H}$ = 8.0 Hz, 4 H, CH_{ar}), 6.39 (s, 2 H, CH_{ar}), 2.56 (s, 3 H, CH_3), 2.52 (s, 3 H, CH_3), 2.34 (s, 6 H, CH_3), 2.33 – 2.06 (br m, 6 H, CH_2).

^{13}C-NMR (126 MHz, $CDCl_3$): δ (ppm) = 150.6, 138.4, 136.5, 135.3, 134.0, 129.3 (*C*H), 125.7 (*C*H), 114.4 (*C*H), 66.7, 59.1, 30.0 (*C*H_3), 29.9 (*C*H_2), 24.2 (*C*H_2), 23.9 (*C*H_3), 21.3 (*C*H_3).

HRMS (ESI+): *m/z* = 440.147 ([M]$^+$, calcd. 440.163 for $C_{29}H_{28}S_2^+$).

Isolation of 1h(c)

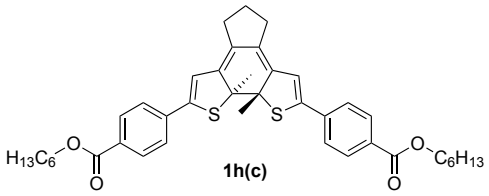

1h(c)

A solution of **1h** (250 mg, 0.37 mmol) in a mixture of 240 mL of acetonitrile and 2 mL of methylene chloride was placed in 6 quartz tubes and irradiated using a Rayonet RPR 100 photochemical reactor equipped with 300 nm lamps over a period of 20 min. After concentration of the solution to 50 mL it was placed in a refrigerator overnight. The formed precipitate was collected by filtration, washed with a small amount of cold acetonitrile and dried *in vacuo* affording **1h(c)** (200 mg, 0.30 mmol, 81%) as a purple solid.

^{1}H-NMR (300 MHz, $CDCl_3$): δ (ppm) = 8.01 (d, $^{3}J_{H,H}$ = 8.4 Hz, 4 H, CH_{ar}), 7.54 (d, $^{3}J_{H,H}$ = 8.4 Hz, 4 H, CH_{ar}), 6.51 (s, 2 H, CH_{ar}), 4.32 (t, $^{3}J_{H,H}$ = 6.6 Hz, 4 H, CH_2), 2.51 (t, $^{3}J_{H,H}$ = 7.2 Hz, 4 H, CH_2), 2.03 (s, 6 H, CH_3), 1.92 (p, $^{3}J_{H,H}$ = 7.2 Hz, 2 H, CH_2), 1.82 – 1.72 (m, 4 H, CH_2), 1.47 – 1.33 (m, 12 H, CH_2), 0.91 (t, $^{3}J_{H,H}$ = 6.9 Hz, 6 H, CH_3).

^{13}C-NMR (76 MHz, $CDCl_3$): δ (ppm) = 166.3, 145.7, 142.0, 138.7, 135.7, 130.0, 129.8 (*C*H), 126.0 (*C*H), 117.8 (*C*H), 66.2, 65.4 (*C*H_2), 31.6 (*C*H_2), 30.1 (*C*H_2), 28.8 (*C*H_2), 27.5 (*C*H_3), 25.8 (*C*H_2), 25.3 (*C*H_2), 22.7 (*C*H_2), 14.2 (*C*H_3).

HRMS (ESI+): *m/z* = 668.294 ([M]$^+$, calcd. 668.299 for $C_{41}H_{48}O_4S_2^+$).

Isolation of 3d(c)

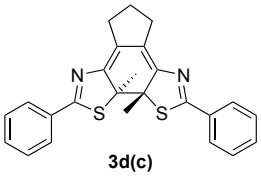

3d(c)

A solution of **3d** (70 mg, 0.17 mmol) in 120 ml of acetonitrile/methylene chloride 4:1 was degassed by evacuating the flask and refilling with argon for several times. It was transferred into quartz tubes, which were purged with argon prior to use, and irradiated in a Rayonet RPR 100 photochemical reactor equipped with 300 nm lamps over a period of 15 min. After

evaporation of the solvent the residue was purified by column chromatography (petrol ether/ethyl acetate 20:1) affording **3d(c)** (54 mg, 0.13 mmol, 77%) as a dark red solid. Crystals suitable for x-ray crystallography were obtained by slow evaporation of a solution of **3d(c)** in methylene chloride at room temperature.

^{1}H-NMR (500 MHz, $CDCl_3$): δ (ppm) = 7.92 - 7.89 (m, 4 H, CH_{ar}), 7.48 - 7.41 (m, 6 H, CH_{ar}), 2.87 - 2.70 (m, 4 H, CH_2), 1.96 (p, $^{3}J_{H,H}$ = 7.5 Hz, 2 H, CH_2), 1.89 (s, 6 H, CH_3).

^{13}C-NMR (126 MHz, $CDCl_3$): δ (ppm) = 169.7, 152.0, 134.0, 132.9, 131.6 (*C*H), 128.7 (*C*H), 128.3 (*C*H), 68.7, 30.1 (*C*H_2), 27.5 (*C*H_3), 25.7 (*C*H_2).

HRMS (ESI+): *m/z* = 415.124 ($[M+H]^+$, calcd. 415.130 for $[C_{25}H_{23}N_2S_2]^+$).

Isolation of 3d(bp)

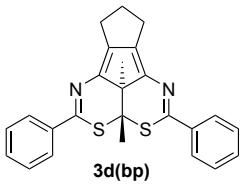

3d(bp)

A solution of **3d** (149 mg, 0.36 mmol) in 250 ml of acetonitrile/methylene chloride 4:1 was degassed by evacuating the flask and refilling with argon for several times. It was transferred into quartz tubes, which were purged with argon prior to use, and irradiated in a Rayonet RPR 100 photochemical reactor equipped with 300 nm lamps over a period of 3 h. After evaporation of the solvent the residue was purified by column chromatography (petrol ether/ethyl acetate 20:1) affording **3d(bp)** (34 mg, 0.13 mmol, 23%) as a dark red solid.

^{1}H-NMR (500 MHz, $CDCl_3$): δ (ppm) = 7.87 – 7.84 (m, 4 H, CH_{ar}), 7.43 - 7.37 (m, 6 H, CH_{ar}), 2.64 – 2.49 (m, 4 H, CH_2), 2.43 (s, 3 H, CH_3), 2.31 (s, 3 H, CH_3), 2.31 – 2.17 (m, 2 H, CH_2).

^{13}C-NMR (126 MHz, $CDCl_3$): δ (ppm) = 155.0, 148.5, 139.0, 138.2, 131.0 (*C*H), 128.6 (*C*H), 126.5 (*C*H), 60.0, 47.3, 34.5 (*C*H_3), 30.1 (*C*H_2), 24.3 (*C*H_2), 21.3 (*C*H_3).

HRMS (ESI+): *m/z* = 415.123 ($[M+H]^+$, calcd. 415.130 for $[C_{25}H_{23}N_2S_2]^+$).

Isolation of 11a(c)

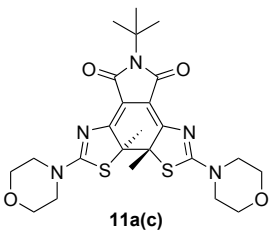

11a(c)

A solution of **11a** (170 mg, 0.33 mmol, 1.0 eq.) in 50 mL of acetonitrile was treated with ceric ammonium nitrate (330 mg, 0.60 mmol, 1.8 eq.) and stirred at room temperature for 5 min. During this time the mixture initially turns dark before it gets an orange color. Then sodium ascorbate (200 mg, 1 mmol, 3.0 eq.) was added and the mixture was stirred for 5 min. After filtration the solvent was removed *in vacuo* and the residue was partioned between 20 mL of

chloroform and 20 mL of water. The organic layer was separated and dried over $MgSO_4$. Evaporation of the solvent yielded 170 mg of a red solid which was determined by UPLC to consist of **11a** (25%), **11a(c)** (47%), and **11a(bp)** (35%). An analytical sample of **11a(c)** could be obtained by separation of the mixture via preparative HPLC (column: Luna Phenomenex, 10 µm, 20 x 250 mm, eluent: methanol/water from 50% to 90% methanol).

^{1}H-NMR (400 MHz, $CDCl_3$): δ (ppm) = 4.05 – 3.40 (broad, 16 H, CH_2), 1.78 (s, 6 H, CH_3), 1.64 (s, 9 H, CH_3).

^{13}C-NMR (101 MHz, $CDCl_3$): δ (ppm) = 172.3, 166.8, 157.7, 103.9, 72.2, 66.4 (*C*H_2), 57.9, 48.6 (*C*H_2), 29.3 (*C*H_3), 26.9 (*C*H_3).

HRMS (ESI+): *m/z* = 518.194 ([M+H]$^+$, calcd. 518.190 for $[C_{24}H_{32}N_5O_4S_2]^+$).

Isolation of 11a(bp)

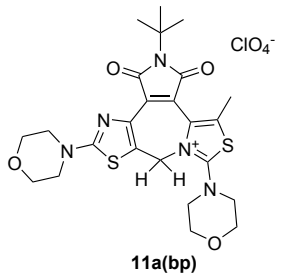

11a(bp)

A solution of **11a** (103 mg, 0.20 mmol) in 75 mL of acetonitrile containing 0.1 M Et_4NClO_4 was oxidized at a potential of 1 V using a divided H-cell with platinum nets as working and counter electrode and a standard calomel electrode (SCE) as reference. After a charge of 2 C/mol was transferred, the mixture was stirred for 2 h at room temperature. The solvent was evaporated and to the residue 20 mL of water were added. After stirring for 30 min at room temperature the remaining solid was filtered off and dried *in vacuo* affording **11a(bp)** (49 mg, 0.08 mmol, 40%) as a red solid. Crystals suitable for x-ray crystallography were obtained by recrystallization from chloroform.

^{1}H-NMR (300 MHz, $CDCl_3$): δ (ppm) = 5.28 (br s, 2 H, CH_2), 3.97 (t, $^3J_{H,H}$ = 4.8 Hz, 4 H, CH_2), 3.79 (t, $^3J_{H,H}$ = 4.8 Hz, 4 H, CH_2), 3.64 (t, $^3J_{H,H}$ = 4.8 Hz, 4 H, CH_2), 3.54 (t, $^3J_{H,H}$ = 4.8 Hz, 4 H, CH_2), 2.49 (s, 3 H, CH_3), 1.65 (s, 9 H, CH_3).

^{13}C-NMR (76 MHz, $CDCl_3$): δ (ppm) = 171.7, 170.5, 167.4, 167.3, 144.4, 133.5, 130.1, 127.3, 126.0, 122.8, 66.1 (*C*H_2), 65.3 (*C*H_2), 59.1, 53.7 (*C*H_2), 48.6 (*C*H_2), 46.5 (*C*H_2), 29.0 (*C*H_3), 14.8 (*C*H_3).

HRMS (ESI+): *m/z* = 516.155 ([M-ClO_4]$^+$, calcd. 516.174 for $[C_{24}H_{30}N_5O_4S_2]^+$).

Isolation of 11b(c)

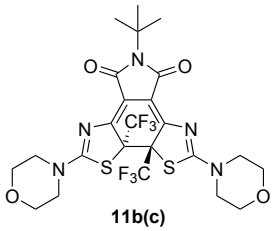

11b(c)

A solution of **11b** (120 mg, 0.19 mmol) in 40 mL of acetonitrile containing 0.1 M Et_4NPF_6 was oxidized at a potential of 1.8 V using a divided H-cell with platinum nets as working and counter electrode and a standard calomel electrode (SCE) as reference. After a charge of 2 C/mol was transferred the mixture was reduced at a potential of -0.2 V. The solvent was removed *in vacuo* and the residue was diluted with 50 mL of water. After extraction with 100 mL of chloroform the organic phase was washed 3x with 30 mL of water and dried over $MgSO_4$. Evaporation of the solvent afforded compound **11b(c)** (80 mg, 0.13 mmol, 67%) as an orange solid.

^{1}H-NMR (500 MHz, $CDCl_3$): δ (ppm) = 4.10 – 3.40 (br, 16 H, CH_2), 1.65 (s, 9 H, CH_3).

^{13}C-NMR (126 MHz, $CDCl_3$): δ (ppm) = 169.4, 165.7, 146.3, 124.6 (q, $^1J_{C,F}$ = 290 Hz, CF_3), 108.0, 72.0 (q, $^2J_{C,F}$ = 26 Hz, CCF_3), 66.4 (CH_2), 58.5, 48.4 (CH_2), 29.1 (CH_3).

^{19}F-NMR (282 MHz, $CDCl_3$): δ (ppm) = -52.7 (s, CF_3).

HRMS (ESI+): *m/z* = 626.139 ($[M+H]^+$, calcd. 626.133 for $[C_{24}H_{26}F_6N_5O_4S_2]^+$).

Isolation of 12(c)

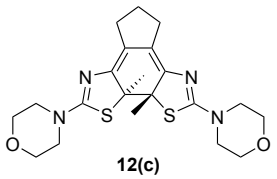

12(c)

A solution of **12** (100 mg, 0.23 mmol) in 40 mL of acetonitrile containing 0.1 M Et_4NPF_6 was oxidized at a potential of 0.8 V using a divided H-cell with platinum nets as working and counter electrode and a standard calomel electrode (SCE) as reference. After a charge of 2 C/mol was transferred, the mixture was reduced at a potential of -0.2 V. Then, the solvent was removed *in vacuo* and the residue was suspended in 200 mL of water. After extraction with 4x 50 mL of chloroform the combined organic phases were dried over $MgSO_4$ and evaporated. Purification by column chromatography (petrol ether/ethyl acetate 2:1) afforded **12(c)** (50 mg, 0.12 mmol, 50%) as a yellow solid.

^{1}H-NMR (500 MHz, $CDCl_3$): δ (ppm) = 3.74 (t, $^3J_{H,H}$ = 5.0 Hz, 8 H, CH_2), 3.54 (t, $^3J_{H,H}$ = 5.0 Hz, 8 H, CH_2), 2.55 – 2.42 (m, 4 H, CH_2), 1.79 (m, 2 H, CH_2), 1.72 (s, 6 H, CH_3).

^{13}C-NMR (126 MHz, $CDCl_3$): δ (ppm) = 165.3, 146.1, 121.8, 70.3, 66.5 (CH_2), 48.5 (CH_2), 29.7 (CH_2), 27.2 (CH_2), 26.1 (CH_3).

HRMS (ESI+): *m/z* = 433.163 ($[M+H]^+$, calcd. 433.173 for $[C_{21}H_{29}N_4O_2S_2]^+$).

6.5 Syntheses of precursors

1,2-Bis(2-methyl-5-(4,4,5,5-tetramethyl-1,3,2-dioxaborolan-2-yl)thien-3-yl)cyclopent-1-ene 29

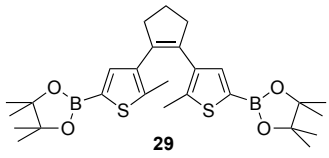

29

1,2-Bis(5-chloro-2-methylthiophen-3-yl)cyclopent-1-ene **16** (1.729 g, 5.30 mmol, 1.0 eq.) was dissolved in 50 mL of anhydrous THF and cooled to 0 °C. *n*-BuLi (2.2 M in cyclohexane, 6.02 mL, 13.25 mmol, 2.5 eq) was added dropwise and the solution was stirred at 0 °C for 45 min. Then, 2-isopropoxy-4,4,5,5-tetramethyl-1,3,2-dioxaborolane (3.24 mL, 15.90 mmol, 3.0 eq.) was added and the mixture was warmed to rt over 20 min. Some drops of MeOH were added, the mixture was poured into 200 mL of a saturated aqueous NH_4Cl solution, and it was extracted 3x with diethyl ether. The combined organic phases were washed with brine, dried over $MgSO_4$, and evaporated affording compound **29** (2.702 g, 5.27 mmol, quant.) as a yellow solid, which was used without further purification.

^{1}H-NMR (500 MHz, $CDCl_3$): δ (ppm) = 7.38 (s, 2 H, CH_{th}), 2.78 (t, $^3J_{H,H}$ = 7.4 Hz, 4 H, CH_2), 2.02 (p, $^3J_{H,H}$ = 7.4 Hz, 2 H, CH_2), 1.81 (s, 6 H, CH_3), 1.32 (s, 24 H, CH_3).

^{13}C-NMR (126 MHz, $CDCl_3$): δ (ppm) = 142.6, 138.5 (*C*H), 137.7, 134.4, 84.0, 39.1 (*C*H_2), 24.9 (*C*H_3), 23.1 (*C*H_2), 14.7 (*C*H_3), one quaternary carbon was not detected due to C-B coupling.

1-Bromo-3,5-di-*tert*-butylbenzene 30[202]

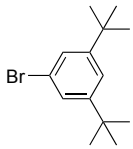

30

Following a literature procedure,[202] 1,3,5-tri-*tert*-butylbenzene (3.70 g, 15.0 mmol, 1.0 eq.) was dissolved in 7.5 mL of CCl_4. To this solution iron powder (0.92 g, 16.5 mmol, 1.1 eq.) was added and the mixture was cooled to 0 °C. Bromine (1.62 mL, 31.5 mmol, 2.1 eq.) was added dropwise and the resulting mixture was stirred at rt for 18 h. Then, the mixture was poured into 100 mL of water and extracted with 3x 25 mL of CH_2Cl_2. The combined organic phases were washed with a sat. aqueous solution of $Na_2S_2O_3$, dried over $MgSO_4$, and evaporated. The residue was taken up in petrol ether, filtered through a pad of silica gel eluting with petrol ether and evaporated affording a colorless liquid. The crude product was distilled under reduced pressure (20 mbar) and fractions boiling at 140 – 150 °C were collected. The material was dissolved in a small amount of petrol ether and stored in a freezer overnight yielding 1-bromo-3,5-di-*tert*-butylbenzene **30** (1.43 g, 5.3 mmol, 36%) as colorless crystals.

^{1}H-NMR (300 MHz, $CDCl_3$): δ (ppm) = 7.34 (ps s, 3 H, CH_{ar}), 1.31 (s, 18 H, CH_3).
^{13}C-NMR (76 MHz, $CDCl_3$): δ (ppm) = 153.1, 125.9 (*C*H), 122.3, 121.2 (CH), 35.1, 31.4 (CH_3).

1,2-Bis(2-methyl-5-(4,4,5,5-tetramethyl-1,3,2-dioxaborolan-2-yl)thien-3-yl)perfluorocyclopent-1-ene 31

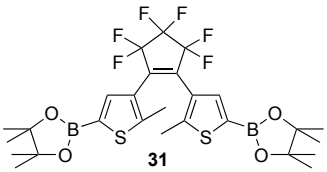

1,2-Bis(2-chloro-5-methylthien-4-yl)perfluorocyclopent-1-ene **18** (1.028 g, 2.35 mmol, 1 eq.) was dissolved in 10 mL of dry diethyl ether and *n*-BuLi (2.2 M in cyclohexane, 2.67 mL, 5.88 mmol, 2.5 eq.) was added dropwise at room temperature over 10 min. The mixture was stirred for further 20 min before 2-isopropoxy-4,4,5,5-tetramethyl-1,3,2-dioxaborolane (0.92 mL, 6.35 mmol, 2.7 eq.) was added. After stirring for 5 min the mixture was diluted with 50 mL of ethyl acetate, washed with brine, dried over $MgSO_4$, and evaporated to dryness affording crude compound **31** (1.305 g, 2.10 mmol, 90%) as a dark-brown solid, which was used without further purification.
^{1}H-NMR (300 MHz, $CDCl_3$): δ (ppm) = 7.61 (s, 2 H, CH_{th}), 1.84 (s, 6 H, CH_3), 1.34 (s, 24 H, CH_3).
^{19}F-NMR (282 MHz, $CDCl_3$): δ (ppm) = -110.5 (t, $^{3}J_{F,F}$ = 5.5 Hz, 4 F, CF_2), -132.2 (p, $^{3}J_{F,F}$ = 5.5 Hz, 2 F, CF_2).

1-(5-Chloro-2-methylthien-3-yl)-2-(5-(4-methoxyphenyl)-2-methylthien-3-yl)cyclopent-1-ene 32[203]

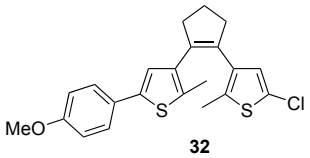

Compound **32** was synthesized following the procedure described for **1a** using 1,2-bis(5-chloro-2-methylthiophen-3-yl)cyclopent-1-ene **16** (2.000 g, 6.07 mmol, 1.0 eq.) in 40 mL of THF, *n*-BuLi (2.2 M in cyclohexane, 2.76 mL, 6.07 mmol, 1.0 eq.), tri(*n*-butyl) borate (2.46 mL, 9.11 mmol, 1.5 eq.), 4-methoxy-1-bromobenzene (0.84 mL, 6.68 mmol, 1.1 eq.) in 20 mL of THF, $Pd(PPh_3)_4$ (0.246 g, 0.21 mmol, 0.035 eq.), and aqueous Na_2CO_3 (2 M, 20 mL, 40.0 mmol, 6.6 eq.). The reaction was performed at 80 °C for 16 h. Column chromatography (petrol ether/ethyl acetate 30:1) afforded compound **32** (1.220 g, 3.04 mmol, 50%) as a white solid.

^{1}H-NMR (500 MHz, $CDCl_3$): δ (ppm) = 7.45 – 7.41 (m, 2 H, CH_{ar}), 6.92 – 6.87 (m, 2 H, CH_{ar}), 6.88 (s, 1 H, CH_{th}), 6.64 (s, 1 H, CH_{th}), 3.83 (s, 3 H, OCH_3), 2.82 (t, $^3J_{H,H}$ = 7.4 Hz, 2 H, CH_2), 2.75 (t, $^3J_{H,H}$ = 7.4 Hz, 2 H, CH_2), 2.06 (ps p, $^3J_{H,H}$ = 7.4 Hz, 2 H, CH_2), 1.99 (s, 3 H, CH_3), 1.90 (s, 3 H, CH_3).

^{13}C-NMR (126 MHz, $CDCl_3$): δ (ppm) = 159.0, 139.8, 136.3, 135.5, 135.3, 133.7, 133.5, 133.4, 127.5, 127.0 (*C*H), 126.7 (*C*H), 125.0, 122.9 (*C*H), 114.3 (*C*H), 55.5 (*C*H_3), 38.6 (*C*H_2), 38.5 (*C*H_2), 23.0 (*C*H_2), 14.5 (*C*H_3), 14.3 (*C*H_3).

1-(5-(3,5-Bis(trifluoromethyl)phenyl)-2-methylthien-3-yl)-2-(5-chloro-2-methylthien-3-yl)cyclopent-1-ene 33

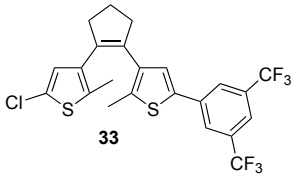

33

Compound **33** was synthesized following the procedure described for **1a** using 1,2-bis(5-chloro-2-methylthiophen-3-yl)cyclopent-1-ene **16** (1.884 g, 5.72 mmol, 1.0 eq.) in 20 mL of THF, *n*-BuLi (2.2 M in cyclohexane, 3.12 mL, 6.86 mmol, 1.2 eq.), tri(*n*-butyl) borate (2.01 mL, 7.44 mmol, 1.3 eq.), 3,5-bis(trifluoromethyl)-1-bromobenzene (1.78 mL, 10.30 mmol, 1.8 eq.) in 30 mL of THF, $Pd(PPh_3)_4$ (0.198 g, 0.17 mmol, 0.03 eq.), and aqueous Na_2CO_3 (2 M, 10 mL, 20.0 mmol, 3.5 eq.). The reaction was performed at 80 °C for 4 h. Column chromatography (petrol ether) afforded compound **33** (0.671 g, 1.32 mmol, 23%) as a pale yellow oil.

HRMS (ESI+): *m/z* = 506.044 (calcd. 506.036 for $[C_{23}H_{17}{}^{35}ClF_6S_2]^+$), 508.043 (calcd. 508.033 for $[C_{23}H_{17}{}^{37}ClF_6S_2]^+$).

(4-*N,N*-Dimethylaminophenyl)-4,4,5,5-tetramethyl-1,3,2-dioxaborolane 34[204]

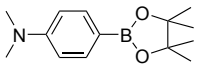

34

4-Bromo-*N,N*-dimethylaniline (8.00 g, 40.00 mol, 1.0 eq.) was dissolved in 150 mL of dry THF and cooled to -78 °C. *n*-BuLi (2.2 M in cyclohexane, 21.82 mL, 48.00 mmol, 1.2 eq.) was added dropwise and the mixture was stirred at -78 °C for 30 min. Then, 2-isopropoxy-4,4,5,5-tetramethyl-1,3,2-dioxaborolane (9.79 mL, 48.00 mmol, 1.2 eq.) was added and the mixture was warmed to room temperature over 45 min. After the addition of 50 mL of water the mixture was extracted 3x with ethyl acetate. The combined organic phases were washed with brine, dried over $MgSO_4$, and evaporated affording compound **34** (8.969 g, 36.29 mmol, 91%) as a yellow solid.

^{1}H-NMR (300 MHz, $CDCl_3$): δ (ppm) = 7.73 – 7.67 (m, 2 H, CH_{ar}), 6.72 – 7.66 (m, 2 H, CH_{ar}), 2.99 (s, 6 H, CH_3), 1.33 (s, 12 H, CH_3).

^{13}C-NMR (76 MHz, $CDCl_3$): δ (ppm) = 152.7, 136.3 (*C*H), 111.4 (*C*H), 83.3, 40.2 (*C*H_3), 25.0 (*C*H_3), one quaternary carbon was not detected due to C-B coupling.

2-(4-(4,4,5,5-Tetramethyl-1,3,2-dioxaborolan-2-yl)phenyl)-4,6-diphenyltriazine 35

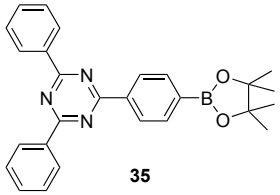

35

In a Schlenk tube equipped with a teflon screw cap 2-(4-bromophenyl)-4,6-diphenyltriazine **36** (1.00 g, 2.58 mmol, 1.0 eq.) and triethylamine (2.15 mL, 15.51 mmol, 6.0 eq.) were dissolved in 20 mL of anhydrous toluene. The solution was degassed by repeated evacuation of the gas phase and refilling with argon for several times. Then, $PdCl_2(PPh_3)_2$ (0.181 g, 0.26 mmol, 0.1 eq.) and 4,4,5,5-tetramethyl-1,3,2-dioxaborolane (0.94 mL, 6.48 mmol, 2.5 eq.) were added, the screw cap was closed, and the mixture was stirred at 120 °C for 8 h. After cooling to room temperature the reaction was quenched by dropwise addition of water (caution: vigorous gas evolution!). The organic phase was washed with brine, dried over $MgSO_4$, and evaporated. Column chromatography (petrol ether/ethyl acetate 20:1) afforded compound **35** (0.226 g) as a mixture with ca. 20% of unreacted starting material, as determined by UPLC. It was used without further purification.

1-(5-(3,5-Di-*tert*-butylphenyl)-2-methylthien-3-yl)-2-(5-chloro-2-methylthien-3-yl)cyclopent-1-ene 37

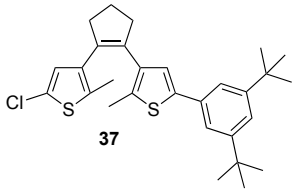

37

Compound **37** was synthesized following the procedure described for **1a** using 1,2-bis(5-chloro-2-methylthiophen-3-yl)cyclopent-1-ene **16** (0.692 g, 2.10 mmol, 1.0 eq.) in 15 mL of THF, *n*-BuLi (2.2 M in cyclohexane, 1.15 mL, 2.52 mmol, 1.2 eq.), tri(*n*-butyl) borate (0.74 mL, 2.73 mmol, 1.3 eq.), 1-bromo-3,5-di-*tert*-butylbenzene **30** (0.678 g, 2.52 mmol, 1.2 eq.) in 6 mL of THF, $Pd(PPh_3)_4$ (0.121 g, 0.11 mmol, 0.05 eq.), and aqueous Na_2CO_3 (2 M, 3.68 mL, 7.35 mmol, 3.5 eq.). The reaction was performed at 80 °C for 20 h. Column chromatography (petrol ether) afforded compound **37** (0.631 g, 1.31 mmol, 62%) as a colorless viscous oil.

^{1}H-NMR (500 MHz, CD_2Cl_2): δ (ppm) = 7.33 (t, $^4J_{H,H}$ = 1.7 Hz, 1 H, CH_{ar}), 7.30 (d, $^4J_{H,H}$ = 1.7 Hz, 2 H, CH_{ar}), 6.94 (s, 1 H, CH_{th}), 6.66 (s, 1 H, CH_{th}), 2.84 (t, $^3J_{H,H}$ = 7.5 Hz, 2 H, CH_2), 2.75 (t, $^3J_{H,H}$ = 7.5 Hz, 2 H, CH_2), 2.06 (ps p, $^3J_{H,H}$ = 7.5 Hz, 2 H, CH_2), 2.05 (s, 3 H, CH_3), 1.91 (s, 3 H, CH_3), 1.34 (s, 18 H, CH_3).

^{13}C-NMR (126 MHz, CD_2Cl_2): δ (ppm) = 151.8, 141.1, 136.6, 136.1, 135.9, 134.5, 134.2, 134.0, 133.9, 127.4 (*C*H), 125.1, 124.2 (*C*H), 121.9 (*C*H), 120.2 (*C*H), 38.64 (CH_2), 38.63 (CH_2), 35.2, 31.5 (CH_3), 23.4 (CH_2), 14.6 (CH_3), 14.3 (CH_3).
HRMS (ESI+): *m/z* = 482.188 ($[M]^+$, calcd. 482.187 for $[C_{29}H_{35}ClS_2]^+$).

1-(5-(3-Bromophenyl)-2-methylthien-3-yl)-2-(5-(3,5-di-*tert*-butylphenyl)-2-methylthien-3-yl)cyclopent-1-ene 38

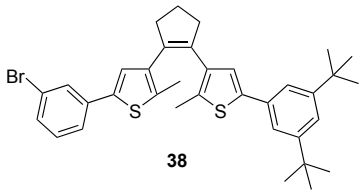

38

Compound **38** was synthesized following the procedure described for **1a** using the monofunctionalized DAE **37** (2.001 g, 4.14 mmol, 1.0 eq.) in 30 mL of THF, *tert*-BuLi (1.9 M in pentane, 2.83 mL, 5.38 mmol, 1.3 eq.), triisopropyl borate (1.012 g, 5.38 mmol, 1.3 eq.), 1-bromo-3-iodobenzene (1.06 mL, 8.28 mmol, 2.0 eq.) in 15 mL of THF, $Pd(PPh_3)_4$ (0.239 g, 0.21 mmol, 0.05 eq.), and aqueous Na_2CO_3 (2 M, 10.8 mL, 21.53 mmol, 5.2 eq.). The reaction was performed at 80 °C for 16 h. Column chromatography (petrol ether/methylene chloride 20:1) afforded compound **38** (0.850 g, 1.41 mmol, 34%) as a white solid.
^{1}H-NMR (500 MHz, $CDCl_3$): δ (ppm) = 7.66 (t, $^4J_{H,H}$ = 1.7 Hz, 1 H, CH_{ar}), 7.43 – 7.40 (m, 1 H, CH_{ar}), 7.36 – 7.33 (m, 1 H, CH_{ar}), 7.32 – 7.30 (m, 3 H, CH_{ar}), 7.19 (t, $^3J_{H,H}$ = 7.9 Hz, 1 H, CH_{ar}), 7.08 (s, 1 H, CH_{th}), 6.95 (s, 1 H, CH_{th}), 2.91 – 2.81 (m, 4 H, CH_2), 2.10 (ps p, $^3J_{H,H}$ = 7.4 Hz, 2 H, CH_2), 2.05 (s, 3 H, CH_3), 2.00 (s, 3 H, CH_3), 1.33 (s, 18 H, CH_3).
^{13}C-NMR (126 MHz, $CDCl_3$): δ (ppm) = 150.3, 139.9, 137.0, 136.2, 135.7, 135.4, 134.6, 134.4, 133.3, 133.1, 132.8, 129.3, 128.8, 127.5, 127.3, 123.9, 123.0, 122.0, 120.5, 119.0, 37.5, 37.4, 34.0, 30.5, 22.2, 13.6, 13.5.
HRMS (ESI+): *m/z* = 602.158 ($[M]^+$, calcd. 602.168 for $[C_{35}H_{39}{}^{79}BrS_2]^+$), 604.156 ($[M]^+$, calcd. 604.166 for $[C_{35}H_{39}{}^{81}BrS_2]^+$).

1-(5-(4-Bromophenyl)-2-methylthien-3-yl)-2-(5-(3,5-di-*tert*-butylphenyl)-2-methylthien-3-yl)cyclopent-1-ene 39

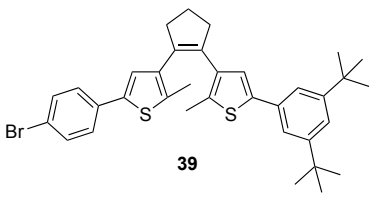

39

Compound **39** was synthesized following the procedure described for **1a** using the monofunctionalized DAE **37** (2.126 g, 4.40 mmol, 1.0 eq.) in 10 mL of THF, *tert*-BuLi (1.9 M in pentane, 3.01 mL, 5.72 mmol, 1.3 eq.), triisopropyl borate (1.32 mL, 5.72 mmol, 1.3 eq.),

1-bromo-4-iodobenzene (2.490 g, 8.80 mmol, 2.0 eq.) in 10 mL of THF, $Pd(PPh_3)_4$ (0.254 g, 0.22 mmol, 0.05 eq.), and aqueous Na_2CO_3 (2 M, 8.80 mL, 17.60 mmol, 4.0 eq.). The reaction was performed at 80 °C for 16 h. Column chromatography (petrol ether/methylene chloride 50:1) afforded compound **39** (1.062 g, 1.76 mmol, 40%) as a white solid.

^{1}H-NMR (500 MHz, $CDCl_3$): δ (ppm) = 7.46 – 7.43 (m, 2 H, CH_{ar}), 7.38 – 7.34 (m, 2 H, CH_{ar}), 7.33 – 7.30 (m, 3 H, CH_{ar}), 7.04 (s, 1 H, CH_{th}), 6.96 (s, 1 H, CH_{th}), 2.90 – 2.81 (m, 4 H, CH_2), 2.09 (ps p, $^3J_{H,H}$ = 7.5 Hz, 2 H, CH_2), 2.05 (s, 3 H, CH_3), 2.01 (s, 3 H, CH_3), 1.33 (s, 18 H, CH_3).

^{13}C-NMR (126 MHz, $CDCl_3$): δ (ppm) = 151.4, 140.9, 138.4, 137.2, 136.4, 135.3, 135.2, 134.4, 134.1, 133.8, 133.6, 131.9 (*C*H), 126.9 (*C*H), 124.6 (*C*H), 124.0 (*C*H), 121.6 (*C*H), 120.7, 120.1 (*C*H), 38.5 (*C*H_2), 38.4 (*C*H_2), 35.0, 31.5 (*C*H_3), 23.2 (*C*H_2), 14.63 (*C*H_3), 14.58 (*C*H_3).

HRMS (ESI+): *m/z* = 602.157 ($[M]^+$, calcd. 602.168 for $[C_{35}H_{39}{}^{79}BrS_2]^+$), 604.155 ($[M]^+$, calcd. 604.166 for $[C_{35}H_{39}{}^{81}BrS_2]^+$).

1-Bromo-2-(5-methyl-2-phenylthiazol-4-yl)cyclopent-1-ene 43

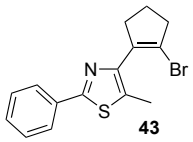

43

The pinacol boronate **42** (2.410 g, 8.00 mmol, 1.0 eq.), $Pd(OAc)_2$ (36 mg, 0.16 mmol, 0.02 eq.), and SPhos (131 mg, 0.32 mmol, 0.04 eq.) were put into a Schlenk tube equipped with a teflon screw cap. The tube was evacuated and refilled with argon twice. Then, 12 mL of toluene were added and the mixture was degassed by repeated evacuation of the flask and refilling with argon. 1,2-Dibromocyclopentene **24** (5.422 g, 24.00 mmol, 3.0 eq.) and K_3PO_4 (ground, 6.793 g, 32.00 mmol, 4.0 eq.) were added and the mixture was stirred at 100 °C for 16 h. After cooling to room temperature the mixture was filtered through a pad of Celite eluting with ethyl acetate, and the filtrate was evaporated. Purification by column chromatography (petrol ether/ethyl acetate 25:1) afforded compound **43** (1.560 g, 4.87 mmol, 61%) as a white solid.

^{1}H-NMR (300 MHz, $CDCl_3$): δ (ppm) = 7.94 – 7.89 (m, 2 H, CH_{ar}), 7.44 – 7.39 (m, 3 H, CH_{ar}), 2.91 – 2.79 (m, 4 H, CH_2), 2.48 (s, 3 H, CH_3), 2.14 (ps p, 2 H, $^3J_{H,H}$ = 7.6 Hz).

^{13}C-DEPT-NMR (76 MHz, $CDCl_3$): δ (ppm) = 129.6 (*C*H), 128.8 (*C*H), 126.3 (*C*H), 41.3 (*C*H_2), 36.4 (*C*H_2), 22.4 (*C*H_2), 13.1 (*C*H_3).

HRMS (ESI+): *m/z* = 320.007 ($[M+H]^+$, calcd. 320.011 for $[C_{15}H_{15}{}^{79}BrNS]^+$), 322.005 ($[M+H]^+$, calcd. 322.009 for $[C_{15}H_{15}{}^{81}BrNS]^+$).

2-(3,5-Bis(trifluoromethyl)phenyl)-5-methylthiazole 49

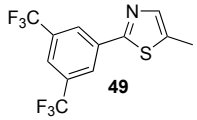

49

In analogy to a literature procedure,[125] zinc (2.649 g, 40.50 mmol, 3.0 eq.) was suspended in 10 mL of dry THF. 1,2-Dibromoethane (0.31 mL, 3.65 mmol, 0.27 eq.) was added and the mixture was heated twice to reflux for 5 min until gas evolution ceased. After the addition of TMSCl (0.21 mL, 1.62 mmol, 0.12 eq.) and stirring for 5 min, a solution of 2-bromo-5-methylthiazole **48** (2.404 g, 13.50 mmol, 1.0 eq.) in 10 mL of THF was added to the reaction mixture via a syringe, and it was stirred for 15 min at room tempreature until TLC indicated consumption of the starting material. Then, 3,5-bis(trifluoromethyl)-1-bromobenzene (5.142 g, 17.550 mmol, 1.3 eq.) and $Pd(PPh_3)_4$ (0.468 g, 0.41 mmol, 0.03 eq.) were added, and the mixture was refluxed at 80 °C for 24 h. After cooling to room temperature it was diluted with ethyl acetate and filtered through a pad of Celite. Then, the organic phase was washed with brine and was dried over $MgSO_4$. After evaporation of the solvent the crude product was purified by column chromatography (petrol ether/ethyl acetate 50:1 to 20:1) affording compound **49** (3.170 g, 10.18 mmol, 75%) as a white solid.

^{1}H-NMR (500 MHz, $CDCl_3$): δ (ppm) = 8.31 (s, 2 H, CH_{ar}), 7.86 (s, 1 H, CH_{ar}), 7.58 (q, $^4J_{H,H}$ = 1.1 Hz, 1 H, CH_{th}), 2.55 (d, $^4J_{H,H}$ = 1.1 Hz, 3 H, CH_3).

^{13}C-NMR (126 MHz, $CDCl_3$): δ (ppm) = 163.0, 142.4 (*C*H), 136.3, 135.9, 132.6 (q, $^2J_{C,F}$ = 34 Hz, *C*CF_3), 126.1 (br, *C*H), 123.2 (q, $^1J_{C,F}$ = 273 Hz, *C*F_3), 122.8 (br, *C*H), 12.2 (*C*H_3).

^{19}F-NMR (471 MHz, $CDCl_3$): δ (ppm) = -63.3 (s, CF_3).

2,4-Dibromo-5-methylthiazole 50[161]

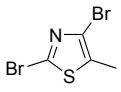

50

2-Bromo-5-methylthiazole **48** (1.460 g, 8.20 mmol, 1.0 eq.) was dissolved in a mixture of 10 mL of HBr (48% in water), 10 mL of water, and 20 mL of acetonitrile. Bromine (1.26 mL, 24.60 mmol, 3.0 eq.) was added, and the mixture was stirred at 80 °C for 2.5 h until TLC indicated consumption of the starting material. The reaction was quenched by adding 10 mL of a saturated aqueous solution of $NaHSO_3$, and the mixture was extracted with 3 x 30 mL of ethyl acetate. The combined organic phases were washed with aqueous $NaHCO_3$ solution and brine and dried over $MgSO_4$. After evaporation of the solvent the crude product was purified by column chromatography (petrol ether/ethyl acetate 9:1) yielding 2,4-dibromo-5-methylthiazole **50** (1.514 g, 5.89 mmol, 72%) as colorless crystals.

^{1}H-NMR (300 MHz, $CDCl_3$): δ (ppm) = 2.36 (s, CH_3).

^{13}C-NMR (75.5 MHz, $CDCl_3$): δ (ppm) = 133.2, 132.9, 123.2, 13.1 (*C*H_3).

HRMS (ESI+): *m/z* = 255.843 ($[M+H]^+$, calcd. 255.843 for $[C_4H_4{}^{79}Br_2NS]^+$), 257.840 ($[M+H]^+$, calcd. 257.841 for $[C_4H_4{}^{79}Br^{81}BrNS]^+$), 259.840 ($[M+H]^+$, calcd. 259.837 for $[C_4H_4{}^{81}Br_2NS]^+$).

2-(3,5-Bis(trifluoromethyl)phenyl)-4-bromo-5-methylthiazole 51

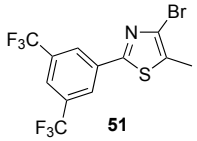

51

In analogy to a literature procedure,[125] zinc (1.08 g, 16.56 mmol, 3.0 eq.) was suspended in 10 mL of dry THF. 1,2-Dibromoethane (0.13 mL, 1.49 mmol, 0.3 eq.) was added and the mixture was heated twice to reflux until gas evolution ceased. After the addition of TMSCl (0.09 mL, 0.66 mmol, 0.1 eq.) and stirring for 5 min, a solution of 2,4-dibromo-5-methylthiazole **50** (1.42 g, 5.52 mmol, 1.0 eq.) in 6 mL of THF was added to the reaction mixture via a syringe, and it was stirred for 25 min at 60 °C until TLC indicated consumption of the starting material. Then, 3,5-bis(trifluoromethyl)-1-bromobenzene (1.94 g, 6.62 mmol, 1.2 eq.) and $Pd(PPh_3)_4$ (0.19 g, 0.17 mmol, 0.03 eq.) were added, and the mixture was refluxed at 80 °C for 18 h. After cooling to room temperature it was diluted with diethylether and filtered through a pad of Celite. Then, the organic phase was washed 2 x with aqueous HCl (1 M), aqueous $NaHCO_3$ solution, and brine, and was dried over $MgSO_4$. After evaporation of the solvent the crude product was purified by column chromatography (petrol ether/methylene chloride 9:1) affording compound **51** (1.12 g, 2.86 mmol, 52%) as a white solid.

^{1}H-NMR (300 MHz, $CDCl_3$): δ (ppm) = 8.30 (s, 2 H, CH_{ar}), 7.90 (s, 1 H, CH_{ar}), 2.49 (s, 3 H, CH_3).

^{13}C-NMR (76 MHz, $CDCl_3$): δ (ppm) = 161.7, 134.8, 132.7 (q, $^2J_{C,F}$ = 34 Hz, *C*CF_3), 131.2, 126.6, 125.9 (*C*H), 123.5 (*C*H), 123.1 (q, $^1J_{C,F}$ = 273 Hz, *C*F_3), 13.3 (*C*H_3).

^{19}F-NMR (282 MHz, $CDCl_3$): δ (ppm) = -63.3 (s, CF_3).

HRMS (ESI+): *m/z* = 389.946 ($[M+H]^+$, calcd. 389.939 for $[C_{12}H_7{}^{79}BrF_6NS]^+$), 391.945 ($[M+H]^+$, calcd. 391.937 for $[C_{12}H_7{}^{81}BrF_6NS]^+$).

(2-(3,5-Bis(trifluoromethyl)phenyl)-5-methylthiazol-4-yl)tributylstannane 52

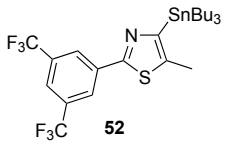

52

2-(3,5-Bis(trifluoromethyl)phenyl)-4-bromo-5-methylthiazole **51** (238 mg, 0.61 mmol, 1.0 eq.) was dissolved in 10 mL of dry THF and cooled to -100 °C. *n*-BuLi (2.2 M in cyclohexane, 0.33 mL, 0.73 mmol, 1.2 eq.) was added dropwise and the mixture was stirred for 10 min. Then, Bu_3SnCl (0.22 mL, 0.79 mmol, 1.3 eq.) was added and the mixture was warmed to room temperature over 45 min. After the addition of 5 mL of an aqueous solution of NH_4Cl the

mixture was extracted 3x with diethyl ether and the combined organic phases were washed with brine, dried over $MgSO_4$, and evaporated. Purification by column chromatography (petrol ether/methylene chloride 9:1) afforded stannane **52** (273 mg, 0.45 mmol, 75%) as a colorless oil.

^{1}H-NMR (300 MHz, $CDCl_3$): δ (ppm) = 8.34 (br s, 2 H, CH_{ar}), 7.83 (br s, 1 H, CH_{ar}), 2.57 (s, 3 H, CH_3), 1.69 – 0.86 (m, 27 H, CH_2, CH_3).

^{13}C-NMR (76 MHz, $CDCl_3$): δ (ppm) = 163.0, 159.7, 141.9, 136.5, 132.3 (q, $^2J_{C,F}$ = 34 Hz, *C*CF_3), 126.4 (br, *C*H), 123.3 (q, $^1J_{C,F}$ = 273 Hz, *C*F_3), 122.2 (br, *C*H), 29.3 (*C*H_2), 27.4 (*C*H_2), 13.9 (*C*H_3), 13.8 (*C*H_3), 10.7 (*C*H_2).

^{19}F-NMR (282 MHz, $CDCl_3$): δ (ppm) = -63.3 (s, CF_3).

2-(3,5-Bis(trifluoromethyl)phenyl)-4-bromo-5-methylthiophene 54

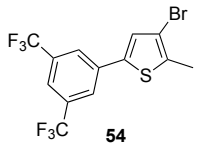

54

2,4-Dibromo-5-methylthiophene **53** (13.803 g, 53.93 mmol, 1 eq.) was dissolved in 135 mL of dry THF and cooled to -78 °C. *n*-BuLi (2.2 M in cyclohexane, 25.50 mL, 56.08 mmol, 1.04 eq.) was added dropwise and the mixture was stirred at -78 °C for 1.5 h. Then, tributylborate (15.13 mL, 56.08 mmol, 1.04 eq.) was added and the mixture was slowly warmed to room temperature over 2 h. Then, 20 mL of water were added before 3,5-bis(trifluoromethyl)-1-bromobenzene (9.300 g, 53.93 mmol, 1 eq.), $Pd(PPh_3)_4$ (1.806 g, 1.56 mmol, 0.03 eq.), and a solution of Na_2CO_3 (22.863 g, 215.71 mmol, 4 eq.) in 90 mL of water were added. The mixture was heated to reflux for 18 h. After cooling to room temperature the mixture was extracted with diethyl ether. The aqueous phase was extracted 2x with diethylether and the combined organic phases were dried over $MgSO_4$ and evaporated. After purification by column chromatography (petrol ether) and recrystallization from acetonitrile compound **54** (17.530 g, 45.05 mmol, 84%) was obtained as a white solid.

^{1}H-NMR (300 MHz, $CDCl_3$): *δ* (ppm) = 7.89 (s, 2 H, CH_{ar}), 7.76 (s, 1 H, CH_{ar}), 7.26 (s, 1 H, CH_{th}), 2.46 (s, 3 H, CH_3).

^{13}C-NMR (76 MHz, $CDCl_3$): *δ* (ppm) = 137.7, 136.4, 135.6, 132.6 (q, $^2J_{C,F}$ = 34 Hz, *C*CF_3), 127.9 (*C*H), 125.2 (*C*H), 123.2 (q, $^1J_{C,F}$ = 273 Hz, *C*F_3), 121.1 (*C*H), 110.8, 15.1 (*C*H_3).

^{19}F-NMR (471 MHz, $CDCl_3$): *δ* (ppm) = -63.3 (s, CF_3).

HRMS (ESI+): *m/z* = 388.941 ($[M+H]^+$, calcd. 388.943 for $[C_{13}H_8{}^{79}BrF_6S]^+$), 390.940 ($[M+H]^+$, calcd. 390.941 for $[C_{13}H_8{}^{81}BrF_6S]^+$).

2,4,5-Triiodoimidazole 56[205]

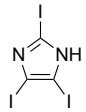

56

Following literature procedures,[205] imidazole (5.00 g, 73.4 mmol, 1.0 eq.) was dissolved in a mixture of 135 mL of dioxane and 135 mL of water. Na_2CO_3 (35.03 g, 330.5 mmol, 4.5 eq.) and iodine (61.52 g, 242.4 mmol, 3.3 eq.) were added and the mixture was stirred at room temperature for 20 h. An aqueous solution of $Na_2S_2O_3$ was added until the dark brown color vanished and water was added until all solids dissolved. The mixture was extracted using diethyl ether, the combined organic phases were washed with brine, dried over $MgSO_4$ and evaporated affording 32.98 g of a yellow-brown solid. The crude material was dissolved in 300 mL of 2 M NaOH, and acetic acid was added until a white precipitate formed. The precipitate was filtered off, washed with 3x 100 mL of water, and dried under high vacuum affording 2,4,5-triiodoimidazole **56** (30.66 g, 68.8 mmol, 94%) as a white solid.

^{13}C-NMR (76 MHz, $CDCl_3$/TFA): δ (ppm) = 85.2, 84.5.

HRMS (ESI+): *m/z* = 446.737 ($[M+H]^+$, calcd. 446.735 for $[C_3H_2I_3N_2]^+$).

Benzyl 3-(2,4,5-triiodoimidazol-1-yl)propylcarbamate 59

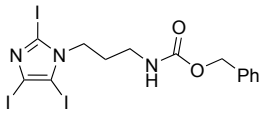

59

2,4,5-triiodoimidazole **56** (28.975 g, 65.00 mmol, 1.0 eq.) was dissolved in 100 mL of DMF. K_2CO_3 (17.967 g, 130.00 mmol, 2.0 eq.) and benzyl 3-bromopropylcarbamate **57** (17.689 g, 65.00 mmol, 1.0 eq.) were added, and the mixture was stirred at room temperature for 72 h. It was filtered through a pad of Celite eluting with ethyl acetate, and the filtrate was concentrated *in vacuo*. The residue was poured into brine, and the mixture was extracted 3x with ethyl acetate. The combined organic phases were washed with brine, dried over $MgSO_4$ and evaporated. Purification by column chromatography (petrol ether/ethyl acetate 1:1) and recrystallization from ethyl acetate afforded compound **59** (28.727 g, 45.10 mmol, 69%) as a pale yellow solid.

^{1}H-NMR (300 MHz, $CDCl_3$): δ (ppm) = 7.38 – 7.28 (m, 5 H, CH_{ar}), 5.12 (s, 2 H, CH_2O), 5.02 (br, 1 H, N*H*), 4.08 (t, $^3J_{H,H}$ = 7.6 Hz, 2 H, CH_2), 3.32 – 3.24 (m, 2 H, CH_2), 1.95 – 1.84 (m, 2 H, CH_2).

^{13}C-NMR (76 MHz, $CDCl_3$): δ (ppm) = 156.6, 136.5, 128.7 (*C*H), 128.4 (2x *C*H), 97.6, 89.5, 84.2, 67.0 (*C*H_2), 50.1 (*C*H_2), 38.2 (*C*H_2), 30.9 (*C*H_2).

HRMS (ESI+): *m/z* = 637.824 ($[M+H]^+$, calcd. 637.830 for $[C_{14}H_{15}I_3N_3O_2]^+$).

5-(Benzyloxycarbonyl)-8,9-diiodo-1,5,7-triazabicyclo[4.3.0]-nona-6,8-diene 60

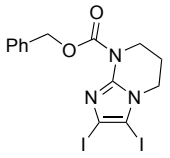

60

In analogy to a literature procedure,[206] imidazole **59** (28.537 g, 44.80 mmol, 1.0 eq.) and K_3PO_4 (19.020 g, 89.60 mmol, 2.0 eq.) were suspended in 400 mL of dioxane. The mixture was degassed by bubbling argon through it for 10 min. Then, CuI (0.683 g, 3.58 mmol, 0.08 eq.) and *trans*-1,2-cyclohexyldiamine (0.43 mL, 3.58 mmol, 0.08 eq.) were added, and the mixture was stirred at 80 °C for 20 h. After cooling to room temperature it was filtered through a pad of Celite eluting with ethyl acetate and evaporated. The residue was dissolved in methylene chloride and washed with diluted aqueous ammonia until the aqueous phase remained colorless. The organic phase was dried over $MgSO_4$ and evaporated to yield 24 g of a yellow solid. Recrystallization from ethyl acetate/chloroform 1:1 afforded compound **60** (17.167 g, 33.72 mmol, 75%) as colorless crystals.

^{1}H-NMR (500 MHz, $CDCl_3$): δ (ppm) = 7.51 – 7.47 (m, 2 H, CH_{ar}), 7.39 – 7.35 (m, 2 H, CH_{ar}), 7.32 – 7.28 (m, 1 H, CH_{ar}), 5.31 (s, 2 H, CH_2O), 3.93 – 3.88 (m, 2 H, CH_2), 3.84 (t, $^3J_{H,H}$ = 6.4 Hz, 2 H, CH_2), 2.15 – 2.09 (m, 2 H, CH_2).

^{13}C-NMR (126 MHz, $CDCl_3$): δ (ppm) = 152.2, 143.8, 135.9, 128.6 (*C*H), 128.1 (*C*H), 127.8 (*C*H), 92.2, 68.5 (*C*H_2), 46.3 (*C*H_2), 43.0 (*C*H_2), 22.5 (*C*H_2), one quaternary carbon signal was not detected due to overlap with solvent signals.

MS (ESI+): *m/z* = 509.9 ([M+H]$^+$, calcd. 509.9 for $[C_{14}H_{14}I_2N_3O_2]^+$).

5-(Benzyloxycarbonyl)-8,9-bis(5-methyl-2-phenylthiazol-4-yl)-1,5,7-triazabicyclo[4.3.0]-nona-6,8-diene 61

5-(Benzyloxycarbonyl)-8-bromo-9-(5-methyl-2-phenylthiazol-4-yl)-1,5,7-triazabicyclo-[4.3.0]-nona-6,8-diene 62

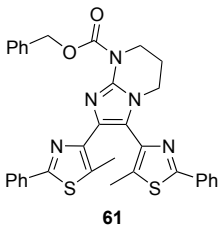

61

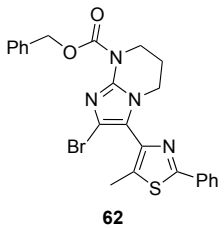

62

Synthesis using $PdCl_2(PPh_3)_2$/Cs_2CO_3 (entry 1 of Table 2):

Pinacol boronate **42** (5.542 g, 18.40 mmol, 3.0 eq.) and dibrominated *N*-Cbz-tbn **27** (2.546 g, 6.13 mmol, 1.0 eq.) were dissolved in 20 mL of DMF and degassed by bubbling argon through the solution for 10 min. $PdCl_2(PPh_3)_2$ (0.129 g, 0.18 mmol, 0.03 eq.) and Cs_2CO_3 (10.084 g, 30.67 mmol, 10.0 eq.) were added and the mixture was stirred at 100 °C for 24 h. After cooling

to room temperature the mixture was filtered through a pad of Celite eluting with ethyl acetate, and the filtrate was evaporated. By column chromatography (methylene chloride/ethyl acetate 4:1, 2% triethylamine) a fraction containing **61** and a fraction containing **62** were separated. Purification of the first fraction by column chromatography (methylene chloride/ethyl acetate 4:1, 2% triethylamine) afforded compound **61** (0.217 g, 0.36 mmol, 6%) as an off-white solid. Purification of the second fraction by column chromatography (petrol ether/ethyl acetate 2:1, 1% triethylamine) afforded compound **62** (0.739 g, 1.45 mmol, 24%) as a pale yellow solid.

Synthesis using $Pd(OAc)_2$/SPhos/K_3PO_4 (entry 5 of Table 2):

Pinacol boronate **42** (3.268 g, 10.85 mmol, 3.5 eq.), dibrominated *N*-Cbz-tbn **27** (1.287 g, 3.10 mmol, 1.0 eq.), $Pd(OAc)_2$ (21 mg, 0.09 mmol, 0.03 eq.), SPhos (89 mg, 0.22 mmol, 0.07 eq.), and K_3PO_4 (ground, dried under high vacuum at 160 °C for 3 d, 4.606 g, 27.70 mmol, 7.0 eq.) were added to a Schlenk tube equipped with a teflon screw cap. The tube was evacuated and refilled with argon twice before 20 mL of anhydrous toluene were added. Water (195 µL, 10.85 mmol, 3.5 eq.) was added and the resulting slurry was heated to 80 °C for 24 h. After cooling to room temperature the mixture was diluted with ethyl acetate and washed with brine. The organic phase was dried over $MgSO_4$ and evaporated. Purification by column chromatography (methylene chloride/ethyl acetate 4:1) afforded compound **61** (0.840 g, 1.39 mmol, 45%) as a pale yellow solid.

Synthesis using microwave irradiation (entry 6 of Table 2):

Pinacol boronate **42** (0.452 g, 1.50 mmol, 3.0 eq.), dibrominated *N*-Cbz-tbn **27** (0.208 g, 0.50 mmol, 1.0 eq.), $Pd(PPh_3)_4$ (29 mg, 0.03 mmol, 0.05 eq.), and K_3PO_4 (ground, 0.425 g, 2.0 mmol, 4.0 eq.) were put into each of two microwave tubes. To each tube 3 mL of dioxane were added and the reaction mixtures were degassed by bubbling argon through the solution for 5 min. The tubes were heated in a microwave (300 W) at 110 °C for 30 min. The contents of both tubes were combined, filtered through a pad of Celite eluting with ethyl acetate, and evaporated. Purification by column chromatography (petrol ether/ethyl acetate 1:1) afforded compound **61** (0.151 g, 0.25 mmol, 25%) as a pale yellow solid.

*Analytical data for **61**:*

^{1}H-NMR (500 MHz, $CDCl_3$): δ (ppm) = 7.98 – 7.95 (m, 2 H, CH_{ar}), 7.77 – 7.75 (m, 2 H, CH_{ar}), 7.57 – 7.55 (m, 2 H, CH_{ar}), 7.47 – 7.39 (m, 3 H, CH_{ar}), 7.38 – 7.28 (m, 6 H, CH_{ar}), 5.38 (s, 2 H, CH_2O), 4.08 – 4.01 (m, 4 H, CH_2), 2.44 (s, 3 H, CH_3), 2.21 – 2.14 (m, 2 H, CH_2), 2.11 (s, 3 H, CH_3).

^{13}C-NMR (126 MHz, $CDCl_3$): δ (ppm) = 164.0, 162.9, 153.3, 146.2, 142.6, 140.5, 136.1, 134.3 134.2, 133.9, 133.2, 130.2, 129.9 (CH), 129.3 (CH), 129.0 (CH), 128.7 (CH), 128.6 (CH),

128.4 (CH), 128.2 (CH), 126.3 (CH), 126.2 (CH), 120.2, 68.5 (CH_2), 43.1 (CH_2), 42.8 (CH_2), 22.4 (CH_2), 12.6 (CH_3), 12.4 (CH_3).

HRMS (ESI+): *m/z* = 604.175 ($[M+H]^+$, calcd. 604.184 for $[C_{34}H_{30}N_5O_2S_2]^+$).

*Analytical data for **62**:*

^{1}H-NMR (500 MHz, $CDCl_3$): δ (ppm) = 7.90 – 7.86 (m, 2 H, CH_{ar}), 7.53 – 7.49 (m, 2 H, CH_{ar}), 7.43 – 7.27 (m, 6 H, CH_{ar}), 5.34 (s, 2 H, CH_2O), 3.97 – 3.89 (m, 4 H, CH_2), 2.51 (s, 3 H, CH_3), 2.11 – 2.05 (m, 2 H, CH_2).

^{13}C-NMR (126 MHz, $CDCl_3$): δ (ppm) = 164.8, 152.4, 140.5, 140.2, 135.9, 134.3, 133.3, 130.0 (C*H*), 128.9 (C*H*), 128.4 (C*H*), 128.0 (C*H*), 127.8 (C*H*), 126.1 (C*H*), 120.3, 114.0, 68.2 (CH_2), 42.84 (CH_2), 42.78 (CH_2), 22.0 (CH_2), 13.2 (CH_3).

MS (ESI+): *m/z* = 509.0 ($[M+H]^+$, calcd. 509.1 for $[C_{24}H_{22}{}^{79}BrN_4O_2S]^+$), 511.0 ($[M+H]^+$, calcd. 511.1 for $[C_{24}H_{22}{}^{81}BrN_4O_2S]^+$).

5-(Benzyloxycarbonyl)-8,9-diphenyl-1,5,7-triazabicyclo[4.3.0]-nona-6,8-diene 64

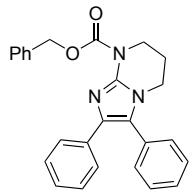

64

Synthesis using Buchwald conditions (entry 6 of Table 3):

Dibrominated *N*-Cbz-tbn **27** (0.429 g, 1.03 mmol, 1.0 eq.), phenylboronic acid (0.378 g, 3.10 mmol, 3.0 eq.), $Pd(OAc)_2$ (7 mg, 0.03 mmol, 0.03 eq.), SPhos (25 mg, 0.06 mmol, 0.06 eq.), and K_3PO_4 (ground, 0.877 g, 4.13 mmol, 4.0 eq.) were put into a Schlenk tube equipped with a teflon screw cap. The tube was evacuated and refilled with argon twice. Then, 3 mL of toluene were added and the mixture was degassed by repeated evacuation of the flask and refilling with argon. The mixture was stirred at 100 °C for 16 h. After cooling to room temperature it was diluted with ethyl acetate and washed with brine. The organic phase was dried over $MgSO_4$ and evaporated. Purification by column chromatography (methylene chloride/ethyl acetate 9:1) afforded compound **64** (0.280 g, 0.68 mmol, 66%) as a white solid.

^{1}H-NMR (300 MHz, $CDCl_3$): δ (ppm) = 7.69 – 7.63 (m, 2 H, CH_{ar}), 7.58 – 7.52 (m, 2 H, CH_{ar}), 7.48 – 7.29 (m, 8 H, CH_{ar}), 7.24 – 7.11 (m, 3 H, CH_{ar}), 5.42 (s, 2 H, OCH_2), 4.00 (t, $^3J_{H,H}$ = 5.8 Hz, 2 H, CH_2), 3.71 (t, $^3J_{H,H}$ = 6.2 Hz, 2 H, CH_2), 2.14 – 2.05 (m, 2 H, CH_2).

^{13}C-NMR (76 MHz, $CDCl_3$): δ (ppm) = 153.3, 139.9, 136.2, 134.7, 134.6, 130.8(*C*H), 130.7, 129.1(*C*H), 128.6(*C*H), 128.5(*C*H), 128.1(*C*H), 128.0(*C*H), 127.7(*C*H), 126.8(*C*H), 126.3 (*C*H), 125.0, 68.4 (O*C*H_2), 43.2 (*C*H_2), 42.4 (*C*H_2), 22.5 (*C*H_2).

2-Morpholinothiazole 66[207]

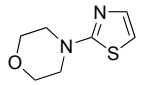

66

2-Bromo-1,1-diethoxyethane (17.60 mL, 117.0 mmol, 1.1 eq.), morpholino-4-carbothioamide **44** (15.00 g, 103.0 mmol, 1.0 eq.), and *p*-toluenesulfonic acid (0.98 g, 5.1 mmol, 0.05 eq.) were dissolved in a mixture of 400 mL of ethanol and 40 mL of water. After stirring for 24 h at 90 °C consumption of the starting material was indicated by TLC. After cooling to room temperature an aqueous solution of Na_2CO_3 was added until gas evolution ceased. The precipitate was filtered off and washed with ethanol. The filtrate was concentrated *in vacuo* and extracted with 3x 100 mL of ethyl acetate. The combined organic layers were washed with brine and dried over $MgSO_4$. Evaporation of the solvent afforded 2-morpholinothiazole **66** (17.0 g, 99.9 mmol, 97%) as a yellow oil.

^{1}H-NMR (300 MHz, $CDCl_3$): δ (ppm) = 7.19 (d, $^3J_{H,H}$ = 3.6 Hz, 1 H, CH_{ar}), 6.58 (d, $^3J_{H,H}$ = 3.6 Hz, 1 H, CH_{ar}), 3.79 (t, $^3J_{H,H}$ = 5.1 Hz, 4 H, CH_2), 3.44 (t, $^3J_{H,H}$ = 5.1 Hz, 4 H, CH_2).

^{13}C-NMR (76 MHz, $CDCl_3$): δ (ppm) = 172.5, 139.7 (*C*H), 107.9 (*C*H), 66.3 (*C*H_2), 48.8 (*C*H_2).

5-Bromo-2-morpholinothiazole 67[208]

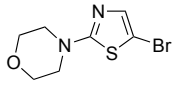

67

In analogy to a literature procedure,[209] 2-morpholinothiazole **66** (5.00 g, 29.4 mmol, 1.0 eq.) was dissolved in 60 mL of glacial acetic acid, and bromine (3.01 mL, 58.7 mmol, 2.0 eq.) was added dropwise. The mixture was stirred at room temperature for 24 h. Then, an aqueous solution of $NaHSO_3$ was added until the dark brown color disappeared and a precipitate formed. The precipitate was filtered off and dried under high vacuum overnight. 5-Bromo-2-morpholinothiazole **67** (4.45 g, 17.8 mmol, 61%) was obtained as a pale yellow solid.

^{1}H-NMR (300 MHz, $CDCl_3$): δ (ppm) = 7.10 (s, 1 H, CH_{ar}), 3.80 (t, $^3J_{H,H}$ = 5.1 Hz, 4 H, CH_2), 3.42 (t, $^3J_{H,H}$ = 5.1 Hz, 4 H, CH_2).

^{13}C-NMR (76 MHz, $CDCl_3$): δ (ppm) = 171.9, 140.3 (*C*H), 95.4, 66.1 (*C*H_2), 48.4 (*C*H_2).

5-Iodo-2-morpholinothiazole 68

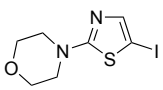

68

2-Morpholinothiazole **66** (2.03 g, 11.9 mmol, 1.0 eq.) was dissolved in 70 mL of dry THF and the mixture was cooled to -80 °C. *n*-Butyllithium (2.2 M in cyclohexane, 5.95 mL, 13.1 mmol, 1.1 eq.) was added dropwise and the mixture was stirred at -80 °C for 20 min and warmed

to -10 °C over 10 min. Then, a solution of iodine (3.62 g, 14.2 mmol, 1.2 eq.) in 10 mL of THF was added and the resulting mixture was stirred at -10 °C for 30 min. After the addition of 20 mL of brine the mixture was extracted with 3 x 50 mL of diethyl ether. The combined organic phases were washed with an aqueous solution of $NaHCO_3$, an aqueous solution of $Na_2S_2O_3$ and brine, and were dried over $MgSO_4$. After evaporation of the solvent the crude product was filtered through a plug of silica eluting with ethyl acetate affording 5-iodo-2-morpholinothiazole **68** (2.95 g, 10.0 mmol, 84%) as a yellow solid.

^{1}H-NMR (500 MHz, $CDCl_3$): δ (ppm) = 7.20 (s, 1 H, CH_{ar}), 3.79 (t, $^3J_{H,H}$ = 5.0 Hz, 4 H, CH_2), 3.42 (t, $^3J_{H,H}$ = 5.0 Hz, 4 H, CH_2).

^{13}C-NMR (126 MHz, $CDCl_3$): δ (ppm) = 175.5, 147.3 (*C*H), 66.2, 55.0 (*C*H_2), 48.6 (*C*H_2).

HRMS (ESI+): *m/z* = 296.941 ([M+H]$^+$, calcd. 296.956 for [$C_7H_{10}IN_2OS$]$^+$).

2-Morpholino-5-trifluoromethylthiazole 69

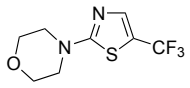

69

In analogy to a literature procedure,[134a] KF (2.23 g, 38.4 mmol, 6.0 eq.) and CuI (1.83 g, 9.6 mmol, 1.5 eq.) were put into a Schlenk tube equipped with a magnetic stirrer and a Teflon-coated screw cap. The tube was evacuated and heated with the heatgun for 5 min until a pale greenish color evolved. Then, 2-morpholino-5-iodothiazole **68** (1.90 g, 6.4 mmol, 1.0 eq.) was added and the tube was evacuated and refilled with argon twice. After the addition of 6 mL of dry DMF and 6 mL of dry NMP the mixture was stirred at room temperature for 5 min. Then, $TMSCF_3$ (1.23 mL, 8.32 mmol, 1.3 eq.) was added, the screw cap was closed, and the tube was heated to 50 °C for 4.5 h. After cooling to room temperature the mixture was poured into 50 mL of a diluted aqueous solution of ammonia and extracted with 3 x 30 mL of diethyl ether. The combined organic phases were washed with diluted ammonia solution until the aqueous phase remained colorless, washed with aqueous $NaHCO_3$ solution and brine, and dried over $MgSO_4$. After evaporation of the solvent the crude product was purified by column chromatography (methylene chloride/ethyl acetate 8:1) affording 2-morpholino-5-trifluoromethylthiazole **69** (0.55 g, 2.3 mmol, 36%) as a white solid.

^{1}H-NMR (300 MHz, $CDCl_3$): δ (ppm) = 7.41 (s, 1 H, CH_{ar}), 3.80 (t, $^3J_{H,H}$ = 5.1 Hz, 4 H, CH_2), 3.49 (t, $^3J_{H,H}$ = 5.1 Hz, 4 H, CH_2).

^{13}C-NMR (76 MHz, $CDCl_3$): δ (ppm) = 173.6, 141.8 (q, $^3J_{C,F}$ = 4 Hz, *C*H), 122.6 (q, $^1J_{C,F}$ = 267 Hz, *C*F_3), 114.0 (q, $^2J_{C,F}$ = 39 Hz, *C*CF_3), 66.0 (*C*H_2), 48.4 (*C*H_2).

^{19}F-NMR (282 MHz, $CDCl_3$): δ (ppm) = -54.0 (s, CF_3).

HRMS (ESI+): *m/z* = 239.040 ([M+H]$^+$, calcd. 239.047 for [$C_8H_{10}F_3N_2OS$]$^+$).

2-Morpholino-4-(tributylstannyl)-5-trifluoromethylthiazole 70

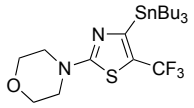

70

2-Morpholino-5-trifluoromethylthiazole **69** (0.47 g, 1.98 mmol, 1.0 eq.) was dissolved in 15 mL of dry THF and cooled to -78 °C. *tert*-BuLi (1.7 M in pentane, 1.40 mL, 2.38 mmol, 1.2 eq.) was added dropwise and the yellow solution was stirred for 25 min at the same temperature. Then, Bu_3SnCl (0.64 mL, 2.38 mmol, 1.2 eq.) dissolved in 2 mL of THF was added and the resulting colorless solution was stirred at -78 °C for 1 h. After warming to room temperature, the reaction was quenched by adding 10 mL of a saturated aqueous NH_4Cl solution and the mixture was extracted with 3x 20 mL of diethyl ether. The combined organic phases were washed with an aqueous $NaHCO_3$ solution and brine and were dried over $MgSO_4$. Evaporation of the solvent gave crude stannane **70** (1.27 g, quant.) as a pale yellow oil that was used without further purification.

^{1}H-NMR (300 MHz, $CDCl_3$): δ (ppm) = 3.81 (t, $^3J_{H,H}$ = 5.1 Hz, 4 H, CH_2), 3.51 (t, $^3J_{H,H}$ = 5.1 Hz, 4 H, CH_2), 1.57 – 1.49 (m, 6 H, CH_2), 1.35 – 1.28 (m, 6 H, CH_2), 1.14 – 1.10 (m, 6 H, CH_2), 0.88 (t, $^3J_{H,H}$ = 7.2 Hz, 9 H, CH_3).

^{13}C-NMR (76 MHz, $CDCl_3$): δ (ppm) = 173.0, 66.2 (*C*H_2), 48.9 (*C*H_2), 29.0 (*C*H_2), 27.4 (*C*H_2), 13.8 (*C*H_3), 11.0 (*C*H_2), three quaternary carbon signals were not detected due to C-F couplings.

^{19}F-NMR (282 MHz, $CDCl_3$): δ (ppm) = -51.0 (s, CF_3).

3-Bromo-1-*tert*-butyl-4-(5-methyl-2-morpholinothiazol-4-yl)-1*H*-pyrrole-2,5-dione 71

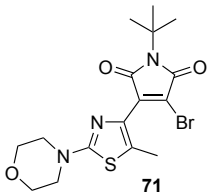

71

5-Methyl-2-morpholino-4-(tributylstannyl)thiazole **47** (1.58 g, 3.33 mmol, 1 eq.) and 3,4-dibromo-1-*tert*-butyl-1*H*-pyrrole-2,5-dione **26** (1.56 g, 5.00 mmol, 1.5 eq.) were dissolved in 40 mL of dry toluene, and the mixture was degassed by bubbling argon through it for 5 min. Then, $Pd(PPh_3)_4$ (0.19 g, 0.17 mmol, 0.05 eq.) was added and the mixture was stirred at 100 °C for 20 h. After cooling to room temperature, the solvent was evaporated and the crude mixture was purified by column chromatography (petrol ether/ethyl acetate gradient from 6:1 to 2:1) affording compound **71** (0.183 g, 0.44 mmol, 13%) as a dark solid. In a second fraction the biscoupled product **11a** (0.250 g, 0.48 mmol, 28%) was isolated.

^{1}H-NMR (300 MHz, $CDCl_3$): δ (ppm) = 3.80 (t, $^3J_{H,H}$ = 5.1 Hz, 4 H, CH_2), 3.43 (t, $^3J_{H,H}$ = 5.1 Hz, 4 H, CH_2), 2.33 (s, 3 H, CH_3), 1.61 (s, 9 H, CH_3).

^{13}C-NMR (76 MHz, $CDCl_3$): δ (ppm) = 66.3 (*C*H_2), 48.4 (*C*H_2), 29.1 (*C*H_3), 13.3 (*C*H_3), quaternary carbon signals were not detected due to low concentration.

HRMS (ESI+): *m/z* = 414.058 ($[M+H]^+$, calcd. 414.049 for $[C_{16}H_{21}{}^{79}BrN_3O_3S]^+$), 416.057 ($[M+H]^+$, calcd. 416.047 for $[C_{16}H_{21}{}^{81}BrN_3O_3S]^+$).

2-Phenylthiazole 72[210]

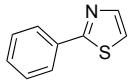

72

2-Bromo-1,1-diethoxyethane (15.78 g, 80.1 mmol, 1.1 eq.), thiobenzamide (10.00 g, 72.9 mmol, 1.0 eq.), and *p*-toluenesulfonic acid (0.63 g, 3.3 mmol, 0.05 eq.) were dissolved in a mixture of 400 mL of ethanol and 20 mL of water. After stirring for 16 h at 100 °C consumption of the starting material was indicated by TLC. The mixture was cooled to room temperature and an aqueous solution of Na_2CO_3 was added until gas evolution ceased. The precipitate was filtered off and washed with ethanol. The filtrate was concentrated *in vacuo* and extracted with 3x 100 mL of methylene chloride. The combined organic layers were washed with brine and dried over $MgSO_4$. Evaporation of the solvent afforded 2-phenylthiazole **72** (11.40 g, 70.7 mmol, 97%) as a yellow oil.

^{1}H-NMR (500 MHz, $CDCl_3$): δ (ppm) = 7.99 – 7.95 (m, 2 H, CH_{ar}), 7.87 (d, $^3J_{H,H}$ = 3.2 Hz, 1 H, CH_{ar}), 7.47 - 7.40 (m, 3 H, CH_{ar}), 7.32 (d, $^3J_{H,H}$ = 3.2 Hz, 1 H, CH_{ar}).

^{13}C-NMR (126 MHz, $CDCl_3$): δ (ppm) = 168.6, 143.9 (*C*H), 133.8, 130.1 (*C*H), 129.1 (*C*H), 126.8 (*C*H), 119.0 (*C*H).

5-Iodo-2-phenylthiazole 73[114a]

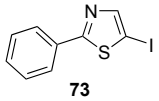

73

Following a literature procedure,[114a] 2-phenylthiazole **72** (4.00 g, 24.8 mmol, 1.0 eq.) was dissolved in 130 mL of dry THF and the mixture was cooled to -80 °C. *n*-Butyllithium (2.2 M in cyclohexane, 13.53 mL, 29.8 mmol, 1.2 eq.) was added dropwise, and the mixture was stirred at -80 °C for 20 min and warmed to -10 °C over 10 min. Then, a solution of iodine (8.17 g, 32.3 mmol, 1.3 eq.) in 10 mL of THF was added and the resulting mixture was stirred at -10 °C for 30 min. After the addition of 20 mL of brine, the mixture was extracted with 3x 50 mL of diethyl ether. The combined organic phases were washed with an aqueous solution of $NaHCO_3$, an aqueous solution of $Na_2S_2O_3$, and brine, and were dried over $MgSO_4$. After evaporation of the solvent the crude product was recrystallized from hexane affording 5-iodo-2-phenylthiazole **73** (5.44 g, 18.9 mmol, 76%) as yellow crystals. The mother liquor was evaporated and purified by column chromatography (petrol ether / ethyl acetate 30:1) giving an additional fraction of **73** (0.39 g, 1.4 mmol, 6%) as a pale yellow solid.

^{1}H-NMR (300 MHz, $CDCl_3$): δ (ppm) = 7.89 – 7.86 (m, 3 H, CH_{ar}), 7.45 – 7.43 (m, 3 H, CH_{ar}).
^{13}C-NMR (76 MHz, $CDCl_3$): δ (ppm) = 151.6 (*C*H), 133.1 (*C*H), 130.6 (*C*H), 129.2 (*C*H), 70.1, two quarternary carbon signals were not detected due to low concentration.
HRMS (ESI+): *m/z* = 287.934 ($[M+H]^+$, calcd. 287.934 for $[C_9H_7INS]^+$).

2-Phenyl-5-trifluoromethylthiazole 74[211]

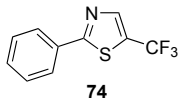

74

In analogy to a literature procedure,[135] CuCl (99 mg, 1.0 mmol, 2.0 eq.) was put into a Schlenk tube equipped with a Teflon-coated screw cap. The tube was evacuated and refilled with argon. Then, 1,10-phenanthroline (180 mg, 1.0 mmol, 2.0 eq.) and KO*t*Bu (112 mg, 1.0 mmol, 2.0 eq.) were added and the tube was evacuated and refilled with argon twice. After the addition of 2 mL of dry DMF the mixture was stirred at room temperature for 30 min. Within this time the initially yellow suspension turned dark brown. Then, $TMSCF_3$ (0.15 mL, 1.0 mmol, 2.0 eq.) was added, the screw cap was closed, and the mixture was stirred for 1 h at room temperature while its color turned to dark red. Afterwards, 5-iodo-2-phenylthiazole **73** (144 mg, 0.50 mmol, 1.0 eq.) was added, the screw cap was tightly closed, and the mixture was stirred at 50 °C for 18 h. After cooling to room temperature, the mixture was diluted with diethyl ether and filtered through a pad of Celite. The organic phase was washed with aqueous HCl (1 M), aqueous $NaHCO_3$ solution, and brine, and was dried over $MgSO_4$. After evaporation of the solvent the crude product was purified by column chromatography (petrol ether/ethyl acetate 9:1) affording 2-phenyl-5-trifluoromethylthiazole **74** (88 mg, 0.38 mmol, 77%) as a white solid.
^{1}H-NMR (500 MHz, $CDCl_3$): δ (ppm) = 8.12 (q, $^{4}J_{H,F}$ = 1.0 Hz, 1 H, CH_{ar}), 7.97 – 7.94 (m, 2 H, CH_{ar}), 7.50 - 7.46 (m, 3 H, CH_{ar}).
^{13}C-NMR (126 MHz, $CDCl_3$): δ (ppm) = 172.1, 144.6 (q, $^{3}J_{C,F}$ = 4 Hz, *C*H_{ar}-C-CF_3), 132.6, 131.5 (*C*H), 129.4 (*C*H), 127.0 (*C*H), 126.4 (q, $^{2}J_{C,F}$ = 39 Hz, *C*-CF_3), 122.2 (q, $^{1}J_{C,F}$ = 269 Hz, *C*F_3).
^{19}F-NMR (471 MHz, $CDCl_3$): δ (ppm) = -54.7 (s, CF_3).
HRMS (ESI+): *m/z* = 230.032 ($[M+H]^+$, calcd. 230.025 for $[C_{10}H_7F_3NS]^+$).

5-Bromo-2-phenylthiazole 75[212]

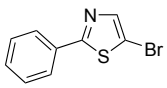

75

In analogy to a literature procedure,[209] 2-phenylthiazole **72** (5.50 g, 34.1 mmol, 1.0 eq.) was dissolved in 70 mL of glacial acetic acid. Bromine (3.50 mL, 68.2 mmol, 2.0 eq) was added dropwise and the mixture was stirred at room temperature for 16 h. Then, it was poured into 300 mL of an aqueous $NaHSO_3$ solution and extracted with 3x 100 mL of methylene chloride.

The combined organic phases were washed with aqueous $NaHSO_3$ and brine and dried over $MgSO_4$. After evaporation of the solvent the crude product was purified by column chromatography (petrol ether/methylene chloride 12:1) affording 5-bromo-2-phenylthiazole **75** (5.26 g, 21.9 mmol, 64%) as a white solid.

^{1}H-NMR (300 MHz, $CDCl_3$): δ (ppm) = 7.88 – 7.85 (m, 2 H, CH_{ar}), 7.74 (s, 1 H, CH_{ar}), 7.46 – 7.43 (m, 3 H, CH_{ar}).

^{13}C-NMR (101MHz, $CDCl_3$): δ (ppm) = 145.0 (*C*H), 133.2, 130.6 (*C*H), 129.2 (*C*H), 126.4 (*C*H), 108.7, one quaternary carbon signal was not detected due to low concentration.

4-Bromo-5-iodo-2-phenylthiazole 76[213]

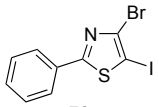

76

In analogy to a literature procedure,[109] 5-bromo-2-phenylthiazole **75** (2.00 g, 8.3 mmol, 1.0 eq.) was dissolved in 20 mL of dry THF and cooled to -78 °C. To this solution LDA, which was freshly prepared by the addition of *n*-BuLi (2.2 M in cyclohexane, 5.68 mL, 12.5 mmol, 1.5 eq.) to a solution of diisopropylamine (1.48 g, 14.6 mmol, 1.75 eq.) in 20 mL of THF at room temperature, was added. The mixture was stirred at -78 °C for 30 min until TLC indicated the completion of the halogen-dance-reaction. Then, iodine (3.20 g, 12.5 mmol, 1.5 eq.) was added in small portions and the mixture was stirred at -78 °C for 30 min. After warming to room temperature it was poured into 150 mL of aqueous HCl (2 M) and the mixture was extracted with 3 x 100 mL of diethyl ether. The combined organic phases were washed 2x with aqueous $Na_2S_2O_3$ solution and brine, and were dried over $MgSO_4$. After evaporation of the solvent the crude product was purified by column chromatography (petrol ether/methylene chloride 3:1) affording 4-bromo-5-iodo-2-phenylthiazole **76** (2.80 g, 7.6 mmol, 92%) as a white solid.

^{1}H-NMR (500 MHz, $CDCl_3$): δ (ppm) = 7.87 – 7.85 (m, 2 H, CH_{ar}), 7.45 – 7.43 (m, 3 H, CH_{ar}).

^{13}C-NMR (126 MHz, $CDCl_3$): δ (ppm) = 173.7, 135.9, 132.4, 131.2 (*C*H), 129.7 (*C*H), 126.3 (*C*H), 71.7.

HRMS (ESI+): *m/z* = 365.835 ($[M+H]^+$, calcd. 365.845 for $[C_9H_6{}^{79}BrINS]^+$), 367.833 ($[M+H]^+$, calcd. 367.843 for $[C_9H_6{}^{81}BrINS]^+$).

4-Bromo-2-phenyl-5-trifluoromethylthiazole 77

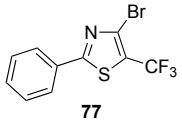

77

In analogy to a literature procedure,[135] CuCl (74 mg, 0.75 mmol, 1.5 eq.) was put into a Schlenk tube equipped with a Teflon-coated screw cap. The tube was evacuated and refilled with argon. Then, 1,10-phenanthroline (135 mg, 0.75 mmol, 1.5 eq.) and KO*t*Bu (84 mg,

0.75 mmol, 1.5 eq.) were added and the tube was evacuated and refilled with argon twice. After the addition of 2 mL of dry DMF the mixture was stirred at room temperature for 15 min. Within this time the initially yellow suspension turned dark brown. Then, $TMSCF_3$ (0.11 mL, 0.75 mmol, 1.5 eq.) was added, the screw cap was closed, and the mixture was stirred for 45 min at room temperature while its color turned to dark red. Afterwards, 4-bromo-5-iodo-2-phenylthiazole **76** (183 mg, 0.50 mmol, 1.0 eq.) was added, the screw cap was tightly closed, and the mixture was stirred at 50 °C for 18 h. After cooling to room temperature, the mixture was diluted with diethyl ether and filtered through a pad of Celite. The organic phase was washed with aqueous HCl (1 M), aqueous $NaHCO_3$ solution, and brine, and was dried over $MgSO_4$. After evaporation of the solvent the crude product was purified by column chromatography (petrol ether/methylene chloride 9:1) affording 4-bromo-2-phenyl-5-trifluoromethylthiazole **77** (124 mg, 0.40 mmol, 80%) as a colorless oil.

^{1}H-NMR (500 MHz, $CDCl_3$): δ (ppm) = 7.93 – 7.91 (m, 2 H, CH_{ar}), 7.52 – 7.47 (m, 3 H, CH_{ar}).

^{13}C-NMR (126 MHz, $CDCl_3$): δ (ppm) = 170.2, 132.1 (*C*H), 131.6, 129.4 (*C*H), 127.9 (q, $^3J_{C,F}$ = 4 Hz, *C*Br-C-CF_3), 126.8 (*C*H), 121.7 (q, $^2J_{C,F}$ = 39 Hz, *C*-CF_3), 121.3 (q, $^1J_{C,F}$ = 270 Hz, *C*F_3).

^{19}F-NMR (471 MHz, $CDCl_3$): δ (ppm) = -54.7 (s, CF_3).

HRMS (ESI+): *m/z* = 307.941 ($[M+H]^+$, calcd. 307.936 for $[C_{10}H_6{}^{79}BrF_3NS]^+$), 309.939 ($[M+H]^+$, calcd. 309.934 for $[C_{10}H_6{}^{81}BrF_3NS]^+$).

2-Phenyl-4-(tributylstannyl)-5-trifluoromethylthiazole 78

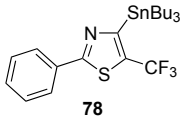

78

*Starting from 2-phenyl-5-trifluoromethylthiazole **74**:* To a solution of 2-phenyl-5-trifluoromethylthiazole **74** (197 mg, 0.86 mmol, 1.0 eq.) in 10 mL of THF at -78 °C LDA was added, which was freshly prepared from diisopropylamine (170 mg, 1.20 mmol, 1.4 eq.) and *n*-BuLi (1.6 M in hexane, 0.64 mL, 1.03 mmol, 1.2 eq.) in 5 mL of THF. The mixture was stirred for 45 min at that temperature before Bu_3SnCl (0.30 mL, 1.12 mmol, 1.3 eq.) was added, and the mixture was warmed to room temperature over a period of 30 min. Then, the reaction was quenched with 20 mL of aqueous NH_4Cl solution and the mixture was extracted with 2x 100 mL of diethyl ether. The combined organic phases were washed with brine, dried over $MgSO_4$, and evaporated. Purification by column chromatography (petrol ether/methylene chloride 9:1) afforded stannane **78** (303 mg, 0.58 mmol, 68%) as a colorless oil.

*Starting from 4-bromo-2-phenyl-5-trifluoromethylthiazole **77**:* To a solution of 4-bromo-2-phenyl-5-trifluoromethylthiazole **77** (126 mg, 0.41 mmol, 1.0 eq.) in 8 mL of dry THF *n*-BuLi (2.2 M in cyclohexane, 0.22 mL, 0.49 mmol, 1.2 eq.) was added at -100 °C. The mixture was

stirred for 45 min and was allowed to warm to -85 °C during this time. Then, Bu_3SnCl (0.13 mL, 0.49 mmol, 1.2 eq.), dissolved in 1 mL of THF, was added and stirring was continued for 10 min at -85 °C. Then, the mixture was warmed to room temperature over a period of 20 min, and the reaction was quenched by adding 10 mL of an aqueous NH_4Cl solution. It was extracted with 3x 50 mL of diethyl ether and the combined organic phases were dried over $MgSO_4$ and evaporated. Purification by column chromatography (petrol ether/methylene chloride 9:1) afforded stannane **78** (98 mg, 0.19 mmol, 46%) as a colorless oil.

^{1}H-NMR (300 MHz, $CDCl_3$): δ (ppm) = 8.02 – 7.98 (m, 2 H, C*H*$_{ar}$), 7.48 – 7.45 (m, 3 H, C*H*$_{ar}$), 1.65 – 1.56 (m, 6 H, C*H*$_2$), 1.41 – 1.22 (m, 12 H, C*H*$_2$), 0.92 (t, $^3J_{H,H}$ = 7.2 Hz, 9 H, C*H*$_3$).

^{13}C-NMR (76 MHz, $CDCl_3$): δ (ppm) = 170.5, 165.9, 133.3, 131.8 (q, $^2J_{C,F}$ = 35 Hz, *C*-CF_3), 130.7 (*C*H), 129.1 (*C*H), 127.3 (*C*H), 123.4 (q, $^1J_{C,F}$ = 269 Hz, *C*F_3), 29.0 (*C*H_2), 27.4 (*C*H_2), 13.8 (*C*H_3), 11.2 (*C*H_2).

^{19}F-NMR (282 MHz, $CDCl_3$): δ (ppm) = -51.1 (s, C*F*$_3$).

2-Chloro-5-iodothiophene 81[139]

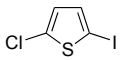

81

Following a literature procedure,[139] in a two-necked flask equipped with a reflux condenser 2-chlorothiophene (11.859 g, 100.00 mmol, 1.0 eq.) and iodic acid (3.694 g, 21.00 mmol, 0.21 eq.) were dissolved in a mixture of 40 mL of acetic acid, 15 mL of water, 20 mL of carbon tetrachloride, and 0.7 mL of sulfuric acid. The mixture was heated to reflux at 85 °C. Then iodine (10.152 g, 40.00 mmol, 0.4 eq.) was added in small portions over a period of 20 min. The resulting mixture was refluxed for further 1.5 h. After cooling to room temperature water and methylene chloride were added, the organic phase was washed with an aqueous solution of $Na_2S_2O_3$, dried over $MgSO_4$, and evaporated. The residue was distilled under membrane pump vacuum and fractions boiling at 95 °C were collected. 2-Chloro-5-iodothiophene **81** (22.576 g, 92.34 mmol, 92%) was obtained as a pale yellow liquid.

^{1}H-NMR (300 MHz, $CDCl_3$): δ (ppm) = 7.06 (d, $^3J_{H,H}$ = 3.9 Hz, 1 H, C*H*$_{ar}$), 6.62 (d, $^3J_{H,H}$ = 3.9 Hz, 1 H, C*H*$_{ar}$).

^{13}C-NMR (76 MHz, $CDCl_3$): δ (ppm) = 136.5 (*C*H), 133.5, 128.0 (*C*H), 70.0.

2-(4-*N*,*N*-Dimethylaminophenyl)thiophene 88[214]

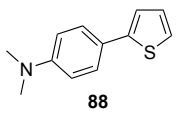

88

Thiophene (1.683 g, 20.00 mmol, 1.0 eq.) was dissolved in 40 mL of anhydrous THF and cooled to -78 °C. *n*-BuLi (2.2 M in cyclohexane, 10.91 mL, 24.00 mmol, 1.2 eq.) was added dropwise and the mixture was stirred at -60 °C for 1 h. Then, tributylborate (7.56 mL,

28.00 mmol, 1.4 eq.) was added and the mixture was allowed to warm to room temperature for 20 min before 30 mL of ethanol, 4-bromo-*N,N*-dimethylaniline (4.802 g, 24.00 mmol, 1.2 eq.), Na_2CO_3 (5.088 g, 48.00 mmol, 2.4 eq.), and $PdCl_2(dppf)\cdot CH_2Cl_2$ (0.490 g, 0.60 mmol, 0.03 eq.) were added. The mixture was degassed by repeated evacuation of the flask and refilling with argon and then stirred at 75 °C for 4 h. After cooling to room temperature the mixture was diluted with diethyl ether and washed with brine. The organic layer was dried over $MgSO_4$ and evaporated. Purification by column chromatography (petrol ether/methylene chloride 9:1) afforded 2-(4-*N,N*-dimethylaminophenyl)thiophene **88** (3.206 g, 15.77 mmol, 79%) as a white solid.

^{1}H-NMR (300 MHz, $CDCl_3$): δ (ppm) = 7.51 (d, $^3J_{H,H}$ = 9.0 Hz, 2 H, C*H*$_{ar}$), 7.18 – 7.15 (m, 2 H, C*H*$_{ar}$), 7.06 – 7.03 (m, 1 H, C*H*$_{ar}$), 6.74 (d, $^3J_{H,H}$ = 9.0 Hz, 2 H, C*H*$_{ar}$), 2.99 (s, 6 H, C*H*$_3$).

^{13}C-NMR (76 MHz, $CDCl_3$): δ (ppm) = 150.1, 145.4, 127.9 (*C*H), 127.0 (*C*H), 123.1, 122.9 (*C*H), 121.0 (*C*H), 112.7 (*C*H), 40.6 (*C*H$_3$).

2-(4-*N,N*-Dimethylaminophenyl)-5-iodothiophene 89

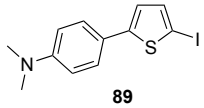

89

2-(4-*N,N*-Dimethylaminophenyl)thiophene **88** (2.135 g, 10.50 mmol, 1.0 eq.) was dissolved in anhydrous THF and cooled to -78 °C. *n*-BuLi (2.2 M in cyclohexane, 7.16 mL, 15.75 mmol, 1.5 eq.) was added and the mixture was stirred at -60 °C for 45 min. Then, iodine (3.198 g, 12.60 mmol, 1.2 eq.) was added in portions, and the mixture was allowed to warm to room temperature for 20 min. The mixture was diluted with diethyl ether and washed with an aqueous solution of $Na_2S_2O_3$ and brine. The organic layer was dried over $MgSO_4$ and evaporated. The crude material was filtered through a plug of silica eluting with methylene chloride. The solvent was evaporated and the residue was recrystallized from acetonitrile affording 2-(4-*N,N*-dimethylaminophenyl)-5-iodothiophene **89** (2.687 g, 8.16 mmol, 78%) as yellow needles. Due to slow decomposition of the product upon storage it should be used immediately.

^{1}H-NMR (500 MHz, $CDCl_3$): δ (ppm) = 7.40 (d, $^3J_{H,H}$ = 8.9 Hz, 2 H, C*H*$_{ar}$), 7.16 (d, $^3J_{H,H}$ = 3.7 Hz, 1 H, C*H*$_{ar}$), 6.82 (d, $^3J_{H,H}$ = 3.7 Hz, 1 H, C*H*$_{ar}$), 6.71 (d, $^3J_{H,H}$ = 8.9 Hz, 2 H, C*H*$_{ar}$), 2.99 (s, 6 H, CH_3).

^{13}C-NMR (126 MHz, $CDCl_3$): δ (ppm) = 151.5, 150.3, 137.8 (*C*H), 126.9 (*C*H), 122.4 (*C*H), 122.1, 112.5 (*C*H), 69.6, 40.5 (*C*H$_3$).

HRMS (ESI+): *m/z* = 329.976 ($[M+H]^+$, calcd. 329.982 for $[C_{12}H_{13}INS]^+$).

2-(4-*N*,*N*-Dimethylaminophenyl)-5-trifluoromethylthiophene 90

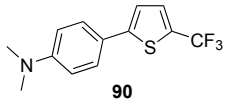

90

In analogy to a literature procedure,[134a] KF (1.394 g, 24.00 mmol, 6.0 eq.) and CuI (1.143 g, 6.00 mmol, 1.5 eq.) were put into a Schlenk tube equipped with a magnetic stirrer and a Teflon-coated screw cap. The tube was evacuated and heated with the heatgun for 5 min until a pale greenish color evolved. Then, iodothiophene **89** (1.317 g, 4.00 mmol, 1.0 eq.) was added and the tube was evacuated and refilled with argon twice. After the addition of 3 mL of dry DMF and 3 mL of dry NMP the mixture was stirred at room temperature for 5 min. Then, $TMSCF_3$ (0.89 mL, 6.00 mmol, 1.5 eq.) was added, the screw cap was closed, and the tube was heated to 55 °C for 16 h. After cooling to room temperature the mixture was poured into 50 mL of a diluted aqueous solution of ammonia and extracted with 3 x 30 mL of diethyl ether. The combined organic phases were washed with diluted ammonia solution until the aqueous phase remained colorless, washed with aqueous $NaHCO_3$ solution and brine, and dried over $MgSO_4$. After evaporation of the solvent the crude product was purified by column chromatography (petrol ether/ethyl acetate 9:1) affording compound **90** (0.750 g, 2.76 mmol, 69%) as a yellow solid.

^{1}H-NMR (300 MHz, $CDCl_3$): δ (ppm) = 7.47 (d, $^3J_{H,H}$ = 8.9 Hz, 2 H, CH_{ar}), 7.34 (dxq, $^3J_{H,H}$ = 3.9 Hz, $J_{H,F}$ = 1.2 Hz, 1 H, CH_{ar}), 7.06 (dxq, $^3J_{H,H}$ = 3.9 Hz, $J_{H,F}$ = 1.1 Hz, 1 H, CH_{ar}), 6.73 (d, $^3J_{H,H}$ = 8.9 Hz, 2 H, CH_{ar}), 3.01 (s, 6 H, CH_3).

^{13}C-NMR (126 MHz, $CDCl_3$): 150.8, 149.7, 129.5 (q, $^3J_{C,F}$ = 4 Hz, *C*H-C-CF_3), 127.5 (q, $^2J_{C,F}$ = 38 Hz, *C*-CF_3), 127.3 (*C*H), 127.1, 122.9 (q, $^1J_{C,F}$ = 269 Hz, *C*F_3), 120.3 (*C*H), 112.5 (*C*H), 40.5 (*C*H_3).

^{19}F-NMR (471 MHz, $CDCl_3$): δ (ppm) = -55.3 (s, CF_3).

MS (ESI+): *m/z* = 272.0 ($[M+H]^+$, calcd. 272.1 for $[C_{13}H_{13}F_3NS]^+$).

2-(4-*N*,*N*-Dimethylaminophenyl)-4-(4,4,5,5-tetramethyl-1,3,2-dioxaborolan-2-yl)-5-trifluoromethylthiophene 91

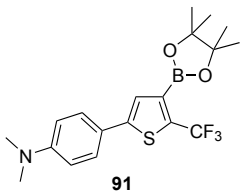

91

Diisopropylamine (0.22 mL, 1.60 mmol, 1.6 eq.) was dissolved in 3 mL of anhydrous THF and cooled to -78 °C. *n*-BuLi (2.2 M in cyclohexane, 0.64 mL, 1.40 mmol, 1.4 eq.) was added, the solution was stirred at -78 °C for 5 min and then warmed to room temperature for 20 min. It was cooled again to -78 °C and a solution of trifluoromethylthiophene **90** (0.271 g, 1.00 mmol, 1.0 eq.) in 2 mL of anhydrous THF was added. The mixture was stirred at -78 °C for 30 min

before 2-isopropoxy-4,4,5,5-tetramethyl-1,3,2-dioxaborolane (0.20 mL, 1.00 mmol, 1.0 eq.) was added. After stirring at -78 °C for 10 min the mixture was allowed to warm to room temperature over 20 min. Some drops of methanol were added, the mixture was diluted with diethyl ether, and it was washed with brine. The organic layer was dried over $MgSO_4$ and evaporated. The resulting yellow solid (0.201 g) mainly contained pinacol boronate **91** and a small amount of the starting material **90,** as determined by UPLC/MS. It was used immediately without any further purification.

MS (ESI+): *m/z* = 398.1 ($[M+H]^+$, calcd. 398.2 for $[C_{19}H_{24}BF_3NO_2S]^+$).

2-Methyl-5-phenylthiophen-3-ylboronic acid 93[215]

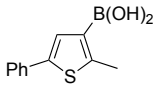

93

3-Bromo-2-methyl-5-phenylthiophene **92** (3.435 g, 13.57 mmol, 1.0 eq.) was dissolved in 50 mL of anhydrous THF and cooled to -78 °C. n-BuLi (2.2 M in cyclohexane, 7.40 mL, 16.28 mmol, 1.2 eq.) was added and the mixture was stirred at -78 °C for 1 h. Tributylborate (4.76 mL, 17.64 mmol, 1.3 eq.) was added and the mixture was allowed to warm to room temperature for 20 min. 20 mL of aqueous HCl (2 M) were added and the mixture was extracted with ethyl acetate. The combined organic layers were dried over $MgSO_4$ and evaporated affording boronic acid **93** (3.632 g, quant.) as a white solid that was used without further purification.

1-Bromo-2-(2-methyl-5-phenylthiophen-3-yl)cyclopent-1-ene 94[26c]

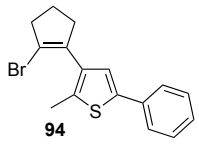

94

Thienyl boronic acid **93** (2.944 g, 13.50 mmol, 1.0 eq.), $Pd(OAc)_2$ (0.061 g, 0.27 mmol, 0.02 eq.), SPhos (0.222 g, 0.54 mmol, 0.04 eq.), and K_3PO_4 (ground, 5.732 g, 27.00 mmol, 2.0 eq.) were dissolved in 75 mL of toluene. 1,2-Dibromocyclopentene **24** (6.100 g, 27.00 mmol, 2.0 eq.) was added annd the mixture was degassed by repeated evacuation of the flask and refilling with argon. The mixture was stirred at 95 °C for 20 h. After cooling to room temperature it was filtered through a pad of Celite eluting with ethyl acetate. The filtrate was evaporated and the residue was purified by column chromatography (petrol ether) to afford compound **94** (0.180 g, 0.56 mmol, 4%) as a pale yellow sticky oil.

^{1}H-NMR (500 MHz, $CDCl_3$): δ (ppm) = 7.57 – 7.54 (m, 2 H, CH_{ar}), 7.38 – 7.34 (m, 2 H, CH_{ar}), 7.26 – 7.23 (m, 1 H, CH_{ar}), 7.14 (s, 1 H, CH_{ar}), 2.83 (t, $^3J_{H,H}$ = 7.6 Hz, 2 H, CH_2), 2.66 (t, $^3J_{H,H}$ = 7.6 Hz, 2 H, CH_2), 2.44 (s, 3 H, CH_3), 2.09 (ps p, $^3J_{H,H}$ = 7.6 Hz, 2 H, CH_2).

^{13}C-NMR (126 MHz, $CDCl_3$): δ (ppm) = 140.1, 136.7, 135.6, 134.6, 134.5, 128.9 (*C*H), 127.2 (*C*H), 125.6 (*C*H), 123.7 (*C*H), 119.0, 41.1 (CH_2), 37.0 (CH_2), 22.6 (CH_2), 15.1 (CH_3).

6.6 Polymerization studies

Polymerization using TBD (0.1 mol%):

Inside of an argon-filled glovebox, TBD (1.0 mg, 0.007 mmol) was placed into an Eppendorf vial and dissolved in 1 mL of freshly distilled CD_2Cl_2. From this solution 150 µL were transferred to a second vial containing 1-pyrenebutanol (2.9 mg, 0.01 mmol). In a flame dried Schlenk tube *L*-lactide (100 mg, 0.70 mmol) was dissolved in 0.9mL of CD_2Cl_2 and 4 pieces of molecular sieves (4 Å) were added. Then, under vigorous stirring 100 µL of the TBD/1-pyrenebutanol solution were added and the mixture was stirred for 30 s. Then, benzoic acid (9 mg, 0.07 mmol) was added, the reaction mixture was transferred to an NMR tube, and an NMR spectrum was recorded.

*Attempted polymerization using DAE **14** (2 mol%):*

Inside of an argon-filled glovebox, *L*-lactide (151.3 mg, 1.05 mmol), 1-pyrenebutanol (2.9 mg, 0.0105 mmol), DAE **14(o)** (9.86 mg, 0.02 mmol), and 5 pieces of molecular sieves (4 Å) were placed into a flame-dried Schlenk tube. To the mixture 1.5 mL of freshly distilled CD_2Cl_2 were added and it was stirred for 3 min. Then the mixture was divided between two NMR tubes, which were tightly closed with a teflon coated screw cap. One of the NMR tubes was irradiated in a Rayonet RPR 100 photochemical reactor equipped with 300 nm lamps for 15 min. NMR spectra were recorded over a period of 17 h.

7. References

[1] R.S. Stoll, S. Hecht, *Angew. Chem. Int. Ed.* **2010**, *49*, 5054-5075.

[2] H. Bouas-Laurent, H. Dürr, *Pure Appl. Chem.* **2001**, *73*, 639-665.

[3] a) R. Göstl, A. Senf, S. Hecht, *Chem. Soc. Rev.* **2014**, *43*, 1982-1996; b) B.M. Neilson, C.W. Bielawski, *ACS Catalysis* **2013**, *3*, 1874-1885; c) D. Samachetty Hema, R. Branda Neil, *Pure Appl. Chem.* **2006**, *78*, 2351-2359.

[4] a) F.M. Raymo, *Phys. Chem. Chem. Phys.* **2013**, *15*, 14840-14850; b) T. Fukaminato, *J. Photochem. Photobiol., C* **2011**, *12*, 177-208; c) J. Cusido, E. Deniz, F.M. Raymo, *Eur. J. Org. Chem.* **2009**, *2009*, 2031-2045; d) M. Heilemann, P. Dedecker, J. Hofkens, M. Sauer, *Laser & Photon. Rev.* **2009**, *3*, 180-202; e) F.M. Raymo, M. Tomasulo, *Chem. Soc. Rev.* **2005**, *34*, 327-336.

[5] a) W. Szymański, J.M. Beierle, H.A.V. Kistemaker, W.A. Velema, B.L. Feringa, *Chem. Rev.* **2013**, *113*, 6114-6178; b) M. Natali, S. Giordani, *Chem. Soc. Rev.* **2012**, *41*, 4010-4029; c) S. Yagai, A. Kitamura, *Chem. Soc. Rev.* **2008**, *37*, 1520-1529.

[6] a) T. Kim, L. Zhu, R.O. Al-Kaysi, C.J. Bardeen, *ChemPhysChem* **2014**, *15*, 400-414; b) D. Bleger, Z. Yu, S. Hecht, *Chem. Commun.* **2011**, *47*, 12260-12266.

[7] a) E. Orgiu, P. Samorì, *Adv. Mater.* **2014**, *26*, 1827-1845; b) T. Tsujioka, M. Irie, *J. Photochem. Photobiol., C* **2010**, *11*, 1-14.

[8] a) M. Irie, *Chem. Rev.* **2000**, *100*, 1685-1716; b) M. Irie, T. Fukaminato, K. Matsuda, S. Kobatake, *Chem. Rev.* **2014**, *114*, 12174-12277.

[9] a) S. Kobatake, M. Irie, *Bull. Chem. Soc. Jpn.* **2004**, *77*, 195-210; b) M. Morimoto, M. Irie, *Chem. Commun.* **2005**, 3895-3905.

[10] R.B. Woodward, R. Hoffmann, *J. Am. Chem. Soc.* **1965**, *87*, 395-397.

[11] a) T. Sumi, Y. Takagi, A. Yagi, M. Morimoto, M. Irie, *Chem. Commun.* **2014**, *50*, 3928-3930; b) M. Irie, K. Sakemura, M. Okinaka, K. Uchida, *J. Org. Chem.* **1995**, *60*, 8305-8309.

[12] a) W. Li, C. Jiao, X. Li, Y. Xie, K. Nakatani, H. Tian, W. Zhu, *Angew. Chem. Int. Ed.* **2014**, *53*, 4603-4607; b) K. Uchida, E. Tsuchida, Y. Aoi, S. Nakamura, M. Irie, *Chem. Lett.* **1999**, *28*, 63-64.

[13] M. Irie, T. Lifka, S. Kobatake, N. Kato, *J. Am. Chem. Soc.* **2000**, *122*, 4871-4876.

[14] a) R.M. Kellogg, M.B. Groen, H. Wynberg, *J. Org. Chem.* **1967**, *32*, 3093-3100; b) K.A. Muszkat, E. Fischer, *J. Chem. Soc. (B)* **1967**, 662-678; c) K.A. Muszkat, D. Gegiou, E. Fischer, *Chem. Commun. (London)* **1965**, 447-448; d) F.B. Mallory, C.S. Wood, J.T. Gordon, *J. Am. Chem. Soc.* **1964**, *86*, 3094-3102.

[15] a) M. Irie, M. Mohri, *J. Org. Chem.* **1988**, *53*, 803-808; b) S. Nakamura, M. Irie, *J. Org. Chem.* **1988**, *53*, 6136-6138.

[16] M. Irie, K. Sayo, *J. Phys. Chem.* **1992**, *96*, 7671-7674.

[17] K. Uchida, Y. Kido, T. Yamaguchi, M. Irie, *Bull. Chem. Soc. Jpn.* **1998**, *71*, 1101-1108.

[18] M. Hanazawa, R. Sumiya, Y. Horikawa, M. Irie, *J. Chem. Soc., Chem. Commun.* **1992**, 206-207.

[19] a) L.N. Lucas, J.J.D. de Jong, J.H. van Esch, R.M. Kellogg, B.L. Feringa, *Eur. J. Org. Chem.* **2003**, *2003*, 155-166; b) J.J.D. de Jong, L.N. Lucas, R. Hania, A. Pugzlys, R.M. Kellogg, B.L. Feringa, K. Duppen, J.H. van Esch, *Eur. J. Org. Chem.* **2003**, *2003*, 1887-1893; c) L. N. Lucas, J. van Esch, R. M. Kellogg, B. L. Feringa, *Chem. Commun.* **1998**, 2313-2314.

[20] a) T. Nakashima, K. Atsumi, S. Kawai, T. Nakagawa, Y. Hasegawa, T. Kawai, *Eur. J. Org. Chem.* **2007**, *2007*, 3212-3218; b) S. Kawai, T. Nakashima, K. Atsumi, T. Sakai, M. Harigai, Y. Imamoto, H. Kamikubo, M. Kataoka, T. Kawai, *Chem. Mater.* **2007**, *19*, 3479-3483; c) T. Kawai, T. Iseda, M. Irie, *Chem. Commun.* **2004**, 72-73.

[21] a) H. Ogawa, K. Takagi, T. Ubukata, A. Okamoto, N. Yonezawa, S. Delbaere, Y. Yokoyama, *Chem. Commun.* **2012**; b) S. Fukumoto, T. Nakashima, T. Kawai, *Angew. Chem. Int. Ed.* **2011**, *50*, 1565-1568; c) S. Fukumoto, T. Nakashima, T. Kawai, *Eur. J. Org. Chem.* **2011**, *2011*, 5047-5053; d) K. Morinaka, T. Ubukata, Y. Yokoyama, *Org. Lett.* **2009**, *11*, 3890-3893.

[22] C.-C. Ko, W.-M. Kwok, V.W.-W. Yam, D.L. Phillips, *Chem. Eur. J.* **2006**, *12*, 5840-5848.

[23] a) B.M. Neilson, C.W. Bielawski, *Organometallics* **2013**, *32*, 3121-3128; b) B.M. Neilson, C.W. Bielawski, *Chem. Commun.* **2013**, *49*, 5453-5455; c) B.M. Neilson, C.W. Bielawski, *J. Am. Chem. Soc.* **2012**, *134*, 12693-12699; d) B.M. Neilson, V.M. Lynch, C.W. Bielawski, *Angew. Chem. Int. Ed.* **2011**, *50*, 10322-10326; e) V.W.-W. Yam, J.K.-W. Lee, C.-C. Ko, N. Zhu, *J. Am. Chem. Soc.* **2009**, *131*, 912-913.

[24] S. Takami, S. Kobatake, T. Kawai, M. Irie, *Chem. Lett.* **2003**, *32*, 892-893.

[25] a) T. Yamaguchi, Y. Kamihashi, T. Ozeki, A. Uyama, J.-i. Kitai, M. Kasuno, K. Sumaru, Y. Kimura, S. Yokojima, S. Nakamura, M. Morimoto, K. Uchida, *Bull. Chem. Soc. Jpn.* **2014**, *87*, 528-538; b) M. Takeshita, E. Mizukami, K. Murakami, Y. Wada, Y. Matsuda, *Eur. J. Org. Chem.* **2014**, *2014*, 3784-3787; c) R. Wang, S. Pu, G. Liu, B. Chen, *Tetrahedron* **2013**, *69*, 5537-5544.

[26] a) H. Cahová, A. Jäschke, *Angew. Chem. Int. Ed.* **2013**, *52*, 3186-3190; b) M. Singer, A. Nierth, A. Jäschke, *Eur. J. Org. Chem.* **2013**, *2013*, 2766-2769; c) M. Singer, A. Jäschke, *J. Am. Chem. Soc.* **2010**, *132*, 8372-8377.

[27] a) T. Kudernac, T. Kobayashi, A. Uyama, K. Uchida, S. Nakamura, B.L. Feringa, *J. Phys. Chem. A* **2013**, *117*, 8222-8229; b) Y. Tatsumi, J.-i. Kitai, W. Uchida, K. Ogata, S. Nakamura, K. Uchida, *J. Phys. Chem. A* **2012**, *116*, 10973-10979; c) K. Uchida, T. Matsuoka, S. Kobatake, T. Yamaguchi, M. Irie, *Tetrahedron* **2001**, *57*, 4559-4565.

[28] a) S. Kobatake, M. Irie, *Chem. Lett.* **2003**, *32*, 1078-1079; b) K. Morimitsu, K. Shibata, S. Kobatake, M. Irie, *J. Org. Chem.* **2002**, *67*, 4574-4578; c) S. Kobatake, K. Uchida, E. Tsuchida, M. Irie, *Chem. Lett.* **2000**, *29*, 1340-1341.

[29] a) S. Takami, T. Kawai, M. Irie, *Eur. J. Org. Chem.* **2002**, *2002*, 3796-3800; b) K. Shibata, S. Kobatake, M. Irie, *Chem. Lett.* **2001**, *30*, 618-619.

[30] K. Higashiguchi, K. Matsuda, Y. Asano, A. Murakami, S. Nakamura, M. Irie, *Eur. J. Org. Chem.* **2005**, *2005*, 91-97.

[31] a) K. Morimitsu, S. Kobatake, M. Irie, *Mol. Cryst. Liq. Cryst.* **2005**, *431*, 451-454; b) K. Morimitsu, S. Kobatake, S. Nakamura, M. Irie, *Chem. Lett.* **2003**, *32*, 858-859.

[32] a) S. Kobatake, Y. Terakawa, *Chem. Commun.* **2007**, 1698-1700; b) S.L. Gilat, S.H. Kawai, J.-M. Lehn, *Chem. Eur. J.* **1995**, *1*, 275-284.

[33] B. Seefeldt, K. Altenhoner, O. Tosic, T. Geisler, M. Sauer, J. Mattay, *Photochem. Photobiol. Sci.* **2011**, *10*, 1488-1495.

[34] a) A. Thomas Bens, D. Frewert, K. Kodatis, C. Kryschi, H.-D. Martin, H.P. Trommsdorff, *Eur. J. Org. Chem.* **1998**, *1998*, 2333-2338; b) M. Irie, T. Eriguchi, T. Takada, K. Uchida, *Tetrahedron* **1997**, *53*, 12263-12271.

[35] a) Y. Ishibashi, M. Fujiwara, T. Umesato, H. Saito, S. Kobatake, M. Irie, H. Miyasaka, *J. Phys. Chem. C* **2011**, *115*, 4265-4272; b) P.R. Hania, A. Pugzlys, L.N. Lucas, J.J.D. de Jong, B.L. Feringa, J.H. van Esch, H.T. Jonkman, K. Duppen, *J. Phys. Chem. A* **2005**, *109*, 9437-9442; c) J. Ern, A.T. Bens, H.-D. Martin, K. Kuldova, H.P. Trommsdorff, C. Kryschi, *J. Phys. Chem. A* **2002**, *106*, 1654-1660.

[36] Y. Ishibashi, T. Umesato, S. Kobatake, M. Irie, H. Miyasaka, *J. Phys. Chem. C* **2012**, *116*, 4862-4869.

[37] D. Dulić, T. Kudernac, A. Pužys, B.L. Feringa, B.J. van Wees, *Adv. Mater.* **2007**, *19*, 2898-2902.

[38] a) Z.S. Valerii, D.V. Lonshakov, A.G. Lvov, M.K. Mikhail, *Russ. Chem. Rev.* **2013**, *82*, 511; b) C. Yun, J. You, J. Kim, J. Huh, E. Kim, *J. Photochem. Photobiol., C* **2009**, *10*, 111-129.

[39] a) M. Ohsumi, M. Hazama, T. Fukaminato, M. Irie, *Chem. Commun.* **2008**, 3281-3283; b) H. Miyasaka, T. Nobuto, M. Murakami, A. Itaya, N. Tamai, M. Irie, *J. Phys. Chem. A* **2002**, *106*, 8096-8102.

[40] Z.R. Grabowski, K. Rotkiewicz, W. Rettig, *Chem. Rev.* **2003**, *103*, 3899-4032.

[41] a) F. Ortica, *Dyes and Pigments* **2012**, *92*, 807-816; b) K. Kuldová, K. Tsyganenko, A. Corval, H.P. Trommsdorff, A.T. Bens, C. Kryschi, *Synth. Met.* **2000**, *115*, 163-166.

[42] A.R. Santos, R. Ballardini, P. Belser, M.T. Gandolfi, V.M. Iyer, L. Moggi, *Photochem. Photobiol. Sci.* **2009**, *8*, 1734-1742.

[43] a) M. Garavelli, P. Celani, M. Fato, M.J. Bearpark, B.R. Smith, M. Olivucci, M.A. Robb, *J. Phys. Chem. A* **1997**, *101*, 2023-2032; b) P. Celani, F. Bernardi, M.A. Robb, M. Olivucci, *J. Phys. Chem.* **1996**, *100*, 19364-19366; c) P. Celani, S. Ottani, M. Olivucci, F. Bernardi, M.A. Robb, *J. Am. Chem. Soc.* **1994**, *116*, 10141-10151.

[44] a) Y. Asano, A. Murakami, T. Kobayashi, A. Goldberg, D. Guillaumont, S. Yabushita, M. Irie, S. Nakamura, *J. Am. Chem. Soc.* **2004**, *126*, 12112-12120; b) M. Boggio-Pasqua, M. Ravaglia, M.J. Bearpark, M. Garavelli, M.A. Robb, *J. Phys. Chem. A* **2003**, *107*, 11139-11152; c) D. Guillaumont, T. Kobayashi, K. Kanda, H. Miyasaka, K. Uchida, S. Kobatake, K. Shibata, S. Nakamura, M. Irie, *J. Phys. Chem. A* **2002**, *106*, 7222-7227.

[45] D. Mendive-Tapia, A. Perrier, M.J. Bearpark, M.A. Robb, B. Lasorne, D. Jacquemin, *Phys. Chem. Chem. Phys.* **2014**, *16*, 18463-18471.

[46] a) J. Piard, Y. Ishibashi, H. Saito, R. Métivier, K. Nakatani, G. Gavrel, P. Yu, H. Miyasaka, *J. Photochem. Photobiol. A* **2012**, *234*, 57-65; b) Y. Ishibashi, M. Mukaida, M. Falkenstrom, H. Miyasaka, S. Kobatake, M. Irie, *Phys. Chem. Chem. Phys.* **2009**, *11*, 2640-2648; c) M. Murakami, H. Miyasaka, T. Okada, S. Kobatake, M. Irie, *J. Am. Chem. Soc.* **2004**, *126*, 14764-14772.

[47] a) H. Nishi, T. Asahi, S. Kobatake, *ChemPhysChem* **2012**, *13*, 3616-3621; b) H. Nishi, T. Asahi, S. Kobatake, *J. Phys. Chem. C* **2011**, *115*, 4564-4570.

[48] a) S. Monaco, M. Semeraro, W. Tan, H. Tian, P. Ceroni, A. Credi, *Chem. Commun.* **2012**, *48*, 8652-8654; b) M.T. Indelli, S. Carli, M. Ghirotti, C. Chiorboli, M. Ravaglia, M. Garavelli, F. Scandola, *J. Am. Chem. Soc.* **2008**, *130*, 7286-7299; c) R.T.F. Jukes, V. Adamo, F. Hartl, P. Belser, L. De Cola, *Coord. Chem. Rev.* **2005**, *249*, 1327-1335; d) R.T.F. Jukes, V. Adamo, F. Hartl, P. Belser, L. De Cola, *Inorg. Chem.* **2004**, *43*, 2779-2792.

[49] R. Murata, T. Yago, M. Wakasa, *Bull. Chem. Soc. Jpn.* **2011**, *84*, 1336-1338.

[50] T. Fukaminato, T. Doi, M. Tanaka, M. Irie, *J. Phys. Chem. C* **2009**, *113*, 11623-11627.

[51] M. Irie, T. Lifka, K. Uchida, S. Kobatake, Y. Shindo, *Chem. Commun.* **1999**, 747-750.

[52] a) H. Shoji, S. Kobatake, *Chem. Commun.* **2013**, *49*, 2362-2364; b) H.-h. Liu, Y. Chen, *New J. Chem.* **2012**, *36*, 2223-2227; c) K. Higashiguchi, K. Matsuda, T. Yamada, T. Kawai, M. Irie, *Chem. Lett.* **2000**, *29*, 1358-1359.

[53] a) T. Hirose, Y. Inoue, J.-y. Hasegawa, K. Higashiguchi, K. Matsuda, *J. Phys. Chem. A* **2014**, *118*, 1084-1093; b) E.C. Harvey, J. Areephong, A.A. Cafolla, C. Long, W.R. Browne, B.L. Feringa, M.T. Pryce, *Organometallics* **2014**, *33*, 447-456; c) T. Sakano, Y. Imaizumi, T. Hirose, K. Matsuda, *Chem. Lett.* **2013**, *42*, 1537-1539; d) H. Ikeda, A. Sakai, A. Kawabe, H. Namai, K. Mizuno, *Tetrahedron Lett.* **2008**, *49*, 4972-4976; e) G. Sevez, J. Gan, J. Pan, X. Sallenave, A. Colin, H. Saadoui, A. Saleh, F. Vögtle, J.-L. Pozzo, *J. Phys. Org. Chem.* **2007**, *20*, 888-893; f) A. Peters, N.R. Branda, *Adv. Mater. Opt. Electron.* **2000**, *10*, 245-249; g) K. Higashiguchi, K. Matsuda, S. Kobatake, T. Yamada, T. Kawai, M. Irie, *Bull. Chem. Soc. Jpn.* **2000**, *73*, 2389-2394.

[54] a) I. Fernández, F.P. Cossío, M.A. Sierra, *Chem. Rev.* **2009**, *109*, 6687-6711; b) M.T. Reetz, *Angew. Chem. Int. Ed.* **1972**, *11*, 129-130.

[55] H. Ikeda, A. Kawabe, A. Sakai, H. Namai, K. Mizuno, *Res. Chem. Intermed.* **2009**, *35*, 893-908.

[56] P.D. Patel, I.A. Mikhailov, K.D. Belfield, A.E. Masunov, *Int. J. Quantum Chem.* **2009**, *109*, 3711-3722.

[57] Y.-C. Jeong, D.G. Park, E. Kim, K.-H. Ahn, S.I. Yang, *Chem. Commun.* **2006**, 1881-1883.

[58] a) A. Staykov, J. Areephong, W. R. Browne, B. L. Feringa, K. Yoshizawa, *ACS Nano* **2011**, *5*, 1165-1178; b) B. He, O.S. Wenger, *J. Am. Chem. Soc.* **2011**, *133*, 17027-17036; c) W.R. Browne, T. Kudernac, N. Katsonis, J. Areephong, J. Hjelm, B.L. Feringa, *J. Phys. Chem. C* **2008**, *112*, 1183-1190; d) J. Areephong, W.R. Browne, N. Katsonis, B.L. Feringa, *Chem. Commun.* **2006**, 3930-3932; e) W.R. Browne, J.J.D. de Jong, T. Kudernac, M. Walko, L.N. Lucas, K. Uchida, J.H. van Esch, B.L. Feringa, *Chem. Eur. J,* **2005**, *11*, 6430-6441; f) W.R. Browne, J.J.D. de Jong, T. Kudernac, M. Walko, L.N. Lucas, K. Uchida, J.H. van Esch, B.L. Feringa, *Chem. Eur. J.* **2005**, *11*, 6414-6429; g) Y. Moriyama, K. Matsuda, N. Tanifuji, S. Irie, M. Irie, *Org. Lett.* **2005**, *7*, 3315-3318; h) G. Guirado, C. Coudret, M. Hliwa, J.-P. Launay, *J. Phys. Chem. B* **2005**, *109*, 17445-17459; i) A. Peters, N.R. Branda, *J. Am. Chem. Soc.* **2003**, *125*, 3404-3405; j) A. Peters, N.R. Branda, *Chem. Commun.* **2003**, 954-955.

[59] a) T. Nakashima, Y. Kajiki, S. Fukumoto, M. Taguchi, S. Nagao, S. Hirota, T. Kawai, *J. Am. Chem. Soc.* **2012**, *134*, 19877-19883; b) S. Lee, Y. You, K. Ohkubo, S. Fukuzumi, W. Nam, *Org. Lett.* **2012**, *14*, 2238-2241; c) T. Koshido, T. Kawai, K. Yoshino, *J. Phys. Chem.* **1995**, *99*, 6110-6114.

[60] a) Y. Liu, C.M. Ndiaye, C. Lagrost, K. Costuas, S. Choua, P. Turek, L. Norel, S. Rigaut, *Inorg. Chem.* **2014**, *53*, 8172-8188; b) Y.-M. Hervault, C.M. Ndiaye, L. Norel, C. Lagrost, S. Rigaut,

Org. Lett. **2012**, *14*, 4454-4457; c) Y. Tanaka, T. Ishisaka, A. Inagaki, T. Koike, C. Lapinte, M. Akita, *Chem. Eur. J,* **2010**, *16*, 4762-4776; d) Y. Lin, J. Yuan, M. Hu, J. Cheng, J. Yin, S. Jin, S.H. Liu, *Organometallics* **2009**, *28*, 6402-6409; e) Y. Liu, C. Lagrost, K. Costuas, N. Tchouar, H.L. Bozec, S. Rigaut, *Chem. Commun.* **2008**, 6117-6119; f) K. Motoyama, T. Koike, M. Akita, *Chem. Commun.* **2008**, 5812-5814; g) G. Guirado, C. Coudret, J.-P. Launay, *J. Phys. Chem. C* **2007**, *111*, 2770-2776.

[61] a) A. Léaustic, E. Anxolabéhère-Mallart, F. Maurel, S. Midelton, R. Guillot, R. Métivier, K. Nakatani, P. Yu, *Chem. Eur. J,* **2011**, *17*, 2246-2255; b) B. Gorodetsky, H.D. Samachetty, R.L. Donkers, M.S. Workentin, N.R. Branda, *Angew. Chem. Int. Ed.* **2004**, *43*, 2812-2815.

[62] B. Gorodetsky, N.R. Branda, *Adv. Funct. Mater.* **2007**, *17*, 786-796.

[63] D.H. Evans, *Chem. Rev.* **2008**, *108*, 2113-2144.

[64] a) S. Lee, Y. You, K. Ohkubo, S. Fukuzumi, W. Nam, *Chem. Sci.* **2014**, *5*, 1463-1474; b) S. Lee, Y. You, K. Ohkubo, S. Fukuzumi, W. Nam, *Angew. Chem.* **2012**, *124*, 13331-13335.

[65] S. Kobatake, S. Takami, H. Muto, T. Ishikawa, M. Irie, *Nature* **2007**, *446*, 778-781.

[66] a) M. Takeshita, M. Hayashi, S. Kadota, K.H. Mohammed, T. Yamato, *Chem. Commun.* **2005**, 761-763; b) M. Takeshita, M. Hayashi, T. Miyazaki, *Chem. Lett.* **2010**, *39*, 82-83.

[67] Y. Odo, K. Matsuda, M. Irie, *Chem. Eur. J,* **2006**, *12*, 4283-4288.

[68] T. Fukaminato, T. Sasaki, T. Kawai, N. Tamai, M. Irie, *J. Am. Chem. Soc.* **2004**, *126*, 14843-14849.

[69] a) M. Morimoto, M. Irie, *J. Am. Chem. Soc.* **2010**, *132*, 14172-14178; b) F. Terao, M. Morimoto, M. Irie, *Angew. Chem. Int. Ed.* **2012**, *51*, 901-904; c) D. Kitagawa, H. Nishi, S. Kobatake, *Angew. Chem. Int. Ed.* **2013**, *52*, 9320-9322.

[70] a) S. Yagai, K. Ishiwatari, X. Lin, T. Karatsu, A. Kitamura, S. Uemura, *Chem. Eur. J,* **2013**, *19*, 6971-6975; b) T. Hirose, M. Irie, K. Matsuda, *Adv. Mater.* **2008**, *20*, 2137-2141; c) T. Hirose, K. Matsuda, M. Irie, *J. Org. Chem.* **2006**, *71*, 7499-7508; d) J.J.D. de Jong, L.N. Lucas, R.M. Kellogg, J.H. van Esch, B.L. Feringa, *Science* **2004**, *304*, 278-281; e) L.N. Lucas, J. van Esch, R.M. Kellogg, B.L. Feringa, *Chem. Commun.* **2001**, 759-760.

[71] a) S.-L. Li, T. Xiao, W. Xia, X. Ding, Y. Yu, J. Jiang, L. Wang, *Chem. Eur. J,* **2011**, *17*, 10716-10723; b) S. Yagai, K. Iwai, M. Yamauchi, T. Karatsu, A. Kitamura, S. Uemura, M. Morimoto, H. Wang, F. Würthner, *Angew. Chem. Int. Ed.* **2014**, *53*, 2602-2606; c) S. Yagai, K. Iwai, T. Karatsu, A. Kitamura, *Angew. Chem. Int. Ed.* **2012**, *51*, 9679-9683; d) S. Yagai, K. Ohta, M. Gushiken, K. Iwai, A. Asano, S. Seki, Y. Kikkawa, M. Morimoto, A. Kitamura, T. Karatsu, *Chem. Eur. J,* **2012**, *18*, 2244-2253.

[72] a) D. Vomasta, C. Högner, N.R. Branda, B. König, *Angew. Chem. Int. Ed.* **2008**, *47*, 7644-7647; b) B. Reisinger, N. Kuzmanovic, P. Löffler, R. Merkl, B. König, R. Sterner, *Angew. Chem. Int. Ed.* **2014**, *53*, 595-598; c) X. Chen, S. Wehle, N. Kuzmanovic, B. Merget, U. Holzgrabe, B. König, C.A. Sotriffer, M. Decker, *ACS Chemical Neuroscience* **2014**, *5*, 377-389; d) C. Falenczyk, M. Schiedel, B. Karaman, T. Rumpf, N. Kuzmanovic, M. Grotli, W. Sippl, M. Jung, B. Konig, *Chem. Sci.* **2014**, *5*, 4794-4799.

[73] a) M. Han, R. Michel, B. He, Y.-S. Chen, D. Stalke, M. John, G.H. Clever, *Angew. Chem. Int. Ed.* **2013**, *52*, 1319-1323; b) M. Takeshita, M. Irie, *J. Org. Chem.* **1998**, *63*, 6643-6649; c) J. Kärnbratt, M. Hammarson, S. Li, H.L. Anderson, B. Albinsson, J. Andréasson, *Angew. Chem. Int. Ed.* **2010**, *49*, 1854-1857; d) D. Sud, T.B. Norsten, N.R. Branda, *Angew. Chem. Int. Ed.* **2005**, *44*, 2019-2021.

[74] S.H. Kawai, S.L. Gilat, J.-M. Lehn, *Eur. J. Org. Chem.* **1999**, *1999*, 2359-2366.

[75] a) M. Herder, diploma thesis, Humboldt-Universität zu Berlin (Berlin), **2010**; b) M. Herder, M. Patzel, L. Grubert, S. Hecht, *Chem. Commun.* **2011**, *47*, 460-462.

[76] a) M. Irie, T. Fukaminato, T. Sasaki, N. Tamai, T. Kawai, *Nature* **2002**, *420*, 759-760; b) M. Pärs, C.C. Hofmann, K. Willinger, P. Bauer, M. Thelakkat, J. Köhler, *Angew. Chem. Int. Ed.* **2011**, *50*, 11405-11408; c) T. Fukaminato, T. Doi, N. Tamaoki, K. Okuno, Y. Ishibashi, H. Miyasaka, M. Irie, *J. Am. Chem. Soc.* **2011**, *133*, 4984-4990.

[77] L. Hou, X. Zhang, T.C. Pijper, W.R. Browne, B.L. Feringa, *J. Am. Chem. Soc.* **2014**, *136*, 910-913.

[78] a) W. Yutaka, H. Ryoma, S. Hoon-Seok, *Sci. Technol. Adv. Mater.* **2014**, *15*, 024202; b) T. Kudernac, N. Katsonis, W.R. Browne, B.L. Feringa, *J. Mater. Chem.* **2009**, *19*, 7168-7177.

[79] N. Katsonis, T. Kudernac, M. Walko, S.J. van der Molen, B.J. van Wees, B.L. Feringa, *Adv. Mater.* **2006**, *18*, 1397-1400.

[80] K. Uchida, Y. Yamanoi, T. Yonezawa, H. Nishihara, *J. Am. Chem. Soc.* **2011**, *133*, 9239-9241.

[81] a) A.C. Whalley, M.L. Steigerwald, X. Guo, C. Nuckolls, *J. Am. Chem. Soc.* **2007**, *129*, 12590-12591; b) C. Jia, J. Wang, C. Yao, Y. Cao, Y. Zhong, Z. Liu, Z. Liu, X. Guo, *Angew. Chem. Int. Ed.* **2013**, *52*, 8666-8670; c) D. Dulić, S.J. van der Molen, T. Kudernac, H.T. Jonkman, J.J.D. de Jong, T.N. Bowden, J. van Esch, B.L. Feringa, B.J. van Wees, *Phys. Rev. Lett.* **2003**, *91*, 207402; d) H. Jin, C. Fan, A.L. Paul, A. Joakim, D.S. Stephen, G. Devens, A.M. Thomas, L.M. Ana, L. Jun, F.S. Otto, M.L. Stuart, *Nanotechnology* **2005**, *16*, 695; e) E.S. Tam, J.J. Parks, W.W. Shum, Y.-W. Zhong, M.E.B. Santiago-Berríos, X. Zheng, W. Yang, G.K.L. Chan, H.D. Abruña, D.C. Ralph, *ACS Nano* **2011**, *5*, 5115-5123; f) Y. Kim, T.J. Hellmuth, D. Sysoiev, F. Pauly, T. Pietsch, J. Wolf, A. Erbe, T. Huhn, U. Groth, U.E. Steiner, E. Scheer, *Nano Lett.* **2012**, *12*, 3736-3742; g) F. Meng, Y.-M. Hervault, L. Norel, K. Costuas, C. Van Dyck, V. Geskin, J. Cornil, H.H. Hng, S. Rigaut, X. Chen, *Chem. Sci.* **2012**, *3*, 3113-3118; h) F. Meng, Y.-M. Hervault, Q. Shao, B. Hu, L. Norel, S. Rigaut, X. Chen, *Nat. Commun.* **2014**, *5*, 3023.

[82] a) M. Ikeda, N. Tanifuji, H. Yamaguchi, M. Irie, K. Matsuda, *Chem. Commun.* **2007**, 1355-1357; b) T. Sakano, H. Yamaguchi, N. Tanifuji, M. Irie, K. Matsuda, *Chem. Lett.* **2008**, *37*, 634-635; c) K. Matsuda, H. Yamaguchi, T. Sakano, M. Ikeda, N. Tanifuji, M. Irie, *J. Phys. Chem. C* **2008**, *112*, 17005-17010; d) S.J. van der Molen, J. Liao, T. Kudernac, J.S. Agustsson, L. Bernard, M. Calame, B.J. van Wees, B.L. Feringa, C. Schönenberger, *Nano Lett.* **2009**, *9*, 76-80.

[83] T. Kudernac, S.J. van der Molen, B.J. van Wees, B.L. Feringa, *Chem. Commun.* **2006**, 3597-3599.

[84] a) E. Kim, M. Kim, K. Kim, *Tetrahedron* **2006**, *62*, 6814-6821; b) H. Lin, Z. Wei, J. Xiang, W. Xu, D. Zhu, *ChemPhysChem* **2009**, *10*, 1996-1999; c) T. Tsujioka, N. Matsui, *J. Mater. Chem. C* **2014**, *2*, 3589-3596.

[85] a) T. Kawai, T. Kunitake, M. Irie, *Chem. Lett.* **1999**, *28*, 905-906; b) T. Kawai, Y. Nakashima, M. Irie, *Adv. Mater.* **2005**, *17*, 309-314; c) H. Choi, H. Lee, Y. Kang, E. Kim, S.O. Kang, J. Ko, *J. Org. Chem.* **2005**, *70*, 8291-8297; d) E. Kim, H.W. Lee, *J. Mater. Chem.* **2006**, *16*, 1384-1389.

[86] a) T. Tsujioka, T. Sasa, Y. Kakihara, *Org. Electron.* **2012**, *13*, 681-686; b) N. Matsui, T. Tsujioka, *Org. Electron.* **2014**, *15*, 2264-2269; c) T. Tsujioka, M. Shimizu, E. Ishihara, *Appl. Phys. Lett.* **2005**, *87*, -; d) T. Tsujioka, H. Kondo, *Appl. Phys. Lett.* **2003**, *83*, 937-939; e) T. Tsujioka, K. Masuda, *Appl. Phys. Lett.* **2003**, *83*, 4978-4980; f) R.C. Shallcross, P.O. Körner, E. Maibach, A. Köhnen, K. Meerholz, *Adv. Mater.* **2013**, *25*, 4807-4813.

[87] a) Z. Zhang, X. Liu, Z. Li, Z. Chen, F. Zhao, F. Zhang, C.H. Tung, *Adv. Funct. Mater.* **2008**, *18*, 302-307; b) P. Zacharias, M.C. Gather, A. Köhnen, N. Rehmann, K. Meerholz, *Angew. Chem. Int. Ed.* **2009**, *48*, 4038-4041; c) R.C. Shallcross, P. Zacharias, A. Köhnen, P.O. Körner, E. Maibach, K. Meerholz, *Adv. Mater.* **2013**, *25*, 469-476.

[88] F.L.E. Jakobsson, P. Marsal, S. Braun, M. Fahlman, M. Berggren, J. Cornil, X. Crispin, *J. Phys. Chem. C* **2009**, *113*, 18396-18405.

[89] R. Hayakawa, K. Higashiguchi, K. Matsuda, T. Chikyow, Y. Wakayama, *ACS Appl. Mater. Interfaces* **2013**, *5*, 3625-3630.

[90] Y. Manabu, S. Kouji, U. Sei, H. Satoshi, T. Noriyuki, K. Takehito, K. Toshihide, *Jpn. J. Appl. Phys.* **2010**, *49*, 04DK09.

[91] T. Koshido, T. Kawai, K. Yoshino, *Synth. Met.* **1995**, *73*, 257-260.

[92] S. Perissinotto, M. Garbugli, D. Fazzi, C. Bertarelli, M. Carvelli, A.R. Srimath Kandada, Z. Yue, K.S. Wong, G. Lanzani, *ChemPhysChem* **2011**, *12*, 3619-3623.

[93] a) P. Andersson, N.D. Robinson, M. Berggren, *Adv. Mater.* **2005**, *17*, 1798-1803; b) P. Andersson, N.D. Robinson, M. Berggren, *Synth. Met.* **2005**, *150*, 217-221; c) X. Guo, D. Zhang, G. Yu, M. Wan, J. Li, Y. Liu, D. Zhu, *Adv. Mater.* **2004**, *16*, 636-640; d) Y. Li, H. Zhang, C. Qi, X. Guo, *J. Mater. Chem.* **2012**, *22*, 4261-4265; e) Y. Ishiguro, R. Hayakawa, T. Chikyow, Y. Wakayama, *J. Mater. Chem. C* **2013**, *1*, 3012-3016; f) Y. Ishiguro, R. Hayakawa, T. Yasuda, T. Chikyow, Y. Wakayama, *ACS Appl. Mater. Interfaces* **2013**, *5*, 9726-9731.

[94] a) A.J. Kronemeijer, H.B. Akkerman, T. Kudernac, B.J. van Wees, B.L. Feringa, P.W.M. Blom, B. de Boer, *Adv. Mater.* **2008**, *20*, 1467-1473; b) D. Kim, H. Jeong, H. Lee, W.-T. Hwang, J. Wolf, E. Scheer, T. Huhn, H. Jeong, T. Lee, *Adv. Mater.* **2014**, *26*, 3968-3973.

[95] a) Q. Shen, L. Wang, S. Liu, Y. Cao, L. Gan, X. Guo, M.L. Steigerwald, Z. Shuai, Z. Liu, C. Nuckolls, *Adv. Mater.* **2010**, *22*, 3282-3287; b) P. Lutsyk, K. Janus, J. Sworakowski, G. Generali, R. Capelli, M. Muccini, *J. Phys. Chem. C* **2011**, *115*, 3106-3114; c) H. Zhang, X. Guo, J. Hui, S. Hu, W. Xu, D. Zhu, *Nano Lett.* **2011**, *11*, 4939-4946.

[96] a) D. Wilson, N.R. Branda, *Angew. Chem. Int. Ed.* **2012**, *51*, 5431-5434; b) H. Iida, N. Umebayashi, E. Yashima, *Tetrahedron* **2013**, *69*, 11064-11069.

[97] M. Morimoto, K. Murata, T. Michinobu, *Chem. Commun.* **2011**, *47*, 9819-9821.

[98] a) H.D. Samachetty, N.R. Branda, *Chem. Commun.* **2005**, 2840-2842; b) H.D. Samachetty, V. Lemieux, N.R. Branda, *Tetrahedron* **2008**, *64*, 8292-8300.

[99] Z. Erno, A.M. Asadirad, V. Lemieux, N.R. Branda, *Org. Biomol. Chem.* **2012**, *10*, 2787-2792.

[100] a) A.M. Asadirad, S. Boutault, Z. Erno, N.R. Branda, *J. Am. Chem. Soc.* **2014**, *136*, 3024-3027; b) V. Lemieux, S. Gauthier, N.R. Branda, *Angew. Chem. Int. Ed.* **2006**, *45*, 6820-6824; c) R. Göstl, S. Hecht, *Angew. Chem. Int. Ed.* **2014**, *53*, 8784-8787.

[101] D. Sud, Tony J. Wigglesworth, Neil R. Branda, *Angew. Chem. Int. Ed.* **2007**, *46*, 8017-8019.

[102] V. Lemieux, M. Spantulescu, K. Baldridge, N. Branda, *Angew. Chem. Int. Ed.* **2008**, *47*, 5034-5037.

[103] T. Nakashima, M. Goto, S. Kawai, T. Kawai, *J. Am. Chem. Soc.* **2008**, *130*, 14570-14575.

[104] a) R. Göstl, B. Kobin, L. Grubert, M. Pätzel, S. Hecht, *Chem. Eur. J,* **2012**, *18*, 14282-14285; b) S. Fredrich, master thesis, Humboldt-Universität zu Berlin (Berlin), **2014**; c) M. Kleinwächter, diploma thesis, Humboldt-Universität zu Berlin (Berlin), **2012**.

[105] S. Iwata, Y. Ishihara, C.P. Qian, K. Tanaka, *J. Org. Chem.* **1992**, *57*, 3726-3727.

[106] G. Szalóki, J.-L. Pozzo, *Chem. Eur. J,* **2013**, *19*, 11124-11132.

[107] L.N. Lucas, J. van Esch, R.M. Kellogg, B.L. Feringa, *Tetrahedron Lett.* **1999**, *40*, 1775-1778.

[108] G. Sevez, J.-L. Pozzo, *Dyes and Pigments* **2011**, *89*, 246-253.

[109] M. Holzweber, M. Schnürch, P. Stanetty, *Synlett* **2007**, *2007*, 3016,3018.

[110] C.-Y. He, S. Fan, X. Zhang, *J. Am. Chem. Soc.* **2010**, *132*, 12850-12852.

[111] S. Hiroto, K. Suzuki, H. Kamiya, H. Shinokubo, *Chem. Commun.* **2011**, *47*, 7149-7151.

[112] A. El Yahyaoui, G. Félix, A. Heynderickx, C. Moustrou, A. Samat, *Tetrahedron* **2007**, *63*, 9482-9487.

[113] a) T. Ishiyama, M. Murata, N. Miyaura, *J. Org. Chem.* **1995**, *60*, 7508-7510; b) M. Murata, S. Watanabe, Y. Masuda, *J. Org. Chem.* **1997**, *62*, 6458-6459.

[114] a) J. Hämmerle, M. Schnürch, N. Iqbal, M.D. Mihovilovic, P. Stanetty, *Tetrahedron* **2010**, *66*, 8051-8059; b) G.R. Dick, D.M. Knapp, E.P. Gillis, M.D. Burke, *Org. Lett.* **2010**, *12*, 2314-2317; c) N. Primas, A. Bouillon, J.-C. Lancelot, H. El-Kashef, S. Rault, *Tetrahedron* **2009**, *65*, 5739-5746; d) E. Tyrrell, P. Brookes, *Synthesis* **2003**, *2003*, 0469-0483.

[115] S.D. Walker, T.E. Barder, J.R. Martinelli, S.L. Buchwald, *Angew. Chem. Int. Ed.* **2004**, *43*, 1871-1876.

[116] A. Lennox, G. Lloyd-Jones, in *New Trends in Cross-Coupling: Theory and Applications*, The Royal Society of Chemistry, **2015**, pp. 322-354.

[117] B.P. Carrow, J.F. Hartwig, *J. Am. Chem. Soc.* **2011**, *133*, 2116-2119.

[118] a) C. Amatore, A. Jutand, G. Le Duc, *Angew. Chem. Int. Ed.* **2012**, *51*, 1379-1382; b) J. Yin, M.P. Rainka, X.-X. Zhang, S.L. Buchwald, *J. Am. Chem. Soc.* **2002**, *124*, 1162-1163.

[119] T.E. Barder, S.D. Walker, J.R. Martinelli, S.L. Buchwald, *J. Am. Chem. Soc.* **2005**, *127*, 4685-4696.

[120] C. Lai, B.J. Backes, *Tetrahedron Lett.* **2007**, *48*, 3033-3037.

[121] H.G. Kuivila, K.V. Nahabedian, *J. Am. Chem. Soc.* **1961**, *83*, 2159-2163.

[122] T. Watanabe, N. Miyaura, A. Suzuki, *Synlett* **1992**, *1992*, 207-210.

[123] a) J. Lozada, Z. Liu, D.M. Perrin, *J. Org. Chem.* **2014**, *79*, 5365-5368; b) S.-J. Ahn, C.-Y. Lee, N.-K. Kim, C.-H. Cheon, *J. Org. Chem.* **2014**, *79*, 7277-7285.

[124] D.W. Robbins, J.F. Hartwig, *Org. Lett.* **2012**, *14*, 4266-4269.

[125] J. Jensen, N. Skjaerbaek, P. Vedso, *Synthesis* **2001**, *2001*, 0128-0134.

[126] M.R. Dobler, *Tetrahedron Lett.* **2003**, *44*, 7115-7117.

[127] M.E. Jung, M.A. Lyster, *J. Chem. Soc., Chem. Commun.* **1978**, 315-316.

[128] M.K. Anwer, A.F. Spatola, *Synthesis* **1980**, *1980*, 929-932.

[129] V.C.R. McLoughlin, J. Thrower, *Tetrahedron* **1969**, *25*, 5921-5940.

[130] O.A. Tomashenko, V.V. Grushin, *Chem. Rev.* **2011**, *111*, 4475-4521.

[131] D.M. Wiemers, D.J. Burton, *J. Am. Chem. Soc.* **1986**, *108*, 832-834.

[132] G.E. Carr, R.D. Chambers, T.F. Holmes, D.G. Parker, *J. Chem. Soc., Perkin Trans. 1* **1988**, 921-926.

[133] C. Liu, Q.-Y. Chen, *Eur. J. Org. Chem.* **2005**, *2005*, 3680-3686.

[134] a) H. Urata, T. Fuchikami, *Tetrahedron Lett.* **1991**, *32*, 91-94; b) F. Cottet, M. Schlosser, *Eur. J. Org. Chem.* **2002**, *2002*, 327-330.

[135] H. Morimoto, T. Tsubogo, N.D. Litvinas, J.F. Hartwig, *Angew. Chem. Int. Ed.* **2011**, *50*, 3793-3798.

[136] a) T. Knauber, F. Arikan, G.-V. Röschenthaler, L.J. Gooßen, *Chem. Eur. J,* **2011**, *17*, 2689-2697; b) E.J. Cho, T.D. Senecal, T. Kinzel, Y. Zhang, D.A. Watson, S.L. Buchwald, *Science* **2010**, *328*, 1679-1681; c) M. Oishi, H. Kondo, H. Amii, *Chem. Commun.* **2009**, 1909-1911.

[137] F. Eisenreich, bachelor thesis, Humboldt-Universität zu Berlin (Berlin), **2012**.

[138] C. Sämann, M.A. Schade, S. Yamada, P. Knochel, *Angew. Chem. Int. Ed.* **2013**, *52*, 9495-9499.

[139] S. Gronowitz, B. Holm, *Acta Chem. Scand., Ser. B* **1976**, *B30*, 423-429.

[140] T. Yamamoto, K. Toyota, N. Morita, *Tetrahedron Lett.* **2010**, *51*, 1364-1366.

[141] G. Gauglitz, in *Photochromism - Molecules and Systems* (Eds.: H. Bouas-Laurent, H. Dürr), Elsevier Science, Amsterdam, **2003**, pp. 15-63.

[142] E. Fischer, *J. Phys. Chem.* **1967**, *71*, 3704-3706.

[143] a) M. Maafi, R.G. Brown, *Photochem. Photobiol. Sci.* **2008**, *7*, 1360-1372; b) S. Delbaere, G. Vermeersch, J.-C. Micheau, *J. Photochem. Photobiol., C* **2011**, *12*, 74-105.

[144] a) H.J. Kuhn, S.E. Braslavsky, R. Schmidt, *Pure Appl. Chem.* **2004**, *76*, 2105-2146; b) M. Montalti, A. Credi, L. Prodi, M.T. Gandolfi, in *Handbook of Photochemistry, Third Edition*, CRC Press, Boca Raton, **2006**, pp. 601-616.

[145] a) G. Gauglitz, S. Hubig, *J. Photochem.* **1985**, *30*, 121-125; b) G. Gauglitz, S. Hubig, *J. Photochem.* **1981**, *15*, 255-257.

[146] C.G. Hatchard, C.A. Parker, *Proc. R. Soc. London, Ser. A* **1956**, *235*, 518-536.

[147] A.P. Glaze, H.G. Heller, J. Whittall, *J. Chem. Soc. Perk. Trans. 2* **1992**, 591-594.

[148] Y. Yokoyama, T. Inoue, M. Yokoyama, T. Goto, T. Iwai, N. Kera, I. Hitomi, Y. Kurita, *Bull. Chem. Soc. Jpn.* **1994**, *67*, 3297-3303.

[149] R.W. Hendler, R.I. Shrager, *J. Biochem. Bioph. Methods* **1994**, *28*, 1-33.

[150] a) L. Zimányi, Á. Kulcsár, J.K. Lanyi, D.F. Sears, J. Saltiel, *Proc. Natl. Acad. Sci.* **1999**, *96*, 4408-4413; b) L. Zimányi, Á. Kulcsár, J.K. Lanyi, D.F. Sears, J. Saltiel, *Proc. Natl. Acad. Sci.* **1999**, *96*, 4414-4419; c) M. Kubista, R. Sjoeback, B. Albinsson, *Anal. Chem.* **1993**, *65*, 994-998.

[151] H. Rau, G. Greiner, G. Gauglitz, H. Meier, *J. Phys. Chem.* **1990**, *94*, 6523-6524.

[152] M.H. Deniel, D. Lavabre, J.C. Micheau, in *Organic Photochromic and Thermochromic Compounds, Vol. 2* (Eds.: J. Crano, R. Guglielmetti), Kluwer Academic, New York, **1999**, pp. 167-209.

[153] K. Uchida, T. Ishikawa, M. Takeshita, M. Irie, *Tetrahedron* **1998**, *54*, 6627-6638.

[154] a) F. Maurel, A. Perrier, D. Jacquemin, *Int. J. Quantum Chem.* **2012**, *112*, 1122-1133; b) D. Jacquemin, E.A. Perpète, F.o. Maurel, A.l. Perrier, *J. Phys. Chem. C* **2010**, *114*, 9489-9497; c) D. Jacquemin, E.A. Perpète, I. Ciofini, C. Adamo, *Acc. Chem. Res.* **2008**, *42*, 326-334.

[155] D. Jacquemin, E.A. Perpète, G.E. Scuseria, I. Ciofini, C. Adamo, *J. Chem. Theory Comput.* **2007**, *4*, 123-135.

[156] W.A. Sheppard, *J. Am. Chem. Soc.* **1962**, *84*, 3072-3076.

[157] R. Göstl, PhD thesis, Humboldt-Universität zu Berlin (Berlin), **2014**.

[158] M. Montalti, A. Credi, L. Prodi, M.T. Gandolfi, in *Handbook of Photochemistry, Third Edition*, CRC Press, Boca Raton, **2006**, pp. 83-351.

[159] a) P.v.R. Schleyer, M. Manoharan, Z.-X. Wang, B. Kiran, H. Jiao, R. Puchta, N.J.R. van Eikema Hommes, *Org. Lett.* **2001**, *3*, 2465-2468; b) P.v.R. Schleyer, C. Maerker, A. Dransfeld, H. Jiao, N.J.R.v.E. Hommes, *J. Am. Chem. Soc.* **1996**, *118*, 6317-6318.

[160] D. Gust, J. Andreasson, U. Pischel, T.A. Moore, A.L. Moore, *Chem. Commun.* **2012**, *48*, 1947-1957.

[161] H. Nishi, T. Namari, S. Kobatake, *J. Mater. Chem.* **2011**, *21*, 17249-17258.

[162] J. Pommerehne, H. Vestweber, W. Guss, R.F. Mahrt, H. Bässler, M. Porsch, J. Daub, *Adv. Mater.* **1995**, *7*, 551-554.

[163] C.M. Cardona, W. Li, A.E. Kaifer, D. Stockdale, G.C. Bazan, *Adv. Mater.* **2011**, *23*, 2367-2371.

[164] A.W. Bott, *Current Separations* **1999**, *18*, 9-16.

[165] Y. Shirota, H. Kageyama, *Chem. Rev.* **2007**, *107*, 953-1010.

[166] a) P. Zacharias, M.C. Gather, M. Rojahn, O. Nuyken, K. Meerholz, *Angew. Chem. Int. Ed.* **2007**, *46*, 4388-4392; b) B.W. D'Andrade, S. Datta, S.R. Forrest, P. Djurovich, E. Polikarpov, M.E. Thompson, *Org. Electron.* **2005**, *6*, 11-20.

[167] H. Sirringhaus, P.J. Brown, R.H. Friend, M.M. Nielsen, K. Bechgaard, B.M.W. Langeveld-Voss, A.J.H. Spiering, R.A.J. Janssen, E.W. Meijer, P. Herwig, D.M. de Leeuw, *Nature* **1999**, *401*, 685-688.

[168] a) E. Orgiu, N. Crivillers, J. Rotzler, M. Mayor, P. Samori, *J. Mater. Chem.* **2010**, *20*, 10798-10800; b) M. Al-Ibrahim, H.K. Roth, M. Schroedner, A. Konkin, U. Zhokhavets, G. Gobsch, P. Scharff, S. Sensfuss, *Org. Electron.* **2005**, *6*, 65-77; c) T. Johansson, W. Mammo, M. Svensson, M.R. Andersson, O. Inganas, *J. Mater. Chem.* **2003**, *13*, 1316-1323; d) J. Hou, T.L. Chen, S. Zhang, L. Huo, S. Sista, Y. Yang, *Macromolecules* **2009**, *42*, 9217-9219.

[169] F.J. Zhang, A. Vollmer, J. Zhang, Z. Xu, J.P. Rabe, N. Koch, *Org. Electron.* **2007**, *8*, 606-614.

[170] A.J. Cascio, J.E. Lyon, M.M. Beerbom, R. Schlaf, Y. Zhu, S.A. Jenekhe, *Appl. Phys. Lett.* **2006**, *88*, 062104.

[171] a) H. Minemawari, T. Yamada, H. Matsui, J.y. Tsutsumi, S. Haas, R. Chiba, R. Kumai, T. Hasegawa, *Nature* **2011**, *475*, 364-367; b) H. Ebata, T. Izawa, E. Miyazaki, K. Takimiya, M. Ikeda, H. Kuwabara, T. Yui, *J. Am. Chem. Soc.* **2007**, *129*, 15732-15733.

[172] B.A. Jones, M.J. Ahrens, M.-H. Yoon, A. Facchetti, T.J. Marks, M.R. Wasielewski, *Angew. Chem. Int. Ed.* **2004**, *43*, 6363-6366.

[173] Z. Chen, Y. Zheng, H. Yan, A. Facchetti, *J. Am. Chem. Soc.* **2008**, *131*, 8-9.

[174] W.A. Velema, W. Szymanski, B.L. Feringa, *J. Am. Chem. Soc.* **2014**, *136*, 2178-2191.

[175] a) A.P. Dove, *Chem. Commun.* **2008**, 6446-6470; b) N.E. Kamber, W. Jeong, R.M. Waymouth, R.C. Pratt, B.G.G. Lohmeijer, J.L. Hedrick, *Chem. Rev.* **2007**, *107*, 5813-5840.

[176] a) R.C. Pratt, B.G.G. Lohmeijer, D.A. Long, R.M. Waymouth, J.L. Hedrick, *J. Am. Chem. Soc.* **2006**, *128*, 4556-4557; b) B.G.G. Lohmeijer, R.C. Pratt, F. Leibfarth, J.W. Logan, D.A. Long, A.P. Dove, F. Nederberg, J. Choi, C. Wade, R.M. Waymouth, J.L. Hedrick, *Macromolecules* **2006**, *39*, 8574-8583; c) A. Chuma, H.W. Horn, W.C. Swope, R.C. Pratt, L. Zhang, B.G.G. Lohmeijer, C.G. Wade, R.M. Waymouth, J.L. Hedrick, J.E. Rice, *J. Am. Chem. Soc.* **2008**, *130*, 6749-6754; d) M.K. Kiesewetter, M.D. Scholten, N. Kirn, R.L. Weber, J.L. Hedrick, R.M. Waymouth, *J. Org. Chem.* **2009**, *74*, 9490-9496.

[177] M.P. Coles, *Chem. Commun.* **2009**, 3659-3676.

[178] H.W. Horn, G.O. Jones, D.S. Wei, K. Fukushima, J.M. Lecuyer, D.J. Coady, J.L. Hedrick, J.E. Rice, *J. Phys. Chem. A* **2012**, *116*, 12389-12398.

[179] A.F. McKay, M.E. Kreling, *Can. J. Chem.* **1962**, *40*, 1160-1163.

[180] B. Maji, D.S. Stephenson, H. Mayr, *ChemCatChem* **2012**, *4*, 993-999.

[181] M. Baidya, F. Brotzel, H. Mayr, *Org. Biomol. Chem.* **2010**, *8*, 1929-1935.

[182] B. Maji, M. Baidya, J. Ammer, S. Kobayashi, P. Mayer, A.R. Ofial, H. Mayr, *Eur. J. Org. Chem.* **2013**, *2013*, 3369-3377.

[183] J.M. Becker, S. Tempelaar, M.J. Stanford, R.J. Pounder, J.A. Covington, A.P. Dove, *Chem. Eur. J,* **2010**, *16*, 6099-6105.

[184] P. Viehmann, PhD thesis, Humboldt-Universität zu Berlin (Berlin), **2014**.

[185] a) I. Leito, T. Rodima, I.A. Koppel, R. Schwesinger, V.M. Vlasov, *J. Org. Chem.* **1997**, *62*, 8479-8483; b) I. Kaljurand, A. Kuett, L. Soovaeli, T. Rodima, V. Maeemets, I. Leito, I.A. Koppel, *J. Org. Chem.* **2005**, *70*, 1019-1028.

[186] J. Massaad, J.-C. Micheau, C. Coudret, R. Sanchez, G. Guirado, S. Delbaere, *Chem. Eur. J,* **2012**, *18*, 6568-6575.

[187] Maike V. Peters, Ragnar S. Stoll, A. Kühn, S. Hecht, *Angew. Chem. Int. Ed.* **2008**, *47*, 5968-5972.

[188] R.A. Kunetskiy, S.M. Polyakova, J. Vavřík, I. Císařová, J. Saame, E.R. Nerut, I. Koppel, I.A. Koppel, A. Kütt, I. Leito, I.M. Lyapkalo, *Chem. Eur. J,* **2012**, *18*, 3621-3630.

[189] F.A. Luzzio, *Tetrahedron* **2001**, *57*, 915-945.

[190] J.M. Bell, D.G. Kubler, P. Sartwell, R.G. Zepp, *J. Org. Chem.* **1965**, *30*, 4284-4292.

[191] a) B. Linton, A.D. Hamilton, *Tetrahedron* **1999**, *55*, 6027-6038; b) G. Müller, J. Riede, F.P. Schmidtchen, *Angew. Chem. Int. Ed.* **1988**, *27*, 1516-1518.

[192] M.J.T. Frisch, G. W.; Schlegel, H. B.; Scuseria, G. E.; Robb, M. A.; Cheeseman, J. R.; Scalmani, G.; Barone, V.; Mennucci, B.; Petersson, G. A.; Nakatsuji, H.; Caricato, M.; Li, X.; Hratchian, H. P.; Izmaylov, A. F.; Bloino, J.; Zheng, G.; Sonnenberg, J. L.; Hada, M.; Ehara, M.; Toyota, K.; Fukuda, R.; Hasegawa, J.; Ishida, M.; Nakajima, T.; Honda, Y.; Kitao, O.; Nakai, H.; Vreven, T.; Montgomery, Jr., J. A.; Peralta, J. E.; Ogliaro, F.; Bearpark, M.; Heyd, J. J.; Brothers, E.; Kudin, K. N.; Staroverov, V. N.; Kobayashi, R.; Normand, J.; Raghavachari, K.; Rendell, A.; Burant, J. C.; Iyengar, S. S.; Tomasi, J.; Cossi, M.; Rega, N.; Millam, J. M.; Klene, M.; Knox, J. E.; Cross, J. B.; Bakken, V.; Adamo, C.; Jaramillo, J.; Gomperts, R.; Stratmann, R. E.; Yazyev, O.; Austin, A. J.; Cammi, R.; Pomelli, C.; Ochterski, J. W.; Martin, R. L.; Morokuma, K.; Zakrzewski, V. G.; Voth, G. A.; Salvador, P.; Dannenberg, J. J.; Dapprich, S.; Daniels, A. D.; Farkas, Ö.; Foresman, J. B.; Ortiz, J. V.; Cioslowski, J.; Fox, D. J. , *Gaussian 09 Rev. A.02, Gaussian Inc.*, Wallingford CT, **2009**.

[193] M. Herder, B.M. Schmidt, L. Grubert, M. Pätzel, J. Schwarz, S. Hecht, *J. Am. Chem. Soc.* **2015**, *137*, 2738-2747.

[194] K. Voigt, P. von Zezschwitz, K. Rosauer, A. Lansky, A. Adams, O. Reiser, A. de Meijere, *Eur. J. Org. Chem.* **1998**, *1998*, 1521-1534.

[195] M. Dubernet, V. Caubert, J. Guillard, M.-C. Viaud-Massuard, *Tetrahedron* **2005**, *61*, 4585-4593.

[196] B.C.D. Salert, A. Wedel, L. Grubert, T. Eberle, R. Anémian, H. Krueger, *Adv. Mater. Sci. Eng.* **2012**, *2012*, 15.

[197] H.A. Davis, R.K. Brown, *Can. J. Chem.* **1971**, *49*, 2321-2335.

[198] H. Hartmann, I. Reuther, *J. Prakt. Chem.* **1973**, *315*, 144-148.

[199] S. Pu, C. Fan, W. Miao, G. Liu, *Dyes and Pigments* **2010**, *84*, 25-35.

[200] K.E. Stensiö, K. Wahlberg, R. Wahren, *Acta Chem. Scand.* **1973**, *27*, 2179.

[201] J.W. Chung, S.-J. Yoon, S.-J. Lim, B.-K. An, S.Y. Park, *Angew. Chem. Int. Ed.* **2009**, *48*, 7030-7034.

[202] P.D. Bartlett, M. Roha, R.M. Stiles, *J. Am. Chem. Soc.* **1954**, *76*, 2349-2353.

[203] J. Areephong, W.R. Browne, B.L. Feringa, *Org. Biomol. Chem.* **2007**, *5*, 1170-1174.

[204] P.-E. Broutin, I. Čerňa, M. Campaniello, F. Leroux, F. Colobert, *Org. Lett.* **2004**, *6*, 4419-4422.

[205] a) B. Iddon, B.L. Lim, *J. Chem. Soc., Perkin Trans. 1* **1983**, 735-739; b) H. Aissaoui, C. Boss, M. Gude, R. Koberstein, T. Sifferlen (Actelion Pharmaceuticals Ltd., Switz.), WO2008078291A1, **2008**.

[206] A. Klapars, J.C. Antilla, X. Huang, S.L. Buchwald, *J. Am. Chem. Soc.* **2001**, *123*, 7727-7729.

[207] H. Grube, H. Suhr, *Chem. Ber.* **1969**, *102*, 1570-1579.

[208] S.L. McDonald, C.E. Hendrick, Q. Wang, *Angew. Chem. Int. Ed.* **2014**, *53*, 4667-4670.

[209] J. Bödeker, S. Hauser, U. Selle, H. Köppel, *J. Prakt. Chem.* **1974**, *316*, 881-885.

[210] H. Erlenmeyer, C. Becker, E. Sorkin, H. Bloch, E. Suter, *Helv. Chim. Acta* **1947**, *30*, 2058-2062.

[211] R. Saijo, K.-I. Kurihara, M. Kawase, *Heterocycles* **2013**, *87*, 2533 - 2553.

[212] M. Begtrup, L.B.L. Hansen, *Acta Chem. Scand.* **1992**, *46*, 372-383.

[213] K. Mouri, S. Saito, S. Yamaguchi, *Angew. Chem. Int. Ed.* **2012**, *51*, 5971-5975.

[214] A.F. Littke, C. Dai, G.C. Fu, *J. Am. Chem. Soc.* **2000**, *122*, 4020-4028.

[215] J. Kühni, V. Adamo, P. Belser, *Synthesis* **2006**, *2006*, 1946-1948.

8. Appendix

8.1 Appendix 1: NMR spectroscopic characterization of by-products

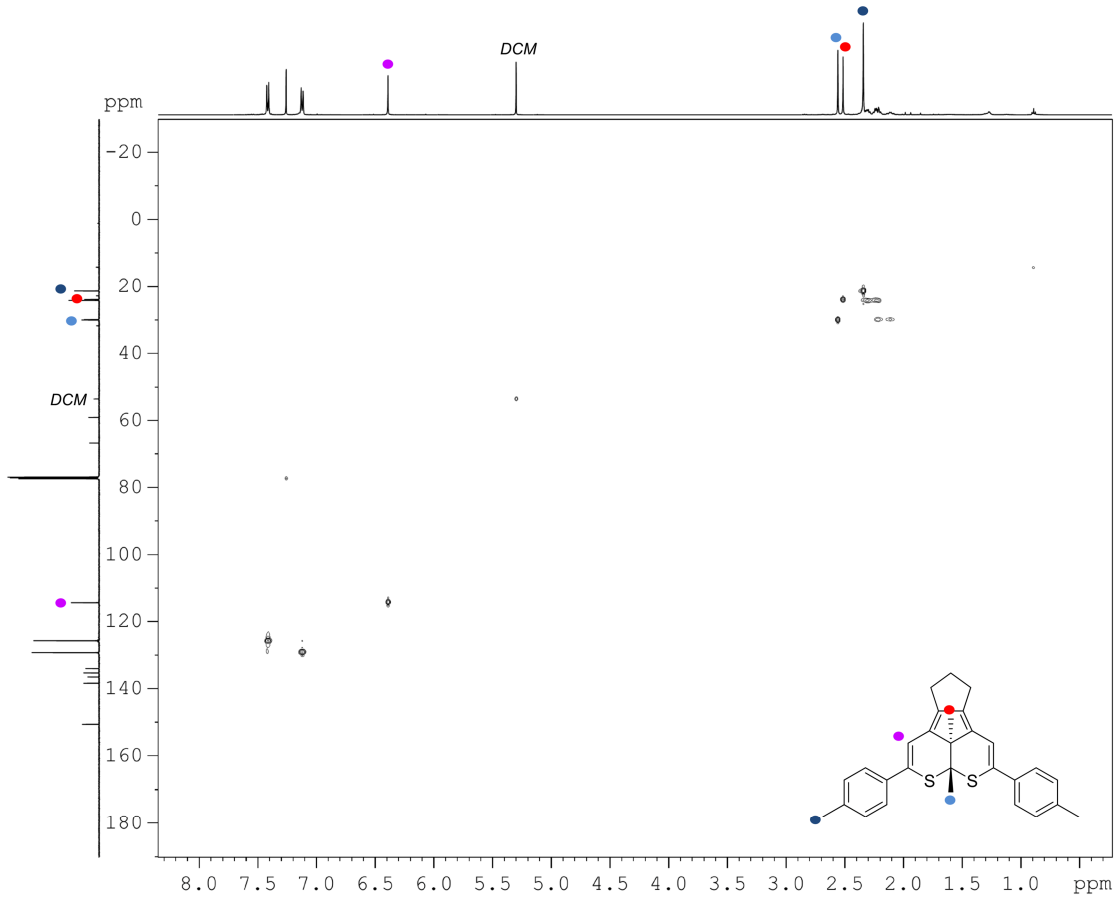

Figure A1-1. $^{1}H,^{13}C$-HSQC ($CDCl_3$, 500 MHz/126 MHz) of **1c(bp)**. Colored labels visualize correlated signals in the one-dimensional ^{1}H-NMR and ^{13}C-NMR spectra, respectively.

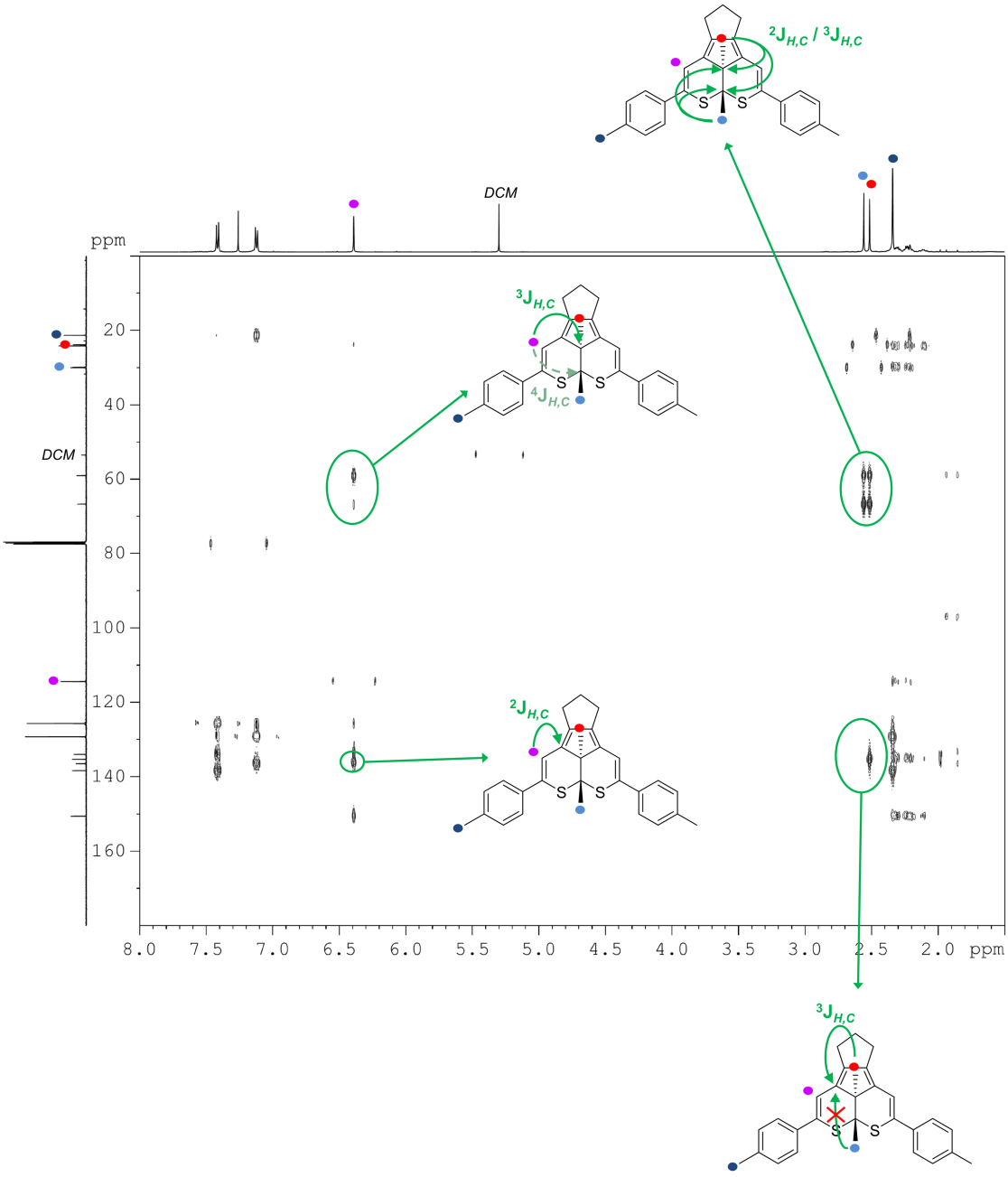

Figure A1-2. ^{1}H,^{13}C-HMBC ($CDCl_3$, 500 MHz/126 MHz) of **1c(bp)**. Colored labels visualize correlated signals in the one-dimensional ^{1}H-NMR and ^{13}C-NMR spectra, respectively. For selected signals the corresponding long-range couplings are shown.

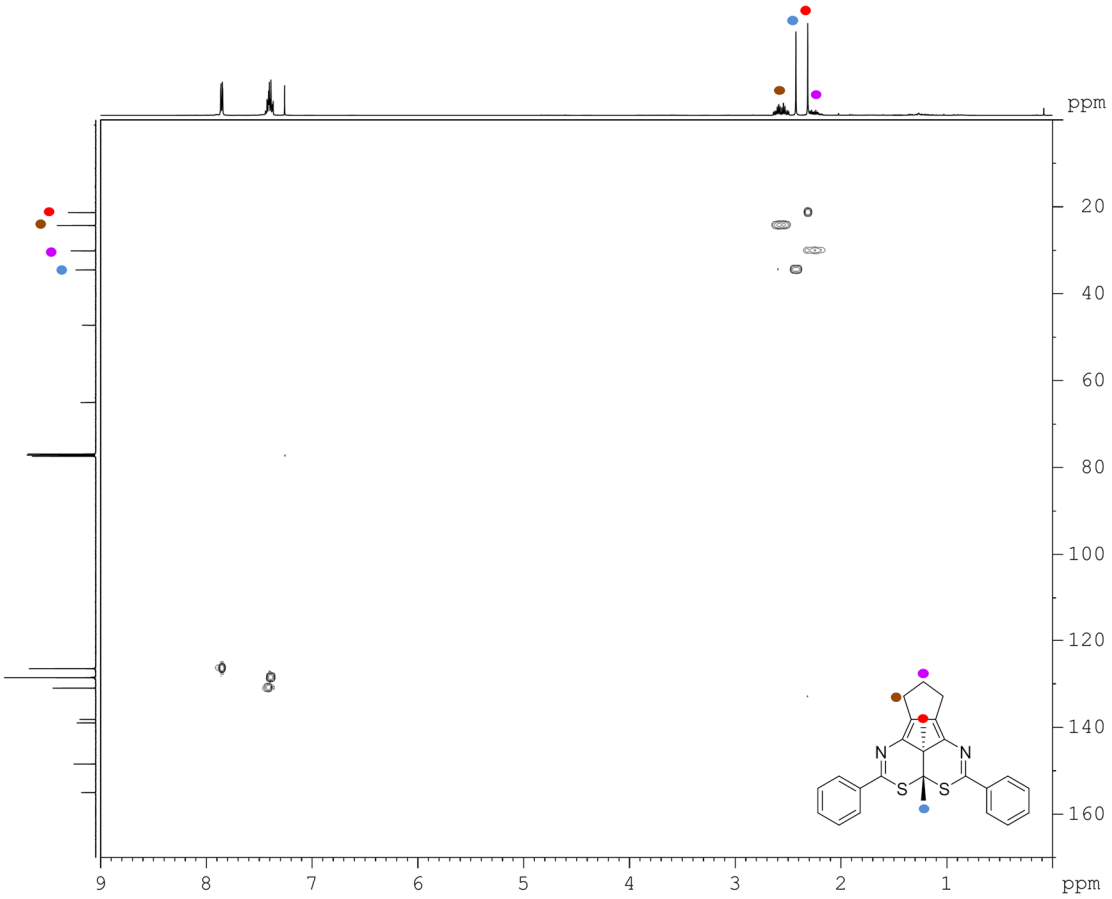

Figure A1-3. $^{1}H,^{13}C$-HSQC ($CDCl_3$, 500 MHz/126 MHz) of **3d(bp)**. Colored labels visualize correlated signals in the one-dimensional ^{1}H-NMR and ^{13}C-NMR spectra, respectively.

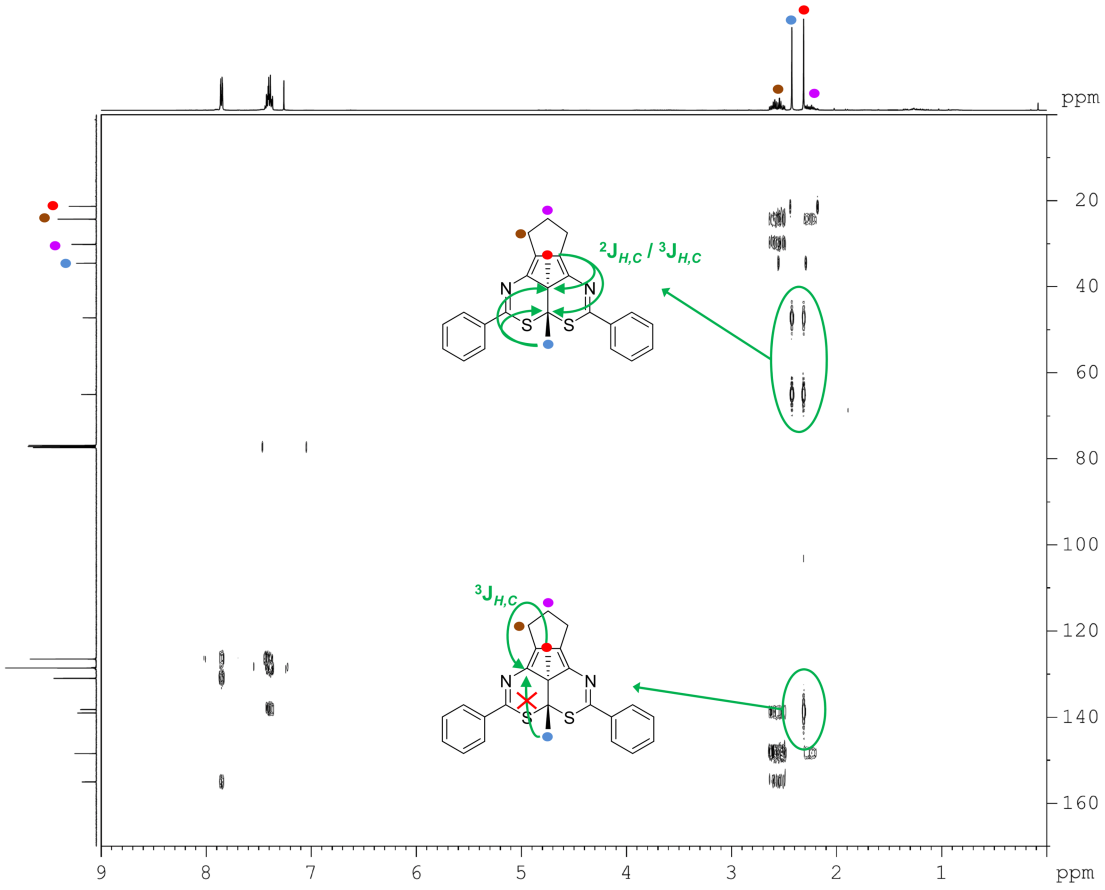

Figure A1-4. ^{1}H,^{13}C-HMBC ($CDCl_3$, 500 MHz/126 MHz) of **3d(bp)**. Colored labels visualize correlated signals in the one-dimensional ^{1}H-NMR and ^{13}C-NMR spectra, respectively. For selected signals the corresponding long-range couplings are shown.

8.2 Appendix 2: UV/Vis spectra of diarylethenes in acetonitrile

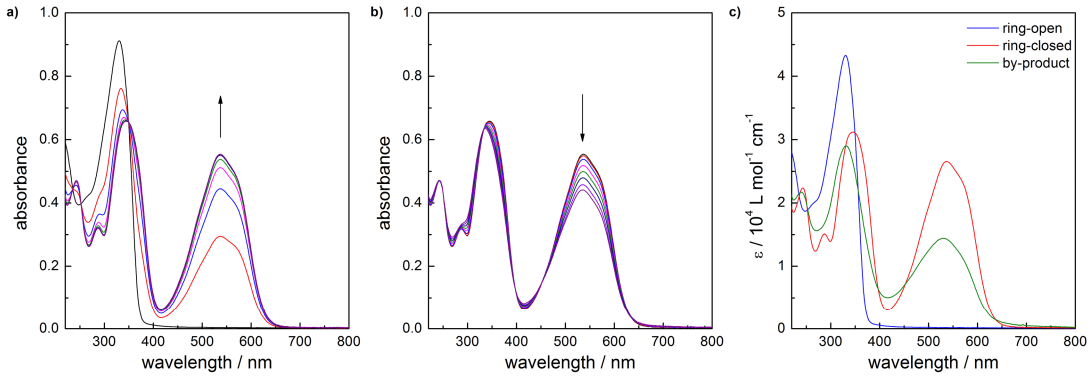

Figure A2-1. UV/Vis spectra of compound **1a** (acetonitrile, $2.11 \cdot 10^{-5}$ M, 25 °C): a) under irradiation with 310 nm light until reaching the PSS, b) under prolonged irradiation with 310 nm light, c) calculated spectra of the pure isomers.

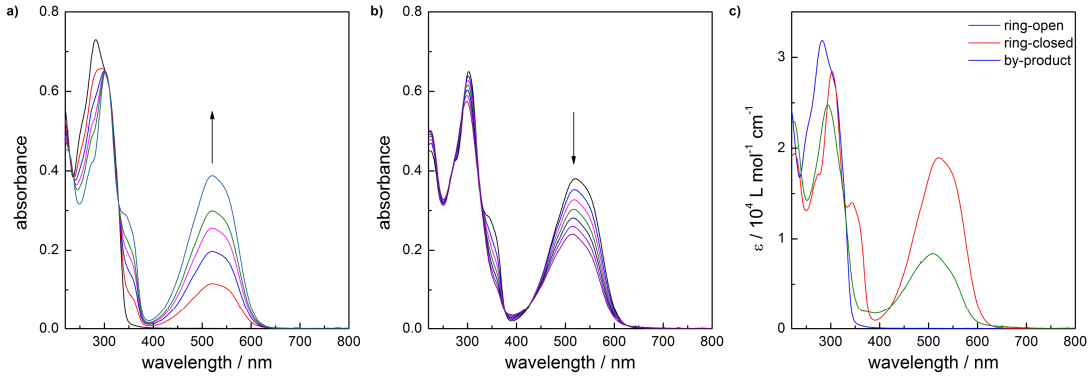

Figure A2-2. UV/Vis spectra of compound **1b** (acetonitrile, $2.29 \cdot 10^{-5}$ M, 25 °C): a) under irradiation with 310 nm light until reaching the PSS, b) under prolonged irradiation with 310 nm light, c) calculated spectra of the pure isomers.

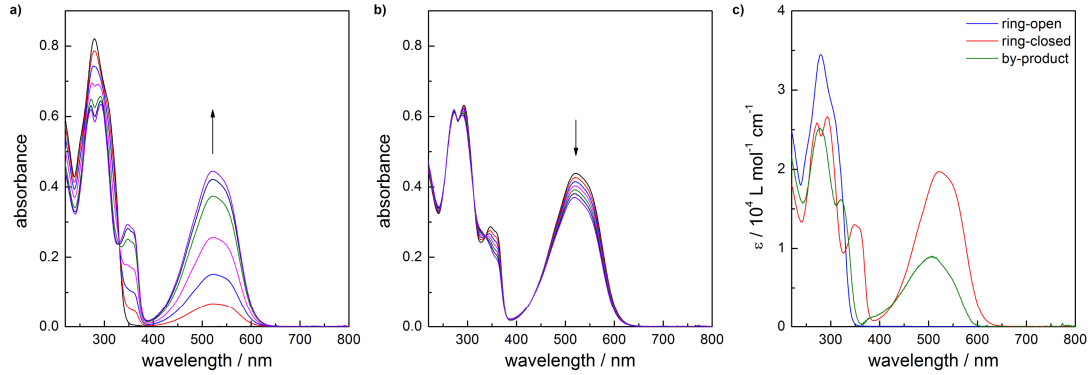

Figure A2-3. UV/Vis spectra of compound **1c** (acetonitrile, $2.38 \cdot 10^{-5}$ M, 25 °C): a) under irradiation with 310 nm light until reaching the PSS, b) under prolonged irradiation with 310 nm light, c) calculated spectra of the pure isomers.

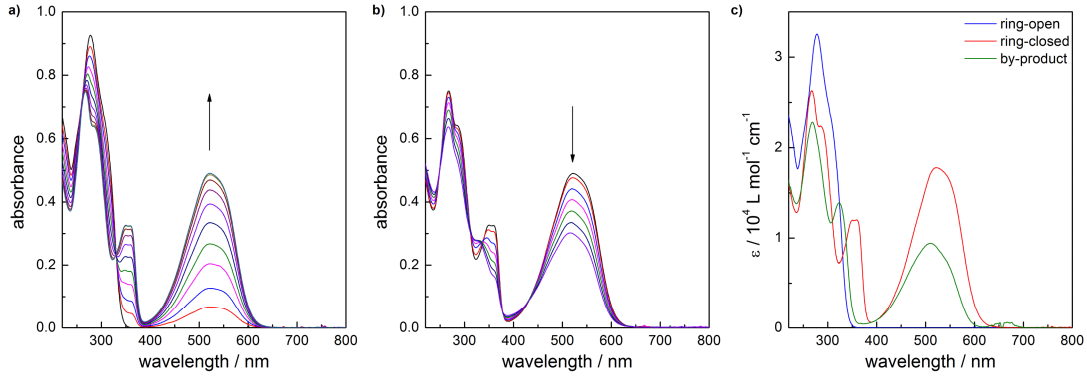

Figure A2-4. UV/Vis spectra of compound **1d** (acetonitrile, $2.85 \cdot 10^{-5}$ M, 25 °C): a) under irradiation with 310 nm light until reaching the PSS, b) under prolonged irradiation with 310 nm light, c) calculated spectra of the pure isomers.

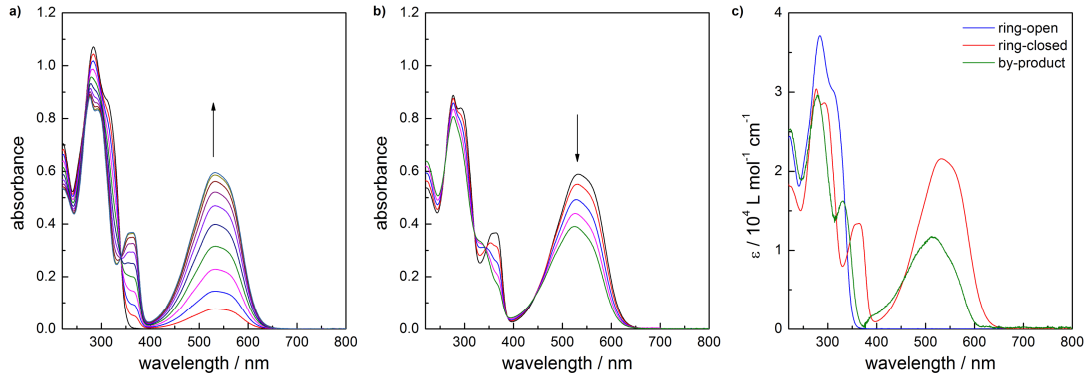

Figure A2-5. UV/Vis spectra of compound **1e** (acetonitrile, $2.89 \cdot 10^{-5}$ M, 25 °C): a) under irradiation with 310 nm light until reaching the PSS, b) under prolonged irradiation with 310 nm light, c) calculated spectra of the pure isomers.

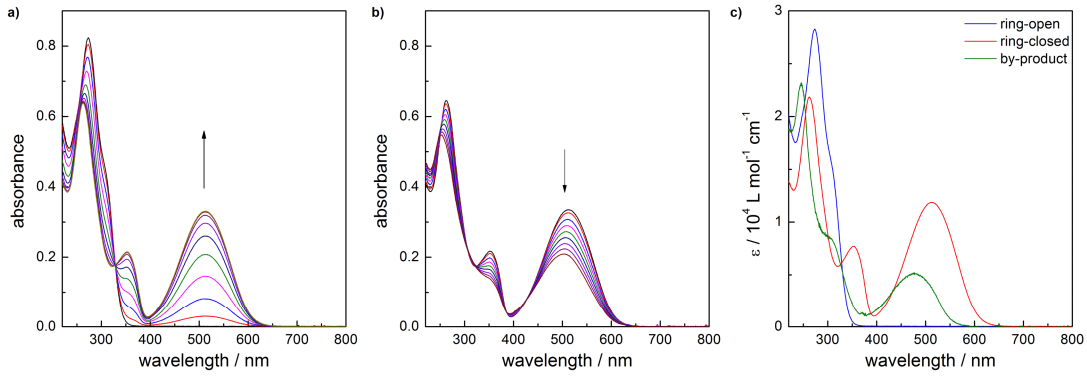

Figure A2-6. UV/Vis spectra of compound **1f** (acetonitrile, $2.91 \cdot 10^{-5}$ M, 25 °C): a) under irradiation with 310 nm light until reaching the PSS, b) under prolonged irradiation with 310 nm light, c) calculated spectra of the pure isomers.

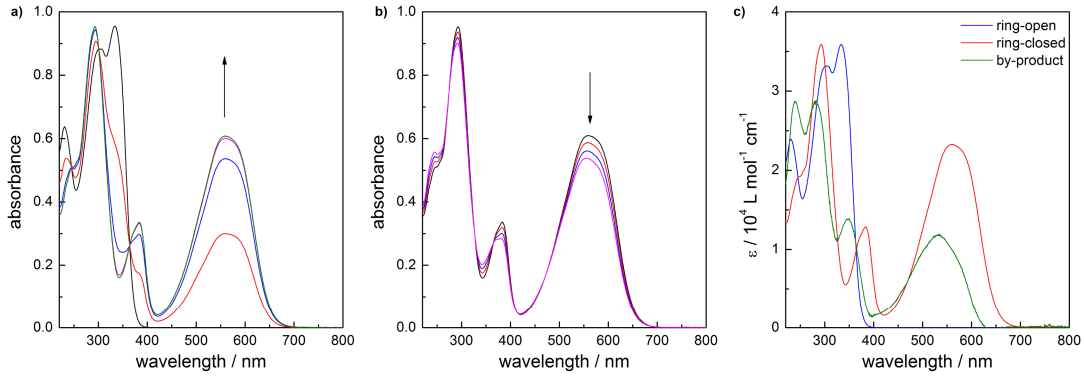

Figure A2-7. UV/Vis spectra of compound **1g** (acetonitrile, $2.66 \cdot 10^{-5}$ M, 25 °C): a) under irradiation with 310 nm light until reaching the PSS, b) under prolonged irradiation with 310 nm light, c) calculated spectra of the pure isomers.

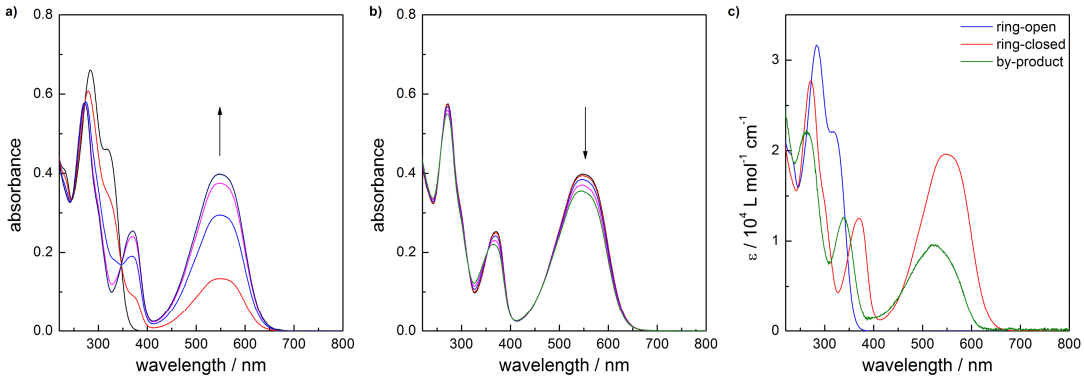

Figure A2-8. UV/Vis spectra of compound **1i** (acetonitrile, $2.09 \cdot 10^{-5}$ M, 25 °C): a) under irradiation with 310 nm light until reaching the PSS, b) under prolonged irradiation with 310 nm light, c) calculated spectra of the pure isomers.

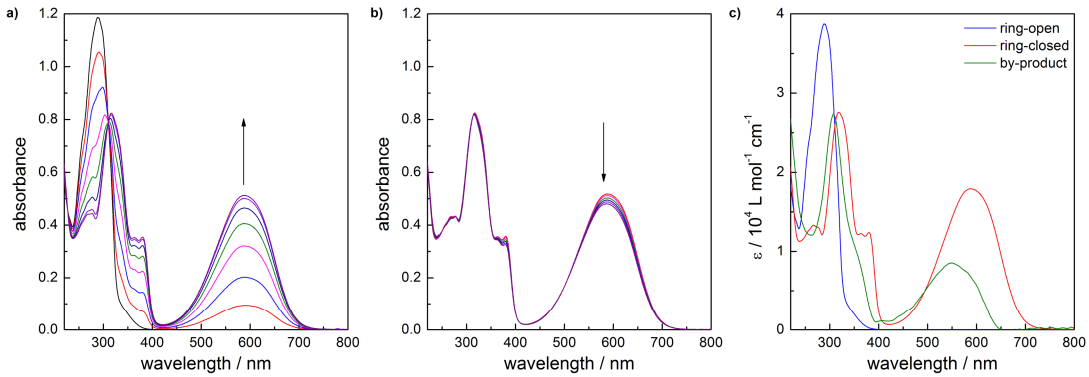

Figure A2-9. UV/Vis spectra of compound **2c** (acetonitrile, $3.06 \cdot 10^{-5}$ M, 25 °C): a) under irradiation with 310 nm light until reaching the PSS, b) under prolonged irradiation with 310 nm light, c) calculated spectra of the pure isomers.

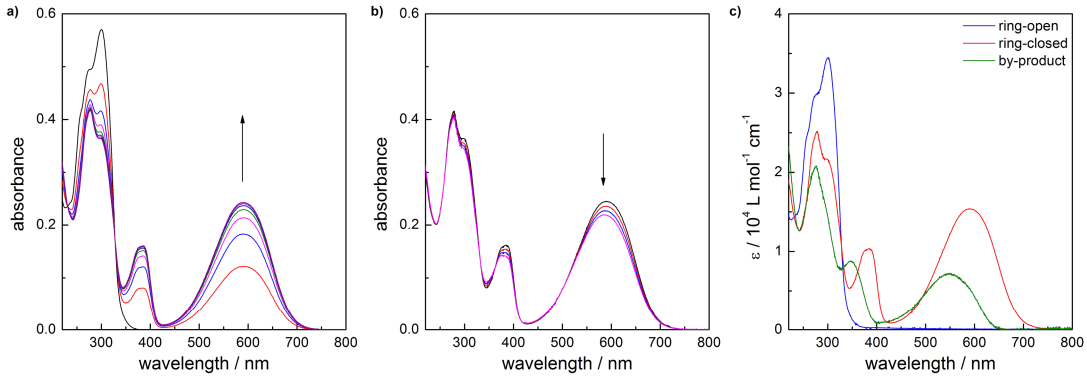

Figure A2-10. UV/Vis spectra of compound **2i** (acetonitrile, $1.68 \cdot 10^{-5}$ M, 25 °C): a) under irradiation with 310 nm light until reaching the PSS, b) under prolonged irradiation with 310 nm light, c) calculated spectra of the pure isomers.

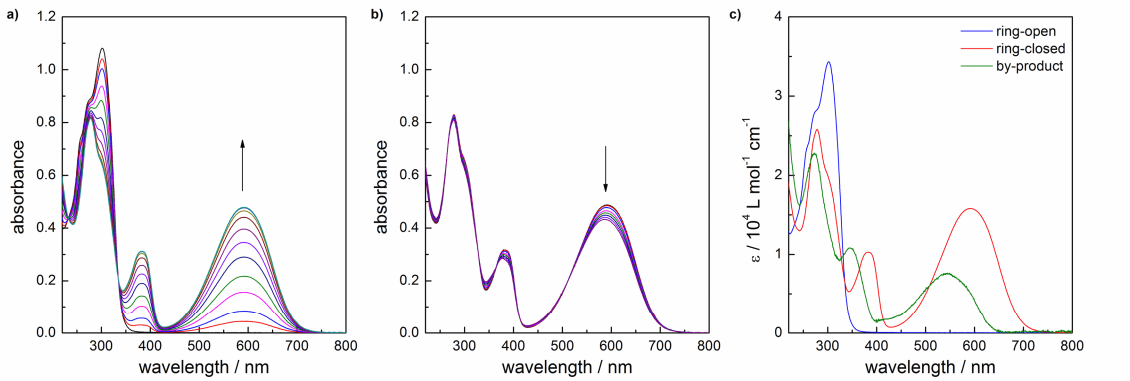

Figure A2-11. UV/Vis spectra of compound **2j** (acetonitrile, $3.15 \cdot 10^{-5}$ M, 25 °C): a) under irradiation with 310 nm light until reaching the PSS, b) under prolonged irradiation with 310 nm light, c) calculated spectra of the pure isomers.

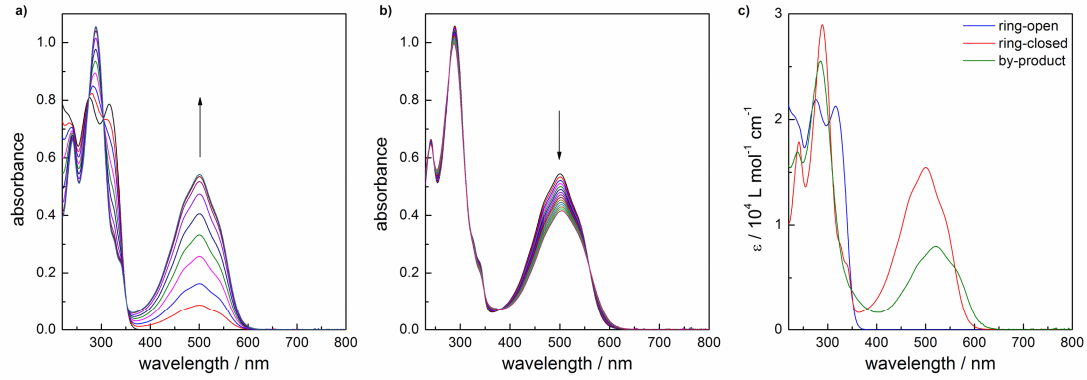

Figure A2-12. UV/Vis spectra of compound **3d** (acetonitrile, $3.70 \cdot 10^{-5}$ M, 25 °C): a) under irradiation with 310 nm light until reaching the PSS, b) under prolonged irradiation with 310 nm light, c) calculated spectra of the pure isomers.

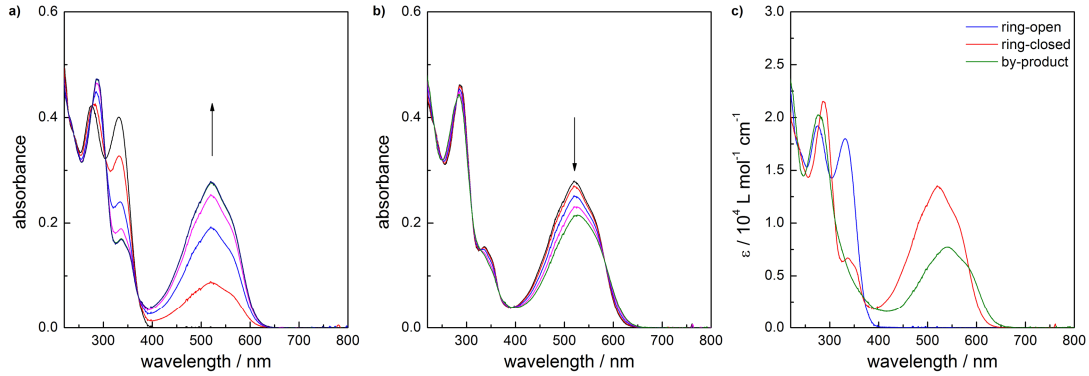

Figure A2-13. UV/Vis spectra of compound **3i** (acetonitrile, $2.16 \cdot 10^{-5}$ M, 25 °C): a) under irradiation with 310 nm light until reaching the PSS, b) under prolonged irradiation with 310 nm light, c) calculated spectra of the pure isomers.

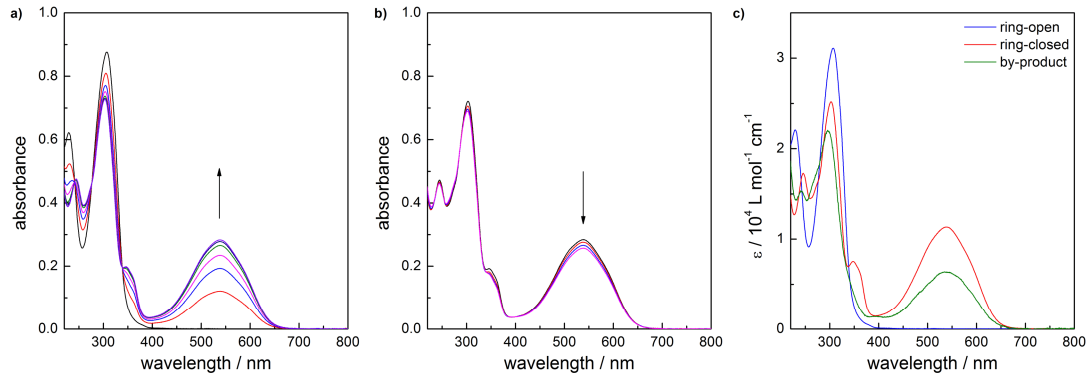

Figure A2-14. UV/Vis spectra of compound **4i** (acetonitrile, $2.82 \cdot 10^{-5}$ M, 25 °C): a) under irradiation with 310 nm light until reaching the PSS, b) under prolonged irradiation with 310 nm light, c) calculated spectra of the pure isomers.

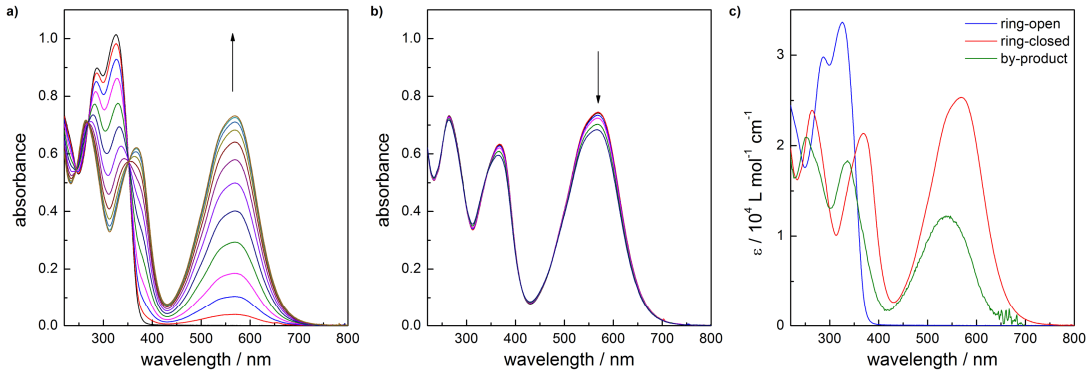

Figure A2-15. UV/Vis spectra of compound **5a** (acetonitrile, $3.02 \cdot 10^{-5}$ M, 25 °C): a) under irradiation with 310 nm light until reaching the PSS, b) under prolonged irradiation with 310 nm light, c) calculated spectra of the pure isomers.

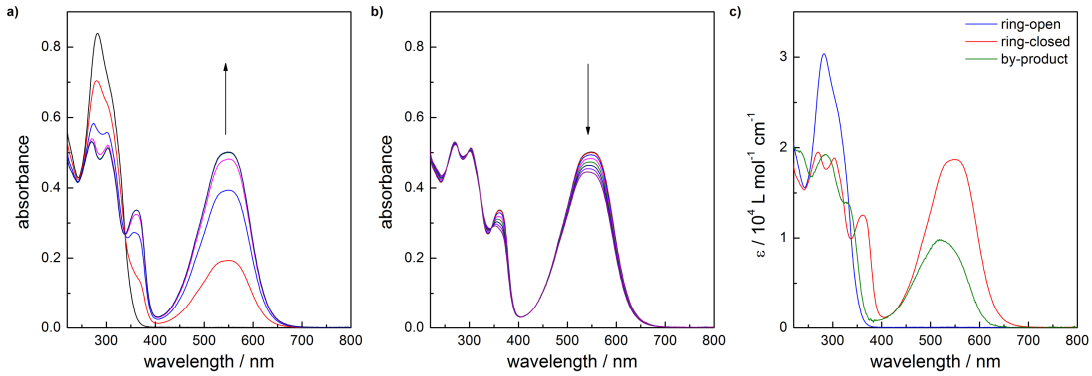

Figure A2-16. UV/Vis spectra of compound **5b** (acetonitrile, $2.71 \cdot 10^{-5}$ M, 25 °C): a) under irradiation with 310 nm light until reaching the PSS, b) under prolonged irradiation with 310 nm light, c) calculated spectra of the pure isomers.

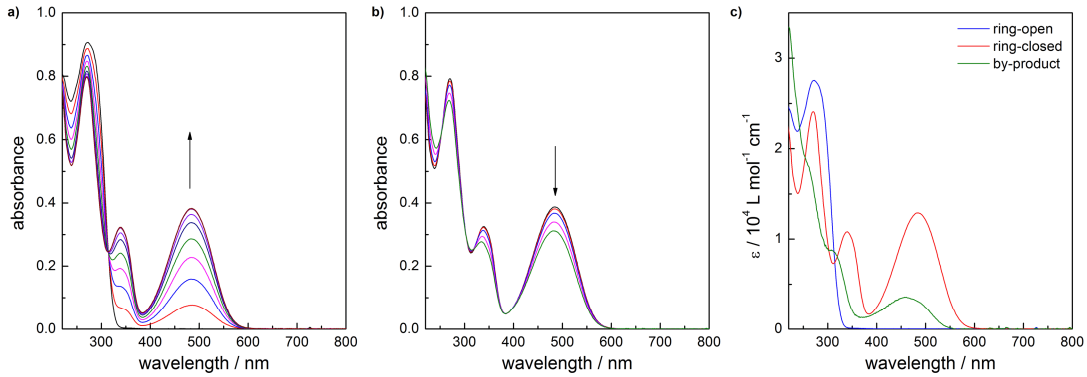

Figure A2-17. UV/Vis spectra of compound **6c** (acetonitrile, $3.18 \cdot 10^{-5}$ M, 25 °C): a) under irradiation with 310 nm light until reaching the PSS, b) under prolonged irradiation with 310 nm light, c) calculated spectra of the pure isomers.

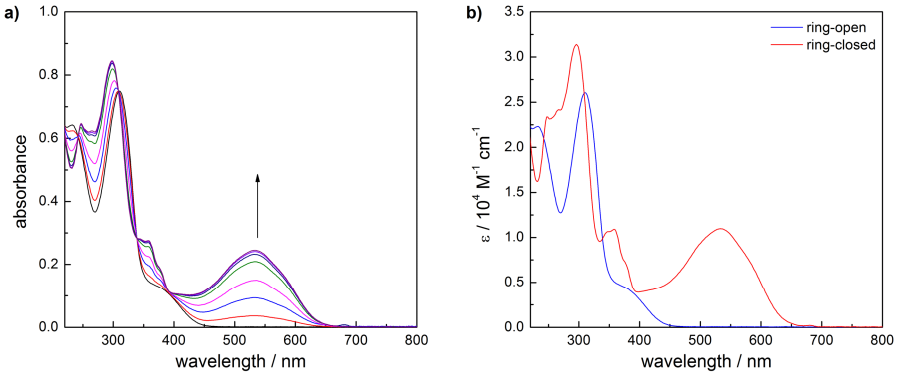

Figure A2-18. UV/Vis spectra of compound **7i** (acetonitrile, $2.88 \cdot 10^{-5}$ M, 25 °C): a) under irradiation with 310 nm light until reaching the PSS, b) calculated spectra of the pure isomers.

8.3 Appendix 3: Vertical transitions of 1c and 3d obtained from TD-DFT

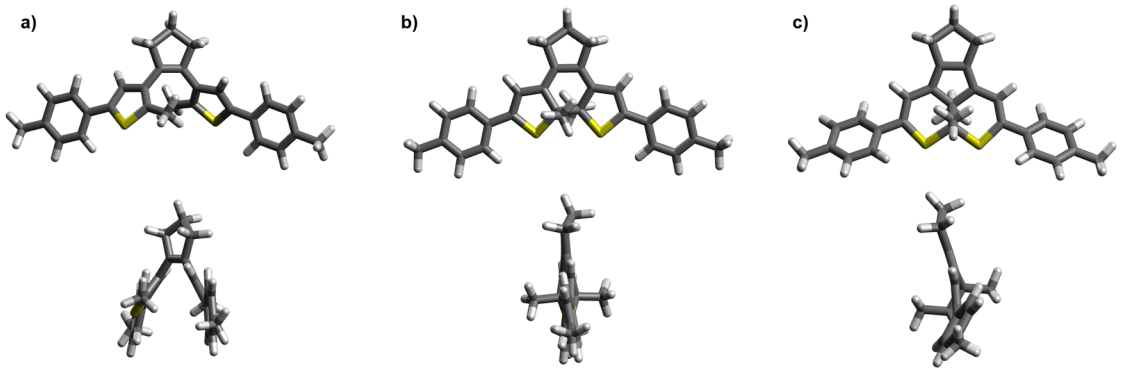

Figure A3-1. Structure of all three isomers of **1c** optimized on the B3LYP/PCM(acetonitrile)/ 6-311G(d,p) level of theory (top: font view, bottom: side view): a) ring-open isomer, b) ring-closed isomer, c) by-product.

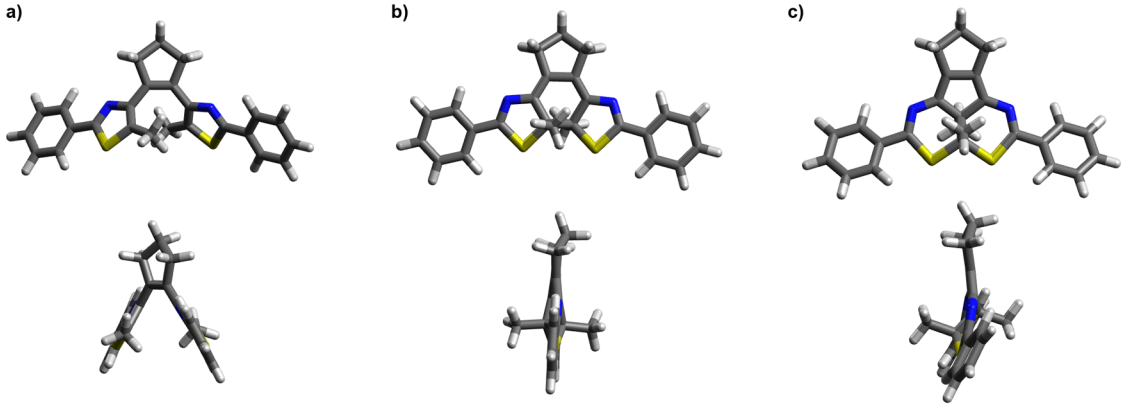

Figure A3-2. Structure of all three isomers of **3d** optimized on the B3LYP/PCM(acetonitrile)/ 6-311G(d,p) level of theory (top: font view, bottom: side view): a) ring-open isomer, b) ring-closed isomer, c) by-product.

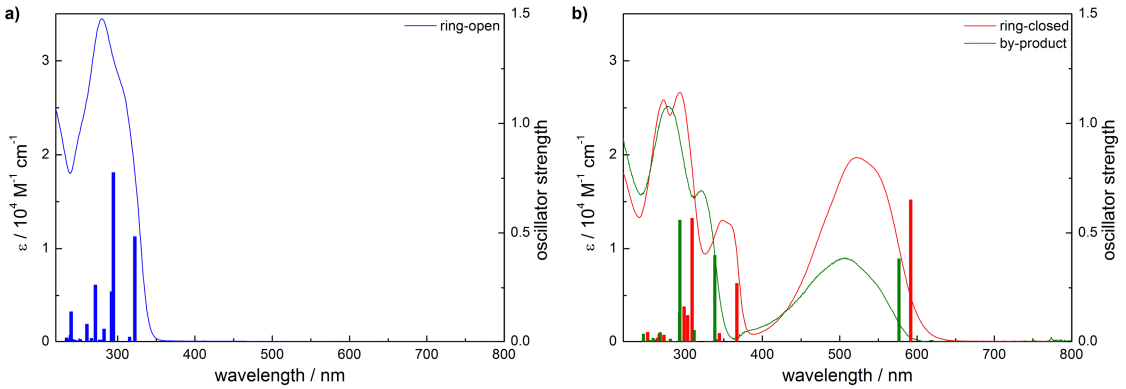

Figure A3-3. Experimental UV/Vis spectra of **1c** (acetonitrile, 25 °C) and vertical transitions computed on the PBE0/PCM(acetonitrile)/6-311+G(2d,p) level of theory: a) ring-open isomer, b) ring-closed isomer and by-product.

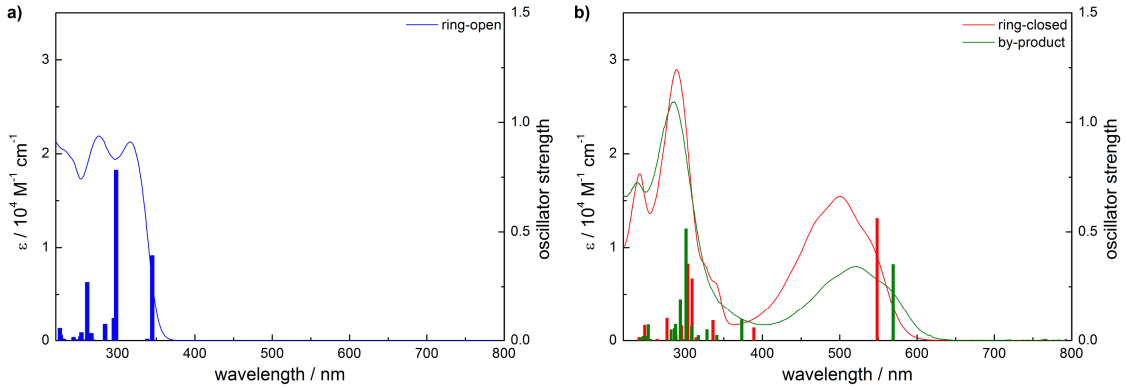

Figure A3-4. Experimental UV/Vis spectra of **3d** (acetonitrile, 25 °C) and vertical transitions computed on the PBE0/PCM(acetonitrile)/6-311+G(2d,p) level of theory: a) ring-open isomer, b) ring-closed isomer and by-product.

Table A3-1. Calculated wavelengths λ and oscillator strengths f of selected intense transitions ($f > 0.1$) of compounds **1c** and **3d**.

	CAM-B3LYP/ PCM(acetonitrile)/ 6-311+G(2d,p)		**PBE0/ PCM(acetonitrile)/ 6-311+G(2d,p)**	
	λ [nm]	**f**	**λ [nm]**	**f**
1c(o)	294.5	0.98	320.9	0.48
	264.9	0.79	293.5	0.78
	233.8	0.10	291.1	0.23
	225.9	0.17	270.6	0.26
			239.6	0.14
1c(c)	523.9	0.65	587.2	0.65
	333.5	0.40	365.0	0.27
	268.7	0.75	307.8	0.57
	261.6	0.13	302.0	0.12
	237.9	0.10	297.6	0.16
1c(bp)	512.5	0.37	572.1	0.38
	306.9	0.55	336.8	0.40
	271.8	0.12	292.2	0.56
	258.6	0.15	291.7	0.13
	253.5	0.57		
3d(o)	307.5	0.79	343.1	0.39
	266.4	0.72	297.0	0.78
	221.2	0.11	294.1	0.10
	213.5	0.13	260.0	0.27
	212.8	0.11		
3d(c)	481.0	0.58	544.1	0.56
	328.4	0.17	307.8	0.29
	272.6	0.50	302.3	0.35
	268.1	0.20	275.7	0.10
	260.7	0.12		
	231.1	0.19		
	228.8	0.11		
3d(bp)	504.6	0.35	564.7	0.35
	320.1	0.23	300.0	0.51
	265.3	0.69	292.8	0.19
	261.7	0.14		
	226.7	0.13		

8.4 Appendix 4: Cyclic voltammetry of DAEs

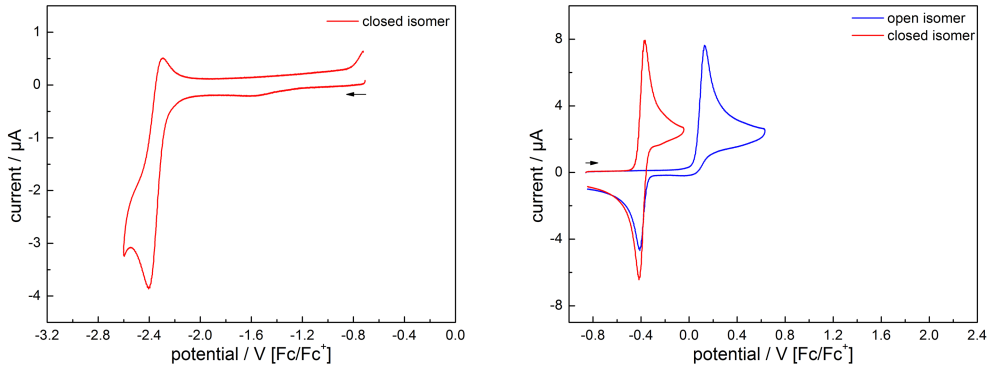

Figure A4-1. Cyclic voltammetry of **1a** (c = $1 \cdot 10^{-3}$ M) in acetonitrile / 0.1 M Bu_4NPF_6, dE/dt = 1 V s^{-1}.

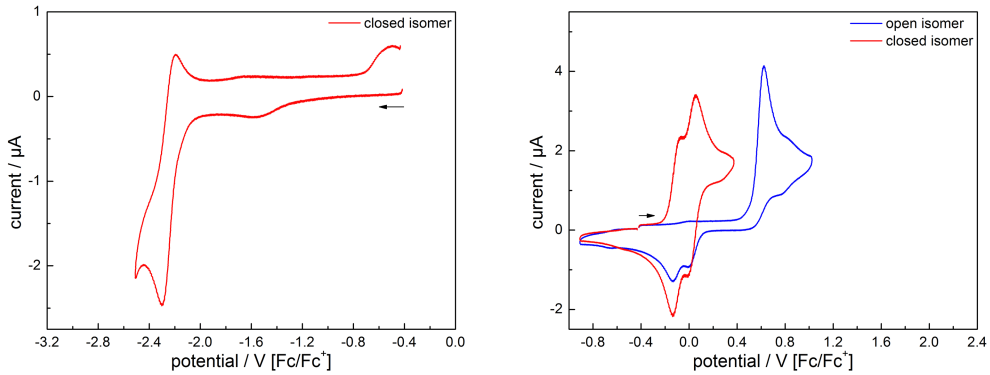

Figure A4-2. Cyclic voltammetry of **1b** (c = $1 \cdot 10^{-3}$ M) in acetonitrile / 0.1 M Bu_4NPF_6, dE/dt = 1 V s^{-1}.

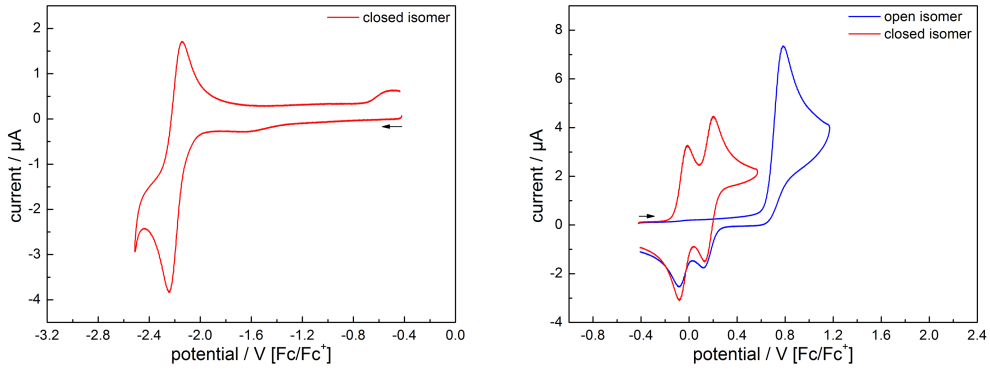

Figure A4-3. Cyclic voltammetry of **1c** (c = $1 \cdot 10^{-3}$ M) in acetonitrile / 0.1 M Bu_4NPF_6, dE/dt = 1 V s^{-1}.

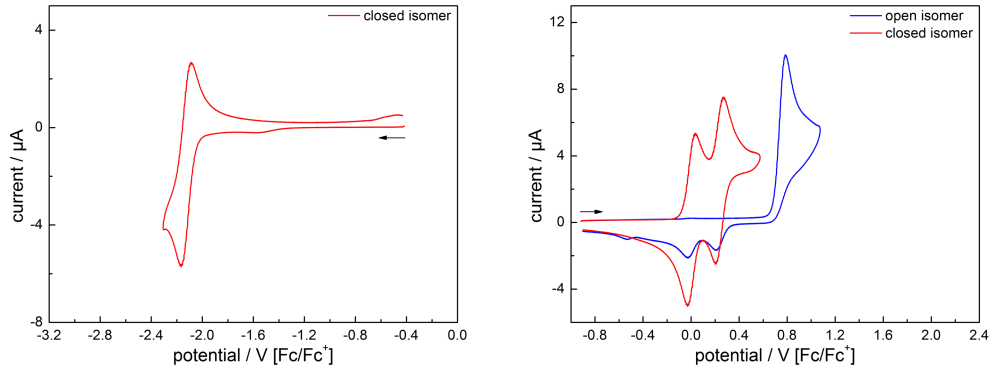

Figure A4-4. Cyclic voltammetry of **1d** (c = $1 \cdot 10^{-3}$ M) in acetonitrile / 0.1 M Bu_4NPF_6, dE/dt = 1 V s^{-1}.

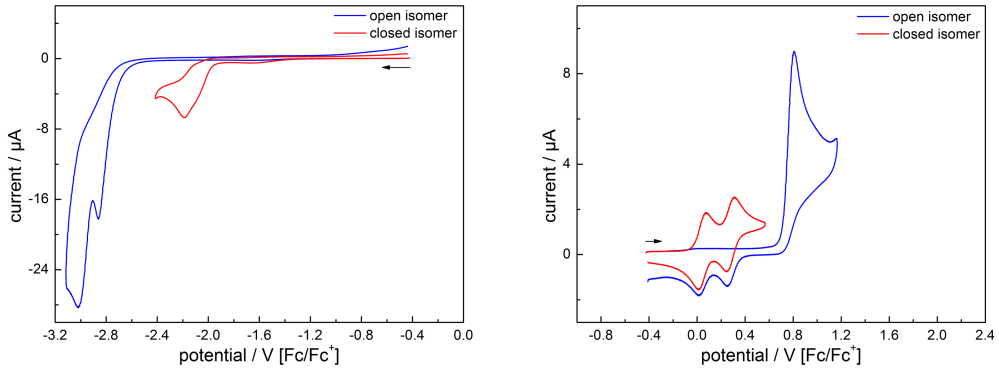

Figure A4-5. Cyclic voltammetry of **1e** (c = $1 \cdot 10^{-3}$ M) in acetonitrile / 0.1 M Bu_4NPF_6, dE/dt = 1 V s^{-1}.

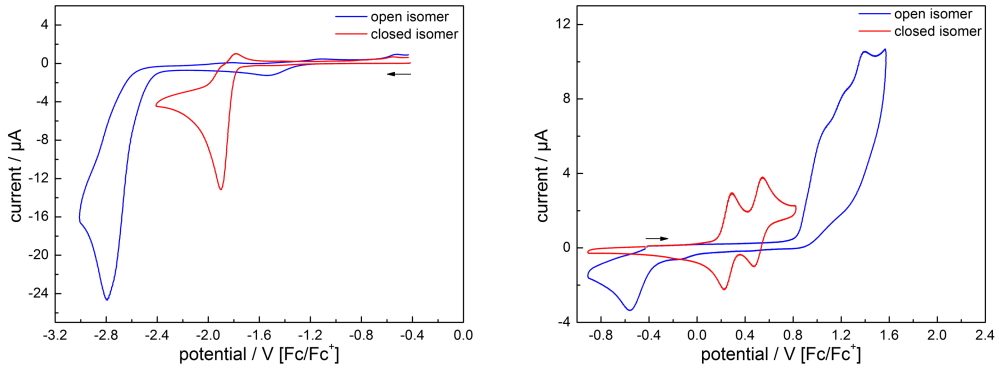

Figure A4-6. Cyclic voltammetry of **1f** (c = $1 \cdot 10^{-3}$ M) in acetonitrile / 0.1 M Bu_4NPF_6, dE/dt = 1 V s^{-1}.

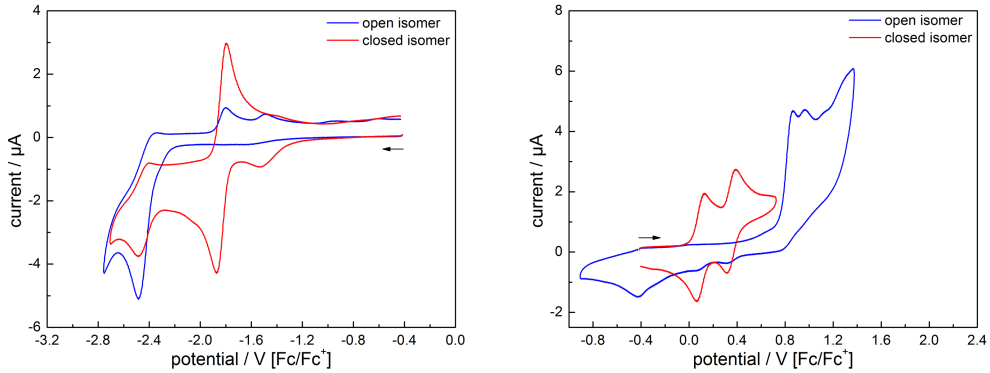

Figure A4-7. Cyclic voltammetry of **1g** (c = $1 \cdot 10^{-3}$ M) in acetonitrile / 0.1 M Bu_4NPF_6, dE/dt = 1 V s^{-1}.

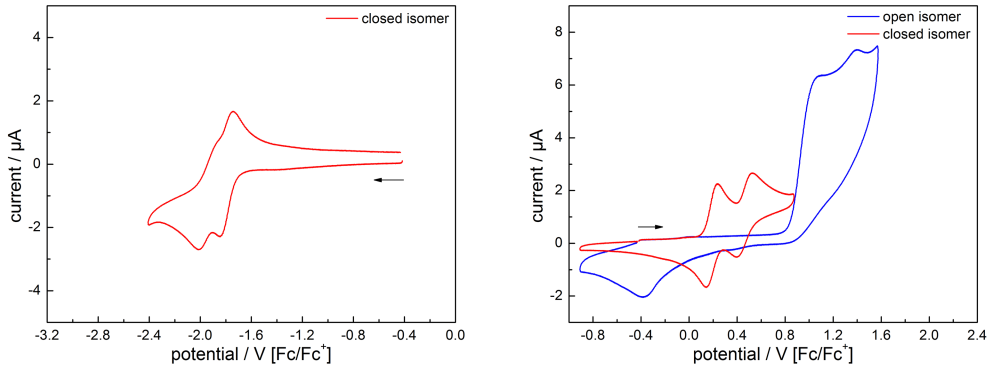

Figure A4-8. Cyclic voltammetry of **1i** (c = $1 \cdot 10^{-3}$ M) in acetonitrile / 0.1 M Bu_4NPF_6, dE/dt = 1 V s^{-1}.

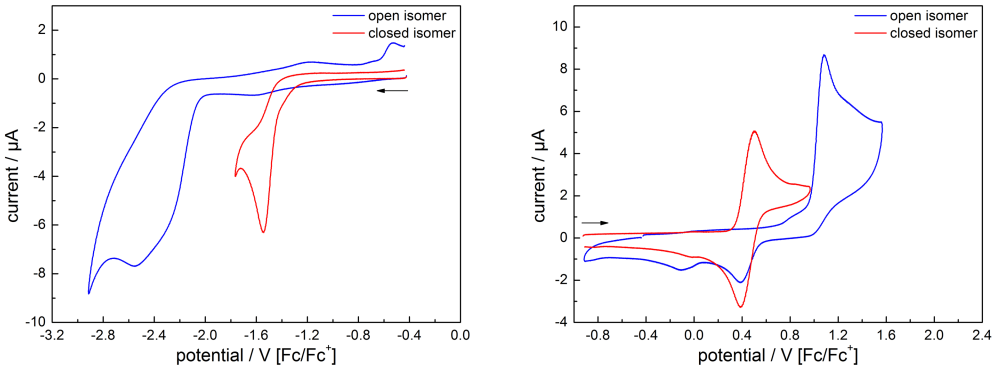

Figure A4-9. Cyclic voltammetry of **2c** (c = $1 \cdot 10^{-3}$ M) in acetonitrile / 0.1 M Bu_4NPF_6, dE/dt = 1 V s^{-1}.

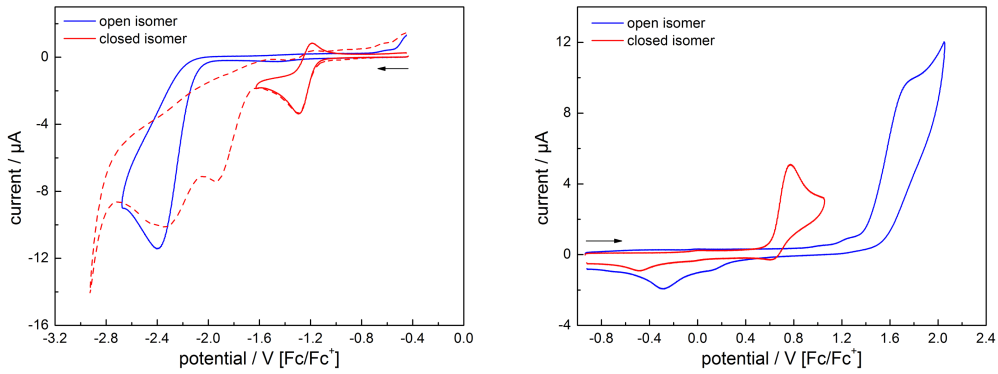

Figure A4-10. Cyclic voltammetry of **2i** (c = $1 \cdot 10^{-3}$ M) in acetonitrile / 0.1 M Bu_4NPF_6, dE/dt = 1 V s^{-1}.

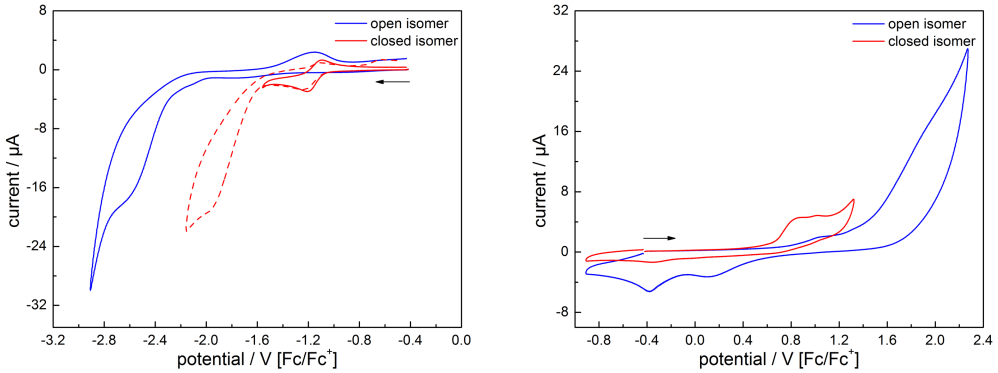

Figure A4-11. Cyclic voltammetry of **2j** (c = $1 \cdot 10^{-3}$ M) in acetonitrile / 0.1 M Bu_4NPF_6, dE/dt = 1 V s^{-1}.

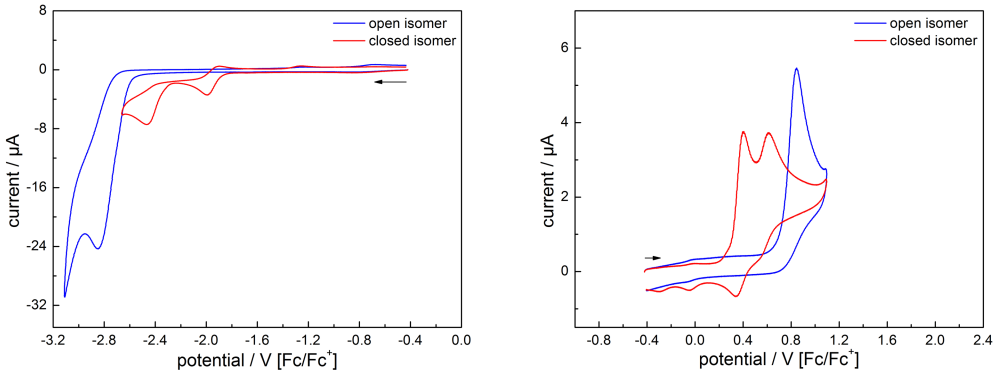

Figure A4-12. Cyclic voltammetry of **3d** (c = $1 \cdot 10^{-3}$ M) in acetonitrile / 0.1 M Bu_4NPF_6, dE/dt = 1 V s^{-1}.

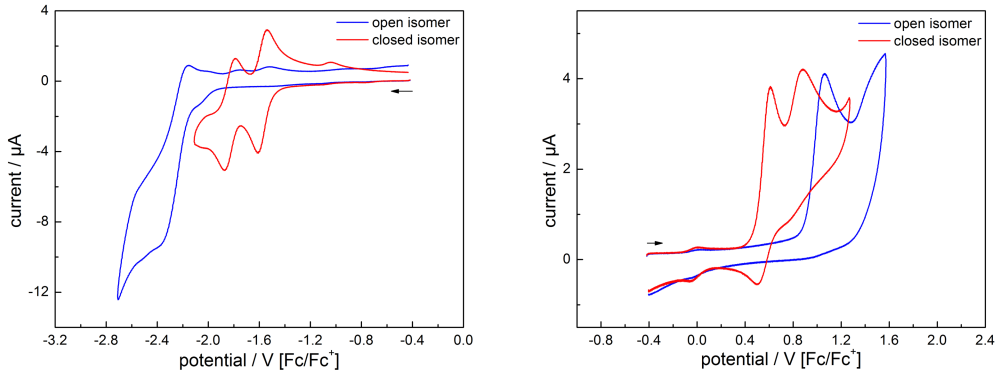

Figure A4-13. Cyclic voltammetry of **3i** (c = $1 \cdot 10^{-3}$ M) in acetonitrile / 0.1 M Bu_4NPF_6, dE/dt = 1 V s^{-1}.

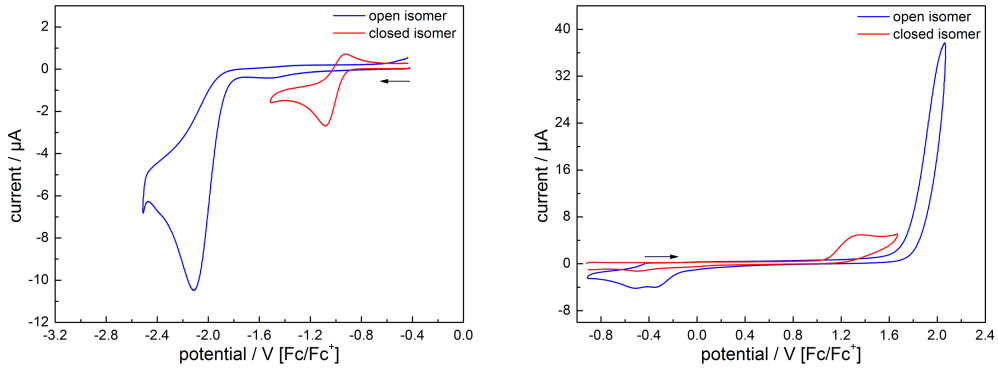

Figure A4-14. Cyclic voltammetry of **4i** (c = $1 \cdot 10^{-3}$ M) in acetonitrile / 0.1 M Bu_4NPF_6, dE/dt = 1 V s^{-1}.

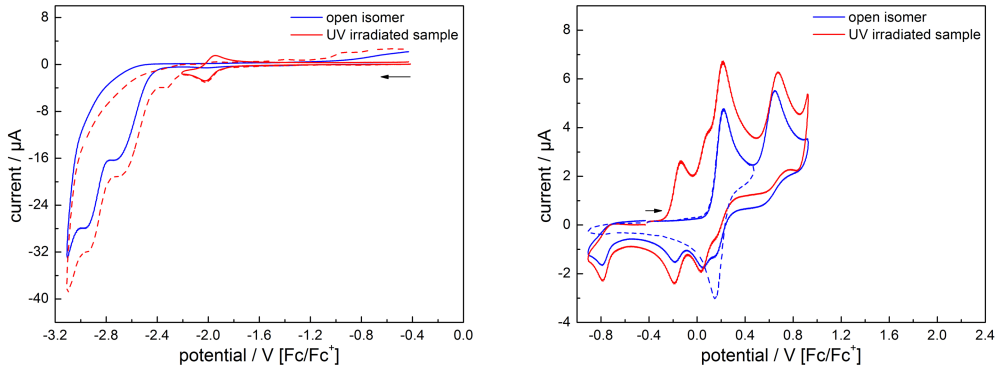

Figure A4-15. Cyclic voltammetry of **5a** (c = $1 \cdot 10^{-3}$ M) in acetonitrile / 0.1 M Bu_4NPF_6, dE/dt = 1 V s^{-1}. Due to low conversion in the electrochemical cell upon UV-irradiation the red line represents a mixture of the ring-open and ring-closed isomers.

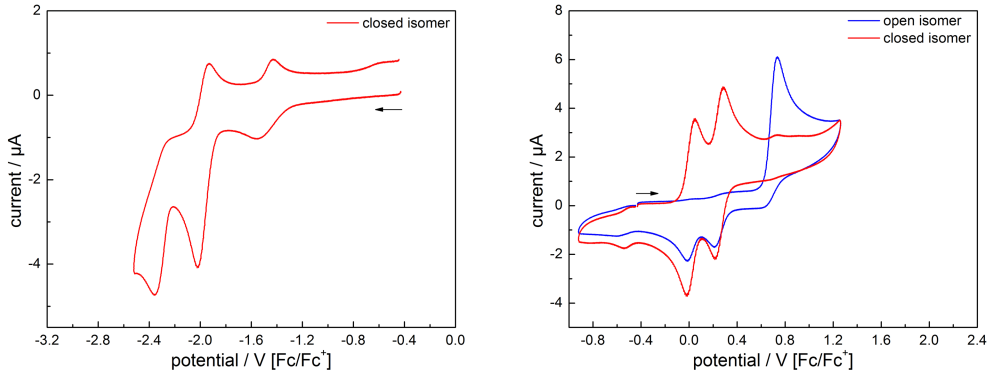

Figure A4-16. Cyclic voltammetry of **5b** (c = $1 \cdot 10^{-3}$ M) in acetonitrile / 0.1 M Bu_4NPF_6, dE/dt = 1 V s^{-1}.

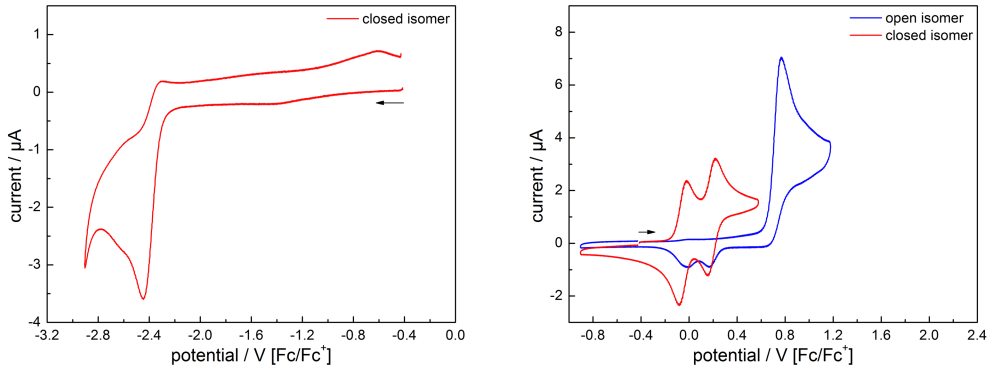

Figure A4-17. Cyclic voltammetry of **6c** (c = $1 \cdot 10^{-3}$ M) in acetonitrile / 0.1 M Bu_4NPF_6, dE/dt = 1 V s^{-1}.

8.5 Appendix 5: Low temperature NMR of 11a(bp)

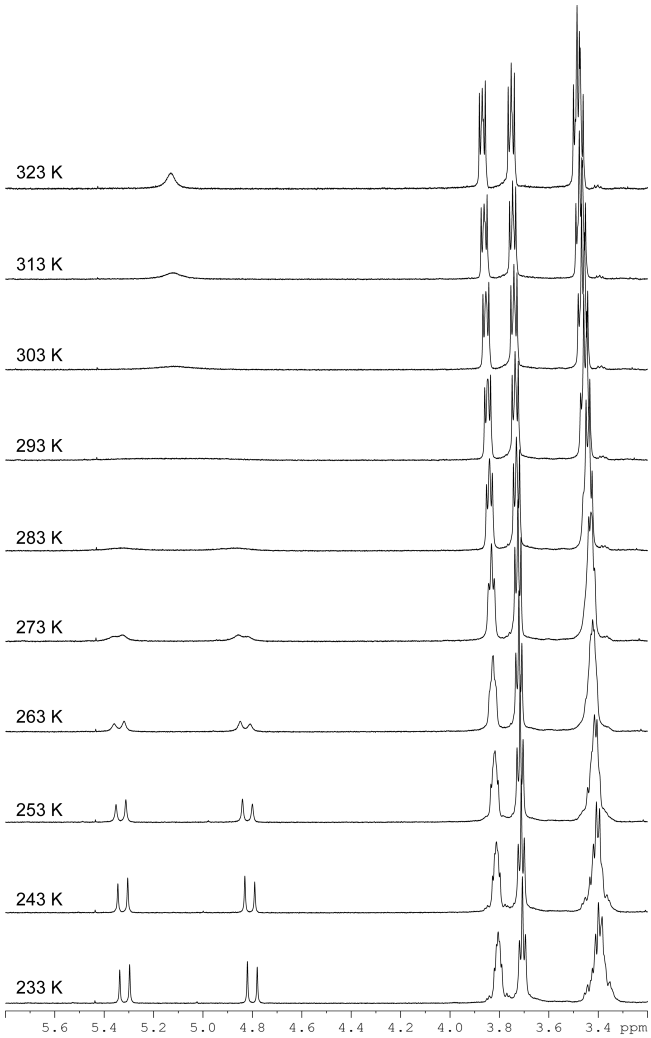

Figure A5-1. Detail of ^{1}H NMR spectra (400 MHz) of **11a(bp)** in CD_3CN at varying temperatures.

8.6 Appendix 6: Single-crystal X-ray data

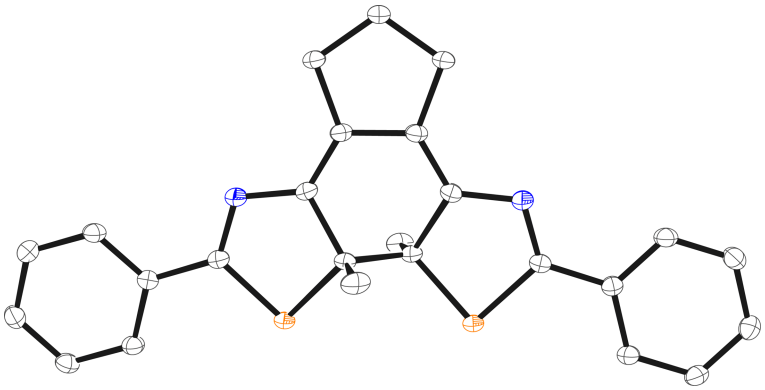

Figure A6-1. ORTEP-drawing (50% probability thermal ellipsoids) of the molecular structure of the ring-closed isomer **3d(c)** in the single-crystal as determined by X-ray diffraction. Hydrogens are omitted for clarity. Only one enantiomer is shown.

Crystal data for **3d(c)**:

Empirical formula	$C_{25}H_{22}N_2S_2$
Formula weight	414.56
Temperature	100(2) K
Wavelength	0.71073 Å
Crystal system, space group	Monoclinic, C2/c
Unit cell dimensions	a = 13.8855(7) Å , b = 19.3733(9) Å, c = 8.1757(4) Å, β = 109.7290(16)°.
Volume	2070.23(18) $Å^3$
Z, Calculated density	4, 1.330 g/cm^3
Absorption coefficient	0.271 mm^{-1}
F(000)	872
Crystal size	0.5 x 0.5 x 0.5 mm
Theta range for data collection	2.785 to 26.369°.
Limiting indices	-17<=h<=17, -24<=k<=24, -10<=l<=9
Reflections collected / unique	17526 / 2122 [R(int) = 0.0230]
Completeness to theta = 26.37	99.8%
Absorption correction	Empirical
Refinement method	Full-matrix least-squares on F^2
Data / restraints / parameters	2122 / 2 / 153
Goodness-of-fit on F^2	1.048
Final R indices [I>2σ(I)]	R_1 = 0.0339, wR^2 = 0.0892
R indices (all data)	R_1 = 0.0357, wR^2 = 0.0909
Largest diff. peak and hole	0.547 and -0.374 e $Å^{-3}$

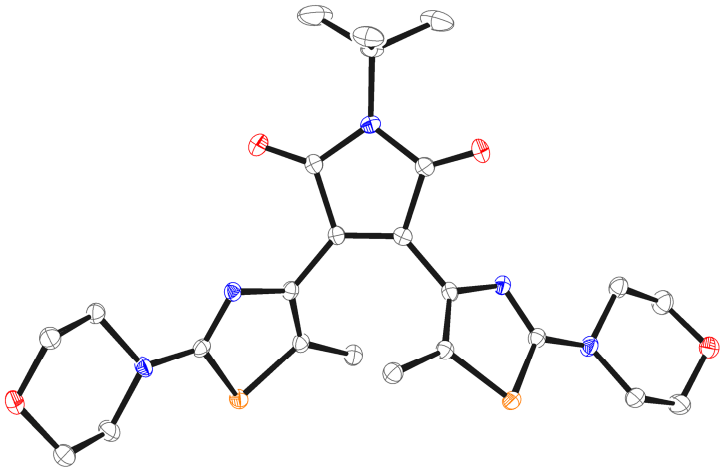

Figure A6-2. ORTEP-drawing (50% probability thermal ellipsoids) of the molecular structure of **11a(o)** in the single-crystal as determined by X-ray diffraction. Hydrogens are omitted for clarity. The unit cell consists of a second molecule of 11a, which only has minor differences in the conformation of one morpholino ring, and an additional solvent molecule (CH_3CN).

Crystal data for **11a** (CCDC: 904567):

Empirical formula	$C_{50}H_{65}N_{11}O_8S_4$
Formula weight	1076.41
Temperature	100(2) K
Wavelength	0.71073 Å
Crystal system, space group	Triclinic, P-1
Unit cell dimensions	a = 9.5692(5) Å, b = 16.6697(9) Å, c = 18.3711(9) Å, α = 114.843(4)°, β = 100.625(4)°, γ = 90.647(4)°
Volume	2600.7(2) $Å^3$
Z, Calculated density	2, 1.375 Mg/m^3
Absorption coefficient	0.248 mm^{-1}
F(000)	1140
Crystal size	0.26 x 0.20 x 0.18 mm
Theta range for data collection	4.69 to 25.00°
Limiting indices	-11<=h<=11, -19<=k<=17, -21<=l<=21
Reflections collected / unique	23457 / 8949 [R(int) = 0.0569]
Completeness to theta = 25.00	97.6%
Absorption correction	None
Refinement method	Full-matrix least-squares on F^2
Data / restraints / parameters	9979 / 6 / 669
Goodness-of-fit on F^2	0.947
Final R indices [I>2σ(I)]	R_1 = 0.0426, wR^2 = 0.0757
R indices (all data)	R_1 = 0.0763, wR^2 = 0.0852
Largest diff. peak and hole	0.466 and -0.308 e $Å^{-3}$

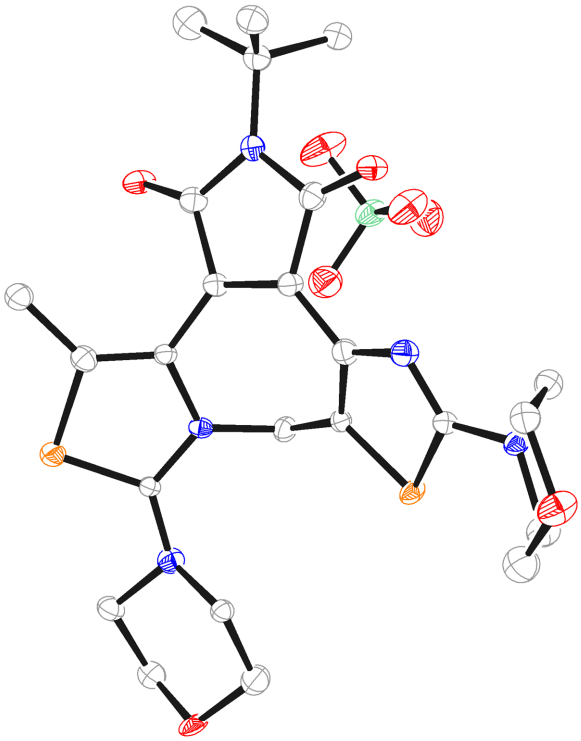

Figure A6-3. ORTEP-drawing (50% probability thermal ellipsoids) of the molecular structure of the ClO_4^- salt of **11a(bp)** in the single-crystal as determined by X-ray diffraction. Hydrogens are omitted for clarity.

Crystal data for **11a(bp)** (CCDC: 904568):

Empirical formula	$C_{24}H_{30}ClN_5O_8S_2$
Formula weight	616.10
Temperature	100(2) K
Wavelength	0.71073 Å
Crystal system, space group	Monoclinic, P 21/n
Unit cell dimensions	a = 10.7226(13) Å, b = 16.7313(14) Å, c = 14.7188(21) Å, β = 90.781(11)°
Volume	2640.4(5) $Å^3$
Z, Calculated density	4, 1.550 Mg/m^3
Absorption coefficient	0.363 mm^{-1}
F(000)	1288
Crystal size	0.20 x 0.06 x 0.05 mm
Theta range for data collection	2.26 to 25.50 °
Limiting indices	-12<=h<=12, -19<=k<=20, -17<=l<=17
Reflections collected / unique	20441 / 4899 [R(int) = 0.1268]
Completeness to theta = 25.50	100%
Absorption correction	None
Refinement method	Full-matrix least-squares on F^2
Data / restraints / parameters	4899 / 174 / 366
Goodness-of-fit on F^2	1.026
Final R indices [I>2σ(I)]	R_1 = 0.1099, wR^2 = 0.2809
R indices (all data)	R_1 = 0.1705, wR^2 = 0.3130
Largest diff. peak and hole	0.738 and -0.500 e A^{-3}

8.7 Compound index

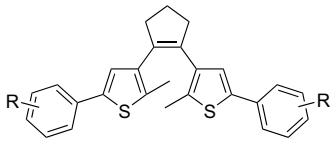

R = 4-Me_2N: **1a**
4-MeO: **1b**
4-Me: **1c**
H: **1d**
4-Br: **1e**
F_5: **1f**
4-EtOOC: **1g**
4-(n-C_6H_{13})OOC: **1h**
3,5-$(CF_3)_2$: **1i**

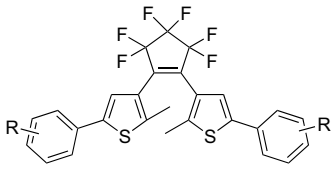

R = 4-Me: **2c**
3,5-$(CF_3)_2$: **2i**
3,5-$(SF_5)_2$: **2j**

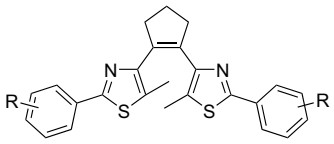

R = H: **3d**
3,5-$(CF_3)_2$: **3i**

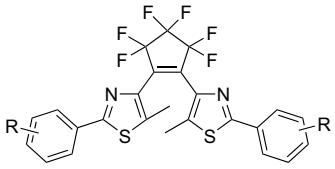

R = 3,5-$(CF_3)_2$: **4i**

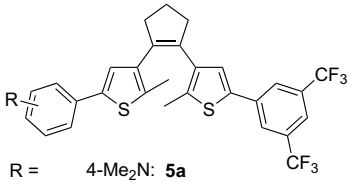

R = 4-Me_2N: **5a**
4-MeO: **5b**

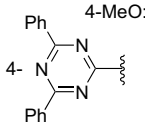

5k

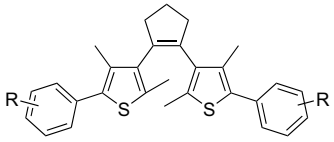

R = 4-Me: **6c**

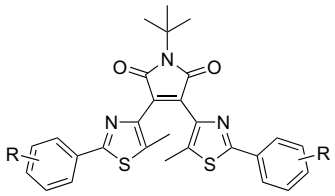

R = 3,5-$(CF_3)_2$: **7i**

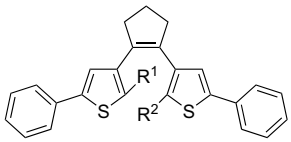

R^1 = R^2 = CF_3: **8b**

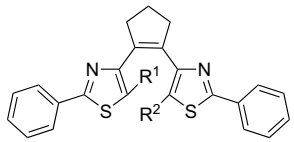

R^1 = R^2 = CF_3: **9b**
R^1 = CF_3, R^2 = CH_3: **9c**

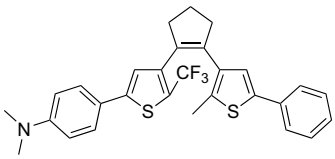

10c

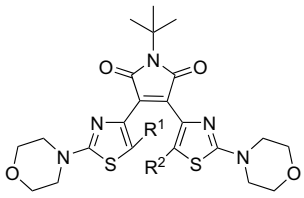

R^1 = R^2 = CH_3: **11a**
R^1 = R^2 = CF_3: **11b**
R^1 = CF_3, R^2 = CH_3: **11c**

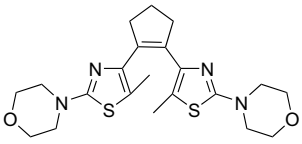

12

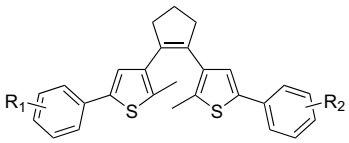

R_1 = R_2 = 3,5-(tBu)$_2$: **13a**
R_1 = 3-SAc, R_2 = 3,5-(tBu)$_2$: **13b**
R_1 = 4-SAc, R_2 = 3,5-(tBu)$_2$: **13c**

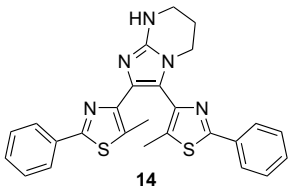

14

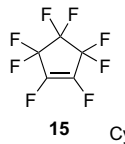

15

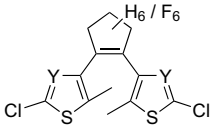

CyH_6, Y = CH: **16**
CyH_6, Y = CCH_3: **17**
CyF_6, Y = CH: **18**

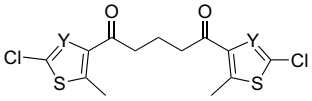

Y = CH: **19**
Y = CCH_3: **20**

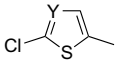

Y = CH: **21**
Y = CCH_3: **22**

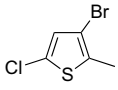

23

24

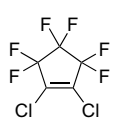

25

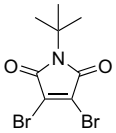

26

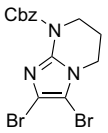

27

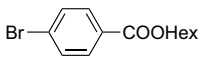

28

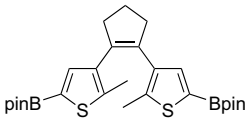

29

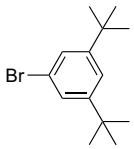

30

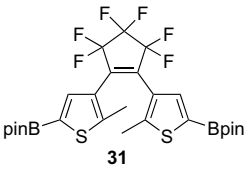

31

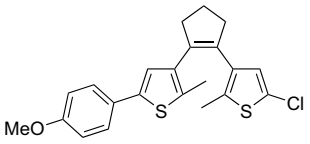

32

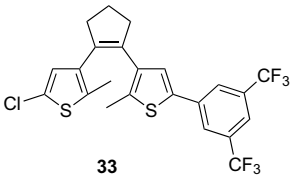

33

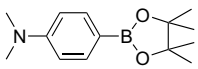

34

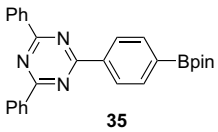

35

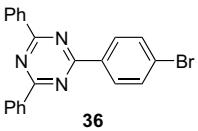

36

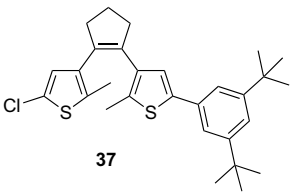

37

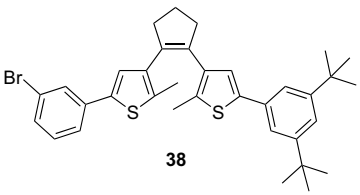

38

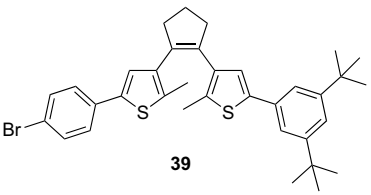

39

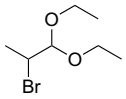

40

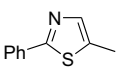

41

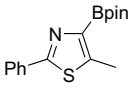

42

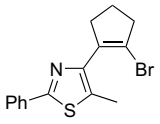

43

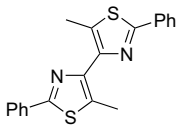

44

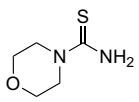

45

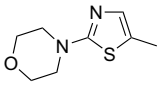

46

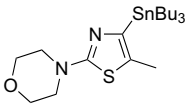

47

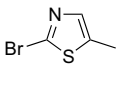

48

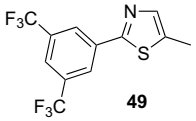

49

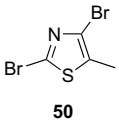

50

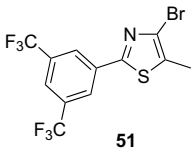

51

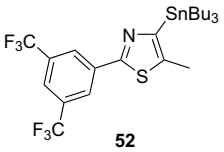

52

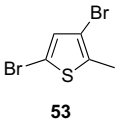

53

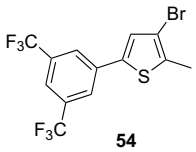

54

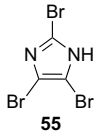

55

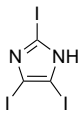

56

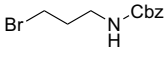

57

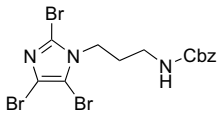

58

59

60

61

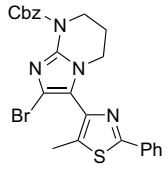

62

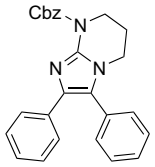

64

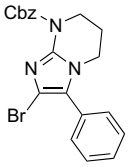

65

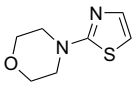

66

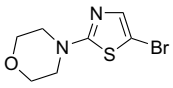

67

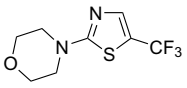

68

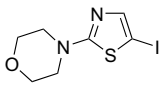

69

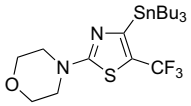

70

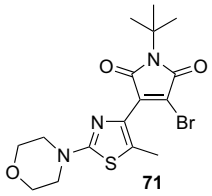

71

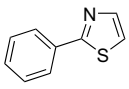

72

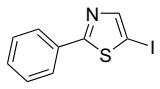

73

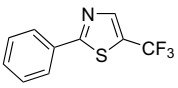

74

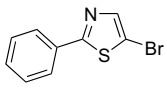

75

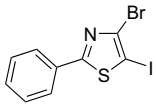

76

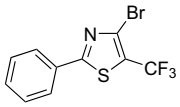

77

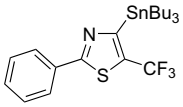

78

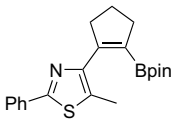

79

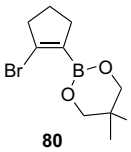

80

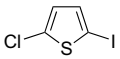

81

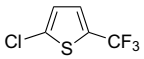

82

83

84

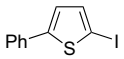

85

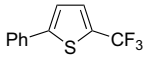

86

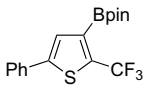

87

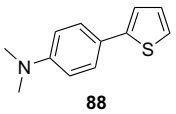

88

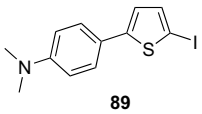

89

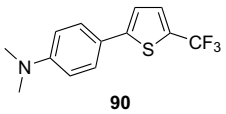

90

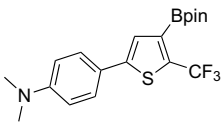

91

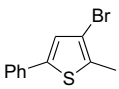

92

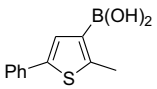

93

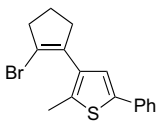

94

8.8 Abbreviations

ABI	2-Amino-1-methylbenzimidazole
Ac	Acyl
AFM	Atomic Force Microscopy
BA	Biacetyl / Butane-2,3-dione
Boc	*tert*-Butyloxycarbonyl
BTBT	2,7-Dodecylbenzothieno(3,2-b)benzothiophene
Cbz	Benzyloxycarbonyl
CT	Charge Transfer
CV	Cyclic Voltammetry
CyF_6	Hexafluorocyclopentene
CyH_6	Cyclopentene
DAE	Diarylethene
DCM	Dichloromethane
DFT	Density Functional Theory
DMAP	4-*N,N*-Dimethylaminopyridine
DMF	Dimethylformamide
DMSO	Dimethylsulfoxide
dppf	1,1′-Bis(diphenylphosphino)ferrocene
DTE	Dithienylethene
EDG	Electron-donating group
EWG	Electron-withdrawing group
Fc	Ferrocene
GIXD	Grazing Incidence X-ray Diffraction
GPC	Gel Permeation Chromatography
HOMO	Highest Occupied Molecular Orbital
ICBA	Indene-C_{60} bisadduct
IE	Ionization Energy
i-Pr	*iso*-Propyl
irr	irreversible
I-*t*Bu	*N*-*tert*-Butylmaleimide
LDA	Lithium diisopropylamide
LUMO	Lowest Occupied Molecular Orbital
MB	Methylene blue
MS	Mass Spectrometry
n-Bu	*n*-Butyl
n.d.	not determined

NHC	N-Heterocyclic Carbene
NICS	Nucleus Independent Chemical Shift
NMP	*N*-Methylpyrrolidone
NMR	Nuclear Magnetic Resonance
OTFT	Organic Thin Film Transistor
P3HT	Poly(3-hexylthiophene)
PCBM	Phenyl-C_{61}-butyric acid methyl ester
PDI	Polydispersity Index
phen	1,10-Phenanthroline
pin	Pinacol / 2,3-Dimethyl-2,3-butandiol
PSS	Photostationary state
qr	quasireversible
rev	reversible
ROP	Ring-Opening Polymerization
rt	room temperature
SCE	Standard Calomel Electrode
SPhos	2-Dicyclohexylphosphino-2',6'-dimethoxybiphenyl
SVD	Singular Value Decomposition
TBD	1,5,7-Triazabicyclo[4.4.0]dec-5-ene
*t*Bu / *tert*-Bu	*tert*-Butyl
THF	Tetrahydrofurane
TICT	Twisted Intramolecular Charge Transfer
TLC	Thin Layer Chromatography
TMS	Tetramethylsilyl
TS	Transition State
UPLC	Ultra-high Performance Liquid Chromatography
UPS	Ultraviolet Photoelectron Spectroscopy

Abbreviations for NMR spectra:

br	broad
d	doublet
m	multiplet
p	pentet
q	quartet
s	singlet
t	triplet

8.9 Publications

Journals:

[1] J. Polte, M. Herder, R. Erler, S. Rolf, A. Fischer, C. Würth, A.F. Thünemann, R. Kraehnert, F. Emmerling: "Mechanistic insights into seeded growth processes of gold nanoparticles", *Nanoscale* **2010**, *2*, 2463-2469.

[2] M. Herder, M. Patzel, L. Grubert, S. Hecht: "Photoswitchable triple hydrogen-bonding motif", *Chem. Commun.* **2011**, *47*, 460-462.

[3] E. Orgiu, N. Crivillers, M. Herder, L. Grubert, M. Pätzel, J. Frisch, E. Pavlica, D.T. Duong, G. Bratina, A. Salleo, N. Koch, S. Hecht, P. Samorì: "Optically switchable transistor via energy-level phototuning in a bicomponent organic semiconductor", *Nat. Chem.* **2012**, *4*, 675-679.

[4] J. Frisch, M. Herder, P. Herrmann, G. Heimel, S. Hecht, N. Koch: "Photoinduced reversible changes in the electronic structure of photochromic diarylethene films", *Appl. Phys. A* **2013**, *113*, 1-4.

[5] M. Herder, M. Utecht, N. Manicke, L. Grubert, M. Pätzel, P. Saalfrank, S. Hecht: "Switching with orthogonal stimuli: electrochemical ring-closure and photochemical ring-opening of bis(thiazolyl)maleimides", *Chem. Sci.* **2013**, *4*, 1028-1040.

[6] M. Herder, B.M. Schmidt, L. Grubert, M. Pätzel, J. Schwarz, S. Hecht: "Improving the Fatigue Resistance of Diarylethene Switches", *J. Am. Chem. Soc.* **2015**, *137*, 2738-2747.

[7] S. Bonacchi, M. El Garah, A. Ciesielski, M. Herder, S. Conti, M. Cecchini, S. Hecht, P. Samorì: "Surface-Induced Selection During In Situ Photoswitching at the Solid/Liquid Interface", *Angew. Chem. Int. Ed.* **2015**, *54*, 4865-4869.

[8] M. El Gemayel, K. Börjesson, M. Herder, D.T. Duong, J.A. Hutchison, C. Ruzié, G. Schweicher. A. Salleo, Y. Geerts, S. Hecht, E. Orgiu, P. Samorì: "Optically switchable transistors by simple incorporation of photochromic systems into small-molecule semiconducting matrices", *Nat. Commun.* **2015**, 6:6330, DOI: 10.1038/ncomms7330.

[9] K. Börjesson, M. Herder, L. Grubert, D.T. Duong, A. Salleo, S. Hecht, E. Orgiu, P. Samorì: "Optically switchable transistors comprising a hybrid photochromic molecule / n-type organic active layer", *J. Mater. Chem. C* **2015**, *3*, 4156-4161.

Talks:

[1] M. Herder, S. Hecht: "Strategies for the intrinsic optimization of diarylethenes as functional elements in light controlled organic electronics", Workshop of the Integrated Research Training group of the SFB 658, Zeuthen, Germany, 2013.

[2] M. Herder, S. Hecht: "Strategies for the intrinsic optimization of diarylethenes as functional building blocks", 8th PHENICS International Network Symposium, Berlin, Germany, 2013.

[3] M. Herder, R. Göstl, S. Hecht: "Diarylethenes: From improving fatigue resistance to controlling surface attachment", Colloquium of the SFB 658, Berlin, Germany, 2014.

Posters:

[1] M. Herder, L. Grubert, M. Pätzel, S. Hecht: "Strategies for the intrinsic optimization of diarylethene switches and their use as functional building blocks", 15th International Symposium on Novel Aromatic Compounds (ISNA-15), Taipei, Taiwan, 2013.

[2] M. Herder, L. Grubert, E. Orgiu, N. Crivillers, P. Samorì, S. Hecht: "Photoswitchable modulation of HOMO and LUMO levels for remote-controlling organic electronics with light", 6th International Meeting on Molecular Electronics (ElecMol'12), Grenoble, France, 2012.

[3] M. Herder, S. Hecht: "Diarylethenes as Functional Units for Remote-controlling Properties and Processes", SFB 658 International Symposium on Molecular Switches, Potsdam, Germany, 2012 and Central European Conference on Photochemistry (CECP 2012), Bad Hofgastein, Austria, 2012.

[4] M. Herder, M. Pätzel, L. Grubert, S. Hecht: "Photoswitchable triple hydrogen-bonding motif", 6th International Symposium on Organic Photochromism (ISOP 2010), Yokohama, Japan, 2010.

Selbstständigkeitserklärung

Hiermit versichere ich, dass ich die vorliegende Arbeit selbstständig und nur unter Verwendung der angegebenen Literatur und Hilfsmittel angefertigt habe.

Berlin, den 24.02.2015

Martin Herder